MM

TP 3987 E

Library and Information Centre / Centre de Documentation (GSLA)
RECEIVED - REÇU LE
APR 6 1983
Transport Canada / Transports Canada

FINAL REPORT

MODELLING THE RESPONSE OF AN LPG-CARRYING RAIL TANK CAR TO AN EXTERNAL FIRE ENVIRONMENT

PHASE I

Prepared For:

TRANSPORT CANADA TRANSPORTATION DEVELOPMENT CENTRE

Prepared By:

DAVIS ENGINEERING LIMITED
CONSULTING ENGINEERS
OTTAWA, CANADA

AUTHORS: T. Currie
D. Millar

APPENDICES C & D Prepared By:

Dr. S. Sjolander
Department of Mechanical & Aeronautical Engineering
Carleton University
Ottawa, Ontario

OCTOBER 1982

"THE CONTENTS OF THIS REPORT REFLECT THE VIEWS OF THE CONTRACTOR AND NOT NECESSARILY THE OFFICIAL VIEWS OR POLICIES OF THE TRANSPORTATION DEVELOPMENT CENTRE OF TRANSPORT CANADA."

REPORT DOCUMENTATION FORM

1. Transport Canada Report No. TP 3987 E	2. TDC Project No. 4559	3. Recipient's Catalogue No.
4. Title and Subtitle Modelling the Response of an LPG-Carrying Rail Tank Car to an External Fire Environment-Phase 1		5. Report Date October 1982 6. Performing Organization Report No.
7. Author(s) Currie, T. and Millar, D.A.J.		8. Transport Canada File No. D 1465-302-6-2
9. Performing Organization Name and Address Davis Engineering Limited, 1481 Cyrville Road, Ottawa, Canada		10. DSS File No. 11SD.T8200-1-1559 11. DSS or Transport Canada Contract No. OSD81-00158
12. Sponsoring Agency Name and Address Transportation Development Centre, 1000 Sherbrooke Street W., Montreal, P.Q.		13. Type of Report and Period Covered Technical 14. Sponsoring Agency Code TDC 4559
15. Supplementary Notes		16. TDC Project Officer D. Dibble

17. Abstract

Thermal, thermodynamic and structural models of an LPG-carrying rail tank car exposed to either an enveloping pool fire or an impinging torch fire are described in this report. Both unprotected tanks and tanks equipped with EXPLOSAFE foil and/or thermal insulation are modelled. The finite-difference method is adopted to analyse the heat flow inside the tank car. A sample computer program implementing the proposed numerical procedures is included.

The proposed thermodynamic model, which predicts changes in the state of the lading, permits the liquid in the tank to be non-isothermal.

The proposed structural model of a tank car in a fire uses a stress-rupture approach to predict failure since creep will be significant if the tank shell is exposed to high temperatures for a prolonged period of time.

The structure of the proposed computer model and the method of implementation is described.

18. Key Words Rail Tank Car, LPG, Pool Fire, Torch Fire, Thermal Computer Model Failure, BLEVE	19. Distribution Statement Copies available from TDC.

20. Security Classification (of this report) NIL	21. Security Classification (of this page) NIL	22. No. of Pages	23. Price NIL

TDC/CDT 79-005

FORMULE DE DOCUMENTATION POUR RAPPORT

1. N° du rapport Transports Canada
TP 3987 E

2. N° de l'étude — CDT
4559

3. N° de catalogue du destinataire

4. Titre et sous-titre
Modelling the Response of an LPG-Carrying Rail Tank Car to an External Fire Environment - Phase 1

5. Date du rapport
Octobre 1982

6. N° du rapport de l'organisme exécutant

7. Auteur(s)
Currie , T. and Millar, D.A.J.

8. N° de dossier Transports Canada
D 1465-302-6-2

9. Nom et adresse de l'organisme exécutant
Davis Engineering Limited,
1481 Cyrville Road,
Ottawa, Ontario

10. N° de dossier — ASC
11SD.T8200-1-1559

11. N° de contrat — ASC ou Transports Canada
OSD81-00158

12. Nom et adresse de l'organisme parrain
Centre de développement des transports
1000 rue Sherbrooke ouest
Montréal, Québec

13. Genre de rapport et période visée
Technique

14. Code de l'organisme parrain
CDT 4559

15. Remarques additionnelles

16. Agent de projet — CDT
D. Dibble

17. Résumé

Ce rapport décrit les modèles mathématiques représentant les contraintes thermiques, thermodynamiques et structurelles s'exerçant à l'intérieur d'un wagon de chemin de fer transportant du gaz de pétrole liquéfié, et soumis à l'action de flammes soit enveloppantes, soit à effet torche. Cette modélisation a voulu figurer des wagons standards et des wagons équipés du système de protection EXPLOSAFE ou d'un calorifugeage ordinaire, ou des deux. L'analyse des flux thermiques à l'intérieur des wagons a été faite par la méthode des différences finies. Le rapport renferme un spécimen du programme informatique mettant en oeuvre la méthodologie numérique proposée.

Le modèle thermodynamique envisagé prend en compte les variations dans l'état du chargement, et permet de la sorte d'éviter une représentation simplement isotherme du fluide véhiculé.

Pour le modèle devant figurer l'état de la structure d'un wagon soumis à l'action des flammes, l'approche suivie pour prédire l'imminence d'une défaillance a été celle du rapport entre les contraintes en jeu et les caractéristiques de rupture des matériaux, étant donné que le fluage devient un facteur important lorsque le corps du wagon est soumis pendant longtemps à des températures élevées.

Enfin ce rapport décrit le processus mathématique utilisé et explique la mise en oeuvre du modèle suggéré.

18. Mots-clés
Wagon citerne, Gaz de pétrole liquéfié, Flammes enveloppantes, Flammes à effet torche, Modélisation des flux thermiques, EXPLOSAFE

19. Diffusion
Un nombre limité d'exemplaires est disponible au CDT.

20. Classification de sécurité (de ce rapport)
AUCUNE

21. Classification de sécurité (de cette page)
AUCUNE

22. Nombre de pages

23. Prix
AUCUN

CDT TDC 79-005

TABLE OF CONTENTS

PAGE:

LIST OF TABLES viii
LIST OF FIGURES ix
NOMENCLATURE xvi

1.0 INTRODUCTION 1

2.0 THERMAL MODELS 6

- 2.1 Finite-Difference Procedure 7
  - 2.1.1 Spatial Difference Equations 8
  - 2.1.2 Time Integrations 20
  - 2.1.3 Linearization Procedures 31
- 2.2 Tank Car Geometry Description & Coordinate Systems 42
- 2.3 Pool Fire Thermal Analysis 50
  - 2.3.1 External Boundary Conditions 51
    - 2.3.1.1 Fire-to-Tank Radiative Heat Transfer 51
    - 2.3.1.2 Fire-to-Tank Convective Heat Transfer 55
  - 2.3.2 Unprotected Tank Car Thermal Analysis 66
    - 2.3.2.1 Internal Boundary Conditions 66
    - 2.3.2.2 Radiative Boundary Conditions in the Ullage 66
    - 2.3.2.3 Convective Heat Transfer to the Propane Vapour 79
    - 2.3.2.4 Heat Transfer from the Liquid-Wetted Tank Wall to the Liquid 90
    - 2.3.2.5 Unprotected Tank Car Thermal Analysis - Model Details 99
  - 2.3.3 EXPLOSAFE-Equipped Tank Car Thermal Analysis 127
  - 2.3.4 EXPLOSAFE Thermal Conductivity Predictions 128
    - 2.3.4.1 Style I EXPLOSAFE 130
    - 2.3.4.2 Style II EXPLOSAFE 135
    - 2.3.4.3 Style III EXPLOSAFE 136

TABLE OF CONTENTS (Cont'd)

PAGE:

2.3.5 EXPLOSAFE Thermal Conductivity Measurements 136

2.3.6 Comparison of Predicted & Measured EXPLOSAFE Thermal Conductivities (Styles I and III) 143

2.3.7 Radiative Heat Transfer in EXPLOSAFE 146

2.3.8 Convective Heat Transport in an EXPLOSAFE Matrix 152

2.3.9 Heat Transfer in a Tank Equipped with EXPLOSAFE- Model Details 155

2.4 Torch Fire Thermal Analysis 162

2.4.1 External Boundary Conditions 162

2.4.2 Dryout Probability and Consequences 188

2.4.3 Torch Fire Thermal Model 192

2.5 Insulation Models 195

3.0 THERMODYNAMIC MODELS 199

3.1 Period Before Pressure Relief 199

3.1.1 Tank Without EXPLOSAFE 199

3.1.2 Tank With EXPLOSAFE 217

3.2 Period After Relief Valve Opens 221

3.2.1 Tank Without EXPLOSAFE 221

3.2.2 Tank With EXPLOSAFE 230

3.3 Discharge Flowrate Calculation - Liquid Stagnation State 233

3.4 Discharge Flowrate Calculation - Vapour Stagnation State 241

4.0 TANK RUPTURE PREDICTION 244

4.1 Pool Fire Rupture Prediction 244

4.2 Stress Calculations 248

4.3 Failure Analyses 259

4.3.1 Comparison of Results of Larson-Miller Rupture Analysis with Experimental Results 269

TABLE OF CONTENTS (Cont'd)

PAGE:

4.4 Torch Fire Rupture Prediction 278
4.5 Finite-Element Rupture Analysis 281

5.0 MODEL SUMMARY 287

6.0 CONCLUSIONS & RECOMMENDATIONS 291

7.0 PROPOSED ACTIVITY SCHEDULE FOR THE DEVELOPMENT OF THE TANK CAR ANALYSIS PROGRAM 294

REFERENCES 296

APPENDICES

Appendix A - Sample Calculation of the Stability-Limited Time Step Size for the Explicit Time Integration Procedure 302

Appendix B - Liquid Level Calculations 305

Appendix C - Outer-Wall Convective Heat Transfer Coefficients for a Tank Car in a Pool Fire 317

Appendix D - Estimating Convective Heat Transfer Coefficients on the Inner Wall of a Propane Tank Lying in a Pool Fire 342

Appendix E - Sample Tank Car Thermal Analysis Program 380

Appendix F - Computer Program for Predicting the Resistance of the Strip AB Shown in Fig. 2-36 451

Appendix G - Calculations of the Nozzle Discharge Conditions for a Midland A-3480 Relief Valve 460

LIST OF TABLES

TABLE NO.	TITLE	PAGE NO.
2-1	Radiation Functions	76
2-2a	Fractions of energy emitted in non-absorbing wavelength ranges ($T_s = 852K$)	77
2-2b	Fractions of energy emitted in absorbing wavelength ranges ($T_s = 852K$)	78
2-3	Values of G (Pr)	84
2-4	Boiling heat transfer data for propane	92
2-5	EXPLOSAFE explosion suppression system material specifications	131
2-6a	Experimental data, Style I EXPLOSAFE	141
2-6b	Experimental data, Style II EXPLOSAFE	141
2-6c	Experimental data, Style III EXPLOSAFE	141
4-1	Limit pressures for pressure vessels with 2:1 ellipsoidal heads - predicted results for differenct tank diameter (D) to crown thickness (t_o) and crown thickness to knuckle thickness (t_1) ratios.	257
4-2	Elevated temperature test results on tank car steel	264
4-3	Results of Larson-Miller rupture analysis for tank car RAX 201	273

LIST OF FIGURES

FIGURE NO.	TITLE	PAGE NO.
2-1	Cylindrical Finite-Difference Grid	10
2-2	Cylindrical Coordinate System Nodal Control Volume	11
2-3	Tank Car Cross-Section Showing Plane of Thermal Symmetry A-A	15
2-4	Boundary Node on a Radial Surface with a Prescribed Heat Flux q"	17
2-5	Tank Outer Surface Node Exchanging Heat by Radiation and Convection With the Flame at Temperature T_f.	19
2-6	Banded Finite-Difference Equations	28
2-7	Convergence of the Newton-Raphson Method	39
2-8	Convergence of the Modified Newton-Raphson Method	40
2-9	Representation of a Tank Car by a Cylinder With Flat Ends	43
2-10	Full-Size DOT 112 (or 114) Tank Car	44
2-11	X-Y-Z Gravitational Coordinate System	46
2-12	Liquid Surface in the X-Y-Z Coordinate System	48
2-13	Global (X-Y-Z) and Tank Car Centered $(r-\theta-z)$ Coordinate Systems Showing Tank Car Roll and Pitch Angles, γ and α	49
2-14	Front Fire Temperatures vs. Time (from reference 10)	53

LIST OF FIGURES

(Cont'd)

FIGURE NO.	TITLE	PAGE NO.
2-15	Tank Car in a Pool Fire	53
2-16	Reynolds Number Increment (ΔRe_D) as a Function of Re_D	62
2-17	Infared Absorption Spectrum for Propane Vapor	70
2-18	(a) Blackbody Emissive Power as a Function of Wavelength and Temperature. (b) Comparison of Emissive Power of Ideal Blackbodies and Gray Bodies With That of a Real Surface	74
2-19	Convection Currents in Tank Ullage	80
2-20	Vapor velocity profile in venting tank	82
2-21	Vapor Velocity Distribution in a Tank With Two Relief Valves	87
2-22	Typical Boiling Curve Showing Wall Heat Flux (q") as a Function of Excess Temperature	91
2-23	Boiling of Propane (99% pure) from a Clean Horizontal Surface - from Cichelli and Bonilla (1945).	91
2-24	Heat Flux Spike at the Liquid/Wall Intersection	94
2-25	Geometry for View Factor Calculation	103
2-26	Elemental Surface area A_1 Viewing an infinitely Long Strip A_2	105

LIST OF FIGURES
(Cont'd)

FIGURES NO.	TITLE	PAGE NO.
2-27	End View of Surfaces 1 and 2 Shown in Fig. 2-26.	106
2-28	Geometric Parameters Needed to Obtain the View Factor for Surface 1 viewing Surface 2.	107
2-29	Geometry for Tank Car View Factor Calculations	109
2-30	Elemental Surface Areas A_1 and A'_1 at the Center and End of a Tank Car Respectively	110
2-31a	Geometry for Determing $\omega (\frac{1}{2} < \omega < 1)$, where $\omega = \frac{1}{2} (\sin \beta + \sin \phi)$	112
2-31b	Elemental Surface Area dA_1 Viewing an Infinitely Long Strip A_2	113
2-32	Geometrical Parameters for View Factor Calculations in a Tilted Tank Car.	116
2-33	Infinitesimal Surface Element dA_1 Viewing Rectangular Surface A_2	118
2-34	Geometrical Parameters for End Cap Elemental Surface Area (dA_1)-to-Liquid Surface (A_2) View Factor Calculations	120
2-35	Heat Transfer Rig Samples	129
2-36	Heat Transfer in Plane of Foil	132
2-37	Expanded View of Strip AB.	133
2-38a	EXPLOSAFE Thermal Conductivity Measuring Apparatus (for Styles I and III).	138

LIST OF FIGURES

(Cont'd)

FIGURES NO.	TITLE	PAGE NO.
2-38b	EXPLOSAFE Thermal Conductivity Measuring Apparatus	139
2-39	Foil Geometry for Radiation Calculations	147
2-40	Peak Wall Temperature vs. Time - All Tests	151
2-41	Finite-Difference Grid Superimposed on Tank Car Cross-Section	157
2-42	Torch Structure	166
2-43	Axial Heat Flux Density Distributions for Various Reynolds numbers	167
2-44	Radial Heat Flux Density Distributions for Various Distances from the Burner Nozzle	167
2-45	Calculated and Measured Heat Flux Density Distributions at the Stagnation Point of Turbulent, Partly premixed Methane-Air Flames	169
2-46	Influence of Probe Surface Temperatures on the Heat Transfer Coefficient for Various Axial Distances Between Plate and Burner	173
2-47	Radial Distribution of Heat Transfer from a Jet Striking a Plane Surface at 90 deg., Compared with the Radial Distributions of Velocity-temperature for a Free Jet (Hinze and van der Hegge Zijnen)	175
2-48	Torch Jet Control Volume	178

LIST OF FIGURES

(Cont'd)

FIGURE NO.	TITLE	PAGE NO.
2-49	Comparison of Measured and Predicted (using Eq. 2-114) Temperature Profiles for the BRL Torch at the Axial Coordinate Where the Torch Centerline Temperature and Velocity are the DOT Standard Values.	182
2-50	Propane Minimum Film Boiling Heat Flux vs. Reduced Pressure-experimental and Predicted Values	191
2-51	Excess Temperature at the Minimum Film Boiling Heat Flux vs. Reduced Pressure-experimental and Predicted Values.	191
2-52	Azimuthal Mesh Structure for Torch Fire Analysis	194
3-1	Internal Energy of Propane Lading in a DOT 112A (or 114A) Full Size Tank Car as a Function of Propane Temperature and Fill Percentage @ 20°C - No Discharge of Propane	201
3-2	Percentage of Liquid Propane in a DOT 112A (or 114A) Full Size Tank Car as a Function of Propane Temperature and Fill Percentage @ 20°C - No Discharge of Propane	202
3-3a	Liquid Temperature Profiles in Tank Car RAX 201.	205
3-3b	Liquid Surface Temperature and Corresponding Propane Vapor Pressure vs. Time	205
3-4	Comparison of Recorded Pressure in Tank Car RAX 201 with the Saturation Pressure of Pure Propane	207
3-5	Stratified Surface Layer Development	210

LIST OF FIGURES
(Cont'd)

FIGURE NO.	TITLE	PAGE NO.
3-6	Liquid Temperature Profiles Measured in a Pool Fire Test of a 1/5 Scale Insulated Tank Car	211
3-7	Growth of Isothermal Surface Layer	225
3-8	Critical Mass Flux of Propane as a Function of Reservoir Quality and Pressure	234
3-9	Midland A-3480 Safety-Relief Value	235
3-10	Critical Mass Flux (G) for Liquid Propane Stagnation State	239
4-1	Tank Car Distortion Due to Overheating of the Top of the Tank	246
4-2	Measured Torospherical Heat Deformations (46)	251
4-3	Stress-Strain Curve for a Rigid-Ideally Plastic Material	252
4-4	Plastic Collapse Pressures for 2:1 Ellipsoidal Head Pressure Vessels Based Upon the von Mises Yield Criterion	254
4-5	TC-128-B Steel Tensile Strength as a Function of Temperature (after RPI-AAR Program Data, RA-11-1-5, Phase 11 Report, 1971, p. 32).	262
4-6	Larson-Miller Plot of Stress-Rupture Data Given in Table 4-2 (for TC-128-B Steel)	265
4-7	Thermocouple Temperature vs. Time	271
4-8	Pressure vs. Time	272

LIST OF FIGURES
(Cont'd)

FIGURE NO.	TITLE	PAGE NO.
4-9	Accumulated life fraction (f_i) from Larson-Miller analysis	274
4-10	Comparison of ultimate strengths measured by Anderson et al. (Table 4-2 for TC-128 steel to RPI-AAR data	276
4-11	Comparison of Larson-Miller rupture analysis results with the stress governing rupture taken to be 1) von Mises stress and, 2) the hoop stress	279
5-1a	Program Flowchart	288
5-1b	Program Flowchart - continued	289
5-1c	Program Flowchart - continued	290

NOMENCLATURE

A	Area or absorbance (use should be obvious from context)
C	Capacitance matrix or local constant
C_p	Specific heat at constant pressure
C_v	Specific heat at constant volume
CHF	Critical heat flux
C.R.	Contraction ratio - ratio of width of EXPLOSAFE foil after expansion to width before expansion
d	Torch nozzle diameter or radiation path length in vapor (use should be obvious from context
D	Tank diameter
E	Young's modulus of elasticity
E.R.	Expansion ratio - ratio of length of EXPLOSAFE foil after expansion to length before expansion
f_i	Stress-rupture life fraction
f_q	Fraction of flame-to-tank heat flow entering the liquid
F_{1-2}	Radiation view factor for surface 1 viewing surface 2
g	Acceleration due to gravity

$G(p_r)$	Function of Prandtl number (see Table 2-3)
h	Enthalpy, heat transfer coefficient or height (use should be obvious from context)
h'	Separation between the bottom of a tank car and the ground (fuel surface)
i	Radial node index
I	Radiation intensity
I_o	Intensity of incident radiation
I_f	Intensity of transmitted radiation
j	Azimuthal node index
J	Jacobian matrix (used in Newton-Raphson method)
k	Thermal conductivity or axial node index (use should be obvious from context)
k_{e1}, k_{e2}, k_{e3}	Effective thermal conductivities of an EXPLOSAFE/vapor matrix in the Style I, II and III directions respectively (for heat transfer by conduction only)
K	Conductance matrix or vapor axial velocity gradient in tank (use should be obvious from context)
K_f	Empirical factor used in expression for torch flame stagnation point heat transfer coefficient
K_λ	Monochromatic extinction coefficient for radiation of wavelength λ
K'	$(C/\Delta t+K)$ - sum of the capacitance matrix (divided by Δt) and the conductance matrix

$K(i,j,k)_{i-1}$	Conductance between node i,j,k and node i-1,j,k. Conductances for other neighbouring nodes are similarly defined
ΣK	Sum of internodal conductances for node i,j,k
L, L_t	Tank car length
L.C.V.	Lower calorific value
M	Total number of nodes in the finite-difference grid, momentum of the torch jet, or the total mass of the lading (use should be obvious from context)
M_i	Initial momentum of the torch jet
M_ℓ	Mass of liquid in the tank car
M_v	Mass of vapor in the tank car
$\dot{m}$	Mass flowrate
n_s	Number of layers of EXPLOSAFE foil per unit depth
Nu	Nusselt number (hD/k or hx/k)
p	Pressure
P_r	Prandtl number ($= \mu C_p/k$)
P_r	Reduced pressure ($= p/p_c$, where p_c is the critical pressure)
q, q'' or $\dot{q}$	Heat flux
Q	Right-hand side heat flow vector for the system of finite-difference equations
$\dot{Q}$	Flame-to-tank heat flow rate

$\dot{Q}_{EX}$	Net rate of heat flow into the EXPLOSAFE/ vapor matrix in a tank car
r	Radial coordinate in the tank car centered coordinate system
r_p	Radius of base of pool fire
R	Gas constant or radiation exchange coefficient (use should be obvious from context)
R_e	Reynolds number ($= U\overline{x}/\nu$, where U is a velocity and $\overline{x}$ is a characteristic length)
R_{it}	Inner radius of tank car
s	Vertical distance measured from the bottom of a tank car
s_t	Vertical distance from the bottom of a tank car to the liquid surface
t	Thickness or time (use should be obvious from context)
T	Temperature (scalar or vector)
$\dot{T}$	Time derivative of T ($= dT/dt$)
T'	Turbulence intensity
u	Specific internal energy or substitution variable in torch fire size calculations (use should be obvious from context)
U	Total internal energy of the lading in a tank car or the velocity of the vapor in a venting tank (use should be obvious from context)
v	Specific volume

V	Total volume or velocity of flame gases (use should be obvious from context)
W	Width
x,y,z	Coordinates
X,Y,Z	Global coordinates
X^*	X-intercept of liquid surface
α	Tank car pitch angle
α_v	Coefficient of thermal expansion (volumetric)
β	Parameter in Falkner-Skan wedge flow description or angle used in tank wall-to liquid surface view factor calculations (see Fig. 2-31a) (use should be obvious from context)
γ	Ratio of specific heats for propane vapor (ie. C_{pv}/C_{vv}) or the roll angle of the tank car (use should be obvious from context)
δ	Gap between the EXPLOSAFE foil and the tank wall inner surface or a boundary layer thickness (use should be obvious from context)
ε	Convergence paramter
$\varepsilon_s, \varepsilon_1, \varepsilon_2$	Surface emissivity
η	$\sigma x/y$ in torch fire size calculations
θ	Angle or boundary layer momentum thickness (use should be obvious from context)

θ_s	Excess temperature (difference between wall and liquid saturation temperatures-needed in boiling heat flux calculations)
κ	Temperature gradient (dT/ds) in liquid propane (see Fig. 3-5)
λ	Wavelength
μ	Dynamic viscosity
ν	Kinematic viscosity
ρ	Density
σ	Mechanical stress or empirical constant (≈15.2) used in torch fire size calculations (use should be obvious from context)
σ_e	Effective stress
σ_h	Hoop Stress
σ_ℓ	Longitudinal Stress
σ_u	Ultimate strength of tank wall material
σ_y	Yield stress
ϕ	Angle used in tank wall-to-liquid surface view factor calculations (see Fig. 2-31a)
ω	See Eq. 2-42.

SUBSCRIPTS

a	ambient, air, atmospheric
al	aluminum
b	back side of plate
c	convective
d	nozzle discharge
D	tank diameter
e	edge of boundary layer or effective
EX	EXPLOSAFE
f	flame
i	inside or initial
l	liquid
m	EXPLOSAFE/vapor matrix
max	maximum
min	minimum
r	radiative
s	surface
st	stagnation point
t	torch
tf	torch flame
v	vapor
w	wall

SUPERSCRIPTS

n	nth estimate of solution vector in Newton-Raphson method
t	quantity evaluated at time t
$t+1$	quantity evaluated at time $t+\Delta t$

1.0 INTRODUCTION

The transportation of flammable materials, in particular those transported in a pressurized state (eg. liquified petroleum gas), is extremely hazardous because of the potentially calamitous consequences of transportation accidents (eg. train derailments) involving such cargoes. At the very least, a huge scorching fireball results when a containment vessel carrying a pressurized fuel ruptures in a fire. Much more serious are "Boiling Liquid Expanding Vapor Explosions" (BLEVE's) which occur if the temperature of a pressurized liquid cargo (not necessarily flammable) is greater than its homogeneous nucleation temperature at atmospheric pressure when the containment vessel ruptures. All of the liquid vaporizes in a few microseconds in that case (ie. the containment vessel effectively explodes) with results that can be devastating if the explosion occurs in an inhabited area, as witnessed by the death toll resulting from the explosion of a propane tank truck in a campground in Spain during the summer of 1978. It is in fact not always clear whether disastrous explosions involving pressurized fuels were true BLEVE's or simply "normal" ruptures and fireballs because the consequences of even normal ruptures can be very serious, particularly when such ruptures involve the "jumbo" (125 kl capacity) LPG carrying rail tank cars in use today.

Even the transport of non-flammable toxic chemicals can be very hazardous if rupture of the vessels carrying the chemicals leads to the release of poisonous gases. When transportation accidents involving such cargoes occur in densely populated areas the result is, at least, very disruptive, as witnessed by the large-scale evacuation of residents of Mississauga, Ontario in November, 1979 following the derailment of a train carrying toxic chemicals in that community.

While hazardous materials must obviously be transported, risks should be minimized by designing containment vessels to withstand severe accident conditions, in particular fires. An RPI-AAR Tank Car Research Committee was established in the United States in 1969 with a mandate to determine specific causes of derailment and tank car damage and develop methods and protection systems to minimize the risks involved in transporting hazardous materials, in particular liquified petroleum gases (LPG) and anhydrous ammonia, by rail. The RPI-AAR research program, in which actual tank car accidents were reviewed and controlled tank car fire tests performed, led to the issuance of DOT Dockets HM109 and HM144 (1) which specified the modifications that had to be made to all new and existing type 112A and 114A (125 kl) tank cars. The changes included redesigned couplers to resist disengagement during derailment, provision of heavy headshields to protect tank car heads from puncture by couplers of other cars, and a thermal protection system to limit heat transfer rates from pool and torch fires to the shell. Candidate thermal protection systems were required to pass simulated pool and torch fire tests specified in HM144 (1) before being approved for use. Several systems were approved, including certain ablative coatings and jacketed insulations (ie. insulative materials incased in steel jackets), but they were all essentially insulations of one form or another applied to the external surface of a tank car shell. Such external insulations can be scraped or torn off the tank surface in a derailment and, in the case of the ablative coatings, are subject to erosion by flame impingement during a fire and by long-term environmental attack. The jacketed insulations can melt, decompose or shrink during a fire thus losing much of their effectiveness.

An alternative method of preventing or at least delaying the rupture of an LPG-carrying tank car in a fire which does not suffer from the deficiencies mentioned previously in connection with external insulation has been proposed which places the protection system inside the tank. In this method, aluminum EXPLOSAFE* mesh is inserted inside the tank to transfer heat away from vapor-covered parts of the tank wall, where tank ruptures usually initiate due to overheating, into the liquid LPG. The high-conductivity EXPLOSAFE mesh enhances the conductivity of the vapor and allows the heat being transferred from the fire to the tank wall in the ullage to be dissipated to the liquid lading, which boils off and is safely released through the relief valve provided the valve is adequately sized.

The EXPLOSAFE tank protection system functioned successfully in pool fire tests of 1/5 scale rail tank cars performed at CFB Suffield, Alberta. Of the six vessels tested in those trials, two were datum vessels which did not contain EXPLOSAFE and four contained EXPLOSAFE in different configurations. Both of the unprotected datum vessels ruptured in the tests, while all of the EXPLOSAFE-equipped vessels remained intact and permitted their propane cargoes to boil off.

---

*Registered trademark of Vulcan Industrial Packaging Ltd.

The results of the tests of the EXPLOSAFE tank protection system were encouraging and indicated that further study of the concept was warranted. This report describes the elements of a thermal model which, once completely developed, will identify optimal orientations of the EXPLOSAFE mesh for full-size tanks and allow the protection offered by the EXPLOSAFE system to be compared with the protection offered by conventional external insulations. Two different fire environments are considered in the model, specifically a pool fire which completely envelopes the tank car and a torch fire which heats the tank locally at some point on its exterior.

The complete analytical model consists of thermal, thermodynamic and structural (failure) models which although each performing a specific function, interact to a certain extent. Heat transfer within the tank and heat transfer from the fire to the tank is calculated in the thermal model, the state of the lading (ie. temperature, pressure) and the volume of liquid remaining in the tank are calculated in the thermodynamic model and, lastly, the structural model predicts tank failure. A two-way interaction exists between the thermal and thermodynamic models in that the thermal model calculates the heat flow rate into the lading for the thermodynamic calculations and the thermodynamic model calculates the liquid level, liquid and vapor temperatures, etc, for the thermal calculations. The structural model obtains the tank wall temperature distribution from the thermal model and the tank pressure from the thermodynamic model for the purpose of predicting tank failure but otherwise is independent of the other two models.

The thermal, thermodynamic and structural models of a tank car in a fire are described in detail in Sects. 2, 3 and 4 respectively and a more detailed discussion of how they interact is given in Sect. 5. A flowchart of the complete model is also provided in Sect. 5. Required and recommended experiments which will reduce uncertainties in the analytical model are outlined in Sect. 6.

2.0 THERMAL MODELS

The tank car thermal models for the pool and torch fire scenarios will use the finite - difference method to solve the heat conduction equation in the tank wall, the external insulation (if present) and the EXPLOSAFE matrix (again, if present) subject to appropriate boundary conditions. The models will be formulated in the cylindrical $(r-\theta-z)$ coordinate system, for which the heat conduction equation can be written in a form applicable to an orthotropic material as,

$$\frac{1}{r}\frac{\partial}{\partial r}\left(r k_r \frac{\partial T}{\partial r}\right) + \frac{1}{r^2}\frac{\partial}{\partial \theta}\left(k_\theta \frac{\partial T}{\partial \theta}\right) + \frac{\partial}{\partial z}\left(k_z \frac{\partial T}{\partial z}\right) + q_v = \rho c \frac{\partial T}{\partial t} \tag{2-1}$$

where k_r, k_θ and k_z are the thermal conductivities of the material in the radial (r), azimuthal (θ) and axial (z) directions respectively, T is temperature, t is time, q_v is the heat generation rate per unit volume, ρ is the material density and c is the material specific heat. The thermal conductivities k_r, k_θ and k_z will be the same for the tank car shell if it is assumed that the shell material is isotropic but these conductivities will not be the same for the EXPLOSAFE/vapor matrix, when present. The conductivities of an EXPLOSAFE/vapor matrix in different orientations are derived in Sect. 2.3.4. External insulations will likely also be isotropic.

The finite-difference calculational procedure that will be used to solve Eq. 2-1 will be the same for all of the specific thermal analyses of a tank car in a fire, such as the analysis of a tank car with EXPLOSAFE in a pool fire or the analysis of a tank car without EXPLOSAFE in a pool fire, etc., although the boundary conditions and heat transfer mechanisms considered in each case will be different. For compactness of presentation, elements of the finite-difference solution procedure that will be common to all analyses will be formulated initially without reference to any specific analysis. The actual heat transfer mechanisms that will be considered in each specific analysis, the boundary conditions that will be imposed and details of the computational model will then be described in later sections for each of those analyses in turn.

The general development of the finite - difference procedure, which is described in the next section, is followed by a description of the coordinate systems needed to formulate the tank car model and, in particular, locate the liquid level in the tank for a specified liquid volume. Details of the pool and torch fire analyses for tank cars with and without EXPLOSAFE are considered next and insulation models are considered last since insulations will be treated in exactly the same manner in all of the pool and torch fire analyses

2.1 Finite-Difference Procedure

Equation 2-1 will be satisfied approximately within the tank car shell and, if present, the EXPLOSAFE lining in the vapor space and/or the external insulation, by expressing it in finite - difference form at a finite number of points, termed nodes or mesh points, within those regions. A finite - difference equation at a given node relates the temperature of that node at any given time to the temperature of the same node at some previous time and the instantaneous temperatures of the nodes around it. Writing the finite - difference equation for each node gives a system of equations that can be solved for all of the nodal temperatures at any instant in time and repeating this procedure for different times, starting from specified initial conditions, provides the temperatures of all of the nodes as functions of time.

The development of the finite - difference procedure that will be applied in the tank car model is described in Sects. 2.1.1, 2.1.2 and 2.1.3 of this report. Sect. 2.1.1 describes the manner in which the spatial derivatives in Eq. 2.1 are approximated in the finite - difference method and the equations derived in that section will be used in all of the thermal analyses. Sec. 2.1.2 discusses different techniques for integrating the spatially differenced equations derived in Sect. 2.1.1 with respect to time and describes the strengths and weaknesses of each technique. The decision as to which time integration procedure will be used in pool fire analyses and which procedure will be used in torch fire analyses will be deferred until after those analyses have been considered in detail in Sections 2.3 and 2.4 respectively, however. Methods that can be used to linearize non-linear finite - difference equations so that those equations can be solved simultaneously at each time step using methods applicable to linear equations are described in Sect. 2.1.3.

2.1.1 Spatial Difference Equations

Finite - difference approximations to the spatial derivatives in Eq. 2.1 can be derived in several ways; for instance, by expressing the temperature at each node as a truncated Taylor series involving the temperatures of surrounding nodes (2), but probably the most straightforward and intuitively appealing approach is the "heat balance" method, described in most elementary heat transfer texts (eg. see Holman (3)). This method considers neighbouring nodes to be connected by fictitious conducting rods with cross-sectional flow areas and lengths obtained from simple geometrical considerations and derives the finite - difference equation for a given node by equating the heat flows entering and leaving a control volume surrounding the node. If the finite - difference nodes are located at points where orthogonal grid lines intersect, as shown in Fig. 2.1 for an orthogonal grid superimposed on a cylinder, the control volume surrounding a node i, j, k located at r_i, θ_j, z_k is constructed as shown in Fig. 2.2 so that its boundaries bisect the distances between node i, j, k and its nearest neighbours. When the conductances between node i, j, k and its neighbours $i \pm 1, j, k$; $i, j \pm 1, k$ and $i, j, k \pm 1$ are designated $K(i, j, k)_{i \pm 1}$, $K(i, j, k)_{j \pm 1}$ and $K(i, j, k)_{k \pm 1}$ respectively and ΣK is the sum of those six conductances, a heat balance equation for the control volume surrounding node i, j, k can be written as:

$$
\begin{aligned}
&K(i, j, k)_{i+1}\,(T(i+1, j, k) - T(i, j, k)) + K(i, j, k)_{i-1} \\
&(T(i-1, j, k) - T(i, j, k)) + K(i, j, k)_{j+1}\,(T(i, j+1, k) \\
&- T(i, j, k)) + K(i, j, k)_{j-1}\,(T(i, j-1, k) - T(i, j, k)) \\
&+ K(i, j, k)_{k+1}\,(T(i, j, k+1) - T(i, j, k)) + K(i, j, k)_{k-1} \\
&(T(i, j, k-1) - T(i, j, k)) = (\rho c \frac{dT}{dt}(i, j, k) - q_v)\, V(i, j, k)
\end{aligned}
\tag{2-2a}
$$

or as,

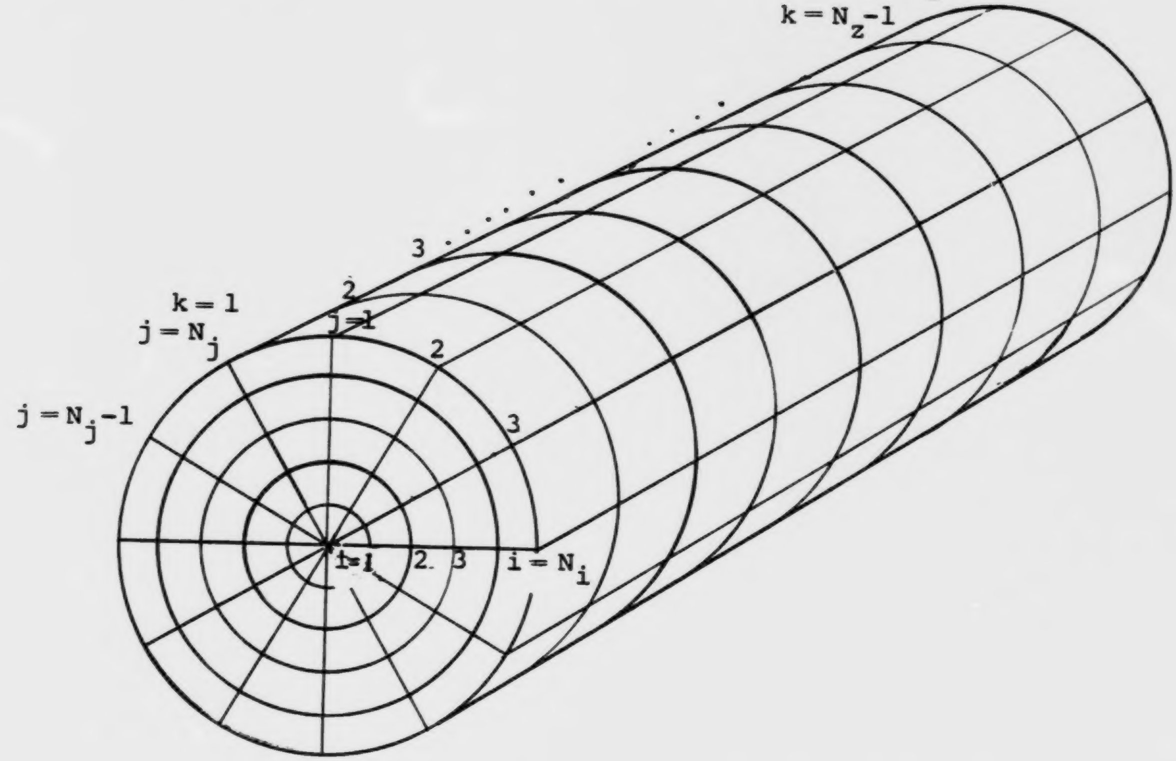
$k = N_z$
$k = N_z - 1$
3 . . . .
2
$k = 1$
$j = N_j$
$j = 1$
2
$j = N_j - 1$
3
$i = 1$
2
3
$i = N_i$

Fig. 2-1: Cylindrical finite-difference grid

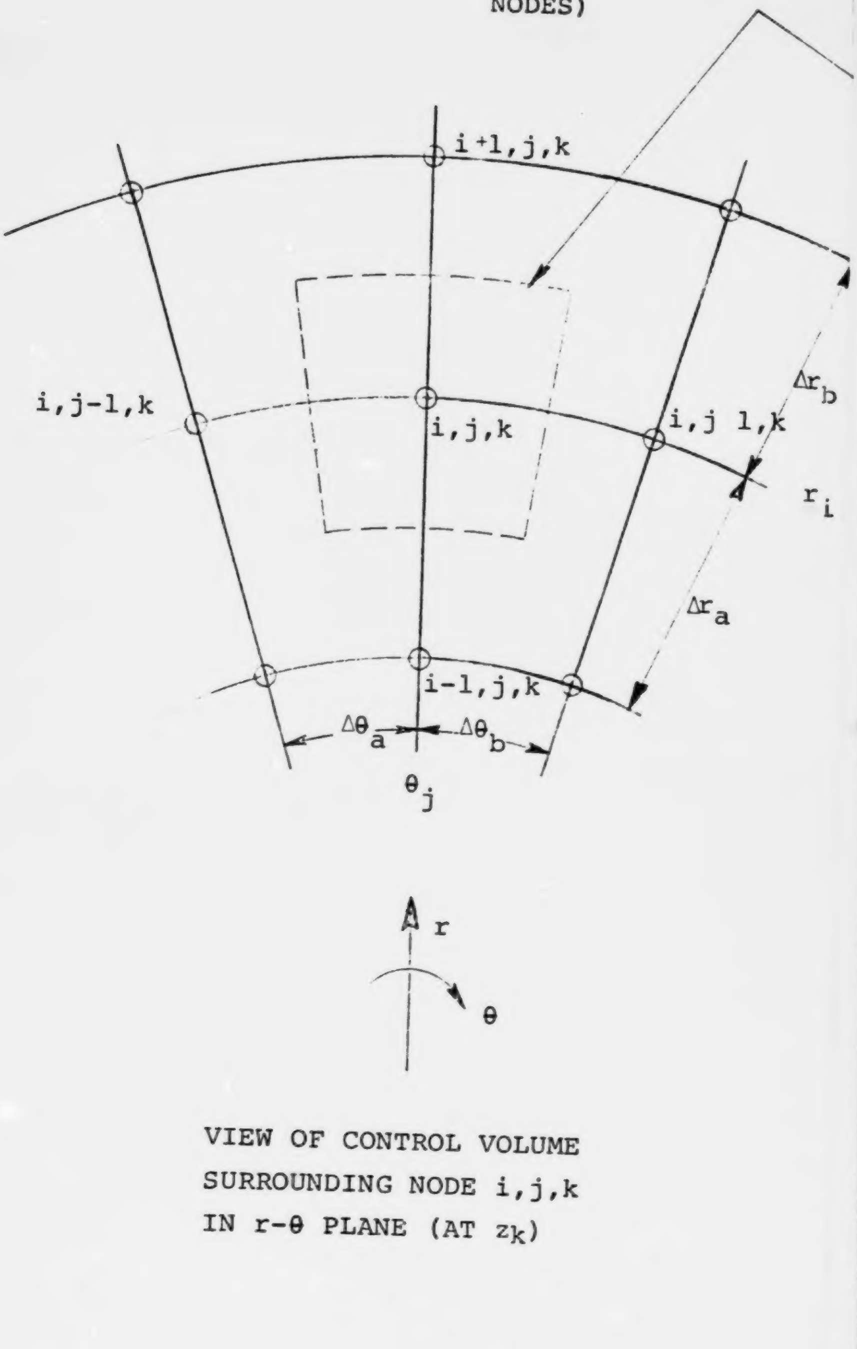
CONTROL VOLUME SURROUN
(BOUNDARIES BISECT DIS
NODES)
i+1,j,k
i,j-1,k
i,j,k
i,j 1,k
Δr_b
r_i
Δr_a
i-1,j,k
$\Delta\theta_a$
$\Delta\theta_b$
θ_j
r
θ

VIEW OF CONTROL VOLUME
SURROUNDING NODE i,j,k
IN r-θ PLANE (AT z_k)

Fig.: 2-2: Cylindrical Coordina

DING NODE i,j,k

TANCES BETWEEN

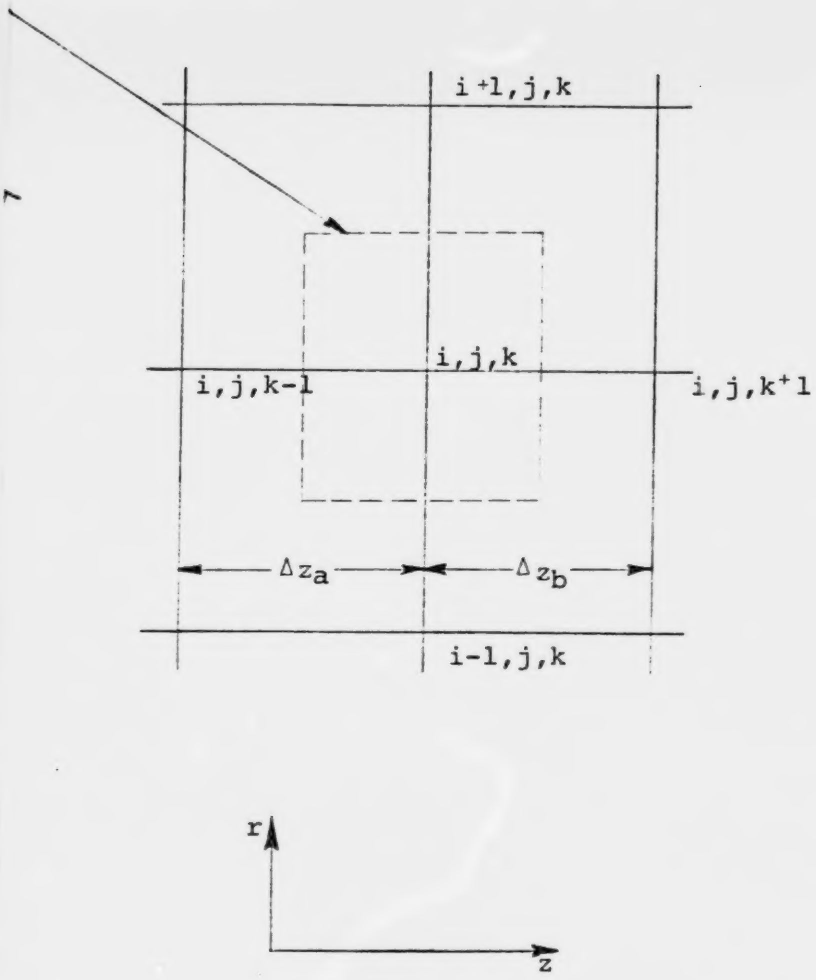
i+1,j,k
i,j,k
i,j,k-1
i,j,k+1
Δz_a
Δz_b
i-1,j,k
r
z

VIEW OF CONTROL VOLUME
SURROUNDING NODE i,j,k
IN r-z PLANE (AT θ_j)

Fig.: 2-2: Cylindrical Coordinate System Nodal Control Volume

e System Nodal Control Volume

$$K(i, j, k)_{i+1} T(i+1, j, k) + K(i, j, k)_{i-1} T(i-1, j, k) + K(i, j, k)_{j+1} T(i, j+1, k) + K(i, j, k)_{j-1} T(i, j-1, k) + K(i, j, k)_{k+1} T(i, j, k+1) + K(i, j, k)_{k-1} T(i, j, k-1) - \Sigma K\, T(i, j, k) = (\rho c \frac{dT}{dt}(i, j, k) - q_v) V(i, j, k) \qquad \text{2-2b}$$

where V(i, j, k) is the volume of the cell surrounding node i, j, k. The volumetric heat generation rate, q_v, will equal zero everywhere in a tank car and hence will be omitted in future equations.

With the geometric grid parameters Δr_a, Δr_b, $\Delta\theta_a$ $\Delta\theta_b$, Δz_a and Δz_b identified in Fig. 2-2, the internodal conductances between node i, j, k and its neighbours are given by the expressions,

$$K(i, j, k)_{i+1} = k_r (r_i + \frac{\Delta r_b}{2}) \overline{\Delta\theta}\ \overline{\Delta z} / \Delta r_b \qquad \text{2-3}$$

$$K(i, j, k)_{i-1} = k_r (r_i - \frac{\Delta r_a}{2}) \overline{\Delta\theta}\ \overline{\Delta z} / \Delta r_a \qquad \text{2-4}$$

$$K(i, j, k)_{j+1} = k_\theta\ \overline{\Delta r}\ \overline{\Delta z} / r_i\ \Delta\theta_b \qquad \text{2-5}$$

$$K(i, j, k)_{j-1} = k_\theta\ \overline{\Delta r}\ \overline{\Delta z} / r_i\ \Delta\theta_a \qquad \text{2-6}$$

$$K(i, j, k)_{k+1} = k_z \overline{\Delta r}\ r_i\ \overline{\Delta\theta} / \Delta z_b \qquad \text{2-7}$$

$$K(i, j, k)_{k-1} = k_z\ \overline{\Delta r}\ r_i\ \overline{\Delta\theta} / \Delta z_a \qquad \text{2-8}$$

where

$$\overline{\Delta r} = (\Delta r_a + \Delta r_b)/2 \qquad \text{2-9}$$

$$\overline{\Delta\theta} = (\Delta\theta_a + \Delta\theta_b)/2 \qquad \text{2-10}$$

$$\overline{\Delta z} = (\Delta z_a + \Delta z_b)/2 \qquad \text{2-11}$$

The volume of the cell associated with node i, j, k. (ie. $V(i, j, k)$) is

$$V(i, j, k) = r_i \overline{\Delta r} \; \overline{\Delta\theta}\overline{\Delta z}. \qquad 2\text{-}12$$

The geometric grid parameters Δr_a, Δr_b, $\Delta\theta a$, $\Delta\theta b$, Δz_a and Δz_b can be varied to give finer spatial discretization in regions where high temperature gradients are expected, such as around the torch in a torch fire analysis, than in other regions. Nodes are conserved in number in this manner because a coarse mesh can be used in regions where temperature gradients are small and / or high accuracy is not required.

Equation 2-2 applies to interior nodes in the finite-difference grid but must be modified for nodes on the boundaries. Boundary conditions take the form of either;

1) a specified temperature, T_o, on the boundary,
2) a specified heat flux, $q''(= -k\nabla T.\hat{n})$, on the boundary, where $\hat{n}$ is the outward facing surface normal,
3) a convective boundary condition, written in general form as $q'' = f(T,T_\infty)$ where T_∞ is the temperature of the medium with which the surface (at temperature T) is exchanging heat. If the functional relationship $f(T,T_\infty)$ is linear we can write $q'' = -k\nabla T.\hat{n} = h(T-T_\infty)$ where $h(\neq g(T)$ is the unit surface conductance. For radiation we have $q'' = R(T^4 - T_\infty{}^4)$ where R is a constant containing the emissivities of the surfaces at temperatures T and T_∞, the view factor between those surfaces, and the Stefan Boltzmann constant (5.669×10^{-8} W/m^2 $^oK^4$). Other non-linear functional relationships, which will be given as they are required later, can be written for boiling, natural convection, etc.

All of the boundary condition types mentioned above will be required in the tank car thermal model. Examples of each type follow. Boundary condition 1.) will be imposed on the uppermost nodes in the liquid - filled EXPLOSAFE mesh in the analysis of an EXPLOSAFE - equipped tank car. The temperatures of those nodes will be fixed at the temperature of the liquid at any given time and the rest of the nodes in the liquid will be eliminated from the model. The uppermost modes in the liquid - filled EXPLOSAFE will thus serve as boundary nodes for the ullage space EXPLOSAFE heat transfer analysis, as described in greater detail in Sect. 2.3.4

Boundary condition 2.) will be required when symmetry is used to reduce the size of the region modelled, in that q" must be set equal to zero on planes of thermal symmetry. When the external boundary conditions and construction of the tank car are such that the heat transfer problem can be assumed to be symmetrical about the plane A-A shown in Fig. 2-3, for instance, the boundary condition $\frac{\partial T}{\partial \theta}=0$ will be prescribed on plane A-A. The $r-\theta$ plane at the tank's axial midpoint could also be a plane of symmetry in certain situations, in which case the boundary condition $\frac{\partial T}{\partial z}=0$ would be prescribed over that plane.

Boundary condition 3.) will be used on the inner surface of the vapor - covered section of the tank wall to account for heat transfer by convection to the propane vapor and heat transfer by radiation to the liquid surface. This type of boundary condition will be prescribed on the inner surface of the liquid - wetted part of the tank wall to model heat transfer to the liquid by boiling

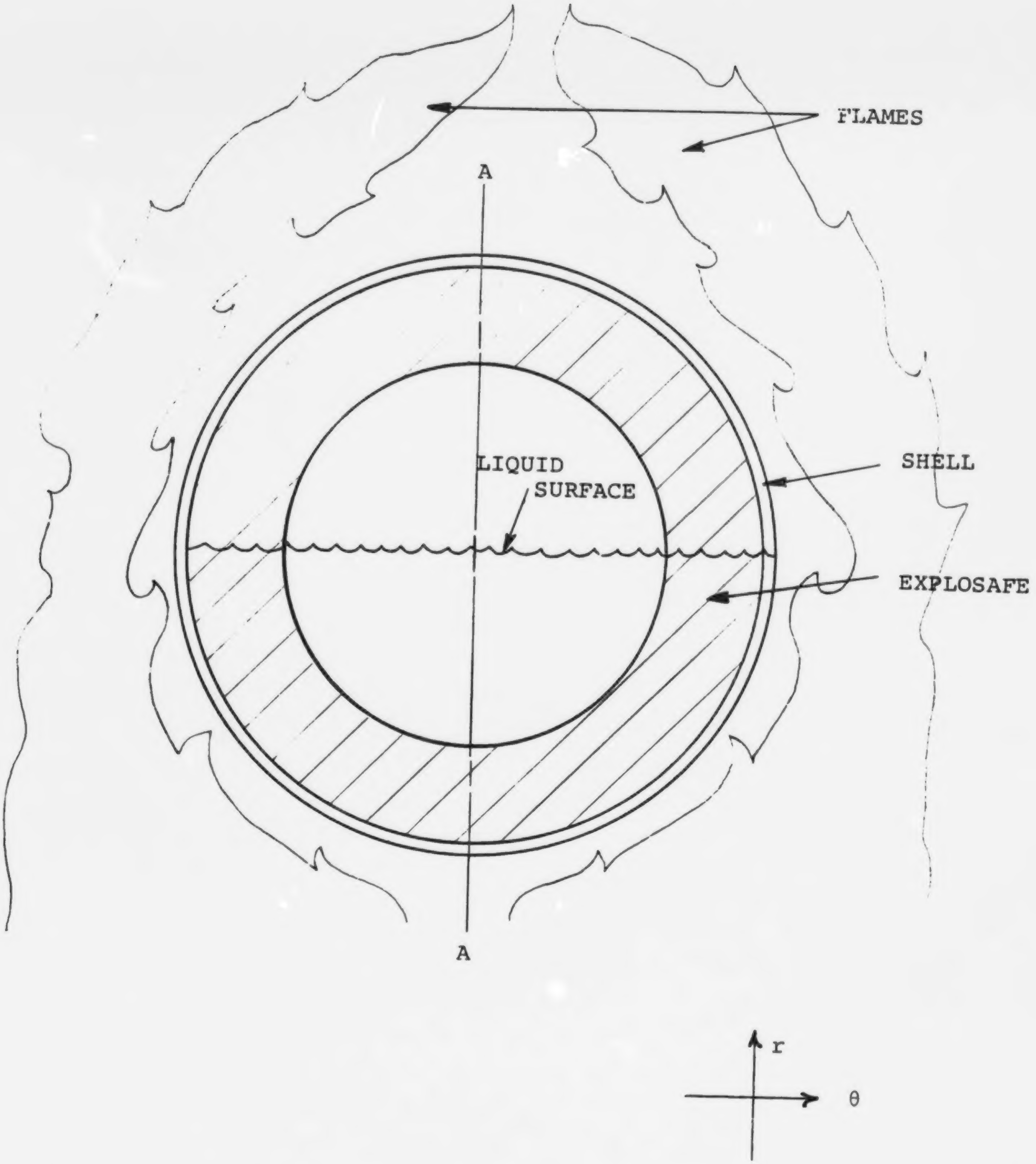
FLAMES
A
LIQUID
SURFACE
SHELL
EXPLOSAFE
A
r
θ

Fig.: 2-3: Tank Car Cross-section Showing Plane of Thermal Symmetry A-A.

at high heat fluxes and by natural convection at low heat fluxes. Boundary conditions of the third type will also be prescribed on the outer surface of the tank wall to model heat transfer between the fire and the tank by radiation and natural convection. All of these boundary conditions are described in greater detail in Sects. 2.3.1 and 2.3.2.

Finite - difference equations applicable to boundary nodes can be obtained by straightforward modification of Eq. 2-2. If the temperature of the node at r_i, θ_{j+1}, z_k is fixed at T_o, for instance, the term associated with that node in Eq. 2-2 is constant and can be transferred to the right-hand side of the equation to give:

$$\begin{aligned}&K(i,\ j,\ k)_{i+1}\ T(i+1,\ j,\ k) + K(i,\ j,\ k)_{i-1}\ T(i-1,\ j,\ k)\\&+K(i,\ j,\ k)_{j-1}\ T(i,\ j-1,\ k) + K(i,\ j,\ k)_{k+1}\ T(i,\ j,\ k+1)\\&+K(i,\ j,\ k)_{k-1}\ T(i,\ j,\ k-1) - \Sigma K\ T(i,\ j,\ k) = \rho c\ V(i,\ j,\ k)\\&\frac{dT}{dt}(i,\ j,\ k) - K(i,\ j,\ k)_{j+1}\ T_o \qquad 2\text{-}13\end{aligned}$$

Similarly, Eq. 2-2 can be applied to a boundary node where q" is prescribed and, for example, the outward facing surface normal $\hat{n}$ is directed in the $+\theta$ direction (ie. in the direction of increasing θ and j), by setting $\Delta\theta_b = 0$, since the region on the $+\theta$ side of node i, j, k does not exist (as seen in Fig. 2-4), and recognizing that the heat flow leaving the node because of the prescribed surface heat flux (q") is $q''A_s(i,j,k)$, where $A_s(i,\ j,\ k) = \Delta r\ \Delta z$ is the surface area of the node. With these modifications Eq. 2-2 becomes

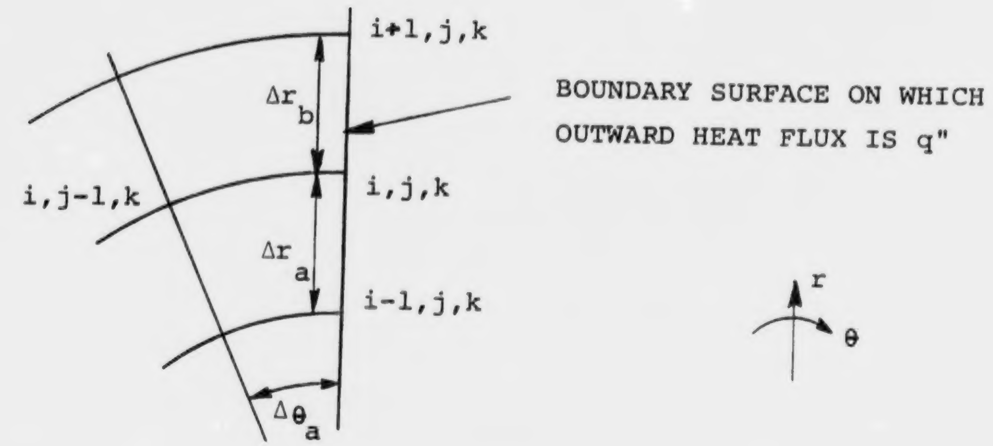
i+1,j,k
Δr_b
BOUNDARY SURFACE ON WHICH OUTWARD HEAT FLUX IS q"
i,j-1,k
i,j,k
Δr_a
i-1,j,k
r
θ
$\Delta\theta_a$

Fig.: 2-4: Boundary node on a radial surface with a prescribed heat flux q"

$$K(i, j, k)_{i+1} T(i+1, j, k) + K(i, j, k)_{i-1} T(i-1, j, k) + K(i, j, k)_{j-1} T(i, j-1, k) + K(i, j, k)_{k+1} T(i, j, k+1) + K(i, j, k)_{k-1} T(i, j, k-1) - \Sigma K\, T(i, j, k) = \rho c V(i, j, k) \frac{dT}{dt} (i, j, k) + q'' A_s(i, j, k) \qquad 2\text{-}14$$

where it should be understood that $\Delta\theta_b$ is set equal to zero in all of the internodal conductances in Eq. 2-14. Similarly, $\Delta r_a = 0$ and $\Delta r_b = 0$ for nodes on internal and external cylindrical surfaces respectively, $\Delta z_a = 0$ and $\Delta z_b = 0$ for nodes on the cylinder ends at the initial and final values of z respectively and $\Delta\theta_a = 0$ on surfaces for which n is directed in the direction of decreasing θ.

As an example of the manner in which a finite-difference equation is obtained for a boundary node where the third type of boundary condition is prescribed, consider a node on the outer surface of a tank car exchanging heat by radiation and convection with an adjacent flame at temperature T_f. Performing a heat balance on such a node, shown in Fig. 2-5, gives the expression ,

$$K(i, j, k)_{i-1} T(i-1, j, k) + K(i, j, k)_{i,\, j+1,\, k} T(i, j+1, k) + K(i, j, k)_{i,\, j-1,\, k} T(i, j-1, k) + K(i, j, k)_{i,\, j,\, k+1} T(i, j, k+1) + K(i, j, k)_{i,\, j,\, k-1} T(i, j, k-1) - \Sigma K T(i, j, k) - (q''_{fc} + q''_{fr}) A_s(i, j, k) = \rho c V(i, j, k) \frac{dT}{dt} (i, j, k) \qquad 2\text{-}15$$

where $\Delta r_a = 0$ in Eqs. 2-4 and 2-9.

q''_{fc} = convective heat flux between the fire and the tank

$= h_f(T(i, j, k) - T_f)$ 2-16

q''_{fr} = radiative heat flux between the fire and the tank

$= R(T(i, j, k)^4 - T_f^{\,4})$ 2-17

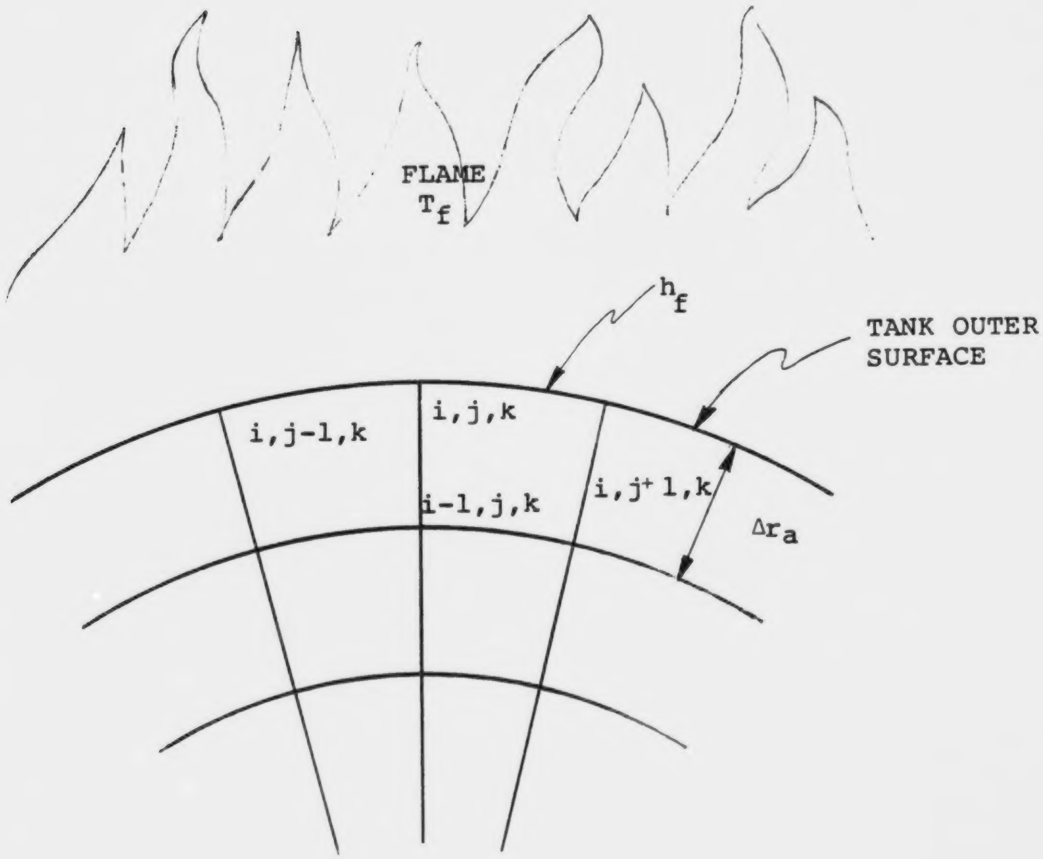
FLAME
T_f
h_f
TANK OUTER SURFACE
i,j-1,k
i,j,k
i-1,j,k
i,j+1,k
Δr_a

Fig.: 2-5: Tank Outer Surface Node Exchanging Heat by Radiation and Convection with the Flame at Temperature T_f.

Expressions for the fire-to-tank convective heat transfer coefficient h_f and the radiation exchange coefficient R are given in Sects. 2.3.1.1 and 2.3.1.2 respectively. Substituting Eqs. 2-16 and 2-17 into Eq. 2-15 and transferring constant terms to the right-hand side of the resulting equation yields the following finite - difference equation for the outer surface node i, j, k.

$$\begin{aligned}
&K(i, j, k)_{i-1}\, T(i-1, j, k) + K(i, j, k)_{j+1}\, T(i, j+1, k) \\
&+K(i, j, k)_{j-1}\, T(i, j-1, k) + K(i, j, k)_{k+1}\, T(i, j+k\ 1) \\
&+k(i, j, k)_{k-1}\, T(i, j\ k-1). \\
&-\left[\Sigma K + (h_f + RT(i, j, k)^3) A_s(i, j, k)\right]\ T(i, j, k) \\
&=\rho c V(i, j, k) \frac{dT}{dt} (i, j, k) \qquad -(h_f + RT_f^3)\ A_s(i, j, k) T_f
\end{aligned} \qquad 2\text{-}18$$

Equation 2-18 is a non-linear equation because T(i, j, k) is raised to the fourth power in the radiation term. The system of finite - difference equations defining temperatures of the nodes in the tank car will be non-linear in general, as discussed in greater detail in Sect. 2.1.3.

2.1.2 Time-Integrations

Finite - difference equations similar to those given previously for an interior node and different types of boundary nodes will be obtained for all of the nodes in the finite - difference grid representing the tank car shell, external insulation and the EXPLOSAFE in the tank ullage, if present. Such a system of finite - difference equations can be written in matrix form as:

$$C\dot{T} = Q - KT \qquad 2\text{-}19$$

or as: $$\dot{T} = C^{-1} (Q - KT) \qquad 2\text{-}20$$

where C is a diagonal capacitance matrix containing the nodal capacitances (ie. $C_{m,\,m} = \rho c V(m)$ and $C^{-1}_{m,\,m} = 1/\rho c V(m)$ for the mth node in the grid, where the value of m corresponding to a given node i, j, k will depend on the order in which the nodes in the grid are numbered), $\dot{T}$ is a vector containing the time derivatives $(dT(m)/dt)$ of the nodal temperatures, Q is a "heat flow" vector containing the constant terms in each nodal equation, K is a conductance matrix containing the internodal conductances (ie. finite - difference coefficients), and T is the vector of nodal temperatures. Equation 2-20, which applies at any instant in time, represents a system of M (M is the total number of nodes in the grid) ordinary differential equations which must be integrated with respect to time, starting with the initial temperature distribution in the tank at the start of the fire, to obtain the desired transient solution.

The system of ordinary differential equations represented by Eq. 2-20 could be integrated with respect to time by applying one of the standard integration methods (eg. Euler, Runge-Kutta, predictor-corrector, etc.), but the integrations are usually performed in heat transfer analyses by expressing the time - derivatives as backward, central, or forward differences. A general expression which includes all of these possibilities can be obtained by expressing the average value of T between times t and $t + \Delta t$ as a weighted average of the forward-difference, $\dot{T}^{t} (= C^{-1}(Q - KT^{t}))$ and the backward - difference, $\dot{T}^{t+1} (= C^{-1}(Q - KT^{t+1}))$* representations of $\dot{T}$. The resulting expression, which is known as the generalized six - point formula (2), is,

---

* The superscript $t+1$ refers to a quantity evaluated at time $t + \Delta t$.

$$\frac{C}{\Delta t}(T^{t+1}-T^{t}) = w(Q - KT^{t+1}) + (1 - w)(Q - KT^{t}) \qquad 2\text{-}21$$

where $w(0 \leq w \leq 1)$ is a weighting parameter. The forward, backward and mid - dfference schemes, which are often referred to as the explicit (or Euler), implicit, and Crank-Nicolson methods respectively, can be obtained from Eq. 2-21 by specifying $w=0$, 1 or ½ respectively. A Galerkin differencing scheme is obtained when $w = 2/3$.

A system of simultaneous equations has to be solved to obtain T^{t+1} from T^{t} when $w = 1$ in Eq. 2-21. This is a serious liability when the number of nodes in the finite - difference model (M) is large because a correspondingly large memory allocation is required to store the necessary elements in the conductance matrix K, round-off errors incurred during the equation solution can ruin the accuracy of the final solution, and computing times required to solve the simultaneous equations can be prohibitively long. The finite - difference equations do not have to be solved simultaneously when $w = 0$, however, because each nodal temperature at time $t + 1$ can be calculated explicitly from the temperatures of the surrounding nodes at time t, explaining the designation "explicit method". The temperature of an interior node i, j, k at time $t + 1$ (ie. $T^{t+1}(i, j, k)$) can be obtained explicitly by forward - differencing the time derivative in Eq. 2-2 to give;

$$
\begin{aligned}
T^{t+1}(i, j, k) = {} & \frac{\Delta t}{\rho c V(i, j, k)} \Big[(K(i, j, k)_{i+1} T^{t}(i+1, j, k) \\
& + K(i, j, k)_{i-1} T^{t}(i-1, j, k) + K(i, j, k)_{j+1} T^{t}(i, j+1, k) \\
& + K(i, j, k)_{j-1} T^{t}(i, j-1, k) + K(i, j, k)_{k+1} T^{t}(i, j, k+1) \\
& + K(i, j, k)_{k-1} T^{t}(i, j, k-1) + \left(\frac{\rho c V(i, j, k)}{\Delta t} - \Sigma K\right) T^{t}(i, j, k) \Big]
\end{aligned}
\qquad 2\text{-}22
$$

for instance. Similar explicit equations for the temperatures of boundary nodes at time $t+\Delta t$ can be easily obtained.

The explicit method is very straightforward to program in that equations similar to Eq. 2-22 can be placed inside nested DO loops which sweep sequentially through the nodal indices i, j and k for interior and boundary nodes. Non-linear terms, such as the term involving $T(i, j, k)^3$ in Eq. 2-18, can be updated using the temperatures at time t to advance to time $t+\Delta t$. The explicit method does have one deficiency, however, which is that the maximum time step size that can be used with the method, designated Δt_{max}, is limited by stability considerations. A fairly accurate estimate of the value of Δt_{max} can be obtained by calculating the value of Δt at which any diagonal entry of the matrix $(C/\Delta t - K)$ becomes negative (2). The mth diagonal entry of this matrix, designated $\lambda(m)$, is given by the expression,

$$\lambda(m) = \frac{\rho c V(m)}{\Delta t} - K \qquad 2\text{-}23$$

so the explicit method is unstable (ie. $\lambda(m)$ is negative) for, $$\Delta t \geqslant \frac{\rho c V(m)}{\Sigma K} \qquad \text{2-24}$$

The term ΣK in Eqs 2-23 and 2-24 is actually the sum of the conductances between node m and neighbouring nodes and any boundary conductances present (eg. $hA_s(i, j, k)$) if node m is a boundary node. For the tank outer surface node to which Eq. 2-18 applies, for example, in Eqs 2-23 and 2-24 would be equivalent to the term contained within the square brackets in Eq. 2-18 (ie. ΣK in Eqs 2-23 and 2-24 is the coefficient of $T(i, j, k)$ in a given finite - difference equation). Examination of Eq. 2-24 shows that Δt_{max} can be increased by reducing ΣK and/or by increasing $V(m)$. It can be shown that $V(m)$ generally increases more rapidly than ΣK, and hence that Δt_{max} increases, when a mesh is made more coarse (ie. when fewer nodes are used to model a given region). Neglecting some of the conductances at a given node, which reduces ΣK, also increases Δt_{max}.

Graves (4) used the explicit method in his tank car analysis program but made certain assumptions to increase the permissible time step size. First, axial conduction was neglected to reduce the value of K at each node. Second, radial heat transfer through the tank wall was modelled in an approximate fashion by assuming that the tank wall temperature varied linearly across the wall thickness in the liquid-wetted region and parabolically across the wall thickness in the vapor - covered region. These assumptions allowed Graves to represent each element of the tank wall by a single temperature (ie. node) so increasing the value of $V(m)$ at each node (by making the mesh effectively very coarse) and hence the value of Δt_{max}.

In the case of a rail tank car equipped with EXPLOSAFE it will be necessary to model not only the heat flow in the tank wall and external insulation, if present, but also the heat flow in the EXPLOSAFE - filled vapor space as well. Thus it will be necessary to superimpose a finite - difference mesh on the tank wall, the external insulation*, if present, and the EXPLOSAFE - filled vapor space and solve for all of the nodal temperatures at each time step. It will not be possible to simplify the model to the extent that Graves did because regions other than the tank wall will have to be modelled and, as a result, the maximum time step size imposed by the stability limit for the explicit method will be quite small. It is shown in Appendix A that Δt_{max} is approximately 0.35 sec. for a node on the inner surface of the liquid-wetted part of the tank wall in a tank similar to one of those tested with and without EXPLOSAFE at CFB Suffield for instance. The value of Δt_{max} cited applies when three nodes are used across the thickness of the tank wall. Since it is expected that time steps of 15-30 seconds will suffice to model temperature changes in a tank car in the later stages of a pool fire transient, when temperatures are changing relatively slowly, 50-100 times more time steps than really necessary will be required to ensure stability of the explicit method if that method is used in the tank car model .

---

*Graves did not superimpose a finite - difference mesh on the insulation but rather modelled it by simply adding its thermal resistance to the outer surface of the tank wall. This approach is only valid under steady-state conditions and should not be used in a transient analysis because insulating materials characteristically have very low thermal diffusitivities, typically two orders of magnitude less than that of steel. The rate at which heat propogates into the insulation should be modelled.

When $w = \frac{1}{2}$ in Eq. 2-24, the resulting integration procedures are unconditionally stable for any size time step (for a linear problem) but as mentioned previously, a system of simultaneous equations has to be solved at each time step to obtain T^{t+1}. Stable (ie. bounded) oscillations in the solution can be obtained when $\frac{1}{2} \leqslant w < 1$, however, so the implicit method, obtained when $w = 1$, will be the only integration technique considered in this analysis other than the explicit method already described. The recursive equation which is used in the implicit method to advance the solution from time t to $t + \Delta t$ is most conveniently written as:

$$\left(\frac{C}{\Delta t} + K\right) T^{t+1} = \frac{C}{\Delta t} T^{t} + Q \qquad 2\text{-}25$$

or alternately as,

$$K' T^{t+1} = Q' \qquad 2\text{-}26$$

where $K' = \frac{C}{\Delta t} + K$ and $Q' = \frac{C}{\Delta t} T^{t} + Q$. Equation 2-25 reduces to the equation governing the steady - state solution (ie. $KT = Q$) if Δt is made very large (ie. as $\Delta t \rightarrow \infty$).

The feasibility of using the implicit method to solve a given problem cannot be properly assessed without roughly estimating the number of nodes that will be required to model the problem. A full-size DOT 112A tank car equipped with both EXPLOSAFE and an external insulation will probably be the largest model considered and for the purposes of this analysis, it is assumed that five, three and ten nodes will be used across the thickness of the insulation, the tank wall and the EXPLOSAFE annulus respectively giving a total of eighteen radial nodes. If azimuthal nodes are spaced 5° apart, there will be 72 azimuthal nodes and 72 x 18 = 1296 nodes in total on each $r - \theta$ plane. If the axial nodes are spaced 1m apart along the 18m length of the tank car, there will be 19 axial nodes in total and a total of 19 x 1296 = 24,624 nodes, neglecting nodes on the end caps, used to represent the entire tank. If the nodes in the tank car are numbered sequentially with the radial, azimuthal and axial node number indices i, j, and k respectively varying from most to least rapidly in that order, the resulting system of finite - difference equations will be banded, as shown in Fig. 2-6, because each node i, j, k in the model only exchanges heat with the six neghbouring nodes at $i \pm 1$, j, k; i, $j \pm 1$, k and i, j, $k \pm 1$ instead of with all of the other nodes in the tank. If axial conduction is not neglected, the half-bandwidth of the matrix, which is the maximum number of entries between and including the first non-zero entry and the diagonal entry in any row, will be equal to the number of nodes on each $r-\theta$ plane, plus one, or 1296 + 1 = 1297 in this example. Assuming the finite - difference equations are calculated so that the conductance matrix (K) is symmetric, a matter which is discussed in the next section, the number of entries within the half - bandwidth of K will be 1297 x 24,624 = 3.2 x 10^7. All of these entries will have to be stored to solve the system of simultaneous equations using a variant of Gaussian elimination (adapted to a banded matrix) so approximately 3.2 x 10^7 words of computer memory will be required to store the banded K matrix in single precision. Since this memory requirement exceeds the high speed

$$\begin{bmatrix} K'_{11} & K'_{12} & K'_{13} & 0 & 0 & 0 & 0 & 0 \\ K'_{21} & K'_{22} & K'_{23} & K'_{24} & 0 & 0 & 0 & 0 \\ K'_{31} & K'_{32} & K'_{33} & K'_{34} & K'_{35} & 0 & 0 & 0 \\ 0 & K'_{42} & K'_{43} & K'_{44} & K'_{45} & K'_{46} & 0 & 0 \\ 0 & 0 & K'_{53} & K'_{54} & K'_{55} & K'_{56} & K'_{57} & 0 \\ 0 & 0 & 0 & K'_{64} & K'_{65} & K'_{66} & K'_{67} & K'_{68} \\ 0 & 0 & 0 & 0 & K'_{75} & K'_{76} & K'_{77} & K'_{78} \\ 0 & 0 & 0 & 0 & 0 & K'_{86} & K'_{87} & K'_{88} \end{bmatrix} T^{t+1} = Q'$$

FIGURE 2-6: Banded finite-difference equations

memory capacity of any computer known to the author, the analysis just described would be impossible or, at the very least, impractical to perform using the implicit method. There are actually only seven non-zero finite - difference coefficients, at the most, in any finite - difference equation, however, because no node exchanges heat with more than six* neighbouring nodes, so all of the information required to advance from one time step to the next using the explicit, method could be stored in less than 7 x 24,624 = 172,368 memory spaces. This memory requirement is well within the capacity of almost any medium-sized or large modern computer. The explicit method could be applied with even less memory than that just mentioned if all of the finite - difference coefficients were recalculated at each time step instead of stored. Finite - difference coefficients containing non-linear terms have to updated at each time step using the most recent nodal temperatures but other coefficients can be stored and re-used repeatedly.

All of the finite - difference coefficients in a model are non-linear if thermal conductivities are allowed to be temperature dependent, otherwise only coefficients in equations for boundary nodes where a radiative or some other non-linear boundary condition (eg. boiling) is prescribed need to be recomputed at each time step. Finite - difference coefficients for interior node equations can and should be stored and re-used when thermal conductivities are constant.

---

* This observation is only valid if radiative heat transfer between nodes is not considered, as discussed in Sect. 2.3.3.

The preceding example showed that the implicit time integration procedure may be impossible to apply in some situations. The conclusion reached in the preceding example can be changed, however, by assuming that axial conduction in the tank wall is negligible (ie. that $K(i, j, k)_{k+1} = K(i, j, k)_{k-1} \approx 0$ at each node i, j, k) since this assumption causes the r-θ planes at different axial nodes to become thermally decoupled, with the result that the formerly 3-D analysis with 19 axial nodes becomes effectively 19 2-D (r-θ) analyses. The half-bandwidth of the conductance matrix (K) for each 2-D analysis is equal to the number of radial nodes plus one, or 18 + 1 = 19 for the hypothetical example considered previously, so the entries contained within the half-bandwidth of the conductance matrix (K) for a single r-θ plane will occupy 19 x 1296 = 24,624 memory spaces. Since neglecting axial conduction will allow the temperature distribution on each r-θ plane to be obtained independently of the temperature distributions on the other r-θ planes (ie. axial nodes), it will really not be necessary to store the K matrix for more than one r-θ plane at any one time. A total of 19 x 24,624 = 467,856 words of memory would be required to store the K matrices for all of the 19 r-θ planes simultaneously but even this memory requirement is within the high-speed core capacity of most large modern computers. The tank car model would be developed on Carleton University's Honeywell Level 66 computing system which consists of six central processing units (CPU's), each with 512,000 words of high speed memory, for instance. This hypothetical example has shown that the implicit time integration procedure could be used in the tank car model if axial heat transfer was neglected, a possibility that is discussed for the pool and torch fire scenarios in later sections.

2.1.3 Linearization Procedures

As noted in Sect. 2.1.1, the finite - difference equations for boundary nodes where non-linear boundary conditions (eg., radiation, boiling, natural convection) are prescribed will contain non-linear terms which must be updated in some manner as the analysis progresses. Even the finite - difference equations for interior nodes will be non-linear if thermal properties (ie. conductivity, specific heat, and density) are allowed to be temperature - dependent, as already mentioned. The simplest way to handle non-linear terms is simply to update them at each time step using T^t, an approach which is consistent with the explicit time integration procedure because T^t is used to evaluate $\dot{T}$ between times t and t + Δ t in that case. Using T^t to update non-linear terms is inappropriate when $\dot{T}$ is evaluated from T^{t+1}, however, as in the implicit method. A linearization technique which is consistent with the use of T^{t+1} to evaluate $\dot{T}$ in the implicit method requires using T^t to evaluate non-linear terms in K' initially so that an initial estimate of T^{t+1} can be obtained, updating the non-linear terms in K' with the value of T^{t+1} thus obtained and subsequently recalculating T^{t+1} with the revised non-linear terms. This process is repeated until consecutive estimates of T^{t+1} differ, with respect to some norm (eg. Euclidean), by less than a user-specified amount (ie. iterations are performed until the solution has converged). The procedure just described, which is known as the method of successive approximations, is not recommended because it often fails to converge. A better approach is to apply the Newton-Raphson (N-R) linearization technique which, while also an iterative procedure, is generally much more powerful than the method of successive approximations.

The Newton-Raphson recursive equation can be written as,

$$J(T^n)\left[T^{n+1} - T^n\right] = Q' - K'T^n \qquad 2\text{-}27$$

or as,

$$\begin{aligned} J(T^n)T^{n+1} &= Q' - K'T^n + J(T^n)T^n \\ &= Q'' \end{aligned} \qquad 2\text{-}28$$

where T^n and T^{n+1} are the nth and (n+1)st estimates of T^{t+1} and $J(T^n)$ is the Jacobian matrix defined by the expression;

$$J(T^n) = \frac{\partial E}{\partial (T^{t+1})^T}\bigg|_{T^n} \qquad 2\text{-}29$$

with $E = K'T^{t+1} - Q'$. The desired solution, T^{t+1}, is obtained when $E = 0$ since $K'T^{t+1} = Q'$ (sec. Eq. 2-26). The superscript T on the term $(T^{t+1})^T$ designates a transposed vector. Using Eq. 2-29, the matrix element J_{rs} can be written as

$$J_{rs} = \frac{\partial E_r}{\partial T_s^{t+1}} \qquad 2\text{-}30$$

Every element of J is evaluated using the most recent estimate of T^{t+1}, in other words T^n. The vector T^n is equated to T^t initially to start the iterative procedure at any time step, as in the method of successive approximations.

The recursive equation for the N-R method (Eq. 2-28) reduces to Eq. 2-26 if $K' \neq f(T)$ since

$$J(T^n) = \frac{\partial E}{\partial (T^{t+1})^T}\Bigg|_{T^n} = \frac{\partial (K'T^{t+1} - Q')}{\partial (T^{t+1})^T}\Bigg|_{T^n} = K' \text{ and}$$

$Q'' = Q' - K'T^n + J(T^n)T^n = Q' - K'T^n + K'T^n = Q'$ in that case. It can also be shown that an entry K'_{rs} in K' is the same as the corresponding entry J_{rs} in J if the $K'_{r\ell}$, $\ell=1,M$ are not functions of T_s^{t+1}. Stated more simply, rows of K' which do not contain any non-linear entries remain unchanged in J.

While the Newton-Raphson method may have appeared to be quite complicated from the preceding discussion, the method is actually very simple to apply in practice. Consider, for instance, the non-linear finite - difference equation for a node on the tank outer surface, given previously by Eq. 2-18 and rewritten here in implicit form as;

$$K(i,j,k)_{i-1}\,T^{t+1}(i-1,j,k) + K(i,j,k)_{j+1}\,T^{t+1}(i,j+1,k)$$
$$+K(i,j,k)_{j-1}\,T^{t+1}(i,j-1,k) + K(i,j,k)_{k+1}\,T^{t+1}(i,j,k+1)$$
$$+K(i,j,k)_{k-1}\,T^{t+1}(i,j,k-1) - \left[\Sigma K + h_f A_s(i,j,k) + \frac{\rho c V(i,j,k)}{\Delta t}\right]$$
$$T^{t+1}(i,j,k) + RA_s(i,j,k)(T_f^{\,4} - T^{t+1}(i,j,k)^4) + h_f A_s(i,j,k) T_f$$
$$+ \frac{\rho c V(i,j,k)}{\Delta t}\,T^t(i,j,k) = E(i,j,k) \qquad 2\text{-}31$$

where $E(i,j,k) = 0$ when T^{t+1} is the correct solution vector. If thermal properties are constant or simply updated using T^t at each time step and not linearized using the Newton-Raphson method*, the only non-linear finite - difference coefficient in Eq. 2-31 is the coefficient for $T^{t+1}(i, j, k)$ (note that T^t and T_f are both known). If the nodes in the tank car model are numbered so that Eq. 2-31 applies to the mth node in the grid (ie. node i, j, k is the same as node m), the only entry in the mth row of J that differs from the corresponding entry in the mth row of K' is the diagonal entry J_{mm} (ie. the coefficient for T^{t+1} (i, j, k), where $T^{t+1}(i, j, k)$ and $T^{t+1}(m)$ are equivalent), which is given by the expression,

$$J_{mm} = \frac{\partial E_m}{\partial T_m{}^{t+1}} \quad \frac{\partial E(i, j, k)}{\partial T^{t+1}(i, j, k)} \quad -\Big[\sum K + h_f A_s(i, j, k) + \frac{\rho c V}{\Delta t}(i, j, k)$$

$$+ 4\, R A_s(i, j, k) T^{t+1}(i, j, k)^3 \Big]$$

2-32

where E_m is the mth entry in E ($= K'T^{t+1} - Q'$). J_{mm} was obtained by differentiating Eq. 2-31 with respect to $T^{t+1}(i, j, k)$ ($= T^{t+1}(m)$). To demonstrate that the remaining entries in the mth now of J are equivalent to the corresponding entries in K', consider the entry $J_{m\ell}$ when the ℓth node is, for instance, node i-1, j, k. $J_{m\ell}$ can be evaluated by differentiating Eq. 2-31 with respect to $T^{t+1}(i-1, j, k)$ $(= T^{t+1}(n))$, viz.

---

*Highly non-linear heat transfer mechanisms, such as radiation, should be linearized using the N-R method but non-linearities arising from temperature-dependent thermal properties are usually not severe and hence can be handled by simply updating the properties periodically during the solution.

$$J_{m\ell} = \frac{\partial E(i, j, k)}{\partial T^{t+1}(i, j, k)} = K(i, j, k)_{i-1}$$

Only the diagonal entries of K' and K are different because $K' = \frac{C}{\Delta t} + K$ and C is a diagonal matrix, so

$K'_{m\ell} = K_{m\ell} = K(i, j, k)_{i-1}$ thus proving that $J_{m\ell}$ and

$K'_{m\ell}$ are equivalent.

The value of T^{t+1} from the previous iteration (ie., T^n), or the previous time step if n=0, is used to evaluate the non-linear term in Eq. 2-32 so

$$J_{mm}\Big|_{T_n} - \Big[K + h_f A_s(i, j, k) + \frac{\rho c V(i, j, k)}{\Delta t} + 4RA_s(i, j, k)T^n(i, j, k)^3\Big] \qquad 2\text{-}33$$

If can easily be shown that the mth entry in the vector Q" on the right-hand side of Eq. 2-28 (ie. $Q"_m$) reduces to the expression,

$$Q"_m = -\Big[h_f A_s(i, j, k)T_f + \frac{\rho c V(i, j, k)T^t(i, j, k)}{\Delta t} + RA_s(i, j, k)(T_f{}^4 + 3T^n(i, j, k)^4\Big] \qquad 2\text{-}34$$

because all of the linear coefficients in $Q' - K'T^n$ $(= -E\big|_{T_n})$

and $J(T^n)T^n$ cancel (note that $Q'' = (Q'-K'T^n) + J(T^n)T^n$ $= -E\big|_{T_n} + J(T^n)T^n)$.

With $J_{mm}\big|_{T^n}$ and Q''_m defined by Eqs. 2-33 and 2-34 respectively, the mth equation in Eq. 2-28 can now be written as,

$$
\begin{aligned}
&K(i,j,k)_{i-1}T^{n+1}(i-1,j,k) + K(i,j,k)_{j+1}T^{n+1}(i,j+1,k) \\
&+K(i,j,k)_{j-1}T^{n+1}(i,j-1,k) + K(i,j,k)_{k+1}T^{n+1}(i,j,k+1) \\
&+K(i,j,k)_{k-1}T^{n+1}(i,j,k-1) - \Big[\Sigma K + h_f A_s(i,j,k) + \frac{\rho c V(i,j,k)}{\Delta t} \\
&+4RA_s(i,j,k)\,T^n(i,j,k)^3\Big]\,T^{n+1}(i,j,k) \\
&= -\Big[h_f A_s(i,j,k)T_f + \frac{\rho c V(i,j,k)}{\Delta t}T^t(i,j,k) + RA_s(i,j,k) \\
&(T_f{}^4 + 3T^n(i,j,k)^4)\Big] \qquad \text{2-35}
\end{aligned}
$$

where T^{n+1} is the (n+1)st estimate of T^{t+1}, as indicated previously. When an equation similar to Eq. 2-35 is written for all of the nodes in the finite - difference grid, the resulting system of equations can be solved for T^{n+1}. An equation similar to Eq. 2-35 but applying to a tank inner surface node where a boiling boundary condition is prescribed is given in Sect. 2.3.2.

When T^{t+1} and T^t do not differ by much (this will be the case unless Δt is large), the convergence properties of the N-R method* are such that iterations do not have to be performed at each time step. The method can, in fact, be programmed to be very fast and economical by using the so-called Modified Newton-Raphson method in which the Jacobian matrix is not updated every iteration or time step. If non-linear terms in the Jacobian are recalculated once every N iterations, where N is specified by the program user based on experience, the Jacobian can be factored after each updating into the product of lower and upper triangular matrices, designated L and U respectively (ie. $J = LU$), using, for instance, Crout decomposition (5). The vector T^{t+1} at each of the N subsequent time steps for which J remains unchanged can be obtaining by recalculating Q", forward substituting to obtain Y from the expression $LY=Q''$ and then backsubstituting to obtain T^{t+1} from the relationship $UT^{t+1}=Y$. The forward and backsubstition steps needed to obtain T^{t+1} at each time step from the factored form of J (ie. LU) can be performed very quickly and the factorization process itself, while relatively laborious, only needs to be performed once every N time steps. The Jacobian must also be re-factored if the time step size (Δt) is changed.

The relationship between the conventional Newton-Raphson method and the modified method can be most easily understood by considering a non-linear function of one variable

---

*The N-R method exhibits quadratic convergence characteristics which, loosely stated, means that the "error" in the solution after any iteration is proportional to the square of the error obtained after the preceding iteration. If the latter error is small, its square (ie. the error for the next iteration) is very small.

(x), say $y = f(x) = q$ where q is a constant. For a function of one variable, the Jacobian matrix (J) in Eq. 2-27 becomes the derivative $\frac{df}{dx}$ and the recursive equation for a non-linear function of several variables, becomes,

$$\left.\frac{df}{dx}\right|_{x^n}(x^{n+1}-x^n)=q-f(x^n)$$

where x^n and x^{n+1} are the nth and (n+1)st estimates of the solution to the equation $f(x)=q$. The manner in which repeated application of the N-R recursive equation locates the solution to the equation $f(x) = q$ is shown diagrammatically in Fig. 2-7. In the modified version of the Newton-Raphson method, the value of $\frac{df}{dx}$ at the first estimate of x (ie. $\left.\frac{df}{dx}\right|_{x^o}$) is used in several, if not all, of the iterations needed to find the correct value of x. The convergence of this method to the correct value of x is shown in Fig. 2-8. The Modified Newton-Raphson method requires more iterations to converge than the conventional version but the saving in computer time made possible by using the factored form of J repeatedly usually more than outweighs the effort involved in performing extra iterations when J is a function of a large number of variables.

The LU factorization of J and the forward and backward substitution steps needed to obtain T^{t+1} from the factored form of J and the right-hand side vector Q" can be performed on most computer installations using standard library subroutines. The IMSL (International Mathematical & Statistical Libraries, Inc.) routine LEQTIB (6), which is available on the computer installation at Carleton

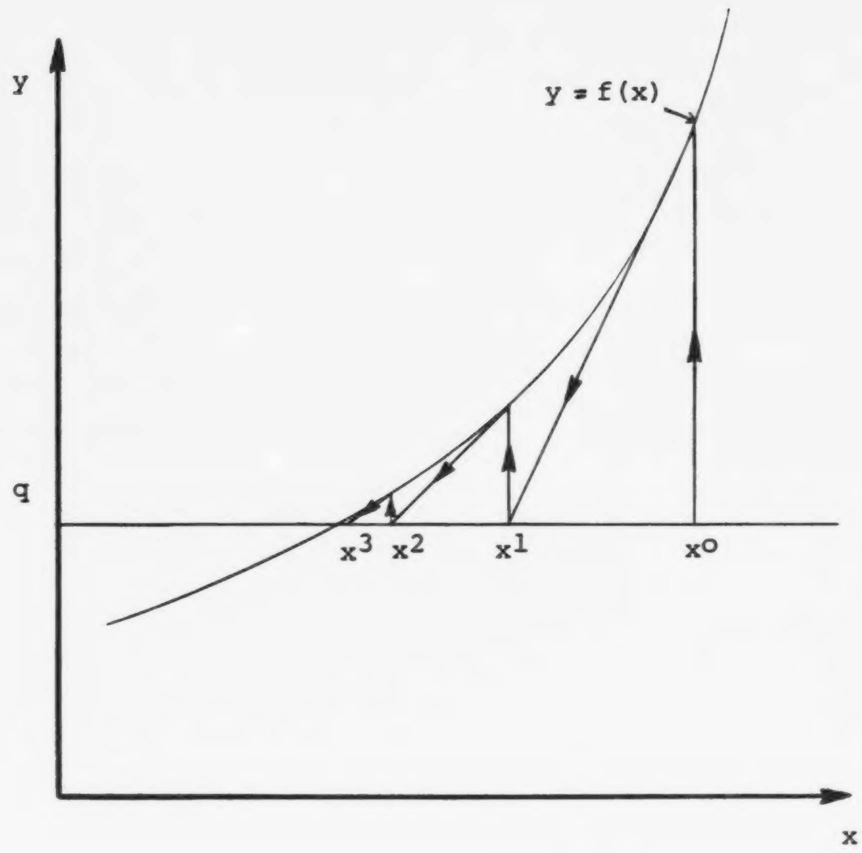
y
y = f(x)
q
x³
x²
x¹
xᵒ
x

Fig.: 2-7: Convergence of the Newton-Raphson Method

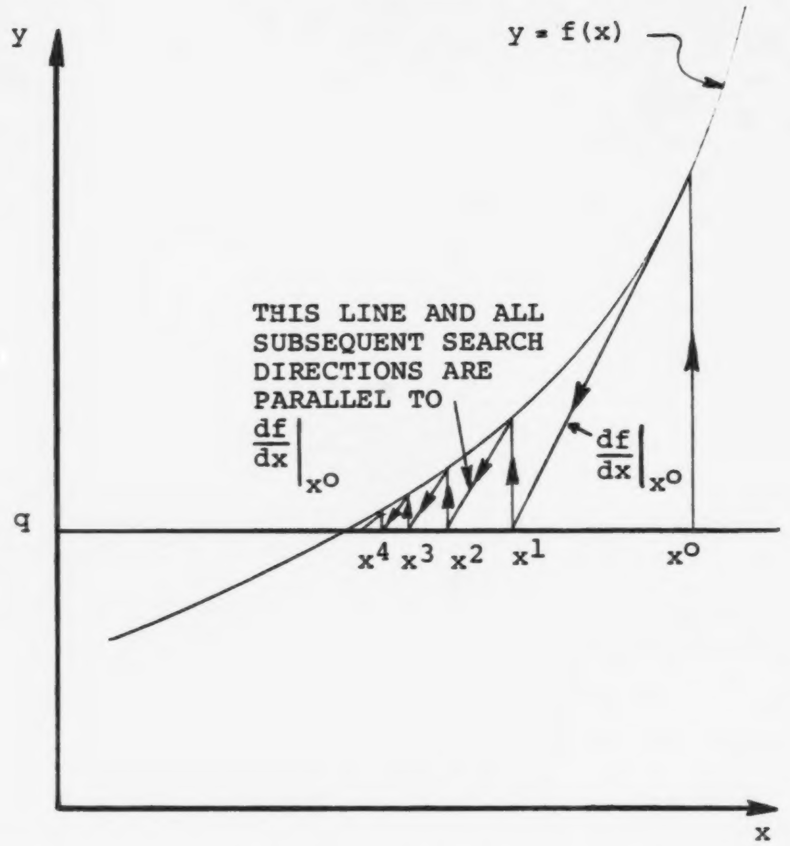
y
y = f(x)
THIS LINE AND ALL SUBSEQUENT SEARCH DIRECTIONS ARE PARALLEL TO
$\left.\frac{df}{dx}\right|_{x^o}$
$\left.\frac{df}{dx}\right|_{x^o}$
q
x^4
x^3
x^2
x^1
x^o
x

Fig.: 2-8: Convergence of the modified Newton-Raphson Method

University where the tank car analysis program would be developed, performs all of these operations on a banded system of equations, for example. The IMSL library routines are available on most computer installations and hence can be used in the DE tank car model without seriously limiting its transportability.

The IMSL routine LEQTIB is applicable to banded systems of equations with non-symmetric coefficient matrices. The Jacobian (J) for the system of finite - difference equations obtained using the heat balance approach described previously will be symmetric, however, unless radiative heat transfer between interior nodes is modelled, as described in Sect. 2.3.3, permitting the finite - difference equations to be solved roughly twice as quickly and with half as much memory as in the non-symmetric case. The IMSL routine LEQTIP could be used to obtain the LU factorization of J and perform the forward and backward substitution phases of the equation solution when J is symmetric*, but routines given by Jennings in (7) will be used to perform these operations in the DE tank car model instead of LEQT1P. Jennings routines are somewhat better than LEQT1P because they permit the bandwidth of the matrix being factored to vary from row to row whereas LEQT1P operates on a constant bandwidth matrix. The band matrix factored by LEQT1P must, therefore, have a bandwidth equal to the largest of the row bandwidths.

---

* The Jacobian (J) must also be positive-definite to apply LEQT1P or any similar routine. Coefficient matrices for finite - difference equations usually satisfy this condition.

The principles and procedures described in the preceding discussion of the finite - difference method will be referred to as they are required in the forthcoming development of the tank car model. The Modified Newton-Raphson method is implemented in a simple computer model of an unprotected tank car in a fire in Appendix E, where results obtained with the conventional and modified versions of the N-R method are compared. The model is introduced in Sect. 2.3.2.2.

2.2 Tank Car Geometry Description And Coordinate Systems

It is assumed for the purpose of developing the tank car thermal and thermodynamic models that a conventional tank car can be adequately modelled as a cylinder with flat ends, as shown in Fig. 2-9 . For 125 kl (33,000 U.S. gal.) railroad tank cars of the DOT 112A or 114A series, which are manufactured with 2:1 ellipsoidal heads, this approximation is quite good, as seen in Fig. 2-10 where a 112A series tank car is shown.

One of the requirements of the tank car thermal model is that it be applicable to a tank car in a pitched attitude. Two degrees of freedom are required to adequately describe the attitude of a tank car for the purposes of a thermal analysis, the first of these being roll, that is rotation of the tank car about its longitudinal axis, and the second being pitch, that is tilt of the longitudinal axis from the horizontal. Roll is important because it affects the position of the relief valve relative to the liquid surface, a parameter which

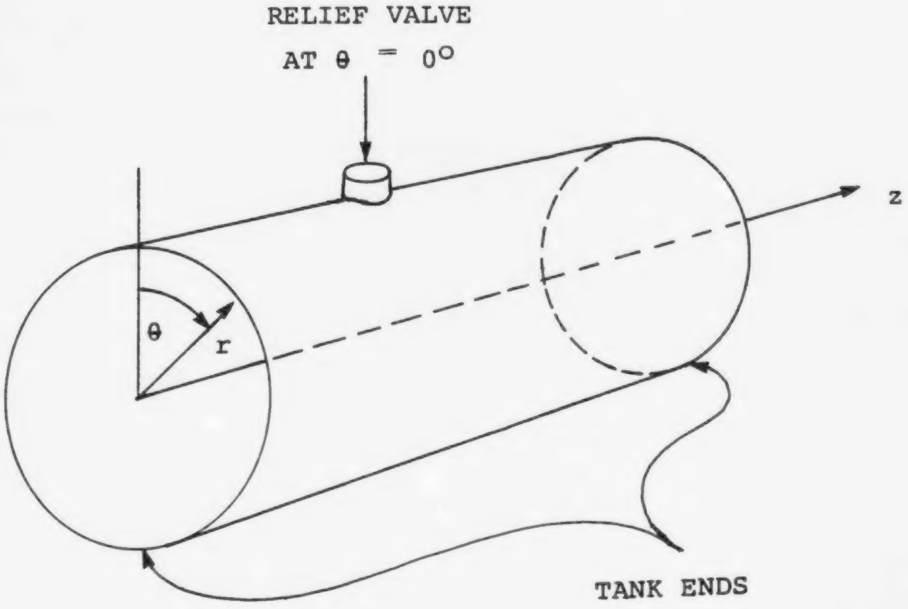
RELIEF VALVE
AT θ = 0°
z
θ
r
TANK ENDS

Fig.: 2-9: Representation of a Tank Car by a Cylinder with Flat Ends

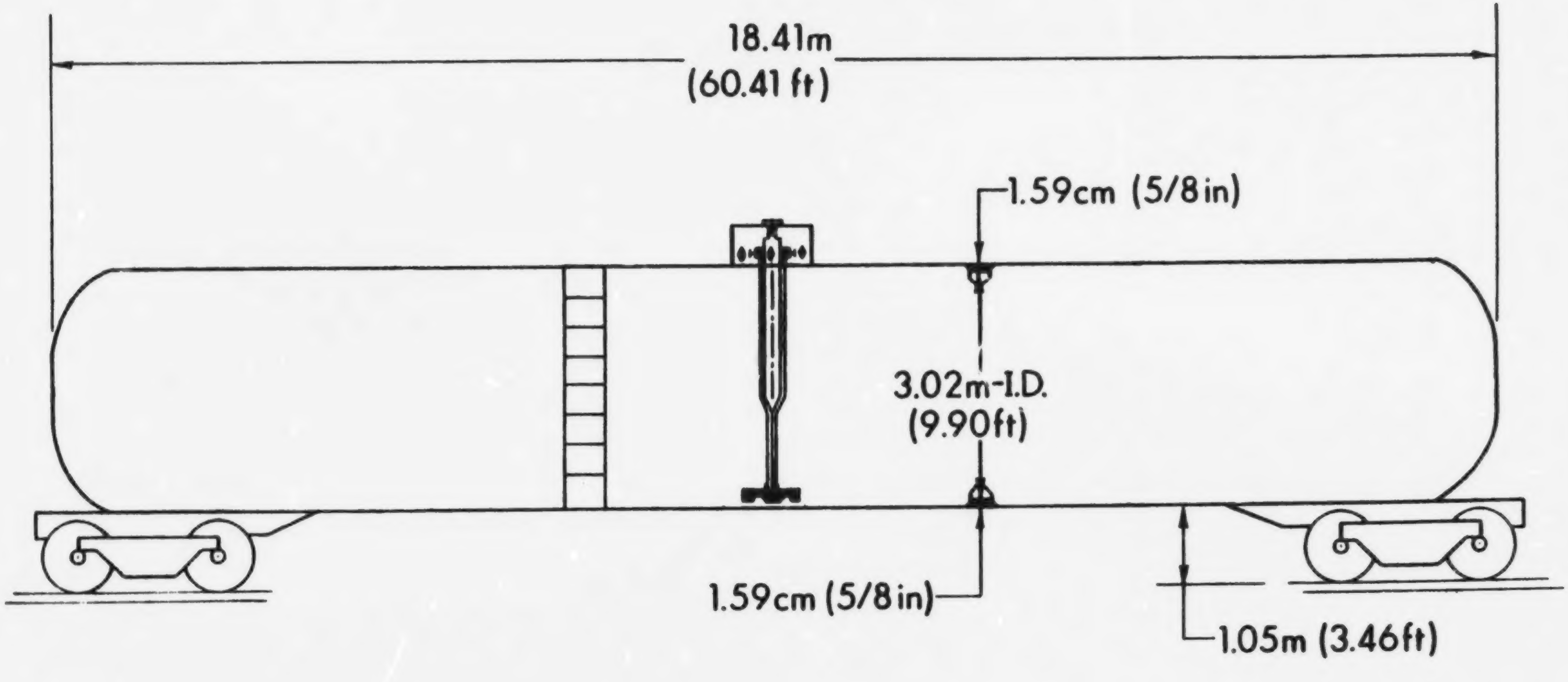
18.41m
(60.41 ft)
1.59cm (5/8 in)
3.02m-I.D.
(9.90ft)
1.59cm (5/8 in)
1.05m (3.46ft)

FIGURE 2-10: Full-size DOT 112 (or 114) tank car

is itself significant because it determines whether vapor or a two-phase mixture of vapor and liquid is discharged from the valve during periods of pressure relief. The flow capacity of the valve defends on the type of fluid discharged. The position of the relief valve is also important because the tank wall adjacent to the valve is cooled by escaping propane vapor during periods of pressure relief when the valve is located above the liquid surface. Heat dissipation by this mechanism in the ullage of the tank is absent when the relief valve is below the liquid surface.

Pitch of the tank car, that is tilt of its longitudinal axis from the horizontal, affects the line of intersection between the liquid surface and the tank wall inner surface and hence the boundary conditions applied to the tank wall inner surface in the thermal model.

Two coordinate systems are required to determine whether a particular point in the tank is above or below the level of the liquid surface. The first of these coordinate systems is the cylindrical (r-θ-z) tank-car centered system shown in Fig. 2-9. The azimuthal coordinate, θ, is meaured in a clockwise sense from the relief valve. If more than one relief valve is used in the tank and the valves do not lie in the same longitudinal plane, one valve must be selected as the datum. The origin of the tank-car centered coordinate system is located at the center of one of the tank end caps.

The second coordinate system needed to impose the proper boundary conditions in the tank car thermal model is the global, gravitational, system shown in Fig. 2-11. The X and Y axes of this coordinate system are aligned with

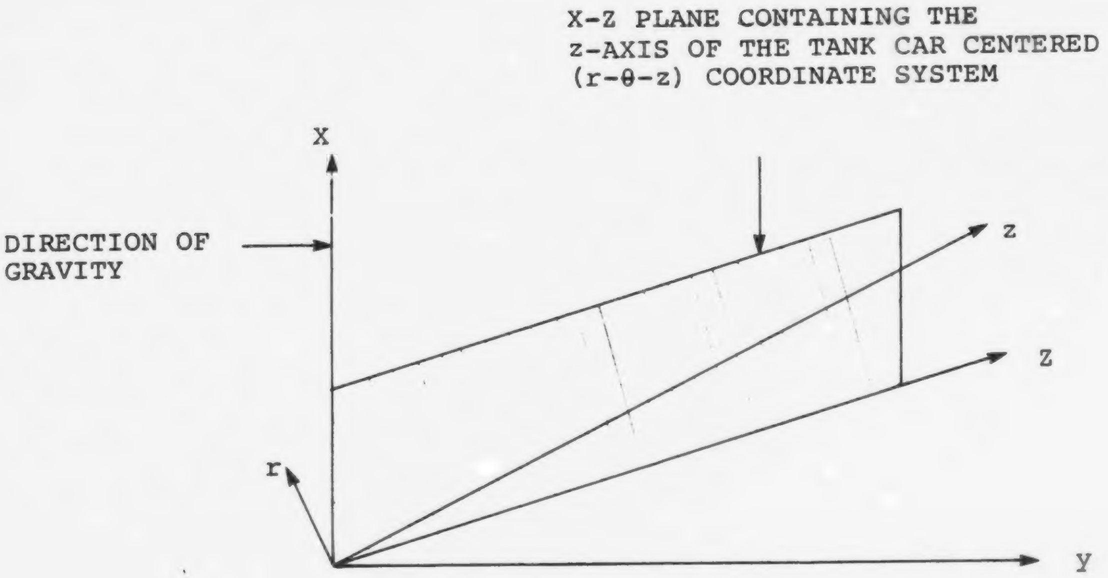
X-Z PLANE CONTAINING THE
z-AXIS OF THE TANK CAR CENTERED
(r-θ-z) COORDINATE SYSTEM
X
DIRECTION OF
GRAVITY
z
Z
r
Y

Fig. 2-11: X-Y-Z GRAVITATIONAL COORDINATE SYSTEM

and normal to the direction of gravity respectively while the X and Z axes form a plane containing the z axis of the tank-car centered system. The origins of the tank-car centered (r-θ-z) and gravitational (X-Y-Z) coordinate systems are coincident. Any liquid surface is parallel to the Y-Z plane of the gravitational coordinate system, as shown in Fig.2-12, so only the X-intercept of the surface, designated X*, is needed to completely specify its position.

Roll and pitch of the tank car are described by the roll and pitch angles, designated γ and α respectively, shown in Fig. 2-13. Setting $\zeta = \gamma + \theta$, the values of X, Y and Z for a point at coordinates r, θ and z in the tank car centered coordinate system can be expressed as,

$$X = z \sin\alpha + r \cos\zeta \cos\alpha \qquad 2\text{-}35$$
$$Y = r \sin\zeta \qquad 2\text{-}36$$
$$Z = z \cos\alpha - r \sin\alpha \cos\zeta \qquad 2\text{-}37$$

Every point in the tank car is located uniquely by its coordinates r, θ and z, so the X, Y and Z coordinates of every point can be determined from Eqn's 2-35 to 2-37 when the roll and pitch angles, γ and α, are specified. When the X coordinate of a particular point has been calculated the question of whether that point is located above the liquid surface or below it is easily answered by comparing its X coordinate to the X-intercept of the liquid surface, X*. If the X coordinate of a particular point is greater than X* the point is above the liquid surface, otherwise it is below the liquid surface.

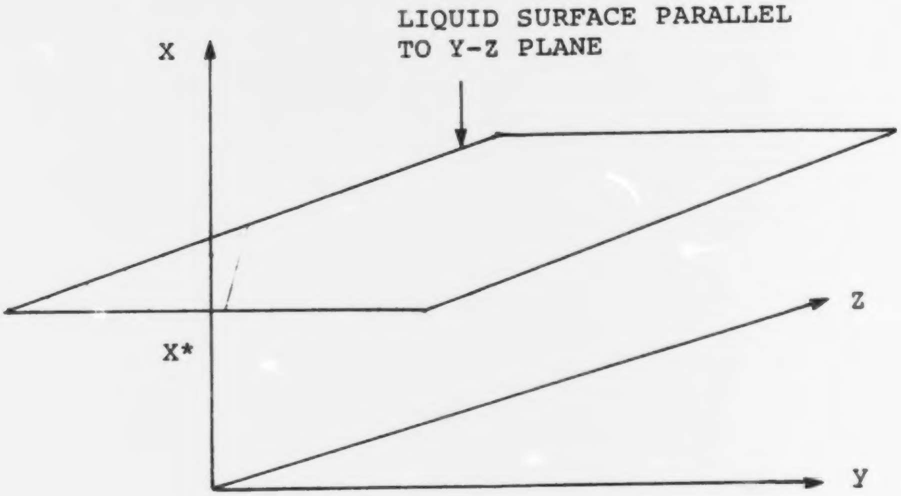
LIQUID SURFACE PARALLEL
TO Y-Z PLANE
X
X*
Z
Y

Fig. 2-12: LIQUID SURFACE IN THE X-Y-Z CO-ORDINATE SYSTEM

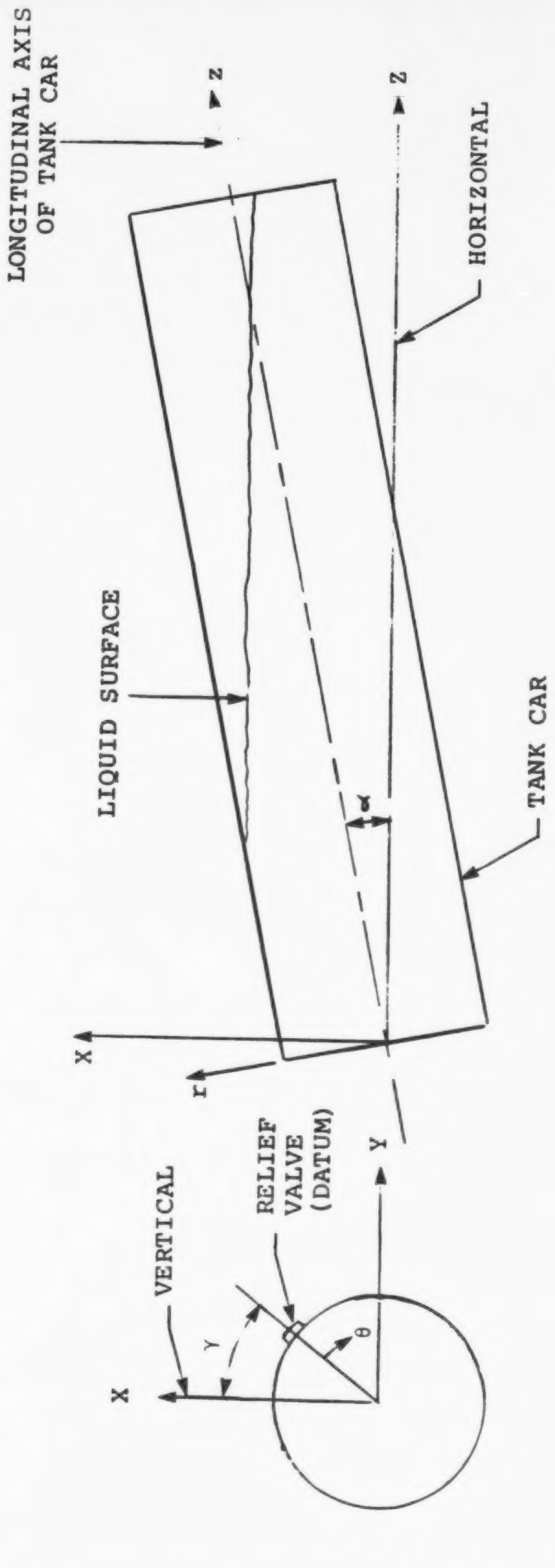
LONGITUDINAL AXIS OF TANK CAR
z
Z
HORIZONTAL
LIQUID SURFACE
TANK CAR
α
X
r
Y
RELIEF VALVE (DATUM)
VERTICAL
X
γ
θ
Y

Fig.: 2-13: Global (X-Y-Z) and Tank Car Centered (r-θ-z) Coordinate Systems showing Tank Car Roll and Pitch Angles, γ and α.

Thermodynamic models of the tank car lading, described in Sects. 3.1 and 3.2, predict the volume of liquid (V_l) remaining at each time step in a pool fire analysis. The X-intercept of the liquid surface, X*, must be calculated from V_ℓ in order to determine the points in the tank that are below the liquid surface and, from this information, specify boundary conditions for the next time step. Mathematical expressions relating V_ℓ to X*, γ and α for a tank of given dimensions are derived in Appendix B and, since this relationship is actually the inverse of the required relationship (ie., X* must be calculated from V_ℓ, γ and α), the half-interval search method is applied in a computer program, described in Appendix B, to obtain X* from V_ℓ, γ and α.

2.3 Pool Fire Thermal Analysis

The thermal model of a tank car in a pool fire will be developed in stages, starting with the analysis of an unprotected tank (ie. a tank without EXPLOSAFE and without external insulation), since this is probably the simplest case to analyse, and progressing to the analysis of an EXPLOSAFE - equipped tank car. The assumptions made in each case will be clearly delineated. Many of the simplifying assumptions, which will increase in number when heat transfer in the EXPLOSAFE is considered and additional heat transfer mechanisms become important, will be made for reasons of computational expediency. The computational consequences of not invoking the suggested simplifications will be described with reference to the material covered in Sects. 2.1.1 to 2.1.3. The external boundary conditions are the same for the protected and unprotected tank car thermal models, of course, and for that reason those boundary conditions are described in the next section before either the protected or the unprotected tank car thermal model is considered. The internal heat flow analysis for an EXPLOSAFE - equipped tank car must differ substantially from the corresponding analysis for a tank without EXPLOSAFE, however, for reasons that will be discussed later. Insulation models will be considered after both the pool fire and torch fire models have been described because insulations will be treated in the same manner in all of the analyses.

2.3.1 External Boundary Conditions

2.3.1.1 Fire-to-Tank Radiative Heat Transfer

Characterizing a pool fire for the purposes of a heat transfer analysis is an exceedingly complex task if approached analytically and, for that reason, heavy reliance must be placed on experimental data. Essentially all of the applicable experimental data available has been obtained in JP-4 fire tests, however, so the consideration of other fuels with markedly different physical and chemical characteristics will be difficult. While Burgess et al (8) and Seeger (9) report that open flame luminous zone temperatures for most liquid and gaseous fuel fires are typically in the 900°C (165°F) to 1250°C (2280°F) range, it should be recognized that this temperature variation corresponds to almost a threefold variation in blackbody emissive power since the latter quantity is proportional to the absolute temperature raised to the fourth power. This variation emphasizes the importance of having an accurate estimate of the effective flame temperature in a radiant heat transfer analysis.

A fire environment is very unsteady, as is evident from the typical fire temperature vs. time record shown in Fig. 2-14, taken from reference 10, where the fire test of the full size DOT 112A tank car referred to as RAX201 in the FRA tank car test series is reported, but the thermal response of a tank car will be slow enough to permit the fire to be represented by a time-average temperature. While the flame temperature alone does not ordinarily provide enough information to evaluate the radiative heat flux from a fire to an object located in its vicinity, such a simple characterization of the flame is possible if it is thick and highly luminous, conditions that will undoubtedly be satisfied for a large pool fire enveloping a tank car. According to Seeger (9), the high luminosity of liquid hydrocarbon fuel fires permits them to be modelled as black or gray bodies with an emissivity (ε_f) between 0.9 and 1.0 if the flames are more than 1m thick. Radiometer and flame temperature measurements reported by Anderson et al. (10) for a JP-4 fire enveloping a full size tank car support this observation in that an average radiant heat flux of 217,000$\frac{W}{m^2}$ was obtained at an average flame temperature of 1130°C. Since the radiant heat flux (q''_r) is related to the flame temperature (T_f) by the expression

$$q''_r = \varepsilon_f \sigma T_f^4 \quad (\sigma \text{ is the Stefan-Boltzmann constant, } 5.669 \times 10^{-8}\ W/m^2K^4) \qquad 2\text{-}38$$

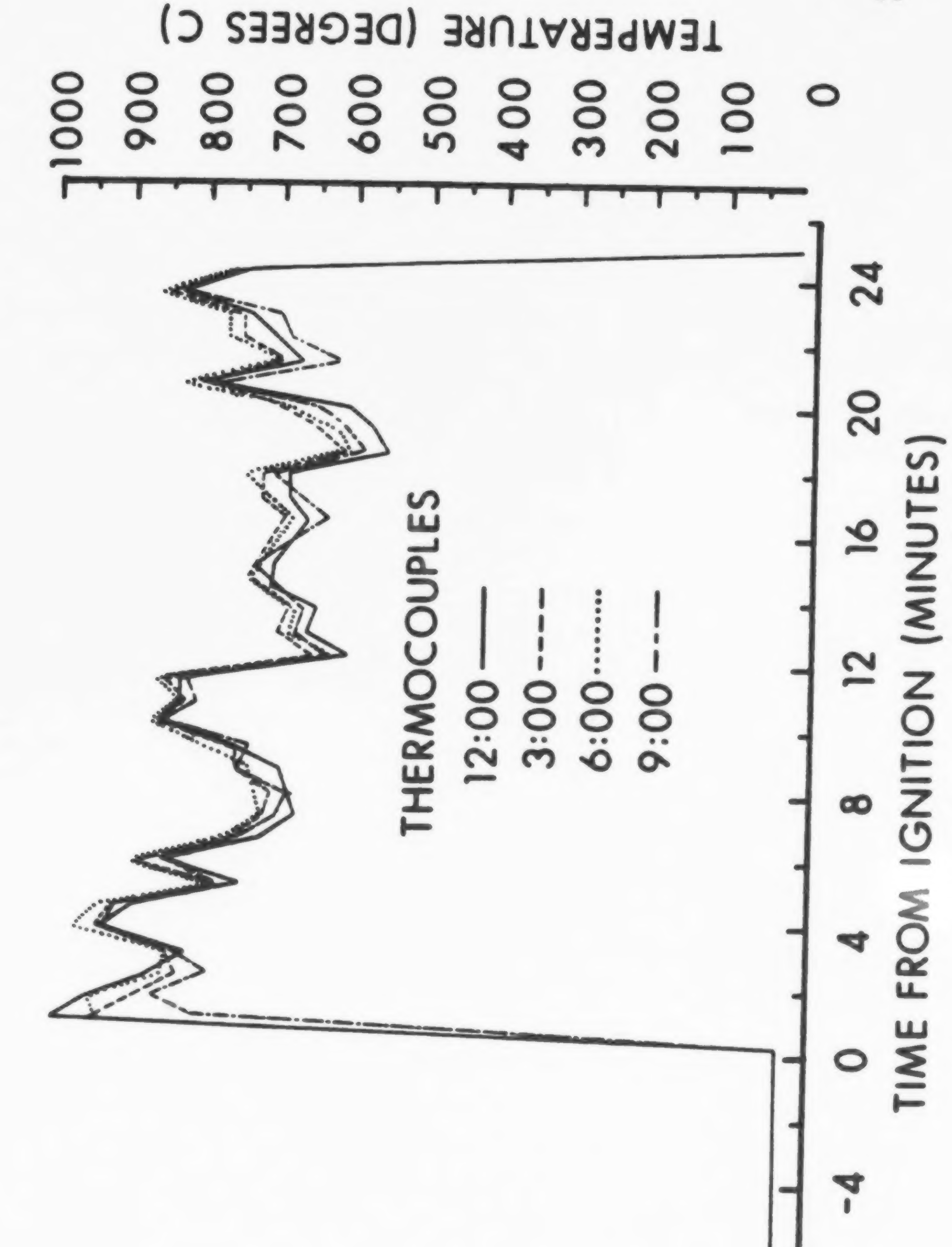

Fig.: 2-14: Front Fire Temperatures vs. Time (from Reference 10) if the flame radiates as a gray body, $\varepsilon_f \simeq 0.97$ for the measured values of q''_r and T_f given previously. This flame emissivity lies within the range mentioned by Seeger.

If it is assumed that the pool fire completely envelopes the tank car, the net radiant heat flux from the flame to a surface element on the tank car outer surface can be expressed as,

$$q''_{ro} = \frac{\sigma(T_f^{\,4} - T_s^{\,4})}{\frac{1}{\varepsilon_f} + \frac{1}{\varepsilon_s} - 1.0} \qquad 2\text{-}39$$

where T_s and ε_s are the temperature and emissivity of the surface element respectively. Equation 2-39 will be used in the thermal model of a tank car in a pool fire to calculate radiative fire-to-tank heat transfer rate. The program user will be permitted to enter either a uniform flame temperature, which will be applied over the entire outer surface of the tank, or an array of flame temperatures, one for each surface element. The second possibility will be permitted as an option. It is expected that most program users will want to use a uniform flame temperature because flame temperatures measured in tank car fire tests under windless conditions have, for the most part, been fairly uniform (ie. not position dependent), as seen in Fig. 2-14 where fire temperatures measured at different positions around the circumference (ie. from 12 o'clock to 6 o'clock) of tank car RAX201 are shown. Almost no circumferential variation in flame temperature is discernible in Fig. 2-14, a result which is consistent with the flame temperature measurements obtained in other tests. Some circumferential variation in fire temperature would probably have been observed if the bottom of the tank car had been located right at the fuel surface, however, since the temperature of a JP-4 pool fire at the fuel surface is only about $500^{o}K$ according to Raj (11). Anderson et al (10) did not mention the distance between the bottom of tank car RAX201 and the fuel surface, a frequent oversight in tank car fire test reports.

2.3.1.2 Fire-to-Tank Convective Heat Transfer

It is usually assumed that the total heat transfer rate from a pool fire to a tank car is approximately 75% radiative and 25% convective, although it is not known how these figures were obtained and they must obviously be subject to fairly large variations because the radiative contribution to the total heat flux is so strongly dependent on flame temperature. Convective heat transfer from the fire to the tank will be modelled in the DE tank car analysis program by specifying convective heat transfer coefficients, designated h_f in Sect. 2.1.1,at the nodes in the finite - difference model of the tank on its outer surface. A procedure for calculating the convective heat transfer coefficient on the tank outer surface as a function of circumferential position is described in detail in Appendix C, where sample calculations show that h_f will, according to the analysis presented, range in value from 5 - $15W/m^{2o}C$ (0.9-2.6 $BTU/hrft^{2o}F$) and vary, at the most, by a factor of two around the tank's circumference. For comparison purposes, the flame-to-tank radiative heat transfer coefficient h_r, defined by the expression

$$h_r = q''_r/(T_f - T_s) \approx \frac{\sigma (T_f^2 + T_s^2)(T_f + T_s)}{1/\varepsilon_f + 1/\varepsilon_s - 1.0} \qquad 2\text{-}40$$

will, for $\varepsilon_f \simeq 0.9$, $\varepsilon_s \simeq 0.8$ (blackened surface) and $T_s = 775K$* (average of 330°K liquid propane temperature and 1200°K flame temperature) have a value of approximately 168W/m^{2}K (29.5 BTU/hrft^{2}F) for $T_f \simeq 1200K$ and an even higher value for higher flame temperatures. If it is assumed that the convective heat transfer coefficient has a value of, say, 10 W/m^{2}K, the radiative heat transfer coefficient of 168W/m^{2}K derived previously represents 94.4% of the total flame-to-tank outer surface conductance instead of 75% as usually assumed. Since it will be difficult to estimate the flame-to-tank radiative heat transfer rate accurately because that heat transfer rate is roughly proportional to T_f^4 and T_f is quite variable, there would appear to be little point in trying to estimate h_f accurately and it might suffice for the purposes of the analysis to specify a uniform value of, say, 15W/cm^2 over the entire outer surface of the tank. To avoid specifying h_f in quite such an arbitrary fashion, the procedure described in Appendix C will be implemented in a simplified manner as described below.

The analysis described in Appendix C combines flame updraft velocities predicted using a simple pool fire model developed by Raj (10) with point-wise heat transfer data obtained by Giedt (12) for cylinders in crossflow at different Reynolds numbers and freestream turbulence levels. According to Raj, the centerline updraft velocity (V) for a plume produced by a circular pool fire, shown in Fig. C-1, can be predicted approximately from the expression,

---

*The radiative heat transfer coefficient, h_r, is not a strong function of T_s when T_s is considerably less than T_f. If T_s is assumed to be 600 K instead of 775 K in the above analysis, $h_r = 135.$/Wm^2°K instead of 168W/m^{2}K, for instance.

$$V=\sqrt{\frac{0.33(1-\omega)gz}{\omega}} \qquad 2\text{-}41$$

where g is the acceleration due to gravity, z is the height above the pool surface, as shown in Fig. C-1, and

$$\omega=\frac{1}{\left[1+\frac{\beta Q}{C_a T_a S}\right]} \qquad 2\text{-}42$$

The parameter β in Eq. 2-42 is an empirical factor introduced to account for incomplete combustion and the loss of energy from the fire by thermal radiation. Raj recommends that β be assigned a value of 0.45 for JP-4 pool fires. The parameters Q, T_a, C_a amd S in Eq. 2-42 are the lower heat of combustion of the fuel, the temperature of the surrounding air (ie. the ambient temperature), the specific heat at constant pressure of air at temperature T_a and the stoichiometric air-fuel mass ratio respectively. For air at a temperature of 290 K, $C_a = 1000$J/kgK while for JP-4 fuel, $Q = 4.65 \times 10^7$J/kg and S = 17(11). Substituting these values into Eq. 2-42 gives $\omega = 0.19$ and Eq. 2-41 then simplifies to:

$$V=1.18\sqrt{gz} \qquad 2\text{-}43$$

or in dimensionless form,

$$\frac{V}{V_{ch}} = 1.18\sqrt{\zeta} \qquad 2\text{-}44$$

where $\zeta = \frac{z}{r_p}$ and $V_{ch} = \sqrt{gr_p}$, with r_p being the radius of the base of the pool, as shown in Fig. C-1.

Equation 2-43 strictly only applies at large distances from the pool surface (z) but it can be shown by comparison with the results of more accurate analyses performed by Raj that it actually predicts V fairly well at all values of z*. The non-dimensional form of Eq. 2-43, viz Eq. 2-44, is plotted in Fig. C-5 for $\beta = 1.0$ (for $\beta = 1.0$, $V/V_{ch} = 1.76\sqrt{\zeta}$).

It is assumed in this analysis that Eq. 2-41 can be used as a first approximation to predict the updraft velocity of combustion gases in a pool fire enveloping a tank car even though such a fire will probably not be circular as assumed in Raj's analysis. Updraft velocities in a flame enveloping a tank car will probably differ from updraft velocities in a flame without a tank car present but such differences will be neglected.

Equation 2-41 will be used to predict the flam updraft velocity at a height above the pool surface (z) coinciding with the mid-height of the tank car. For a tank located a distance h above the pool surface, $z = D/2 + h'$ as shown in Fig. 2-15. As mentioned in Sect. 2.3.1.1 the value of h' is usually not provided in tank car fire test reports but it will probably be ≈0 in most accident situations. The updraft velocity

---

*Equation 2-43 is obviously not applicable as $z \to \infty$ because V must approach zero for large heights.

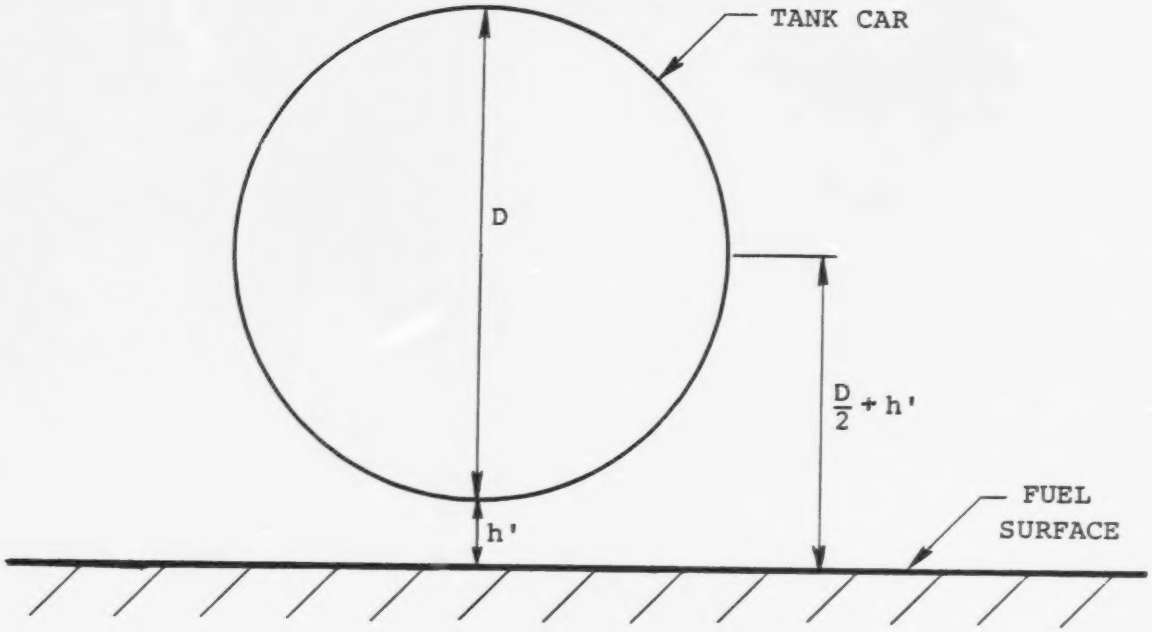
TANK CAR
D
$\frac{D}{2} + h'$
h'
FUEL SURFACE

Fig.: 2-15: Tank Car in Pool Fire

at the tank mid-height will be used to calculate the Reynolds number (Re_D) of the flow of combustion gases around the tank from the equation,

$$Re_D = \frac{VD}{\nu} \qquad 2\text{-}45$$

where ν is the kinematic viscosity of the combustion gases evaluated at the average of the local value of the tank outer surface temperature (T_s) and the user-specified flame temperature T_f (ie. ν will be evaluated at the film temperature, T_{film}, where $T_{film} = (T_s + T_f)/2$). It will be assumed that the kinematic viscosity of the combustion gases is approximately the same as that of air, which is given conveniently by the expression:

$$\nu = 6.6568 \times 10^{-11}\, T^2 \quad 5.95036 \times 10^{-8}\, T - 8.162203 \times 10^{-6} (m^2/s) \qquad 2\text{-}46$$

Equation 2-46 which is valid for 200 K $\leqslant$ T $\leqslant$ 1300 K, was obtained by fitting a quadratic curve to values of ν given by Holman (3).

Unless explicitly stated otherwise, most correlations for convective heat transfer coefficients in external flows apply to flows in which the freestream turbulence intensity (T') is fairly low, typically 1% or less. A procedure is described in Appendix C whereby pointwise heat transfer data obtained by Giedt (12) for a cylinder in cross-flow at different Reynolds numbers but at a freestream turbulence level of only about 1% can be applied to more turbulent flows by simply increasing the actual Reynolds number to obtain an "effective" Reynolds number. Figure C-3 is used in the manner described in Appendix C to obtain the effective Reynolds number for given values of T' and Re_D. It is assumed in Appendix C that the freestream turbulence intensity in a pool fire is approximately 3% and that this value should be increased by an additional 1% (ie. to obtain T'=4%) to account for the fact that the lower stagnation points on a cylinder in a pool fire will not be at $\theta=0^{\circ}$ (see Fig. C-9) as they are for a cylinder in cross-flow. The higher stagnation points in the pool fire case will cause the thermal and hydrodynamic boundary layers at a given value of θ to be thinner than the corresponding boundary layers at the same value of θ for a cylinder in cross-flow, thus increasing local heat transfer coefficients. It will be assumed for the purposes of this analysis that the "effective" Reynolds number for a tank car in a pool fire is the Reynolds number calculated from Fig. C-8 with T'= 4%. The curves shown in Fig. C-8 for T' = 4% (for the fire) and T'= 1% (for Giedt's or similar data) can be used to obtain a plot of the Reynolds number increment, designated ΔRe_D, that must be added to Re_D to obtain the effective Reynolds for T'= 4%, as a function of Re_D. The plot of ΔRe_D vs. Re_D obtained from Fig. C-8 is shown in Fig. 2-16. The following expression for ΔRe_D in terms of Re_D can be obtained from Fig. 2-16.

$$\Delta Re_D = 29.07 \times 10^3 + 9.33 \times 10^{-2}\ Re_D \qquad 2\text{-}47$$

from which,

$$Re_{D_{effective}} = Re_D \quad Re_D = 29.07 \times 10^3 + 1.0933\ Re_D \qquad 2\text{-}48$$

The procedure described in this section for predicting h_f has so far paralleled the procedure described in

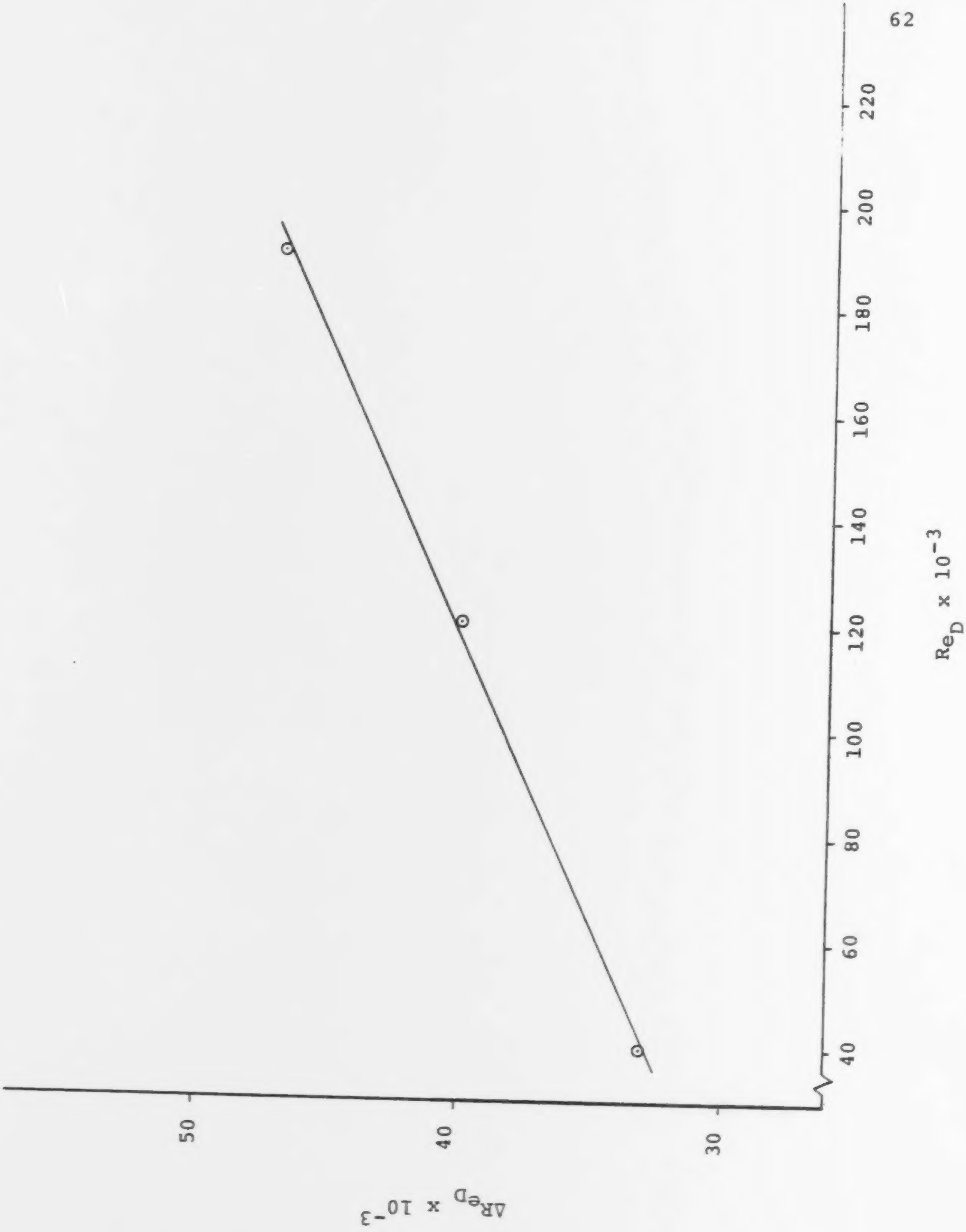

Fig.: 2-16: Reynolds Number Increment (ΔRe_D) as a Function of Re_D

Appendix C except that Eq. 2-41 is used to predict the updraft velocity (V) instead of Fig. C-5 and the flame temperature (T_f) is assumed to be user-specified instead of obtained from Fig. C-5. Also, the properties of the combustion gases are evaluated at T_{film} instead of T_f and the procedure for calculating Re_D effective has been simplified. The analyses will differ after this point, however, in that Re_D effective will be used in the tank car model to define an average convective heat transfer coefficient for the entire tank surface instead of local values as in Appendix C. This simplication of the procedure described in Appendix C is justifiable because the circumferential variation in h_f shown in Figs C-11 and C-12 is probably not as large as the uncertainty in h_f introduced by the approximations and simplifications made in its estimation. Also, predicting the value of h_f accurately will be most important for the tank outer surface at the top of the tank (ie. at large values of θ, where $\theta = 180^\circ$ at the top of the tank) because tank wall temperatures are usually highest in that region. Since it can be seen from Figs. C-11 and C-12 that h_f for $140^\circ \leq \theta \leq 180^\circ$ is probably close to its average value for the entire cylinder, the latter value serves as a good estimate of h_f in regions where that parameter in most important. Thus a uniform value of h_f for the entire circumference of the tank will be calculated from the expression,

$$Nu = \frac{h_f D}{k_a} = 0.0239 (Re_{D_{effective}})^{0.805} \qquad 2\text{-}49$$

which applies to cylinders in cross-flow for $40,000 \leq Re_{D_{effective}} \leq 400,000$ (13) . The thermal conductivity of the combustion gases, k_a, assumed the same as that of air, will be evaluated at T_{film} in the tank car model.

The thermal conductivity of air is given approximately by the expression

$$k_a = 8.9201 \times 10^{-3} + 5.7733 \times 10^{-5} T(K)\ (W/mK) \qquad 2\text{-}50$$

for $200K \leqslant T \leqslant 1300K$ so Eqs. 2-43, 2-45, 2-46, 2-48 and 2-50 can be combined and substituted into Eq. 2-49* to give the following expression for h_f.

$$h_f = \frac{(2.132 \times 10^{-4} + 1.38 \times 10^{-6}\ T_{film})}{D} \times$$

$$\left[29.07\text{x}10^{3} + \frac{4.039\sqrt{zD}}{6.6568\text{x}10^{-11} T^2_{film} + 5.9504\text{x}10^{-8} T_{film} - 8.1622\text{x}10^{-6}}\right]^{0.805}$$

where D and z are in meters. 2-51

For the following typical values-

$$\left.\begin{array}{l} T_f = 1200K \\ T_s = 775K \end{array}\right\} \quad T_{film} = 990K$$

$$\left.\begin{array}{l} h' = 0 \\ D = 3m\ \text{(DOT 112A tank car)} \end{array}\right\} \quad z = 1.5m,$$

Eqn. 2-51 gives $h_f = 8.1\ W/m^2K$ as the average heat transfer coefficient for the tank outer surface. This value of h_f is in fairly good agreement with local values given in Appendix C so Eq. 2-51 will be used in the DE tank car analysis program to predict h_f for each node on the tank car outer surface.

---

* Equation 2-49 is strictly only applicable when the cylinder for which h_f is being calculated is isothermal, so it can only be used to obtain a first approximation to h_f in the tank car model.

2.3.2 Unprotected Tank Car Thermal Analysis

2.3.2.1 Internal Boundary Conditions

The boundary conditions that must be prescribed on the inner surface of a tank car in a pool fire are all of the third type mentioned in Sect. 2.1.1, that is they are all defined by an equation of the form,

$$q'' = f(T, T_\infty) \qquad 2\text{-}52$$

where q'' $(= -k \nabla T.\hat{n})$ is the wall heat flux. The function $f(T, T_\infty)$ adopts different forms for natural convection, boiling, radiation etc. and is a non-linear function of T in general as discussed previously.

Heat transfer from the vapor-covered parts of a tank wall to the tank contents occurs by convection and radiation to the propane vapor and by radiation alone to the liquid while heat transfer from the liquid-wetted wall to the liquid lading occurs by either boiling, or natural convection depending on the wall heat flux and the degree of subcooling, if any, of the liquid. All of the heat transfer mechanisms mentioned above will be modelled by prescribing appropriate boundary conditions on the vapor-covered and liquid-wetted parts of the tank wall. The boundary conditions needed to model these mechanisms are described in subsequent sections.

2.3.2.2 Radiative Boundary Conditions In The Ullage

Radiation from the inner surface of the tank wall to the surface of the liquid LPG will be most significant when the temperature of the wall is high because radiation is proportional to T^4. To put this heat transfer mechanism into the proper perspective, consider a case in which the temperature of the tank wall is 922 K(1200°F), since this is about the maximum temperature that tank cars walls have withstood in tank car fire tests without rupturing, and the liquid LPG is at its saturation temperature corresponding to a tank pressure of 2.07 MPa (300psig), specifically approximately 334K(142°F). Assuming that the propane vapor is optically transparent* (ie. that it does not absorb or emit radiation), the radiative heat flux from the inner surface of the tank wall in the ullage (assumed isothermal) to the liquid LPG surface is given by the expression,

$$q''_{ri} = \frac{\sigma(T_1^{\,4} - T_2^{\,4})}{\frac{1-\varepsilon_1}{\varepsilon_1} + \frac{1}{F_{1-2}} + \frac{(1-\varepsilon_2)}{\varepsilon_2} \quad \frac{A_1}{A_2}} \qquad 2\text{-}53$$

where the subscripts 1 and 2 identify parameters associated with the tank wall inner surface and the liquid surface respectively, A is the area of a surface and F_{1-2} is the view factor for the tank wall inner surface viewing the liquid surface. If the tank is half-full of liquid,

$A_1 = \pi R_{it}$ (R_{it} is the inner radius of the tank)

$A_2 = 2R_{it}$

and since $A_1F_{1-2} = A_2F_{2-1}$ where $F_{2-1} = 1$ (ie. the liquid surface "sees" only the tank wall). $F_{1-2} = \frac{2}{\pi} = 0.637$.

---

* The validity of this assumption will be discussed later

The value of ε_1 will depend on the surface finish and condition (ie., degree of corrosion) of the tank inner surface and could vary over quite a wide range for that reason but it will be assumed that $\varepsilon_1 = 0.6$ for the purposes of this analysis. It will also be assumed that $\varepsilon_2 = 0.8$, since $\varepsilon = 0.82$ for an infinitely thick layer of "oil" according to data published by McAdams (14). Substituting the values of T_1, T_2, F_{1-2} and ε_2 mentioned previously into Eq. 2-53 we obtain,

$$q''_{ri} = 15{,}300\text{W/m}^2 \ (4{,}850\frac{\text{BTU}}{\text{hrft}^2}),$$

which, for a temperature difference of (922-334) = 588K. corresponds to a radiative heat transfer coefficient (h_r) of 26W/m^{2}K. By way of comparison, the heat flux from a fire with a flame temperature of 1200K (927°C) to the outer surface of the tank wall (assumed to be at the same temperature as the inner surface, 922K) can be shown by applying Eq. 2-39 to be;

$$q''_{ro} = 56{,}200\text{W/m}^2 (17{,}800\text{BTU/hrft}^2).$$

when $\varepsilon_f = 0.9$ and $\varepsilon_s = 0.8$ as assumed in Sect. 2.3.1.2. Thus the radiative heat flux from the inner surface of the tank wall to the liquid surface for the assumed conditions is only 27% (ie. (15,300/56200)x100) of the flame-to-tank radiative heat flux and the temperature of the tank wall will still be increasing rapidly under the assumed conditions for that reason.

The inner surface of the tank wall was assumed to be isothermal in the preceding analysis for the purpose of estimating the radiative heat flux from that surface to the liquid LPG. That assumption will not be valid in general and a procedure for incorporating the radiative heat transfer calculations into a finite - difference model of the tank wall is described in Sect. 2.3.2.2.

It was also assumed in the preceding analysis that the LPG vapor in the tank ullage is optically transparent and hence that radiant energy being transferred from vapor-covered parts of the tank wall to the liquid is not attenuated by absorption in the vapor. The LPG vapor will actually participate in the exchange of radiant energy to some extent but modelling the absorption and emission of radiation by the vapor would be very difficult and hence will not be attempted in the DE tank car model. It can be demonstrated fairly easily that the LPG vapor will be effectively transparent to the radiation emitted by the tank wall in any case by examining the infrared absorption spectrum for propane vapor* shown in Fig. 2-17 (taken from (15)). Figure 2-17 shows the absorbance (A) of propane vapor as a function of the wavelength (λ) and the wavenumber (N) of the incident radiation (note that $\lambda = 10^4/N$ when λ and N have the units μm and cm^{-1} respectively) for a path length of 5cm and propane partial pressures of 25mm Hg (for $3\,\mu m < \lambda < 3.7\,\mu m$ only) and 150 mm Hg at a reference temperature of 20°C. The propane vapor was mixed with an inert diluent gas (N_2) such that the

---

* Liquefied petroleum gases (LPG) typically contain small percentages of ethane, butane, etc. in addition to propane but most of the hydrocarbon fractions present in small percentages are more volatile than propane and hence will boil off rapidly in a pool fire leaving essentially pure propane vapor in the ullage.

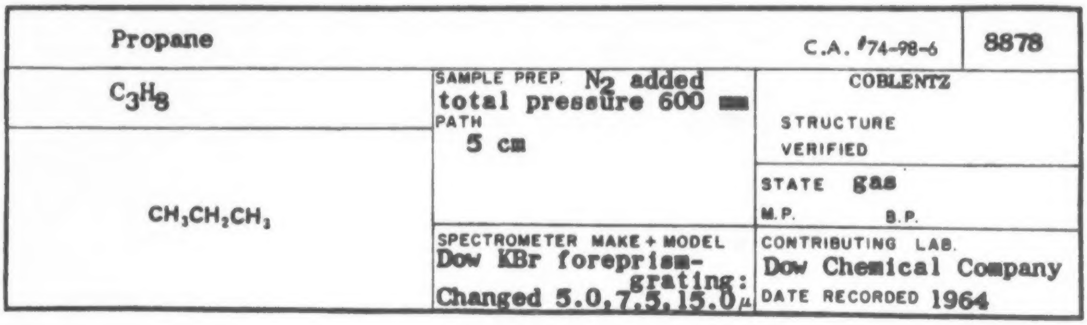

Propane	C.A. #74-98-6	8878
C_3H_8	SAMPLE PREP. N_2 added total pressure 600 mm PATH 5 cm	COBLENTZ STRUCTURE VERIFIED
$CH_3CH_2CH_3$		STATE gas M.P. B.P.
	SPECTROMETER MAKE + MODEL Dow KBr foreprism-grating: Changed 5.0,7.5,15.0μ	CONTRIBUTING LAB. Dow Chemical Company DATE RECORDED 1964

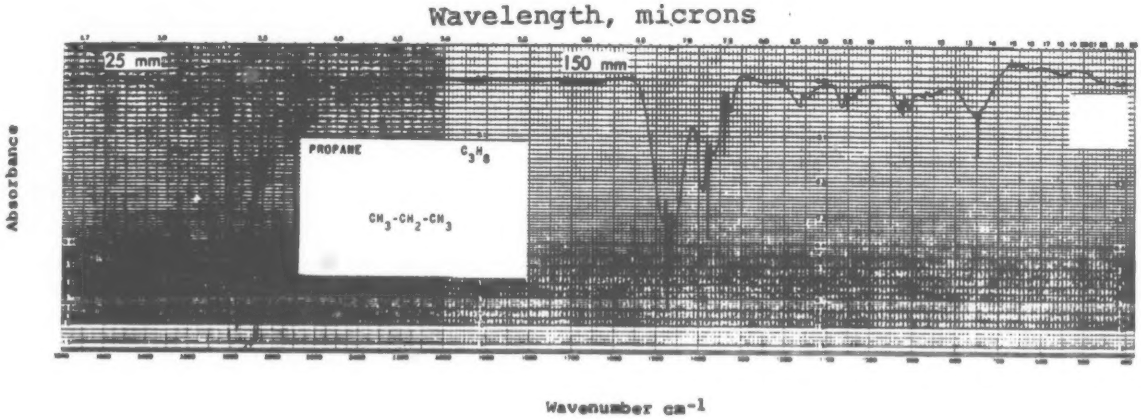

Fig. 2-17: Infrared absorption spectrum for propane vapor.

total pressure of the gas mixture was 600 mmHg, as noted in Fig. 2-17. A diluent gas is used in a spectroscopic analysis to reduce the concentration (partial pressure) of the absorbing gas and does not absorb radiation itself. The absorbance of the propane vapor was measured at two partial pressures (ie. 25mm and 150mmHg) in the wavelength range $3\mu m < \lambda < 3.7\mu m$ because the absorbance for the higher partial pressure (150mmHg) went off scale at $\lambda = 3.4\mu m$.

The absorbance (in absorbance units) of a gas (vapor) layer of a given thickness d ($d = 5$cm for the spectrum shown in Fig. 2-17) is defined by the expression,

$$A = \log_{10} \left(\frac{I_o}{I_f}\right) \tag{2-54}$$

where I_o is the intensity of monochromatic radiation of wavelength λ entering the layer and I_f is the intensity of the radiation (of wavelength λ) leaving the layer. According to the Lambert-Bouguer law (16),

$$\frac{I_f}{I_o} = e^{-K_\lambda . d} \tag{2-55}$$

where K_λ is the monochromatic extinction coefficient of the gas. Substituting Eq. 2-55 into Eq. 2-54 we obtain the expression

$$A = 0.4343\ K_\lambda . d \tag{2-56}$$

which, when combined with the results shown in Fig. 2-17, can be used to obtain a rough estimate of the absorption strength of the propane vapor in the ullage of a tank car for different values of λ. Consider the worst possible case, for example, when the wavelength of the radiation passing through the vapor is ≃3.38μm so that the absorbance of the vapor is a maximum, as seen in Fig. 2-17. The value of A shown in Fig. 2-17 for this wavelength and a propane partial pressure of 25mm Hg is 1.0(unit) so,

$$A = 1 = 0.4343\, K\lambda . d$$

where $d = 5$cm. Solving for K_λ we obtain

$$K_\lambda = 0.4605 \text{ cm}^{-1}$$

Assuming that K_λ is a function only of the number of propane molecules present per unit volume, which is only approximately correct, the value of K_λ (for $\lambda = 3.38$μm) at a propane pressure of ≃2MPa (ie. a typical venting pressure for a tank car in a fire) can be obtained from its value at a pressure of 25mmHg and 20°C by multiplying the latter value by the ratio of the propane vapor densities for those conditions. It can be shown that the ratio of the density of saturated propane vapor at 2MPa to the vapor density at 25mmHg and 20°C is ≃ 800 so,

$$(K_\lambda)_{2MPa} \simeq 800 \times 0.4605 \text{ cm}^{-1} = 368.4 \text{ cm}^{-1}$$

The thickness of a layer of saturated propane vapor at 2MPa that would be required to reduce the intensity of 3.38 μm wavelength radiation to only 1% of its original value (ie. effectively absorb all of the incident radiation) can be obtained by setting $A = 2$ in Eq 2-56 and solving for d with $K_\lambda = 368.4 \text{ cm}^{1-}$. This calculation gives $d = 0.125$ mm which shows that the absorption of 3.38μm wavelength radiation by the propane vapor will be almost immediate.

While the result of the foregoing analysis indicates that propane vapor can be strongly absorbing, it should be recognized that the vapor only absorbs radiation strongly within narrow wavelength intervals. Propane vapor is effectively transparent to radiation with wavelengths between $3.7\mu m$ and $6.5\mu m$, for instance, so the absorbing characteristics of propane have to be discussed with reference to the spectrum of the radiation passing through it. Radiant energy emitted by the hot tank wall will, at any wall temperature, have a spectrum which peaks at some wavelength λ_{max}, as shown in Fig. 2-18 (taken from (3)) for black and gray $(\varepsilon = 0.6)$ surfaces at a temperature of 1922K. The value of λ_{max} is related to the surface temperature (T_s) by Wien's displacement law, written as;

$$\lambda_{max} T_s = 2897.6\mu m.K \qquad 2\text{-}57$$

The propane vapor in the ullage of a tank car in a fire will absorb radiation emitted by the tank wall most strongly when the wall temperature (T_s) is such that λ_{max} at that temperature coincides with one of the strongly absorbing wavelengths shown in Fig. 2-17. The absorption strength of propane vapor in the infrared spectrum peaks at wavelengths of approximately $3.4\mu m$ and $6.8\mu m$ according to Fig. 2-17, so Wien's displacement law gives the result that radiation emitted by the tank wall at wall temperatures of 852K (for $\lambda_{max} = 3.4\mu m$) and 426K (for $\lambda = 6.8\mu m$) will be the most highly absorbed. The lower wall temperature (426K); for which $\lambda_{max} = 6.8\mu m$, is not of interest in this analysis because the emissive power of the tank wall will be very low at that temperature but the higher wall temperature (852K) is high enough to be of concern since the optically

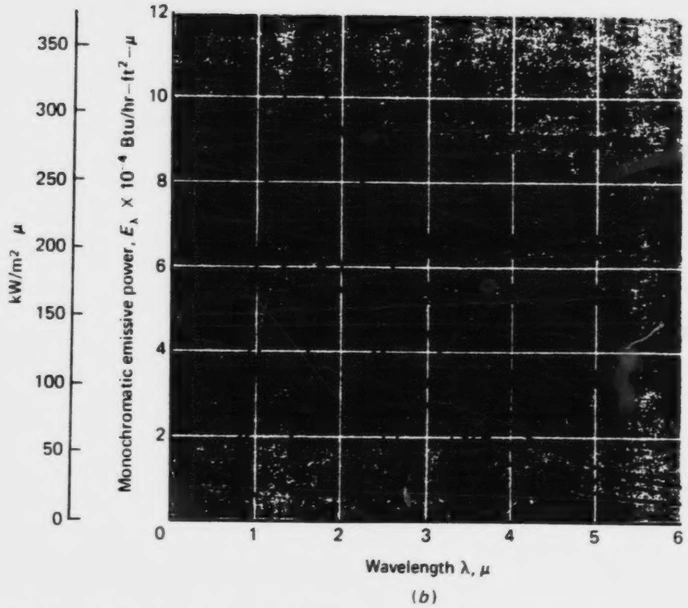

Fig. 2-18: (*a*) Blackbody emissive power as a function of wavelength and temperature. (*b*) Comparison of emissive power of ideal blackbodies and gray bodies with that of a real surface.

transparent vapor assumption made previously could be invalid for wall temperatures at or near to that value.

In order to determine whether the propane vapor can be considered optically transparent when the tank wall temperature is at or near 852K, an estimate of the fraction of the emitted radiation that will absorbed by the vapor when the wall temperature is at or near to that value must be obtained. It will be assumed for the purpose of estimating that fraction that radiation with wavelengths in the ranges $3.3\mu m < \lambda < 3.6\mu m$ and $6.5\mu m < \lambda < 7.7\mu m$ (ie. with wavelengths in the strongly absorbing intervals seen in Fig. 2-17) will be totally absorbed by the propane vapor in the tank ullage and that radiation with wavelengths outside of these ranges (but within the spectrum covered by Fig. 2-17) will be transmitted unattenuated. It can be shown that radiation with a wavelength of $\simeq 6.8\mu m$ would be 99% absorbed by saturated propane vapor at a pressure of $\simeq 2$MPa within a path length of 0.25 cm, compared to the corresponding path length of 0.125 mm derived previously for 3.4μm wavelength radiation, so path lengths in the ullage of a full size DOT 112A tank car, which has an inner diameter of 3 m, will obviously be long enough to absorb most of the 6.5μm - 7.7μm radiation as assumed.

The energy radiated by a blackbody at temperature T_s within a specified wavelength range, say between $\lambda = \lambda_1$ and $\lambda = \lambda_2$ (where $\lambda_2 > \lambda_1$), can be calculated as a fraction of the total energy radiated by computing the difference between appropriate values of the radiation fraction, $f_{\lambda T}$, given in Table 2.1 (taken from Holman (3)) as a function of λT. The energy radiated by a blackbody at temperature T_s between the wavelengths λ_1 and λ_2 would be the difference between the values of $f\ \lambda_T$ at $\lambda T = \lambda_2\ T_s$ and $\lambda T = \lambda_1\ T_s$ when expressed as a fraction of the total energy radiated, for instance. The total

TABLE 2-1: Radiation Functions

λT		$E_{b\lambda}/T^5$		$\frac{E_{b0-\lambda T}}{\sigma T^4}$
μm·°R	μm·°K	$\frac{\text{Btu}}{\text{h}\cdot\text{ft}^2\cdot{}^\circ\text{R}^5\cdot\mu\text{m}}$ $\times 10^{15}$	$\frac{\text{W}}{\text{m}^2\cdot{}^\circ\text{K}^5\cdot\mu\text{m}}$ $\times 10^{11}$	
1,000	555.6	0.000671	0.400×10^{-5}	0.170×10^{-7}
1,200	666.7	0.0202	0.120×10^{-3}	0.756×10^{-6}
1,400	777.8	0.204	0.00122	0.106×10^{-4}
1,600	888.9	1.057	0.00630	0.738×10^{-4}
1,800	1,000.0	3.544	0.02111	0.321×10^{-3}
2,000	1,111.1	8.822	0.05254	0.00101
2,200	1,222.2	17.776	0.10587	0.00252
2,400	1,333.3	30.686	0.18275	0.00531
2,600	1,444.4	47.167	0.28091	0.00983
2,800	1,555.6	66.334	0.39505	0.01643
3,000	1,666.7	87.047	0.51841	0.02537
3,200	1,777.8	108.14	0.64404	0.03677
3,400	1,888.9	128.58	0.76578	0.05059
3,600	2,000.0	147.56	0.87878	0.06672
3,800	2,111.1	164.49	0.97963	0.08496
4,000	2,222.2	179.04	1.0663	0.10503
4,200	2,333.3	191.05	1.1378	0.12665
4,400	2,444.4	200.51	1.1942	0.14953
4,600	2,555.6	207.55	1.2361	0.17337
4,800	2,666.7	212.32	1.2645	0.19789
5,000	2,777.8	215.06	1.2808	0.22285
5,200	2,888.9	216.00	1.2864	0.24803
5,400	3,000.0	215.39	1.2827	0.27322
5,600	3,111.1	213.46	1.2713	0.29825
5,800	3,222.2	210.43	1.2532	0.32300
6,000	3,333.3	206.51	1.2299	0.34734
6,200	3,444.4	201.88	1.2023	0.37118
6,400	3,555.6	196.69	1.1714	0.39445
6,600	3,666.7	191.09	1.1380	0.41708
6,800	3,777.8	185.18	1.1029	0.43905
7,000	3,888.9	179.08	1.0665	0.46031
7,200	4,000.0	172.86	1.0295	0.48085
7,400	4,111.1	166.60	0.99221	0.50066
7,600	4,222.2	160.35	0.95499	0.51974
7,800	4,333.3	154.16	0.91813	0.53809
8,000	4,444.4	148.07	0.88184	0.55573
8,200	4,555.6	142.10	0.84629	0.57267
8,400	4,666.7	136.28	0.81163	0.58891
8,600	4,777.8	130.63	0.77796	0.60449
8,800	4,888.9	125.15	0.74534	0.61941
9,000	5,000.0	119.86	0.71383	0.63371
9,200	5,111.1	114.76	0.68346	0.64740
9,400	5,222.2	109.85	0.65423	0.66051
9,600	5,333.3	105.14	0.62617	0.67305
9,800	5,444.4	100.62	0.59925	0.68506
10,000	5,555.6	96.289	0.57346	0.69655
10,200	5,666.7	92.145	0.54877	0.70754
10,400	5,777.8	88.181	0.52517	0.71806
10,600	5,888.9	84.594	0.50261	0.72813
10,800	6,000.0	80.777	0.48107	0.73777
11,000	6,111.1	77.325	0.46051	0.74700
11,200	6,222.2	74.031	0.44089	0.75583
11,400	6,333.3	70.889	0.42218	0.76429
11,600	6,444.4	67.892	0.40434	0.77238
11,800	6,555.6	65.036	0.38732	0.78014
12,000	6,666.7	62.313	0.37111	0.78757
12,200	6,777.8	59.717	0.35565	0.79469
12,400	6,888.9	57.242	0.34091	0.80152
12,600	7,000.0	54.884	0.32687	0.80806
12,800	7,111.1	52.636	0.31348	0.81433
13,000	7,222.2	50.493	0.30071	0.82035
13,200	7,333.3	48.450	0.28855	0.82612
13,400	7,444.4	46.502	0.27695	0.83166
13,600	7,555.6	44.645	0.26589	0.83698
13,800	7,666.7	42.874	0.25534	0.84209
14,000	7,777.8	41.184	0.24527	0.84699
14,200	7,888.9	39.572	0.23567	0.85171
14,400	8,000.0	38.033	0.22651	0.85624
14,600	8,111.1	36.565	0.21777	0.86059
14,800	8,222.2	35.163	0.20942	0.86477
15,000	8,333.3	33.825	0.20145	0.86880
16,000	8,888.9	27.977	0.16662	0.88677
17,000	9,444.4	23.301	0.13877	0.90168
18,000	10,000.0	19.536	0.11635	0.91414
19,000	10,555.6	16.484	0.09817	0.92462
20,000	11,111.1	13.994	0.08334	0.93349
21,000	11,666.7	11.949	0.07116	0.94104
22,000	12,222.2	10.258	0.06109	0.94751
23,000	12,777.8	8.852	0.05272	0.95307
24,000	13,333.3	7.676	0.04572	0.95788
25,000	13,888.9	6.687	0.03982	0.96207
26,000	14,444.4	5.850	0.03484	0.96572
27,000	15,000.0	5.139	0.03061	0.96892
28,000	15,555.6	4.532	0.02699	0.97174
29,000	16,111.1	4.012	0.02389	0.97423
30,000	16,666.7	3.563	0.02122	0.97644
40,000	22,222.2	1.273	0.00758	0.98915
50,000	27,777.8	0.560	0.00333	0.99414
60,000	33,333.3	0.283	0.00168	0.99649
70,000	38,888.9	0.158	0.940×10^{-3}	0.99773
80,000	44,444.4	0.0948	0.564×10^{-3}	0.99845
90,000	50,000.0	0.0603	0.359×10^{-3}	0.99889
100,000	55,555.6	0.0402	0.239×10^{-3}	0.99918

energy radiated by the inner surface of the wall of a tank car will be less than the energy radiated by a blackbody at the same temperature, of course, but the dependence of the radiation fraction, $f_{\lambda T}$, on wavelength should be roughly the same as for a blackbody. Thus it is assumed that the data given in Table 2-1 can be used to calculate the energy radiated by the tank wall inner surface in a given wavelength interval as a fraction of the total energy radiated. The results of such a spectral analysis, summarized in Tables 2-2a and 2-2b, indicate that roughly 14.4% of the total energy radiated by the tank wall inner surface (at $T_s = 852K$) will be absorbed by the propane vapor in the wavelength ranges $3.3 < \lambda < 3.6\mu m$ and $6.5 < \lambda < 7.7\mu m$, and 73.1% of the radiation

TABLE 2-2a: Fractions of energy emitted in non-absorbing wavelength ranges ($T_s = 852K$)

WAVELENGTH	RANGE	FRACTION OF ENERGY EMITTED
λ_1	λ_2	(percent)
2.6$^{1 = 1}$	3.3	12.6
3.6	6.5	40.6
7.7	22.0^2	19.9
		$\Sigma = 73.1\%$

1. Lowest wavelength in Fig. 2-17
2. Highest wavelength in Fig. 2-17

TABLE 2-2b: Fractions of energy emitted in absorbing wavelength ranges (T_s = 852K)

WAVELENGTH RANGE		FRACTION OF ENERGY EMITTED
λ_1	λ_2	(percent)
3.3	3.6	5.7
6.5	7.7	8.7
		Σ =14.4%

will be transmitted unattenuated within the wavelength intervals $2.6\ \mu m < \lambda < 3.3 \mu m$, $3.6 \mu m < \lambda < 6.5 \mu m$ and $7.7 \mu m < \lambda < 22 \mu m$. Radiation with wavelengths less than 2.6μm and greater than 22μm, which constitutes 12.5% of the total, cannot be accounted for because these wavelengths lie outside of the range covered by Fig. 2-17.

The preceding analysis showed that at least 73% of the energy radiated by the inner surface of a tank wall at 852°C will reach the liquid surface and hence that it can be assumed, without introducing serious error, that the vapor is optically transparent. Note that the radiation absorbed by the vapor will be absorbed within very short path lengths and, as a result, will tend to heat the vapor close to the wall. This will increase the rate of heat transfer to an EXPLOSAFE liner if such a liner is fitted, although probably not very significantly.

2.3.2.3 Convective Heat Transer To The Propane Vapor

Convective heat transfer to the propane vapor in the ullage of a tank car in a fire occurs by both free and forced convection. Density gradients in the bulk of the vapor must be predominantly stable because it has been observed in experiments that the temperature of the vapor increases in the upward vertical direction (ie. the vapor is hottest at the top of the tank and coolest at the vapor/liquid interface), thus inhibiting free convection, but some free convection must nevertheless occur at the sides of the tank as relatively cool vapor is heated by the hot tank wall. It is expected that the convection currents induced by the upward movement of heated vapor at the sides of the tank would appear as shown in Fig. 2.19. The convective motion of the vapor must slow down and eventually cease at the top of the tank, however, since the heated vapor will only flow up a surface which is inclined (the tank wall at the top of the tank is horizontal) and the tank wall is symmetrical about the 12 o'clock position. Since free convection will not assist in the removal of heat from the top of the tank, which is usually the region that governs rupture because it is generally the hottest part of the tank, free convection in the ullage will not be modelled in the DE tank car analysis program.

Heat transfer to the propane vapor is augmented by forced convection when the relief value is venting unless, of course, the relief valve is located below the level of the liquid surface. It will be assumed in the DE tank car model that the flow of propane-vapor in the ullage is quasi-steady during venting and an expression for the convective heat transfer coefficient on the tank inner surface under those conditions

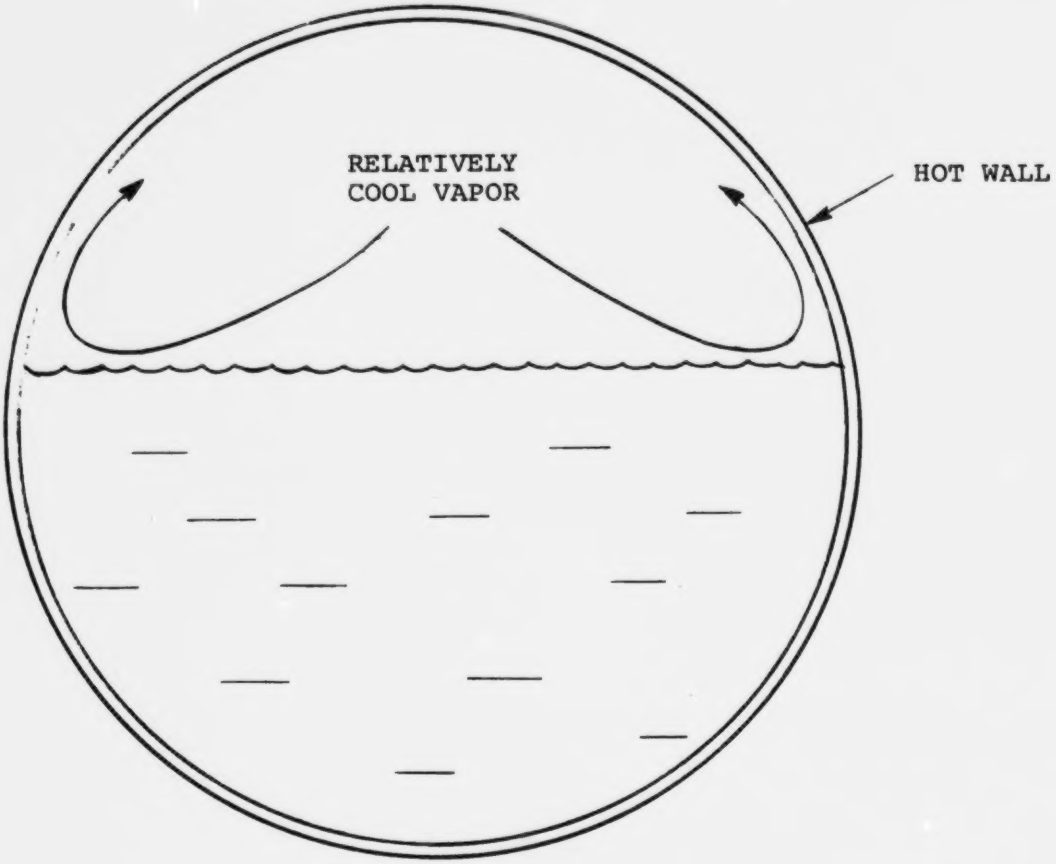
RELATIVELY
COOL VAPOR
HOT WALL

Fig. 2-19: Convection currents in tank ullage

is derived in Appendix D. The analysis described in Appendix D is briefly summarized below.

Considering first a level tank car with a single relief valve located at the tank center, as shown in Fig. 2-20; the velocity of the propane vapor flowing towards the relief valve will vary linearly from zero at the tank ends to some value U_c at the tank center (also shown in Fig. 2-20) if the propane boil-off rate per unit length is constant along the length of the tank. The latter condition should be approximately satisfied for a tank car in a pool fire since it is assumed that the fire completely envelopes the tank. The linear velocity distribution shown in Fig. 2-20 will obviously be incorrect in the immediate vicinity of the relief valve where the vapor flow will be constricted as it flows out of the valve, resulting in very high vapor velocities. Convective cooling will therefore be very high on the tank surface around the relief valve but the actual magnitude of the heat transfer coefficient in that region cannot be estimated easily. It would only be necessary to obtain an accurate estimate of the heat transfer coefficient distribution around the relief valve if the cooling provided by high heat transfer rates in that region had a significant effect on the peak wall temperature obtained, say, midway between the relief valve and one of the tank ends since tank ruptures usually initiate in regions well removed from the relief valve. A sensitivity analysis is described in Appendix E which indicates that high heat transfer rates and the resulting low wall temperatures around the relief valve have very little effect on peak wall temperatures at axial locations more than one tenth of a tank diameter away from the relief valve, and hence that an accurate estimate of the heat transfer coefficient distribution around the relief valve is not required. The axial

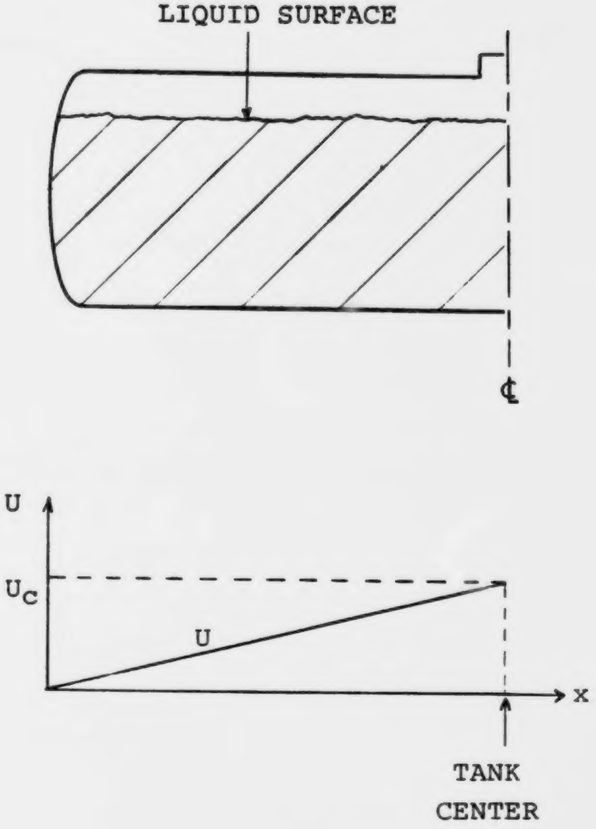
LIQUID SURFACE
℄
U
U_C
U
x
TANK CENTER

Fig. 2-20: Vapor velocity profile in venting tank

extent of the region affected by low wall temperatures around the relief valve will depend on the tank wall thickness, the thermal conductivity of the shell material, etc., however, so users of the DE model of an unprotected tank car will be permitted to specify an arbitrarily high heat transfer coefficient over a circular area on the tank inner surface around the relief valve. The radius of the circular area will be user specified. These provisions will permit the user of the tank car model to assess the model's sensitivity to assumed conditions around the relief valve for a given tank construction. It is expected that the sensitivity will be minimal in most cases.

As pointed out in Appendix D, the linear vapor velocity distribution in the ullage, shown in Fig. 2-20, is identical to the velocity distribution obtained in plane stagnation flow when the stagnation point for the stagnation flow is taken to be at the tank end cap, as shown in Fig. D-3. If the boundary layer on the inner surface of the tank wall remains laminar from the end cap to the relief valve, and the analysis given in Appendix D indicates that it probably will under most conditions for a tank without EXPLOSAFE, the convective heat transfer coefficient (h_i) on the tank inner surface is independent of position and is given exactly by the expression,

$$h_i = \frac{G(Pr)}{Pr} \rho_v C_{p_v} \sqrt{K\nu} \qquad \text{2-58}$$

where G(Pr) is given in Table 2-3 as a function of the Prandtl number (Pr) of the propane vapor, ρ_v, C_{p_v} and ν are the density, specific heat and kinematic viscosity of the vapor at the film conditions (ie. at the prevailing tank pressure and at the average of the tank wall inner surface and propane temperatures) and

TABLE 2-3: VALUES OF G (Pr)

Pr	G(Pr)
0.6	0.466
0.72	0.501
1.0	0.570
2.0	0.744

$$K = \frac{2U_c}{L} \qquad 2\text{-}59$$

where L is the length of the tank car. The vapor velocity at the center of the tank, U_c, is given by the expression,

$$U_c = \dot{m}_v / 2\rho_v A_{flow}, \qquad 2\text{-}60$$

so

$$K = \dot{m}_v / L\rho_v A_{flow}. \qquad 2\text{-}61$$

where $\dot{m}_v$ is the mass discharge rate of the vapor, calculated by the thermodynamic model of an unprotected tank car described in Sec. 3.1.2 (note that $h_i = 0$ when the tank is not venting), ρ_v is the bulk vapor density (ie. not the density at the film conditions), and A_f is the vapor cross-sectional flow area which, for a level tank, is given by the expression,

$$A_{flow} = R_{it}^2 \left[\cos^{-1}\left(\frac{X^*}{R_{it}}\right) - \frac{X^*}{R_{it}^2} \sqrt{R_{it}^2 - X^{*2}} \right] \qquad 2\text{-}62$$

where R_{it} is the tank inner radius.

Sample calculations described in Appendix D indicate that h_i will have values of approximately 8W/m^{2}K and 17W/m^{2}K for full and 1/5 scale tanks respectively when the tanks are 80% full of liquid and the heat flux incident on the tank outer surface is the pool fire standard heat flux (maximum value) of 108,000W/m^2 (34,500BTU/hrft^2). A tank pressure of 1.93MPa (280psia) was assumed in the calculations. Both of these heat transfer coefficients are less than the radiative heat transfer coefficient of 26W/m^{2}K derived in the preceding section for radiation from the inner surface of the tank wall at 922K (1200^{o}F) to the liquid surface. It is pointed out in Appendix D that the values of h_i for the full and 1/5 scale tanks will be 2-4 times the values just mentioned if the boundary layer becomes turbulent, a possibility that the analysis in Appendix D shows to be remote for a 1/5 scale tank but conceivable for a full-size tank under the assumed conditions. The vapor velocity and hence the likelihood of the boundary layer undergoing transition to turbulence will be reduced when the tank is less than 80% full of liquid, because the vapor flow area is inceased in that case. Since it is unlikely that the tank will rupture when the volume occupied by the liquid is equal to or greater than 80%* of the tank's total volume it will be assumed in the thermal model of an unprotected tank car that the boundary layer on the tank inner surface will remain laminar and hence that Eq. 2-58 can be used to predict h_i for a level tank under all conditions.

It should be noted that K, defined by Eqs. 2-59 and 2-61, is just the axial velocity gradient ($\frac{dU}{dz}$) of the vapor flow in the tank which, in turn, is simply the vapor volumetric discharge flowrate per unit length ($\dot{m}_v/\rho_v L$) divided by the vapor flow area (A_{flow}). The absolute value of K is thus independent of the number of relief valves in the tank and Eq. 2-58 can be used to predict h_i for a tank with any number of valves.

---

* The tank will rupture if it goes shell-full and the relief value is inadequately sized, of course.

The vapor velocity distribution in a tank with two relief valves would appear as shown in Fig. 2-21, for instance, and K_A and K_B would have the same absolute value (defined by Eq. 2-61).

The procedure needed to determine values of the heat transfer coefficient on the inner surface of a tilted tank car is fairly complicated compared to the procedure just described for a level tank. The procedure for defining the heat transfer coefficient distribution on the inner surface of a tilted tank is described in detail in Appendix D and hence will only be summarized here.

The analysis described in Appendix D shows that h_i at a distance x' from a stagnation point (ie. a point where $U=0$) is given approximately by the expression:

$$h_i(x') = \left[\frac{k_v^2 \quad U(x')^{2.27}}{8.15\nu \int_0^{x'} U(x)^{1.27} dx} \right]^{\frac{1}{2}} \qquad 2\text{-}63$$

where k_v is the thermal conductivity of the propane evaluated at the local film conditions.* The vapor velocity U(x) is given by the expression,

$$U(x) = \frac{\dot{m}_{vx}}{\rho v A_{flow}(x)} \qquad 2\text{-}64$$

where $\dot{m}_{vx}$ is the mass flowrate of vapor through the cross-section at x and $A_{flow}(x)$ is the vapor flow area at that point. The value of $\dot{m}_{vx}$ can be calculated by assuming that

---

* The propane vapor will always be superheated at the film conditions, in which case its conductivity is given (approximately) by the expression,

$$k_V = -1.2673\text{x}10^{-2} + 8.6147\text{x}10^{-5}T + 5.52278\text{x}10^{-8}T^2 \quad (T \text{ inK}, k \text{ inW/mK})$$

which is valid for $300 \leqslant T \leqslant 1000$ according to Ehya et al. (23).

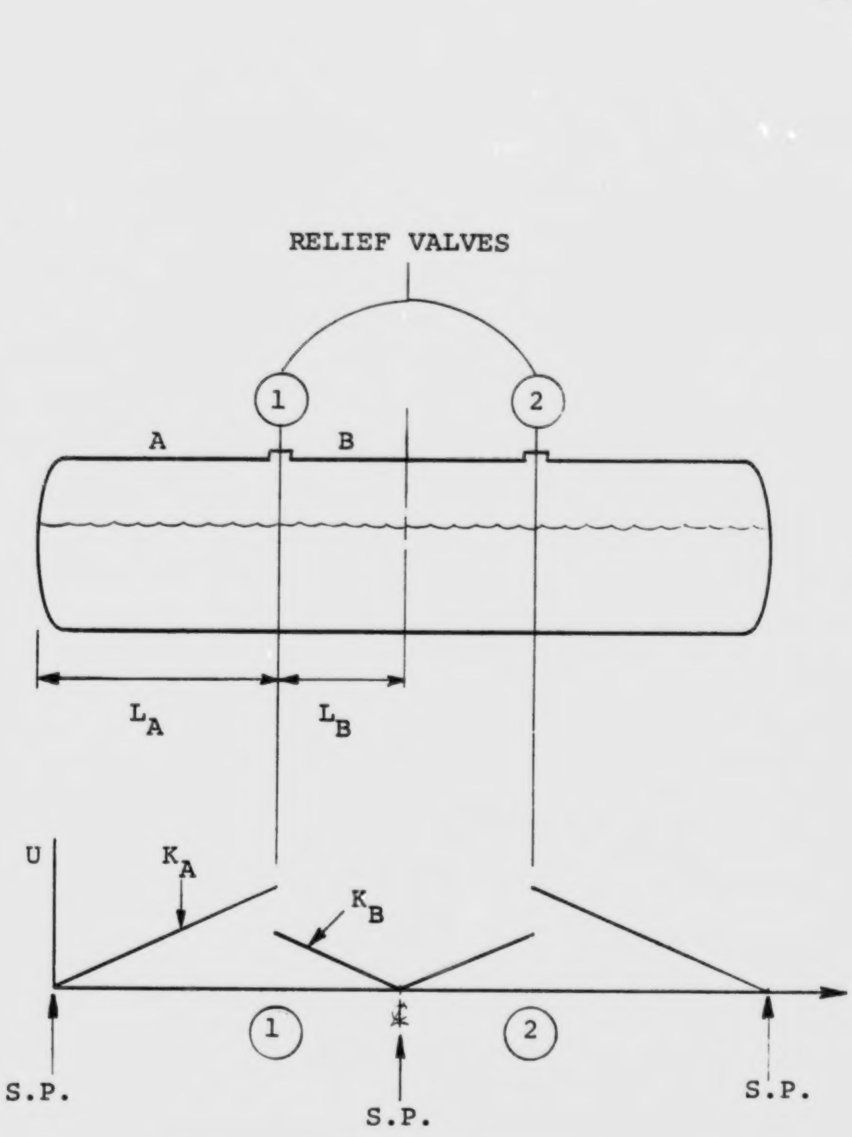
RELIEF VALVES
1
2
A
B
L_A
L_B
U
K_A
K_B
1
2
S.P.
S.P.
S.P.

S.P. - STAGNATION POINT

Fig. 2-21: Vapor velocity distribution in a tank with two relief valves

vapor evolution occurs uniformly over the free surface area of the liquid (A_{surf}), in which case

$$\dot{m}_{vx} = \left(\frac{\dot{m}_V}{A_{surf}}\right) A_{0 \rightarrow x} \qquad 2\text{-}65$$

where $A_{O \rightarrow x}$ is the area of the free surface between the stagnation point (at $x = 0$) and the point x. Integrals defining A_{surf} and $A_{O \rightarrow x}$ for a tilted tank are given in Appendix D. The value of $A_{flow}(x)$ can be calculated from the expression,

$$A_{flow}(x) = R_{it}^2 \left[\cos^{-1}\left(\frac{Y^*}{R_{it}}\right) - \frac{Y^*}{R_{it}^2} \sqrt{R_{it}^2 - Y^{*2}}\right] \qquad 2\text{-}66$$

where $Y^* = X^* - z(x) \sin \alpha$. The value of $z(x)$ is the value of z in the tank car coordinate system (see Sect. 2.2) corresponding to the location x, where x is measured from a stagnation point. The coordinate x would be measured from the left tank end for regions to the left of the relief valve and from the right tank end for regions to the right of the relief valve for a tank with only one relief valve, for instance, since the tank ends are the only stagnation points of that case.

Equation 2-63 was derived using a Prandtl number (Pr) of 0.81 for the propane vapor at the film conditions. The Prandtl number of propane vapor ranges from $\simeq 0.83$ at 111°C (200°F) superheat to $\simeq 0.81$ at 356°C (640°F) at a pressure of 1.94MPa (280psia), although it is almost independent of pressure (and also of temperature as seen from the figures quoted) so Eq. 2-63 should be applicable to all cases of interest. Heat transfer coefficients usually only vary according to the one-third power of the Prandtl number (ie. $h \sim Pr^{1/3}$ in general) in any case.

The integral in the denominator of Eq. 2-63 will be evaluated numerically in the DE tank car model since the integral can only be evaluated exactly when $U(x)$ is a simple function of x. Sample calculations of h_i for a tilted tank are given in Appendix D.

It can be shown that values of h_i obtained by applying Eq. 2-63 to a level tank agree almost exactly with values predicted using Eq. 2-58 since, in the level tank case, $U = Kx$ and Eq. 2-63 becomes:

$$h_i(x') = \left[\frac{k_v^2 (Kx')^{2.27}}{8.15\nu \int_0^{x'} (Kx)^{1.27}\, dx}\right]^{\frac{1}{2}}$$

$$= \left[\frac{k_v^2 K^{2.27} x'^{2.27}}{8.15\nu\, K^{1.27} \cdot \frac{x'^{2.27}}{2.27}}\right]^{\frac{1}{2}}$$

$$= 0.5277 \frac{k_v}{\sqrt{\nu}} \sqrt{K}$$

2-67

Also, $Pr = \frac{C_{pv}\mu}{k_v}$ and $G(Pr) = 0.524$ when $Pr = 0.81$ (interpolated from Table 2-3) so Eq. 2-58, giving h_i for a level tank, can be written as:

$$h_i = \frac{0.524}{Pr} \rho_v C_{pv} \sqrt{\nu} \sqrt{K}$$

$$= 0.524 \frac{k_v}{\sqrt{\nu}} \sqrt{K}$$

2-68

since $\nu = \mu/\rho$. This expression is in excellent agreement with Eq. 2-67, which was obtained using the expression for h_i in a tilted tank (ie. Eq. 2-63).

2.3.2.4 Heat Transfer From The Liquid-Wetted Tank Wall To The Liquid

Heat transfer from the liquid-wetted tank wall to the liquid lading will occur either by boiling or by natural convection, depending on the wall heat flux and the degree of subcooling of the liquid. The excess temperature (θ_s), which is the difference between the wall temperature and the liquid's saturation temperature at the prevailing pressure, will depend qualitatively on the wall heat flux in the manner shown in Fig. 2-22 when the propane liquid is saturated. At very low heat fluxes, such as might be obtained with an insulated tank, heat transfer to the liquid will occur by natural convection and the difference between the wall and liquid temperatures will be of the order of a few degrees. Nucleate boiling at the wall/liquid interface will start at higher heat fluxes and further increases in wall temperature will only be obtained with very large increases in heat flux because heat transfer coefficients in the nucleate boiling regime are very high. According to experimental boiling data obtained by Cichelli and Bonilla (17) for propane, tabulated (in part) in Table 2-4 and shown in Fig. 2-23, the wall heat flux for propane boiling at, say, 1.69MPa (245psia), increases from 53,600W/m^2 ($17000\frac{BTU}{hrft^2}$) at $\theta_s = 8.2^\circ C$ ($14.7^\circ F$) to approximately 208,000W/m^2 ($66{,}000\frac{BTU}{hrft^2}$) at $\theta_s = 12.9^\circ C$ ($23.3^\circ F$). Thus the wall heat flux increases by approximately 154,500W/m^2 ($49{,}000\frac{BTU}{hrft^2}$) (ie. by a very large amount, both in absolute and relative terms) with a change in wall temperature of only

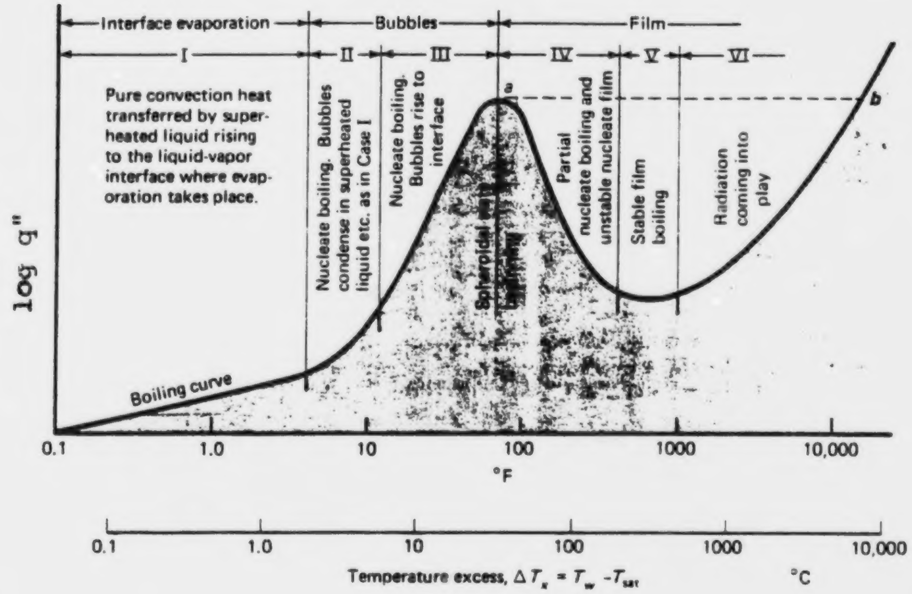

Fig. 2-22: Typical boiling curve showing wall heat flux (q") as a function of excess temperature.

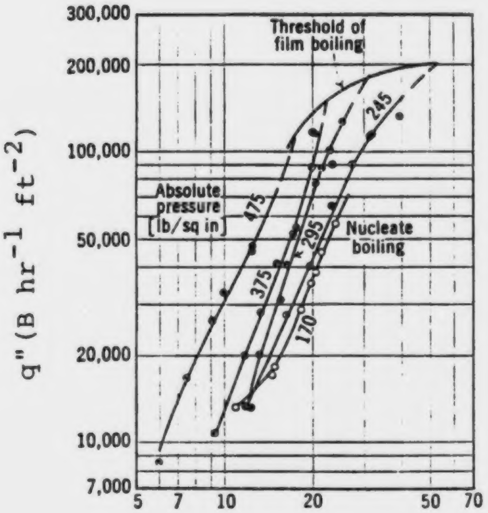

Fig. 2-23: Boiling of Propane (99% pure) from a Clean Horizontal Surface - from Cichelli and Bonilla (1945).

Experimental Data from Reference 17		
Pressure - psia	θ_s, Temperature Difference, Wall and Liquid Bulk - °F	$\dot{q}$, Heat Transfer Rate - Btu/ft^2-hr
168	18.4	28,850
170	14.9	19,380
168	11.0	13,180
245	23.3	65,600
240	19.5	40,300
248	16.1	27,600
245	14.7	17,060
295	15.6	31,200
295	13.3	20,100
378	15.2	41,200
375	19.9	88,300
375	17.7	54,750
375	13.3	28,100

TABLE 2-4: Boiling heat transfer data for propane

4.7°C (8.5°F). It can be seen from Fig. 2-23 that θ_s would not exceed approximately 28°C (50°F) even for a wall heat flux of 630,000W/m^2 (200,000$\frac{BTU}{hrft^2}$). Since wall heat fluxes measured in tank car fire tests have typically been in the 22,000W/m^2 (7000$\frac{BTU}{hrft^2}$) - 142,000W/m^2 (45,000$\frac{BTU}{hrft^2}$) range, (for uninsulated tanks), it is quite apparent that the inner surface of the tank will not exceed the saturation temperature of the propane lading at the prevailing tank pressure by more than 10-12°C. This observation may be invalid at one location on the tank inner surface, however, that being the point at which the tank shell intersects the liquid surface since the heat flux will peak at that point just below the liquid surface, as shown in Fig. 2-24. It is conceivable that the heat flux at that point, which peaks because of circumferential conduction from the hot, vapor-covered section of the tank wall to the cooler, liquid-wetted section, could exceed the heat flux at point a in Fig. 2-22, known as the critical heat flux (CHF). The curve labelled "Threshold of film boiling" in Fig. 2-23 defines the critical heat flux for propane* as a function of pressure. The critical

---

* While the relationship between q"and θ_s in the nucleate boiling regime is not a strong function of the geometry and inclination of the heated surface, these parameters can have quite a pronounced effect on the critical heat flux, as noted by Rohsenhow (18). The CHF for vertical surfaces is generally less than the CHF for horizontal surfaces (18), to which the results shown in Fig. 2-23 apply, so CHF data for propane boiling on inclined surfaces may eventually be needed in the tank car model. Performing experiments to obtain this data should not be contemplated until it has been demonstrated that heat fluxes greater than approximately 315,000W/m^2 (100,000$\frac{BTU}{hrft^2}$) can be obtained on the tank inner surface under certain circumstances, however.

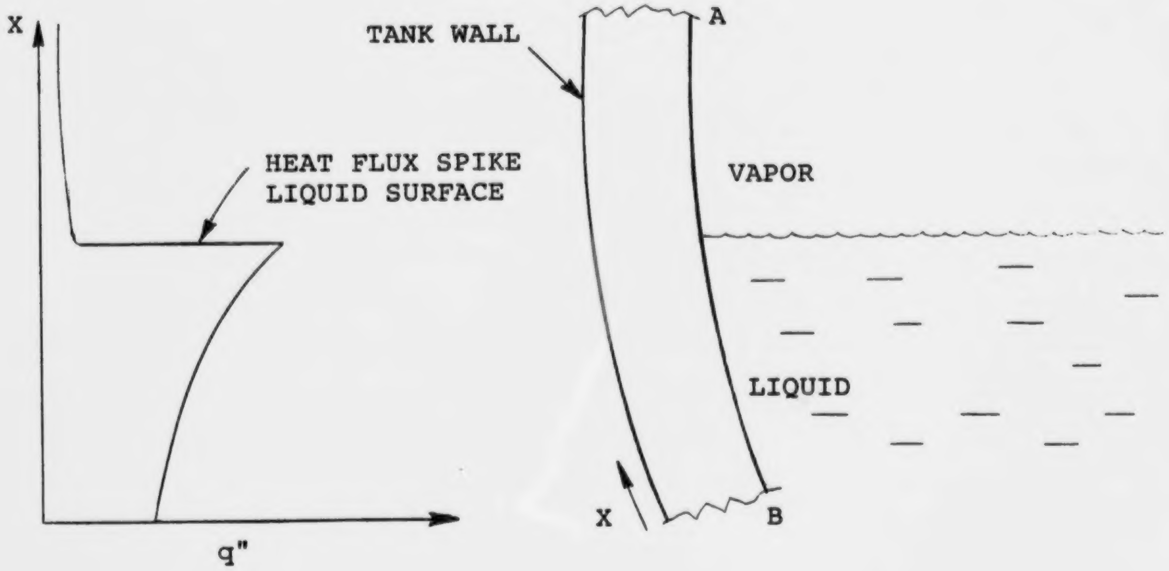
X
HEAT FLUX SPIKE
LIQUID SURFACE
q"
TANK WALL
A
VAPOR
LIQUID
X
B

q" - Heat flux on tank inner surface

Fig. 2-24: Heat flux spike at the liquid/wall intersection

heat flux appears to vary from about 410,000W/m^2 $(130{,}000\frac{BTU}{hrft^2})$ at a pressure of 2.58MPa (375psia) to approximately 630,000W/m^2 $(200{,}000\frac{BTU}{hrft^2})$ at a pressure of 1.69MPa (245psia). These values are quite high so it is not considered likely that localized dryout* of the tank wall at the liquid/tank wall intersection will occur. This possibility will nevertheless, have to be investigated because CHF would presumably be exceeded at the liquid/tank wall intersection if the thermal conductivity of the tank wall material was sufficiently high. A very fine finite-difference mesh will have to be superimposed on the tank wall at the liquid/wall intersection in order to model the heat flux "spike" at that location accurately so initial analyses will be performed using such a mesh to obtain an estimate of the size of the "spike". If those analyses indicate that dryout is very unlikely, the fine mesh at the liquid/wall interface will not be used in subsequent analyses performed with the same tank wall material and under similar conditions.

As noted previously, the temperature of the inner surface of the tank wall will be very close to the temperature of the liquid propane unless CHF is exceeded. Since the difference between the temperature of the liquid-wetted part of the tank wall and the adjacent flame will ordinarily be hundreds of degrees, likely variations in the temperature of the liquid-wetted part of the tank wall will have almost no effect on the flame-to-tank heat transfer rate. Incorporating several correlations into the tank car model to determine the liquid/wall heat transfer coefficient in the natural convection heat transfer regime (which will prevail at low wall heat fluxes) and the nucleate boiling regime for both saturated and subcooled conditions is therefore not considered worthwhile and a single expression applicable to saturated nucleate boiling will be used in all cases. Such an expression is given by Graves (4) as,

---

* The liquid cannot wet the wall when CHF is exceeeded so the condition is termed dryout.

$$h_b = \frac{q''}{\theta_s} = (15.0 + 0.0642\text{x}10^{-6} p^{3.347})\theta_s^{1.55}, \qquad 2.69$$

for θ_s in ^{o}F, p in psia and q" in BTU/hrft^2.

Note that,

$$q'' = h_b\theta_s = (15.0 + 0.0642\text{x}10^{-6} p^{3.347})\theta_s^{2.55} \qquad 2.70$$

In metric units, Eqs. 2-69 and 2-70 should be replaced by the expressions,

$$h_b = (211.8 + 15.543p^{3.347})\theta_s^{1.55}, \qquad 2.71$$

and $$q'' = (211.8 + 15.543p^{3.347})\theta_s^{2.55}, \qquad 2.72$$

for h_b in $\frac{W}{m^{2\,o}C}$, q" in W/m^2, p in MPa and θ in ^{o}C (or K).

With the boiling heat flux (q") defined by Eq. 2-72, the finite-difference (heat-balance) equation for a node on the inner surface of the tank wall in the liquid-wetted region can be written as,

$$K(i,j,k)_{i+1}T^{t+1}(i+1,j,k)+K(i,j,k)_{j+1}T^{t+1}(i,j+1,k)$$

$$+K(i,j,k)_{j-1}T^{t+1}(i,j-1,k)+K(i,j,k)_{k+1}T^{t+1}(i,j,k+1)$$

$$+K(i,j,k)_{k-1}T^{t+1}(i,j,k-1)-\left[\Sigma K+\frac{\rho cV(i,j,k)}{\Delta t}\right]T^{t+1}(i,j,k)$$

$$-(211.8+15.543p^{3.347})(T^{t+1}(i,j,k)-T_{ps})^{2.55}A_s(i,j,k)$$

$$+\frac{\rho cV(i,j,k)}{\Delta t}T^{t}(i,j,k)=E(i,j,k)=0 \qquad 2\text{-}73$$

where T_{ps} is the saturation temperature of propane at the prevailing tank pressure. If node i,j,k is the mth node in the grid then, by analogy with the analysis given in Sect. 2.1.3 for an outer surface node exchanging heat by radiation and convection with an adjacent flame, we can write,

$$J_{mm}\Big|_{T^n}=-\Big[\Sigma K+\frac{\rho cV}{\Delta t}(i,j,k)$$

$$+2.55A_s(i,j,k)(211.8+15.543p^{3.34})(T^n(i,j,k)-T_{ps})^{1.55}\Big]$$

$$2\text{-}74$$

and $$Q''_m\Big|_{T^n}=-\Big[\frac{\rho cV}{\Delta t}(i,j,k)T^t(i,j,k)-A_s(i,j,k)(211.8+15.543p^{3.347})$$

$$\times(T^n(i,j,k)-T_{ps})^{2.55}+2.55(T^n(i,j,k)-T_{ps})^{1.55}T^n(i,j,k))\Big],$$

$$2\text{-}75$$

for the tank inner surface node in the liquid-wetted region.

The equation in the Newton-Raphson recursive relationship (ie.

Eq. 2-28) applying to the tank inner surface node (ie. the mth equation), can now be written as,

$$
\begin{aligned}
&K(i,j,k)_{i+1}T^{n+1}(i+1,j,k) + K(i,j,k)_{j+1}T^{n+1}(i,j+1,k) \\
&+K(i,j,k)_{j-1}T^{n+1}(i,j-1,k) + K(i,j,k)_{k+1}T^{n+1}(i,j,k+1) \\
&+K(i,j,k)_{k-1}T^{n+1}(i,j,k-1) + J_{mm}\big|_{T^n}T^{n+1}(i,j,k) = Q_m''\big|_{T^n},
\end{aligned}
\qquad 2\text{-}76
$$

where $J_{mm}\big|_{T^n}$ and $Q_m''\big|_{T^n}$ are defined by Eqs 2-74 and 2-75 respectively.

Note that the propane temperature (T_{ps}) and pressure (p) in Eqs. 2-74 and 2-75 will probably not be constant and therefore should, strictly speaking, both be written with the superscript t+1 to indicate that their values at time $t+\Delta t$ are needed to evaluate $\dot{T}$. If simple equations relating T_{ps}^{t+1} and p^{t+1} to the temperatures at time $t+\Delta t$ of all of the nodes in the finite-difference model of the tank car could be obtained, it would be possible to include those two variables in the vector of nodal temperatures (ie. unknowns) and solve for their values and those of the nodal temperatures simultaneously at each time step. The thermodynamic models will be too complicated to do this in general, however, so the heat flow into the tank at time t and the state of the lading at the same time will be used to obtain a first estimate of the state of the lading at time $t+\Delta t$ (ie. T_{ps}^{t+1} and p^{t+1}) for use in equations such as Eq. 2-76. Thus the state of the lading at time $t+\Delta t$ will be obtained explicitly from the state of the state of the lading at time t and subsequently used to calculate the nodal temperatures at time $t+\Delta t$ implicity. The heat flow into the tank at time t+Δt will be calculated from the nodal temperatures at that time, after they have been obtained, and compared to the heat flow at time t that was used to obtain a first estimate of T_{ps}^{t+1} and p^{t+1}. If those heat flows are found to be significantly different, the new heat flow will be used to recalculate T_{ps}^{t+1}, p^{t+1} and, subsequently, T^{t+1}. This procedure will be repeated until consistent values of T_{ps}^{t+1}, p^{t+1} and T^{t+1} are obtained. It is fully expected that iterations will not be needed in practice because the heat flow rate into the tank will not change significantly from one time step to the next unless time steps that are too large to model other effects properly (eg. the discharge of propane vapor through the relief value when the tank is venting) are used. This matter is discussed further in Sect. 3.1.

2.3.2.5 Unprotected Tank Car Thermal Analysis-Model Details

To develop a rigorous thermal model of even an unprotected tank car in a fire is a formidable task for several reasons. First, all of the surface elements on the inner surface of the tank in the ullage space see each other and hence exchange heat by radiation. A rigorous model of radiative heat exchange in the tank ullage would consider the directional dependence of radiative surface properties (ie. emissivity, absorptivity and reflectivity) and take into account the absorption and emission of radiation by the propane vapor in the ullage space. Such a model would be exceedingly complex and would, in addition, require detailed surface property data that are essentially unavailable .

To simplify the analysis of radiative heat exchange in the ullage, it will be assumed that

a) the propane vapor is optically transparent (ie. non-absorbing and non-emitting).

b) the tank inner surface emits, absorbs and reflects radiation diffusely.

c) the tank inner surface can be considered "gray", ie. it is assumed that the emissivity (ε) and absorptivity (α) of the surface are equal and independent of the wavelength of the emitted or absorbed radiation.

Assumptions b) and c) together constitute the "gray-diffuse" surface assumption made in most radiative heat transfer analyses. This assumption usually provides results which are sufficiently accurate for most purposes. The implications of assumption a) have already been discussed.

Since each surface element on the tank inner surface in the ullage exchanges heat with all of the other vapor-covered surface elements, the heat balance equation for each node in the discretized model of the tank car shell in the ullage will contain heat flow contributions from all of the other nodes of that type. If a 112A (or 114A) series tank car that is half full of liquid propane is discretized using 5° circumferential subdivisions, as assumed in Sect. 2.1.3, the inner surface of the tank in the ullage will be represented by approximately $180^\circ/5^\circ = 36$nodes on each r-θ plane. If, as assumed in Sect. 2.1.3, 19 nodes are used in the axial (z) direction to model the 18.4m (60.4ft) length of the tank*, a total of $36 \times 19 = 684$ nodes, excluding those used on the tank end caps, will be used on the inner surface of the cylindrical shell in the ullage. If there are, say, 150 nodes on vapor-covered sections of the endcaps, a total of $684 + 150 = 834$ nodes will be used on the tank inner surface in the vapor space. The heat balance equation for each of these 834 nodes will contain heat flow contributions from the other 833 nodes, creating a completely unmanageable system of non-linear equations defining the nodal temperatures because $834^2 = 695{,}556$ memory spaces would be required just to store the finite-difference coefficients for the equations. To reduce the problem to one that is manageable, it will be assumed that the heat transferred from each tank inner surface element in the ullage to all of the other such elements is negligible compared to the heat transferred from each surface element to the liquid surface. This assumption is equivalent to assuming that variations in the temperature of the vapor-covered tank wall will be small compared to the difference between the vapor-covered tank wall and liquid temperatures, which should be true in most instances. Radiative heat fluxes in the ullage will be almost insignificant over most of the transient anyway, since it has already been shown (in Sect. 2.3.2.1) that the radiative heat flux from the inner surface of the tank wall to the liquid surface will be approximately 1/4 of the flame-to-tank heat flux at a wall temperature of 922K (1200^oF). It can be shown that the corresponding ratio at a tank wall temperature of 628K, which is the average of the liquid propane temperature of 334K used in the example given in Sect. 2.3.2.1 and the previously used wall temperature of 922K, will be only 1/26th (ie. less than 4%) of the flame-to-tank heat flux for the liquid level, etc. used in the example given in Sect. 2.3.2.1. Thus radiation from the tank wall in the ullage to the liquid surface will have almost no effect on the rate at which the tank wall temperature increases over most of the transient and hence is not worth modelling with high accuracy for that reason.

---

* More than 19 axial nodes would be required if in the axial conduction component was large for some reason.

When radiation between nodes on the inner surface of the tank wall in the ullage is neglected, the heat balance equation for each such node can be written as,

$$
\begin{aligned}
&K(i,j,k)_{i+1}T^{t+1}(i+1,j,k)+K(i,j,k)_{j+1}T^{t+1}(i,j+1,k)\\
&+K(i,j,k)_{j-1})T^{t+1}(i,j-1,k)+K(i,j,k)_{k+1}T^{t+1}(i,j,k+1)\\
&+K(i,j,k)_{k-1}T^{t+1}(i,j,k-1)-\left[\sum K+\frac{\rho cV}{\Delta t}(i,j,k)\right]T^{t+1}(i,j,k)\\
&-q''_{ri}A_s(i,j,k)+\frac{\rho cV}{\Delta t}(i,j,k)T^{t}(i,j,k)=E(i,j,k)=0\ ,
\end{aligned}
\qquad 2\text{-}77
$$

where q''_{ri} is given by Eq. 2-53 with the subscripts 1 and 2 identifying parameters associated with the surface areas of node i,j,k and the liquid respectively. The temperature T_1 in Eq. 2-53 is $T^{t+1}(i,j,k)$.

The view factor for the surface area of node i,j,k viewing the liquid surface, viz. F_{1-2}, must be obtained in order to evaluate q''_{ri}. The value of F_{1-2} for any node on the tank inner surface in the ullage could be obtained by integrating the well-known double cosine formula (3), written as,

$$
F_{1-2}=\frac{1}{A_1}\int\!\!\int_{A_1A_2}\frac{\cos\theta_1\cos\theta_2\,dA_1dA_2}{\pi r^2}\ , \qquad 2\text{-}78
$$

either numerically or, perhaps, exactly. The geometric parameters θ_1, θ_2 and r are shown in Fig. 2-25. Solutions to Eq. 2-78 are available in the literature for a large number of common geometries but the author has not seen a published

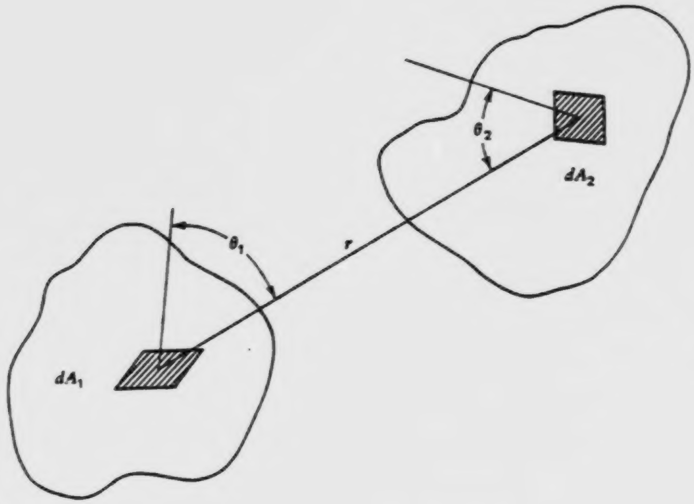
θ_2
dA_2
θ_1
r
dA_1

Fig. 2-25: Geometry for view factor calculation.

solution that would be applicable to the case of a surface element on the inner surface of a tank car's cylindrical shell viewing the liquid. Performing the integrations in Eq. 2-78 numerically for this case would be extremely tedious so an approximate expression for F_{1-2} will be used in the tank car model, as described below.

Consider the elemental surface A_1 and the infinitely long surface A_2 shown in Fig. 2-26. The surface normals for surfaces A_1 and A_2 are both perpendicular to the z axis which means that the generating lines for both surfaces are parallel to that axis and an "end view" of the surfaces would appear as shown in Fig. 2-27. The surface A_2 can be considered "infinitely" long when the ratio of its length to some characteristic distance between surfaces A_1 and A_2, say the distance r shown in Fig. 2-27, is extremely large. When this condition is satisfied, the view factor for surface 1 viewing surface 2, designated $F_{1-2\infty}$, is given by the expression,

$$F_{1-2\infty} = \frac{(d_1 + d_2) - (d_3 + d_4)}{2\ell_1} \qquad 2\text{-}79$$

when the geometric parameters d_1, d_2, d_3, d_4 and ℓ_1 are identified in Fig. 2-28. This method of determining shape factors is known as "Hottel's crossed string" method (13) because Eq. 2-79 can be written as,

$$F_{1-2\infty} = \frac{(\text{sum of crossed strings}) - (\text{sum of uncrossed strings})}{2\,(\text{width of } A_1)},$$

when the dashed lines in Fig. 2-28 are considered to be taut strings. Looking endwise at a tank car with the positions of the ends of the surfaces A_1 (the tank inner surface element) and A_2 (the liquid surface) defined by the angles θ_{1i}, θ_{1f}, θ_{2i}

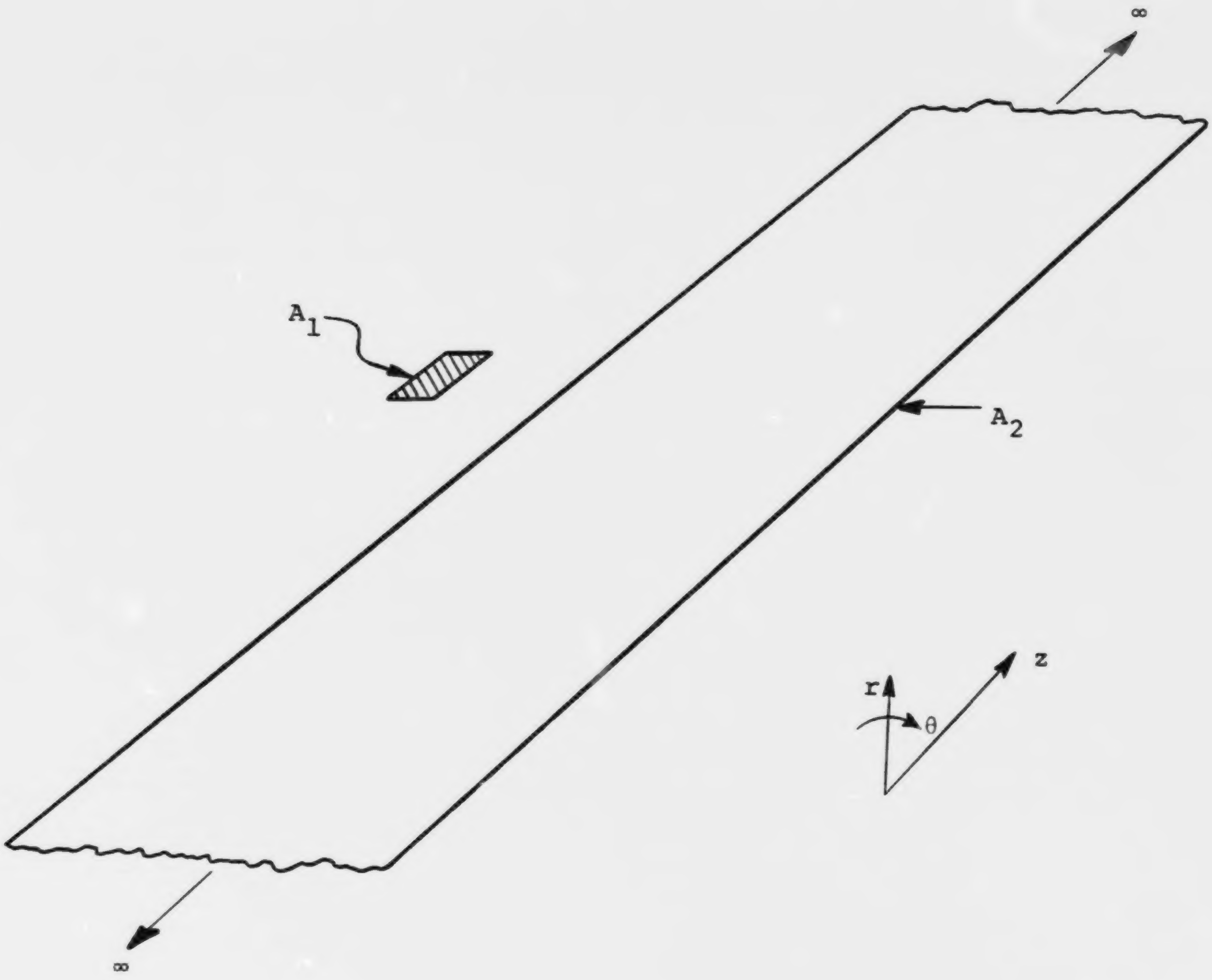

Fig. 2-26: Elemental surface area A_1 viewing an infinitely long strip A_2

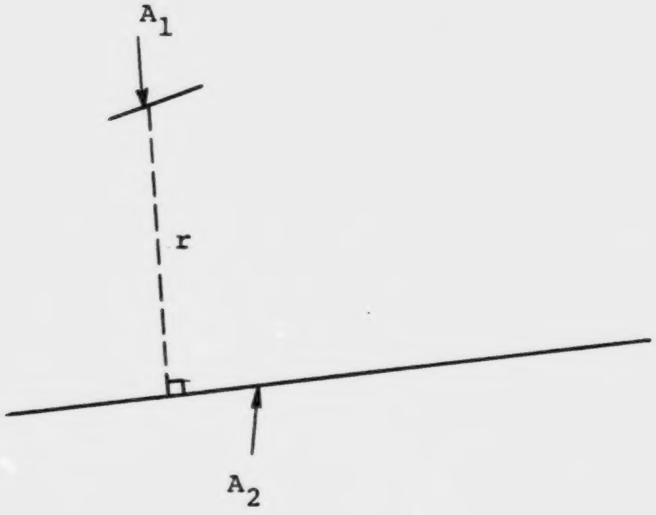

Fig. 2-27: End view of surfaces 1 and 2 shown in Fig. 2-26.

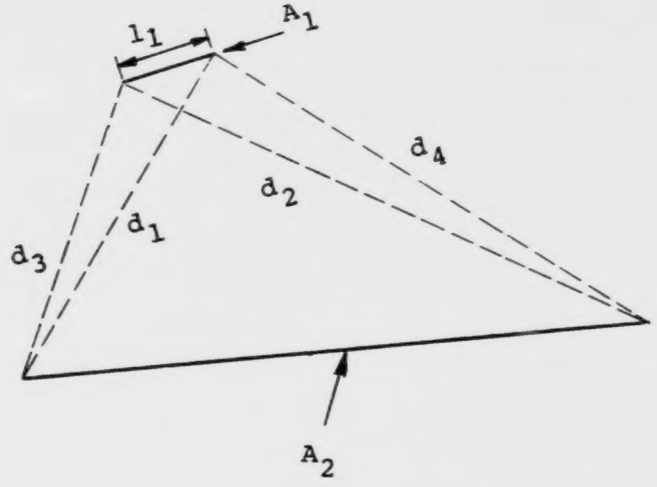
l_1
A_1
d_4
d_2
d_1
d_3
A_2

Fig. 2-28: Geometric parameters needed to obtain the view factor for surface 1 viewing surface 2.

θ_{2f} shown in Fig. 2-29, it is easily verified by applying Hottel's crossed-string method that,

$$F_{1-2\infty} = \frac{1}{\sqrt{2}(\theta_{1f}-\theta_{1i})} \Big[\sqrt{1-\cos(\theta_{2f}-\theta_{1f})} + \sqrt{1-\cos(\theta_{2i}-\theta_{1i})} - \sqrt{1-\cos(\theta_{2f}-\theta_{1i})} - \sqrt{1-\cos(\theta_{2i}-\theta_{1f})} \qquad \text{2-81}$$

Equation 2-81 is actually only approximate because the parameter ℓ_1 in Eq. 2-79 was taken to be the length of the arc between points 1i and 1f instead of the length of the chord between those two points, which is really the correct interpretation of ℓ_1. There is very little difference between the length of the arc and the length of the chord between points 1i and 1f when $(\theta_{if}-\theta_{1i})$ is small, as it will be for a typical surface element, however.

Since the length of a DOT 112A tank car is 18.4m while its diameter is only 3m, one would expect $F_{1-2\infty}$, defined by Eq. 2-81, to be a good approximation to F_{1-2} for an elemental area (A_1) on the tank inner surface at the tank center, as seen in Fig. 2-30. If the tank is, say, half-full of liquid, the ratio of the length of A_2 (the liquid surface) to the characteristic distance between A_1 and A_2, assumed to be R_{it} (= 1.5m), will be approximately 12. It is expected that this ratio, while not infinite, will nevertheless be large enough to make $F_{1-2\infty}$ a good approximation to F_{1-2}, as mentioned previously. Similarly the value of F_{1-2} for a surface element A_1 at one end of the cylindrical shell, shown in Fig. 2-30, will probably be closely approximated by $\frac{F_{1-2\infty}}{2}$ since this is the view factor for an elemental sur-

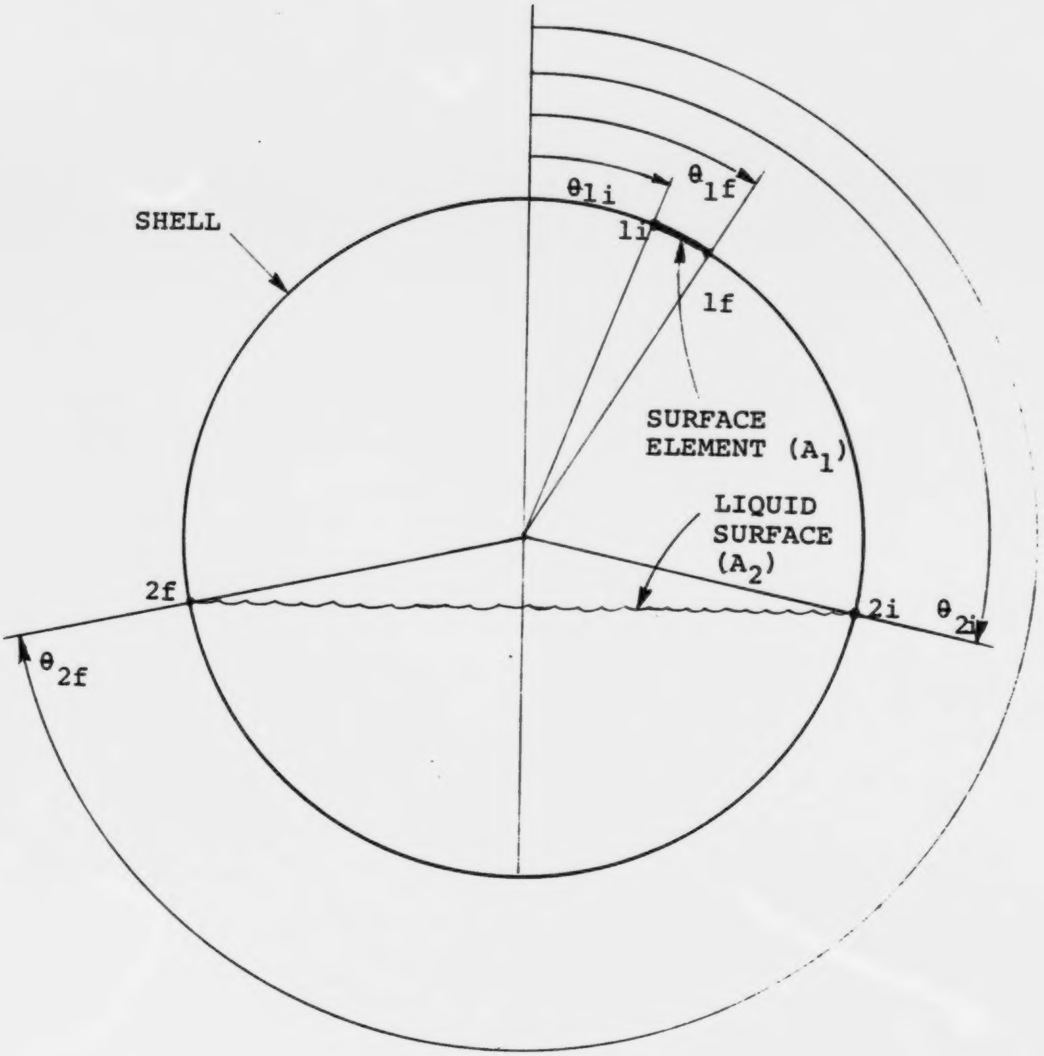
θ_{1i}
θ_{1f}
SHELL
1i
1f
SURFACE ELEMENT (A_1)
LIQUID SURFACE (A_2)
2f
2i
θ_{2i}
θ_{2f}

Fig. 2-29: Geometry for tank car view factor calculations.

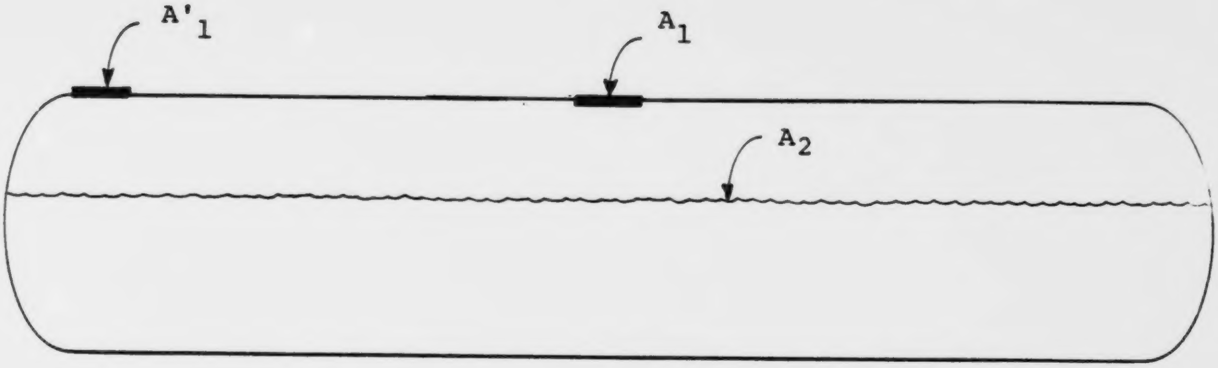

Fig. 2-30: Elemental surface areas A_1 and A'_1 at the center and end of a tank car respectively

face area viewing one-half (of the length) of an infinitely long strip A_2*. Approximate expressions that can be used to determine view factors (F_{1-2}) for nodes at the center and ends of the cylindrical shell have now been determined, but similar expressions applying to elemental areas (A_1) between those points must be obtained in some manner. It will be assumed for the purposes of this analysis that the value of F_{1-2} for any node on the inner surface of the cylindrical shell is defined by the expression;

$$F_{1-2} = \omega F_{1-2\infty} , \qquad 2\text{-}82$$

where $\omega = \frac{1}{2}(\sin\beta + \sin\emptyset)$, β is the angle between a ray normal to A_1 and a ray lying in a plane normal to the liquid surface and joining the center of A_1 to the left end cap/liquid intersection point, and $\emptyset$ is similarly defined for a ray going to the right end cap/liquid intersection point. The angles β and $\emptyset$ are shown in Fig. 2-31a. The factor $\omega = \frac{1}{2}(\sin\beta + \sin\emptyset)$ is actually the view factor for an elemental surface area dA_1 viewing an infinitely long strip A_2, as shown in Fig. 2-31b, when the surface normals for A_1 and A_2 are both perpendicular to the z-axis. The view factor ω is simply the limiting value of $F_{1-2\infty}$, defined by Eq. 2-79, as $\ell_1 \to 0$. The view factor ω should really only be used when the width of the liquid surface in the tank (ie. the length of A_2 in this case) is very large compared to the distance r shown in Fig. 2-27, a condition that will be satisfied less and less satisfactorily for the surface elements at the top of the tank as the liquid level drops. When the tank is half-full of liquid, for instance, the ratio of the length of A_2 to r for a node at $\theta = 0^\circ$ will be only 2 and its value will be even lower for lower liquid levels. The factor ω nevertheless has the desired characteristics in that $\omega \to \frac{1}{2}$ when one of the angles β and $\emptyset$ is 90°, and the other is 0°.

---

* From the strip center.

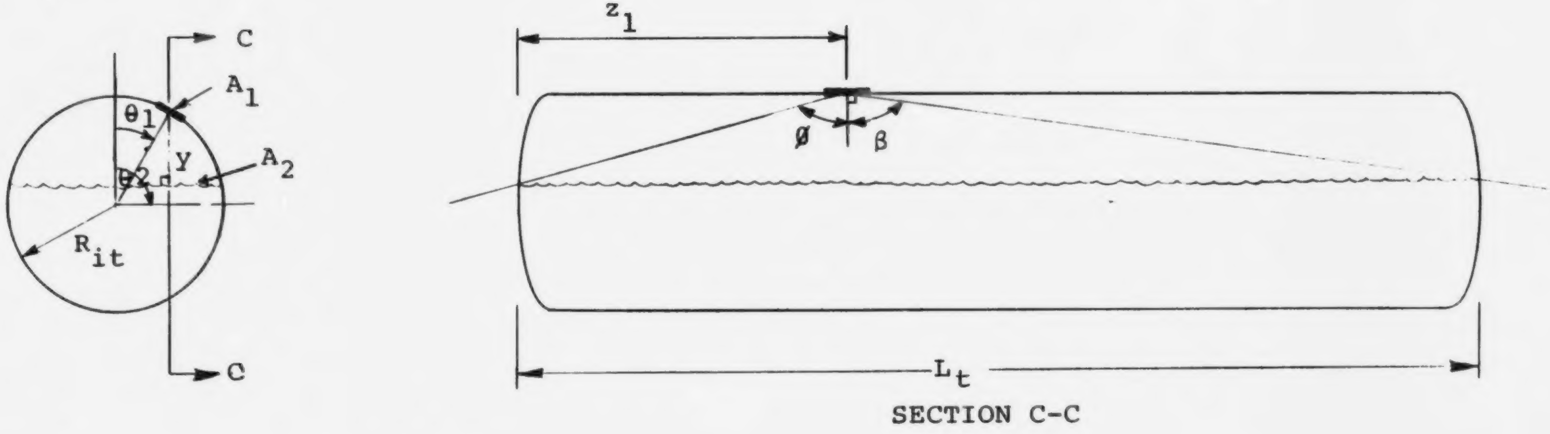
C
C
A_1
A_2
θ_1
θ_2
y
R_{it}
z_1
ϕ
β
L_t
SECTION C-C

Fig. 2-31a: Geometry for determing $\omega(\frac{1}{2} < \omega < 1)$, where $\omega = \frac{1}{2}(\sin\beta + \sin\phi)$

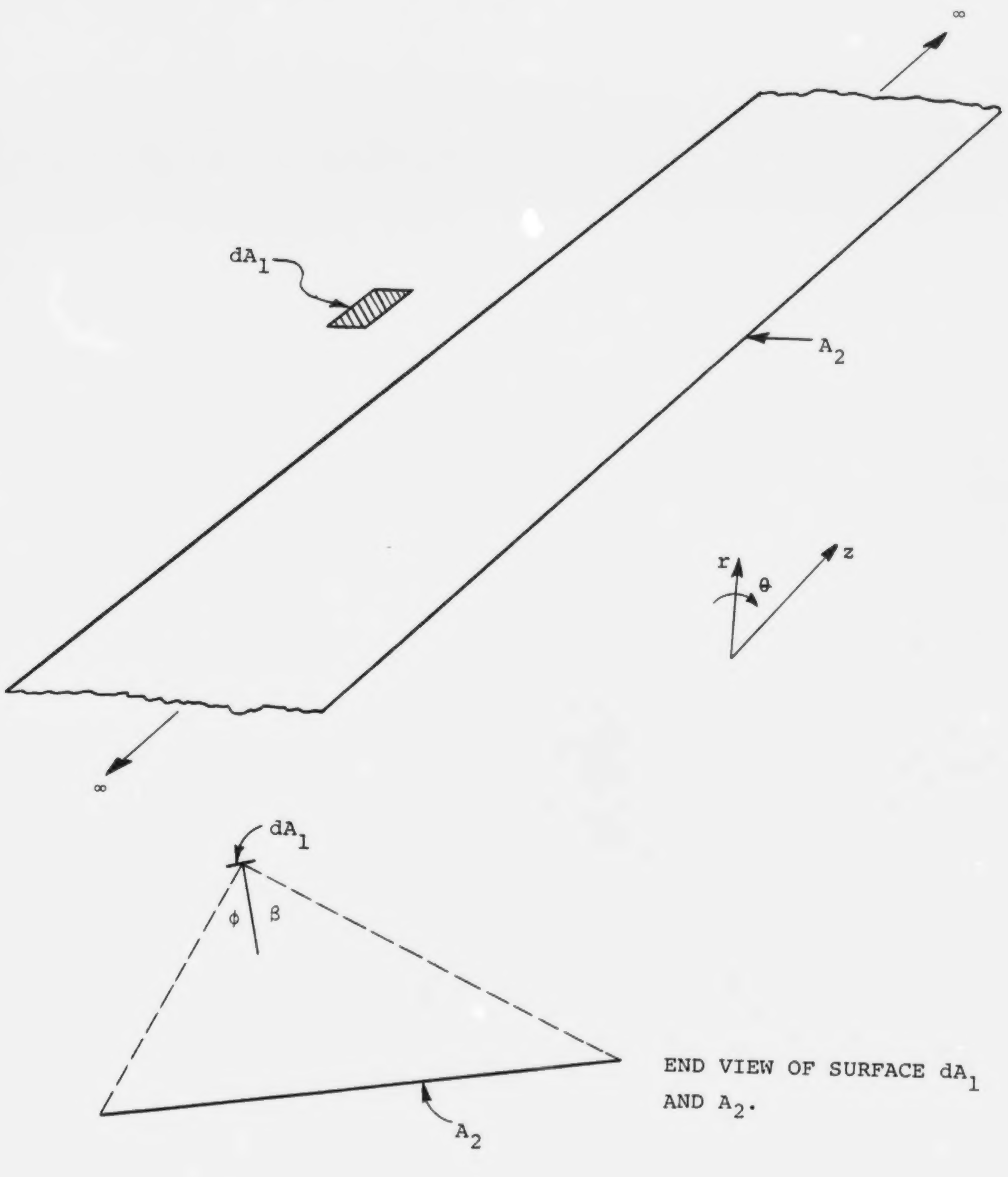
∞
dA_1
A_2
r
θ
z
∞
dA_1
φ
β
END VIEW OF SURFACE dA_1 AND A_2.
A_2

Fig. 2-31b: Elemental surface area dA_1 viewing an infinitely long strip A_2.

Thus the view factor (F_{1-2}) for an area (A_1) located at one end of an infinitely long tank and viewing the liquid surface in the tank would be $F_{1-2\infty}/2$ according to Eq. 2-82, as it actually is. Also, $\omega \to 1$ when $\beta \to 90^\circ$ and $\phi \to 90^\circ$ (ie. when the tank length approaches ∞ and A_1 is not located at one end of the tank), a result which is also correct.

The angles β and ϕ are defined by the expressions,

$$\beta = \tan^{-1}\left(\frac{L_t - z_1}{y}\right) , \qquad 2\text{-}83$$

and,

$$\phi = \tan^{-1}\left(\frac{z_1}{y}\right) , \qquad 2\text{-}84$$

where,

$$y = R_{it}(\cos\theta_1 - \cos\theta_2) , \qquad 2\text{-}85$$

and the geometric parameters z_1, R_{it}, L_t, θ_1 and θ_2 are identified in Fig. 2-31.

It can be shown that $F_{1-2} = 0.986$ according to Eq. 2-82 when the surface element (A_1) is located at the top center (ie. $\theta_1 = 0^\circ$, $z_1 = \frac{L_t}{2}$) of a DOT 112A tank car that is half-full of liquid. Also, $F_{1-2} = 0.498F_{1-2\infty}$ according to Eq. 2-82 when A_1 is located at one end of the same tank car (ie. for $\theta_1 = 0^\circ$, $z_1 = 0$ or L_t). These values seem reasonable when compared to the limiting values given previously for these two cases.

While the expression defining $F_{1-2\infty}$ was derived subject to the condition that surface normals to A_1 and A_2 both be perpendicular to the z-axis, a condition that will not be satisfied in the case of a tilted tank car*, it is nevertheless assumed that the factor ω in Eq. 2-82 accounts for the effect of tilt and hence that Eq. 2-82 can be used to obtain values of F_{1-2} in a tilted tank car. Radiation in the tank ullage will not be very significant, as discussed previously, so this approach should provide results of acceptable accuracy. The value of $F_{1-2\infty}$ will be evaluated using the values of θ_{1i}, θ_{1f}, θ_{2i} and θ_{2f} at the axial coordinate of A_1 in the tank-car centered coordinate system (z_1) and $\emptyset$ and β for the tilted tank case will be defined by the expressions,

$$\beta \simeq 90^{\circ} \qquad \text{for } ZRR < L_t,\ -\text{ve}\,\alpha, \qquad \text{2-86a}$$

$$\beta = \tan^{-1}\left[\frac{ZRR - z_1}{R_{it}(1 + \cos\theta_1)}\right] \qquad \text{for } ZRR < L_t,\ +\ \text{ve}\,\alpha, \qquad \text{2-86b}$$

$$\beta = \tan^{-1}\left[\frac{L_t - z_1}{R_{it}\cos\theta_1 + Z_1\sin\alpha - \frac{X^*}{\cos\alpha}}\right] \qquad \text{for } ZRR = L_t, \qquad \text{2-86c}$$

$$\emptyset = \tan^{-1}\left[\frac{z_1}{R_{it}\cos\theta_1 + Z_1\sin\alpha - \frac{X^*}{\cos\alpha}}\right] \qquad \text{for } ZRL = 0, \text{2-87a}$$

$$\emptyset \simeq 90^{\circ} \qquad \text{for } ZRL > 0,\ +\ \text{ve}\,\alpha, \qquad \text{2-87b}$$

$$\emptyset = \tan^{-1}\left[\frac{z_1 - ZRL}{R_{it}(1 + \cos\theta_1)}\right] \qquad \text{for } ZRL > 0,\ -\ \text{ve}\,\alpha, \qquad \text{2-87c}$$

where the z coordinates of the left and right liquid/shell intersection points, designted ZRL and ZRR respectively, are calculated in the routine LIQLEV described in APPENDIX B. The angles $\emptyset$ and β and the points ZRL and ZRR are shown in Fig. 2-32.

---

*Another condition that will not be satisfied in the case of a tilted tank car is the condition that A_2 (the liquid surface) have parallel sides.

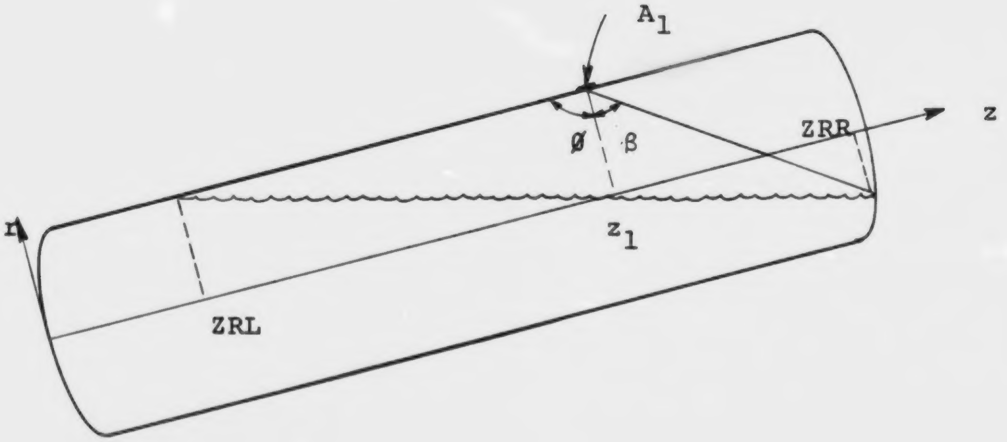
A$_1$
z
ZRR
Ø
β
r
z$_1$
ZRL

Fig. 2-32: Geometrical parameters for view factor calculations in a tilted tank car.

View factors for surface elements on the tank end caps viewing the liquid surface remain to be determined. The tank heads will be modelled as flat caps (ends) on a cylindrical shell in the tank car model and, if it is assumed that the surface areas ($A_s(i,j,k)$) of the nodes (i,j,k) on the end caps will be small and hence can be regarded as differential areas (dA_1), the view factor (F_{1-2}) for each $A_s(i,j,k)$ (ie. dA_1) viewing the liquid surface (A_2) can be obtained from an equation derived by Hamilton and Morgan (19) for the geometry shown in Fig. 2-33. According to Hamilton and Morgan, the view factor for the differential surface element dA_1 viewing the surface A_2 is,

$$F_{dA_1-A_2}$$

$$= \frac{1}{2\pi}\left\{\tan^{-1}M + \left(\frac{H\cos\phi-1}{\sqrt{1+H^2-2H\cos\phi}}\right)\tan^{-1}\left(\frac{M}{\sqrt{1+H^2-2H\cos\phi}}\right)\right.$$

$$\left. + \left(\frac{M\cos\phi}{\sqrt{M^2+\sin^2\phi}}\right)\tan^{-1}\left(\frac{H-\cos\phi}{\sqrt{M^2+\sin^2\phi}}\right) + \tan^{-1}\left(\frac{\cos\phi}{\sqrt{M^2+\sin^2\phi}}\right)\right\} \qquad \text{2-88}$$

where $H=\frac{a}{c}$ and $M=\frac{b}{c}$ for the dimension a,b and c shown in Fig. 2-33. Equation 2-88 can only be used to predict $F_{dA_1-A_2}$ when dA_1 is located at a corner of the rectangle bounded by the dashed lines in Fig. 2-33, but it can easily be used to predict the view factor for an elemental area dA_1 on an end cap viewing the liquid surface (A_2) by writing that view factor as,

$$F_{dA_1-A_2} = F_{dA_1-A'_2} \pm F_{dA_1-A''_2} \qquad \text{2-89}$$

when the areas A'_2 and A''_2 ($A'_2 + A''_2 \equiv A_2$) are obtained as

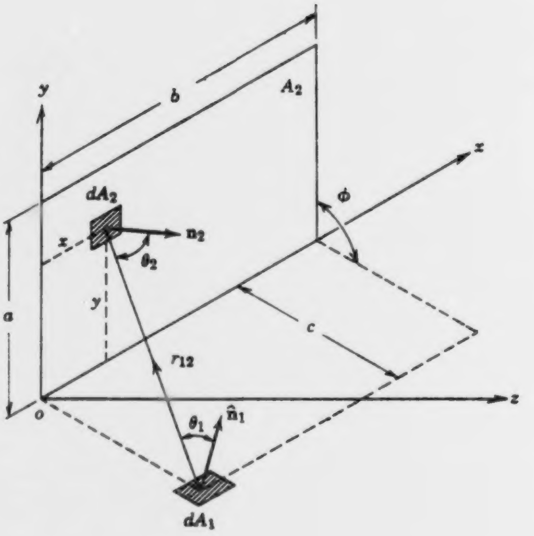
y
b
A_2
x
Φ
dA_2
x
n_2
θ_2
a
y
c
r_{12}
o
z
θ_1
$\hat{n}_1$
dA_1

Fig. 2-33: Infinitesimal surface element dA_1 viewing rectangular surface A_2.

shown in Fig. 2-34. The view factors $F_{dA_1-A'_2}$ and $F_{dA_1-A''_2}$ can both be predicted (separately) from Eq. 2-88 by using the substitutions $b = b'$ and $b = b''$ to evaluate $F_{dA_1-A'_2}$ and $F_{dA_1-A''_2}$ respectively. Note that Eqs. 2-88 and 2-89 can be used to predict end cap view factors for a tilted tank by setting $\emptyset = 90^\circ - \alpha$ ($\emptyset = 90^\circ$ for a level tank).

Modelling radiative heat transfer in the ullage of a tank car is obviously fairly involved, even when the analysis is simplified as just described. Analysing conduction in the tank wall will, by contrast, be very straightforward and the finite-difference techniques described in Sects. 2.1.1 - 2.1.3 will be used for that purpose. The implicit time integration procedure, to which finite-difference equations such as Eqs. 2-35 and 2-76 apply, will be used instead of the explicit method to avoid the stability problems encountered with the latter technique when the time step size (Δt) is too large. The Jacobian matrix for the system of finite-difference equations will be symmetric when the simplified radiation model already described is used. The user of the tank car analysis program will be allowed to either include the axial conductances in the finite-difference equations (ie. model axial conduction in the tank wall) or leave them out (ie. neglect axial conduction). An example which showed the implicit method to be impractical in 3-D analyses was discussed in Sect. 2.1.2, but it will be remembered that a tank car equipped with both external insulation and EXPLOSAFE was considered in the example and, as a result, it was assumed that a total of eighteen radial nodes would be required to model radial heat transfer in the tank. It was assumed that only three of those nodes would be used across the thickness of the tank wall, however, and considering the approximations made in most of the other aspects of

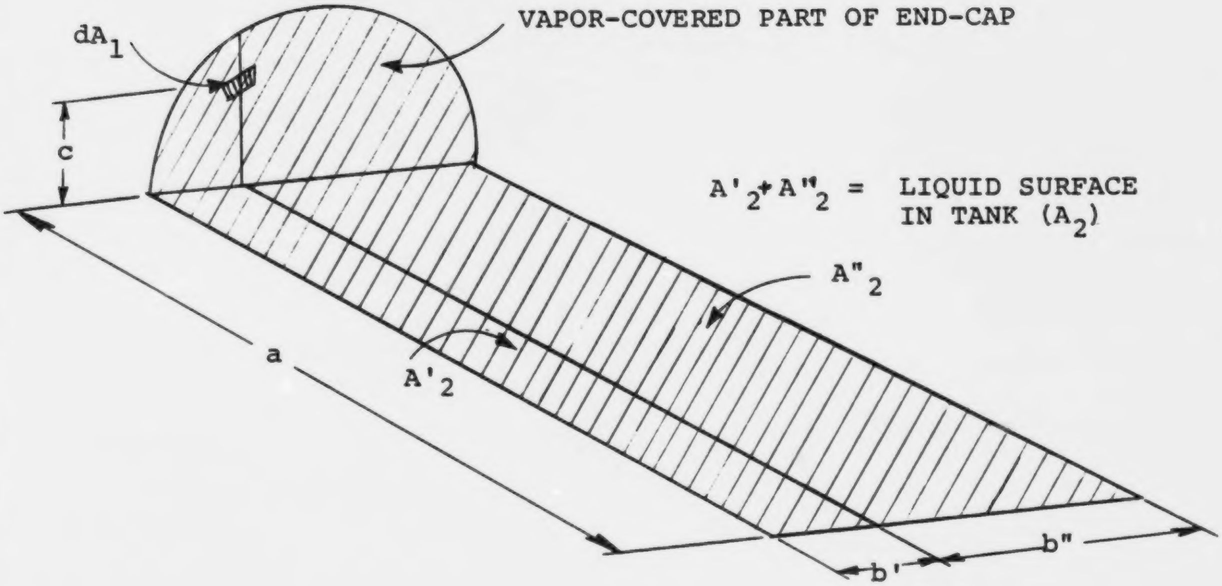
VAPOR-COVERED PART OF END-CAP
dA_1
c
$A'_2+A''_2$ = LIQUID SURFACE IN TANK (A_2)
A''_2
a
A'_2
b'
b"

Fig. 2-34: Geometrical parameters for end cap elemental surface area (dA_1)-to-liquid surface (A_2) view factor calculations.

the thermal analysis, even fewer nodes than this would probably suffice. The user of the tank car analysis program will be permitted to use any number of nodes across the thickness of the tank wall, but the number of nodes chosen will influence the feasibility of performing a full 3-D analysis. The feasibility of performing a full 3-D analysis will also depend on the size of the region modelled, in other words whether the entire tank car is modelled or only one-half or one-quarter of it. Options will be provided in the finite-difference model that will permit the user of the tank car analysis program to reduce the model size by taking advantage of planes of thermal symmetry when such planes exist. It will be possible to declare,

1) the vertical diametral plane A-A shown in Fig. 2-3, and/or
2) the r-θ plane at the tank's axial midpoint (ie. at $z=L_{t/2}$), as planes of thermal symmetry.

Options 1) and 2) will probably both be used in most analyses of level tanks, meaning that only one-quarter of the tank will be modelled in such cases.

The tank car analysis program will check the user-supplied values for the number of radial, circumferential and axial nodes to determine the order in which nodes in the finite-difference grid should be numbered, since that order affects the bandwidth of the Jacobian matrix and hence the time needed to factor the matrix into the desired LU form. It can be shown, in fact, that the number of arithmetic operations needed to factor a banded matrix, such as the Jacobian matrix for a system of finite-difference equations, is proportional to N^2M where N is the bandwidth (or half-bandwidth) of the matrix and M is the total number of equations. Since the operations count for the factorization process varies according to N^2 and N is, in turn, affected by the order in which nodes in the finite-difference grid are numbered, the ordering strategy must obviously be selected carefully. If N_i,N_j and N_k are the number of radial, circumferential, and axial nodes respectively, the nodes in the finite-difference grid representing the tank car should be ordered so that the nodal index ℓ, where $\ell = i$ or j or k, varies least rapidly when N_ℓ is the largest of N_i,N_j and N_k. If, for instance, N_j is greater than either N_i or N_k, the finite-difference equations for the nodes in the tank car would be assembled by three nested DO loops arranged in the order,

```
  L=O
DO 1 j = 1, $N_j$
  DO 2 i = 1,$N_i$
    DO 3 k = 1,$N_k$
      L = L + 1

3 CONTINUE
2 CONTINUE
1 CONTINUE
```

or

```
  L=O
DO 1 j = 1,$N_j$
  DO 2 k = 1,$N_k$
    DO 3 i = 1,$N_i$
      L = L + 1

3 CONTINUE
2 CONTINUE
1 CONTINUE
```

since in either case the circumferential subscript (j) will vary least frequently in any array written in an equivalent singly-subscripted form with the subscript L (eg. every entry T(L) in the vector of nodal temperatures T will correspond to an entry T(i,j,k) in the triply-subscripted representation of T). Note that the half-bandwidth of the Jacobian matrix for the example just given would be $(N_i N_k + 1)$ or simply the number of nodes on an r-z plane plus one. If three nodes are used across the thickness of the tank wall (ie. $N_i = 3$) and nineteen axial nodes (ie. $N_k = 19$) are used to represent one-half of the length of the tank car (ie, it is assumed that the r-θ plane at the tank's axial midpoint is a plane of thermal symmetry), the half-bandwidth of the resulting Jacobian matrix will be $3 \times 19 \times 1 = 58$. If, in addition, 72 azimuthal nodes are used to model the entire circumference of the tank car (ie. it is assumed in this example that the thermal problem is not symmetrical about the plane A-A shown in Fig. 2-3), the entire finite-difference model will contain $3 \times 19 \times 72 = 4104$ nodes and a total of approximately $58 \times 4104 = 238{,}000$ memory spaces will be needed to store one-half of the Jacobian matrix in banded form. Only one-half of the matrix needs to be stored because it is symmetric. The aforementioned memory requirement is less than one-half of the high speed memory capacity of the Carleton CP-6 computing system, on which the DE tank car model would be developed, thus demonstrating that it will be possible to model axial conduction in an unprotected tank car.

It was assumed in the preceding example that the entire circumference of the tank car will be modelled. The liquid-wetted section of the tank wall will be maintained at a temperature very close to that of the liquid (unless CHF is exceeded) however, for reasons discussed in Sect. 2.3.2.1, so the circumferential extent of the tank wall segment modelled could be reduced considerably by modelling only vapor-covered parts of the wall. The temperature of the tank wall at the intersection of the liquid surface and the tank wall would be set at the temperature of the liquid propane at each time step in that case. The only drawback associated with eliminating the liquid-wetted part of the tank shell from the thermal model as just described is that the boundary of the modelled region will change position as the liquid level changes. The strategy described by Crank (20) for modelling a boundary which is moving through a fixed finite-difference grid would probably be the best approach to use in the tank car model, but that strategy will not be described here because it is felt that its implementation in the tank car analysis program would not be worthwhile unless the program was to be applied primarily to unprotected tanks. Heat transfer in the segment of the tank shell below the level of the liquid surface will be modelled in thermal analyses of EXPLOSAFE-equipped tank cars, where the benefit of deleting the liquid-wetted segment of the tank wall from the thermal model will be reduced because most of the nodes in the finite-difference model will be needed to model heat transfer in the EXPLOSAFE/vapor matrix, so to prevent the thermal models of unprotected and protected tank cars from becoming too dissimilar, heat transfer in liquid-wetted sections of the tank wall will also be modelled in unprotected tank car analyses.

If the program user elects to perform the thermal analysis with axial conductances deleted from the finite-difference equations (ie. with axial conduction in the tank wall neglected), the heat transfer analyses in the N_k axial segments used to represent the tank car will be thermally decoupled and the analysis of heat transfer in the entire tank will become effectively N_k two-dimensional (r-θ) analyses. The bandwidth of the Jacobian matrix for each of these r-θ analyses will be only $N_i + 1$ (eg. $3 + 1 = 4$ if three nodes are used across the thickness of the tank wall), assuming that N_i will be less than either N_j or N_k, so it will be possible to perform the separate r-θ analyses very rapidly because, as noted previously, the operations count for the LU factorization of the Jacobian matrix is proportional to N^2, where $N = N_i + 1$ in this case. The user of the tank car analysis program will be permitted to perform the tank car heat transfer analysis with the N_k axial segments either thermally coupled or decoupled as just described, and an additional option will be provided that will permit the program user to perform the analysis at only one user-specified axial location in the tank and obtain the information needed in the thermodynamic and rupture analyses from the thermal solution at that location alone. This option will be provided because it is expected that the temperature distribution obtained in an r-θ heat transfer analysis performed at, say, the axial location midway between the relief value and one end of a level tank, will be representative of the temperature distributions prevailing at other axial locations. This result is expected because the heat transfer coefficient for convection between the tank wall and the propane vapor will be independent of axial position except in the immediate vicinity of the relief valve, as already noted, and radiative heat exchange between the tank wall and the liquid surface will be insignificant during most of the transient, so the axial variations in the tank wall-to-liquid view factors (F_{1-2}) will have only a small effect on wall temperatures.

A simple computer program that predicts tank wall temperatures in an unprotected tank car for a fixed (constant) liquid level is described in Appendix E, where sample analyses are performed comparing the modified and unmodified forms of the Newton-Raphson method and estimating the axial extent of the region affected by high convective heat transfer rates around a venting relief valve. Only one node is used across the thickness of the tank wall in the program and the tank wall is not modelled below the level of the liquid surface. The model assumes that thermal symmetry exists about the diametral plane A-A shown in Fig. 2-3 and the $r-\theta$ plane at the tank's axial midpoint. View factors for nodes on the end cap viewing the liquid surface are all set to a single, average, value instead of being calculated from Eqs. 2-88 and 2-89.

2.3.3 EXPLOSAFE - Equipped Tank Car Thermal Analysis

An obvious prerequisite to the thermal analysis of an EXPLOSAFE - equipped tank car is an analysis of the mechanisms by which heat is transferred in an EXPLOSAFE/vapor matrix. It will not be possible to correctly assess the effectiveness of the EXPLOSAFE thermal protection system unless the dominant heat transfer mechanisms in an EXPLOSAFE/vapor matrix are identified and characterized quantitatively. It should be recognized, however, that the process of identifying the important heat transfer mechanisms in an EXPLOSAFE matrix should be an evolutionary one, that is, the heat transfer mechanisms which it is felt will be the most significant should be the only ones modelled initially. If predicted and experimental temperature-time histories for EXPLOSAFE - equipped tank cars are in good agreement with only those mechanisms considered, it can be assumed that only secondary heat transfer mechanisms have been neglected. If the predicted and experimental results are not in good agreement initially and it is felt that the EXPLOSAFE heat transfer model is the cause of the poor agreement, that model will have to be improved, either by improving the modelling of mechanisms already considered or by including other mechanisms. Needless to say, the staged analysis just described cannot be performed properly at this time because a preliminary computer model of heat transfer in an EXPLOSAFE - equipped tank car is not available.

Of the three possible modes of heat transfer in an EXPLOSAFE/vapor matrix, namely conduction, convection (free and forced) and radiation, the first, conduction, is the easiest to analyse, followed by radiation and then convection. A rigorous analysis of either of the last two modes is actually very difficult to perform and it is felt that those analyses should probably not be attempted until it has been demonstrated, by comparing results of the 1/5 scale tests to analytical results obtained using a preliminary computer model in which only conduction in the EXPLOSAFE/vapor matrix is considered, that conduction alone could not have been responsible for the success of the EXPLOSAFE concept in those tests. Heat transfer by conduction in an EXPLOSAFE/vapor matrix can be analysed using the finite-difference techniques described in Sect. 2.1 once the thermal conductivity of the matrix in different directions has been determined, so expressions for predicting those thermal conductivities are derived in the next section. Comparisons of predicted thermal conductivities with values measured for different EXPLOSAFE configurations are given in Sect. 2.3.6. The significance of radiative heat transfer within the matrix is estimated in Sect. 2.3.7 and the role played by convection is discussed qualitatively in Sect. 2.3.8. A description of the complete model of heat transfer in an EXPLOSAFE - equipped tank car is given after the possible heat transfer mechanisms in an EXPLOSAFE/vapor matrix have been analysed.

2.3.4 EXPLOSAFE Thermal Conductivity Predictions

An EXPLOSAFE/vapor matrix is an orthotropic medium with a principal thermal conductivity in each of the three heat flow directions shown in Fig. 2-35. The heat flow direction is parallel to the layers of foil in Styles I and III and normal to the foil layers in Style II so the designations used here for the different matrix configurations are the same as those used by Appleyard in TP2740 (21). The thermal conductivities of the three EXPLOSAFE styles are considered separately in the next three sections.

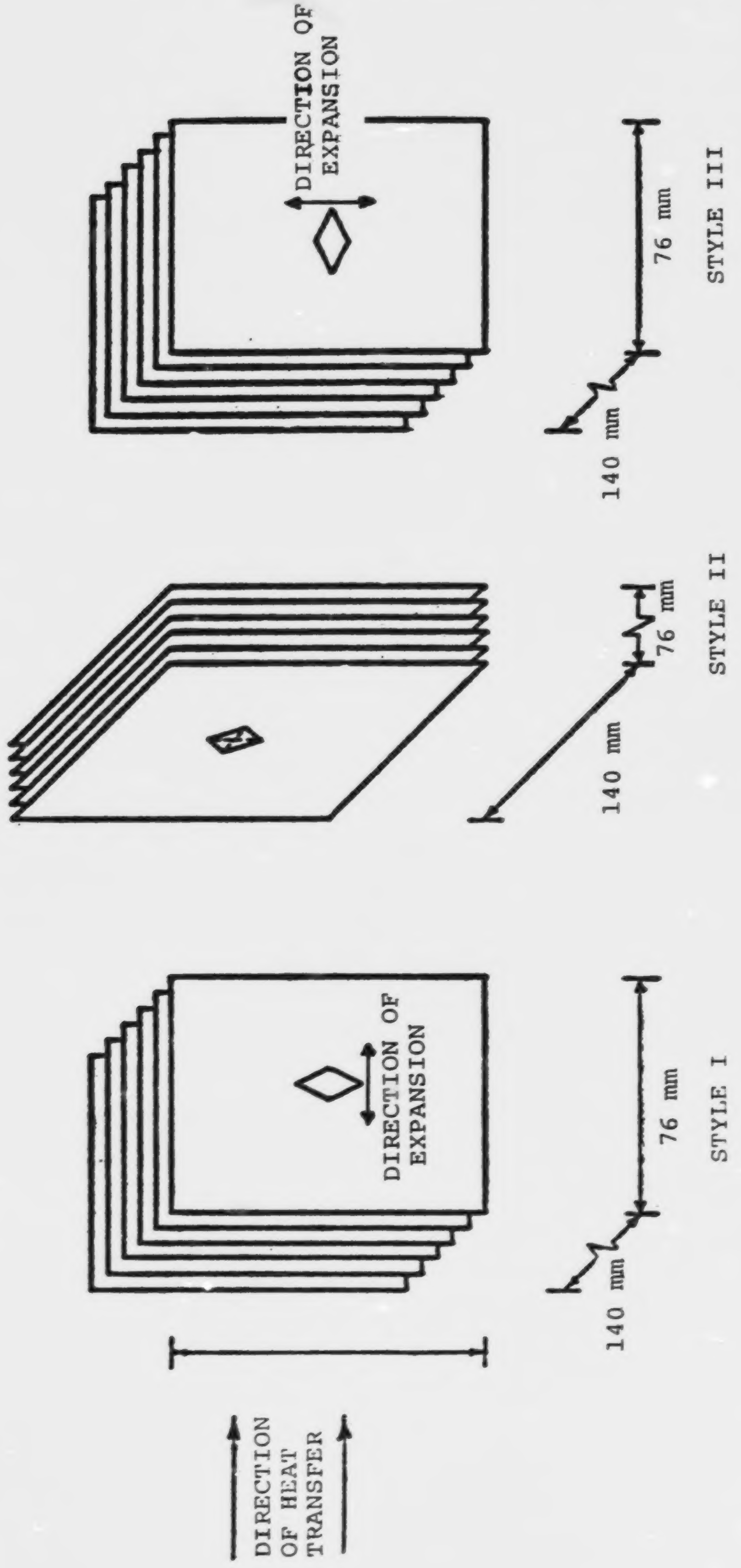
DIRECTION OF EXPANSION
76 mm
140 mm
STYLE III
76 mm
140 mm
STYLE II
DIRECTION OF EXPANSION
76 mm
140 mm
STYLE I
DIRECTION OF HEAT TRANSFER

Fig.: 2-35: Heat Transfer Rig Samples

2.3.4.1 Style I EXPLOSAFE

The thermal conductivity of Style I EXPLOSAFE can be predicted by considering the manner in which heat is conducted in a single plane of foil for the Style I heat flow direction. When a single plane of foil is expanded as shown in Fig. 2-36, the heat is forced to flow through series and parallel combinations of strips similar to the double cross-hatched strip AB. The resistance of that strip between the isothermal patches shown at temperatures T_o and T_1 in Fig. 2-36 is thus the basic resistance that can be used to predict the effective thermal conductivity of a Style I EXPLOSAFE matrix. The patches over which the temperatures T_o and T_1 are prescribed in Fig. 2-36 will be isothermal because of symmetry considerations and the remaining surfaces of the strip can be considered insulated (adiabatic).

An enlarged view of the strip AB is shown in Fig. 2-37. The strand width (w) shown in Fig. 2-37 is generally quoted by the manufacturer for a particular EXPLOSAFE sample and is typically 0.1375cm (0.055 inches). The dimensions $\bar{S}$ and L_1 are typically 0.15cm and 1.0cm respectively (values obtained by direct measurement) and the thickness (t) of the foil is generally in the 0.04 to 0.08mm range. Materials specifications for EXPLOSAFE foil are given in Table 2-5. The thermal conductivity (k_{al}) of the AA 3003-H24 aluminium alloy from which EXPLOSAFE foil is fabricated is not given in Table 2-5, nor could the author find its value in standard sources (eg. 22), but it is estimated that it must lie in the 170 W/m^{o}C - 190 W/m^{o}C range and a value of 180 W/m^{o}C will be assumed for the purposes of the analysis.

TABLE 2-5: EXPLOSAFE EXPLOSION SUPPRESSION SYSTEM

MATERIAL SPECIFICATIONS

RAW MATERIALS

Alloy	AA 3003	AA 3003
Temper	H24	H24
Thickness	.0015 to .003 in	0.04 to 0.08 mm
Tensile Strength	20,000 to 23,000 psi	137,900 to 158,600 kPa
Elongation	2% to 6% in 2 inches	2% to 6% in 50 mm
Melting Temperature	1170°F	632°C

EXPANDED MATERIALS

PHYSICAL DATA	MIN.	MAX.	UNITS (U.S.)	MIN.	MAX.	UNITS (SI)
Specific Weight (Density)	1.5	4.0	lb/cu ft	24	64	kg/m^3
	3.2	8.6	oz/gal	.024	.064	kg/l
Layer Count	12	15	layers/in	472	590	layers/m
Surface Area Per Unit Volume	110	212	sq ft /cu ft	361	696	m^2/m^3
Expanded Web Width	26	42	in	660	1067	mm
Strand Width	.055		in	1.4		mm
PERFORMANCE						
Displacement	.65	2.5	%	.65	2.5	%
Retention Gasoline	1.0	1.3	%	1.0	1.3	%
Self-Supporting Height (5% compaction)		48	ft		15	m
AVAILABILITY	L W H			L W H		
Standard Batt	36 x 22 x 12		in	915x560 x305		mm
Non-Standard						
Rectangular: min.	6 x 6 x 2		in	150x150 x 50		mm
max.	36 x 39 x 38		in	915x1000x960		mm
Cylindrical: min.	6 x 6 diam		in	150x150 diam		mm
max.	39 x 36 diam		in	1000x910 diam		mm

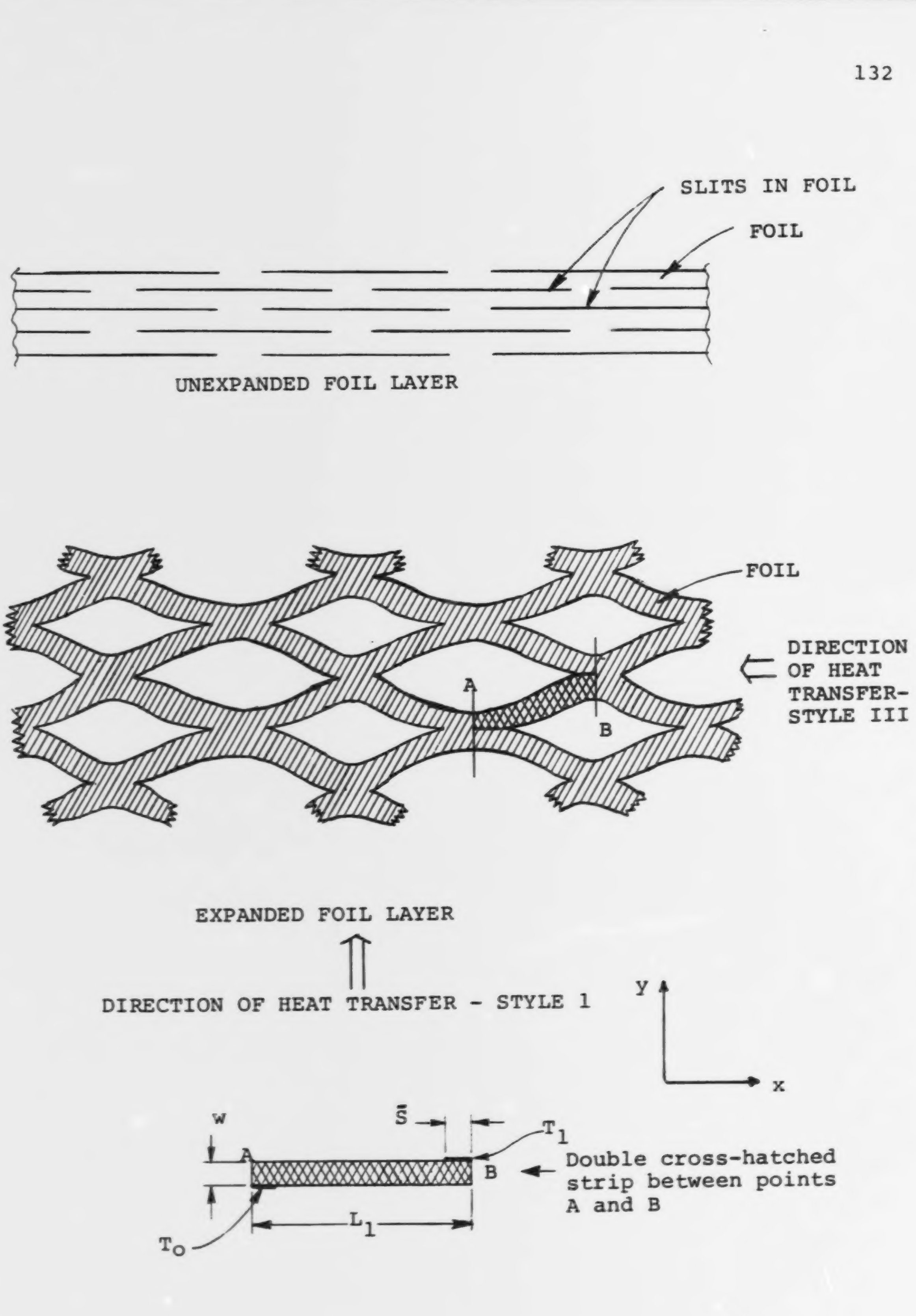
SLITS IN FOIL
FOIL
UNEXPANDED FOIL LAYER
FOIL
DIRECTION OF HEAT TRANSFER-STYLE III
A
B
EXPANDED FOIL LAYER
DIRECTION OF HEAT TRANSFER - STYLE 1
y
x
w
S̄
T_1
A
B
Double cross-hatched strip between points A and B
L_1
T_o

Fig.: 2-36: Heat Transfer in Plane of Foil

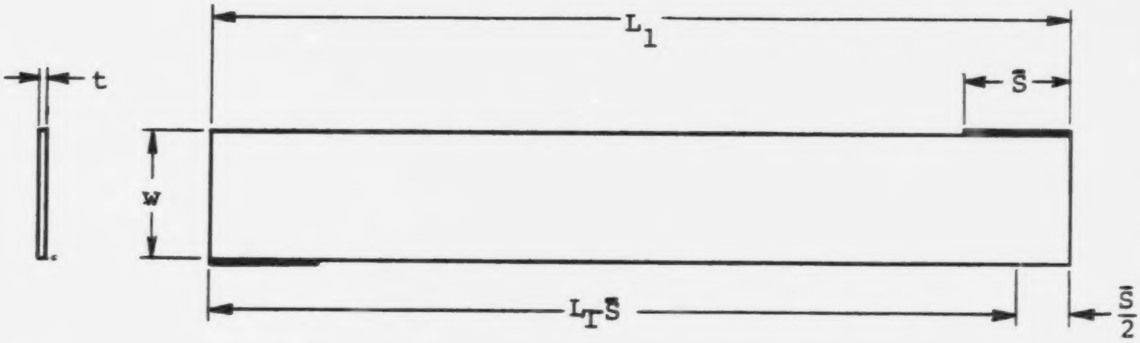
t
w
L_1
$\bar{S}$
$L_T\bar{S}$
$\frac{\bar{S}}{2}$

Fig. 2-37: Expanded view of strip AB.

A finite-difference computer program, given in Appendix F, was written to obtain the resistance of the strip AB between the isothermal patches at temperatures T_o and T_1, designated R_s for convenience. For $w = 1.4$mm, $\bar{S} = 0.15$cm, $L_1 = 1.0$cm, $t = 0.075$mm and $k_{al} = 180$ W/m°C, the computer program predicted a value for R_s of 446.0°C/W. The author was unable to obtain an exact solution for R_s, but R_s can be predicted quite accurately without using the finite-difference program given in Appendix F by applying the expression,

$$R_s = \frac{(L_1 - \bar{S})}{k_{al} w t} \qquad 2\text{-}90$$

which is just the resistance of a substitute strip with cross-sectional dimensions w and t and a length $(L-\bar{S})$. The latter dimension is the separation between the midpoints of the patches at temperatures T_o and T_1, as indicated in Fig. 2-37. For the values of $w, \bar{S}, L_1, t$ and k_{al} given previously, Eq. 2-90 predicts a resistance (R_s) of 449.7°C/W for the strip AB, which is only 0.8% different from the computer predicted value of 446.0°C/W. The computer predicted value of R_s and the value obtained by applying Eq. 2-90 are in good agreement in this case because the dimensions $\bar{S}$ and w are similar but the agreement would be poor if the dimension $\bar{S}$ was, say, much smaller than w because the heat flow would be constricted at the patches in that case. Eq. 2-90 would not account for the increase in R_s produced by the thermal constrictions and hence would tend to underpredict the value of R_s.

The value of R_s can be used to predict the thermal conductivity of Style II EXPLOSAFE in the following manner. Consider a rectangular piece of foil measuring L_{xi} and L_{yi} in the x and y directions respectively before expansion and L_{xf} and L_{yf} in the x and y directions after expansion. The x and y directions are perpendicular to and parallel to the heat flow direction for Style I EXPLOSAFE respectively, as shown in Fig. 2-36. With the contraction and expansion ratios, designated C.R. and E.R. respectively, defined by the expressions,

$$C.R = \text{Contraction ratio} = L_{xf}/L_{xi} ,$$

and

$$E.R = \text{Expansion ratio} = L_{yf}/L_{yi} ,$$

it is easily shown that the effective thermal conductivity of Style I EXPLOSAFE, designated k_{el}, is given by the expression,

$$k_{el} = \frac{w(E.R.)n_s}{L_1(C.R.)R_s} + k_v \qquad 2\text{-}91$$

where N_s is the number of foil layers per unit depth of foil (always quoted in EXPLOSAFE specifications) and k_v is the thermal conductivity of the propane vapor. The resistances of the EXPLOSAFE foil and the vapor were combined in parallel to obtain Eq. 2-91. The expansion ratio (E.R.) can always be determined from EXPLOSAFE specifications but the corresponding contraction ratio (C.R.) must be determined experimentally. The contraction ratio for the type A EXPLOSAFE mesh used in the heat transfer experiments reported by Appleyard in TP2740 (21) was measured by the author and found to be approximately 0.92, for instance, for the quoted expansion ratio of 2.14. The contraction ratio will probably always be close to unity so its effect on k_{el} will usually be fairly small.

2.3.4.2 Style II EXPLOSAFE

The effective thermal conductivity of a Style II EXPLOSAFE/vapor matrix cannot be predicted analytically because it depends on the degree of contact, or lack thereof, between the foil layers and hence on the degree of compression of the

EXPLOSAFE. It is expected that a semi-empirical model could be developed relating the conductivity of a Style II EXPLOSAFE/ vapor matrix to either the compressive strain of the matrix or the compressive load per unit area (compressive stress) plus various parameters describing the geometry of the foil layers and material properties, etc., but experiments to obtain the data needed to develop such a model have not been performed. It can be said as a general observation, however, that the thermal conductivity of Style II EXPLOSAFE, designated k_{e2}, will be lower than that of Style I or Style III because heat cannot flow between the foil layer as easily as it can flow within the planes of the layers. Measured conductivities supporting this observation are given in Sect. 2.3.5.

2.3.4.3 Style III EXPLOSAFE

The effective thermal conductivity of Style III EXPLOSAFE, designated k_{e3}, is,

$$k_{e3} = \frac{k_{a1}(C.R.)n_s t}{E.R.} + k_v \qquad 2.92$$

where, as in the case of Style I EXPLOSAFE, it is assumed that the foil and vapor resistances act in parallel. While the value of k_{e3} will generally be larger than the value of k_{e1} or k_{e2}, the value of k_{e3} decreases with increasing expansion ratio (E.R.) while the value of k_{e1} increases, so k_{e1} could be greater than k_{e3} at large expansion ratios.

2.3.5 EXPLOSAFE Thermal Conductivity Measurements

The thermal conductivity of EXPLOSAFE in Styles I, II and III was measured with air present using an apparatus similar to the guarded hot plate apparatus commonly used to measure the thermal conductivities of insulating materials. The experimental apparatus consisted of an electrically heated copper plate sandwiched between two effectively identical layers of EXPLOSAFE foil (with air present), as shown in Fig. 2-38 and Fig. 2-38b. The heat source was fabricated by inserting three 12.7cm (5") longx0.952cm (3/8") O.D. Chromalox C-207 cartridge heaters into holes drilled through one of the large dimensions of a 15.2x15.2x2.5cm (6"x6"x1") copper plate. Guard heaters were not used to reduce heat losses from the edge of the plate. The heat source and the two layers of EXPLOSAFE/air, which were nominally 14cmx14cm in cross-section and 7.6cm thick, were, in turn, sandwiched between two water-cooled copper heat sinks, each of which was fabricated by soldering three loops of 0.952cm (3/8") O.D. copper tubing to one side of a 15.2x15.2x1.25cm (6"x6"x½") copper plate. Municipal water was used for cooling purposes. The multi-tiered test assembly just described was contained in a square styrofoam duct with 2.5cm (1") wall thickness, as shown in Figs. 2.38a and 2.38b, and the effective thermal conductivity of the EXPLOSAFE/air matrix was estimated by measuring the electrical power supplied to the heat source and the heat source and sink temperatures. The electrical power for the heat source was supplied by an A.C. variac and chromel-alumel thermocouples were used to measure all temperatures. A thermally conducting grease, specifically type Z9 silicone heat sink compound manufactured by GC Electronics, was applied to the heat source and sink surfaces to minimize contact resistances between the surfaces and the EXPLOSAFE. Styrofoam shims, approximately 0.63cm (¼") thick, were inserted between the heat source and the heat sinks around the edges of the plates to maintain the desired gap (nominally 7.6cm as mentioned previously) between the plates. The shim heights, nominally 7.6cm, were varied to achieve dif-

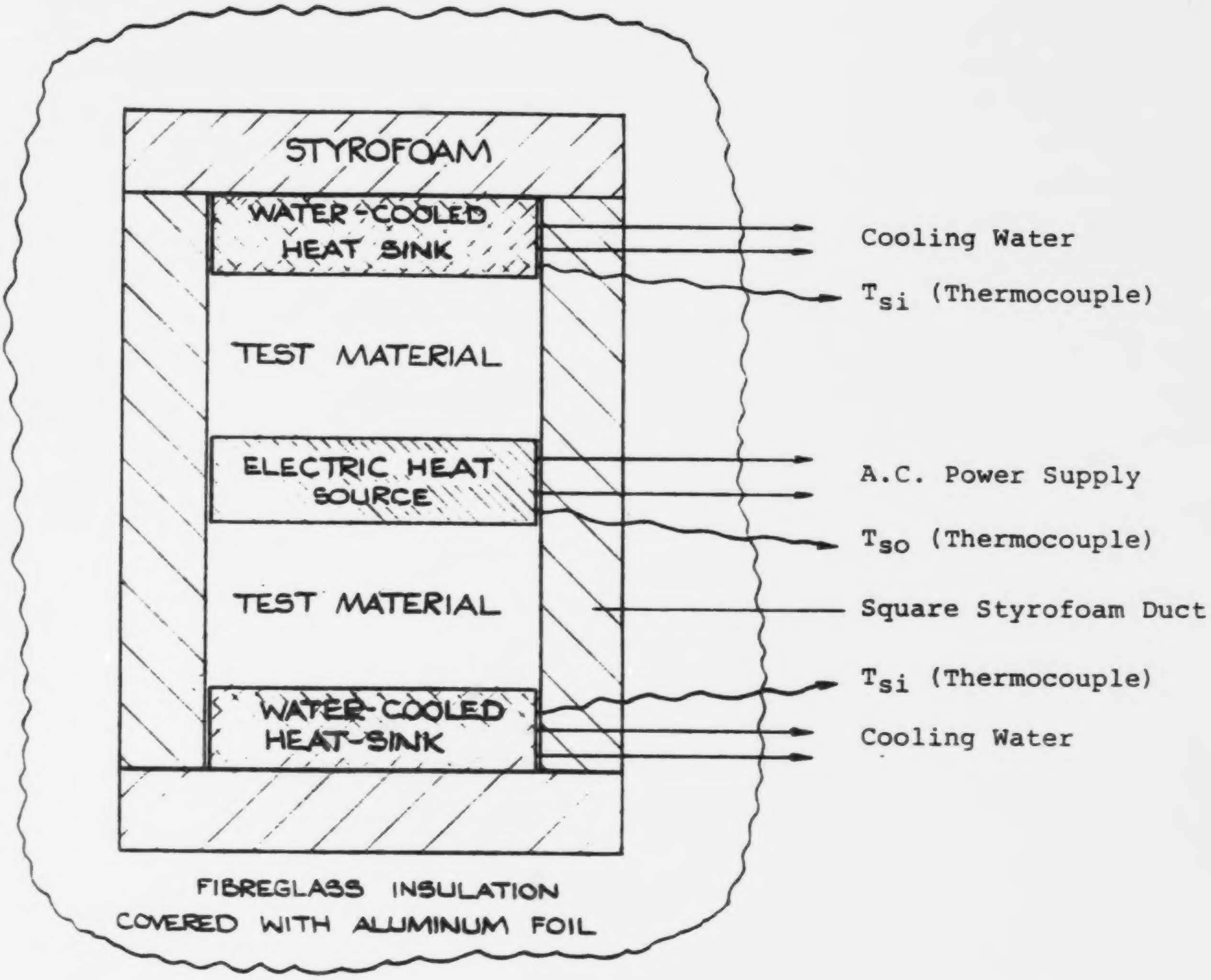
STYROFOAM
WATER-COOLED HEAT SINK
TEST MATERIAL
ELECTRIC HEAT SOURCE
TEST MATERIAL
WATER-COOLED HEAT-SINK
FIBREGLASS INSULATION COVERED WITH ALUMINUM FOIL
Cooling Water
T_{si} (Thermocouple)
A.C. Power Supply
T_{so} (Thermocouple)
Square Styrofoam Duct
T_{si} (Thermocouple)
Cooling Water

$$k_{effective} \sim \frac{P}{(T_{so} - T_{si})}$$

where P = power supplied to heater

T_{so} = heat source temperature

T_{si} = heat sink temperature

Fig. 2-38a: EXPLOSAFE thermal conductivity measuring apparatus (for Styles I and III).

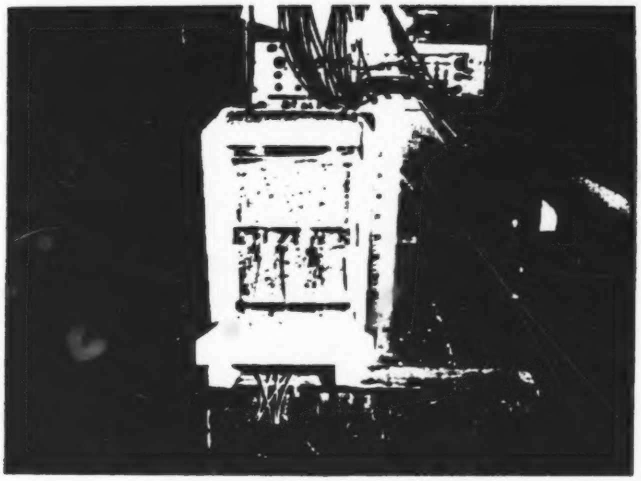

Fig. 2-38b: EXPLOSAFE thermal conductivity measuring apparatus.

ferent degrees of compression of the Style II EXPLOSAFE samples.

The EXPLOSAFE samples tested were supplied precut to the proper size by Vulcan Industrial Packaging Ltd., the manufacturer of EXPLOSAFE foil. The samples tested were manufactured to the specifications of the type A EXPLOSAFE used in the laboratory heat transfer experiments performed by Appleyard and reported in TP 2740 (21). This material has the following, nominal, specifications.

Density - 60.9kg/m^3
Layers/meter (n_s) - 571
Stands/meter - 333
Strand width (w) - 1.375mm
Expansion ratio (E.R.) - 2.14
Foil thickness - 0.075mm
Material - AA 3003-H24 aluminum

Note that the number of strands/meter = (1/w)/E.R. when w is measured in meters because (1/w) is the number of strands/meter before expansion and expanding the foil simply reduces the strands/meter count by the factor 1/E.R.

Results of the EXPLOSAFE thermal conductivity measurements are tabulated in Tables 2-6a, 2-6b and 2-6c for the Style I,II and III samples respectively. The Style I and Style III thermal conductivities were both measured at two different power levels and the Style II thermal conductivity was measured at two different compressions, as shown in the tables. Two thermocouples were attached to the heat source so their temperature readings were averaged to obtain $\overline{T}_{source}$. The two source temperature measurements never differed by more than 0.2°C. The tem-

TABLE 2-6a: Experimental data, Style I EXPLOSAFE

TRIAL #	POWER (P),W	$\overline{T}_{source}$ °C	$\overline{T}_{sink}$ °C	$\overline{H}$ m	k_e W/m°C
1	10.55	54.4	16.1	0.072	0.50
2	14.51	67.7	15.7	0.072	0.51

TABLE 2-6b: Experimental data, Style II EXPLOSAFE

TRIAL #	COMPRESSION %	POWER (P),W	$\overline{T}_{source}$ °C	$\overline{T}_{sink}$ °C	$\overline{H}$ m	k_e W/m°C
1	8	5.76	64.0	19.2	0.0746	0.24
2	16	9.19	74.2	17.3	0.0630	0.26

TABLE 2-6c: Experimental data, Style III EXPLOSAFE

TRIAL #	POWER (P),W	$\overline{T}_{source}$ °C	$\overline{T}_{sink}$ oC	$\overline{H}$ m	k_e W/m°C
1	35.6	44.0	20.1	0.079	3.01
2	71.4	68.3	20.5	0.079	3.05

peratures of the upper and lower heat sinks also never differed by more than 0.2^{o}C so those two temperatures were averaged to obtain $\overline{T}_{sink}$. The measured thicknesses of the upper and lower EXPLOSAFE samples, which were nominally about 7.6cm, were averaged in each test to obtain the values of $\overline{H}$ tabulated in Table 2-6a - 2-6c. The effective thermal conductivity (k_e) of the EXPLOSAFE sample being tested was then calculated from the equations,

$$k_e = \frac{P\overline{H}}{2A_{cs}(\overline{T}_{source}-\overline{T}_{sink})} \qquad 2\text{-}93$$

where A_{cs} = the cross-sectional area of the sample = 14cmx14cm=196cm^2 = .0196m^2 in all cases. Values of k_e calculated using Eq. 2-93 are tabulated in Tables 2-6a - 2-6c.

As seen in Table 2-6b, the effective thermal conductivity of Style II EXPLOSAFE was 0.24 W/m^{o}C when the compressive strain of the matrix was 8% and 0.26 W/m^{o}C when the strain was 16%. The compressive strain in this case was defined as the ratio of the change in height of the matrix, obtained by compressing it, to the original height. The original height of a Style II EXPLOSAFE matrix is difficult to estimate unless a small preload is applied because the foil layers do not lie flat so the original height was measured with a 14cmx14cm piece of 1.25cm (½") thick plywood placed on top of the stack of foil layers. The stack of foil layers was compressed by placing weights on top of the upper heat sink. Compressive strains of approximately 8% and 16% were obtained with unit loadings of approximately 0.23 N/cm^2 and 0.41 N/cm^2 so the stiffness (= load per unit area/compressive strain) of the type of EXPLOSAFE tested must have been approximately

2.55-2.88 N/cm^2 in a direction normal to the foil layers for compressive strains in the 0-16% range. The foil matrix did not return to its original height after it had been compressed 16% so some yielding of the matrix must have occurred.

2.3.6 Comparison Of Predicted And Measured EXPLOSAFE Thermal Conductivities (Styles I and III)

The thermal conductivity of an EXPLOSAFE foil matrix manufactured to the specifications given in the preceding section is approximately 0.50 $W/m^{o}C$ for the Style I configuration and approximately 3.03 $W/m^{o}C$ for the Style III configuration according to the experimental data given in that section. These thermal conductivities apply when the temperature of the air in the matrix is in the $32^{o}C$-$46^{o}C$ range, although the thermal conductivity of air at temperatures in this range is only about 0.027 $W/m^{o}C$ so the amount of heat transferred through the air must have been almost negligible compared to the amount transferred through the foil in the experiments.

As mentioned previously, the author obtained a contraction ratio (C.R.) of 0.92 by expanding a sample of EXPLOSAFE foil to approximately 2.14 times its original length (ie. to an expansion ratio, E.R. of 2.14). Also, a value of $446^{o}C/W$ was predicted for R_s when the foil strand dimensions given in the preceding section for type A EXPLOSAFE material were used in the computer program given in Appendix F. This value of R_s, the measured value of C.R. and the values of E.R., w and n_s for the type A EXPLOSAFE material can be substituted into Eq. 2-91 to give

$$k_{el} = \frac{w(E.R.)n_s}{(C.R.)R_s} + k_v$$

$$= \frac{.001375\text{m}(2.14)571}{0.01\text{m}(0.92)446^{\circ}\text{C/W}} + 0.027\ \text{W/m}^{\circ}\text{C}$$

$$= .436\text{W/m}^{\circ}\text{C},$$

as the thermal conductivity of Style I EXPLOSAFE when $L_1 = 1\text{cm}$ (0.01m) and $k_v = 0.027\text{W/m}^{\circ}\text{C}$. This value is approximately 13% less than the measured conductivity of $0.50\text{W/m}^{\circ}\text{C}$.

The author counted the number of layers in the Style III EXPLOSAFE sample and found that the number corresponded to a layer count (n_s) of approximately 544 layers/meter instead of 571 as specified. Substituting this value of n_s into Eq. 2-92 gives

$$k_{e3} = \frac{k_{al}(\text{C.R.})n_s t}{\text{E.R.}} + k_v$$

$$= 3.184\text{W/m}^{\circ}\text{C},$$

as the thermal conductivity of Style III EXPLOSAFE. This value is approximately 5% greater than the measured conductivity of $3.03\ \text{W/m}^{\circ}\text{C}$ (average).

The agreement obtained between the predicted and measured thermal conductivities of the Style I and III EXPLOSAFE configurations is considered quite good and demonstrates that the conductivity of EXPLOSAFE can be predicted fairly accurately when the direction of heat flow is parallel to the layers of foil, as it is for Styles I and III. The conductivity of the air in the matrix contributed almost nothing to the overall conductivity of the matrix in either configuration and the overall conductivity of the matrix was thus almost directly proportional to k_{al} in both cases. The thermal conductivity of saturated propane vapor at a saturation pressure of 1.93 MPa (280psia) is, at 0.025W/m^{o}C, almost exactly the same as that of the air present in the experiments so the effective thermal conductivity of an EXPLOSAFE/propane vapor matrix will also be almost directly proportional to k_{al}. If EXPLOSAFE foil transfers heat away from a hot tank wall primarily by conduction, then manufacturing the foil from a material like stainless steel, which typically has a thermal conductivity less than one-tenth that of aluminum, would seriously affect the effectiveness of the EXPLOSAFE thermal protection system.

2.3.7 Radiative Heat Transfer In Explosafe

While the effective thermal conductivity of an EXPLOSAFE/vapor matrix will be increased by radiation at high temperatures, it is fairly difficult to predict the amount of the increase accurately because the geometry of the foil is quite complex. It will be shown in this section that the "radiative" thermal conductivity of the matrix, which can be added to the conductivity calculated in Sect. 2.3.4 for heat transfer by conduction alone, will probably be fairly small compared to the latter conductivity for heat flows in the Style I, II and III directions and hence that radiation in the matrix does not need not to be modelled with high accuracy. Conservative assumptions will be made in the forthcoming analysis to obtain upper bound estimates for the "radiative" thermal conductivities.

To obtain a rough estimate of the "radiative" thermal conductivity of Style I EXPLOSAFE, consider the foil strands containing the points numbered "1" and "2" in Fig. 2-39. The two points numbered "1" are assumed to be at approximately the same temperature, as are the two points numbered "2". If the view factor between the upper strand of foil containing the two points numbered "1" and the lower strand of foil containing the two points numbered "2" is assumed, conservatively,* to be unity, then the radiative heat transfer coefficient (h_r)

---

* This assumption leads to an overestimation of the view factor because each strand "sees" itself to a certain extent. This assumption would also only be strictly correct if there were no gaps between the layers of foil and the strands in different layers perfectly aligned.

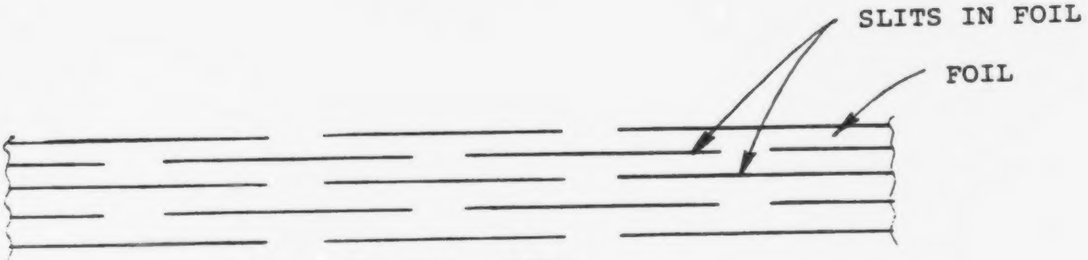
SLITS IN FOIL
FOIL

UNEXPANDED FOIL LAYER

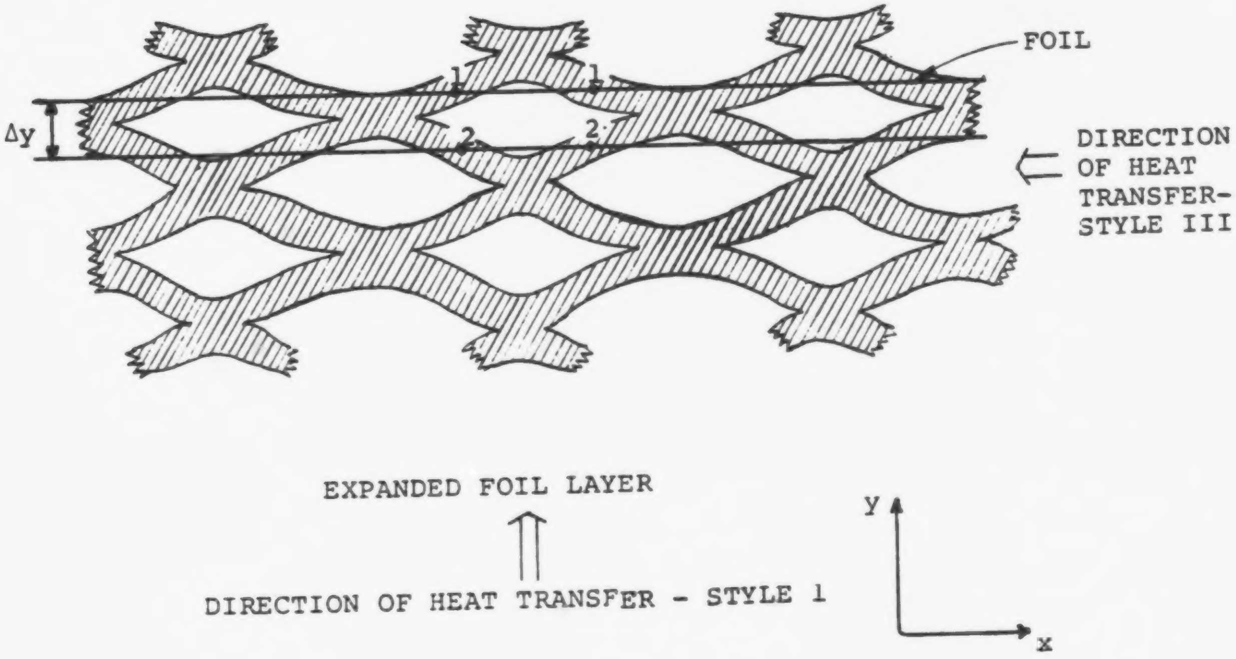
FOIL
1
1
Δy
2
2
DIRECTION OF HEAT TRANSFER-STYLE III
DIRECTION OF HEAT TRANSFER - STYLE 1
y
x

EXPANDED FOIL LAYER

Fig.: 2-39: Foil Geometry for Radiation Characteristics between the upper and lower strands is given approximately by the expression,

$$h_r = \frac{\sigma(T_2{}^4 - T_1{}^4)}{\frac{1}{\varepsilon_1} + \frac{1}{\varepsilon_2} - 1} / (T_2 - T_1) \qquad \text{2-94a}$$

$$= \frac{\sigma(T_2{}^2 + T_1{}^2)(T_2 + T_1)}{\frac{1}{\varepsilon_1} \quad \frac{1}{\varepsilon_2} - 1} \qquad \text{2-94b}$$

where ε_1 and ε_2 are the emissivities of surfaces 1 and 2 respectively. It is assumed that T_1 and T_2 are the average temperatures of the upper and lower strands respectively. If T_1 and T_2 have approximately the same value, Eq. 2-94 simplifies to,

$$h_r = \frac{4\sigma\ \overline{T}^3}{\frac{1}{\varepsilon_1} + \frac{1}{\varepsilon_2} - 1} \qquad \text{2-95}$$

where $\overline{T} = (T_1 + T_2)/2$. The heat transfer coefficient h_r defined by Eq. 2-95 causes heat to be transferred across a distance Δy (see Fig. 2-39) on average, so the radiative thermal conductivity of EXPLOSAFE in the Style I heat flow direction, designated k_{r1}, can be obtained from the expression,

$$\frac{k_{r1}}{\Delta y} = h_r \qquad \text{2-96a}$$

or

$$k_{r1} = \frac{4\sigma\overline{T}^3\,\Delta y}{\frac{1}{\varepsilon_1} + \frac{1}{\varepsilon_2} - 1} \qquad \text{2-96b}$$

where $\Delta y = w \times E.R.$ When $\bar{T} = 922K$ ($1200^{\circ}F$), $W = 0.14cm$, $E.R. = 2.14$ and $\varepsilon_1 = \varepsilon_2 = 0.05$ (value for polished aluminum, from Holman (3)), Eq. 2-96b gives a value for k_{r1}, of,

$$k_{r1} = \frac{4 \times 5.669 \times 10^{-8} \frac{W}{m^2K^4}(922K)^3(0.0014m)2.14}{\frac{1}{.05} + \frac{1}{.05} - 1}$$

$$= 0.014 \frac{W}{mK}$$

which is negligible compared to the thermal conductivity of approximately $0.05 \frac{W}{mK}$ obtained previously for Style I EXPLOSAFE (with the same values of w and E.R.) for heat transfer by conduction alone.

Equation 2-96b can also be used to obtain an upper bound estimate of the radiative thermal conductivity of EXPLOSAFE in the Style III heat flow direction (k_{r3}) if Δy is calculated from the expression, $\Delta y = L_1 \times C.R.$ since this is the spacing between the two points numbered "1" or the two points numbered "2" in Fig. 2-39. It can easily be shown that k_{r3} will generally be negligible compared to k_{e3} (ie. the thermal conductivity for heat transfer by conduction alone).

The radiative thermal conductivity of Style II EXPLOSAFE (k_{r2}) could also be estimated from Eq. 2-96b if Δy for that style of EXPLOSAFE could be evaluated in some manner. Using the EXPLOSAFE samples obtained for the thermal conductivity experiments, the author observed that approximately ten layers of foil, which represents a total thickness of about 2cm, was required to block all transmission of light through the matrix. An upper bound estimate for k_{r2} can be obtained by making the obviously unrealistic assumption that radiant energy is transferred unattenuated across that distance since this assumption maximizes Δy in Eq. 2-96b and hence also k_{r2}. Thus substituting $\Delta y = 0.02\text{m}$ into Eq. 2-96b with $\overline{T} = 922\text{K}$ and $\varepsilon_1 = \varepsilon_2 = 0.05$ as before, we obtain the value of k_{r2} as,

$$k_{r2} = \frac{4\text{x}5.669\text{x}10^{-8}\,\dfrac{\text{W}}{\text{m}^2\text{K}^4}\,(922\text{K})^3(0.02\text{m})}{\dfrac{1}{.05} + \dfrac{1}{.05} - 1}$$

$$= .091\,\frac{\text{W}}{\text{mK}}$$

which is not negligible compared to the measured value of k_{e2} of approximately $0.25\frac{\text{W}}{\text{mK}}$. This value of k_{r2} is an upper bound estimate, of course, and the true value of k_{r2} will probably be closer to $0.091/2 = 0.045\frac{\text{W}}{\text{mK}}$ than to $0.091\frac{\text{W}}{\text{mK}}$ because the average transmission length for radiant energy in the matrix in the Style II heat flow direction must be approximately one-half of the value of Δy used previously (ie. $.02/2 = .01\text{m}$). Thus it will be assumed initially in the DE tank car model that radiation is not a significant heat transfer mechanism in any direction in an EXPLOSAFE/vapor matrix.

There is actually some experimental justification for neglecting radiation in the ullage of an EXPLOSAFE-equipped tank car. It is quite evident from the behaviour of the temperature vs. time traces shown in Fig. 2-40 for the bare tank ENIGMA and the EXPLOSAFE-equipped tanks DRES SPECIAL, NOVA and DIABLO that radiation in the EXPLOSAFE does not need to be modelled because wall temperatures in the EXPLOSAFE-equipped tanks increased much more slowly than the wall temperature in ENIGMA

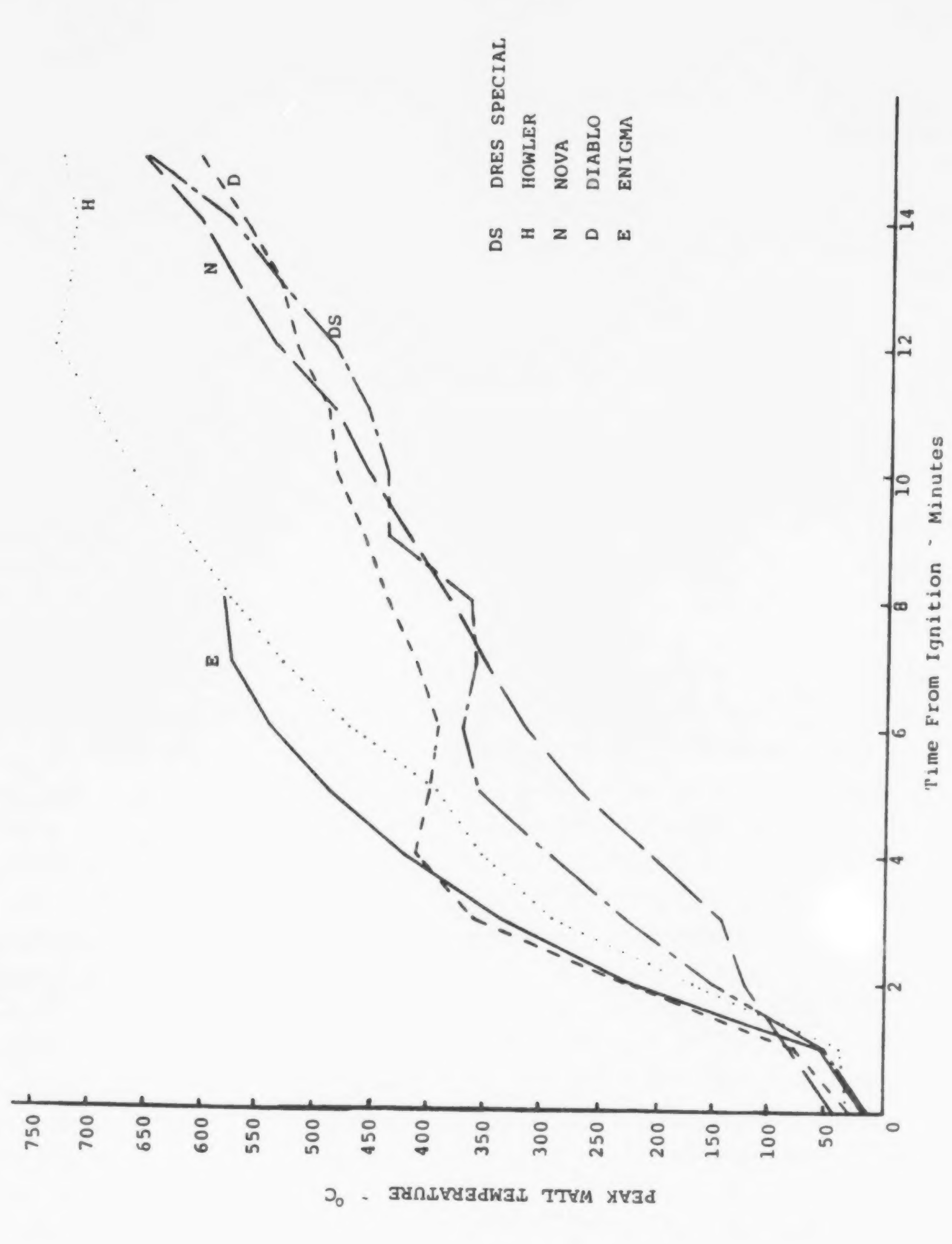

Fig.: 2-40: Peak Wall Temperature vs. Time - All Tests even in the early stages of the transients. Wall temperatures were low during those periods so radiation in the ullage, which would not have been significant at those temperatures, could not have been responsible for the reduced rates of temperature rise measured at those times in the tests of the EXPLOSAFE-equipped tanks.

It was assumed that the emissivity of the EXPLOSAFE foil will be essentially the same as that of polished aluminium (ie. 0.05) in the preceding order of magnitude estimates of k_{r1}, k_{r2} and k_{r3}. The surface of the foil may lose its polish as the foil ages in a tank car, however, and it is conceivable that the emissivity of the surface could be as high as 0.2 instead of 0.05 as assumed. The values of k_{r1} and k_{r3} would still be negligible compared to k_{e1} and k_{e3} in that case, but k_{r2} would become comparable in magnitude to k_{e2}. Sensitivity analyses will be performed using the tank car model, once developed, to see how variations in k_{e2} affect predicted peak wall temperatures and predicted rupture times.

2.3.8 Convective Heat Transport In An EXPLOSAFE Matrix

Since EXPLOSAFE foil undoubtedly offers a fairly high resistance to flow, it can safely be assumed that the vapor in an EXPLOSAFE matrix in a tank car will be largely stagnant when only an annular lining of EXPLOSAFE is used since the vapor evolved at the liquid surface during venting periods will tend to escape through the voided core in that case. The vapor will obviously be forced to flow through the EXPLOSAFE matrix when the tank is fully packed with the material and lateral diversion of the flow by the strands of foil will cause the vapor to be laterally well-mixed. The amount of heat transferred in the EXPLOSAFE/

vapor matrix by convective effects, in other words by axial and laterally-diverted flows, could easily exceed the amount transferred by pure conduction in a fully-packed tank. Some assumption would have to be made regarding lateral mixing rates in a fully-packed tank in order to model heat transfer in the tank and it could be assumed, initially anyway, that lateral mixing rates (ie. lateral eddy diffusivities) are negligible. The thermal model of a fully-packed tank car would undoubtedly be quite sensitive to assumptions in this area, however, and experimental measurements of lateral eddy diffusivities in an EXPLOSAFE matrix would have to be made if initial predictions of peak wall temperatures, etc. did not agree with the results of the 1/5 scale tests performed at DRES Suffield. Modelling the heat transfer process in a tank fully-packed with EXPLOSAFE would be fairly difficult for the reasons just mentioned and, since it is felt that packing a tank completely with EXPLOSAFE is not a practical possibility, only annular EXPLOSAFE linings will be considered in the DE tank car model.

It will be assumed initially in the DE tank car model that the propane vapor in an EXPLOSAFE annulus is stagnant and in thermal equilibrium with the mesh and hence that heat is transferred in the matrix by conduction alone. The author suspects that the model predicated on this assumption will be unable to predict the fairly low peak wall temperatures measured in the 1/5 scale tests of EXPLOSAFE-equipped tank cars, however, because it can be shown, for instance, that the 7.6cm (3") thick EXPLOSAFE annulus used in NOVA would have less than halved the thermal resistance of the circumferential conducting path to the liquid surface. Stated another way, if pure conduction had been responsible for the demonstrated effectiveness of EXPLOSAFE foil in the test of NOVA, then even better results could have been obtained by simply doubling the thickness of the tank wall (or the conductivity of the wall material) because that would have produced a greater reduction in the resistance of the conducting path to the liquid surface than was obtained by adding the EXPLOSAFE annulus. Results obtained with the computer program described in Appendix E suggest that circumferential conduction in the tank wall is not a very significant heat removal mechanism, although it is recognized that circumferential conduction may have a much greater effect on the peak wall temperature vs. time relationship in a real tank car analysis in which the fraction of the tank volume occupied by liquid is initially quite large (eg. 85%) and decreases as time progresses. Thus the question of whether the demonstrated effectiveness of the EXPLOSAFE thermal protection system is attributable only to the high conductivity of an EXPLOSAFE/vapor matrix, compared to that of the vapor alone, cannot be answered until a preliminary version of the tank car model has been developed.

If results obtained with the initial tank car model do not agree with the results of the 1/5 scale tests of EXPLOSAFE-equipped tank cars,* it will be assumed that the vapor in an EXPLOSAFE annulus is not stagnant and hence that convective effects significantly increase the effective thermal conductivity of the matrix. If some axial flow of the vapor in the matrix occurs when the tank is venting, axially-moving fluid particles will be diverted by the strands of EXPLOSAFE foil and effective lateral mixing of the vapor will result. Heat will also be transported in the matrix as a result of fluid motion caused by changes in tank pressure since fluid particles will move closer together when the tank pressure increases and further apart when the pressure decreases. The fluid particles will transfer heat from one part of the matrix to another with each such change of position.

---

* Only the results of the test of NOVA will be used because all of the other EXPLOSAFE-equipped tanks tested were fully packed with EXPLOSAFE.

The EXPLOSAFE annulus will therefore be ventilated and its effective thermal conductivity increased to a certain extent by pressure changes and the transfer of heat within the EXPLOSAFE/vapor matrix by this mechanism could be quite significant if the tank pressure varied rapidly, as a result of high frequency relief valve cycling for instance. While relief valve cycling occurred for significant periods of time during the 1/5 scale tests of EXPLOSAFE-equipped tank cars, relatively little cycling has been observed in full scale tank car fire tests. Propane vapor motion caused by changes in tank pressure and the consequent changes in vapor density may therefore be of quite different significance in 1/5 scale and full-scale tanks, if indeed such motion is ever significant.

As mentioned previously, heat transfer by fluid motion in an EXPLOSAFE/vapor matrix will be ignored until it has been demonstrated, by comparing analytical results obtained initially with just conduction considered to the results of the 1/5 scale tests, that convective effects in the matrix are probably significant.

2.3.9 Heat Transfer In A Tank Equipped With EXPLOSAFE-Model Details

Axial heat transfer in a level tank car in an all-enveloping pool fire will almost undoubtedly be negligible compared to r-θ heat transfer. It is expected that this observation will apply even when the flame temperature varies moderately in the axial direction, as it often does, and/or the tank is tilted.* The sample analyses described in Appendix E show that even r-θ conduction is not significant at points in the tank wall more than about ten wall thicknesses away from the line of intersection of the liquid surface and the tank shell in an unprotected tank. Since adding an EXPLOSAFE liner to the tank should improve the r-θ conduction and make axial conduction even less important as a heat transfer mechanism in most cases, axial conduction will be neglected in the thermal model of an EXPLOSAFE-equipped tank car in a pool fire and the implicit method described in Sect. 2.1.2 will be used to integrate the heat conduction equation with respect to time. The program user will be allowed to use planes of thermal symmetry to reduce the size of the region modelled, as in the analysis of an unprotected tank car, and the user will also be allowed to choose between performing the thermal analysis at only one axial location in the tank or performing it in N_k thermally decoupled axial segments. Heat transfer in a level tank car equipped with EXPLOSAFE will be analysed at only one axial location as a strictly two-dimensional (r-θ) analysis, however, since as discussed below, the internal boundary conditions in the tank will, initially anyway, be assumed to be independent of the z coordinate.

A finite-difference grid will be superimposed over the EXPLOSAFE and the tank wall in the thermal analysis of an EXPLOSAFE-equipped tank car, as shown in Fig. 2-41. The pro-

---

* Axial conduction will be significant in regions near the line of intersection of the liquid surface and the tank shell in a tilted or untilted tank but those regions are of little interest because they will not be where the highest wall temperatures are obtained.

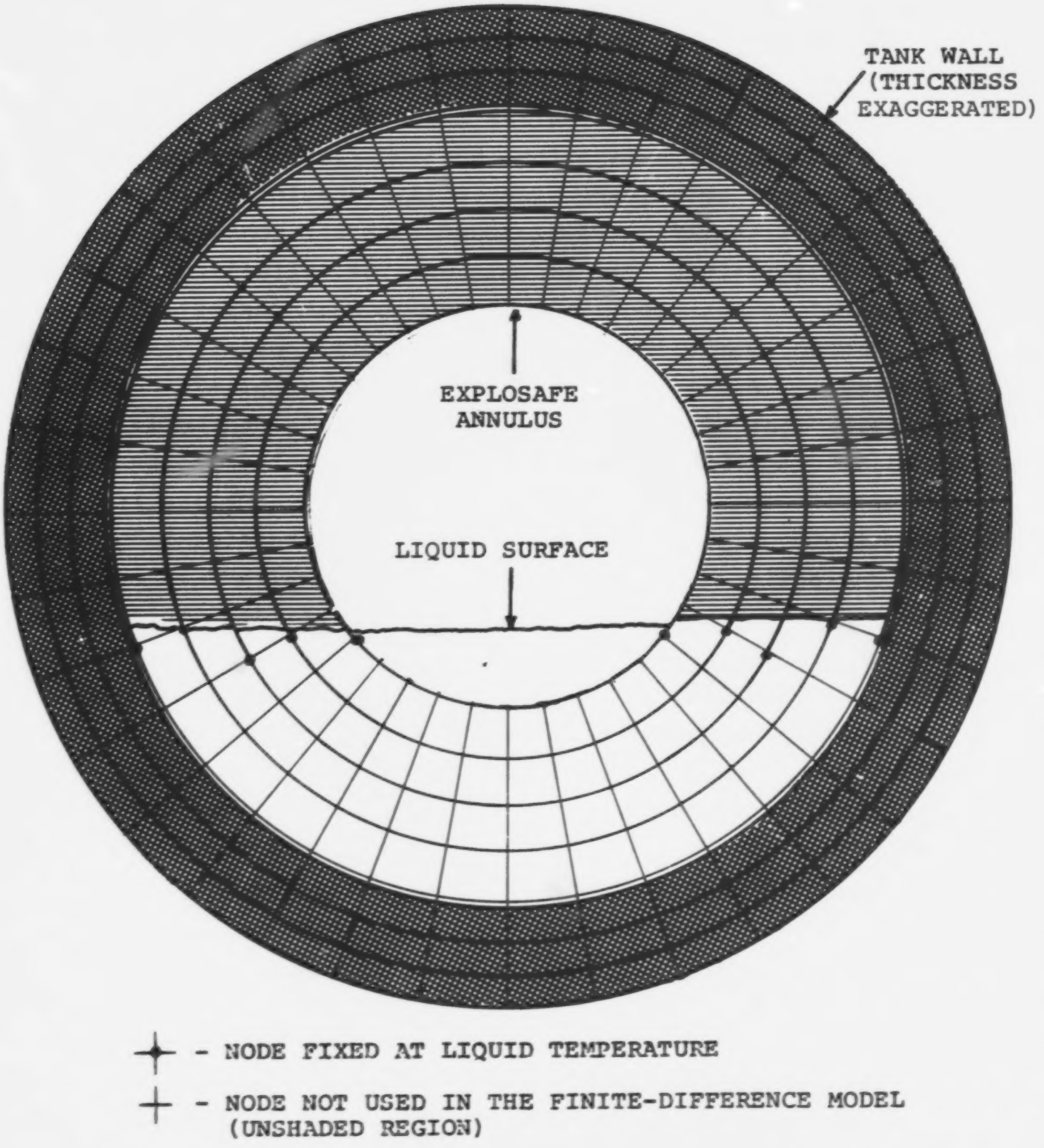
TANK WALL (THICKNESS EXAGGERATED)
EXPLOSAFE ANNULUS
LIQUID SURFACE
- NODE FIXED AT LIQUID TEMPERATURE
- NODE NOT USED IN THE FINITE-DIFFERENCE MODEL (UNSHADED REGION)

FIG. 2-41: FINITE-DIFFERENCE GRID SUPERIMPOSED ON TANK CAR CROSS-SECTION

gram user will be required to specify the inner radius of the EXPLOSAFE annulus (R_{iE}), the inner radius of the tank wall (R_{it}), the thickness of the tank wall (t_w), the number of radial subdivisions in the EXPLOSAFE (n_{rE}), the number of radial subdivisions in the tank wall (n_{rt}) and the number of azimuthal subdivisions to completely define the r-θ grid structure. The user will also be required to specify whether or not the plane A-A in Fig. 2-3 is to be considered a plane of symmetry, of course. The grid definition data just mentioned will be used to calculate equi-sized radial subdivisions in the EXPLOSAFE annulus, equi-sized radial subdivisions in the tank wall, and equi-sized azimuthal subdivisions around the tank circumference, thus defining the geometric parameters needed in the finite-difference equations.

The X-coordinate of the liquid surface (ie. X^*), calculated by the program LIQLEV described in Appendix B, will be compared to the X-coordinate of each node in the EXPLOSAFE annulus, calculated using Eq. 2-35, to determine which nodes are located above the liquid surface and which nodes are located below the liquid surface at each time step. The temperatures of the uppermost nodes in the liquid will be fixed at the liquid temperature and the rest of the nodes will be eliminated from the model at each time step causing the fraction of the EXPLOSAFE annulus modelled to vary as the liquid level varies. The uppermost nodes in the liquid will thus serve as boundary nodes for the ullage space heat transfer analysis, as mentioned in Sect. 2.1.1, and frequent updatings of the Jacobian matrix will be required to model the constantly changing grid size and boundary conditions. The Jacobian can be factored very rapidly when axial conduction is neglected, however, because the bandwidth of the matrix is small in that case, so the need to update and refactor it frequently will not be a serious liability.

Radiative heat transfer in the EXPLOSAFE matrix will not be modelled, as already discussed, and radiation from the EXPLOSAFE matrix to the liquid surface will also not be modelled because the emissivity of EXPLOSAFE foil is very low. Convective heat transfer from the inner surface of the EXPLOSAFE annulus to the propane vapor will be modelled when the tank is venting, however, by calculating convective heat transfer coefficients for the EXPLOSAFE inner surface nodes. The inner surface of the EXPLOSAFE mesh will appear to the flow of propane vapor to be a very rough surface, as discussed in Appendix D, so the boundary layer between the vapor and the mesh will likely be turbulent over most of the length of the tank car as a result. While the equations given previously for the inner surface heat transfer coefficient (h_i) (ie. Eqs. 2-58 and 2-63) cannot be applied to a turbulent boundary layer, obtaining an accurate estimate of the turbulent convective heat transfer coefficient using the techniques described in Appendix D would be a major undertaking that should not be attempted until it has been demonstrated, by performing sensitivity analyses with the tank car model, once developed, that an accurate estimate of the convective heat transfer coefficient on the inner surface of the EXPLOSAFE mesh is required. An order of magnitude estimate of the turbulent convective heat transfer coefficient will be obtained by multiplying the value of h_i, predicted using Eq. 2-58 for a level tank and Eq. 2-63 for a tilted tank, by a user-specified factor. The convective heat transfer for a turbulent boundary layer will likely be 2-4 times the value of h_i for a laminar boundary layer, as noted in Appendix D, so the user-specified factor will typically lie in the range 2-4.

The program user will be required to specify the size of the gap (δ) between the EXPLOSAFE/vapor matrix and the tank wall for use in calculating the contact conductance (h_{int}) at the tank wall/EXPLOSAFE interface. The value of h_{int} will be calculated by the program from the equation,

$$h_{int} = \frac{k_v}{\delta} + \frac{\sigma(T_1{}^2 + T_2{}^2)(T_1 + T_2)}{\frac{1}{\varepsilon_1} + \frac{1}{\varepsilon_2} - 1} \qquad 2\text{-}97$$

where k_v is the thermal conductivity of propane vapor evaluated at the average of the tank wall inner surface temperature (T_1) and the EXPLOSAFE outer surface temperature (T_2) and ε_1 and ε_2 are the emissivities of the tank wall inner surface and EXPLOSAFE matrix outer surface respectively. The values of ε_1 and ε_2 will be specified by the program user along with δ. While the value of δ could easily be input as a function of azimuthal position, a circumferentially uniform value will be used initially because this parameter cannot be predicted and hence will have to be specified arbitrarily. The gap (δ) will have to be assigned a value greater than zero, of course, but it will be possible to simulate an essentially negligible interfacial resistance by setting δ to a very small value.

As mentioned previously, it will be assumed that the propane vapor is stagnant within, and in thermal equilibrium with, the EXPLOSAFE mesh. All of the thermal properties of the EXPLOSAFE/vapor matrix, including its density and specific heat, will have to be calculated by combining the properties of the EXPLOSAFE foil and the propane vapor appropriately in that case. The density of an EXPLOSAFE/vapor matrix (ρ_m) can be calculated simply by summing the density of the expanded EXPLOSAFE foil (ρ_{EX}), which is always specified by the manufacturer and is typically approximately 50kg/m^3, to the density of the propane vapor (ρ_v) because the volume occupied by the foil is negligible (the fluid displacement factor is typically 1-2%).

The density of saturated propane vapor at a typical tank venting pressure of 2.03MPa (295psia) is 47kg/m^3, for instance, so the density of the EXPLOSAFE/vapor matrix would be $50+47=97\text{kg/m}^3$ if the density of the expanded EXPLOSAFE foil was that mentioned previously (ie. 50kg/m^3).

The specific heat of an EXPLOSAFE/vapor matrix, designated C_{EX}, can be calculated from the equation,

$$C_{EX} = \frac{\rho_{EX}}{\rho_m} C_{al} + \frac{\rho_v}{\rho_m} C_{pv} \qquad \text{2-98}$$

where C_{al} is the specific heat of aluminium, typically $0.89\text{kJ/kg}^\circ\text{C}$, and C_{pv} is the specific heat (at constant pressure) of propane vapor. The value of C_{pv} will be obtained in the tank car model from the equation.

$$C_{pv} = \left.\frac{\partial h}{\partial T}\right|_p \qquad \text{2-99}$$

where the enthalpy (h) of the vapor will be available in tabular form as a function of pressure (p) and temperature (T) and Eq. 2-99 will be evaluated as a finite-difference at the prevailing values of p and T. The thermodynamic property tables prepared by Sallett and Palmer (24) for propane will be used in the model.

Except for the differences explicitly mentioned in this section, the thermal model of an EXPLOSAFE-equipped tank car will be the same as that of an unprotected tank car. It will therefore be assumed, for instance, that the equation given previously relating the wall heat flux to the excess temperature for boiling propane (ie. Eq. 2-70) applies even to an EXPLOSAFE-equipped tank car.

2.4 Torch Fire Thermal Analysis

The principal difference between the thermal analysis of a tank car enveloped by a pool fire and a tank car heated locally by a torch fire relates, of course, to the external boundary conditions. The pool fire and torch fire thermal models will be the same in most respects so the forthcoming discussion of the torch fire analysis will be relatively brief. The external boundary conditions for the torch fire analysis are considered in the next section and the section after that deals with the effect that EXPLOSAFE foil will likely have on the probability and consequences of dryout of the liquid-wetted tank wall. Dryout of the tank wall as a result of torch impingement is considered unlikely, for reasons that will be discussed later, but it is a possibility that cannot be completely discounted. Other differences between the pool and torch fire thermal models are considered in Sect. 2.4.3.

2.4.1 External Boundary Conditions

The external boundary conditions needed in the torch fire analysis are, of course, those associated with the torch itself. Characterizing a torch fire for the purpose of estimating heat transfer rates from the torch to a surface in its path is, unfortunately, a matter that has received very little attention in the heat transfer literature. Kremer et al. (25) measured heat transfer rates from turbulent free jet flames to plane surfaces and, while they obtained some results that can be used in this study as will be shown shortly, they did not present enough information to calculate stagnation point heat transfer coefficients without having a priori knowledge of jet velocities. A complete model would predict jet velocities as well as the resulting heat transfer coefficients, of course. Heat transfer from an axisymmetric jet to a flat or concave surface in its path has been studied by several investiagtors, for instance Martin (26), Chan (27), Gardon and Akfirat (28), Hrycak (29), Vallis et al. (30), Perry (31) and Gardon and Cobonpue (32), but a torch cannot be represented as a hot non-reacting gas jet except at large distances from the fuel source (ie. outside of the reaction zone) and it is difficult, even then, to determine the parameters needed to apply the axisymmetric gas jet heat transfer correlations to the torch heat transfer analysis. It is probably not impossible to characterize a torch at large distances from its origin in terms of the parameters used to characterize a hot gas jet, which are usually the nozzle Reynolds number (ie. a Reynolds number based on the nozzle diameter and the velocity and kinematic viscosity of the fluid at the throat of the nozzle), the distance from the nozzle to the surface placed in its path, the nozzle diameter and the radial distance from the axis of the jet to some point on the surface in its path, but it is considered outside of the scope of this investigation to attempt to do so. While the nozzle Reynolds number is important because it affects the level of turbulence in the jet, it is difficult to relate the nozzle Reynolds number, or equivalently the turbulence level, in a combustible jet before combustion to either an effective Reynolds number, or the turbulence level, of the jet after combustion, for instance. The mass flow rate of propane vapor feeding a torch can often be calculated - it would be approximately 28kg/sec. for a torch fed by propane escaping from a full-size tank car at 2.07MPa (300psia) through the standard 50.7cm^2 (7.86in^2) relief valve area for instance - but it is extremely difficult to relate the known nozzle conditions to the torch temperature and heat transfer coefficients on a surface located an arbitrary distance from the nozzle. It is this relationship that would be desirable, of course. Because the heat transfer characteristics of torch fires are highly variable, it is proposed that a simple, largely empirical, model of those characteristics be used until addtitional experimental data becomes available.

A torch fire in a tank car derailment situation will be fed by flammable fluid (eq. LPG) escaping from either a punctured tank or an open pressure relief device (ie. a safety valve, rupture disc, or fusible plug). The fuel source for the torch could be either vapor or liquid depending on whether the aperture through which the fluid was being discharged was located above or below the surface of the liquid in the feed tank. A liquid-fed torch would probably not be as serious as a vapor-fed torch, as noted by Mandl (33), because the liquid would have to vaporize before it could mix with the surrounding air and ignite. The vaporization process would absorb large amounts of heat from the surrounding air, thereby lowering the temperature of the air and slowing reaction rates with the fuel. Combustion would likely be very incomplete under those circumstances. Combustion will also be incomplete with a vapor-fed torch due to imperfect mixing of the fuel with the air but reaction rates will nevertheless be much more rapid than in the liquid-fed case because the fuel will already be in the vapor state when it is discharged from the feed tank. Since a vapor-fed torch is envisaged as being more serious than a liquid-fed torch and since, in addition, a small amount of experimental data is available for a torch of the former type while none is available for the latter, only the vapor-fed torch will be considered further.

For the purpose of describing the structure of a torch and modelling its heat transfer characteristics, reference will be made to the torch-centered coordinate system shown in Fig. 2-42. It is assumed that the torch is axisymmetric and radial and axial coordinates, designated x and y respectively, are defined relative to the origin of the torch (ie. the puncture or pressure relief device). Axial coordinates are measured along the axis of the torch, of course. It will be assumed that the torch impinges on any surface (ie. the tank surface) placed in its path at right angles.

Competing mechanisms cause the heat transfer characteristics of a torch to vary markedly both along its axis and radially. The velocity of the torch and hence convective heat transfer coefficients on any surface placed in its path are very high at the torch origin but the torch temperature is low at that point because combustion has not yet started.

The net result of these factors is that heat transfer rates to a surface placed in the path of a torch are low near the torch origin. Flame temperatures and hence heat transfer rates to the surface increase initially as y increases, and reaction rates peak, but then start to decrease, not necessarily simultaneously, as reaction rates slow and entrainment of the surrounding air causes gas velocities in the torch to drop. The result of these effects is that the heat transfer rate to a surface placed in the path of the torch rises to a maximum value at some distance from the torch origin and then falls off, as shown in Fig. 2-43 (taken from the paper by Kremer et al. (25)) for a partly premixed methane-air torch. The heat transfer rate is usually a maximum at the axis (ie. at $x = 0$) at a given value of y, as seen in Fig. 2-44 (also taken from (25)) which shows the ratio of the local heat flux $\dot{q}$ to the peak heat flux ($\dot{q}_{max}$) shown in Fig. 2-43 (ie. approximately 38.5×10^4 kcal/m^{2}h or 447,000 W/m^2 $Re_d = 22700$) as a function of x/d for different values of y/d,

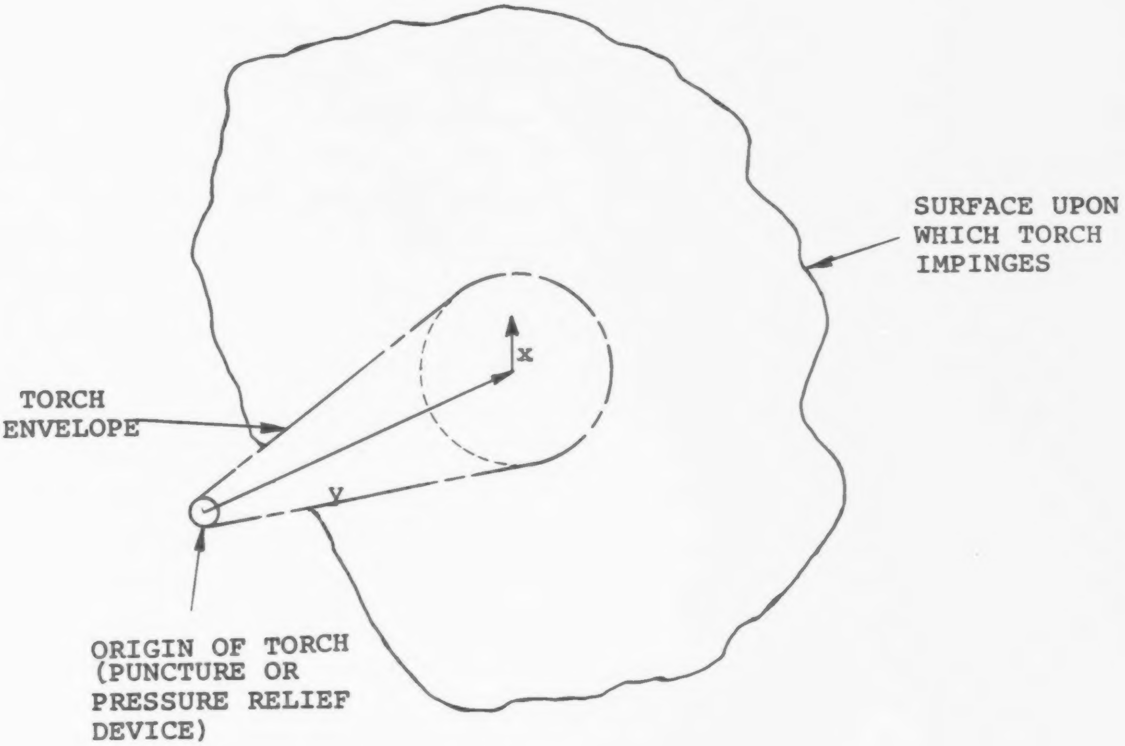
SURFACE UPON
WHICH TORCH
IMPINGES
x
TORCH
ENVELOPE
y
ORIGIN OF TORCH
(PUNCTURE OR
PRESSURE RELIEF
DEVICE)

Fig. 2-42: Torch Structure

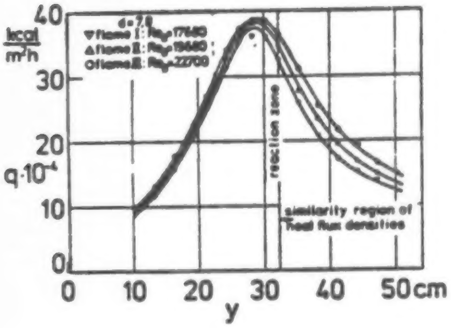

Fig. 2-43:

Axial heat flux density distributions for various Reynolds numbers

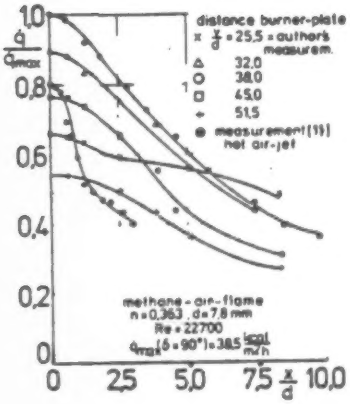

Fig. 2-44:

Radial heat flux density distributions for various distances from the burner nozzle

where d is the diameter of the nozzle orifice.

According to Kremer et al (25), the heat flux ($\dot{q}$) at the stagnation point (ie. at $x=0$) of a torch (or really any hot gas jet) impinging on a flat surface at right angles is given by the expression,

$$\dot{q} = 0.195 K_f (P_r)^{-0.6} \rho_e V_{st} \, \Delta h \qquad 2\text{-}100$$

where Pr is the Prandtl number of the torch gases, ρ_e is the density of the torch gases at the torch temperature (T_{tf}), V_{st} is the centerline velocity of the torch jet as it approaches the surface (before impingement) and Δh is defined by the expression,

$$\Delta h = h_e - h_s \qquad 2\text{-}101$$

where h_e is the enthalpy of the torch (combustion) gases at the torch temperature T_{tf} and h_s is the enthalpy of the same gases at the temperature of the surface on which the torch impinges (T_s). The factor K_f in Eq. 2-100 is an empirical factor which Kremer et al. found to have a value of 0.19 for partly premixed methane-air torch flames. Figure 2-45 shows the agreement Kremer et al. obtained between measured and predicted (using Eq. 2-100) stagnation point heat fluxes at different values of y for different nozzle Reynolds numbers (the value of V_{st} depends on the nozzle Reynolds number, Re_d) using measured values of T_{tf}, T_s and V_{st}. The agreement between the predicted and experimental results is obviously quite good.

Equation 2-100 can be used to predict the stagnation point heat flux for a torch impinging on a flat surface at right angles if the values of T_{tf}, T_s and V_{st} are known. The

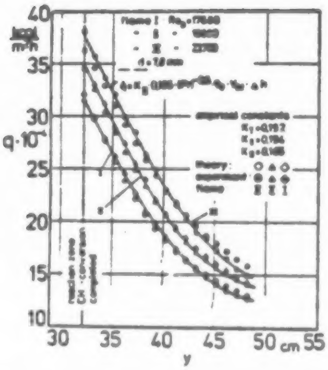

Fig. 2-45:

Calculated and measured heat flux density distributions at the stagnation point of turbulent, partly pre-mixed methane-air flames

stagnation point heat transfer coefficient (h_{st}) can be obtained easily from Eq. 2-100 if the specific heat of the torch gases (C_{pt}) is not strongly temperature dependent in the temperature range $T_s \leqslant T \leqslant T_{tf}$ because Δh can be written in the form,

$$\Delta h = \bar{C}_{pt}(T_{tf} - T_s) \tag{2-102}$$

in that case, where $\bar{C}_{pt}$ is the torch gas specific heat evaluated at $T = (T_{tf} + T_s)/2$. This simplification allows h_{st} to be written as,

$$h_{st} = 0.195K_f(Pr)^{-0.6}\ \rho_e V_{st}\bar{C}_{pt} \tag{2-103}$$

Equation 2-103 (or Eq. 2-100) can be evaluated for the DOT standard torch because the values of T_{tf} and V_{st} are specified for that torch in DOT Docket HM-144 (1).
The HM-144 specifications require that the torch centerline velocity (V_{st}) be 40 miles per hour (17.8m/s) plus or minus 10 miles per hour and that the torch temperature (T_{tf}) be 2200°F (1204°C or 1477K) plus or minus 100°F during the duration of the torch test. Assuming that the thermophysical properties of the torch gases are approximately the same as those of air, the specific heat of the gases will vary from 1008 J/kg°C at an assumed minimum surface temperature of 325K to 1226 J/kg°C (3) at the specified flame temperature of 1477K. Since this variation is not large, an average specific heat ($\bar{C}_{pt}$) of $(1008+1226)/2 = 1117$ J/kg°C can be used in Eq. 2-103 to evaluate h_{st}. Taking ρ_e to be the density of air at 1477K, which is 0.239 kg/m^3, the stagnation point heat flux for the DOT standard torch can be calculated as,

$$\begin{aligned} h_{st} &= (0.195)(0.19)(0.696)^{-0.6}(0.2392\ \mathrm{kg/m^3})(17.8\ \mathrm{m/s})(1117\ \mathrm{J/kg^{\circ}} \\ &= 219\ \mathrm{W/m^{2\circ}C} \end{aligned}$$

when K_f is assigned the value of 0.19 obtained by Kremer et al. The Prandtl number used in the preceding calculation (ie. 0.696) is the Prandtl number of air at an assumed film temperature of $(1477+325)/2=901K$. The Prandtl number of air varies from 0.702 at 325K to a minimum of 0.680 at 500-600K and then back up to 0.705 at 1477K so its variation within the temperature range of interest is almost negigible.

Experimentally determined values of h_{st} for the torch used to evaluate candidate tank car thermal insulations at the FRA/BRL Torching Facility in Aberdeen, Maryland are given by Eggers et al. in (34). The FRA/BRL torch satisfies the DOT standard torch specifications prescribed in HM-144 so the values of h_{st} measured for that torch can be compared directly to the previously predicted value of 219 $W/m^2{}^oC$. Eggers et al. obtained values of h_{st} for the FRA/BRL torch from heating rate data given by Anderson (35) for a 1.59cm (5/8") thick steel plate (with insulation only on the back side) being heated from 20^oC to 427^oC (800^oF) by the torch. Anderson's experimental data indicated that the torch heat flux ($\dot{q}$) was related to the temperature of the backside of the plate (T_b) by the equation,

$$\dot{q}=2.1x10^5-279.9T_b \qquad 2\text{-}104$$

for $\dot{q}$ in W/m^2 and T_b in ^oC. Eggers et al. simply divided $\dot{q}$ by the temperature difference $(T_{tf}-T_b)$, where $T_{tf} = 1204^oC$, to obtain h_{st} at a given plate temperature, a procedure which is not completely correct because h_{st} should have been calculated from the temperature of the front surface of the plate rather than from the temperature of the back surface. It can be shown that these two temperatures would not have differed by more than about 20^oC, however, so calculating h_{st} from T_b would have introduced little error. Equation 2-104 is only applicable for $20^{\circ}C \leqslant T_b \leqslant 427^{\circ}C$ and gives values for h_{st} of 173 $W/m^2{}^{\circ}C$ at $20^{\circ}C$ and 117 $W/m^2{}^{\circ}C$ at $427^{\circ}C$. These values agree with the values of h_{st} given be Eggers et al., who used Eq. 2-104 to obtain h_{st} at temperatures beyond its range of applicability (ie. at temperatures greater than $427^{\circ}C$). Equation 2-104 is clearly incorrect at high temperatures because, according to it, $\dot{q} = 0$ at $T_b = 750^{\circ}C$ whereas, in reality, $\dot{q}$ will not be zero until the flame temperature ($1204^{\circ}C$) and T_b are approximately equal. Furthermore, Kremer et al. measured torch heat fluxes at different surface temperatures and found that the stagnation point heat transfer coefficient (h_{st}) was essentially independent of surface temperature, as shown in Fig. 2-46. The value of h_{st} obtained from Eq. 2-104 with $T_b = 20^{\circ}C$ (ie. 173 $W/m^2{}^{\circ}C$) is in fairly good agreement with the value of 219 $W/m^2{}^{\circ}C$ predicted using Eq. 2-103 in that it is only 21% less than the latter value. The value of 117 $W/m^2{}^{\circ}C$ obtained for h_{st} from Eq. 2-104 with $T_b = 427^{\circ}C$ is not in good agreement with the predicted value of 219 $W/m^2{}^{\circ}C$,but the author feels that the accuracy of Eq. 2-104 at high temperatures is very questionable for the reasons given previously. Equation 2-103 will therefore be used in the DE tank car model to predict the torch flame stagnation point heat transfer coefficient (h_{st}) for user-specified values of $\bar{C}_{pt}$ ρ_e, K_f, and V_{st}.

The variation of the torch-to-surface heat transfer coefficient (h_t) with x (ie. with radius) remains to be determined. The temperature of the radially deflected flames sweeping across the surface will obviously also vary with x but values of h_t are usually calculated by dividing the local heat flux ($\dot{q}$) by the difference between the centerline torch temperature (T_{tf}) and the local surface temperature (T_s) since this eliminates the need to know both the flame temperature and h_t as functions of x. Thus h_t is expressed as,

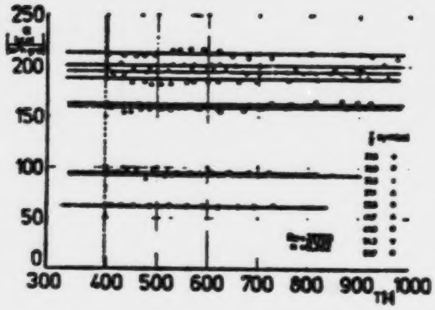

Fig. 2-46: **Influence of probe surface temperatures on the heat transfer coefficient for various axial distances between plate and burner**

$$h_t = \frac{\dot{q}}{T_{tf} - T_s} \qquad 2\text{-}105$$

and $\dot{q}$ can be calculated if $h_t(x)$ is known.

The functional relationship between h_t and x is more difficult to predict than the stagnation point heat transfer coefficient. It is well known that the ratio $h_t(x)/h_{st}$ is a function only of x/y for a fully-developed turbulent free jet so if x, y (the distance between the surface and the jet origin) and h_{st} (at y) are known the value of $h_t(x)$ can be calculated. The relationship between $h_t(x)/h_{st}$ and x/y is shown in Fig. 2-47 (taken from Perry (31)). Since the $h_1(x)/h_{st}$ vs. x/y plot shown in Fig. 2-47 applies at all values of y (ie. at all axial positions along the jet), the $h_t(x)/h_{st}$ profiles are said to be similar at all values of x/y and Fig. 2-47 is termed a similarity plot. Kremer et al. note in Fig. 2-43 that the similarity region for a torch flame (ie. the region in which $h_t(x)/h_{st}$ profiles are similar) starts at the end of the reaction zone (ie. after combustion has stopped.). The h_t/h_{st} profile in Fig. 2-47 could only be applied to a torch flame if an effective value of y for the torch (this value of y would be the value for a turbulent free jet having the same velocity profile as the torch jet) could be obtained in some manner. Assuming a value of y for the torch would suffice to determine the entire $h_t(x)/h_{st}$ vs. x distribution, where h_{st} is assumed known (from Eq. 2-103) of course.

---

* The distance y for a turbulent free jet is actually measured from the "apparent" jet origin, which is the apex of the conical envelope surrounding the fully developed jet. The locations of the apparent jet origin and the real jet origin (the nozzle) are usually only spaced a few nozzle diameters apart so the distinction between these two origins is only important in regions very close to the nozzle.

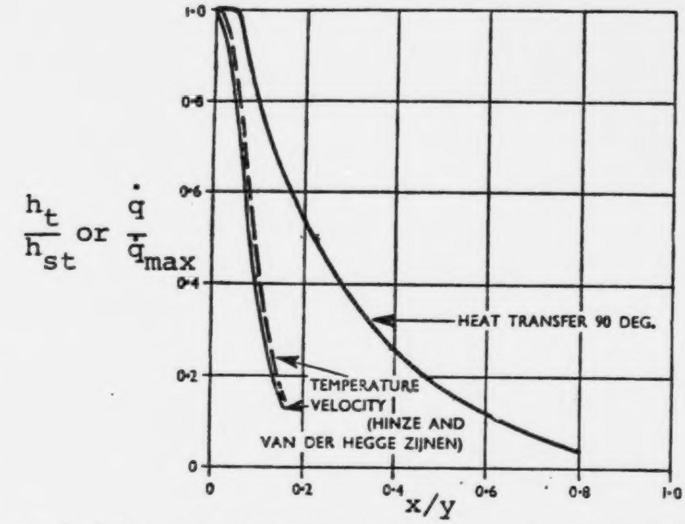

Fig. 2-47: Radial Distribution of Heat Transfer from a Jet Striking a Plane Surface at 90 deg., Compared with the Radial Distributions of Velocity-temperature for a Free Jet (Hinze and van der Hegge Zijnen)

The value of y for a turbulent free jet having the same velocity profile (at y) as the DOT standard torch can be calculated in the following manner. First, it will generally be possible to calculate the momentum of the torch jet at the nozzle discharge from the geometry of the nozzle and the state of the propane lading in the feed tank. For the BRL torch fire apparatus, which uses a 0.952 cm (3/8") diameter orifice fed by saturated propane at a pressure of approximately 1.45 MPa (210 psia), it can be shown that the mass flow rate of vapor through the nozzle must be approximately 0.237 kg/sec. and that the velocity of the vapor at the nozzle exit must be approximately 250 m/sec (assuming that the nozzle is a sharp-edged orifice and that the propane expands isentropically to the nozzle pressure without condensing at all), for instance. The momentum of the vapor jet leaving the nozzle, designated M_i, is thus approximately 0.237 kg/sec x 250 m/sec. =59.25 N for the BRL torch. The pressure at the nozzle exit (p_d), which must be greater than atmospheric pressure (p_d) because the nozzle is choked, can be calculated approximately from the equation for the critical pressure ratio, viz.

$$\frac{p_d}{p_o} = \left(\frac{\gamma+1}{2}\right)^{\gamma/1-\gamma} \qquad 2\text{-}106$$

where p_o is the reservoir pressure (1.447 MP_a) and γ is the ratio of specific heats for propane vapor ($= 1.14$) Substituting the appropriate values of γ and p_o into Eq. 2-106, we obtain $p_d = 0.576 \times 1.447 = 0.834$ MP_a (121 psia). Expansion waves will form outside of the nozzle to reduce the jet pressure from p_d to atmospheric. With the conditions at the nozzle discharge known, a momentum balance can be performed in the y direction on a control volume cutting through the vapor jet at the nozzle discharge and cutting through the torch at some distance $\bar{y}$ from the nozzle, where the static pressure in the torch jet is assumed to be atmospheric and the total momentum of the jet is M. The remaining boundaries of the control volume are assumed to be far enough away from the torch axis so that no fluid passes through them, as shown in Fig. 2-48. Performing a momentum balance in the y-direction on the control volume shown in Fig. 2-48, we obtain the equation,

$$M = (p_d - p_a)A_d + M_i \qquad 2\text{-}107$$

where A_d is the nozzle discharge area ($= 7.13 \times 10^{-5}\,m^2$ for the 0.952 cm diameter BRL nozzle). The momentum, M, of the torch jet at the distance $\bar{y}$ from the nozzle can be calculated from the known nozzle discharge conditions by applying Eq. 2-107. For convenience, the sum of the terms on the right-hand side of that equation will be termed the effective initial momentum of the jet, designated M_{ie}, so Eq. 2-107 indicates that the jet momentum, M, is constant and equal to M_{ie} once the jet pressure has dropped to atmospheric. Note that $p_d = p_a$ if the nozzle is not underexpanding and that the jet momentum is constant at all values of y in that case. For the BRL nozzle,

$$\begin{aligned} M_{ie} &= (p_d - p_a)A_d + M_i \\ &= .733 \times 10^6 \frac{N}{m^2} \times 7.13 \times 10^{-5}\,m^2 + 59.25\,N \\ &= 111.5\,N \end{aligned}$$

If the centerline velocity and temperature of the torch jet are known at $y = \bar{y}$, where it is assumed that the distribution of h_t is required, and if the velocity and temperature profiles

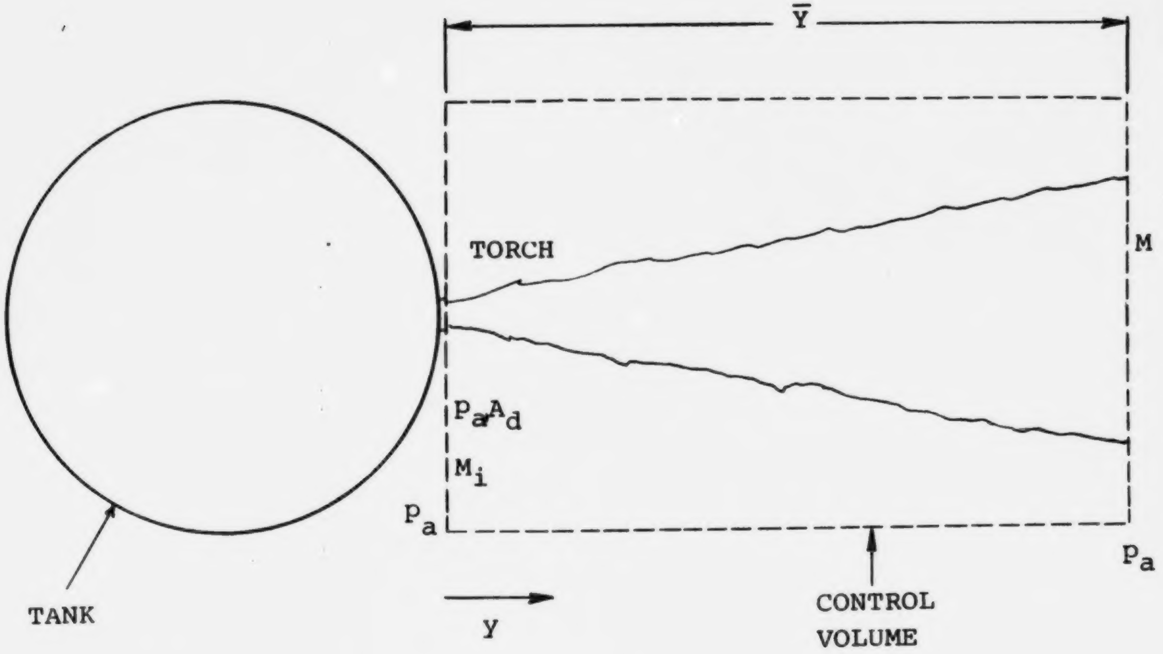

$\overline{Y}$
TORCH
M
$p_a A_d$
M_i
p_a
p_a
TANK
y
CONTROL VOLUME

Fig. 2-48: Torch jet control volume

at $\overline{y}$ can be obtained as functions of x and one other paramter, say the value of y for a non-combustible turbulent free jet which has the same velocity and temperature profiles as the torch jet does at $\overline{y}$, then the value of that parameter (y) can be obtained from Eq. 2-107 in the following manner. According to Görtler (36), the velocity profile in a turbulent free jet is given by the expression,

$$\frac{V}{V_{st}} = \left(1 + \frac{\eta^2}{4}\right)^{-2} \qquad 2\text{-}108$$

where $\eta = \sigma x/y$, $\sigma \approx 15.2$ and V is the local axial velocity at x. Since Hinze and van der Hegge Zijnen (37) demonstrated that the velocity and temperature profiles in a fully-developed turbulent free jet are similar (see the velocity and temperature distributions plotted in Fig. 2-47), we can also write,

$$\frac{T - T_a}{T_{max} - T_a} = \left(1 + \frac{\eta^2}{4}\right)^{-2} \qquad 2\text{-}109$$

where T_{max} $(= T_{tf})$ is the torch centerline temperature, T is the temperature at x, and T_a is the ambient temperature. Assuming that the gas in the jet behaves as a perfect gas, the gas density (ρ_g) at temperature T is given by the expression,

$$\rho_g = \frac{p_a}{RT} = \frac{p_a}{R\left(T_a + \frac{(T_{max} - T_a)}{(1 + Cx^2)^2}\right)} \qquad 2\text{-}110$$

where p_a is atmospheric pressure, R is the gas constant $(= 0.287$ kN-m/kg K for air and assumed the same for the torch gases) and $C = \sigma^2/4y^2 = 57.76/y^2$ for $\sigma = 15.2$. The total momentum of the jet, designated M, can now be calculated from the expression,

$$M = \int_{o}^{x_{max}} \rho_g V^2 2\pi \quad xdx$$

$$= \frac{2\pi p_a V_{st}^2}{R} \int_{o}^{x_{max}} \frac{xdx}{T_a(1+Cx^2)^4 + (T_{max}-T_a)(1+Cx^2)^2}$$

2-111

where x_{max} is the radius of the outer boundary of the jet. Evaluating the integral in Eq. 2-111 gives M as,

$$M = \frac{-\pi p_a V_{st}^2}{CR} \left[\frac{1}{(T_{max}-T_a)u} + \frac{\sqrt{T_a}}{(T_{max}-T_a)^{3/2}} \tan^{-1} u \sqrt{\frac{T_a}{T_{max}-T_a}} \right]_{u=1}^{u=u_{max}}$$

2-112

where $u = 1 + \eta^2/4 = 1 + Cx^2$ ($u = 1$ whene $x = 0$ and $u = 1 + Cx^2_{max}$ when $x = x_{max}$). According to White (38), $\eta \simeq 3.2$ at the outer boundary of a turbulent free jet (this result was obtained experimentally) so $u = 1 + \eta^2/4 = 3.56$ at $x = x_{max}$. Thus the upper limit of integration in Eq. 2-112 (U_{max}) can be replaced by 3.56. Substituting values of p_a, V_{st}, R, T_a and T_{max} into Eq. 2-112 allows M to be expressed as a function of C and equating M to the initial effective momentum of the torch jet at the nozzle exit gives the value of $C (= 57.76/y^2)$ and thus the required value of y. For the DOT standard torch, $V_{st} = 17.8$ m/sec., $T_{max} = 1477$ K, $T_a = 293$ K (assumed), $p_a = 101$ Kp$_a$ (assumed) and $R = 0.287$ kN-m/kg K, so Eq. 2-112 simplifies to,

$$M = \frac{125.2}{C} \qquad 2\text{-}113$$

Equating M to M_{ie} ($=111.5$ N), we obtain $C = 1.123$ and $y = \sqrt{57.76/C} = 7.2$ m for the BRL torch. This value of y is how long a non-combustible turbulent free jet would have to be in order to have the same velocity and temperature profiles at its end as the BRL torch has at the target plate and hence is the value of y that should be used with the h_t/h_{st} vs. x/y profile given in Fig. 2-47 to obtain h_t as a function of x.

Since the target plate in the BRL torch fire test facility is located 3.7 m from the nozzle discharge, the effective value of y just calculated (7.2 m) seems reasonable. This value can be checked however, because Anderson et al. (35) measured the temperature profile in the BRL torch at the point where the torch temperature and velocity were the DOT standard values of 1204°C and 17.8 m/sec. respectively. The torch temperature profile measured by Anderson et al. should agree with the profile predicted using Eq. 2-109, written here as,

$$\frac{T-T_a}{T_{max}-T_a} = \left(1 + \frac{\eta^2}{4}\right)^{-2}$$

$$= (1 + 1.123x^2)^{-2} \qquad 2\text{-}114$$

for $y = 7.2$ m. Results obtained using Eq. 2-114 are compared to the experimental results given by Anderson et al. in Fig. 2-49 and, considering the approximate nature of the analysis and the complexity of the phenomenon being modelled,

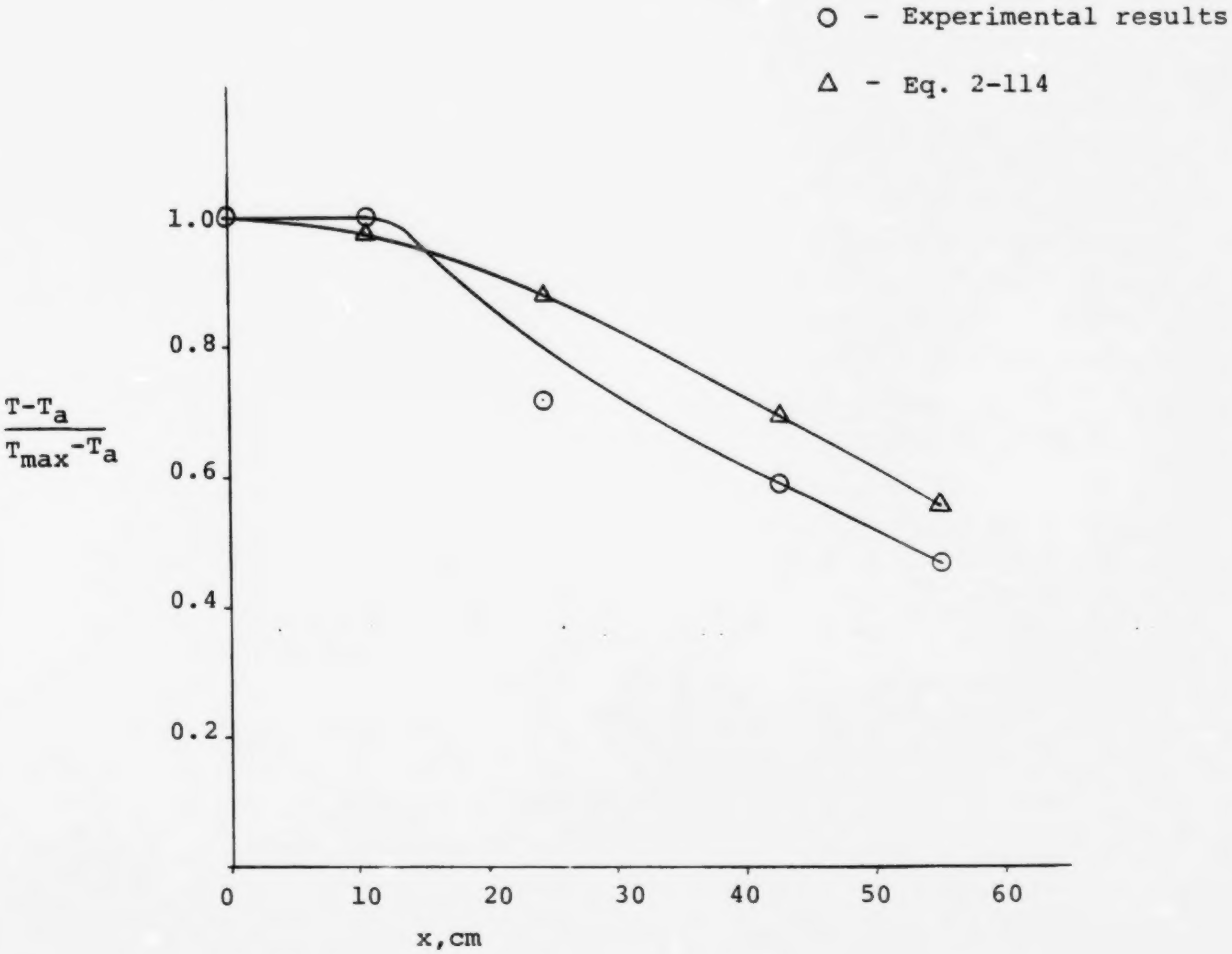

Fig. 2-49: Comparison of measured and predicted (using Eq. 2-114) temperature profiles for the BRL torch at the axial coordinate where the torch centerline temperature and velocity are the DOT standard values.

the agreement is considered quite good. Thus the effective value of y needed to obtain h_t as a function of x from Fig. 2-47 will be evaluated using Eq. 2-112 for user-specified values of $T_{tf}(=T_{max})$, T_a and V_{st} in the DE tank car model. Note that the effective value of y for the BRL torch could have been obtained by finding the value of y which, when substituted into the equation for the torch temperature profile (ie. Eq. 2-109), gave the best agreement with the measured profile shown in Fig. 2-49. The value of y thus obtained would only have applied to the BRL torch, however, whereas Eq. 2-112 permits y to be calculated for any torch if M_{ie} (ie. the nozzle discharge conditions), V_{st} and T_{tf} are known. It is also possible to obtain an estimate of the effective value of y by performing an energy balance on the torch jet and, since the energy analysis follows easily from the momentum analysis just described and can serve as a check on the correctness of the latter analysis, the energy balance approach will be considered briefly.

If it is assumed for simplicity that,

a) combustion of the propane vapor issuing from the nozzle is complete,

b) the radiative heat loss from the torch to the surroundings is negligible,

c) the properties of the torch gases are the same as those of air,

d) kinetic energies are negligble compared to thermal and chemical energies, and

e) water produced as a by-product of combustion is present as a vapor in the torch (ie. the torch temperature, T_{tf}, is greater than 100^oC at any point of interest),

then the energy balance equation for the torch jet can be written as,

$$\dot{m}(L.C.V = \int_{0}^{x_{max}} \pi 2 \, \rho_g V \, \bar{C}_{pt}(T-T_a)\, x \, dx \qquad 2\text{-}115$$

where $\dot{m}$ is the mass flow rate of propane vapor issuing from the nozzle and L.C.V. is the lower calorific value of gaseous propane (= 46,353 kJ/kg). The left-hand side of Eq. 2-115 is simply the combustion energy of the fuel while the right-hand side is the thermal energy of the jet at some cross-section past the end of the reaction zone. Substituting Eqs. 2-108 to 2-110 into Eq. 2-115 we obtain,

$$\dot{m}(LCV = \frac{2\pi}{R} \, \bar{C}_{pt} \, P_a \, V_{st} \, (T_{max}-T_a) \int_{0}^{x_{max}} \frac{x dx}{T_a(1+Cx^2)^4 + (T_{max}-T_a)(1+Cx^2)^2} \qquad 2\text{-}116$$

The integral in Eq. 2-116 is the same as that in Eq. 2-111 so the former equation can be rewritten as,

$$\dot{m}(L.C.V. = -\frac{\pi \bar{C}_{pt} \, P_a \, V_{st} \, (T_{max}-T_a)}{CR} \left[\frac{1}{(T_{max}-T_a)u} + \frac{\sqrt{T_a}}{(T_{max}-T_a)^{3/2}} \tan^{-1} u\sqrt{\frac{T_a}{T_{max}-T_a}} \right]_{u=1}^{u=3.56} \qquad 2\text{-}117$$

For LCV = 46,353 kJ/kg, V_{st} = 17.8 m/sec., T_{max} = 1477 K, T_a = 293 K, P_a = 101 kP_a, $\bar{C}_{pt}$ = 1117 J/kgK and R = 0.287 kN-m/kgK Eq. 2-117 simplifies to

$$\dot{m} = \frac{0.2007}{C} \qquad 2\text{-}118$$

where $C = 57.76/y^2$ as before. For the BRL nozzle, $\dot{m} \simeq 0.237$ kg/sec. so solving Eq. 2-118 for C gives $C = 0.847$ or $y = \sqrt{57.76/C} = 8.26$ m. This result is in reasonably good agreement with the value of y obtained previously in the momentum balance analysis (ie. 7.2 m).

Note that Eqs. 2-112 and 2-117 are two equations that can be solved simultaneously to obtain the values of two unknowns. Since the nozzle discharge conditions can be calculated, the only unknowns are $T_{max}(= T_{tf})$, V_{st} and $y(=\sqrt{57.76/C})$ and, if y is specified, Eqs. 2-112 and 2-117 can be solved simultaneously to obtain T_{max} and V_{st}. Performing the calculations for several values of y would give T_{max} and V_{st} both as functions of y. For a given discharge flowrate ($\dot{m}$), there will probably be only one nozzle discharge velocity (V_d) that results in the DOT standard torch temperature (1204°C) and jet velocity (17.8 m/sec.) being obtained on the jet centerline at the same value of y (ie. simultaneously). Since the values of y calculated from Eqs. 2-113 and 2-118 for the BRL torch are in fairly good agreement, it can be assumed that the nozzle discharge conditions used to calculate the momentum of the jet at the nozzle discharge are approximately correct.

It is shown in Appendix G that the nozzle discharge velocity for a Midland A-3480 relief valve, which is the type of valve commonly used on full-size tank cars, must be approximately 408 m/sec. when the valve is fully open and the tank pressure is 2.07 Mp_a (300 psia). The mass flow rate of propane is approximately 28 kg/sec. for the stated conditions so the initial momentum of the jet (M_i) is roughly $28 \times 408 = 11424$ N. The nozzle discharge pressure (p_d) will be approximately atmospheric, as shown in Appendix G so the effective initial momentum (M_{ie}) will also be 11424 N. Setting M equal to

11424 N in Eq. 2-113 and solving for C, we obtain $C = 0.0109$ so $y = \sqrt{57.76/C} = 72.6$ m*. From the results obtained previously for the BRL torch, we would expect the DOT standard conditions ($V_{st} = 17.8$ m/sec., $T_{tf} = 1204^{o}C$) to prevail at a distance of approximately (3.7 m/ 7.2 m) x 72.6 m = 37.3 m (122') from the discharging relief valve since the nozzle-to-target plate distance and effective value of y for the BRL torch were 3.7 m and 7.2 m respectively. Considering the large mass flow rate of the valve torch (28 kg/sec. or 118 times the flow rate for the BRL torch), this distance seems reasonable and it is also reasonable as the distance the torch might have to travel before impinging on another tank car. Since $\eta = \sigma\, x/y = 15.2\, x/77.5 \approx 3.2$ at the outer boundary of the torch jet at the point where the torch centerline velocity and temperature are the DOT standard values, the radius of the torch (x_{max}) at that point will be approximately $72.6 \times 3.2/15.2 = 15.3$ m. Since the diameter of a DOT 112 or 114 tank car is only 3 m, the diameter of a large valve-fed torch may be much greater than the diameter of the tank on which it impinges, at least according to the results of the preceding analysis. This would be a very serious situation. It can be shown that the diameter of the BRL torch must be about 3 m, so even this relatively small torch would heat a large area on a full-size tank.

The rapid growth and large size of a valve torch shown in Fig. 25 in TP2740 (21) lends credibility to the torch size calculations given here. The valve torch photograph also shows that almost no smoke was produced by the torch, in contrast to the dense black smoke produced by the pool fire, and hence suggests that combustion in the torch was essentially complete. The highly luminous part of a torch presumably defines the reaction zone where, because of the flame luminosity, radiation must be a significant heat transfer mechanism (at least for large torches with correspondingly large flame thicknesses). Since Eq. 2-100 really only defines the convective heat transfer rate between a torch jet and a surface (at the torch stagnation point), radiative heat transfer between the torch and the surface would have to be calculated in the manner described previously for the pool fire heat transfer analysis if the surface was located inside the torch's luminous zone. The effective flame emissivity would be difficult to determine in such an analysis, however. It will be assumed, initially anyway, that the DOT standard conditions prevail at a point where radiation between the torch jet and the tank surface is of secondary importance.

---

* The energy conservation equation (ie. Eq. 2-118) gives $y = 89.8$ m

It was assumed in the preceding analysis that heat transfer data for a jet impinging on a flat plate can be applied to the case of a jet impinging on a convex curved surface (ie. a tank car surface). Since data given by Hrycak (29) and Chan (27) comparing boundary layer velocity profiles around a jet impinging on a convex hemispherical surface to those for a jet impinging on a flat plate indicate that the boundary layer velocity profiles for these flows are very similar, it is reasonable to assume that the corresponding heat transfer coefficients will be very similar also, at least near to the stagnation point.

2.4.2 Dryout Probability And Consequences

From the results given in the preceding section, it appears that the stagnation point heat transfer coefficient (h_{st}) for a torch flame similar to the DOT standard torch impinging on a flat surface will lie between 175 $W/m^2 {}^oC$ and 220 $W/m^2 {}^oC$. Taking the higher value and assuming that the torch temperature is approximately 1200^oC, the resulting heat flux to a surface at approximately 20^oC (ie. ambient temperature) will be $220x(1200-20) = 259{,}600\ W/m^2$. Since the critical heat flux for propane boiling at a pressure of 0.82 MPa (120 psia), which is the saturation pressure of propane at 20^oC, is likely greater than 631,000 W/m^2 (200,000 $BTU/hrft^2$) according to the data shown in Fig. 2-23, it is considered extremely unlikely that a torch impinging on the wall of an LPG-carrying tank car below the level of the liquid surface will cause the wall to dryout. It cannot be stated conclusively that dryout of an EXPLOSAFE-equipped tank car wall will not occur, of course, because it is not known how the presence of EXPLOSAFE foil in the propane will affect the CHF and, as noted in Sect. 2.3.2.4, the data shown in Fig. 2-23 applies to a horizontal surface and may not be valid for an inclined tank car surface. Dryout would also be more probable if the center of the torch coincided, approximately, with the level of the liquid surface because a heat flux "spike" similar to that shown in Fig. 2-24 would be present at the line of intersection of the liquid surface and the tank shell in that case. If the torch impinges on the tank wall below the level of the liquid surface and dryout does not occur, the tank wall inner surface temperature will not exceed the liquid temperature by more than about $15^{o}C$ and tank rupture will not occur because the strength of the tank car steel will not be degraded.

If dryout of the tank wall does occur for some reason, a thin vapor gap will separate the tank wall surface from the liquid and heat transfer between the wall and the liquid will occur by conduction across the vapor gap and by radiation. Radiation will only become significant if the tank wall temperature reaches a high value. Since EXPLOSAFE foil greatly increases the thermal conductivity of propane vapor, film boiling heat transfer coefficients will be much higher with EXPLOSAFE present than without it. It is shown below, however, that the consequences of dryout would probably not be catastrophic even if the tank car in question was not equipped with EXPLOSAFE or if EXPLOSAFE was present but had no effect on the film boiling heat transfer coefficients.

The minimum heat transfer coefficient in the film boiling regime is obtained when the film boiling heat flux is also a minimum (this occurs in region V in Fig. 2-22) so a "worst case" estimate of the consequences of dryout can be obtained by using the minimum film boiling heat transfer coefficient to obtain an estimate of the tank wall temperature under dryout conditions. An estimate of the minimum film boiling heat transfer coefficient for saturated propane at a temperature of 20^oC (68^oF) and a pressure of 0.82 MPa (120 psia) can be readily obtained from curves prepared by Sciance and Colver (39) showing the minimum film boiling heat flux for propane (q_{min}) and the corresponding excess temperature at the minimum heat flux point (ΔT_{min}) as functions of the reduced pressure, $P_r (= p/p_c$, where p_c, the critical pressure, is 4.26MPa for propane). Those curves are shown in Figs. 2-50 and 2-51. Equations giving $\dot{q}_{min}$ and ΔT_{min} in terms of fluid properties are given in (39).

At a tank pressure of 0.82 MPa, $P_r = 0.82/4.26 = 0.192$ so $q_{min} = 22{,}000$ BTU/hrft^2 from Fig. 2-50 and $\Delta T_{min} = 270^oF$ from Fig. 2-51. The minimum film boiling heat transfer coefficient is therefore $22{,}000/270 = 81.5$ BTU/hrft^{2}F = 463 W/m^2^oC. Neglecting the thermal resistance of the tank wall and taking the torch flame stagnation point heat transfer coefficient to be 220 W/m^2^oC and the torch flame temperature to be 1200^oC, the equilibrium temperature of the tank wall (T_w) for one-dimensional heat flow through the wall can be calculated from the heat balance equation,

$$220(1200-T_w) = 463(T_w-20) \qquad 2\text{-}119$$

for the assumed liquid temperature of 20^oC. Equation 2-119 predicts a wall temperature (T_w) of 400^oC (752^oF).

It can be shown (see Fig. 4-5) that the strength of the most commonly used tank car steel, TC-128, is still near its maximum value at this temperature so it can be stated almost categorically that a tank car will not rupture if a torch impinges on the tank wall below the level of the liquid

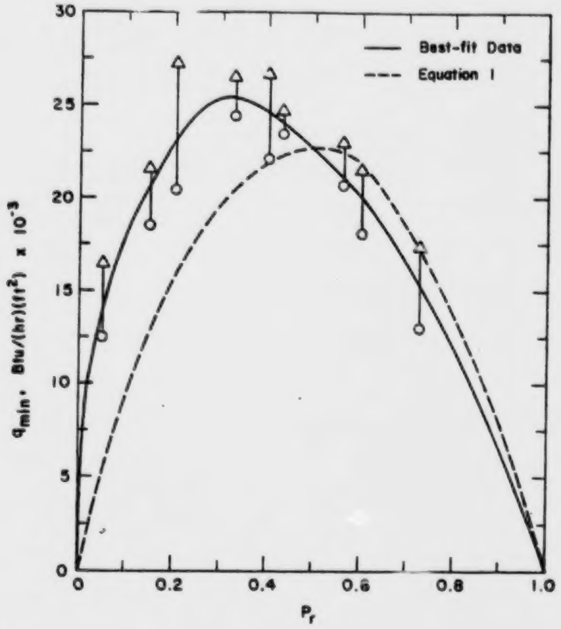

Fig. 2-50: Propane minimum film boiling heat flux vs. reduced pressure-experimental and predicted values

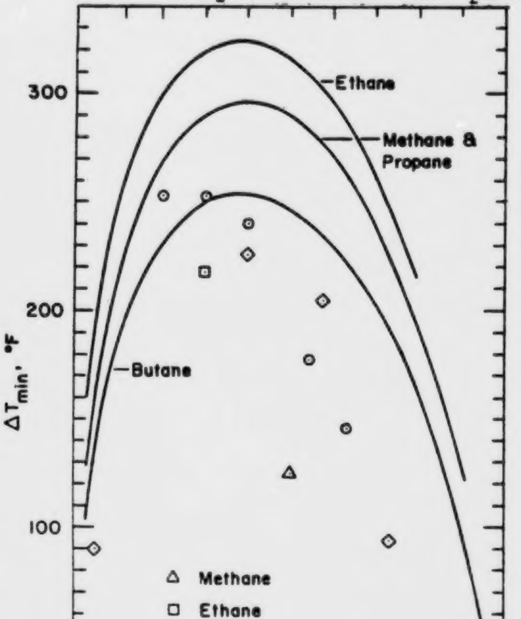

Fig. 2-51: Excess temperature at the minimum film boiling heat flux vs. reduced pressure-experimental and predicted values

surface, even if the tank wall dries out within the torch impingement area. It is therefore recommended that the case of a torch impinging on the tank wall below the level of the liquid surface be excluded as a possible case of interest.

While a liquid temperature of $20^{\circ}C$ was used in the preceding analysis, it can be shown that similar results would have been obtained with an assumed propane temperature of $57^{\circ}C$, for which the saturation pressure is 2 MPa (typical tank venting pressure), since P_r would have been 0.47 in that case and the values of $\dot{q}_{min}$ and ΔT_{min} obtained from Figs. 2-50 and 2-51 would have been almost the same as the values obtained with $P_r = 0.192$.

2.4.3 Torch Fire Thermal Model

The thermal analysis of a tank car heated locally by an impinging torch fire will be performed in three-dimensions unless the torch is very large. A large torch will produce predominantly 2-D ($r-\theta$) heat flow in a tank car which it will be possible to model in the manner already described for a pool fire (with the boundary conditions modified appropriately, of course). Since a three-dimenstional model will be used to analyse heat transfer in an unprotected tank car in a pool fire, as already discussed, the torch fire analysis for an unprotected tank car will be performed using the same model, only with torch fire boundary conditions. The user will be required to specify the location of the center of the torch on the tank surface and the other torch-related variables mentioned in Sect. 2.4.1. Grid definition subroutines similar to DTHW and DZR described in Appendix E will permit the user to refine the finite-difference grid locally in the neighbourhood of the torch impingement area and thereby model the large temperature gradients that will prevail in that region with high accuracy. Variable subdivision sizes will be permitted in the azimuthal (subroutine DTHW) and axial (subroutine DZR) directions but equi-sized subdivisions will be used across the thickness of the tank wall (ie. in the radial direction). Since a small torch will cause the liquid level to change very slowly, it will probably also be possible to refine the azimuthal mesh in a sufficiently large region around the line of intersection of the liquid surface with the tank shell to avoid having the liquid level drop below the refined region during the time period of interest. Temperature gradients and heat fluxes around the line of intersection of the liquid surface and the tank shell will be accurately modelled throughout the transient in that case. The azimuthal mesh structure for a small torch might appear, typically, like that shown in Fig. 2-53.

The thermal analysis of a protected tank car (ie. a tank car with EXPLOSAFE and/or insulation) heated locally by a small torch fire will also have to be performed in three-dimensions but it will be impossible to perform such an analysis using the implicit (backward-difference) time integration procedure for the reasons discussed in Sect. 2.1.2. The time integrations in analyses of this type will, therefore, be performed using the explicit (forward-difference) time integration method. The model will be similar in other respects to the protected tank car model described previously for the pool fire analysis and, as in the case of the model just described for an unprotected tank car subjected to a torch fire, variable azimuthal and axial subdivisions will be permitted.

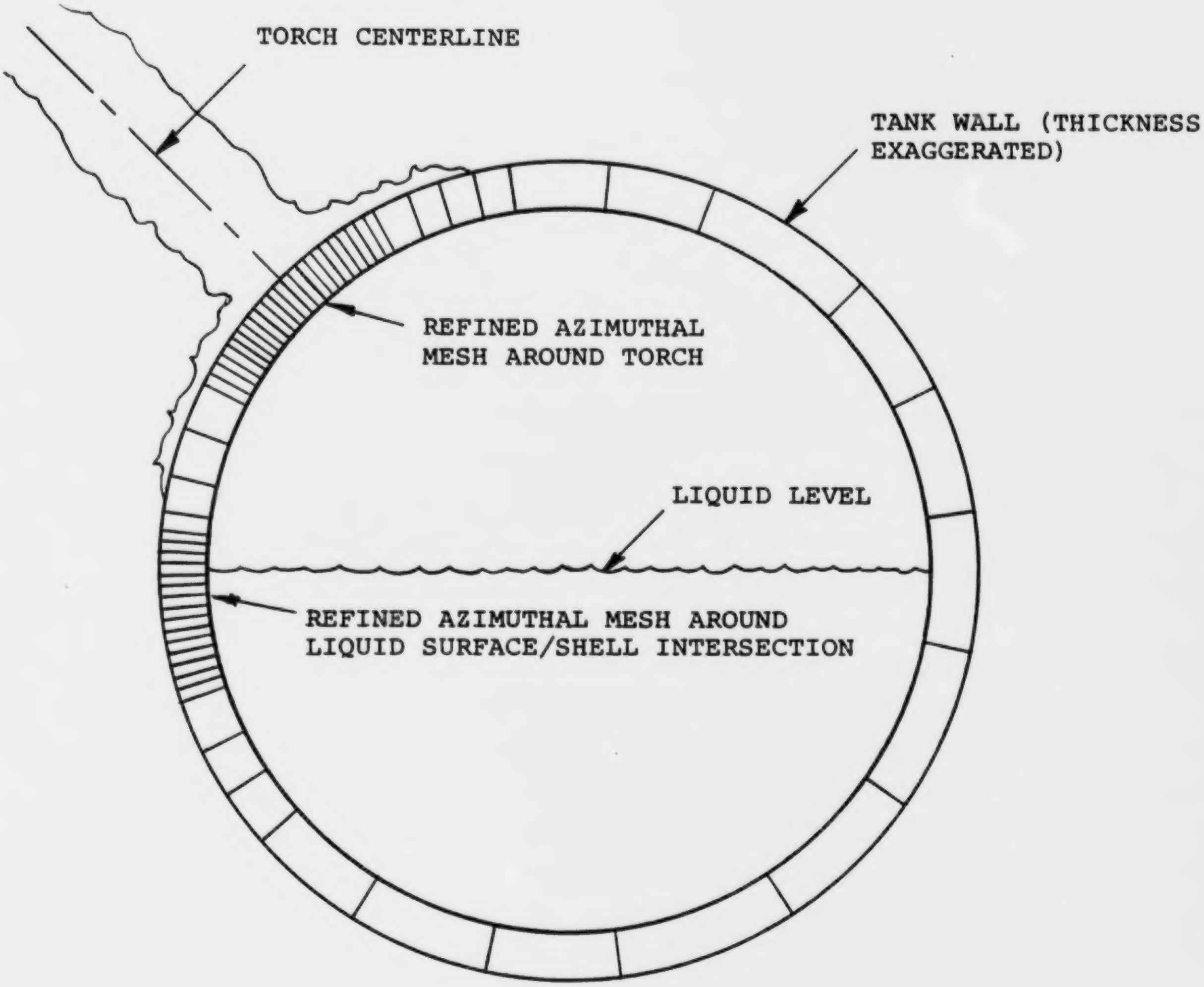
TORCH CENTERLINE
TANK WALL (THICKNESS EXAGGERATED)
REFINED AZIMUTHAL MESH AROUND TORCH
LIQUID LEVEL
REFINED AZIMUTHAL MESH AROUND LIQUID SURFACE/SHELL INTERSECTION

Fig. 2-52: Azimuthal mesh structure for torch fire analysis

2.5 Insulation Models

Two types of thermal protection systems are used on DOT 112 and 114 tank cars, specifically the spray-on coatings used on the 112T and 114T tank cars and the jacketed thermal insulations applied to the 112J and 114J cars. Insulating materials must pass pool and torch fire exposure tests specified in DOT Docket HM-144 (1) in order to be approved for use on tank cars. A typical jacketed insulation system is the system described in HM-144, consisting of Delta-board* insulation with a minimum thickness of 2.5cm (1") encased in an 11-gauge (0.119") steel jacket. Chartek 59** applied as a 0.46cm (0.18") thick coating and Thermolag 330-1*** applied as a 0.42cm (0.165") coating are approved spray-on thermal shield materials mentioned in HM-144. Chartek 59 is a charring ablative material, which means that the original, virgin material is replaced by char as it decomposes at high temperatures, while Thermolag 330-1 is a compound which sublimes and hence slowly disappears when exposed to a high incident heat flux. Other insulating materials have been approved since the issuance of DOT Docket HM-144.

Heat transfer in a jacketed insulation can be modelled using the finite-difference procedures described in Sects. 2.1.1 - 2.1.3, that is by superimposing a grid over the insulation and substituting the appropriate geometric parameters and thermal properties into the finite-difference equations for the nodes in the grid. The steel casing for the insulation will be represented by a single node in the DE tank car analysis program and the program user will be required to specify the thicknesses of the steel jacket and the insulation along with all necessary thermal properties and the number of radial subdivisions to be used across the insulation. The thermal conductivity of an insulating material is usually strongly temperature dependent so this dependence will be modelled as a linear relationship in the program. The program user will be required to specify the intercept and the slope of the thermal conductivity vs. temperature correlation. Degradation of the insulation by melting or shrinking at high temperatures will not be modelled, although a warning will be printed if the temperature of the insulation exceeds a user-specified maximum (ie. the melting temperature) at any time during the transient. An insulation which melts during a pool or torch fire should be judged unacceptable unless, as is the case with certain melting ablators (eg. Teflon), the molten material is very viscous and remains on the surface of the unmelted material to protect it.* Such materials are essentially non-porous and the low-density, highly porous insulating materials used in jacketed thermal protection systems cannot be included in that category.

---

* Manufactured by Rockwell Manufacturing Company, Leeds, Alabama.

** Manufactured by Avco, Lowell, Massachusetts.

*** Manufactured by TSI-Inc., St. Louis, Missouri.

The spray-on coatings, which are typically less than 0.5cm in thickness, are, to the author's knowledge, all ablative materials of some kind. Chartek 59 and Korotherm are charring ablative materials while Thermolag 330-1 is a subliming ablator, as mentioned previously. The thermal analysis of a subliming ablator must be performed differently from that of a charring ablator and even this classification is too simple because almost any ablator is eventually consumed by some combination of melting, charring, sublimation, oxidation and spallation. The general problem of predicting material ablation in a high heat flux environment requires the consideration of several complex degradation processes which generally interact and hence cannot be considered separately. These include thermal decomposition of the material below the surface, production of a variety of decomposition gas species, percolation of these gases through a solid-phase surface char layer, and chemical interaction between decomposition gases and the porous char near and at the char surface. Char consumption can occur by sublimation, erosion due to surface shear forces, oxidation and spallation resulting from vibration, thermal stresses and internal pressures produced by escaping decomposition gases. To solve almost any ablation problem requires a variety of detailed thermal, chemical and mechanical property data and a very sophisticated computer program that models all of the chemical,thermal and mechanical effects mentioned previously. Some programs for performing simplified ablation analyses are available but it is quite possible that as much effort would be required to properly model ablative spray-on coatings as would be required to model all other phenomena in the tank car model combined. It is also quite probable that most of the property data for commercially available ablative coatings is proprietary and hence difficult to obtain.

---

* The surface of the melt layer is usually gradually consumed so the protection offered is not indefinite.

Because spray-on coatings vary so widely in their characteristics, it is proposed that only provisions for modelling a constant thickness (ie. non-decomposing) coating with constant thermal properties be included in the tank car model initially. Heat transfer in such a coating can be analysed in a very straightforward manner using the finite-difference techniques discussed previously in this report. The program user will be required to specify the thickness and thermal properties of the coating and the number of radial subdivisions that are to be used to model it. It is expected that placing one node at the coating/tank wall interface and one node at the outer surface of the coating (ie. using one radial subdivision to model the insulating layer) will generally suffice to model such coatings because of their thinness. The simple constant thickness, constant thermal property coating model should represent a charring ablator fairly well provided the char layer remains intact and has a thermal conductivity similar to that of the virgin material.

3.0 THERMODYNAMIC MODELS

3.1 Period Before Pressure Relief

3.1.1 Tank Without EXPLOSAFE

The heat input ($\dot{Q}$) into the tank from the fire (pool or torch) simply raises the internal energy of the tank contents in the period before pressure relief, as expressed by the first law,

$$\dot{Q} = \frac{d}{dt}\left(\int_V \rho u dV\right) = \frac{dU}{dt} \qquad 3\text{-}1$$

where V is the volume of the tank, ρ and u are the local density and internal energy of the fluid in the tank respectively and $U = \int_V \rho u dV$. Since $V = V_\ell + V_v$, where V_ℓ is the volume occupied by the liquid in the tank and V_v is the volume occupied by the vapor, we can rewrite the expression defining the total internal energy in the tank (U) as,

$$U = \int_{V_\ell} \rho_\ell u_\ell dV_\ell + \int_{V_v} \rho_v u_v dV_v \qquad 3\text{-}2$$

where the subscripts ℓ and v identify quantities associated with the liquid and vapor phases respectively. If the liquid and vapor phases are assumed to be in saturated equilibrium, Eq. 3-2 can be rewritten as

$$U = M_\ell u_\ell + M_v u_v \qquad 3\text{-}3$$

where $M_\ell (= \rho_\ell V_\ell)$ and $M_v (= \rho_v V_v)$ are the masses of liquid and vapor respectively in the tank. The total mass in the tank (M) remains constant before venting starts so the expressions,

$$M_\ell + M_v = M \qquad 3\text{-}4$$

and

$$\frac{M_\ell}{\rho_\ell} + \frac{M_v}{\rho_v} = V \qquad 3\text{-}5$$

can be solved simultaneously for M_ℓ and M_v when ρ_ℓ and ρ_v are known. If a value is chosen for either the temperature (T) or the pressure (p) of the saturated mixture in the tank, then ρ_ℓ and ρ_v can both be obtained from saturation tables for propane, M_ℓ and M_v can be calculated by solving Eqs. 3-4 and 3-5 simultaneously (M and V are assumed known of course) and U can then be calculated from Eq. 3-3 using the values of u_ℓ and u_v for the assumed saturation conditions.

If the internal energy of the lading is computed at different lading temperatures before the start of the thermal analysis and stored in tabular form as a function of lading temperature, the change in the temperature of the lading from time t to time $t + \Delta t$ can be calculated from the change in internal energy, ΔU, $(= \dot{Q}\,\Delta t)$ by interpolating from the tables. The total internal energy of the propane lading in a full size DOT 112A tank car is shown as a function of the liquid fill percentage at $20^{\circ}C$ and the temperature of the tank contents in Fig. 3-1. The volume of liquid in the tank can also be obtained as a function of the liquid fill fraction at the inital temperature, say $20^{\circ}C$, and the propane temperature, as shown in Fig. 3-2.

As discussed in Sect. 2.1.2, the implicit time integration procedure, when used, will need the lading conditions at time $t + \Delta t$ in order to advance from time t to $t + \Delta t$. A heat balance equation which contained heat flow contributions

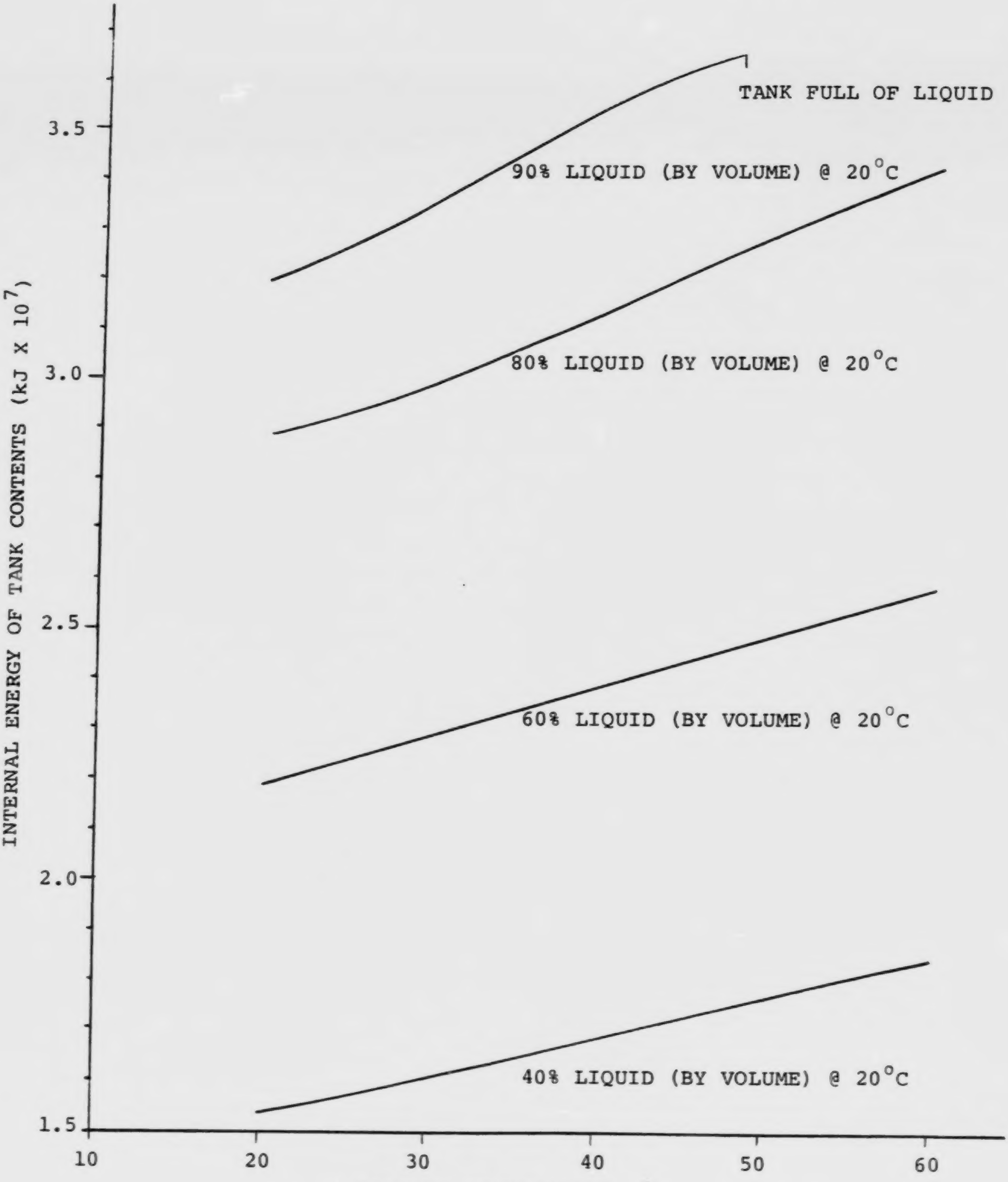

FIG. 3-1: INTERNAL ENERGY OF PROPANE LADING IN A DOT 112A (OR 114A) FULL SIZE TANK CAR AS A FUNCTION OF PROPANE TEMPERATURE AND FILL PERCENTAGE @ 20°C - NO DISCHARGE OF PROPANE

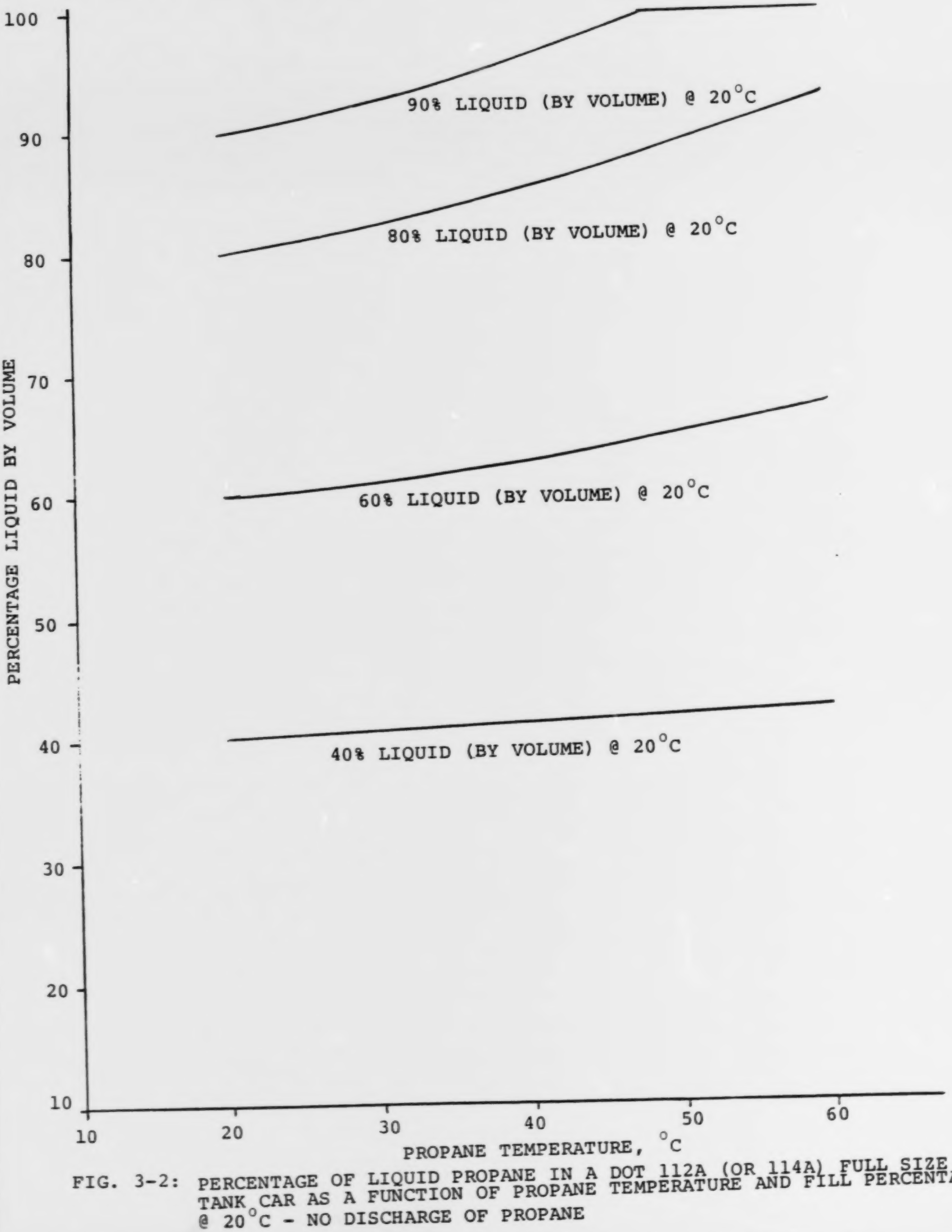

FIG. 3-2: PERCENTAGE OF LIQUID PROPANE IN A DOT 112A (OR 114A) FULL SIZE TANK CAR AS A FUNCTION OF PROPANE TEMPERATURE AND FILL PERCENTAGE @ 20°C - NO DISCHARGE OF PROPANE

from all of the tank inner surface nodes could be written for the propane lading and solved simultaneously along with the other finite-difference equations, for the lading conditions at time $t+\Delta t$. The sum of the heat flow contributions would equal

$$\frac{U^{t+1}-U^{t}}{\Delta t}$$

which would, in turn, be approximately equal to $\frac{dU}{dT_p}\frac{(T_p^{t+1}-T_p^{t})}{\Delta t}$ for current and future (at time $t+\Delta t$) lading temperatures T_p^{t} and T_p^{t+1} respectively. The value of $\frac{dU}{dT_p}$ would be obtained from the internal energy vs. propane temperature table (ie. from the slope of a U vs. T_p curve, similar to one of those shown in Fig. 3-1, stored in tabular form). This approach is not considered practical because the heat balance equation for the propane lading would contain a large number of terms and hence would destroy the banded structure of the finite-difference equations. A more practical alternative is to calculate the lading temperature at time $t+\Delta t$ explicitly from the heat flow rate ($\dot{Q}$) into the tank at time t and then use the resulting value of T_p^{t+1} as a boundary temperature in the finite-difference equations used to advance to time $t+\Delta t$. This approach, which was described in Sect. 2.3.2.4, will give good results provided $\dot{Q}$ does not change significantly from time t to time $t+\Delta t$. A value of $\dot{Q}$ which is consistent with the tank temperatures at time $t+\Delta t$ can be obtained by iterating, as described in Sect. 2.3.2.4, if $\dot{Q}$ changes significantly. It is fully expected that iterations will not be required, however. The explicit calculation of U^{t+1} and hence T_p^{t+1} from the value of $\dot{Q}$ at time t will be used to obtain the nodal temperatures in the tank wall implicitly in the DE tank car model.

It was assumed in the preceding discussion of the thermodynamic model applying to the period before pressure relief that the vapor and liquid phases will both be isothermal and in thermal equilibrium. The vapor will actually become slightly superheated near the tank wall but this effect can undoubtedly be ignored. Tank temperature distributions measured in pool fire tests of tank cars have shown that the liquid phase cannot be considered isothermal, however, because the large coefficient of thermal expansion of liquid propane* causes the liquid heated at the tank wall to flow up the sides of the tank and stratify on top of the cooler bulk fluid. This is clearly shown in Fig. 3-3a, where tank centerline temperatures measured in the test of tank car RAX 201 by Anderson et al. (10) are plotted against s, where S is the vertical distance above the tank bottom. Where a large temperature difference was shown between the highest wet thermocouple and the lowest "dry" one in the tank temperature distributions given in (10), the gradient in the liquid was continued up to the presumed surface of the liquid.

As seen in Fig. 3-3a, the liquid propane eventually becomes isothermal at some time after the opening of the relief valve (the safety valve opened after about 2 minutes in the test of tank car RAX 201). The stratification of the liquid that

---

* At 50°C, the coefficient of thermal expansion of liquid propane is about nine times that of water at the same temperature.

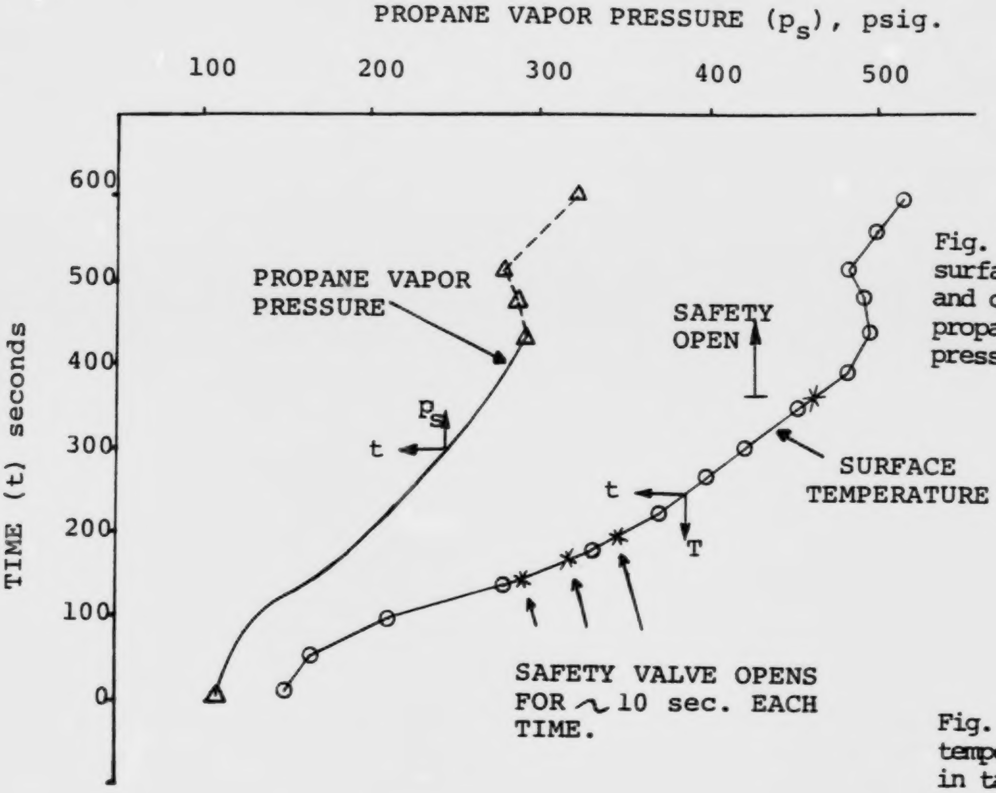

Fig. 3-3b: Liquid surface temperature and corresponding propane vapour pressure vs. time

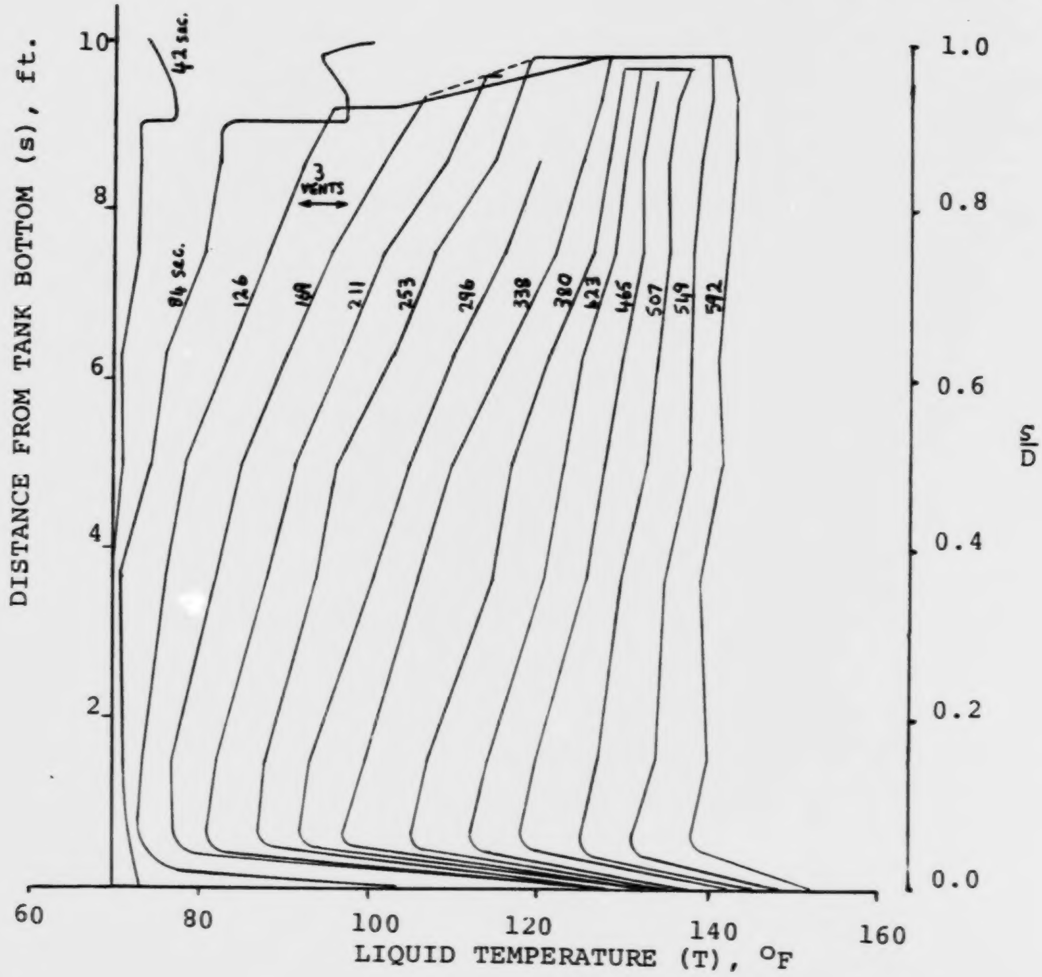
Fig. 3-3a: Liquid temperature profiles in tank car RAX 201

occurs during the first few minutes of the transient could probably be ignored were it not for the fact that the pressure in the tank car is set by the temperature of the surface layer of liquid (i.e., the tank pressure must equal the saturation pressure corresponding to the temperature of the surface layer). This fact is itself significant because thermal stratification of the liquid causes the tank pressure to increase much more rapidly than would be the case if the liquid was isothermal, thus causing the relief valve to open much earlier than would otherwise be the case. The boil-off of liquid that accompanies the early opening of the pressure relief valve may prevent the tank from becoming shell-full and thus prevent the rupture that occurs unless the liquid flow capacity of the valve is greater than the rate of volumetric expansion of the liquid.

The liquid surface temperature shown in Fig. 3-3a is plotted as a function of time-after-ignition in Fig. 3-3b along with the corresponding saturation pressure (at the measured surface temperature) of pure propane. When the resulting pressure-time curve for pure propane is plotted against the measured pressure-time curve for tank car RAX 201 in the manner shown in Fig. 3-4, it is quite apparent that the tank pressure during the first few minutes of the test must have been governed by the vapor pressures of the lighter fractions (e.g., ethane) initially present in the LPG, not by the vapor pressure of pure propane. This is shown by the fact that at the time when the safety valve first opened, at 270 psig, the saturation pressure of propane at the prevailing surface layer temperature would only have been 170 psig. Even before ignition, the pressure in the tank (125 psig) was greater than the saturation pressure of pure propane (110 psig) at the measured liquid temperature. It can be seen from Fig. 3-4 that the tank pressure equalled the saturation pressure of pure propane at the prevailing surface temperature at times greater than about six minutes into the transient, however,

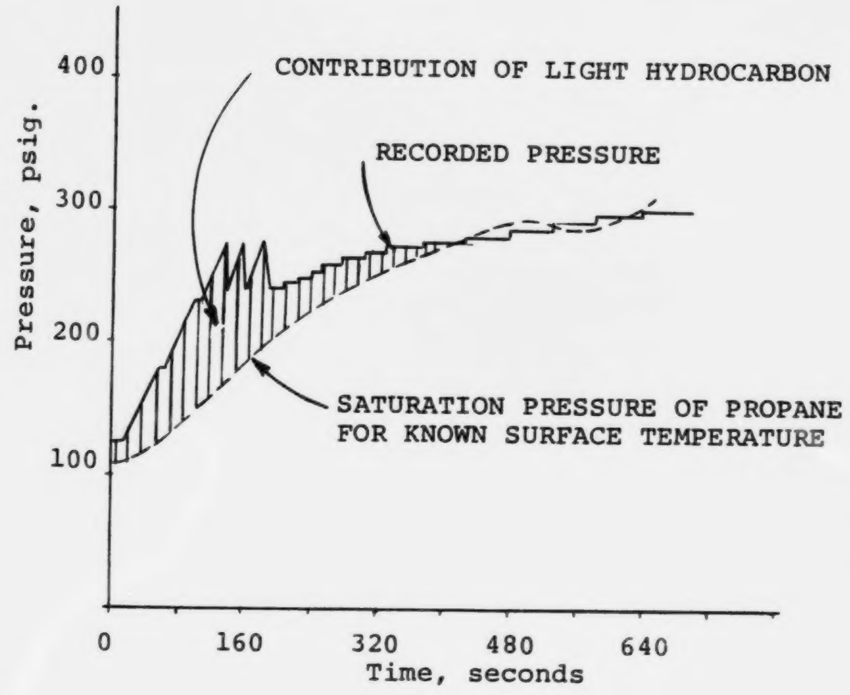

Fig.: 3-4: Comparison of Recorded Pressure in Tank Car RAX 201 with the Saturation Pressure of Pure Propane indicating that all of the lighter fractions had boiled off.

While a saturation curve for the initial LPG lading could be calculated from the concentrations and partial pressures of the constituent hydrocarbons, the calculation of saturation curves for the LPG after the lighter fractions had started to boil off would be difficult and hence will not be undertaken in the DE tank car model. Instead, it will be assumed that the lading is pure propane. Modelling the thermal stratification of the liquid in a rigorous manner would also be a difficult undertaking which probably should not be attempted until it has been demonstrated that thermal stratification of the liquid during the early stages of a pool fire has a significant effect on the time at which a tank car eventually ruptures. While it is true that thermal stratification of the liquid causes the relief valve to open early and, by so doing, possibly prevents the tank from rupturing as a result of becoming shell-full, shell-full ruptures are presumably of little interest in this study because EXPLOSAFE cannot be expected to prevent such ruptures. Any tank will quickly become shell-full in a pool fire if the initial fill fraction is large enough, regardless of whether thermal stratification occurs or not, and the likelihood of tank rupture at that time will depend totally on how the liquid flow capacity of the relief valve compares to the rate of volumetric expansion of the liquid. Presumably, a fair assessment of the effectiveness of EXPLOSAFE can only be made if input data for the computer model (e.g., the initial fill percentage) are purposefully selected to prevent the tank car from becoming shell-full. This observation would not be valid if the presence of EXPLOSAFE in a tank car inhibited thermal stratification of the liquid in some manner, thereby increasing the probability of a shell-full type tank failure, but the tank temperature distributions given in TP2740 (21) for the EXPLOSAFE-equipped and bare tanks do not show any evidence that EXPLOSAFE inhibits thermal stratification.

To permit the program user to determine whether thermal stratification of the liquid could have a significant effect on predicted rupture times, the user will be required to specify the temperature gradient (dT/ds) in the surface layer of liquid and it will be assumed that all of the heat supplied by the fire is used to increase the thickness of the surface layer and not to heat the cool liquid at the bottom of the tank. With the temperature gradient in the hot surface layer of liquid maintained at the user-specified value (κ) at all times, the temperature profile in the liquid will vary in the manner shown in Fig. 3-5 for times $t = 0$, $t = t_1$ and $t = t_2$ ($t_2 > t_1 > 0$) for an initial liquid temperature T_i. Setting κ to a large value will cause the surface temperature of the liquid to rise rapidly and the relief valve to open early while setting $\kappa = 0$ will cause the liquid to be isothermal (i.e., the model will default to the isothermal equilibrium model described previously when $\kappa = 0$). When the surface temperature of the liquid reaches the saturation temperature of propane corresponding to the relief valve opening pressure, the surface temperature will be held fixed until the liquid propane becomes isothermal. The thermodynamic model applying to the period following the start of venting is described in Section 3.2.1.

Since the pressure relief valve opened after about two minutes in the pool fire test of tank car RAX 201, the only temperature gradients in Fig. 3-3a that can be used to obtain an average value of κ for a full-size unprotected tank car are the gradients at times of 42, 84, and 126 seconds after ignition. The temperature gradients at 42 and 84 seconds are not very well defined and the temperature gradient at 126 seconds after ignition appears to be approximately $7.3^{\circ}C/m$ ($4^{\circ}F/ft$) on average. In contrast to this result, Fig. 3-6 shows the liquid temperature distributions measured at different times in a pool fire test of a 1/5 scale insulated tank car (40) and, as seen in the figure, the temperature gradients in the liquid are an order of magnitude

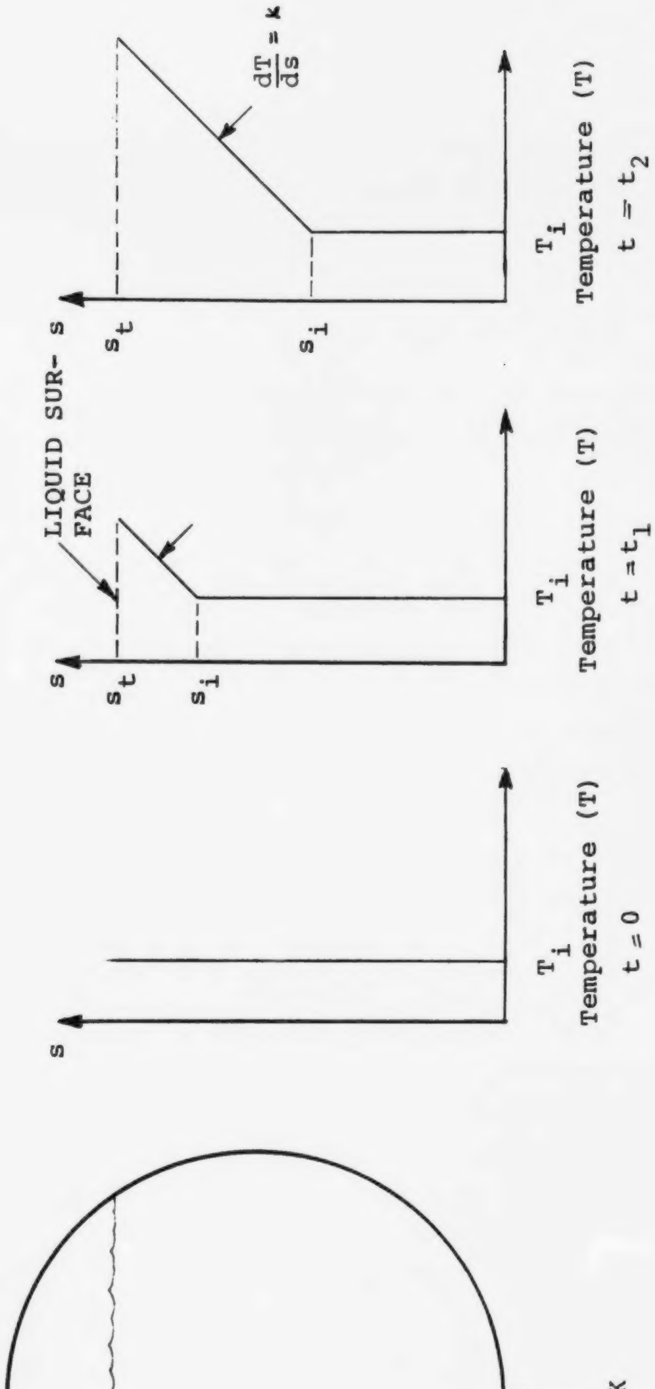
TANK
s
T_i
Temperature (T)
t = 0
s
s_t
s_i
LIQUID SUR- FACE
T_i
Temperature (T)
t = t_1
s
s_t
s_i
dT/ds = k
T_i
Temperature (T)
t = t_2

Fig.: 3-5: Stratified Surface Layer Development

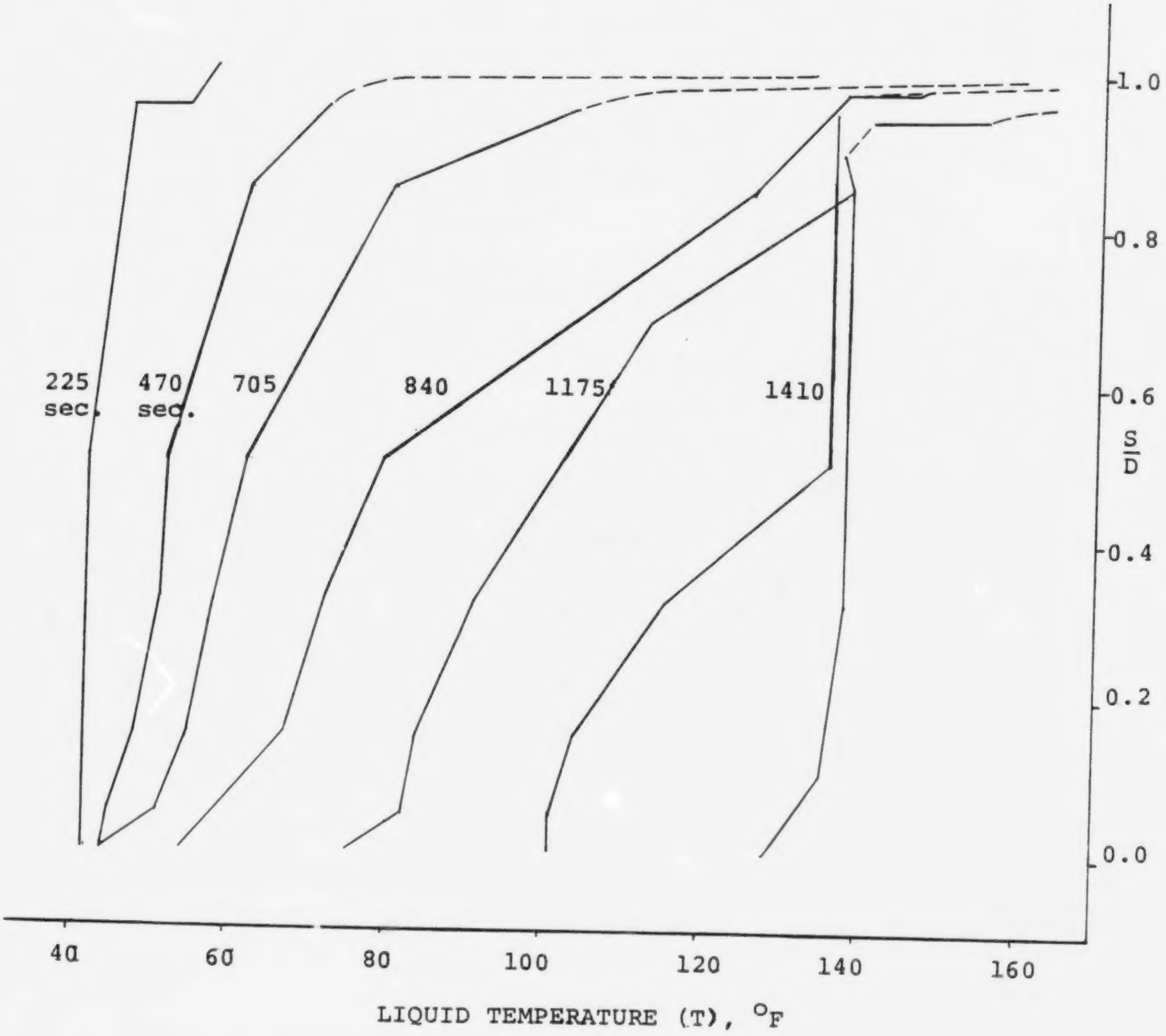

Fig. 3-6: Liquid temperature profiles measured in a pool fire test of a 1/5 scale insulated tank car

higher (i.e., about $70^{\circ}C/m$ or $40^{\circ}F/ft$ on average) in this case than those shown in Fig. 3-3a for tank car RAX 201. It is expected that the very large temperature gradients measured by Anderson et al (40) in the test of the 1/5 scale insulated tank stemmed from the large reduction in the flame-to-tank-heat flux that the insulation produced. The average flame-to-tank-heat flux was only 18,600 W/m^2 (5900 $BTU/hrft^2$) during the test compared to 104,800 W/m^2 (33,230 $BTU/hrft^2$) for tank car RAX 201. Boiling at the tank wall/propane interface would therefore have been much more vigorous in the test of tank car RAX 201 than in the test of the insulated tank, resulting in more effective mixing of the liquid and less thermal stratification. The markedly different degrees of thermal stratification observed in the tests of the insulated tank car and tank car RAX 201 indicate that the value of κ will have to be varied over quite a wide range in the sensitivity analyses in order to properly assess the significance of thermal stratification.

Since the temperature gradient in the heated surface layer of liquid is held constant at all times in the simple non-equilibrium thermodynamic model, the state of lading in the tank can be specified completely as a function of only one variable. The most convenient variable to use is either the temperature of the propane vapor (assumed the same as the temperature of the liquid surface) or its pressure. If, say, the temperature of the propane vapor is specified, then its density (ρ_v) can be obtained from a table of thermodynamic properties and the mass of propane vapour in the tank (M_v) can be calculated from the equation,

$$M_v = \rho_v \, {}^{V}s_t\text{-}D \qquad 3\text{-}6$$

where ${}^{V}s_t - D$ is the volume of the tank between $s = s_t$ and $s = D$ (s_t is the value of s at the liquid surface, as shown in Fig. 3-5). It can easily be shown that ${}^{V}s_t\text{-}D$ is given by the equation,

$$^{V}s_t - D = R_{it}^2 L_t \Big[\pi - 1/2\Big[2\Big(\pi - \cos^{-1}\Big(\frac{s_t}{R_{it}} - 1\Big)\Big) - \sin 2\Big(\pi - \cos^{-1}\Big(\frac{s_t}{R_{it}} - 1\Big)\Big]\Big] \qquad 3\text{-}7$$

It can be seen that $^{V}s_t$ - D, and hence M_v, is only a function of s_t, which is not known at this stage in the calculations. Since the temperature gradient (dT/ds) in the hot surface layer of liquid is assumed known (dT/ds = κ, where κ is specified by the user), the location of the bottom of the layer (i.e., s_i) can be expressed in terms of s_t as follows,

$$s_i = \frac{T_i - T_s}{\kappa} + s_t \qquad 3\text{-}8$$

where T_i and T_s (the surface temperature of the liquid and the temperature of the propane vapor) are also known. If the coefficient of thermal expansion of the liquid is designated α_v, then the density of the liquid (ρ_ℓ) at some point s between s_i and s_t is given by the expression,

$$\rho_\ell(s) = \frac{\rho_{\ell s}}{1 + \alpha_v(T(s) - T_s)}$$

$$= \frac{\rho_{\ell s}}{1 + \alpha_v \kappa(s - s_t)} \qquad 3\text{-}9$$

where $\rho_{\ell s}$ is the density of the liquid at the known surface temperature and the temperature of the liquid at s (i.e., T(s)) is defined by the expression,

$$T(s) = T_s + \kappa(s - s_t) \qquad 3\text{-}10$$

or

$$T(s) - T_s = \kappa (s - s_t)$$

The total mass of liquid in the tank (M) can now be obtained from the equation,

$$M_\ell = \rho_{\ell_i} V_{0-s_i} + \int_{V_{s_i-s_t}} \rho_\ell \, dV \qquad 3\text{-}11$$

where ρ_{ℓ_i} is the density of the liquid at the initial temperature T_i, V_{0-s_i} is the volume of the tank between $s = 0$ and $s = s_i$ and $V_{s_i-s_t}$ is similarly the volume between $s = s_i$ and $s = s_t$. The volume V_{0-s_i} is defined by the equation,

$$V_{0-s_i} = \frac{R_{it}^2 L_t}{2} [2(\pi - \cos^{-1}(\frac{s_i}{R_{it}} - 1)) - \sin 2(\pi - \cos^{-1}(\frac{s_i}{R_{it}} - 1))] \qquad 3\text{-}12$$

and hence is only a function of s_t because s_i is related to s_t by Eq. 3-8. The integral in Eq. 3-11 can be written in expanded form as,

$$\int_{V_{s_i-s_t}} \rho_\ell \, dV = 2L_t \int_{s_i}^{s_t} \frac{\rho_{\ell s} \sqrt{2sR_{it} - s^2}}{1 + \alpha v \kappa (s - s_t)} \, ds \qquad 3\text{-}13$$

where Eq. 3-9 has been substituted for ρ_ℓ. It may be necessary to evaluate the integral in Eq. 3-13 numerically but it is quite apparent that the value of the integral will be a function only of s_t (for user-specified values of R_{it}, κ, etc.). Thus M_ℓ and M_v are both functions of s_t only when a value for the propane temperature (or pressure) is chosen and the correct value of s_t

will be the one for which,

$$M_\ell + M_v = M \qquad 3\text{-}14$$

where M is assumed known. It is not possible to obtain an explicit expression for s_t so it will be evaluated numerically, using the half-interval search technique, in the DE tank car model.

With the value of s_t and hence M_ℓ and M_v evaluated for a specified propane temperature in the manner just described, the total internal energy of the lading (U) can be calculated from the expression,

$$U = M_v u_v + \rho_{\ell i} u_{\ell i} V_{0-s_i} + \int_{V_{s_i-s_t}} \rho_\ell u_\ell dV \qquad 3\text{-}15$$

where u_v is the internal energy of saturated propane vapor at the specified propane temperature and $u_{\ell i}$ is the internal energy of liquid propane at the temperature T_i. The liquid at temperature T_i will actually be subcooled (compressed) but its internal energy will be negligibly different from that of saturated liquid propane at the same temperature. The liquid density (ρ_ℓ) in the integral on the right-hand side of Eq. 3-15 is given as a function of s by Eq. 3-9 and the internal energy (u_ℓ) can be expressed in terms of s as,

$$u_\ell = u_{\ell s} + C_v(T(s) - T_s)$$

$$= u_{\ell s} + C_v\kappa(s - s_t) \qquad 3\text{-}16$$

where $u_{\ell s}$ is the internal energy of liquid propane at T_s and

$C_v (= \frac{\partial u_\ell}{\partial T})$ is the specific heat (at constant volume) of propane. With Eqs. 3-9 and 3-16 defining ρ_ℓ and u_ℓ respectively, the integral in Eq. 3-15 can be written in expanded form as,

$$\int_{V_{s_i - s_t}} \rho_\ell u_\ell \, dV = 2L_t \int_{s_i}^{s_t} \frac{\rho_{\ell s}}{1 + \alpha_v \kappa (s - s_t)} \left(u_{\ell s} + C_v \kappa (s - s_t) \right) \sqrt{2sR_{it} - s^2} \, ds \tag{3-17}$$

This integral will probably have to be evaluated numerically. Note that the first term on the right-hand side of Eq. 3-11 and the second term on the right-hand side of Eq. 3-15 will not have to be evaluated if the heated liquid layer extends to the bottom of the tank.

Using the procedure just described, it will be possible to evaluate U, V_ℓ , (and hence X*), p (pressure), s_i and s_t at different propane vapor temperatures and store the results in tabular form before the thermal analysis is started. All of these variables will be calculated explicitly from the heat flow rate into the tank at time t to obtain the boundary conditions needed to advance the thermal analysis to time t + Δ t, as described previously for the simple isothermal liquid/vapor thermodynamic model. A tilted tank will be treated as though it is a level tank for the purposes of the thermodynamic analysis but the liquid temperatures needed as boundary temperatures for the liquid-wetted tank wall nodes will be calculated from the local liquid level and the user-specified value of dT/ds (i.e., κ).

3.1.2 Tank with EXPLOSAFE

The thermodynamic model for an EXPLOSAFE-equipped tank during the pre-venting period will be obtained by modifying the model described in the preceding section in the simplest possible manner. The main effect that the EXPLOSAFE will have on the tank car thermodynamics will be to allow the vapor in the EXPLOSAFE annulus to become superheated, but this effect will undoubtedly be of minor importance during the pre-venting period since the fraction of the tank volume occupied by vapor during that period is typically about 15% initially and decreases until the relief valve opens. The mass and thermal capacity of the vapor in the tank will therefore be very small during the pre-venting period. Also, the tank temperature distributions measured in the pool fire tests of the 1/5-scale EXPLOSAFE-equipped tank cars at DRES Suffield show very little superheating of the vapor (above the temperature of the liquid surface) in the tank cars before the start of venting. These results suggest that the model described in the preceding section really needs almost no modification in order to be applied to an EXPLOSAFE-equipped tank, except perhaps to include the thermal capacity of the EXPLOSAFE foil (which will be quite small) in the vapor and liquid internal energy calculations. Only Eq. 3-15 needs to be modified to accomplish this. If the internal energy of the aluminum foil is taken to be zero at some convenient reference temperature, say T_i, then the total internal energy of the vapor space (formerly $M_v u_v$) becomes $(M_v u_v + M_{EX} C_{al.} (T_s - T_i)$ with EXPLOSAFE in the tank, where M_{EX} is the mass of aluminum foil in the volume ${}^{V}s_t$ - D. The terms representing the internal energy of the liquid in Eq. 3-15 can be modified to include the internal energy of the aluminum foil in a similar manner.

Only one other change will be made to the thermodynamic model described in the preceding section to apply it to an EXPLOSAFE equipped tank. Since most of the net heat flow into the EXPLOSAFE/vapor matrix (i.e., the total heat flow into the matrix less the heat flow from the matrix into the liquid) affects the tank car thermodynamics by superheating the vapor and foil in the EXPLOSAFE/vapor matrix above the temperature T_s, that heat flow (less an amount that will be discussed shortly) will be subtracted from the total flame-to-tank heat flow to obtain the heat flow rate used to calculate the state of the lading at time $t + \Delta t$. The net heat flow into the EXPLOSAFE/vapor matrix causes the temperatures of the "control volumes" in the finite-difference model of the EXPLOSAFE/vapor matrix to increase from one time step to the next and it is by that mechanism that its effect on the tank car thermodynamics (i.e., its contribution to increases in internal energy) is taken into account. The constant volume specific heat of the vapor $C_{vv}(=\partial u/\partial T)$ will be used to calculate the specific heat of the EXPLOSAFE/vapor matrix in Eq. 2-98 instead of the constant pressure specific heat (C_{pv})* during the pre-venting period and the density of the propane vapor (ρ_v) used to calculate the density and specific heat of each EXPLOSAFE/vapor control volume will be updated at each time step using the current temperature of the control volume and the prevailing tank pressure.

---

* The values of C_{pv} and C_{vv} differ by a small amount (e.g., by 14% for saturated propane vapor at 2 MPa).

To recapitulate and to elaborate on the manner in which the presence of EXPLOSAFE foil will be accounted for, the procedure described in Section 3.1.1 will be used to evaluate U, V_ℓ, p, s_i and s_t at different propane temperatures before the thermal analysis is started. The results of the thermodynamic analysis will be stored in tabular form as indicated in Section 3.1.1. The only way in which this part of the analysis will differ from the analysis already described in Section 3.1.1 is that the internal energy of the aluminum foil will be included in Eq. 3-15 by writing $(M_v u_v + M_{EX} C_{al.}(T_s - T_i)$ instead of $M_v u_v$, etc. Then, when the thermal analysis has been started and the total heat flow rate into the tank at some time t has been calculated, the net heat flow rate into the EXPLOSAFE/vapor matrix at time t $(\dot{Q}^t_{EX})$ will be subtracted from the total flame-to-tank heat flow-rate $(\dot{Q}^t)$ to obtain the change in internal energy from time t to t + Δt (i.e., $\Delta U = (\dot{Q}^t - \dot{Q}^t_{EX})\Delta t$. If the temperature of the liquid surface in the tank changes from T^t_s at time t to T^{t+1}_s at time t + Δt, then really only that fraction of $\dot{Q}^t_{EX}$ that is used to change the temperature of the vapor (and the EXPLOSAFE in the vapor space) by more than the amount $(T^{t+1}_s - T^t_s)$ should be subtracted from $\dot{Q}_t$ to obtain the heat flow needed to calculate ΔU from the tabulated results of the isothermal vapor/non-isothermal liquid thermodynamic analysis. This must be the case because if the heat flow into the EXPLOSAFE/vapor matrix at each time step was such that the matrix temperature always changed by an amount $(T^{t+1}_s - T^t_s)$ then the vapor would always be isothermal and the isothermal vapor/non-isothermal liquid thermodynamic model would be directly applicable without reducing $\dot{Q}^t$ by the amount $\dot{Q}^t_{EX}$. To account for this effect, the heat flow $(\dot{Q}^t - \dot{Q}^t_{EX})\Delta t$ will be used to obtain an initial estimate of T^{t+1}_s from the tabulated results of the isothermal vapor/non-isothermal liquid thermodynamics analysis. The internal energy increment,

$$\Delta U_{EX} = \sum_{i=1}^{N} \rho^t_{mi} C^t_{EX_i} V_i (T^{t+1}_s - T^t_s) \qquad \text{3-17a}$$

will then be added to the value of ΔU obtained initially from the expression $(\dot{Q}^t - \dot{Q}^t_{EX})\Delta t$ to obtain a new value of ΔU for use in obtaining final values of T_s^{t+1}, P^{t+1}, V_ℓ^{t+1}, etc., from the tabulated results of the simple thermodynamic analysis described previously. The index i in Eq. 3-17a refers to a finite difference control volume in the EXPLOSAFE/vapor matrix and $\rho^t_{m_i}$, $C^t_{EX_i}$, and V_i are the density, specific heat (obtained from Eq. 2-98 with C_{vv} substituted for C_{pv}) and volume of the i^{th} control volume respectively at time t. The total number of control volumes in the EXPLOSAFE/vapor matrix at time t is designated N in Eq. 3-17a.

Nodes in the EXPLOSAFE/vapor matrix will be gradually uncovered (by the liquid) if and when the liquid level in the tank starts to drop (not likely in the period before pressure relief). Since newly uncovered nodes will be added to the finite-difference model of the EXPLOSAFE/vapor matrix in the tank ullage, their temperatures will have to be initialized to some value when they first become part of the model (i.e., for the first time step after their uncovery). The logical temperature to assign to the newly uncovered nodes is the prevailing temperature of the liquid surface, T_s^t.

3.2 Period After Relief Valve Opens

3.2.1 Tank Without EXPLOSAFE

When the tank is venting, the first law energy conservation equation, given formerly as Eq. 3-1, must be rewritten as,

$$\dot{Q} = \frac{d}{dt} \left(\int_V \rho u \, dV \right) + \dot{m} \, h_o = \frac{dU}{dt} + \dot{m} \, h_o \qquad 3\text{-}18$$

where h_o is the stagnation enthalpy of the fluid (which may be liquid, vapor, or a two-phase mixture) being discharged from the valve and $\dot{m}$ is the fluid mass flowrate. The manner in which the value of $\dot{m}$ can be calculated from the prevailing tank pressure and lading conditions for a relief valve (or other pressure relief device) of specified geometry is described in Sections 3.3 and 3.4.

In order to predict the state of the lading as a function of time, the first law energy conservation equation (Eq. 3-18) and the mass conservation equation,

$$\frac{d}{dt} \left(\int_V \rho dV \right) = \frac{dM}{dt} = - \dot{m} \qquad 3\text{-}19$$

must be solved simultaneously. Equations 3-18 and 3-19 will be solved in finite-difference form in the tank car model. Assuming the total internal energy and the state of the lading in the tank are known at time t, the total internal energy of the lading at time t + Δt (i.e., U^{t+1}) can be calculated from the equation,

$$U^{t+1} = U^t + \Delta t(\dot{Q}^t - \dot{m}^t h_o^t) \qquad 3\text{-}20$$

where all of the quantities written with the superscript t are evaluated at time t. The manner in which $\dot{m}^t$ is calculated from the prevailing tank pressure (p^t) when the relief valve is located below the liquid surface (i.e., for liquid stagnation conditions) is described in Section 3.3 and the calculation of $\dot{m}$ for a relief valve located above the liquid surface (i.e., for vapor stagnation) is described in Section 3.4. The mass conservation equation written as,

$$M^{t+1} = M^t - \dot{m}^t \Delta t \qquad 3\text{-}21$$

defines the total mass of propane in the tank at time t + Δt (i.e., M^{t+1}) explicitly in terms of the mass at time t (M^t) and the mass discharge rate, $\dot{m}^t$.

With the mass of propane in the tank and the total internal energy of the lading at time t + Δt known, the state of the lading (e.g., its pressure, temperature, the volume of liquid, etc.) at that time can be obtained iteratively in the following manner. First, it is fairly obvious that the problem is, at this point, essentially, the same as that described in Section 3.1.1, in other words, we have a known mass of propane in the tank and we know the total internal energy of the lading. Choosing a tank pressure (and hence temperature) permits the internal energy of the lading to be calculated in the manner described in Section 3.1.1 and, if the guessed tank pressure is correct, the calculated internal energy of the lading should equal the known internal energy. If the calculated and known internal energies are not equal, other tank pressures can be tried until the correct one is found. The search for the correct tank pressure (i.e., the pressure which causes the calculated and known total internal energies to be equal) will be performed using the half-interval search technique (used in Appendix B to determine X* for a known liquid volume) in the DE tank car model. It will be assumed that the search has converged to the correct pressure when the absolute value of the difference between two consecutive estimates of the pressure is less than some user-specified amount (ε). The calculated lading conditions at time t + Δt will then be used to define the boundary conditions in the implicit finite-difference equations used to obtain the temperatures of the nodes in the finite-difference model of the tank car at time t + Δt.

The thermodynamic analysis of a venting tank car can be performed exactly in the manner just described when the vapor and liquid phases in the tank car are isothermal and in thermal equilibrium. Determing the lading internal energy at a given propane pressure (or temperature) for a known total mass of propane is very straightforward in that case, as described at the beginning of Section 3.1.1. The analysis is more difficult, of course, when the phases are non-isothermal. Since the tank wall-to-propane vapor convective heat transfer analysis presented in Appendix D indicates that the boundary layer on the inner surface of the tank wall in the ullage will be extremely thin when the tank is venting, it can be assumed without introducing significant error that the vapor is isothermal throughout the tank. It is also known from the results of tank car tests that the liquid in a tank car becomes isothermal within a few minutes after the start of venting, but a method must be found to permit the liquid, which will be non-isothermal at the start of venting if a non zero value is assigned to κ (i.e., the user-specified temperature gradient in the hot surface layer of liquid) in the pre-venting thermodynamic calculations, to eventually become isothermal. In order to allow the liquid to become isothermal, a user-specified fraction (f_q) of the total heat flow rate into the tank will be used to increase the internal energy of the liquid until the liquid temperature becomes uniform. The total internal energy of the lading at time t + Δt (i.e., U^{t+1}) will still be calculated from Eq. 3-20, but an additional calculation will also give the internal energy of the liquid at time t + Δt (i.e., U^{t+1}) as,

$$U_\ell^{t+1} = U_\ell^t + f_q \dot{Q}^t \Delta t \tag{3-22}$$

and hence the internal energy of the vapor (U_v^{t+1}), as,

$$U_v^{t+1} = U^{t+1} - U_\ell^{t+1} \tag{3-23}$$

The preceding calculations will give the values of U_ℓ^{t+1}, U_v^{t+1}, and M^{t+1} (from Eq. 3-21) from which the complete state of the lading at time t + Δt must be calculated.

If it is assumed that the liquid heated at the wall of the tank stratifies on the liquid surface at the saturation temperature of propane corresponding to the venting pressure, then the liquid will become isothermal from the top downwards as shown in Fig. 3-7. The isothermal surface layer shown in Fig. 3-7 is not discernible in Fig. 3-3a but it is clearly visible in the temperature profiles shown in Fig. 3-6 for times greater than about 600 seconds. With the assumption that the liquid becomes isothermal from the top downwards, the state of the lading for the known values of U_ℓ, U_v, and M can be obtained iteratively by first guessing a tank pressure and then solving the equations,

$$U_v = u_v M_v \tag{3-24}$$

and,

$$M_v = \rho_v V_v \tag{3-25}$$

for M_v and then V_v. The values of u_v and ρ_v can be obtained for the chosen tank pressure from tables of thermodynamic properties for propane, of course. The mass of liquid (M_ℓ) in the tank is subsequently available from the expression,

$$M_\ell = M - M_v \tag{3-26}$$

and the volume of liquid is also available as,

$$V_\ell = V - V_v \tag{3-27}$$

The volume of liquid (V_ℓ) can be used to calculate the distance from the bottom of the tank to the liquid surface (i.e., s_t) from the equation,

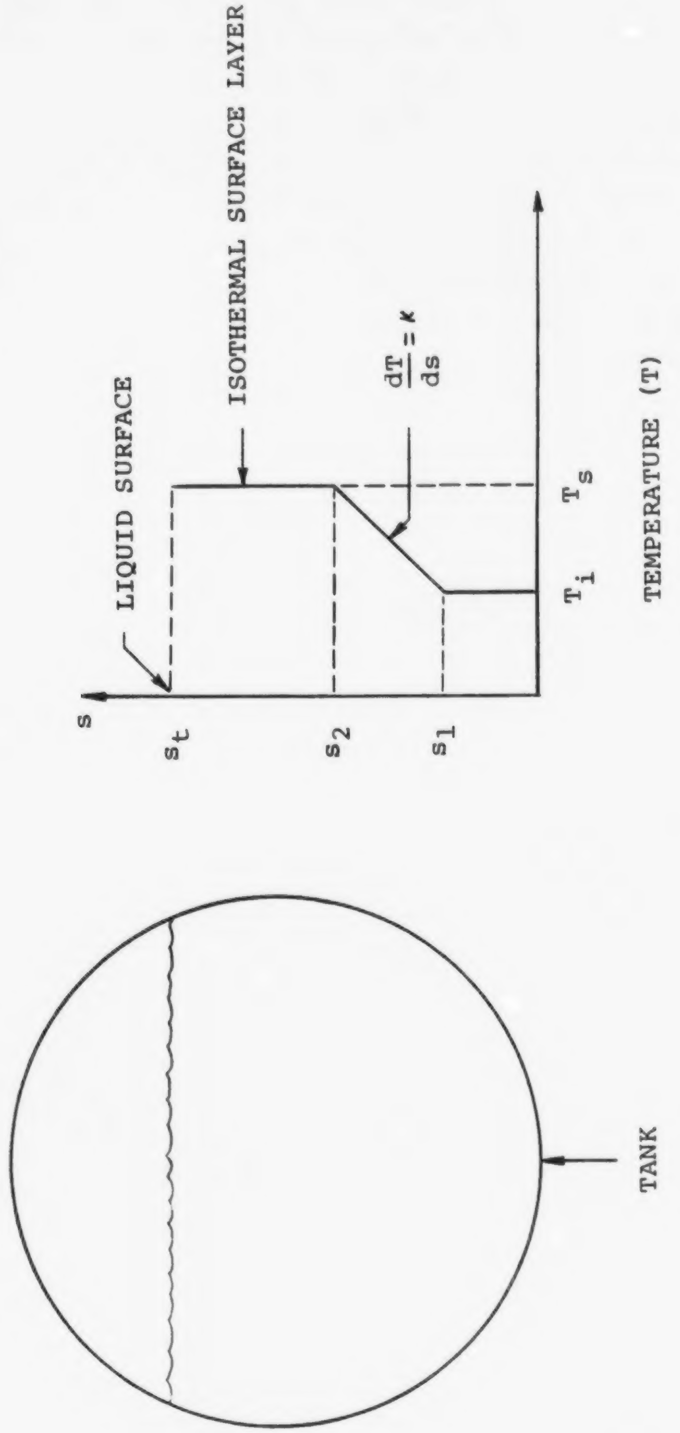
s
s_t
s_2
s_1
LIQUID SURFACE
ISOTHERMAL SURFACE LAYER
$\frac{dT}{ds} = \kappa$
T_i
T_s
TEMPERATURE (T)
TANK

Fig.: 3-7: Growth of Isothermal Surface Layer

$$V_\ell = \frac{R_{it}^2 L_t}{2} \left[2\left(\pi - \cos^{-1}\left(\frac{s_t}{R_{it}} - 1\right)\right) - \sin 2\left(\pi - \cos^{-1}\left(\frac{s_t}{R_{it}} - 1\right)\right)\right] \qquad 3\text{-}28$$

which cannot be rewritten to give s_t explicitly but which can be solved for s_t using the half-interval search technique. If it is assumed that the temperature gradient (dT/ds) in the non-isothermal layer of liquid shown in Fig. 3-7 remains at the user-specified value κ, then,

$$s_1 = s_2 + \frac{T_i - T_s}{\kappa} \qquad 3\text{-}29$$

where the variables s_1 and s_2 are identified in Fig. 3-7 and T_s is the saturation temperature of propane corresponding to the chosen tank pressure p (i.e., T_s is the temperature of the isothermal layer at the top of the liquid). The density of the liquid at any location s in the non-isothermal layer can be calculated from the equation,

$$\rho_\ell = \frac{\rho_{\ell s}}{1 + \alpha_v \kappa (s - s_2)} \qquad 3\text{-}30$$

by analogy with Eq. 3-9 and the value of s_2 can then be obtained by solving the equation,

$$M_\ell = \rho_{\ell i} V_{0-s_1} + \int_{V_{s_1-s_2}} \rho_\ell \, dV + \rho_{\ell s} V_{s_2-s_t}$$

$$= \rho_{\ell i} V_{0-s_1} + 2L_t \int_{s_1}^{s_2} \frac{\rho_{\ell s} \sqrt{2sR_{it} - s^2}}{1 + \alpha_v \kappa (s - s_2)} \, ds + \rho_{\ell s} V_{s_2-s_t} \qquad 3\text{-}31$$

with the half-interval search technique. The value of V_{0-s_1} can be obtained from Eq. 3-28 by substituting s_1 for s_t and the value of $V_{s_2-s_t}$ is defined by the expression:

$$V_{s_2-s_t} = \frac{R_{it}^{2} L_t}{2} [2(\cos^{-1}(\frac{s_2}{R_{it}} -1) - \cos^{-1}(\frac{s_t}{R_{it}} - 1)$$

$$+ \sin 2(\pi - \cos^{-1}(\frac{s_2}{R_{it}} - 1)) - \sin 2(\pi - \cos^{-1}(\frac{s_t}{R_{it}} - 1))] \qquad 3\text{-}32$$

Note that the right-hand side of Eq. 3-31 is only a function of s_2 because s_1 is related to s_2 by Eq. 3-29. The first term on the right-hand side of Eq. 3-31 can be omitted and the lower limit of integration in the integral set to 0 (instead of s_1) when all of the liquid at temperature T_i has disappeared (i.e., when s_1 reaches the bottom of the tank).

With the values of s_1, s_2, and s_t calculated in the manner just discussed the internal energy of the liquid can be obtained from the expression,

$$U_\ell = \rho_{\ell i} u_{\ell i} V_{0-s_1} + \int_{V_{s_1-s_2}} \rho_\ell u_\ell \, dV + \rho_{\ell s} u_{\ell s} V_{s_2-s_t} \qquad 3\text{-}33$$

where the integral on the right-hand side is given by Eq. 3-17 when s_1 and s_2 are substituted for s_i and s_t in that equation.

If the value of U_ℓ calculated using Eq. 3-33 does not agree with the value obtained from Eq. 3-22, another tank pressure can be chosen and the value of U_ℓ recalculated by applying the procedure just described. This procedure will be repeated and the half interval search technique applied in the DE tank car model until the absolute value of the difference between two consecutive estimates of the tank pressure is less than some user-specified amount (ε). The state of the lading (i.e., temperature, volume, etc.) will be available at that time for use in calculating the boundary conditions for the implicit finite-difference equations defining the temperatures of the nodes in the tank wall at time $t + \Delta t$.

An appropriate range of values for the factor f_q (see Eq. 3-22) will be found by comparing the times required for the liquid to become isothermal with different values of f_q to the corresponding times observed in tank car tests. Large values of f_q (i.e., values close to unity) will cause the liquid to become isothermal rapidly. The liquid temperature typically has not become uniform until several minutes after the start of venting in tank car fire tests.

The manner in which the quantities $\dot{Q}^t$ and h_o^t in Eq. 3-20 should be evaluated deserves mention since a small fraction of total heat flow into the lading will be transferred by convection from the tank wall to the venting vapor (assuming the relief valve is located above the liquid surface). The propane vapor being discharged from the pressure relief device will be slightly superheated as a result of this heat transfer and will therefore have a stagnation enthalpy (h_o^t) defined by the expression,

$$h_o^t = h_{vs}^t + \frac{\dot{Q}_v^t}{\dot{m}^t} \qquad 3\text{-}34$$

where h_{vs}^t is the enthalpy of saturated propane vapor at the prevailing tank pressure (p^t) and $\dot{Q}_v^t$ is the heat transferred by convection from the tank wall to the venting vapor. If $\dot{Q}_\ell$ is the rate of heat transfer to the liquid, then $\dot{Q}^t = \dot{Q}^t_\ell + \dot{Q}_v^t$ and Eq. 3-20 can be rewritten as,

$$U^{t+1} = U^t + \Delta t(\dot{Q}^t_{\ell} + \dot{Q}^t_v - \dot{m}^t(h^t_{vs} + \frac{\dot{Q}^t_v}{\dot{m}^t}))$$

$$= U^t + \Delta t(\dot{Q}^t_{\ell} - \dot{m}^t h^t_{vs}) \qquad 3\text{-}35$$

so h^t_{vs} can be substituted for h^t_o in Eq. 3-20 if $\dot{Q}^t$in that equation is replaced by $\dot{Q}^t_{\ell}$.

Equations 3-24 and 3-35 only apply when the venting relief valve is located above the liquid surface. When the valve is located below the liquid surface, the enthalpy of the liquid propane at the level of the relief valve (i.e., at the temperature corresponding to that level if the liquid temperature is non uniform) should be used as the reservoir stagnation enthalpy h^t_o.

3.2.2 Tank With EXPLOSAFE

Since it is assumed that the vapor in the EXPLOSAFE/vapor matrix will be stagnant during venting, as discussed in Sect. 2.3.8, the thermodynamic model of an EXPLOSAFE - equipped tank car during periods of venting will be the same as the model described in the preceding section except that the internal energy of the EXPLOSAFE foil will be included in Eq. 3-33 (as described in Sect. 3.1.2) and the term $\dot{Q}^t$ in Eq. 3-20 will be replaced by $(\dot{Q}^t - \dot{Q}^t_{EX})$ to obtain an initial estimate of U^{t+1}. The procedure described in the preceding section will then be used to obtain an estimate of T_s^{t+1} from the known values of U^{t+1} and M^{t+1} and the value of T_s^{t+1} thus obtained will be used to evaluate $\Delta U_{EX.}$, defined by Eq. 3-17a. The value of U^{t+1} will then be recalculated by adding ΔU_{EX} to the initial value and another estimate of T_s^{t+1} will be obtained for the corrected U^{t+1} and the known mass of the lading (M^{t+1}). Thus the procedure will be:

1) Calculate U^{t+1} from the expression,

$$U^{t+1} = U^t + \Delta t \ (\dot{Q}^t - \dot{Q}^t_{EX} - \dot{m}^t h^t_o$$

2) Calculate T_s^{t+1} from U^{t+1} and M^{t+1} (given by Eq. 3-21).
3) Recalculate U^{t+1} using the expression,

$$U^{t+1} = U^t + \Delta t (\dot{Q}^t - \dot{Q}^t_{EX} - \dot{m} h^t_o) + \Delta U_{EX}$$

4) Recalculate T_s^{t+1} from the corrected value of U^{t+1} and the value of M^{t+1} used previously.
5) Use the values of V_ℓ, s_t, etc. obtained in the solution for T_s^{t+1} to define the boundary conditions in the finite-difference equations for the nodal temperatures at time $t + \Delta t$ and then solve those equations.
6) Repeat steps 1-5 for the next time step.

Note that ΔU_{EX} will be zero in value if the tank pressure does not change from time t to t+Δt because $T_s^{t+1} = T_s^t$ in that case.

The net rate of heat transfer into the EXPLOSAFE foil, $\dot{Q}_{EX}^{t}$, will be the total rate of heat transfer into the foil less the sum of the heat transferred by conduction from the foil to the liquid and the heat transferred by convection from the inner surface of the EXPLOSAFE annulus to the venting propane vapor ($\dot{Q}_V$). It is assumed, as in Sect. 3.1.2, that most of the net heat flow into the EXPLOSAFE/vapor matrix is used to superheat the vapor and the foil and that the increase in internal energy resulting from that heat transfer appears in the form of elevated temperatures in the finite-difference model of the matrix. The heat flow rate ($\dot{Q}_{EX}$-ΔU_{EX}/Δt should therefore not be used to calculate U^{t+1} when U^{t+1} is the internal energy of the lading with the vapor temperature assumed to be T_s.

The constant pressure specific heat of the vapor (C_{pv}) will be used to calculate the specific heat of the EXPLOSAFE/vapor matrix, as seen in Eq. 2-98, since the tank pressure will probably remain fairly constant after the tank has started venting. The density of the propane vapor in each "control volume" found in the finite-difference representation of the EXPLOSAFE/vapor matrix will be updated periodically during the transient to account for pressure and temperature changes.

It should be evident that essentially the same modifications will be made to the thermodynamic model described in Sect. 3.2.1 to apply it to a tank with EXPLOSAFE as were made to the pre-venting thermodynamic model described in Sect. 3.1.1 to achieve the same objective.

As mentioned in Sect. 3.1.2, the temperatures of newly uncovered (by liquid) nodes in the EXPLOSAFE/vapor matrix will be initialized to the temperature of the liquid surface for the first time step after their uncovery.

3.3 Discharge Flowrate Calculation - Liquid Stagnation State

When initially liquid propane flows through the safety valve, and its pressure drops to atmospheric pressure, the state of the propane will change. If the process occurs slowly, part of the liquid will flash to vapor, and at the minimum area of the valve a two phase mixture will exist. The flow rate could be computed if one assumed the two phases had the same velocity (homogeneous) and were in equilibrium; this is called the homogeneous equilibrium model. Such a model has been used by Sallet (41) to calculate the maximum, or critical, mass flux ($G = \dot{m}/A$) of propane as a function of reservoir stagnation pressure (p_o) and quality (x') and figure 3.8 shows his calculated results. While it seems unlikely that equilibrium could exist during such a rapid process, Sallet states that full scale tests (at Edwards AFB) and model tests (by Sallet) support the validity of his calculations.

On the other hand, for flow through sharp-edged orifices, Henry (43) states that the pressure drops so rapidly that phase equilibrium is not maintained, and a subcooled or saturated liquid does not flash to vapor until it reaches atmospheric pressure. The flow rate ($\dot{m}$) can thus be calculated by applying the Bernoulli equation (which gives $\dot{m} = A\sqrt{2\rho_\ell(p_o - p_a)}$ for a discharge flow area A) to the liquid flow as it drops from tank pressure to atmospheric pressure through the orifice. The flow rate predicted by this method is about four times than given by Sallet at typical venting pressures.

To try to reconcile these discrepancies, it is useful to examine figure 3.9, taken from reference (42), which shows

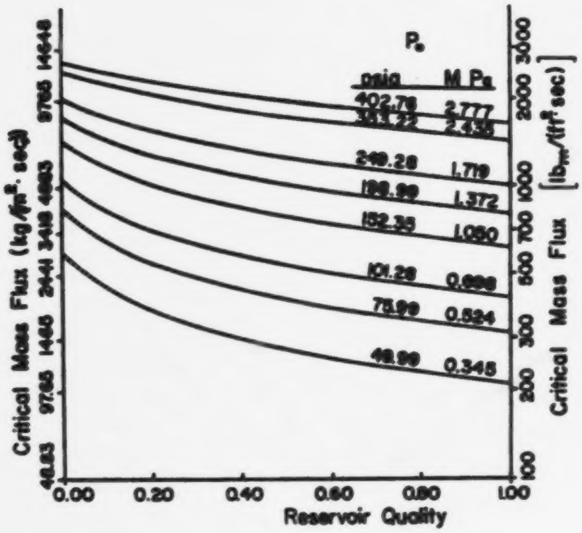

Fig. 3-8: Critical mass flux of propane as a function of reservoir quality and pressure.

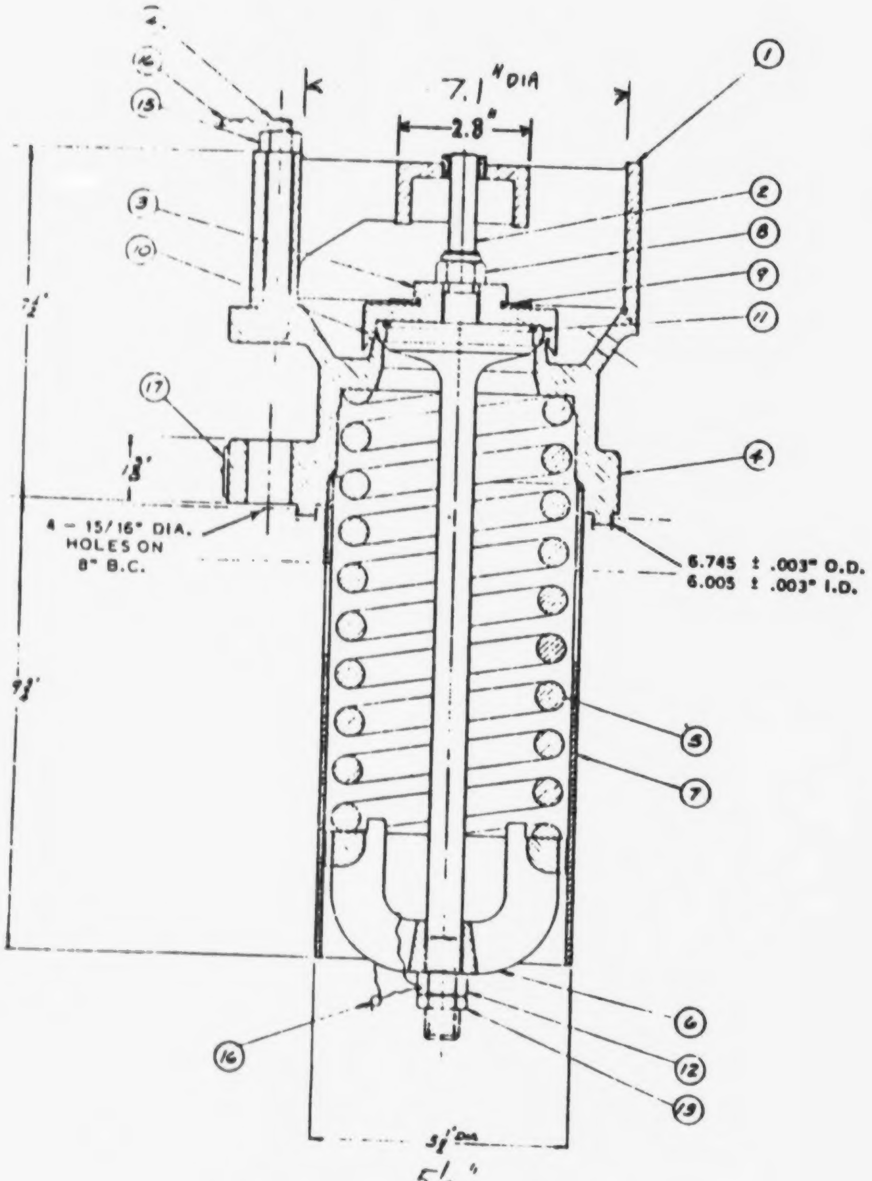

ITEM NO.	NO. REQD.	PART NAME	MATERIAL	PART NO.
1	1	TOP GUIDE	STEEL WITH S.S. INSERT	34-1-XS
2	1	STEM	STAINLESS STEEL	31-2-SS
3	1	RETAINER	STEEL, CAD. PLATED	31-3-CS
4	1	BODY	STEEL	34-41-CS
5	1	SPRING	ALLOY STL., CAD.PLATE	SEE TABLE
6	1	FOLLOWER	STEEL, CAD. PLATED	34-6-CS
7	1	SPRING GUIDE	STEEL	34-71-CS
8	1	TOP LOCK NUT	STEEL, CAD. PLATED	23-8-CS
9	1	WASHER	LAMINATED NEOPRENE	23-9-LN
10	1	SEAT "O" RING	BUNA N 70D*	31-10-BN
11	1	STEM "O" RING	BUNA N 70D*	31-11-BN
12	1	BOTT.ADJ.NUT	STEEL, CAD. PLATED	23-12-CS
13	1	BOTT.LOCK NUT	STEEL, CAD. PLATED	23-13-CS
14	4	STUD	ALLOY STEEL	31-14-AS
15	4	STUD NUT	STEEL	23-15-CS
16	2	SEAL	LEAD WITH S.S. WIRE	23-7-PB
17	1	NAME PLATE	STAINLESS STEEL	SEE TABLE

*ALTERNATE MATERIAL AVAILABLE.

PRESSURE SETTING	CFM AIR	SPRING NO.	VALVE NO.	NAME PLATE
150	20500	34-150-AS	A-3450	34-18-SS
255	33300	34-255-AS	A-3455	34-19-SS
280.5	36640	34-280-AS	A-3490	34-17-SS
300	38700	34-300-AS	A-3400	34-20-SS
330	42900	34-300-AS	A-3430	34-21-SS

Fig.: 3-9: Midland A-3480 Safety-Relief Valve a cross-section of the Midland A-3480 safety valve commonly used on DOT 112A (or 114A) tank cars. The entrance to the actual valve seat is seen to be through a short tube (enclosing the spring) having a flow area less than twice that of the valve port area. Hence the liquid will accelerate and its pressure will drop before it reaches the final constriction, much as it would in a nozzle. Henry (43) discusses the flow through an ideal nozzle, and shows that the pressure at the throat is well above atmospheric, signifying a choking phenomenon as in a compressible flow, and implying the formation of vapour at or before the throat is reached. For a nozzle flow, Henry suggests a model (the Henry-Fauske model) in which no vapour is formed until the flow reaches the throat, where partial flashing occurs to produce a mixture of phases in equilibrium at the observed critical pressure ratio of 0.85 (p_{th}/p_o where p_{th} is the pressure at the nozzle throat) for a saturated liquid. The flow will therefore be incompressible up to the throat, and the flow velocity can again be determined from Bernoulli's equation, but for a pressure drop from p_o to 0.85 p_o only. The Henry-Fauske model determines the flow rate by assuming the saturated liquid density to exist at the throat. If this is done, a flow rate is predicted which exceeds that given by Sallet by a factor of nearly 2. However, to be consistent with the assumption that vapour has formed at the throat, a mixture density corresponding to an equilibrum mixture at the throat pressure should be used to determine the mass flux, $\dot{m}/A$ or ρV. The mass flux determined by this modified H-F model agrees reasonably well with the Sallet model prediction, being about 20% lower. This discrepancy can be accounted for by a probable difference in flow coefficient, to be discussed later.

Of the four methods just discussed, two appear to give similar results, while the others predict mass fluxes about twice and four times as high. The H-F orifice model, predicting the highest flow rate, is probably not applicable to the type of safety valve now in use, though it would be applicable to a rupture disc type of emergency device if these are used in the future. The H-F nozzle model, which would seem to be appropriate, is based on actually observed two phase flow behavior and predicts actual nozzle flows quite well, as reported by Henry (43). However, the inconsistency between the physical model proposed, and the density used in the evaluation of the mass flux, is disturbing. The modified H-F nozzle method seems more rational, but would not agree well with the nozzle flow data quoted by Henry. Finally, the Sallet method, which uses a rather simplistic homogeneous equilibrium model, is said (by Sallet) to agree well with observed tests of actual valves, even though similar methods have been shown by Henry (43) and by Fauske (44) to badly under predict flow rates of very low quality steam/water mixtures through nozzles (43) and pipes (44). The reasonable agreement between the Sallet prediction and the modified H-F nozzle flow prediction is encouraging however, so that in the absence of actual valve test data, the Sallet method is recommended.

Using the mass flux data given in figure 3-8, the flow through a particular valve is given by

$$\dot{m} = C_D A G \qquad 3\text{-}36$$

where $G = f(p_o, x_o')$ ($x_o' = 0$ for a saturated liquid stagnation state) and C_D and A are the valve flow coefficient and minimum area, respectively. A plot of G vs. p_o given by Graves in (4) and shown here as Fig. 3-10 indicates the relationship between G and p_o for the saturated liquid stagnation state more clearly than Fig. 3-8 and hence is more suitable for obtaining a curve fit to the relationship. The critical mass flux curve shown in Fig. 3-10 can be approximated (within the readability of the graph) by the expression,

$$G = -0.0292\ p_o^2 + 24.1\ p_o - 1602.0 \qquad 3\text{-}37$$

for $200 \le p_o \le 450$ psia. The mass flux (G) predicted by Eq. 3-37 is in lbm/ft^2 sec. In metric units, Eq. 3-37 can be rewritten as

$$G = -2998.87\ p_o^2 + 17065.77\ p_o - 7821.78 \qquad 3\text{-}38$$

for $1.38 \le p_o \le 3.10$ MPa (the units of G are kg/m^2 sec.). Equation 3-38 will be used in the DE tank car model to predict G for a submerged pressure relief valve.

Finding suitable values for C_D and A in Eq. 3-36 presents considerable difficulty. Consider the area A first. The safety valve shown in figure 3-9 is a spring loaded poppet valve which is forced open by the internal pressure and does not appear to have either a toggle action or a latching mechanism. Reference 42, from which figure 3-9 was taken, shows the valve opening history during a tank car fire. The valve, a Midland A-3480, had a port opening area of 5100mm^2 (7.85 in^2), but for valve lifts less than about 20mm, the poppet and its seat defined a smaller opening. The valve-lift trace on a recorder showed that during the test the valve opened fully during the initial five minutes of blowdown, but for the remaining 17 minutes, the lift was only 18mm or so. While this lower reading might have been due to thermal

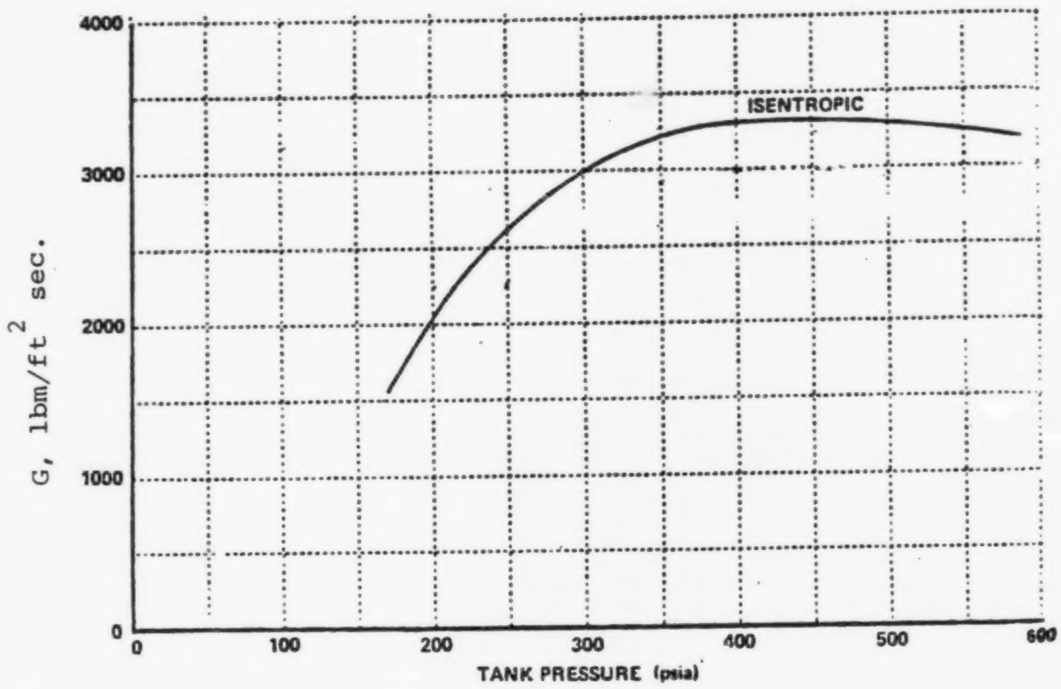

Fig. 3-10: Critical mass flux (G) for liquid propane stagnation state.

drift in the transducer used, it might also have been caused by the reduced task pressure in the later stages of blowdown. In any case, the user of the DE tank car model will be required to provide a valve area vs. tank pressure schedule, $A(p_o)$, for the relief valve being modelled to ensure that the venting process is modelled accurately. Defining the flow coefficient C_D for the valve presents further difficulties. Sallet (41) quotes a value of 0.64 for liquid flow, and 0.88 for air flow through the valve. However, it is well known that the flow coefficient for compressible flow through an orifice is not constant but depends on the pressure ratio, increasing from about 0.61 to about 0.85, as the pressure ratio drops from 1 to 0.15. The valve opening is annular, and the coefficient for an annular orifice is larger than for a circular one, and is also pressure ratio dependent. The annular orifice flow coefficient varies from 0.65 to about 0.95 as pressure ratio varies from 1 to 0.3.

It seems likely that the coefficient changes continuously, at a given pressure ratio, as initial quality varies from 0 to 1. However, in view of the fact that even for saturated liquid at the inlet, the void fraction will be over 0.6 at the valve constriction using Sallet's equilibrium process, the flow coefficient will almost certainly exceed 0.7 at this inlet condition.

In the absence of any more specific information, a value of 0.75 is suggested for this coefficient when the valve is submerged in saturated or subcooled liquid propane. (It is interesting to note that using a value of 0.75 with the Sallet model, and the appropriate value of about 0.98 for the H-F nozzle model, brings the mass flow rate prediction of these two models into very close agreement).

To summarize, the mass flow rate through a submerged safety valve can be calculated from

$$\dot{m} = 0.75\ A(p_o)\ G(p_o) \qquad 3\text{-}39$$

where $A(p_o)$ is the minimum valve area specified as a function of tank pressure and $G(p_o)$ is given by Eq. 3-38.

3.4 Discharge Flowrate Calculation - Vapor Stagnation State

The stagnation state of the fluid discharged by the relief valve or other pressure relief device will be vapor if the valve is located above the liquid surface and if no liquid spray is entrained in the discharge flow. If the vapor is saturated initially, an isentropic expansion to the minimum flow area will result in some condensation and/or supersaturation of the vapor. In steam turbine nozzles, for example, the Willams line, which lies about 40^oF below the saturation line on a temperature-pressure (T-p) plot, defines the lowest pressure that initially saturated steam can be expanded to (rapidly) without some condensation occurring. The vapor is in a state of metastable equilibrium between the Willams line and the saturation line.

It will be assumed that the vapor being discharged from a relief valve does not condense at all during its expansion to the pressure at the valve port since this permits the discharge flowrate to be calculated very easily. The vapor will usually be somewhat superheated because of the heat transferred to it from the hot tank wall so it is possible that the vapor would expand without condensing even if the expansion occurred slowly.

The critical pressure ratio for propane vapor was shown to be approximately 0.576 in Sect. 2.4.1 (see Eq. 2-106) so the relief valve or other pressure relief device will be choked for all cases of interest. The mass flowrate through the relief valve can be calculated from Eq. 3-36 in this case, as before, only with the critical mass flux G (for an isentropic expansion) defined by the expression,

$$G = \sqrt{\frac{p_o}{v_o}}\sqrt{\gamma\left(\frac{2}{\gamma+1}\right)^{\frac{\gamma+1}{\gamma-1}}}$$

$$= 0.637\sqrt{\frac{p_o}{v_o}} \qquad (\text{kg/m}^2\ \text{sec.}),\ \text{for } p_o \text{ in Pa},\ v_o \text{ in m}^3/\text{kg} \qquad 3\text{-}40$$

instead of by Eq. 3-38. The ratio of specific heats (γ) was assumed to be 1.14 for propane to obtain the factor of 0.637 in Eq. 3-40.

The superheat of the propane vapor produced by heat transfer from the tank wall will be taken into account when its specific volume (v_o) is calculated for the purpose of evaluating Eq. 3-40. If the saturation temperature of the vapor at the prevailing tank pressure is T_s, then the stagnation temperature (T_o) of the venting vapor at the relief valve will be,

$$T_o = T_s + \frac{\dot{Q}_v}{\dot{m}C_{pv}} \qquad 3\text{-}41$$

when the tank-to-vapor heat flow rate is $\dot{Q}_v$ (this heat flow rate will be calculated by the thermal model) and the constant pressure specific heat of the vapor at the temperature $(T_o+T_s)/2$ (ie. at its average temperature) is C_{pv}. Assuming that the vapor behaves, to a first approximation, as a perfect gas, its stagnation specific volume at the relief valve (v_o) is calculable from the expression,

$$v_o = v_s \frac{T_o}{T_s} \tag{3-42}$$

where v_s is the specific volume of saturated propane vapor at the temperature T_s. The value of v_s will be obtained from thermodynamic property tables for propane.

As in the case of the liquid flowrate calculation, the valve throat area (A) in Eq. 3-36 will have to be specified as a function of the tank pressure by the program user. For the valve flow coefficient (C_D), Sallet (41) recommends that it be assigned a value of 0.88 to evaluate the critical vapor flowrate through a typical relief valve. By analysing the rate at which the liquid level changed during the test of tank car RAX 201, Anderson et al. (10) determined that the valve coefficient for the Midland A-3480 relief valve used on that tank must have been approximately 0.86 on average during the venting period. Since this flow coefficient agrees quite well with Sallet's recommended value of 0.88, a flow coefficient of 0.87 will be used in the DE tank car model to predict vapor discharge flowrates.

4.0 TANK RUPTURE PREDICTION

The methods that will be used to predict if and when a pressurized tank car will rupture when it is enveloped by a pool fire or heated locally by a torch fire are described in Sects. 4.1 to 4.4. The DE proposed approach does not use the finite - element method to predict tank rupture in either the pool fire or the torch fire scenario but a procedure by which the finite - element method could be used to predict rupture in either of those cases is described in Sect. 4.5. The finite - element formulation that would be required to predict tank rupture reliably is outlined in that section.

4.1 Pool Fire Rupture Prediction

Determining if and when a tank car ruptures in a pool fire requires, as a first step, that the stresses in the tank wall be estimated and then that the stresses in the wall be used to predict failure in some manner. Neither task is easy if approached rigorously for several reasons. First, it is not clear whether thermal strains will contribute significantly to tank failure. Thermal strains will probably be comparable in magnitude to the elastic strains produced by internal tank pressure and, for that reason, thermal stresses will likely be comparable to pressure induced stresses when deformations are elastic. In support of this observation, consider a scenario in which the wall temperature of a tank car in a fire is approximately 600°C (this is a typical rupture temperature) in the ullage space and approximately 80°C* below the level of the liquid surface. The resulting temperature difference of 520^{o}C between the top and bottom sections of the tank wall will produce a differential thermal strain (ε_t) of $\simeq 6.1 \times 10^{-3}$ m/m (calculated using a coefficient of thermal expansion, α_t, of $1.17 \times 10^{-5}\,{}^{o}C^{-1}$) which will, in turn, produce an axial compressive stress (σ_z) of 420 MPa (61,000 psi)* at the top of the tank if the bottom (ie. liquid - wetted) part of the tank wall inhibits axial expansion of the top and if, in addition, wrinkling of the upper part of the tank wall does not occur. If the tank is, say, half-full of liquid, the bottom half of the tank will be much stiffer than the top half because Young's modulus of elasticity for steels is typically 207GPa (30×10^{6}psi) at 80^{o}C and less than 69GPa (10×10^{6}psi) at 600^{o}C. The upper part of the tank will not be completely restrained (axially) by the bottom half, of course, so the axial compressive stress in that section will be less than the value of 420MPa mentioned previously. Thermal expansion of the top part of the tank relative to the bottom part will cause the entire tank to bow slightly, as shown in Fig. 4-1. Even if the axial compressive stress induced by thermal expansion of the top of the tank is only half of that mentioned previously (ie. only 210MPa), however, it will still be comparable in magnitude to typical pressure - induced stresses. The hoop stress in a full-size DOT 112A or 114A tank car at an internal pressure of 1.93MPa (280psig), which is a typical relief valve pressure, is 184MPa(26,600psi) by way of comparison.

---

* Estimated average wall temperature at a tank pressure of 2.0MPa (290 psiq). The saturation temperature of propane at this pressure is 60°C.

Thermal strains and hence elastic thermal stresses will also be produced by the temperature gradient across the tank wall and temperature - induced changes in the curvature of the

---

* Calculated using a Young's modulus of 69GPa (10×10^{6}psi)

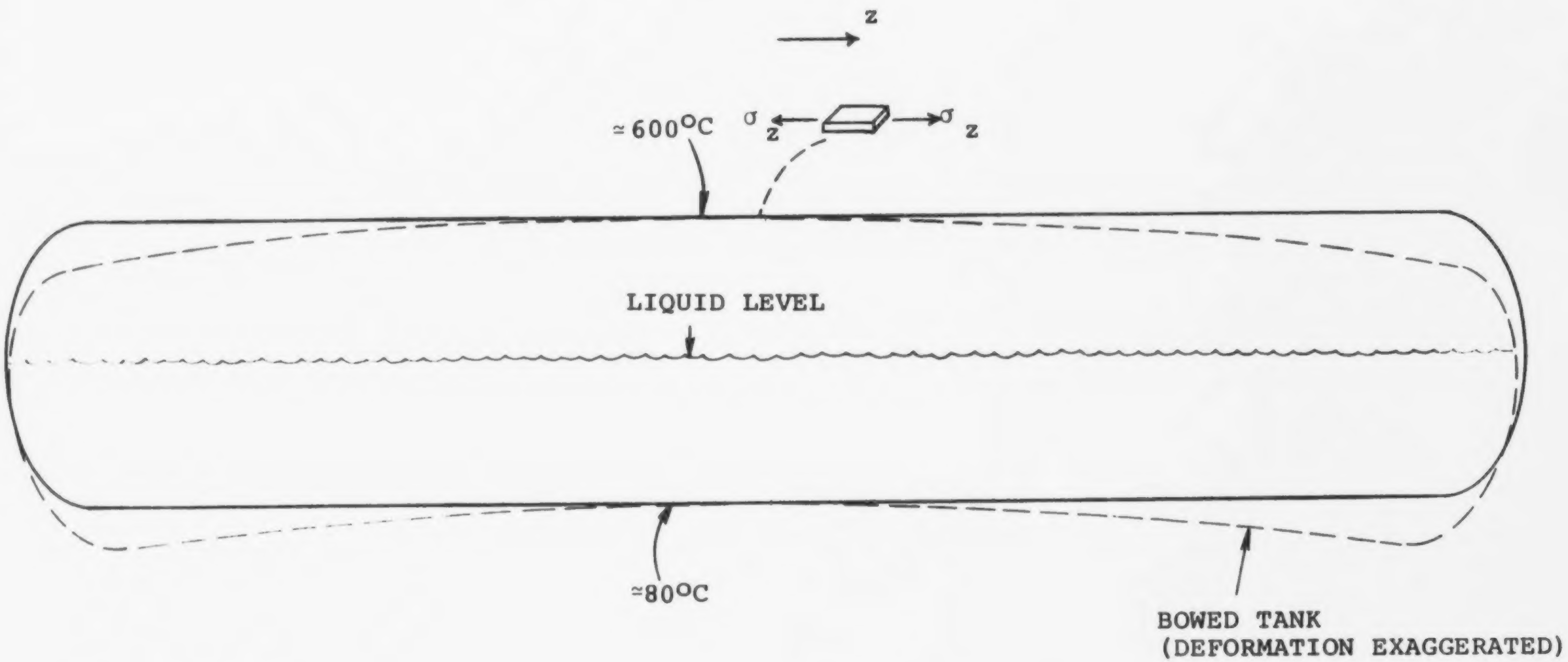
z
≃600°C
σ_z
σ_z
LIQUID LEVEL
≃80°C
BOWED TANK
(DEFORMATION EXAGGERATED)

Fig.: 4-1: Tank car distortion due to overheating of the top of the tank hot part of the tank wall relative to the cool part, etc., but there is no way that any of these stresses can be determined without modelling the *entire* tank using the finite - element method. The axial and hoop (circumferential) thermal stresses at the inner and outer surfaces of a thin-walled cylinder subjected to *axisymmetric* thermal loading can both be calculated from the equation

$$\sigma = \pm \frac{E \ \alpha_T \ \Delta T}{2(1-\nu)},$$

(-ve (compressive) stresses are found at the botter surface) 4-1

ν = Poisson's ratio

when the temperature difference between the inner and outer surfaces is ΔT and the temperature gradient is linear across the wall, but the axisymmetric thermal loading stipulation will not be satisfied in the case of a tank car that is partially filled with LPG because thermal gradients across the tank wall will be higher below the level of the liquid surface than above it. Equation 4-1 cannot be used to estimate thermal stresses in the tank car analysis because of this lack of axisymmetry, although it was used for that purpose by Graves (4). The curvature of the tank wall remains constant and uniform at all circumferential positions when the thermal loading is axisymmetric but it will be circumferentially non-uniform in the tank car case (ie. the tank will not remain circular in cross-section).

The preceding discussion of thermal strains demonstrated that they will be comparable in magnitude to elastic strains cause by internal tank pressure. Rupture of a tank car occurs as the result of inelastic strains brought about by yielding and/or creep, however, as proven by the substantial reductions in wall thickness that have been observed along fracture paths in failed tanks. While thermal strains can contribute significantly to the fracture of very brittle materials, such as glass, where almost no inelastic deformation occurs before failure, they cannot generally cause ductile materials to rupture because such materials yield to accommodate the thermal strains when those strains produce excessively high stresses. The action of-pressure-induced stresses is quite different, however, in that they are produced by forces which do not decrease in value when yielding occurs. Stresses produced by invariant loads (eq. pressure forces) are commonly referred to as primary stresses while thermal stresses are an example of secondary (or self-limiting) stresses (45). Harvey (45) observes in his book "Pressure Component Construction" (1980, p. 72) that "They (thermal stresses) will not cause failure by rupture in ductile materials upon their first application irrespective of their magnitude, but they will cause failure by repeated cycling, ie. fatigue. It is important to recognize this distinction (between thermal and primary stresses) in appraising the significance of thermal stresses". Since loads imposed by internal tank pressure can provide the energy needed to cause ductile tank car steels (eg. TC-128-B) to deform (thin) and eventually rupture while thermal stresses and strains can contribute relatively little energy, it will be assumed in this analysis that tank rupture is caused by and hence can be predicted from pressure - induced stresses alone.

4.2 Stress Calculations

Only pressure-induced stresses will be used to predict tank failure in this analysis, as mentioned previously. The pressure-induced membrane stresses in the cylindrical section of a thin-walled tank car shell are, of course, the hoop and longitudinal stresses, designated σ_h and σ_ℓ respectively. These two stresses can be calculated from the well-known equations

$$\sigma_h = \frac{pR_{it}}{t} \qquad 4\text{-}2$$

$$\sigma_\ell = \frac{pR_{it}}{2t} \qquad 4\text{-}3$$

in which p is the internal tank pressure, R_{it} is the inner radius of the tank, and t is the shell's wall thickness.

Tank cars manufactured to DOT 112A (or 114A) specification use 2:1 ellipsoidal heads fabricated from plate with a thickness equal to that of the wall of the cylindrical shell with the result being that the maximum membrane stresses in the heads and the cylindrical shell are the same. Tank ruptures in tank car fire tests performed with level (horizontal) tanks have always initiated in the cylindrical shell rather than in the heads, to the author's knowledge, so it is proposed that tank rupture by head failure not be considered in the tank car model. This simplification is deemed necessary because it is impossible to predict tank head failure when part of the head is below the level of the liquid surface and part is above it without using a very sophisticated finite - element program. Failure of a tank head can only be predicted, without performing a sophisticated finite - element analysis, when the head is approximately isothermal so that its ultimate strength is the same at all points, a proviso that will only be satisfied (approximately) when the head is either completely covered by liquid or completely uncovered. The latter condition might arise at the high end of a tilted tank, for instance, while the former situation could prevail at the low end depending on the angle of tilt. Even a failure analysis performed under these restrictive conditions is not simple, however, because expressions for the membrane stresses in the head obtained using the undeformed head geometry, and expressions for the discontinuity stresses at the head-to-shell joint, which are actually secondary or self-limiting stresses (similar to thermal stresses) because they result from mis-matched deformations between the cylindrical shell and the head, are of almost no value in predicting the rupture of a tank head fabricated from a ductile steel because such a head undergoes extreme deformations before rupturing. In support of this observation, Fig. 4-2 (taken from (46)) shows the measured deformations before rupture of a torospherical head with a geometry similar to that of the 2:1 ellipsoidal head design commonly used on tank cars. The curvature of the head in a meridional plane (the profile shown in Fig. 4-2 is a cross-sectional view through a meridional plane) actually changed sign in the knuckle region in that it went from being concave in, initially, to being concave out at the rupture pressure. The rupture pressure of approximately $63 kg/cm^2$ was more than three times the pressure at which the head started to yield, which was approximately $20 kg/cm^2$. It can be seen from Fig. 4-2 that the change in head geometry from the initial, undeformed, configuration to the final deformed configuration resulted primarily from bending of the tank wall in the knuckle region. Only a very advanced finite - element code would be able to model the large scale yielding and changes in geometry that preceded the failure of the head shown in Fig. 4-2. The application of finite - element techniques to such problems is discussed in Sect. 4.5.

The rupture pressure of a head which undergoes large deformations before failing can be calculated approximately by performing a limit analysis, in the manner described by Gerdeen and Hutula in reference (47), when material properties are uniform throughout the head. A limit analysis predicts the limit pressure of a pressure vessel component which, by definition, is the pressure at which the component would undergo unrestrained deformation if it was fabricated from a rigid - ideally plastic material. The stress-strain curve for such an idealized material is shown in Fig. 4-3. Elastic

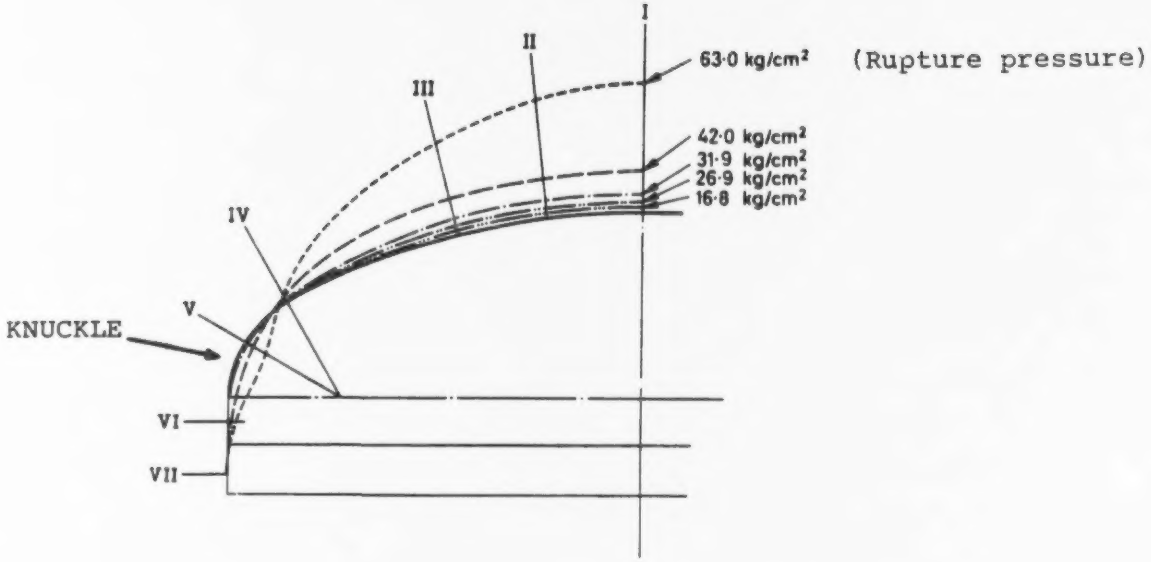
I
II
III
IV
V
KNUCKLE
VI
VII
63·0 kg/cm²
(Rupture pressure)
42·0 kg/cm²
31·9 kg/cm²
26·9 kg/cm²
16·8 kg/cm²

Fig. 4-2: Measured Torospherical Head Deformations (46).

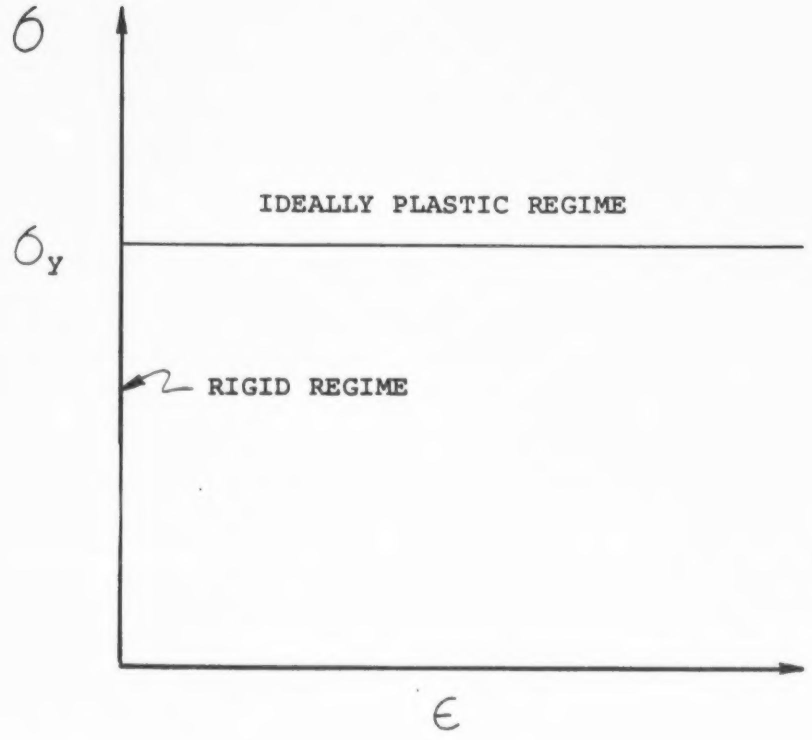
σ
IDEALLY PLASTIC REGIME
σ_y
RIGID REGIME
ε

Fig.: 4-3: Stress-strain curve for a rigid-ideally plastic material strains, which are generally small compared to plastic strains in a ductile material at the time of rupture, are neglected in such an analysis because of the assumed rigid-ideally plastic stress-strain relationship. Strain hardening effects are also ignored. While a tank car steel is obviously not really rigid-perfectly plastic, such steels are usually sufficiently ductile to give the limit pressure concept genuine significance when the ultimate or yield strength of the steel is uniform throughout the head.

The results of Gerdeen's limit analysis for a 2:1 ellipsoidal head design of the type commonly used in tank cars are summarized in Fig. 4-4, taken from (47). The curve labelled "Upper Bound, Mode II,$p_u z$" is based upon von Mises yield criterion (von Mises yield criterion is described briefly in the next section). A "Mode II" failure occurs in the head. Changes in stress resulting from changes in geometry during yielding were not considered in the limit analysis, a simplification which it can be shown leads to a slight underestimation of the limit pressure for the head. The curve labelled "Membrane Theory, Lower Bound" is not of particular interest in this analysis because it defines the pressure at which yielding begins, as predicted from the membrane stresses in the head without considering interaction with the cylinder. The line drawn parallel to the abscissa at $\frac{pD}{2\sigma_y t} = 1.155$ and labelled "Collapse Pressure for Infinite Cylinder with Rigid Heads" indicates the pressure at which a long cylinder attached to the head would burst, again based on von Mises failure theory. It can be seen from this curve and the "Upper Bound; Mode II,p_u" curve that the cylindrical shell of a long cylindrical pressure vessel will fail before the head when the inner diameter/ thickness (D/t) ratio is less than approximately 100 and that

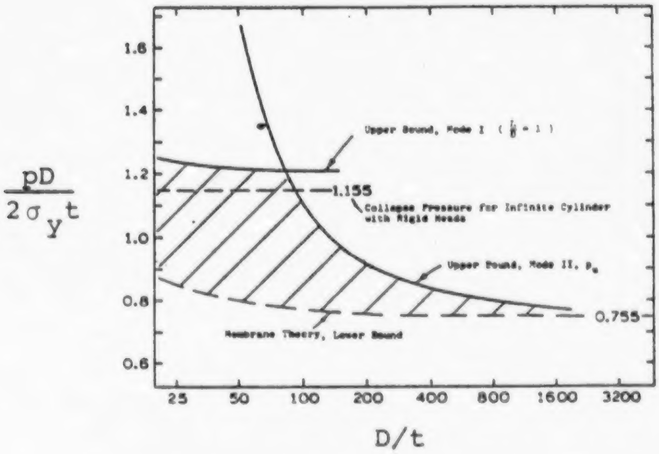

Fig. 4-4: Plastic collapse pressures for 2:1 ellipsoidal head pressure vessel based upon the von Mises yield criterion.

the head will fail before the cylinder at D/t ratios greater than this value. It is assumed that the head and the cylindrical shell have the same wall thickness. The head reinforces the cylindrical shell slightly when the cylinder is short and hence increases the burst pressure of the cylinder, as seen from the curve labelled "Upper Bound, Mode I, (L/D = 1)", where L is the length of the cylinder. A "Mode I" failure occurs in the cylindrical shell.

The D/t ratio for a DOT 112A tank car is 189 (D = 3m, t = 1.59cm) so the curves shown in Fig. 4-4 indicate that the 2:1 ellipsoidal head on such a tank would fail (before the shell) when $\frac{pD}{2\sigma_y t} = 0.925$. Gerdeen performed a more accurate analysis, described in (48), which indicated that a 2:1 ellipsoidal head with D/t = 189 would fail when $\frac{pD}{2\sigma_y t} = 0.99$. The head and shell materials were assumed to be elastic-perfectly plastic in the analysis described in (48) instead of rigid - perfectly plastic as previously assumed and changes in stress resulting from changes in head geometry during failure were taken into account.

Hydrostatic burst tests of a 2:1 ellipsoidal head attached to a cylindrical skirt were performed by Foster-Wheeler and, for the D/t ratio of 192 used in those tests (D/t = 189 for a DOT 112A tank car), failure occurred in the cylindrical shell rather than in the head as predicted by Gerdeen's analysis. The Foster-Wheeler tests are described by Berman et al. in (49). The 2:1 ellipsoidal head used in the Foster-Wheeler tests was commercially fabricated in the manner in which all such heads are produced, by hot spinning, and it was found that the hot spinning process caused the wall thickness of the head to be highly non-uniform. The wall thickness in the knuckle region of the hot spun head was 50% greater than the wall thickness at the crown. Since yielding in a 2:1 ellipsoidal head occurs initially in the knuckle region, the greater-than-normal thickness of the knuckle in the Foster-Wheeler head would have caused Gerdeen's predicted failure pressure, which assumed a uniform head thickness, to be too low. Gerdeen predicted the limit pressures of a large number of 2:1 ellipsoidal heat with different knuckle-to-crown wall thickness ratios (t_1/t_o) for several tank inner diameter-to-crown wall thickness ratios (D/t_o) and obtained the results tabulated in Table 4-1. The limit pressure ($\overline{p}_\ell$) given in that table is actually the value of $\frac{pD}{2\sigma_y t}$ at the rupture pressure. The wall thicknesses of the cylindrical shell and the crown of the head were assumed to be the same in the analysis. The results given in Table 4-1 for $t_1/t_o = 1.5$*, and $D/t_o = 192$, which are the appropriate values of those parameters for the head/cylinder combination tested by Foster-Wheeler, predict that the Foster-Wheeler pressure vessel would have failed by head rupture at $\frac{pD}{2\sigma_y t} \simeq 1.08$. Since the value of $\frac{pD}{2\sigma_y t}$ is quite close to the value at which rupture would have occurred in the cylinder instead of the head (rupture would have occurred in the cylinder at $\frac{pD}{2\sigma_y t} \simeq 1.155$) and since Berman et al. noted that the head was severely deformed at the time of rupture, Gerdeen's analysis probably cannot be faulted for failing to predict the point of rupture correctly. If the ultimate tensile strength (σ_u) of the steel used in the Foster-Wheeler tests is substituted for

---

* Limit pressures are not given for t_1/t_o 1.429 in Table 4-1, so the tabulated values were extrapolated slightly to obtain the limit pressure for $t_1/t_o = 1.5$

TABLE 4-1: Limit pressures for pressure vessels with 2:1 ellipsoidal heads - predicted results for different tank diameter (D) to crown thickness (t_o) and crown thickness to knuckle thickness (t_1) ratios.

$\frac{D}{t_o}$	$\frac{t_o}{t_1}$	$\frac{t_1}{t_o}$	$\bar{p}_v$	$\bar{p}_\ell$
80	0.7	1.4286	0.736	1.143
	0.8	1.2500	0.728	1.128
	0.9	1.1111	0.720	1.113
	1.0	1.0	0.708	1.095
100	0.7	1.4286	0.736	1.128
	0.8	1.2500	0.730	1.109
	0.9	1.1111	0.714	1.087
	1.0	1.0	0.702	1.070
150	0.7	1.4286	0.747	1.093
	0.8	1.2500	0.726	1.067
	0.9	1.1111	0.711	1.038
	1.0	1.0	0.689	1.015
200	0.7	1.4286	0.751	1.063
	0.8	1.2500	0.731	1.034
	0.9	1.1111	0.704	1.005
	1.0	1.0	0.685	0.981
300	0.7	1.4286	0.763	1.036
	0.8	1.2500	0.732	0.999
	0.9	1.1111	0.706	0.969
	1.0	1.0	0.681	0.943
400	0.7	1.4286	0.772	1.018
	0.8	1.2500	0.742	0.982
	0.9	1.1111	0.706	0.950
	1.0	1.0	0.678	0.918
800	0.7	1.4286	0.799	0.998
	0.8	1.2500	0.755	0.958
	0.9	1.1111	0.721	0.921
	1.0	1.0	0.684	0.884
Membrane theory	0.7	1.4286	0.94	0.94(lb)
	0.8	1.2500	0.88	0.88(lb)
	0.9	1.1111	0.82	0.82(lb)
	1.0	1.0	0.76	0.76(lb)

$\bar{p}_y = \frac{p_y D}{2 \sigma_y t_o}$, ($p_y$ = pressure at which yielding starts)

$\bar{p} = \frac{p_r D}{2 \sigma_y t_o}$, ($p_r$ = pressure at which rupture occurs)

σ^*_y in the parameter $\frac{pD}{2\sigma_y t}$, the value of 1.08 given previously for $\frac{pD}{2\sigma_y t}$ corresponds to a failure pressure of 9.75MPa (1414psi) for the Foster-Wheeler pressure vessel. That pressure agrees well with the actual rupture pressure of 10.17MPa(1475psi) obtained in the burst test. Failure of the cylinder would have occurred for $\frac{pD}{2\sigma_y t} \approx 1.155$ or $p = 10.42$MPa(1511psi), a pressure which is, again, in excellent agreement with the observed rupture pressure of 10.17MPa.

The foregoing example of the use of Table 4-1 indicates that the limit pressures tabulated in Table 4-1 for different values of D/t_o and t_1/t_o are probably suitable for predicting the limit pressure of a 2:1 ellipsoidal head** when σ_u is approximately uniform throughout the head. The latter proviso will not be satisfied when temperatures within the head vary over a wide range because of the dependence of ultimate strength on temperature so it is not likely that the tabulated data will be applicable to a head which is exposed to flames on its external surface but partly covered by liquid propane on its internal surface. The liquid-wetted section of the head will likely be much cooler, and hence stronger, than the vapor-covered section under those conditions and hence will reinforce the hot section in contact with the vapor.

Thus it is recommended, as mentioned previously, that failure be predicted from the temperature and stress conditions in the cylindrical shell alone since it is has been observed experimentally that tank ruptures do not initiate in tank heads when the heads are partly covered by liquid. It is likely that the head at the high end of a tilted tank will rapidly become approximately isothermal (and hence of uniform strength) if and when the liquid level drops below the bottom of the head so the values of $\bar{p}_\ell (= \frac{pD}{2\sigma_y t_o})$ in Table 4-1 could be used to predict head rupture after that time. The value of $\bar{p}_\ell$ corresponding to given values of D/t_o and t_1/t_o would be used in that case to define an effective stress in the head, designated σ_e, where

---

* Steels are not perfectly plastic so the ultimate tensile strength of a steel is a better measure of its rupture strength than σ_y.

** The well-known Shield and Drucker equation (46) can be used to predict the limit pressure of a torospherical head of arbitrary dimensions.

$$\sigma_e = \frac{pD}{2\bar{p}_\ell t_o} \qquad 4\text{-}4$$

At the limit pressure (ie. when $\bar{p}_\ell = \frac{pD}{2\sigma_u t_o}$), $\sigma_e = \sigma_u$

An effective stress in the cylindrical shell will be defined in the next section, where the actual manner in which rupture will be predicted from effective stresses is described in detail.

4.3 Failure Analysis

Equation 4-2 and 4-3 can be used to predict the membrane stresses in the cylindrical shell of a pressurized tank car. The cylindrical shell is under a biaxial state of stress at all points so a decision as to which stress constitutes the "effective stress" governing failure must be made. For ductile materials, this stress is generally taken to be either the maximum shear stress or the octahedral shear stress at a point, with the corresponding failure theories being known as the maximum shear stress (or Tresca's) theory and von Mises (or the maximum distortion energy) theory respectively. The maximum shear stress theory predicts failure by yielding when $\sigma_1 - \sigma_2 \geqslant \sigma_y$, where σ_1 and σ_2 are the maximum and minimum principal stresses at a point. For a biaxially stressed material with positive principal stresses $\sigma_2 = 0$, however, so the Tresca yield criterion reduces to $\sigma_1 \geqslant \sigma_y$, where $\sigma_1 = \sigma_h$ for a pressurized cylindrical shell. Thus the hoop stress, σ_h can be taken as the effective stress (σ_e) governing rupture if it is assumed that Tresca's failure criterion applies to tank car steels. Von Mises theory predicts failure by yielding when $\sigma_m \geqslant \sigma_y$, (for failure by rupture, σ_u should be substituted for σ_y) where $\sigma_m = \sqrt{\sigma_1^2 + \sigma_2^2 - \sigma_1 \sigma_2}$ for a biaxially stressed material. For a pressurized cylinder, $\sigma_1 = \sigma_h$ and $\sigma_2 = \sigma_\ell = \frac{\sigma_h}{2}$ so $\sigma_m = \sqrt{\sigma_h^2 + (\sigma_h/2)^2 - \sigma_h^2/2}$ $= 0.866\sigma_h$.* Von Mises stress (σ_m) can be taken as the effective stress governing rupture if it is assumed that tank car steels fail according to von Mises criterion (ie. rupture occurs when $\sigma_m \geqslant \sigma_u$). Since $\sigma_e = \sigma_h$ and $\sigma_e = 0.866\sigma_h$ for materials obeying Tresca's yield criterion and von Mises yield criterion respectively, the maximum shear stress (Tresca's) theory predicts a lower rupture pressure for a cylindrical shell than von Mises theory and hence is usually used for design purposes (because it is more conservative). The results of failure tests performed with ductile materials generally agree somewhat better with von Mises theory than they do with Tresca's theory, however, so it will be assumed in this analysis that the von Mises stress (σ_m) is the effective stress (σ_e) governing the rupture of a cylindrical tank car shell. It will be shown later, however, that similar rupture times are predicted for a full-size unprotected tank car in a fire when σ_h is taken to be the stress governing rupture instead of σ_m(ie. when it is assumed that the tank car steel obeys Tresca's failure criterion instead of von Mises). Equation 4-4 will be used to calculate the effective stress in a 2:1 ellipsoidal head if temperature variations and hence variations in ultimate strength within the head are small, as discussed in Sect. 4-2.

---

* Since von Mises theory predicts that a pressurized cylinder will rupture when $\sigma_m \geqslant \sigma_u$, where $\sigma_m = .866\sigma_h = .866\frac{pD}{2t}$, rupture occurs by this theory when $\bar{p}_\ell = \frac{pD}{2\sigma_u t} = \frac{1}{0.866} = 1.155$. This result is in agreement with the collapse pressure of an infinitely long cylinder shown in Fig. 4-4.

The stress chosen as the stress governing rupture (ie. σ_e) can be used to predict rupture in one of two possible ways depending on whether or not creep (stress-rupture) effects are judged to be important. If such effects are not considered to be important, it can be assumed that the tank will rupture when σ_e exceeds the ultimate tensile strength of the tank car steel at the prevailing wall temperature. A plot of the ultimate tensile strength of the most commonly used tank car steel, TC-128-B, is shown as a function of temperature in Fig. 4-5. The simple rupture criterion (von Mises) mentioned previously would predict failure of a TC-128 tank car shell stressed to 159MPa (23,000psi), which is the von Mises stress in the cylindrical section of a full-size DOT 112A tank car at an internal pressure of 1.93MPa (280psig), at a temperature of approximately 680°C (1250°F), for example. If creep of the tank car steel before rupture is expected to be significant, however, a stress-rupture approach must be used to predict failure. A stress-rupture approach will be used to predict failure of tank cars in this analysis

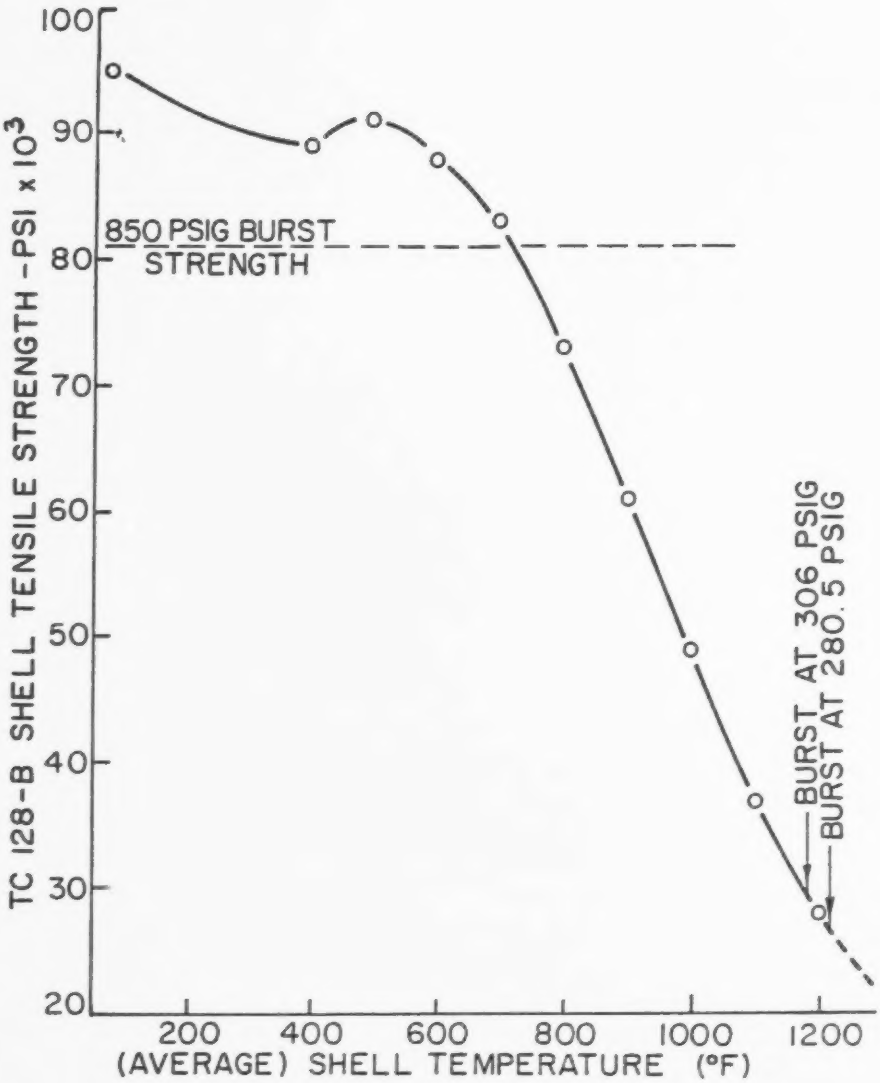

Fig. 4-5: TC-128-B Steel Tensile Strength As a Function of Temperature (after RPI-AAR Program Data, RA-11-1-5, Phase II Report, 1971, p. 32).

since it defaults to the first approach if creep is not important. Also, the requirement that the analytical model be applicable to tanks with differing degrees of thermal protection over a wide variety of accident conditions means that creep cannot be ruled out as a significant mechanism under all circumstances. Slow heating (temperature rise) rates, such as will be obtained with insulated tanks, will tend to make creep more important, for example, because the tank car steel may conceivably be at high temperatures, where creep rates are correspondingly high, for extended periods of time.

Creep will be taken into account in the tank car failure analysis by applying the results of stress-rupture tests, which are simply tests in which a specimen is held at a constant known temperature, at a constant known stress (tensile) until it breaks. Such tests are performed at different temperatures and stress levels and the life of the specimen (ie. time to rupture) is recorded for each set of test conditions to produce data such as that shown in Table 4-2 (taken from (50)). The results shown in Table 4-2 were obtained in tests of TC-128 steel specimens.

The stress-rupture data obtained in the manner described previously can be presented in the form of a Larson-Miller curve in which stress is plotted against the Larson-Miller parameter P, where

$$P = T(20 + \ln(t)) \qquad 4\text{-}5$$

The variables T and t in Eq. 4-5 are the temperature of the stressed material and the life of the material at that temperature respectively. The Larson-Miller curve for the test results given in Table 4-2 is shown in Fig. 4-6. Assuming the Larson-Miller correlation technique (described in (51)) is

TABLE 4-2

ELEVATED TEMPERATURE TEST RESULTS ON TANK CAR STEEL

Spec Ident.	Temperature		Stress		Time to Failure (min)	Elongation (%)
	(^oC)	(^oF)	($10^8 \cdot$ dynes/cm^2)	($10^3 \cdot$ lbs/in^2)		
9T	482.2	900	52.9	76.7	(a)	31.1
9AS	482.2	900	42.7	62.0	244	21.5
9BS	482.2	900	45.0	65.2	16	24.7
10T	565.6	1050	41.4	60.0	(a)	29.8
10AS	565.6	1050	34.0	49.3	52	22.6
10BS	565.6	1050	28.8	41.8	138	16.3
12T	648.9	1200	33.6	48.7	(a)	24.7
12AS	648.9	1200	21.0	30.4	36	22.4
12BS	648.9	1200	13.7	19.8	115	23.5
S	648.9	1200	22.1	32.1	6	(b)

(a) Tensile Test

(b) Data not reported

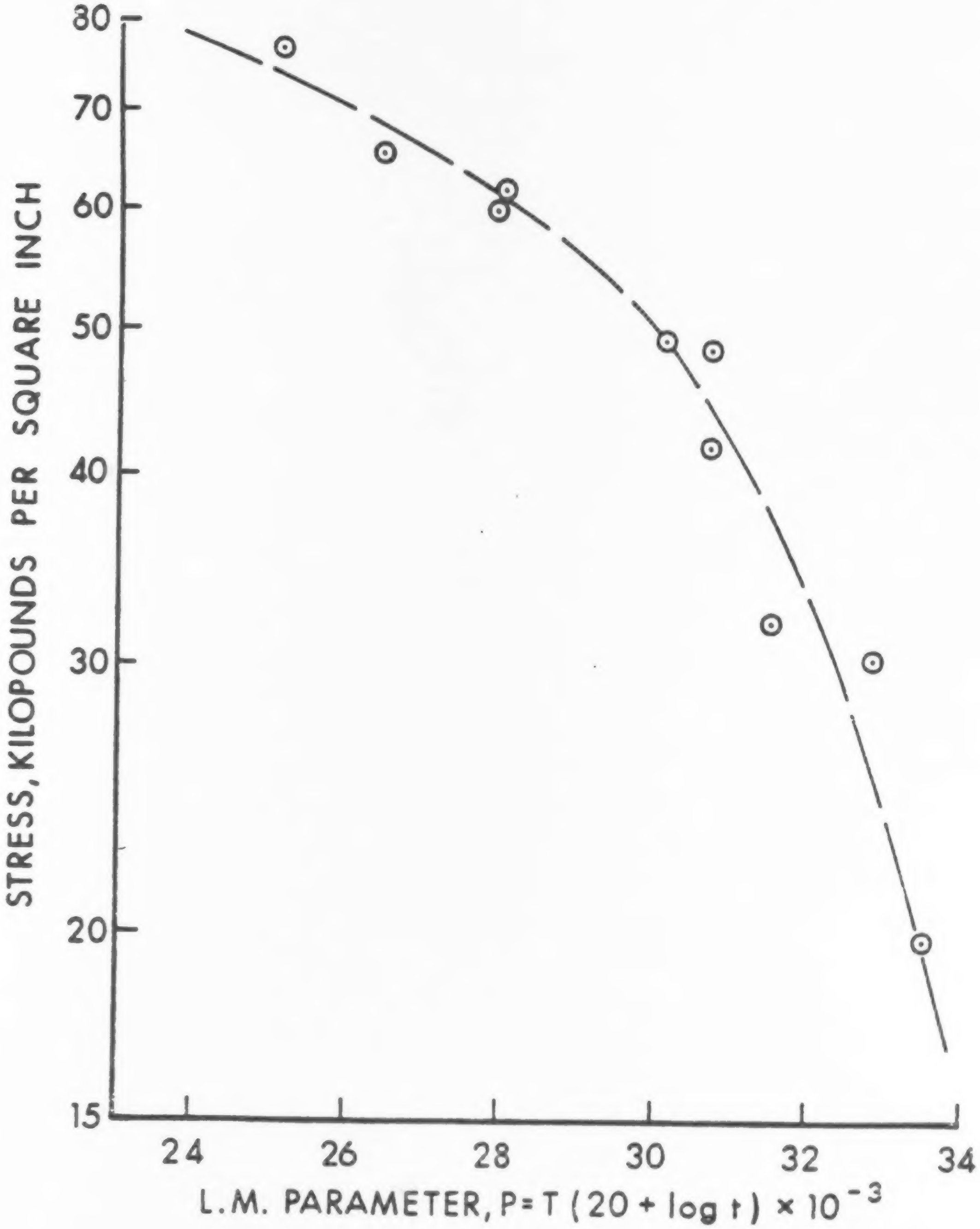

Fig. 4-6: Larson- Miller plot of stress-rupture data given in Table 4-2 (for TC-128-B steel)

valid, a curve such as that shown in Fig. 4-6 can be used to predict the life (t) of a part at any combination of stress and temperature. The value of the Larson-Miller parameter (P) is obtained from the curve for the specified stress and Eq. 4-5 is subsequently used to calculate the life (t) of the part at the specified temperature (T) or, alternately, the temperature required to produce a specified life.

Ultimate tensile strength data are used to obtain some of the points on a Larson-Miller curve by assuming that the failure time of a material stressed to its ultimate strength is not zero but rather is some specified (small) value. Values of the Larson-Miller parameter (P) for the ultimate tensile strengths given in Table 4-2 (specimens 9T, 10T and 12T) were calculated by assuming that those strengths correspond to a life (t) of 108 seconds (0.03hrs), for example. It is because ultimate tensile strength data are included in the data used to construct a Larson-Miller curve that a stress-rupture failure analysis performed using that curve can predict failure even when creep is not important (ie. when failure is by yielding alone). A Larson-Miller rupture analysis will not predict instantaneous failure of a part stressed to its ultimate strength, of course,* but the ultimate strength of a material, as determined in a standard tensile test, is not the strength that the material would have at very high strain rates (such as would be required to produce failure that was effectively "instantaneous") anyway.

---

* The Larson-Miller curve shown in Fig. 4-5 would predict a rupture life of 108 seconds for a specimen stressed to its ultimate strength.

The thermal and thermodynamic models of a tank car in a pool fire will provide the tank wall temperature distribution and the tank pressure respectively as functions of time. The tank pressure will be used to evaluate membrane stresses which will, in turn, be used to compute the effective stresses defined previously. If the average wall temperature at a point where the effective stress has been calculated is $\overline{T}_i$ over the ith time step, a Larson-Miller curve for the tank car steel in question (eg. Fig. 4-6 for TC-128 steel) will be used to calculate the total life expectancy $(t_{rup})_i$ (ie. time to rupture) of the steel at the stress $(\sigma_e)_i$ and temperature $\overline{T}_i$. The ratio of the size of the ith time step, Δt_i, to the total life expectancy of the steel under the conditions prevailing during that time step, $(t_{rup})_i$, will then represent the fractional life (f_i) of the tank under those conditions. It will be assumed that rupture occurs when $\sum_i f_i = 1$ (ie. when a running sum of the f_i for the conditions prevailing during each time step equals unity). This procedure, which is similar in concept to Miner's rule (used in fatigue life calculations), assumes that the creep rate is more or less constant at a particular set of conditions and that the creep strains resulting from exposure to different stresses and temperatures for different lengths of time can simply be summed to obtain the total accumulated creep strain at any time. This procedure is known as the "life-fraction rule" (45) and is not exact.

The foregoing procedure will have to be applied at several points on the tank to predict where rupture initiates (ie. a running sum of the f_i will have to be kept at more than one location). The user of the tank car analysis program will be offered a choice of two possible ways of specifying the locations on the tank where stress-rupture analyses are to be performed. In the first of these methods, the user will be required to provide all of the test locations, in the form of pairs of circumferential and axial node numbers since each such pair will define a grid point and hence a position on the tank wall, as input. The circumferential and axial node number indices of several nodes along the length of the tank at the 12 o'clock position might be specified as the test locations, for instance, since wall temperatures and hence the probability of rupture will normally be highest at those locations. It is expected that spacing the test locations approximately 1-2m apart on an 18.4m long tank (ie. a DOT 112A or 114A design) will probably provide adequate resolution of the stress and temperature fields in the tank wall, meaning that there will be 10-20 test locations in total.

As an option to the procedure just described for specifying the stress-rupture test locations, it will also be possible to have the tank car analysis program determine possible rupture points automatically. The program will determine possible rupture points during the course of the analysis by comparing nodal temperatures to a user-specified "creep initiation" temperature, which will simply be the temperature at which the user expects creep to become significant. When the temperature of a particular node exceeds the creep initiation temperature, values of f_i will be calculated and summed at that node in subsequent time steps. As mentioned previously, it will be assumed that rupture occurs when the integrated value of f_i at one of the test locations equals unity. This method of determining stress-rupture test locations will be less efficient than the method in which those locations are specified by the program user because it will probably lead to f_i sums being accumulated at a relatively large number of nodes, many of which may be experiencing similar temperature and stress histories, in the later stages of the transient. Values of f_i will be easy to compute and sum, however, so the use of a large number of stress-rupture test locations should not increase the total computing effort significantly.

The value chosen for the creep initiation temperature will not be critical provided it is not too high. The rupture life of TC-128 steel at a stress of 159MPa (23,000psi), which is the von Mises stress in the cylindrical section of a full-size DOT 112A tank car at an internal pressure of 1.93MPa (280psig), is approximately 6000hrs at a temperature of 900^{o}F (according to Fig. 4-6), for example, so creep rates at that temperature and stress level will not contribute significantly to the failure of a tank car in a fire, which typically occurs after exposure times of 20-120 minutes. Thus 900^{o}F could be selected as the creep initiation temperature because creep of a TC-128 tank car steel would be insignificant (during the time period of interest) below that temperature. The rupture life of TC-128 steel is approximately 320hrs at 900^{o}F when the stress is double that mentioned previously (ie. 2x159 MPa = 318 MPa = 46,000psi) so 900^{o}F would be an acceptable creep initiation temperature even for the much higher stress level.

4.3.1 Comparison Of Results of Larson-Miller Rupture Analysis With Experimental Results

The specimens used to obtain the stress-rupture data given in Table 4-2 were taken from a tank car designated RAX 201 by the Federal Railroad Administration (U.S.) and the Association of American Railroads in their tank car test series. Metallurgical aspects of the test of RAX 201 are examined by

Anderson et al. in reference 50, from which the data given in Table 4-2 and Fig. 4-6 were taken, but all of the remaining data related to the test, such as temperature and pressure measurements, are reported by Anderson et al. in reference (10)) Figures 4-7 and 4-8 (taken from (10)) show the peak wall temperature, which was recorded at the top of the tank (ie. at 12 o'clock) at a point located midway between the center of the tank and one end, and the tank pressure as functions of time (after the start of the test) respectively. The Larson-Miller failure analysis procedure described previously can be applied to the failure analysis of tank car RAX 201 with the information given in Figures 4-6 to 4-8.

The results of a Larson-Miller rupture analysis performed using Figures 4-6 to 4-8 in the manner described previously are tabulated in Table 4-3 and a plot of the accumulated value of f_i is shown as a function of time in Fig. 4-9. The von Mises stress $(\sigma_m)_i$ was calculated from the hoop and longitudinal stresses in the cylindrical shell (ie. using Eqs. 4-2 and 4-3) because it was concluded from an analysis of the fracture paths in (50) that rupture probably initiated in the cylindrical shell at a point located 3.5m (11.5ft.) from one of the head-to-shell welds. The Larson-Miller analysis did not predict rupture of tank car RAX 201 before or when it actually occurred (at 24.5 minutes) so the temperature and pressure traces given in Figures 4-7 and 4-8 respectively were extrapolated to times greater than 24.5 min. using the slopes of those traces at the time of failure. The tank pressure was held constant at 2.27MPa (330psig) for times greater than 24.5 minutes, as seen in Table 4-3, while the peak wall temperature was assumed to increase at a rate of 13.9°C/min. (25°F/min). The rupture time of 29 minutes predicted by the Larson-Miller analysis

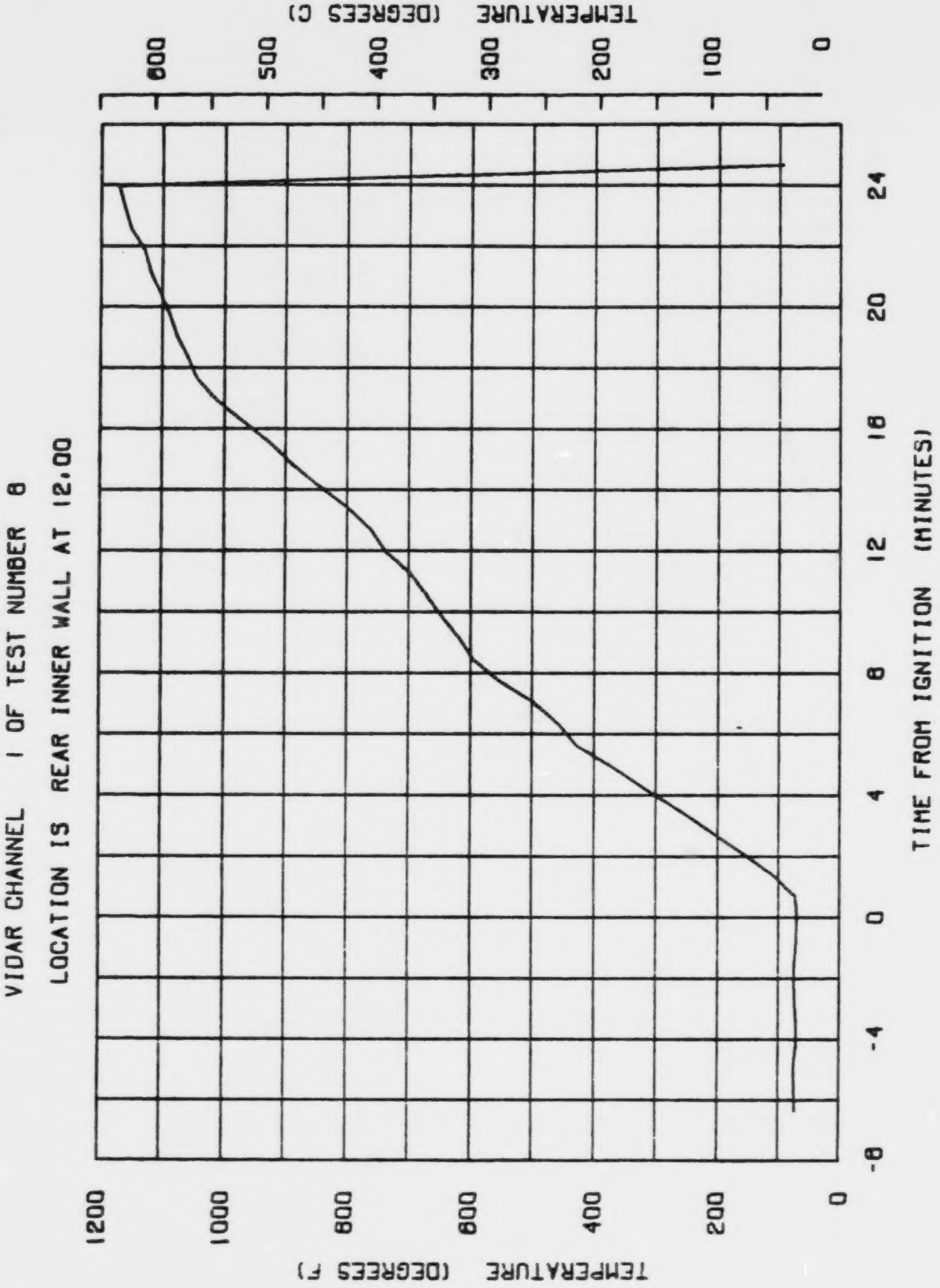

Fig.: 4-7: Thermocouple Temperature Vs. Time

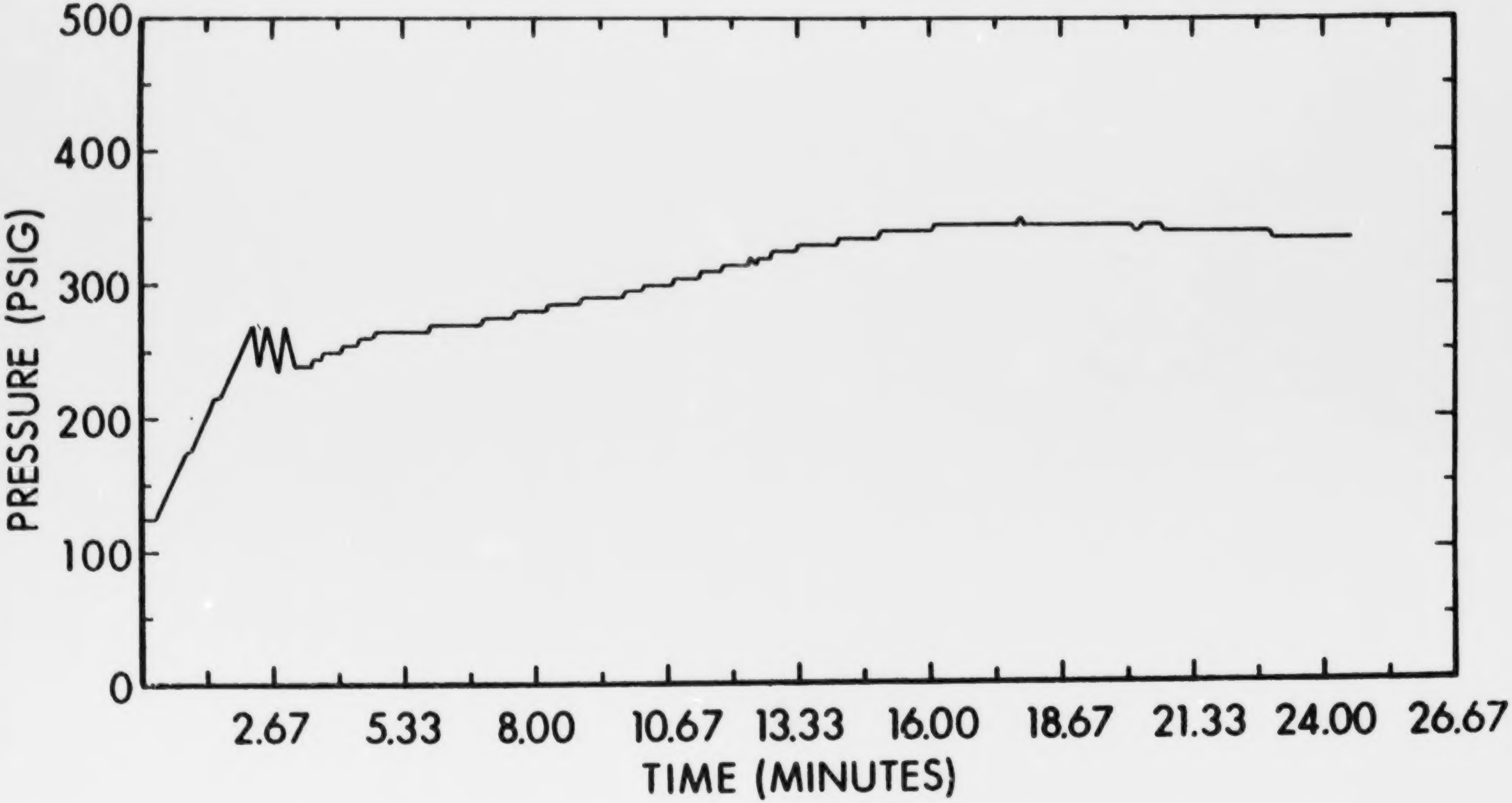

Fig. 4-8: Pressure vs. Time

TABLE 4-3: RESULTS OF LARSON-MILLER RUPTURE ANALYSIS FOR TANK CAR RAX 201

TIME PERIOD # i	TIME INTERVAL MIN.	$\overline{T}$ ^{o}F	$\overline{P}_i$ psig	$(\sigma_m)_i$ ksi	LARSON-MILLER PARAM. p	$(t_{rup})_i$	f_i	Σf_i
1	0-5	193	225	18.7	33.65			
2	5-10	525	280	23.3	33.0			
3	10-15	720	315	26.15	32.7			
4	15-18	980	340	28.2	32.4	7839	.0004	.0004
5	18-20	1070	340	28.2	32.4	406	.0041	.0045
6	20-21	1110	340	28.2	32.4	163	.0061	.0106
7	21-22	1125	340	28.2	32.4	110	.009	.0196
8	22-23	1150	340	28.2	32.4	59.1	.0169	.0365
9	23-24	1173	330	27.4	32.5	37	.0270	.0635
10	24-25	1200	330	27.4	32.5	19.9	.0503	.1138
11	25-26	1225	330	27.4	32.5	11.4	.0875	.2013
12	26-27	1250	330	27.4	32.5	6.7	.1487	.3500
13	27-28	1275	330	27.4	32.5	4.04	.2476	.5976
14	28-29	1300	330	27.4	32.5	2.47	.4043	1.0019

RUPTURE PREDICTED AT 29 MINS.

Fig. 4-9: Accumulated life fraction (f_i) from Larson-Miller analysis

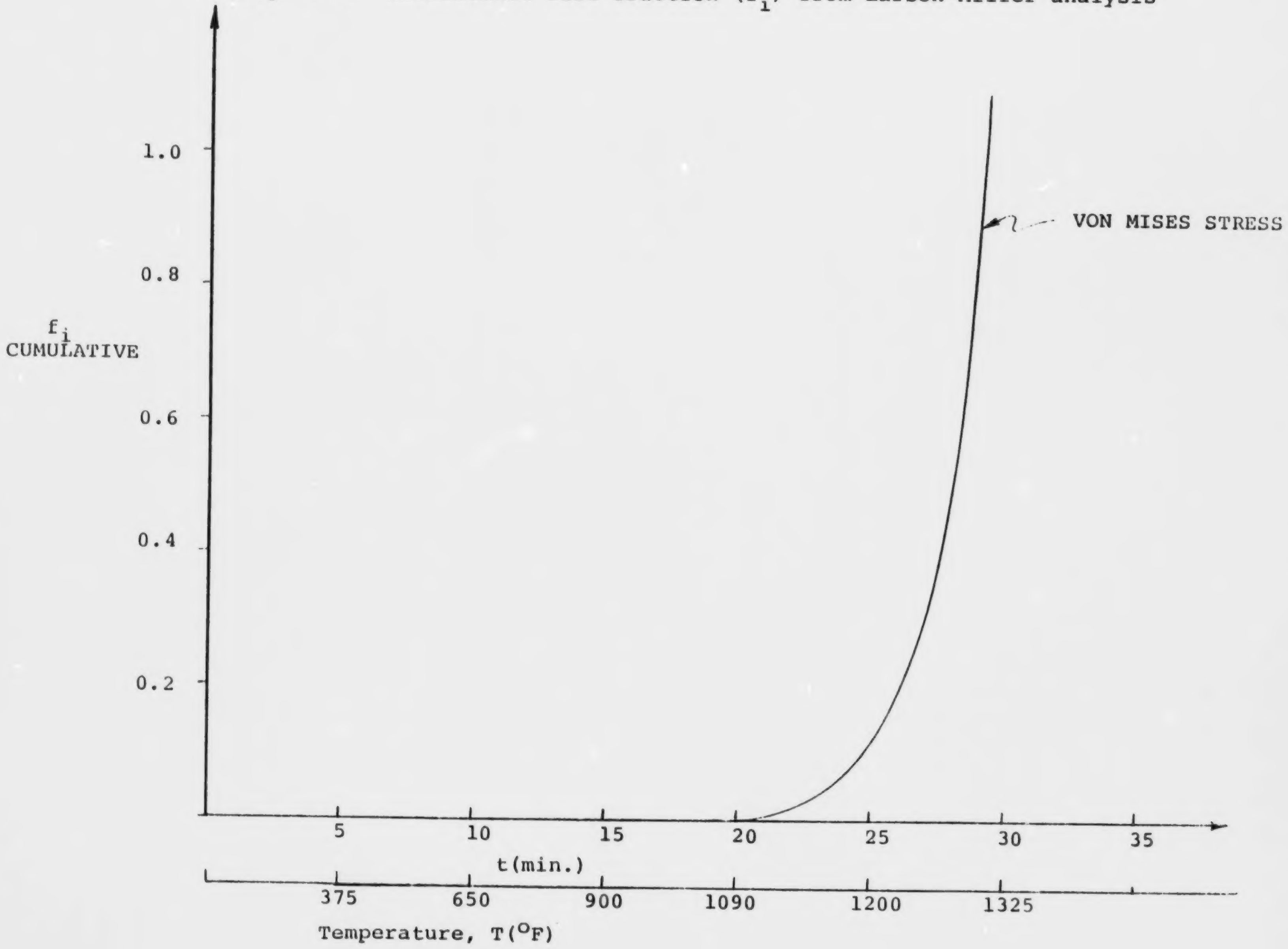

differed significantly from the actual rupture time of 24.5 minutes but there are at least two possible reasons for the poor agreement. First, it was noted by Anderson et al. in (50) that rupture initiated within a region which had an acicular microstructure and that rupture of the tank was premature, perhaps by as much as several minutes, for that reason. The steel samples used in the stress rupture tests were taken from a region of the tank where the more normal pearlite plus blocky ferrite microstructure existed so the stress-rupture data obtained by Anderson et al. (Table 4-2) would not have applied to the region where rupture initiated. Anderson et al. suspected that the acicular microstructure had been produced by rapid localized heating of the tank wall, perhaps by a torch during the installation of the test instrumentation (ie. thermocouples, bracket mounts, etc.).

Another possible explanation for the failure of the Larson-Miller analysis to predict the rupture time accurately relates to the accuracy of the stress-rupture data obtained by Anderson et al. The ultimate tensile strength data obtained in tests 9T, 10T and 12T, given in Table 4-2, are compared in Fig. 4-10 to the RPI-AAR ultimate tensile strength vs. temperature curve given in (52) for TC-128-B steel. The ultimate tensile strengths measured by Anderson et al. can be seen to be substantially higher than the strengths from the other source, in particular at 650°C (1200°F) where the strength measured by Anderson et al. is almost 80% greater than the RPI-AAR value. Since the cumulative f_i vs T curve in Fig. 4-9 shows that strains increase rapidly at temperatures above $\simeq$ 600°C (1100°F), the ultimate strength data governs, to a large extent, the time at which the Larson-Miller failure analysis predicts rupture. If unrealistically high ultimate tensile strengths were used to obtain the Larson-Miller plot shown in Fig. 4-6, using that plot to predict rupture would result in correspondingly long

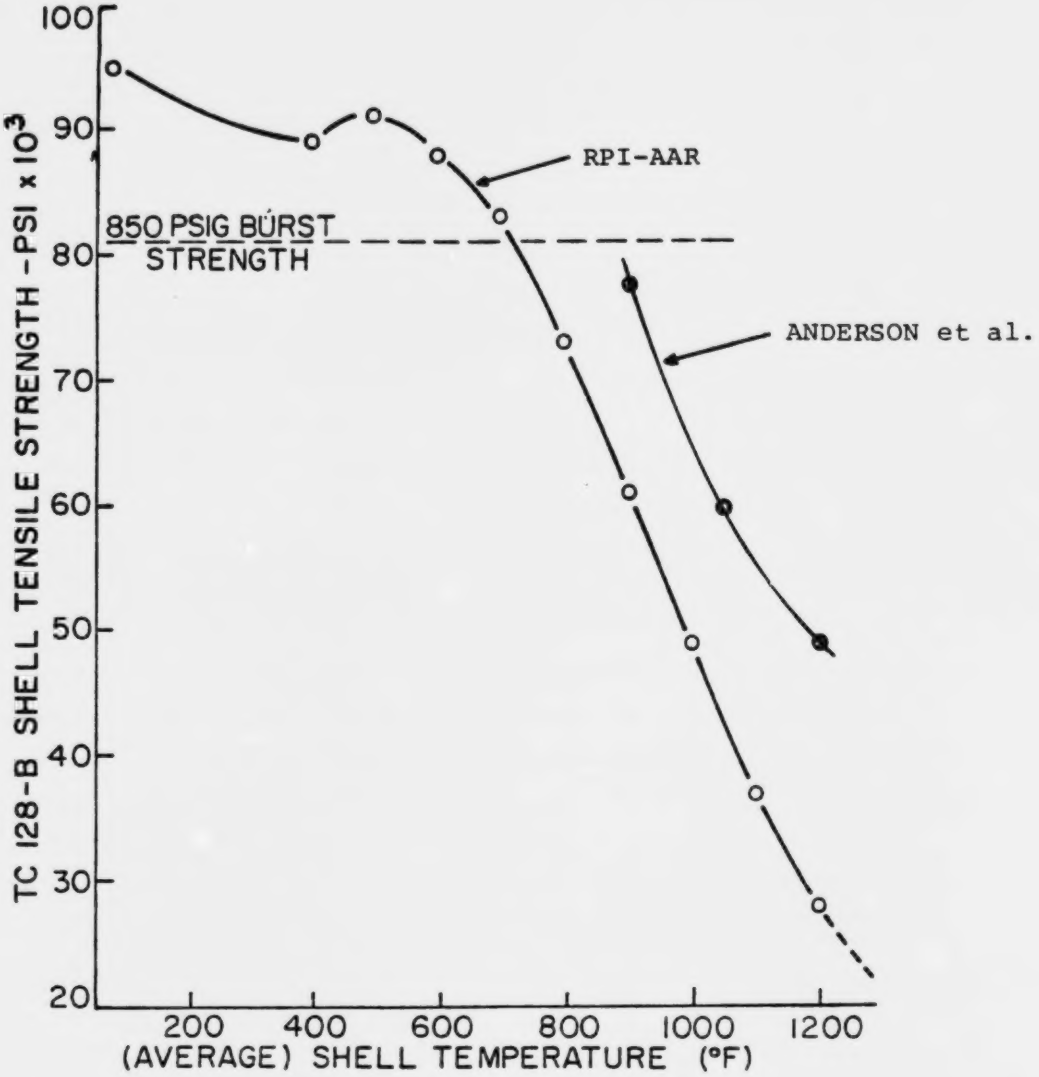

Fig. 4-10: Comparison of ultimate strengths measured by Anderson et al. (Table 4-2) for TC-128 steel to RPI-AAR data.

rupture times. It should be noted that the actual failure time of tank car RAX 201 (ie. 24.5 min.) can be predicted quite accurately by simply comparing the RPI-AAR tensile strength vs. temperature curve shown in Fig. 4-5 (or 4-10) to the von Mises stresses and temperatures given in Table 4-3. The von Mises stress of 188.9MPa (27.4ksi) obtained in the cylindrical shell at times greater than ≈23 min. corresponds to the ultimate strength of TC-128-B steel at ≈ 650°C (1200°F) according to the RPI-AAR tensile strength vs. temperature curve given in Fig. 4-5. The peak wall temperature vs. temperature trace given in Fig. 4-7 indicates that a temperature of 1200°F would have been obtained, and hence that failure would have occurred, at a time of ≈25.5 min. This result is in close agreement with the actual rupture time of 24.5 min.

The rapid increase in strain (ie. cumulative f_i) observed in Fig. 4-9 at temperatures above ≈600°C (1100°F) indicates that creep strains were probably not very significant before rupture occurred and hence that using a stress-rupture approach to predict failure was probably not worthwhile for tank car RAX 201. The rapid predicted increase in strain before rupture occurred because the wall temperature was still increasing rapidly at the time of rupture.

While this result would probably always be obtained in analyses of unprotected tank cars in pool fires, temperature rise rates and hence strain rates will be lower for protected tank cars (ie. tank cars with EXPLOSAFE and/or thermal insulation) making the use of stress-rupture failure analyses almost mandatory. Creep will be important if the tank wall temperature is high (but nevertheless less than the temperature required to produce almost instantaneous failure of the tank wall at the prevailing tank pressure) for extended periods of time .

As an example of this, a rupture analysis based only on the ultimate tensile strength vs. temperature data tabulated in Table 4-2 would not have predicted the rupture of specimen 12AS (tested at a temperature of 649°C (1200°F) and a stress of 210MPa (30.4ksi)) because the stress to which that specimen was subjected was much less than the ultimate tensile strength of 336MPa (48.7ksi) measured at 649°C in test 12T. Specimen 12AS, which was chosen for this example because it was subjected to a stress similar to the von Mises stresses given in Table 4-3 for times greater than 15 minutes, actually lasted only 36 minutes before it failed by stress rupture. This example demonstrates that creep must be considered in the tank car failure analysis because it is entirely plausible that a protected tank car could experience temperature and stress conditions similar to those experienced by specimen 12AS in the stress-rupture tests.

It was mentioned previously that similar results (ie. predicted rupture times) are obtained when the hoop stress in the tank wall is taken to be the stress governing rupture instead of the von Mises stress. Taking σ_h to be the stress governing rupture instead of σ_m produced a predicted rupture time for tank car RAX 201 that was only 45 seconds less than that obtained with σ_m, for instance, as seen in Fig. 4-11 where cumulative values of f_i for both cases are plotted against time and temperature. Greater sensitivity to the assumed stress values would be obtained at lower rates of temperature rise, however, such as would be obtained with protected tanks.

4.4 Torch Fire Rupture Prediction

It will be difficult to predict rupture times for a tank car exposed to a torch fire because thermal stresses and distor-

Fig.: 4-11: Comparison of Larson-Miller rupture analysis results with the stress governing rupture taken to be
1) von Mises stress and,
2) the hoop stress

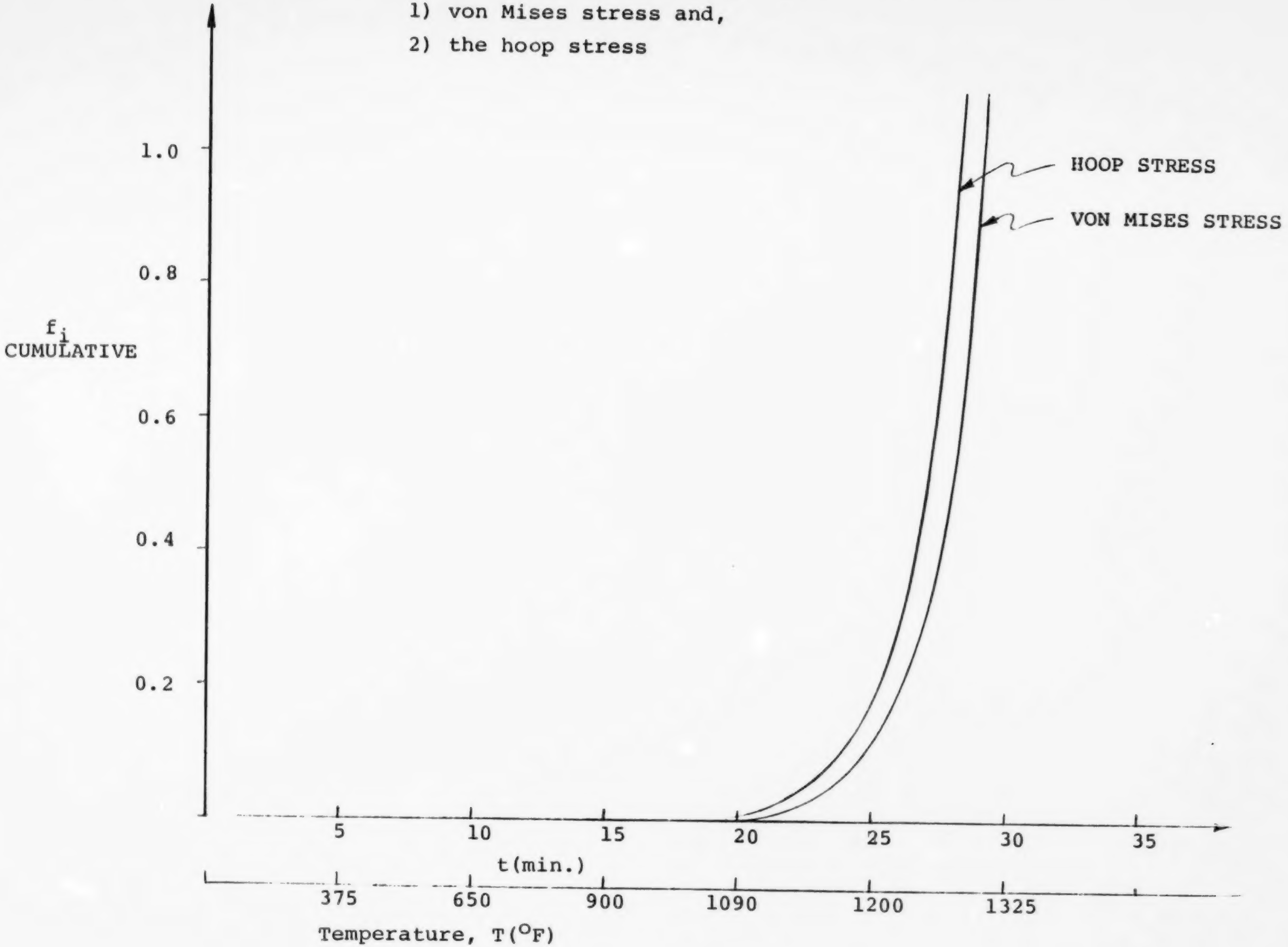

tions, which were neglected in the pool fire rupture analysis described in Sects. 4.1-4.3, will probably play a part in promoting tank failure in the torch fire case. The thermal strains will still be small compared to the inelastic strains that occur before failure, however, so tank rupture will again be predicted from pressure-induced stresses alone based on the arguments presented in Sect. 4.1. The method that will be used to predict rupture will be exactly the same as that used in the pool fire failure analysis and it will be assumed, in particular, that the membrane stresses throughout the cylindrical shell, including the region inside and near the torch impingement area, can be predicted from Eqs. 4-2 and 4-3. Some of the pressure-induced loads acting on the hot part of the tank wall within and near the torch impingement area will be transferred to the cooler and hence stronger parts of the shell when the hot part starts to yield*, making Eqs. 4-2 and 4-3 inapplicable within and near the hotspot after that time, but it is expected that this load transferral will be slight if the diameter of the hotspot is of the same order of magnitude as the tank diameter. Since the diameter of the torch itself will likely be at least equal to the tank diameter and since the heating effect of the torch will extend over several torch diameters, load transferral from the hotspot to cooler regions of the wall will probably be slight. It would only be possible to obtain a better estimate of the stresses and deformations resulting from the impingment of a torch fire on a pressurised tank car by performing a sophisticated finite-element analysis, as described in the next section.

---

* Some load transferral will occur even before the hotspot starts to yield because the steel within the hotspot will have a lower modulus of eslasticity than the surrounding steel. Load transferral will also occur when the steel within the hotsport expands of course.

4.5 Finite-Element Rupture Analysis

Relatively simple methods for predicting if and when a pressurized tank car will rupture when it is envelcped by a pool fire or heated locally by a torch fire were developed in Sects. 4.1 - 4.4 without recourse to the finite-element method. Use of the finite-element method was deliberately avoided because a finite-element analysis of tank rupture in either the pool or torch fire case would have to be very sophisticated to provide realistic results. A simple elastic analysis of thermal and pressure-induced stresses performed using the finite-element method would be of little use in predicting tank rupture because, as mentioned previously, tank rupture is usually preceded by large inelastic strains. Somewhat better results could be obtained by performing an elastic / plastic analysis of the tank deformations with stress changes caused by changes in tank geometry neglected for simplicity. Since the yield surface of a strain - hardening material (such as a tank car steel) is a function of the material's deformation history, stresses and strains would have to be computed periodically during the transient to obtain that history. In other words, the entire deformation history of the tank would have to be known to predict the stresses and strains in the tank at any given time. Plasticity is a material non-linearity (ie. stress is not directly proportional to strain) so elastic / plastic analyses have to be performed iteratively. Ignoring changes in stress caused by changes in tank geometry (ie. ignoring geometrical non-linearities) simplifies the solution procedure in that iterations do not have to be performed to account for those changes but this simplification, which is only valid when deformations are small, would give poor results in the rupture analysis of a tank head, for example, where very large deformations can occur before failure as seen in Fig. 4-2. Geometrical non-linearities would, therefore, have to be accounted for, by performing a so-called large displacement / large rotation analysis. Most finite-element programs that perform large displacement / large rotation analyses consider strains to be small since this permits the finite-element formulation to be simplified considerably. The small strain assumption would not be acceptable in the tank car rupture analysis, however, so a large displacement / large rotation / finite strain formulation of the finite-element method would have to be used. Finally, an analysis which considered creep (ie. a viscoplastic analysis) would have to be performed since it was demonstrated in Sect. 4-3 that creep may be important in some situations. A viscoplastic analysis allowing large displacements, large rotations and finite strains would permit direct modelling of the failure process, including the bulging and thinning of the tank wall.

It would be necessary to model the entire tank using the finite-element method to predict tank rupture in a pool fine analysis. It is estimated that a full-sized tank car could be modelled with 100-200 curved shell elements, similar to Irons' semi-loof element (53). Flat shell elements, which are the only shell elements available in many finite-element programs (eg. ANSYS and STARDYNE), should not be used because they are more expensive to use (for the same accuracy) than curved elements. An estimate of the number of elements that would be required in the torch fire analysis cannot be given at this time because the discretization used would depend on the temperature distribution in the tank wall near the torch and the desired accuracy. It would be preferable to model the entire tank in the torch fire analysis rather than isolate a section of it near the torch since the latter approach would necessitate selecting appropriate boundary conditions for the isolated section. Appropriate boundary conditions for isolated sections are not always obvious and hence are frequently selected incorrectly in finite-element analyses. A very coarse mesh (ie. large elements) could be used in regions remote from the torch so neglecting those regions in the finite-element model would give only a slight and hence not worthwhile, improvement in computing speed. Very few finite-element programs are capable of performing the type of sophisticated analysis that would be needed to model failure of a tank car in a fire, that is a viscoplastic analysis allowing large displacements, large rotations and finite strains. Several programs, such as the ABAQUS code* maintained by Control Data Canada Ltd., can perform viscoplastic analyses considering large displacements, large rotations and small strains, but the application of one of those programs to the tank car failure analysis would be a major and expensive undertaking which would not be worthwhile for several reasons. First, even such sophisticated finite-element programs will produce results of questionable accuracy because strains in a tank car will not be small and hence will violate the small strain assumption used to develop the programs. Second, tank wall temperatures and tank pressures predicted using the thermal and thermodynamic models will likely not be accurate enough, owing to uncertainties in predicted fire-to-tank heat transfer rates, etc., to warrant using such sophisticated techniques to predict tank rupture. Third, the tank car model will not be self-contained, transportable and easy to use if a commercially available finite-element program is used to perform the structural analysis of the tank. Performing the structural analysis with a finite-element program would require storing the tank wall temperature distribution and tank pressure predicted by the thermal and thermodynamic models as functions of time on a magnetic tape or other data storage device and then using the information on the tape as input data for the finite-element program. The output from the thermal and thermodynamic models would have to be supplied to the finite-element program in the proper input format, for the latter program, of course. While such a two-stage analysis would be by no means impossible to perform, it would nevertheless complicate the analysis considerably and would probably discourage potential users of the tank car analysis program who had never performed very advanced finite-element analyses from using the program. It should be mentioned that it would be almost impossible to automate the use of the finite-element program so that the user would not have to, at least, prepare the finite-element model of the tank car shell (ie. divide the shell into elements). This task would be difficult for the casual user to perform, in particular for a torch fire analysis, where finer discretization would have to be used in regions near the torch impingement point than in regions remote from it. Several analyses would probably have to be performed with different meshes to determine when the mesh was sufficiently refined.

---

* ABAQUS has curved shell elements of the type needed to model a tank car efficiently.

In contrast to the fairly complex two-stage analytical procedure just described, use of the simple rupture models described in Sects. 4.1 - 4.4 will permit the tank car analysis program to be completely self-contained and easy to use. The simple rupture models will probably be able to predict rupture of the cylindrical shell adequately but, as mentioned in Sect. 4.2, it will not be possible to predict rupture of a tank head accurately without performing a sophisticated finite-element analysis unless the ultimate strength of the head material is approximately uniform throughout the head. It will not be possible to predict, at least accurately, if and when a tank head heated by a torch fire, will rupture for instance, without using the finite-element method. If analyses of this nature are required, the task of predicting tank failure will be given to Dr. J. Goldak of Carleton University, Ottawa since Dr. Goldak is a finite-element specialist who performs difficult elastic / plastic analyses routinely. Dr. Goldak has developed an extremely sophisticated finite-element program, ASGARD, which has an element library of over 50 elements, including state-of-the-art curved shell elements. Estimated computing costs for a viscoplastic finite-element analysis of tank failure allowing for large displacements, large rotations and finite strains are $1,000. to $10,000. per run (with ASGARD) for either a pool or torch fire. These cost estimates will have to be verified by performing sample analyses, however, and costs will vary depending on the degree of discretization required to obtain accurate results.

The extent to which Dr. Goldak's services will be required cannot be estimated without knowing specific details of the cases that are to be run, although it is expected that the simple rupture models described in Sects. 4.1 4.4 will suffice for the majority of analyses. If preliminary analyses of specific cases performed using the thermal model (once developed) and the rupture models described in Sects 4.1 - 4.4 suggest that tank head rupture is possible, ASGARD will have to be used to obtain an accurate estimate of the time and point of initiation of rupture. It should be possible to obtain a great deal of useful information about the effectiveness of EXPLOSAFE in preventing tank car ruptures without ever using ASGARD, however.

It is not proposed that ASGARD be included with the tank car analysis program as a package. Any advanced finite-element structural analysis program capable of performing geometrically non-linear viscoplastic analyses of shells with thermal and pressure loads could be substituted for ASGARD.

5.0 MODEL SUMMARY

Detailed descriptions of the thermal, thermodynamic and structural models that will together represent the complete DE tank car model have been given in the preceding sections. In terms of the computer program implementing those models, the thermal and thermodynamic calculations will be much more involved than the structural calculations because the structural model described in Sec. 4 is comparatively simple. A flowchart summarizing many of the calculations described in the preceding sections and placing them in the order in which they will be performed in the program is included as Fig. 5-1.

FIGURE 5-1a: PROGRAM FLOWCHART

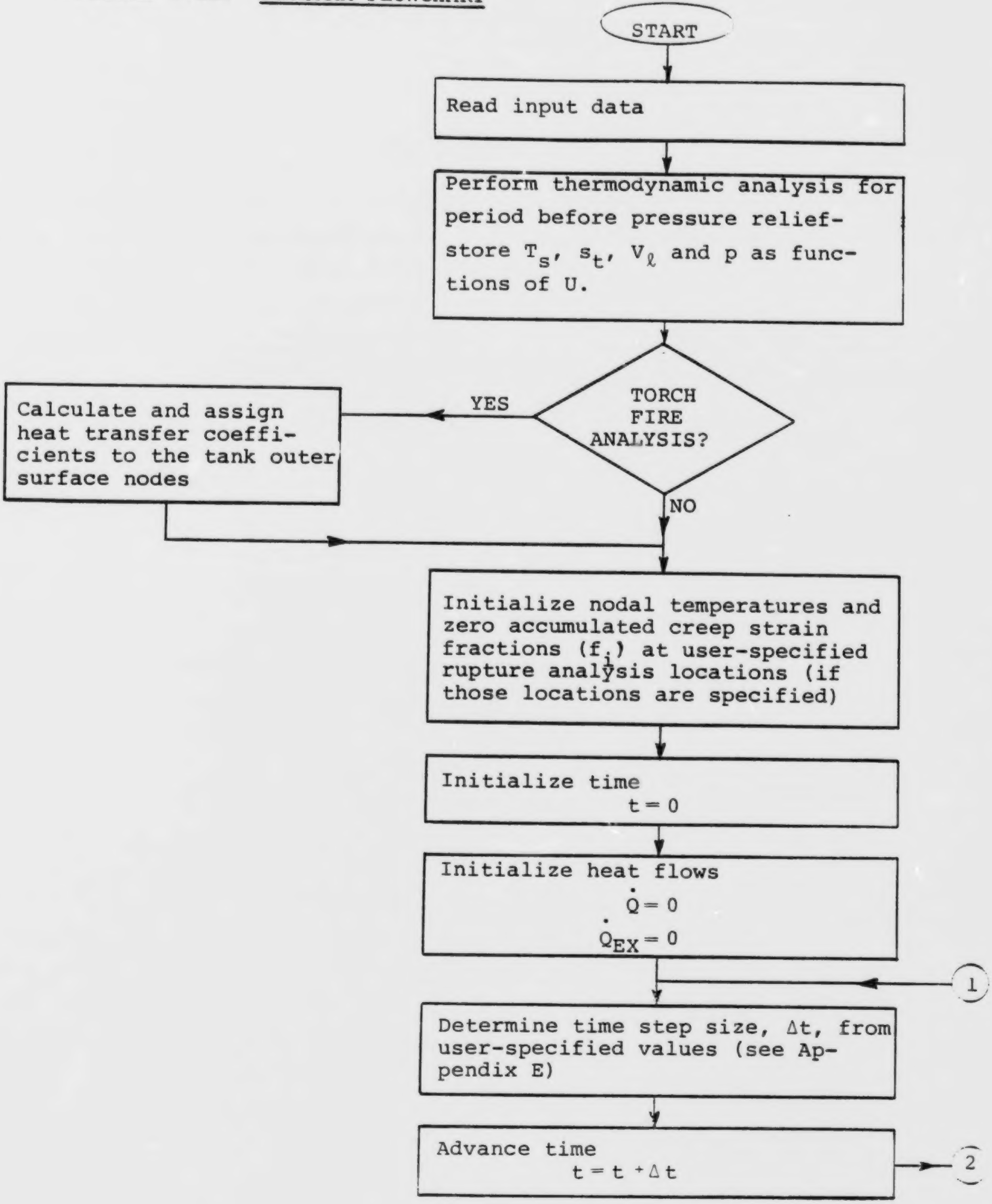
START
Read input data
Perform thermodynamic analysis for period before pressure relief- store T_s, s_t, V_ℓ and p as functions of U.
TORCH FIRE ANALYSIS?
YES
Calculate and assign heat transfer coefficients to the tank outer surface nodes
NO
Initialize nodal temperatures and zero accumulated creep strain fractions (f_i) at user-specified rupture analysis locations (if those locations are specified)
Initialize time $t = 0$
Initialize heat flows $\dot{Q} = 0$ $\dot{Q}_{EX} = 0$
1
Determine time step size, Δt, from user-specified values (see Appendix E)
Advance time $t = t + \Delta t$
2

FIGURE 5-1b: PROGRAM FLOWCHART - continued

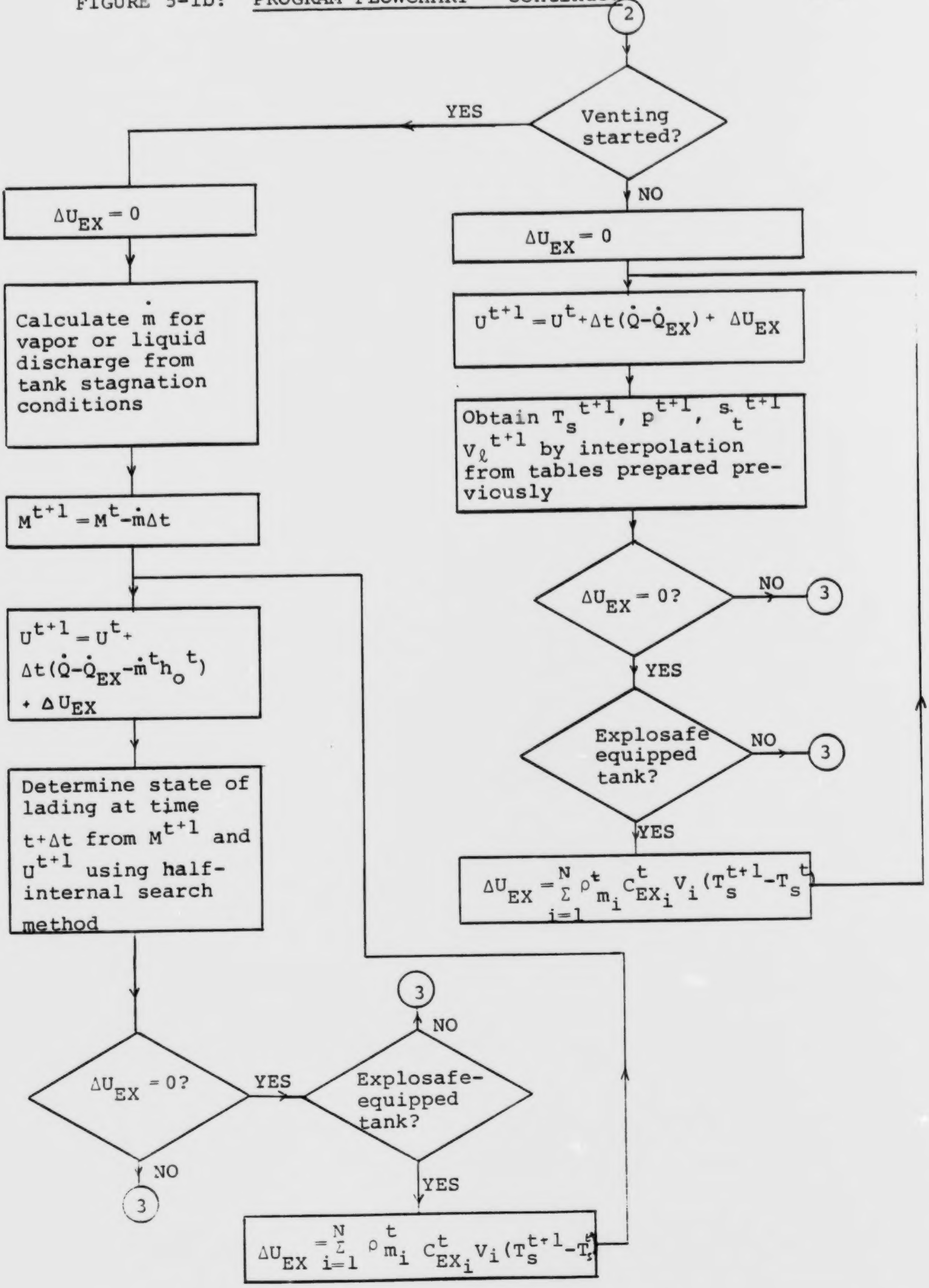
2
Venting started?
YES
NO
$\Delta U_{EX} = 0$
$\Delta U_{EX} = 0$
Calculate $\dot{m}$ for vapor or liquid discharge from tank stagnation conditions
$M^{t+1} = M^t - \dot{m}\Delta t$
$U^{t+1} = U^t + \Delta t(\dot{Q} - \dot{Q}_{EX} - \dot{m}^t h_o^t) + \Delta U_{EX}$
Determine state of lading at time $t+\Delta t$ from M^{t+1} and U^{t+1} using half-internal search method
$U^{t+1} = U^t + \Delta t(\dot{Q} - \dot{Q}_{EX}) + \Delta U_{EX}$
Obtain T_s^{t+1}, p^{t+1}, s_t^{t+1} V_ℓ^{t+1} by interpolation from tables prepared previously
$\Delta U_{EX} = 0?$
NO
3
YES
Explosafe equipped tank?
NO
3
YES
$\Delta U_{EX} = \sum_{i=1}^{N} \rho^t_{m_i} C^t_{EX_i} V_i (T_s^{t+1} - T_s^t)$
$\Delta U_{EX} = 0?$
YES
NO
3
Explosafe-equipped tank?
NO
3
YES
$\Delta U_{EX} = \sum_{i=1}^{N} \rho^t_{m_i} C^t_{EX_i} V_i (T_s^{t+1} - T_s^t)$

FIGURE 5-1c: PROGRAM FLOWCHART - continued

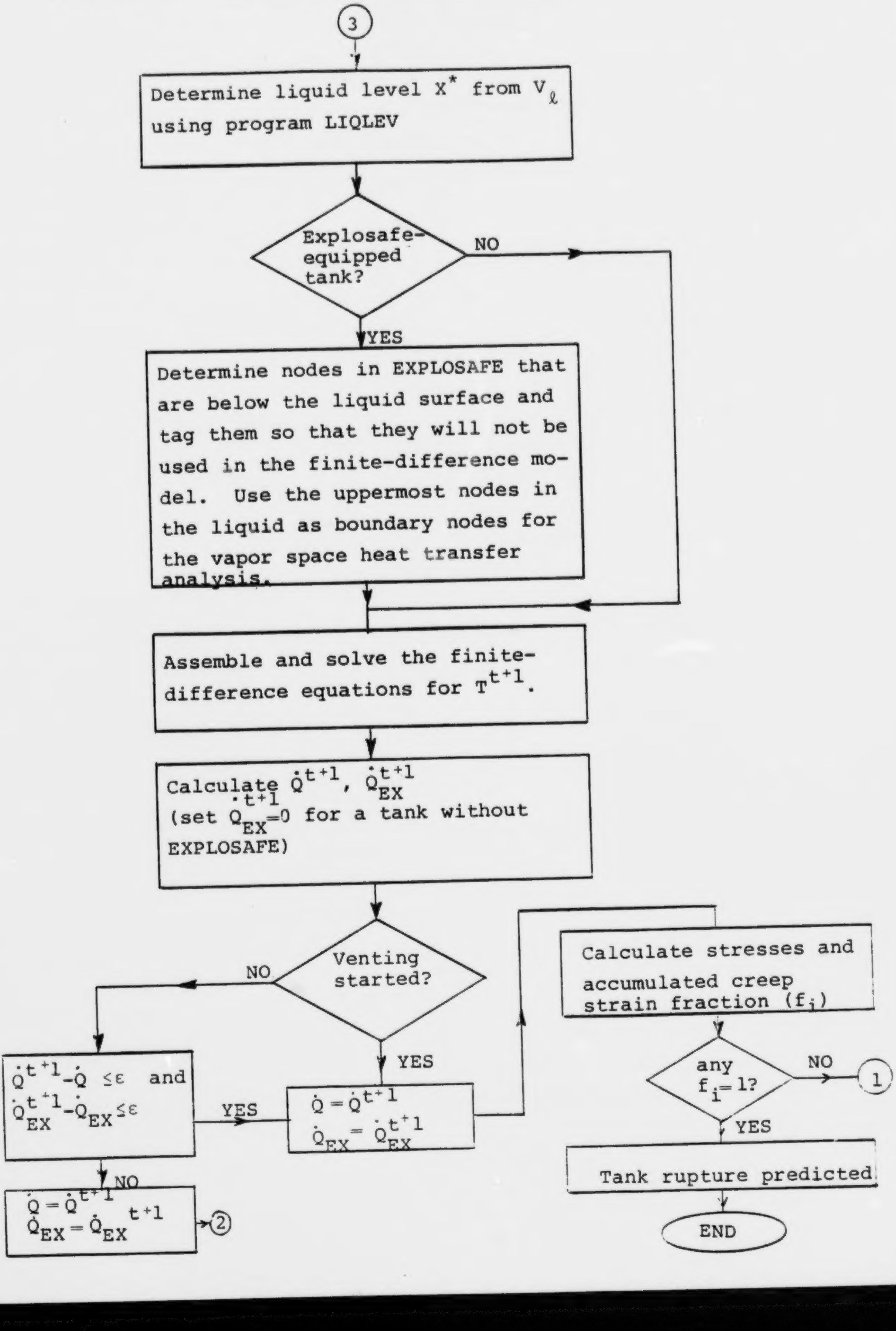
3
Determine liquid level X^* from V_ℓ using program LIQLEV
Explosafe-equipped tank?
NO
YES
Determine nodes in EXPLOSAFE that are below the liquid surface and tag them so that they will not be used in the finite-difference model. Use the uppermost nodes in the liquid as boundary nodes for the vapor space heat transfer analysis.
Assemble and solve the finite-difference equations for T^{t+1}.
Calculate $\dot{Q}^{t+1}$, $\dot{Q}_{EX}^{t+1}$ (set $\dot{Q}_{EX}^{t+1}=0$ for a tank without EXPLOSAFE)
Venting started?
NO
YES
$\dot{Q}^{t+1}-\dot{Q} \leq \varepsilon$ and $\dot{Q}_{EX}^{t+1}-\dot{Q}_{EX} \leq \varepsilon$
YES
NO
$\dot{Q}=\dot{Q}^{t+1}$ $\dot{Q}_{EX}=\dot{Q}_{EX}^{t+1}$
$\dot{Q}=\dot{Q}^{t+1}$ $\dot{Q}_{EX}=\dot{Q}_{EX}^{t+1}$
2
Calculate stresses and accumulated creep strain fraction (f_i)
any $f_i = 1$?
NO
1
YES
Tank rupture predicted
END

6.0 CONCLUSIONS AND RECOMMENDATIONS

The thermal, thermodynamic and structural models that together constitute the complete DE tank car model have been described in considerable detail in the preceding sections of this report. Particular attention has been devoted to defining the boundary conditions for the pool fire and torch fire analyses as accurately as possible since the results obtained in the analyses will depend strongly on those conditions. The pool fire and torch fire analyses will, as described, differ primarily in the prescribed boundary conditions and only minor changes to the input data for, say, a pool fire, will be needed to analyse a torch fire.

As indicated in the discussion of the torch fire analysis, a large valve torch would represent a serious threat to the integrity of a tank car upon which it impinged. A puncture torch would probably also be quite serious unless the distance between the puncture and the tank car upon which the torch impinged was small enough so that combustion of the fluid (most likely liquid) discharged through the puncture was very incomplete. The latter comment applies to any torch, of course. It is recommended that either 1/5 scale or full-scale torch fire tank car tests be performed to obtain some experimental results with which to compare the predictions of the analytical model once developed, since no experimental data that can be used for model verification purposes is available at this time.

While it is important to provide tank cars with thermal protection of some sort to minimize the likelihood of a tank rupturing when exposed to a pool or torch fire, it is also worthwhile searching for measures that could mitigate the consequences of a rupture should one occur. The most serious type of tank rupture is a BLEVE, which occurs when the liquid temperature is above its homogeneous nucleation temperature at atmospheric pressure when the tank ruptures. Although a true BLEVE could not be prevented by providing nucleation sites throughout the bulk of the liquid because nucleation sites are not needed for vapor formation when the homogeneous nucleation temperature is exceeded, it has nevertheless been speculated that "near BLEVE's" could be avoiding by providing extra nucleation sites in the liquid in some manner. Crevices and imperfections in the surfaces of EXPLOSAFE foil strands in the liquid would provide such sites, for example. While the effect that EXPLOSAFE would have on the BLEVE mechanism cannot be properly assessed without performing experiments, the results of recent experiments performed by Buivid and Sussman (54) indicate that the idea of preventing BLEVE's by providing extra nucleation sites in the liquid is not viable. They showed that the experimental superheat-limit (homogeneous nucleation) temperature for liquids was not greatly affected by "loading" the liquid with nucleation sites in the form of suspended hydrophobic or hydrophilic particles. As noted by Reid (55), only measures which cause the nucleation sites to be very closely spaced together will likely have much effect on the BLEVE mechanism. The relatively large volumes of liquid between the foil strands in an EXPLOSAFE/liquid matrix will not have any sites where heterogeneous boiling can start in the event of a rapid pressure drop so it is expected that the effect of EXPLOSAFE on the BLEVE mechanism will be minimal.

It is felt that experiments to determine critical heat fluxes for propane boiling in the presence of EXPLOSAFE should not be performed until preliminary results obtained with the analytical model, once developed, show that dryout is a possibility and that its consequences could be serious. Similarly, experiments to assess the significance of various heat transfer mechanisms (other than conduction) in an EXPLOSAFE/vapor matrix should not be undertaken until it has been demonstrated that conduction alone could not have been responsible for the effectiveness of the EXPLOSAFE thermal protection system in the 1/5 scale tank car tests.

As noted in Sect. 4.3, the tank car structural model will require a Larson-Miller curve (this curve will be input to the computer program in tabular form) for the tank car steel in question. Stress-rupture data, from which a Larson-Miller curve can be obtained, will therefore be required for the SA-285 steel used to fabricate the 1/5 scale tank cars tested at DRES Suffield and also a typical TC-128 steel sample since this steel is the most common tank car steel in use today (in Canada and the U.S.). The Larson-Miller plot obtained by Anderson et al. (50) and shown in Fig. 4-5 could be used to perform the rupture analysis of tank cars fabricated from TC-128 steel but the accuracy of that plot is suspect, as mentioned in Sect. 4.3. Stress-rupture data will have to be obtained by government laboratories. While this data is not needed to develop the tank car model, it will be needed to use it.

7.0 PROPOSED ACTIVITY SCHEDULE FOR THE DEVELOPMENT OF THE TANK CAR ANALYSIS PROGRAM

The tasks required to complete this project are outlined briefly below. A cost estimate and schedule for the remaining work will be prepared if the evaluators consider the technical approach described in this report to be satisfactory.

TASK 1.0 - Project Initiation

Members of the DE analysis group and TDC representatives and project evaluators will meet to discuss-the project and specify in detail the capabilities that the tank car analysis program should have.

TASK 2.0 - Preliminary Computer Model Development

A computer program capable of performing the thermal thermodynamic and structural analyses described in the preceding sections of this report will be developed.

TASK 3.0 - Comparison of Predicted & Experimental Results

Results obtained with the preliminary computer model will be compared to available experimental data, permitting an assessment of the models' completeness and accuracy.

TASK 4.0 - Refinement of Computer Models

The computer models will be refined based on the results of Activity 3.0

TASK 5.0 - Simulation Runs

Simulation runs using the complete validated computer model will be performed for a full-sized tank car. Cases of interest will be specified after consulting with TDC representatives.

TASK 6.0 - Assessment of EXPLOSAFE as an Explosion Suppressing System for LPG Tank Cars

The effectiveness of EXPLOSAFE as an explosion supressing system for full-size tank cars will be assessed. Optimal design configurations of the EXPLOSAFE material will be identified.

TASK 7.0 - Final Report & Computer Program Documentation

A draft report discussing the results of the analysis and making recommendations for further development and testing of the EXPLOSAFE concept will be prepared and submitted to the Transportation Development Centre, along with complete documentation of the computer program(s) and details of the analytical procedure. A final report will be issued after the contents of the draft have been evaluated by TDC.

REFERENCES

1. Department of Transportation Docket No. HM-144; Amendment Nos. 173-106, 179-19 by Materials Transportation Bureau (DOT). Published in the Federal Register, Vol. 42, No. 179 - Thursday, Sept. 15, 1977.

2. Razelos, P., Methods of Obtaining Approximate Solutions, Sect. 4, Handbook of Heat Transfer, edited by Rohsenow, W.M. and Hartnett, J.P., McGraw-Hill, 1973.

3. Holman, J.P., Heat Transfer, Fourth Edition, McGraw-Hill, 1976.

4. Graves, K.W., Development of a Computer Program for Modeling the Heat Effects on a Railroad Tank Car, FRA-OR&D report #75-53, January 1973, NTIS #PB-241-365.

5. Stewart, G., Introduction to Matrix Computations, Academic Press, 1973.

6. IMSL (International Mathematical & Statistical Libraries, Inc.) Documentation, Edition 8, Vol. 2, Section L, June, 1980.

7. Jennings, A., Matrix Computation for Engineers and Scientists, John Wiley & Sons, 1977.

8. Burgess, D., and Hertzberg, M., Radiation from Pool Flames, Ch. 27 in Heat Transfer in Flames, edited by Afgan, N.H., and Beer, J.M., John Wiley & Sons, 1974.

9. Seeger, P.G., Heat Transfer by Radiation from Fires of Liquid Fuels in Tanks, Ch. 28 in Heat Transfer in Flames, edited by Afgan, N.H., and Beer, J.M., John Wiley & Sons, 1974.

10. Anderson, C., Townsend, W., Zook, J. and Cowgill, G., The Effects of a Fire Environment on a Rail Tank Car Filled with LPG FRA-OR&D report #75-31, Sept., 1974.

11. Raj, P.K., Analysis of JP-4 Fire Test Data and Development of a Simple Fire Model ASME Paper 81-HT-17, Aug., 1981.

REFERENCES (Cont'd)

12. Giedt, W.H., *Investigation of Variation of Point Unit Heat Transfer Coefficient Around a Cylinder Normal to an Air Stream*, Trans. ASME, May 1949, pp. 375-381.

13. Welty, J.R., *Engineering Heat Transfer*, John Wiley & Sons, 1974.

14. McAdams, W.H., *Heat Transmission*, McGraw-Hill Book Co., 2nd edition, 1942.

15. Craver, C.D., *Gases and Vapors - A Special Collection of Infrared Spectra*, The Coblenty Society, Inc., 1980.

16. Howell, J.R., and Siegel, R., *Thermal Radiation Heat Transfer*, McGraw-Hill Book Co., 1972.

17. Cichelli, M.T., and Bonilla, C.F., Trans. Am. Inst. Chem. Engrs., 41, p. 755, A45.

18. Rohsenow, W.M., *Boiling*, Sect. 13, *Handbook of Heat Transfer*, edited by Rohsenow, W.M. and Hartnett, J.P., McGraw-Hill, 1973.

19. Hamilton, D.C. and Morgan, W.R., *Radiant Interchange Configuration Factors*, NACA TN 2836, 1952.

20. Crank, J., *How to Deal with Moving Boundaries in Thermal Problems*, Ch. 9, in *Numerical Methods in Heat Transfer*, edited by Lewis, R.W., Morgan, K. and Zienkiewicz, O.C., John Wiley & Sons, 1981.

21. Appleyard, R.D., *Testing and Evaluation of the EXPLOSAFE System as a Method of Controlling the Boiling Liquid Expanding Vapor Explosion (BLEVE)*, Transport Canada Research & Development Centre, Report #TP2740, Prepared by the EXPLOSAFE Division of Vulcan Industrial Packaging Ltd., August 1980.

22. Touloukian, Y.S., Powell, R.W., Ho, C.Y. and Klemens, P.G. (Editors) *Thermal Conductivity-Metallic Elements and Alloys* Thermophysical Properties of Matter, Vol. 1, IFI/Plenum, 1970.

23. Ehya, H., Faubert, F.M. and Springer, G.S., *Thermal Conductivity Measurements of Propane and N-Butane in the Range 300 to 1000 deg. K.* ASME Journal of Heat Transfer, August, 1982, pp. 262-265.

REFERENCES (Cont'd)

24. Sallett, D.W., and Palmer, M.E., The Calculation of the Thermodynamic Properties of Propane, Propylene, N-Butane and Ethylene, FRA-OR&D report #76-300, April, 1980.

25. Kremer, H., Buhr, E. and Haupt, T., Heat Transfer from Turbulent Free-Jet Flames to Plane Surfaces, Ch. 31 in Heat Transfer in Flames, edited by Afgan, N.H., and Beer, J.M., John Wiley & Sons, 1974.

26. Martin, H., Heat and Mass Transfer between Impinging Gas Jets and Solid Surfaces, Ch. 1 in Advances in Heat Transfer, Vol. 13, edited by Hartnett, J.P., and Irvine, T.F., Academic Press, 1977.

27. Chan, D., Axisymmetric Air Jet Impinging on a Convex Hemispherical Plate, M.S. Thesis, N.J.I.T., Newark, New Jersey, 1979.

28. Gardon, R. and Akfirat, J.C., The Role of Turbulence in Determining the Heat-Transfer Characteristics of Impinging Jets, Int. J. Heat Mass Transfer, Vol. 8, pp. 1261-1272, Pergamon Press, 1965.

29. Hrycak, P., Heat Transfer from a Row of Impinging Jets to Concave Cylindrical Surfaces, Int. Journ. Heat Mass Transfer, Vol. 24, Pergamon Press, 1981, pp. 407-419.

30. Vallis, E.A., Patrick, M.A. and Wragg, A.A., Radial Distribution of Convective Heat Transfer Coefficient between an Axisymmetric Turbulent Jet and a Flat Plate Held Normal to the Flow, Proceedings 6th International Heat Transfer Conference, Toronto, Canada, 1978.

31. Perry, K.P., Heat Transfer by Convection from a Hot Gas Jet to a Plane Surface, Proc. Inst. Mech. Engrs., Vol. 168, 1954, pp. 775-784.

32. Gardon, R. and Cobonpue, J., Heat Transfer between a Flat Plate and Jets of Air Impinging on it, International Developments in Heat Transfer, pp. 454-460, A.S.M.E., 1962.

33. Mandl, L.J., Thermal Protection Criteria for Tank Car, Appendix E in Phase II Report on Full Scale Fire Tests, Report #RA-11-6-31 (AAR R-201), Dec. 12, 1975.

REFERENCES (Cont'd)

34. Eggers, PE., Crawford, H.L., Trujillo, A.A., Pope, R.A. and Yoshimura, H.R., Thermal Analysis of HNPF Spent Fuel Shipping Container in Torch Environments ASME paper 80-HT-37.

35. Anderson, C. et al., Comparison of Various Thermal Systems for the Protection of Rail Tank Cars Tested at the FRA/BRL Torching Facility, Interim Memorandum Report #459, USA Ballistic Research Laboratories, Aberdeen Proving Gound, Maryland, Dec., 1975.

36. Görtler, H., Z. Angew, Math. Mech., Vol. 22, 1942, pp. 244-254.

37. Hinze, J.O. and van der Hegge Zijnen, B.G., 1949 Applied Scientific Research, Vol. A1, p. 435.

38. White, F.M., Viscous Fluid Flow, McGraw-Hill Book Co., 1974.

39. Sciance, T.C. and Colver, P.C., Minimum Film-Boiling Point for Several Light Hydrocarbons, ASME Journal of Heat Transfer, Nov. 1970, pp. 659-661.

40. Anderson, C., Townsend, W., Zook, J., Wright, W. and Cowgill, G., Railroad Tank Car Fire Test: Test No. 7, FRA-OR&D report #75-37, December, 1973.

41. Sallet, D.W., On the Sizing of Pressure Relief Valves for Pressure Vessels Which are used in the Transport of Liquified Gases, ASME paper 78-WA/HT-39.

42. Phase II Report on Full Scale Fire Tests, Report # RA-11-6-31 (AAR R-201), Dec. 12, 1975.

43. Henry, R.E., Two-Phase Compressible Flow EPRI Workshop Proceedings, Basic Two-Phase Flow Modelling in Reactor Safety and Performance, EPRI WS-78-143, Vol. 2, pp. 9-68 to 9-106, 1980.

44. Fauske, H.K., Two-Phase Two-and One-Component Critical Flow, Proc. of Symp. on Two-Phase Flow, Univ. of Exeter, Exeter, England, 1965, p. G101.

45. Harvey, J.F., Pressure Component Construction, Van Nostrand Reinhold Co., 1980.

REFERENCES (Cont'd)

46. Gill, S.S. (editor), The Stress Analysis of Pressure Vessels and Pressure Vessel Components, Pergamon Press, 1970.

47. Gerdeen, J.C. and Hutula, D.N., Plastic Collapse of ASME Ellipsoidal Head Pressure Vessels, ASME Journal of Engineering for Industry, Nov. 1970, pp. 797-804.

48. Gerdeen, J.C., The Effect of Geometrical Variations on the Limit Pressures for 2:1 Ellipsoidal Head Vessels under Internal Pressure, Welding Research Council Bulletin #215, May, 1976.

49. Berman, I., Henschel, R. and Horowitz, J.M., Elastic-Plastic Behaviour to Burst of Commercially Fabricated Pressure Vessel Heads with Attached Cylinders, Report for the Pressure Vessel Research Committee (PVRC) of the Welding Research Council (WRC).

50. Anderson, C. and Norris, E.B., Fragmentation and Metallurgical Analysis of Tank Car RAX201, FRA-OR&D report #75-30, April 1974.

51. Faupel, J.H., Engineering Design, John Wiley & Sons, 1964.

52. Phase II Report on Effects of Fire on LPG Tank Cars Report #RA-11-1-5, April 19, 1971.

53. Irons, B., Techniques of Finite-Elements, Hemisphere Publishing Co., 1980.

54. Buivid, M.G. and Sussman, M.V., Nature (London), 275, 203 (1978).

55. Reid, R.C., Some Theories on Boiling Liquid Expanding Vapor Explosions, Fire, March 1980, pp. 525-526.

APPENDICES

APPENDIX A: SAMPLE CALCULATION OF THE STABILITY-LIMITED TIME STEP SIZE FOR THE EXPLICIT TIME INTEGRATION PROCEDURE

The stability-limited time step size for a node on the inner surface of a 1/5 scale tank car similar to one of the tanks tested with and without EXPLOSAFE at CFB Suffield is calculated in this appendix. It will be assumed when calculating the stability-limited time step size for this node that,

1) three nodes are used across the thickness of the tank wall because this number of nodes would permit the roughly parabolic (quadratic) temperature distribution expected to exist in vapor-covered parts of the tank wall to be modelled accurately.
2) azimuthal nodes are located at 5° intervals (ie. 72 nodes are used to model the entire tank circumference).
3) axial conduction is negligible, so that axial conductances can be neglected. It will be assumed, however, that the tank is divided into thermally decoupled axial segments (as in Graves' model) of 1m length*.
4) the node is located below the liquid surface so that, with an assumed wall heat flux of $63{,}000 \mathrm{W}/_{\mathrm{m}^2}$ $\left(20{,}000 \frac{\mathrm{BTU}}{\mathrm{hrft}^2}\right)$ and a tank pressure of 2.03MPa (295psia), the heat transfer coefficient between the wall and the liquid propane (h_{ℓ}) is $\approx 8745 \frac{\mathrm{W}}{\mathrm{m}^{2\,\circ}\mathrm{C}}$ $\left(1540 \frac{\mathrm{BTU}}{\mathrm{hrft}^{2\,\circ}\mathrm{F}}\right)$. This value was obtained from Fig. 2-23 which indicates that the wall-to-liquid (assumed saturated) temperature difference (θ_s) for the assumed heat flux and pressure is $\approx 7.2^{\circ}\mathrm{C}$ ($13^{\circ}\mathrm{F}$) and hence that the heat transfer coefficient is $63{,}000/7.2 = 8725 \frac{\mathrm{W}}{\mathrm{m}^{2\,\circ}\mathrm{C}}$ as assumed.

---

* The value of Δt_{max} is not a function of the assumed length of the axial segments if axial conductances are neglected.

5) the properties of SA-285 steel, from which the 1/5 scale tanks were fabricated, are as follows.

$$\rho = 780 \text{ kg/m}^3$$
$$c = 480 \text{ J/kg}^\circ\text{C}$$
$$K = 50 \text{ W/m}^\circ\text{C}$$

The node in question is shown in Fig. A-1. For a 0.80cm (5/16") wall thickness and a 61 cm tank outer diameter (values appropriate to the 1/5 scale tanks used in the Suffield tests), the internodal conductances between node i,j,k and the neighbouring nodes are:

$$K(i,j,k)_{i+1} = 670.0 \text{ W/}^\circ\text{C},$$
$$K(i,j,k)_{j+1} = 1.866 \text{ W/}^\circ\text{C},$$
$$K(i,j,k)_{j-1} = 1.866 \text{ W/}^\circ\text{C},$$
$$h_\ell A_s(i,j,k) = 465 \text{ W/}^\circ\text{C}.$$

Also, $V(i,j,k) = 1.056\text{x}10^{-4}\text{m}^3$,

so $\Sigma K = 670.0 + 1.866 + 1.866 + 465 = 1138.7$,

and $\Delta t_{max} = \dfrac{7800\text{x}480\text{x}1.056\text{x}10^{-4}}{1138.7} = 0.347\text{sec.}$

Thus 0.347sec. is the maximum time step size that could be used in the explicit method without exceeding the stability limit for this node.

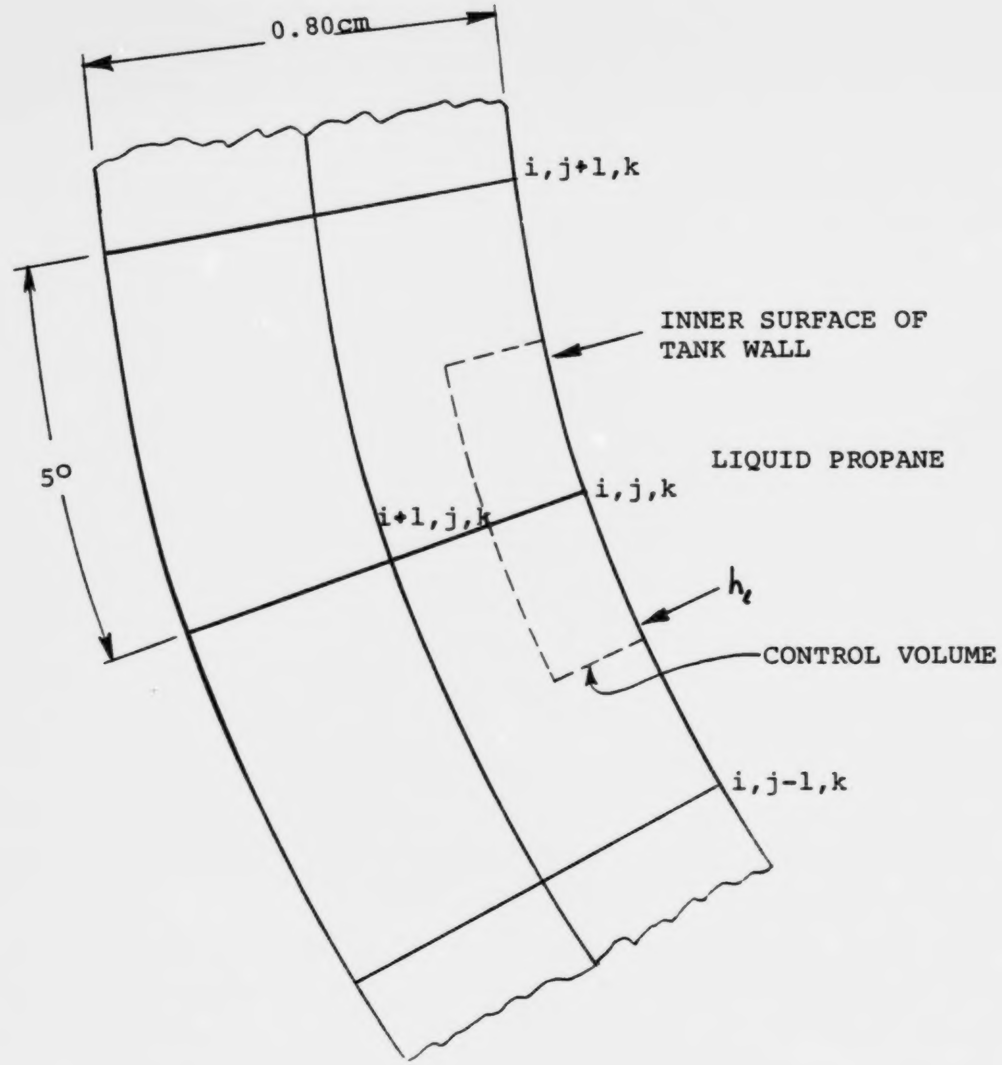
0.80cm
i,j+1,k
INNER SURFACE OF TANK WALL
5°
LIQUID PROPANE
i,j,k
i+1,j,k
h_ℓ
CONTROL VOLUME
i,j-1,k

Fig.: A-1: Tank wall inner surface node

APPENDIX B: LIQUID LEVEL CALCULATIONS

The liquid level, X*, in a cylindrical tank of given dimensions containing a known volume of liquid, V_ℓ, can only be obtained by solving the inverse problem first (ie. by obtaining V_ℓ from X*) and then applying a search technique to find the value of X* corresponding to a given value of V_ℓ. If the tank is horizontal (ie. $\alpha = 0^\circ$) it is easily shown the volume of liquid in the tank, V_ℓ, can be calculated from the expression,

$$V_\ell = L_t R_{it}^{\ 2} \left[\pi - \cos^{-1}\left(\frac{X^*}{R_{it}}\right) + \frac{X^*}{R_{it}^{\ 2}} \sqrt{R_{it}^2 - X^{*2}} \right] \qquad \text{B-1}$$

where L_t = the length of the tank

and R_{it} = the inner radius of the tank

When the tank is horizontal, X* is simply the height of the liquid surface above the center of the tank, as shown in Fig. B-1, because the origins of the global (X-Y-Z) and tank car centered coordinate systems are coincident, as discussed in Sect. 2.2. When the tank's longitudinal axis is not horizontal, Eqn. B-1 can still be used to predict the differential volume of liquid, dV_ℓ, in a differential length of the tank, dz, when X* is replaced by ($X^* - z \sin\alpha$), which is the height of the liquid surface above the center of the tank at axial location z, as seen in Fig. B-2. The variables V_ℓ and L_t must be replaced by dV_ℓ and dz respectively, of course, giving

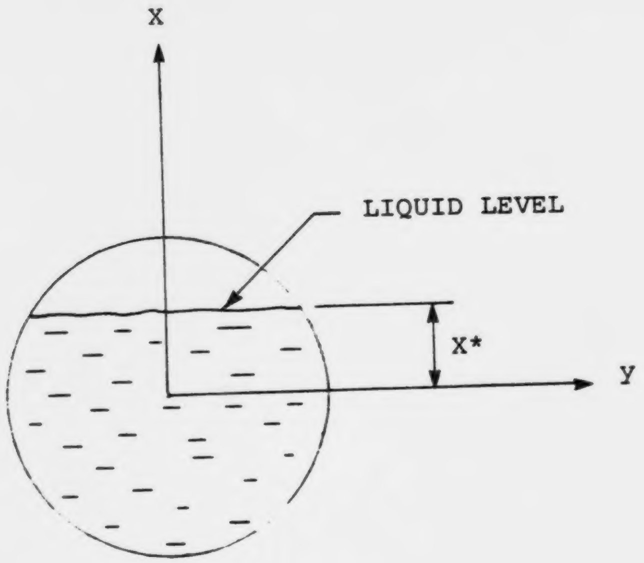
X
LIQUID LEVEL
X*
Y

Fig. B-1: LOCATION OF THE LIQUID SURFACE IN A HORIZONTAL TANK

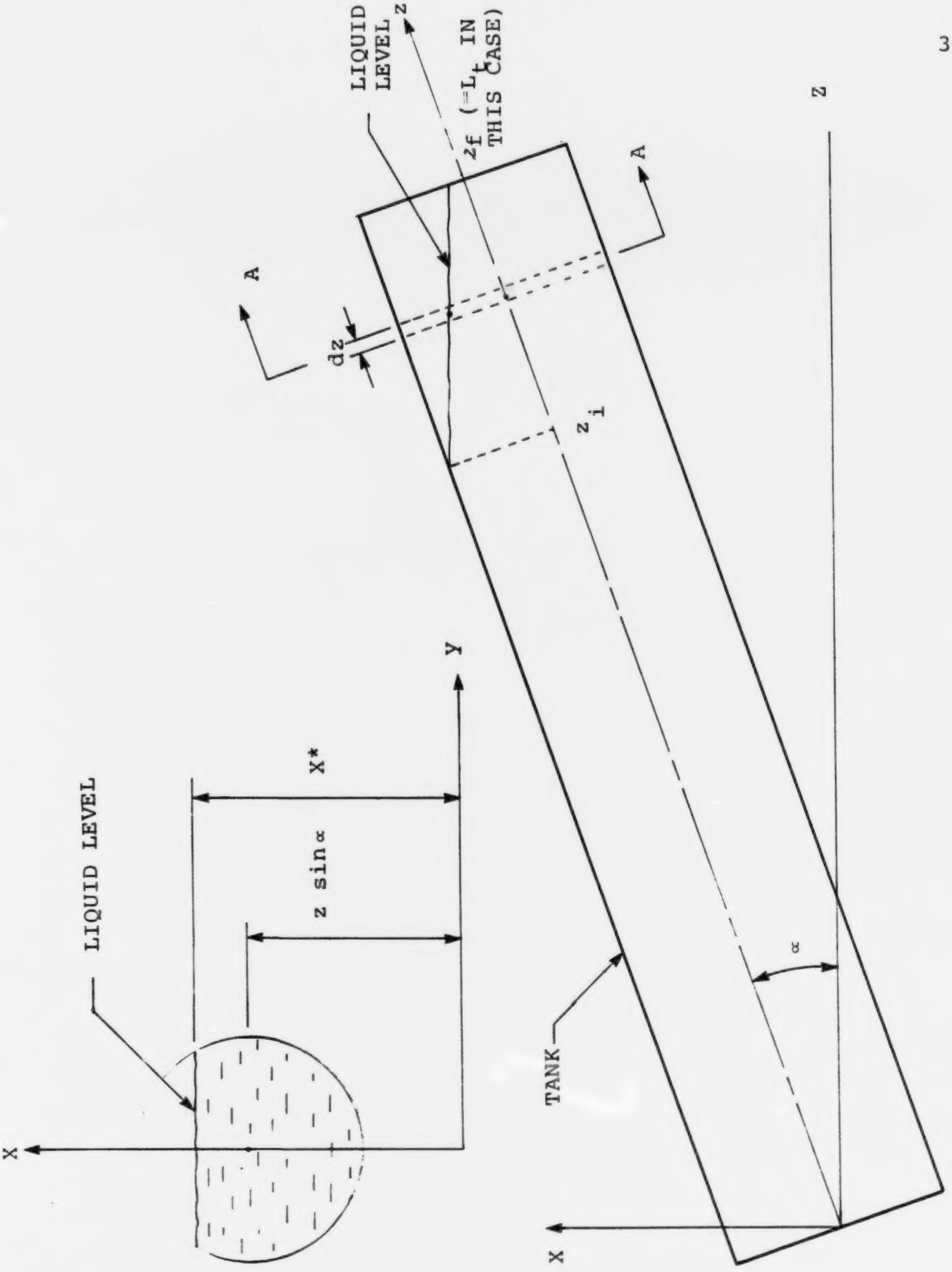
LIQUID LEVEL
z
z_f ($=L_t$ IN THIS CASE)
z
A
A
dz
z_i
y
X*
z sinα
LIQUID LEVEL
α
TANK
X
X
SECTION A-A

Fig.: B-2: Geometry for Differencial Liquid Volume Calculations in a Non-Horizontal Cylindrical Tank

$$dV_{\ell} = R_{it}^{2}\left[\pi - \cos^{-1}\left(\frac{X^{*} - z\sin\alpha}{R_{it}}\right) + \left(\frac{X^{*} - z\sin\alpha}{R_{it}^{2}}\right)\sqrt{R_{it}^{2} - (X^{*} - z\sin\alpha)^{2}}\right]dz \qquad \text{B-2}$$

as the volume of liquid contained in the axial slice of thickness dz. Equation B-2 is only applicable in differential axial segments that are partially filled with liquid. If the axial region of the tank that is partially filled with liquid starts at z_i and ends at z_f, the total volume of liquid in that region designated V_{ℓ}', is the integral of Eqn. B-2 from z_i to z_f, or,

$$V_{\ell}' = \int_{z_i}^{z_f} dV_{\ell}$$

$$= \int_{z_i}^{z_f} R_{it}^{2}\left[\pi - \cos^{-1}\left(\frac{X^{*} - z\sin\alpha}{R_{it}}\right) + \left(\frac{X^{*} - z\sin\alpha}{R_{it}^{2}}\right)\sqrt{R_{it}^{2} - (X^{*} - z\sin\alpha)^{2}}\right]dz \qquad \text{B-3}$$

Equation B-3 can be integrated to give,

$$V_{\ell}' = R_{it}^{2}\left[\pi(z_f - z_i) + \frac{R_{it}}{\sin\alpha}\left\{\left(\frac{X^{*} - z_f\sin\alpha}{R_{it}}\right)\cos^{-1}\left(\frac{X^{*} - z_f\sin\alpha}{R_{it}}\right) - \left(\frac{X^{*} - z_i\sin\alpha}{R_{it}}\right)\cos^{-1}\left(\frac{X^{*} - z_i\sin\alpha}{R_{it}}\right) - \sqrt{1 - \left(\frac{X^{*} - z_f\sin\alpha}{R_{it}}\right)^{2}} + \sqrt{1 - \left(\frac{X^{*} - z_i\sin\alpha}{R_{it}}\right)^{2}}\right\}\right.$$

$$+\frac{1}{3R_{it}^{2}\sin\alpha}\left\{\left(R_{it}^{2}-(X^{*}-z_{f}\sin\alpha)^{2}\right)^{3/2}-\left(R_{it}^{2}-(X^{*}-z_{i}\sin\alpha)^{2}\right)^{3/2}\right]\qquad \text{B-4}$$

While V_ℓ' is only the volume of liquid in the partially filled part of the tank, the volume of liquid in the filled region (ie. the region between $z=0$ and $z=z_i$ in Fig. B-2) can be easily calculated and added to V_ℓ' to obtain V_ℓ. Equation B-4 is applicable to both positive and negative pitch angles (α) but it cannot be used when $\alpha=0^\circ$ because the terms with $\sin\alpha$ in the denominator blow up in that case. Equation B-1 must be used to predict V_ℓ when $\alpha=0^\circ$.

It is obviously impossible to invert Eqn. B-4 to calculate X* explicitly from V_ℓ' so a search technique must be used to find the value of X* corresponding to a given value of V_ℓ' (or V_ℓ). The computer program provided in the appendix uses the half-interval search technique, described in reference B-1, to find the appropriate zero of Eqn. B-4 (ie. X*) when V_ℓ is specified.

DESCRIPTION OF THE PROGRAM LIQLEV

The program LIQLEV calculates the liquid level (X*) in a cylindrical tank, which may or may not be horizontal, when the volume of liquid in the tank (V_ℓ) is specified. Input variables read by line 9 of LIQLEV are VOLIQ ($=V_\ell$), TLEN ($=L_t$), TRADI ($=R_{it}$), ALPHA ($=\alpha$) and EPSLN. The last input variable (EPSLN) is a convergence parameter compared to the absolute value of the difference between consecutive estimates of X*, at each iteration, designated DIFF in the program. It is assumed that the search for X* has converged to the correct result when DIFF $\leqslant$ EPSLN.

Lines 13-19 in LIQLEV calculate the highest and lowest possible values of the liquid level, designated LLEVH and LLEVL respectively, since these values are needed to start the search for the true level. The values of LLEVH and LLEVL are simply taken to be the highest and lowest points in the tank respectively. The iteration loop for the half-interval search starts at statement 90 (line 22) where the midpoint of the search interval (AVLEV) is calculated. Lines 23-53 then proceed to calculate the liquid volume in the tank for $X^* = \text{AVLEV}$. Lines 24-33 calculate the values of z_i and z_f, designated ZRL and ZRR respectively in the program, along with the volume of liquid in the completely filled part of the tank, designated VOLUM. Lines 44-52 calculate the volume of liquid in the partially filled part of the tank (ie. V_ℓ') which is subsequently added to VOLUM in line 53 to obtain the total volume of liquid in the tank. The calculated volume of liquid is compared to the specified volume (VOLIQ) in lines 56-58 to determine whether AVLEV should be used as the liquid level upper limit or lower limit in the next iteration (interval halving step) and lines 59-62 make the appropriate assignments. Lines 63-64 perform the convergence test described previously and direct the program back to the start of the iteration loop (statement 90) to perform another interval halving step if the convergence test indicates that the desired accuracy has not been achieved. If the result has converged to the required accuracy the results are printed by line 65.

VERIFICATION OF THE LIQUID LEVEL MODEL

The liquid level calculational procedure was verified over a wide range of positive and negative pitch angles (α) for a tank of typical tank car dimensions by choosing X^* in each case to coincide with the X- coordinate of the tank centroid in the X-Z plane. For a given value of α, X^* equals the X- coordinate of the tank centroid in the X-Z plane when $X^* = \frac{L_t}{2} \sin\alpha$, as seen in Fig. B-3. The volume of liquid in the tank must always be one-half of the total volume of the tank when X^* is chosen in this manner, regardless of the value of α. As a further test of the liquid level calculational procedure, the volume of liquid in the tank was calculated for $X^* = 0.0$ and $\alpha = \pm\alpha'$. When $X^* = 0.0$ and $\alpha = 0$ the tank is obviously half-full and the volume of liquid in the tank when $\alpha = -\alpha'$ should be greater than the half-full volume by the same amount that the volume of liquid in the tank is less than the half-full volume when $\alpha = +\alpha'$ (α' is some constant angle). The program LIQLEV passed all of the tests of this type.

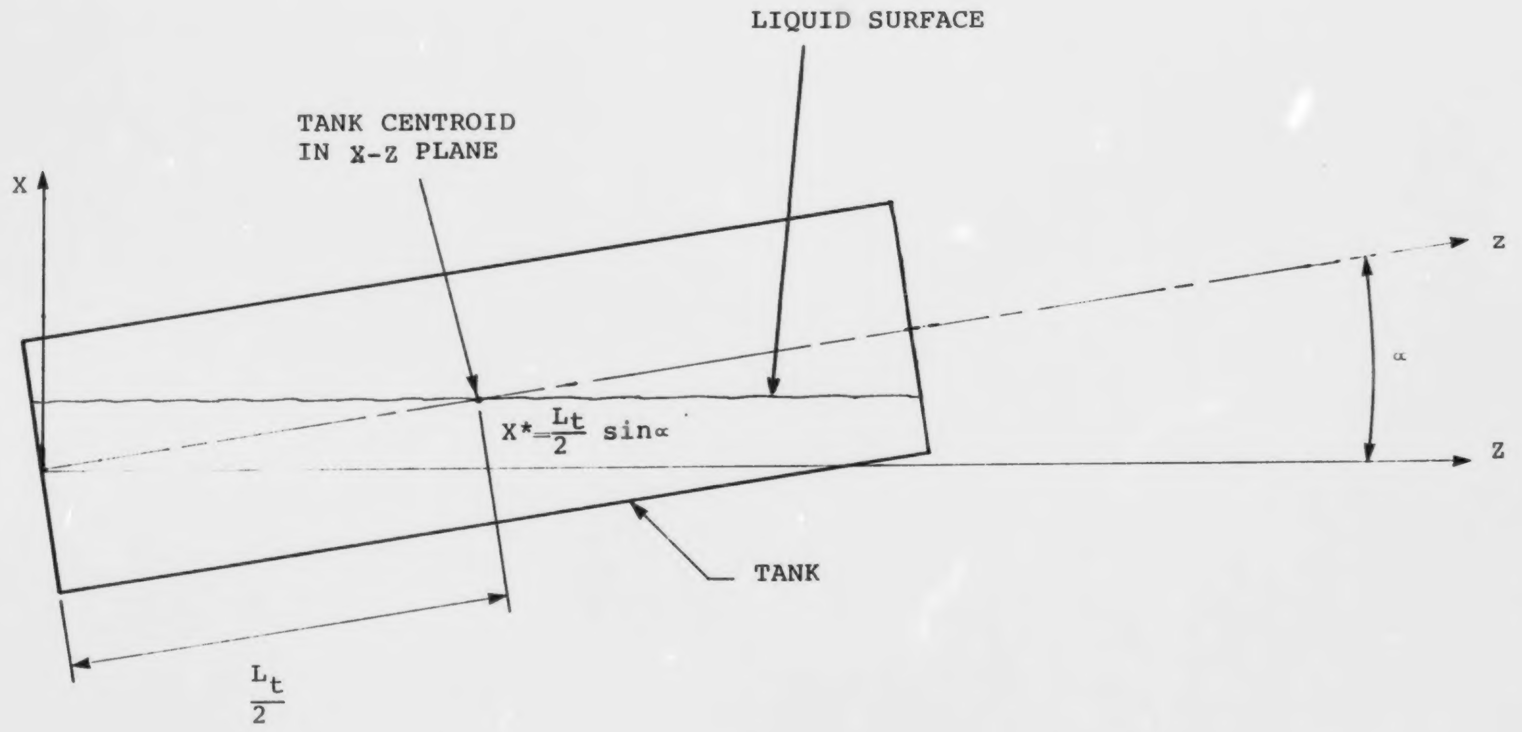
LIQUID SURFACE
TANK CENTROID IN X-Z PLANE
X
z
α
Z
$X^* = \frac{L_t}{2} \sin\alpha$
TANK
$\frac{L_t}{2}$

Lig. B-3: LIQUID LEVEL COINCIDING WITH THE TANK CENTROID IN THE X-Z PLANE

References

B-1 Southworth, R.W. and Deleeuw, S.L. "Digital Computation and Numerical Methods' McGraw-Hill, 1965.

```
FORTRAN IV      V02.1-1    Thu 15-Jul-82 15:03:14              PAGE 001

0001            PROGRAM LIQLEV
          C
          C     THIS PROGRAM CALCULATES THE LIQUID LEVEL IN AN INCLINED
          C     CYLINDRICAL TANK WHEN THE VOLUME OF LIQUID IN THE TANK IS
          C     SPECIFIED.
          C
0002            IR=5
          C
0003            REAL FNAME(4),LLEV,LLEVL,LLEVH
          C
          C     GET INPUT DATA FILE NAME
          C
0004            WRITE(7,7)
0005      7     FORMAT(1X,'ENTER FILE NAME'$)
          C
0006            READ(7,8) FNAME
0007      8     FORMAT(4A4)
          C
0008            OPEN(UNIT=5,TYPE='OLD',NAME=FNAME)
          C
          C     READ LIQUID VOLUME (VOLIQ), TANK LENGTH (TLEN), TANK INNER
          C     RADIUS (TRADI), ANGLE BETWEEN TANK LONGITUDINAL AXIS AND
          C     HORIZONTAL (ALPHA-RADIANS), AND CONVERGENCE CRITERION FOR
          C     HALF-INTERVAL ROOT SEARCH (EPSLN).
          C
0009            READ(IR,100) VOLIQ,TLEN,TRADI,ALPHA,EPSLN
0010      100   FORMAT(5F10.5)
          C
          C     CALCULATE LOW AND HIGH VALUES OF LIQUID LEVEL (LLEVL & LLEVH)
          C     TO START HALF-INTERVAL SEARCH FOR ACTUAL LIQUID LEVEL (LLEV)
          C     CORRESPONDING TO SPECIFIED LIQUID VOLUME.
          C
0011            SALPH=SIN(ALPHA)
0012            CALPH=COS(ALPHA)
          C
0013            IF(ALPHA.GT.0.0) LLEVL=-TRADI*CALPH
0015            IF(ALPHA.GT.0.0) LLEVH=TLEN*SALPH+TRADI*CALPH
0017            IF(ALPHA.LE.0.0) LLEVL=TLEN*SALPH-TRADI*CALPH
0019            IF(ALPHA.LE.0.0) LLEVH=TRADI*CALPH
          C
          C     START HALF-INTERVAL SEARCH FOR LIQUID LEVEL.
          C     CALCULATE DIFFERENCE BETWEEN LIQUID VOLUME AT LOW LIQUID LEVEL
          C    (WHICH IS ZERO INITIALLY) AND SPECIFIED VOLUME.
          C
0021                VOL1=-VOLIQ
          C
          C     CALCULATE AVERAGE OF HIGH AND LOW LIQUID LEVELS.
          C    (IE. INTERVAL MIDPOINT)
          C
0022      90    AVLEV=(LLEVL+LLEVH)/2.0
          C
          C     CALCULATE LIQUID VOLUME AT INTERVAL MIDPOINT
          C
0023            VOLUM=0.0
```

```
      ZRL=0.0
      ZRR=TLEN
      HT=TRADI*CALPH
      HTN=-HT
      HT1=TLEN*SALPH+HT
      HT2=TLEN*SALPH+HTN
C
      IF(ALPHA) 25,30,35
C
 25   IF(AVLEV.LT.HTN) ZRL=(AVLEV-HTN)/SALPH
      IF(AVLEV.GT.HT1) ZRR=(AVLEV-HT)/SALPH
      IF(AVLEV.GT.HT1) VOLUM=(TLEN-ZRR)*3.14159*(TRADI**2.0)
      GO TO 40
C
 35   IF(AVLEV.GT.HT) ZRL=(AVLEV-HT)/SALPH
      IF(AVLEV.GT.HT) VOLUM=ZRL*3.14159*(TRADI**2.0)
      IF(AVLEV.LT.HT2) ZRR=(AVLEV+HT)/SALPH
C
 40   C1=(AVLEV-SALPH*ZRR)/TRADI
      C2=C1*ACOS(C1)
      C3=(AVLEV-SALPH*ZRL)/TRADI
      C4=C3*ACOS(C3)
      C5=SQRT(1.-C1**2.0)
      C6=SQRT(1.-C3**2.0)
      C7=(TRADI**2.-(AVLEV-ZRR*SALPH)**2.)**1.5
      C8=(TRADI**2.-(AVLEV-ZRL*SALPH)**2.)**1.5
C
      VOL=(TRADI**2.)*((3.14159*(ZRR-ZRL)+(TRADI/SALPH)*(C2-C4-C5+C6))
     $+((1.0/(3.0*SALPH*(TRADI**2.)))*(C7-C8)))
C
      VOL=VOL+VOLUM
      GO TO 48
C
 30   VOL=TLEN*(TRADI**2.0)*(3.14159-ACOS(AVLEV/TRADI)+AVLEV
     $*SQRT(TRADI**2.-AVLEV**2.)/(TRADI**2.))
C
C     COMPUTE DIFFERENCE BETWEEN ACTUAL VOLUME OF LIQUID IN TANK
C     (AT LIQUID LEVEL AVLEV) AND SPECIFIED LIQUID VOLUME.
C
 48   VOLM=VOL-VOLIQ
C
C     COMPUTE NEW UPPER AND LOWER LIQUID LEVELS (IE. NEW INTERVAL
C     CONTAINING CORRECT LEVEL).
C
      PROD=VOL1*VOLM
      IF(PROD) 50,60,70
C
 50   LLEVH=AVLEV
      GO TO 80
C
 70   VOL1=VOLM
      LLEVL=AVLEV
C
C     CHECK FOR CONVERGENCE
```

```
      C
0063  80    DIFF=LLEVH-LLEVL
0064        IF(DIFF-EPSLN) 60,60,90
      C
      C     PRINT THE RESULTS
      C
0065  60    WRITE(6,200) VOLIQ,TLEN,TRADI,ALPHA,EPSLN,AVLEV
0066  200   FORMAT(1X,'VOLIQ=',F10.5,4X,'TLEN=',F10.5,4X,'TRADI='
           $,F10.5,/1X,'ALPHA=',F10.5,4X,'EPSLN=',F10.5,4X,'AVLEV='
           $,F10.5)
0067        STOP
0068        END
```

APPENDIX C: OUTER-WALL CONVECTIVE HEAT TRANSFER COEFFICIENTS FOR A TANK CAR IN A POOL FIRE

C-1.0 INTRODUCTION

Estimates are made for the convective heat transfer coefficient on the outer-wall of a tank car lying in a pool of JP-4 or similar fuels.

There appear to be few data in the literature which deal directly with this problem, no doubt because of the experimental difficulties involved. Russell & Cranfield (1973) estimated the "perimeter-mean" convective heat transfer coefficient for a small cylinder well above a very large pool of burning JP-5, but these results obviously cannot readily be applied to a large cylinder lying directly in or close to the pool.

The approach used here is therefore an indirect one, combining data for fires with data for the heat transfer characteristics of single cylinders in cross flow.

C-2.0 GENERAL FLOW CHARACTERISTICS

C-2.1 Behaviour of Fire

The fire is modelled using the data of Raj (1981) who made measurements on a large circular pool of burning JP-4. Details of the fire geometry are shown in Fig. C-1.

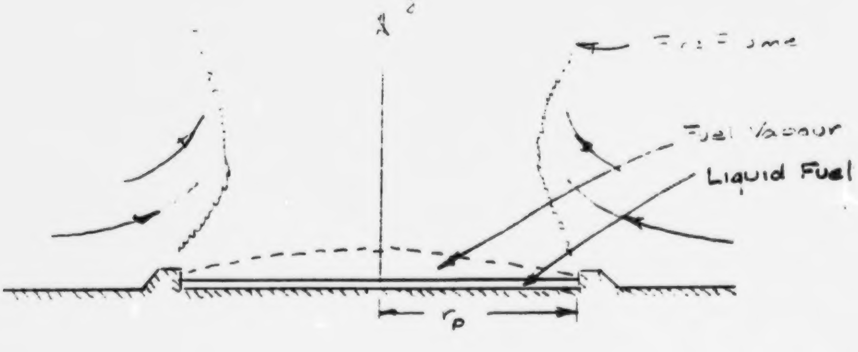

Fig. C-1: Circular pool fire geometry and structure

Unfortunately, there are some errors and internal inconsistencies in Raj's paper, but with some reasonable assumptions it is possible to arrive at an empirical model which predicts the centreline velocity and temperature distributions for pool fires of arbitrary radius. Figures C-2 and C-3 show predicted and measured centerline velocity and temperature distributions obtained by Raj for a fire with a base diameter of 15.2 m.

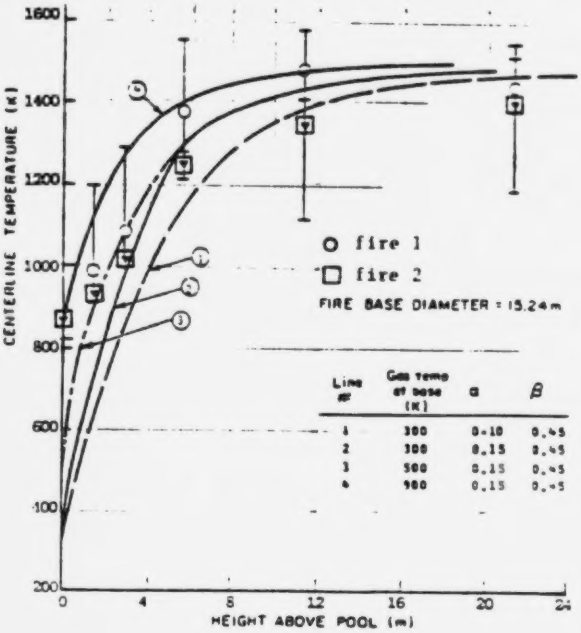

Line #	Gas temp at base (K)	α	β
1	300	0.10	0.45
2	300	0.15	0.45
3	500	0.15	0.45
4	900	0.15	0.45

Fig. C-2: Comparison of Experimental Centerline Temperature Data and Model Predictions

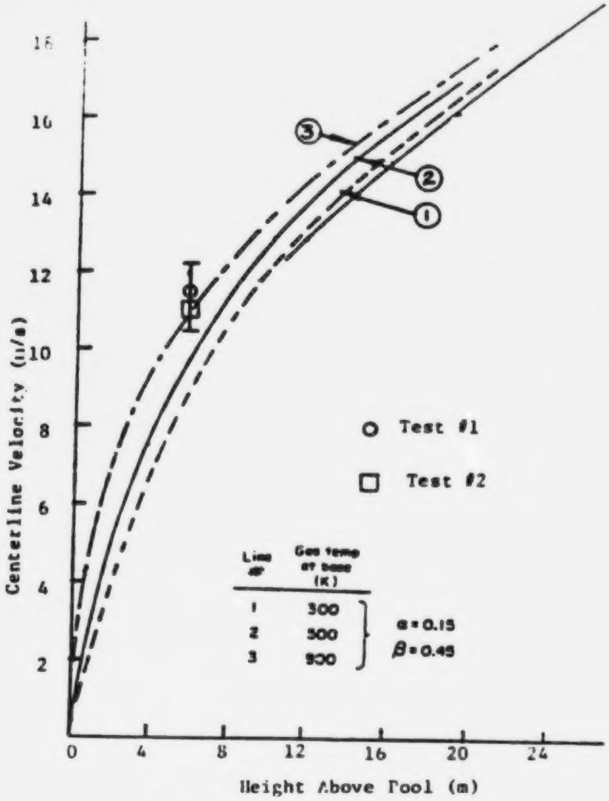

Fig. C-3: Comparison of Experimental Velocity Data and Theoretical Predictions

Raj also derived a simple analytical model of the fire vehicle predicted the distributions of the following non-dimensional variables:

$\xi = \frac{z}{r_p}$ (height above pool)

$\eta = \frac{r}{r_p}$ (radius of plume)

T_o = temperature at bottom of plume

$v = \frac{V}{V_{ch}}$

$V_{ch} = \sqrt{g r_p}$ ("characteristic" velocity)

and obtained the results shown in Fig. C-4.

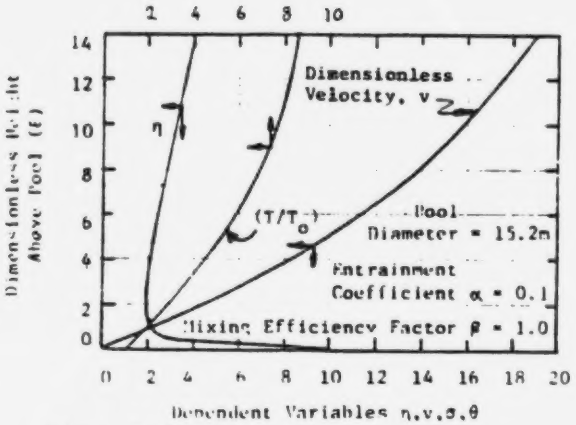

Fig. C-4: Variation of Dimensionless Variables with Height Within the Fire

According to Raj, the model results are in good agreement with the experimental measurements. However, cross-comparison with Figs. C-2 & C-3 shows that there must be several errors in Fig. C-4. If the ξ and (η, v, σ, θ) scales are divided by 10 then the variations of η and v are reasonable. On the other hand, the T/T_o line is clearly incorrect and the problem is not simply one of scale labelling. It will therefore be assumed that a universal curve of T/T_o does exist and it will be rederived from Fig. C-2.

Although Raj does not make this clear, T_o, the temperature at the bottom of the gas plume, should presumably be the ignition temperature of the fuel at atmospheric pressure. For JP-4, $T_o \approx 500^oK$. Using this value of T_o, curve 3 in Fig. C-2 provides the flame temperature vs. height above pool data shown in Table C-1.

TABLE C-1: FLAME TEMPERATURES AT DIFFERENT ACTUAL AND DIMENSIONALESS DISTANCES FROM THE POOL

(m) z	$\xi\left(=\frac{z}{7.62}\right)$	T (^oK)	T/T_o ($T_o = 500^oK$)
0	0	500	1.0
2.0	0.262	1000	2.0
4.0	0.525	1200	2.4
6.0	0.787	1310	2.62
8.0	1.050	1370	2.74
10.0	1.312	1410	2.82
12.0	1.575	1430	2.86
16.0	2.100	1460	2.92

The revised temperature vs. height correlation is plotted in Fig. C-5. Note that Raj's data implies that the temperature in the plume is asymptotic to some maximum value. This is clearly not correct since once combustion is complete, continued dilution by entrained air should begin to reduce the temperature. However, this should occur well above the region which is of interest for the tank car problem.

Most of the combustion characteristics (stoichiometric air-fuel ratio, calorific value etc.) are very similar for all hydrocarbon fuels. It thus seems reasonable to assume that the characteristics of plumes produced by fires involving fuels other than JP-4 will be very similar to, and hence can be inferred from, the available JP-4 plume characteristics.

C-2.2. Cylinders in Cross-Flow

The heat transfer characteristics of cylinders in cross-flow have been studied extensively: for a detailed list of references, see Morgan (1975).

For the present case data is taken from two papers by Giedt (1949, 1951). Fig. C-6 shows the Nusselt number distribution around the cylinder as a function of Reynolds number, for a low turbulence stream (according to the author, "T' = 1% or less" - it will be assumed to be 1%). Fig. C-7 shows the effect of increasing turbulence intensity (T') to 4%.

Fig. C-5

NON-DIMENSIONAL PLUME CHARACTERISTICS (JP-4 FIRE DATA)

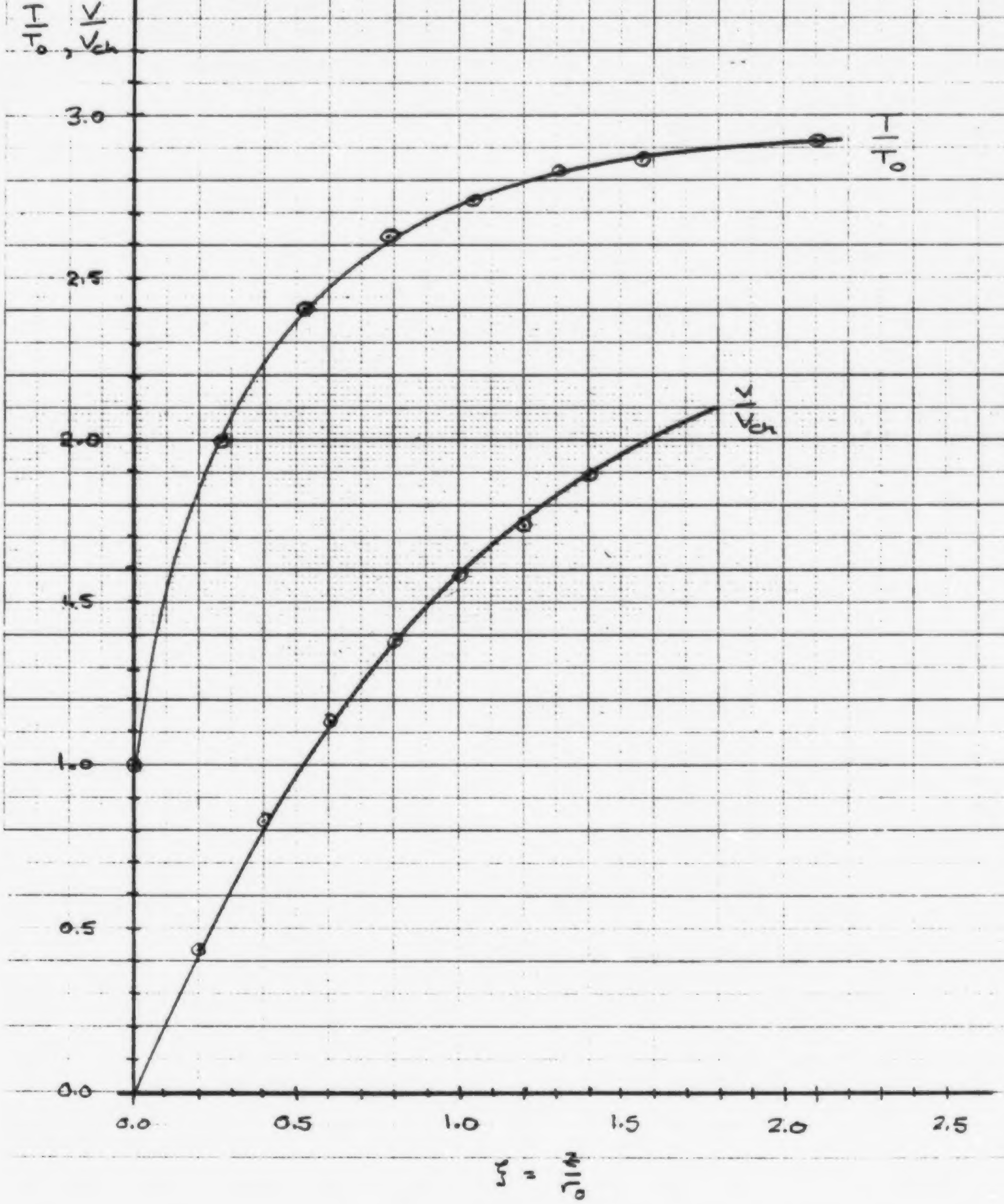

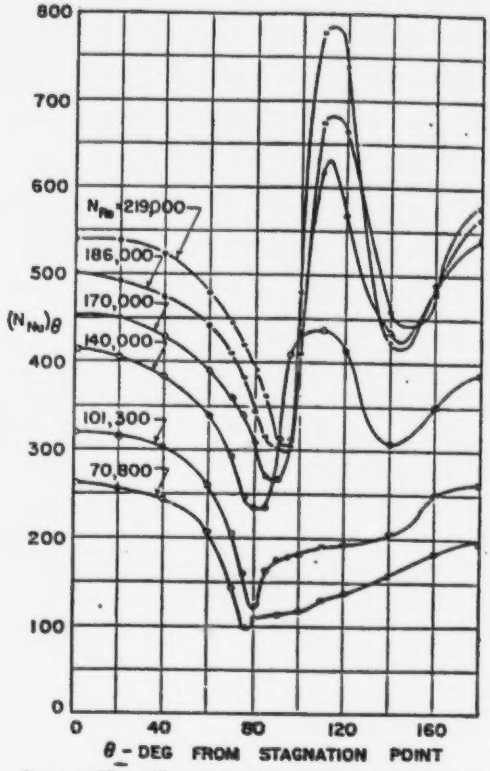

Rate of Heat-Transfer Distribution Around Cylinder Circumference for Different Values of Reynolds Modulus;

Fig. C-6

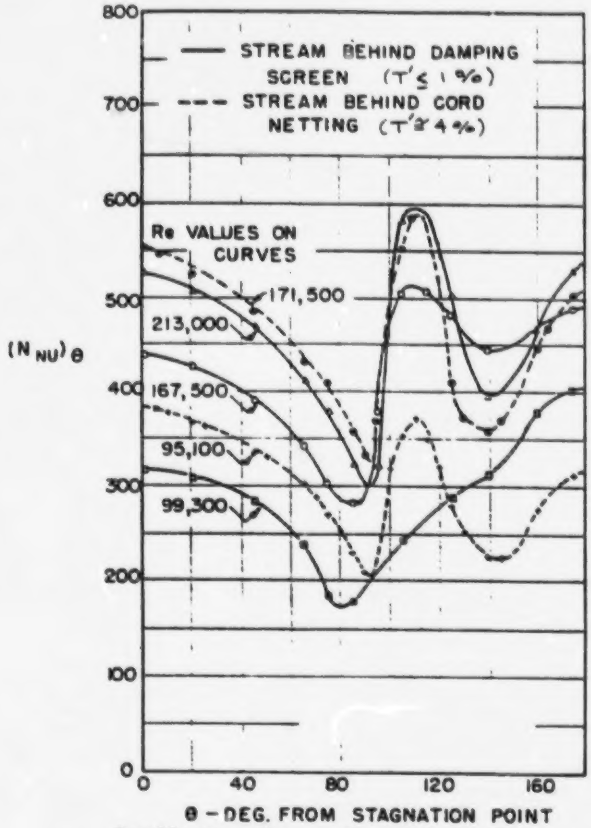

Local heat transfer around a cylinder for different Reynolds Numbers.

Fig. C-7

The turbulent freestream data is included here since the flow in the plume is undoubtedly highly turbulent. As seen from the figures, freestream turbulence has several related effects. In the first place, the resulting increased turbulence intensity inside the boundary layer increases the local wall shear stress and thus the convective heat transfer coefficient. In addition, early transition is promoted and separation is delayed. All of these effects can be lumped together as an increase in the effective Reynolds number.

The following approach will therefore be used to evaluate the heat transfer coefficients for the tank car:

(i) A nominal Reynolds number will be calculated, using flow conditions derived from the fire data.

(ii) The effective Reynolds number will then be estimated, based on an assumed value of freesteam turbulence.

(iii) The N_u distribution corresponding to the effective R_e will then be read from Fig. C-6.

The relationship between nominal and effective Reynolds numbers and turbulence intensity is derived from Fig. C-6 and C-7 using the stagnation point Nusselt numbers, as shown in Table C-2

TABLE C-2: STAGNATION POINT Nu AS A FUNCTION OF Re_D AND T'

T' %	Re_D	Nu (STAGNATION POINT)	SOURCE
1.0 (ASSUMED)	70800	265	Fig. C-6
	101300	320	
	140000	415	
	170000	450	
	186000	500	
	219000	540	
	99300	315	Fig. C-7
	167500	440	
	213000	525	
4.0	95100	385	Fig. C-7
	171500	550	

The resulting correlation is shown in Fig. C-8. Lines for other values of T' have been interpolated on the assumption that Nu tends to some limit as T' increases. Use of Fig. C-8 is illustrated in the next section.

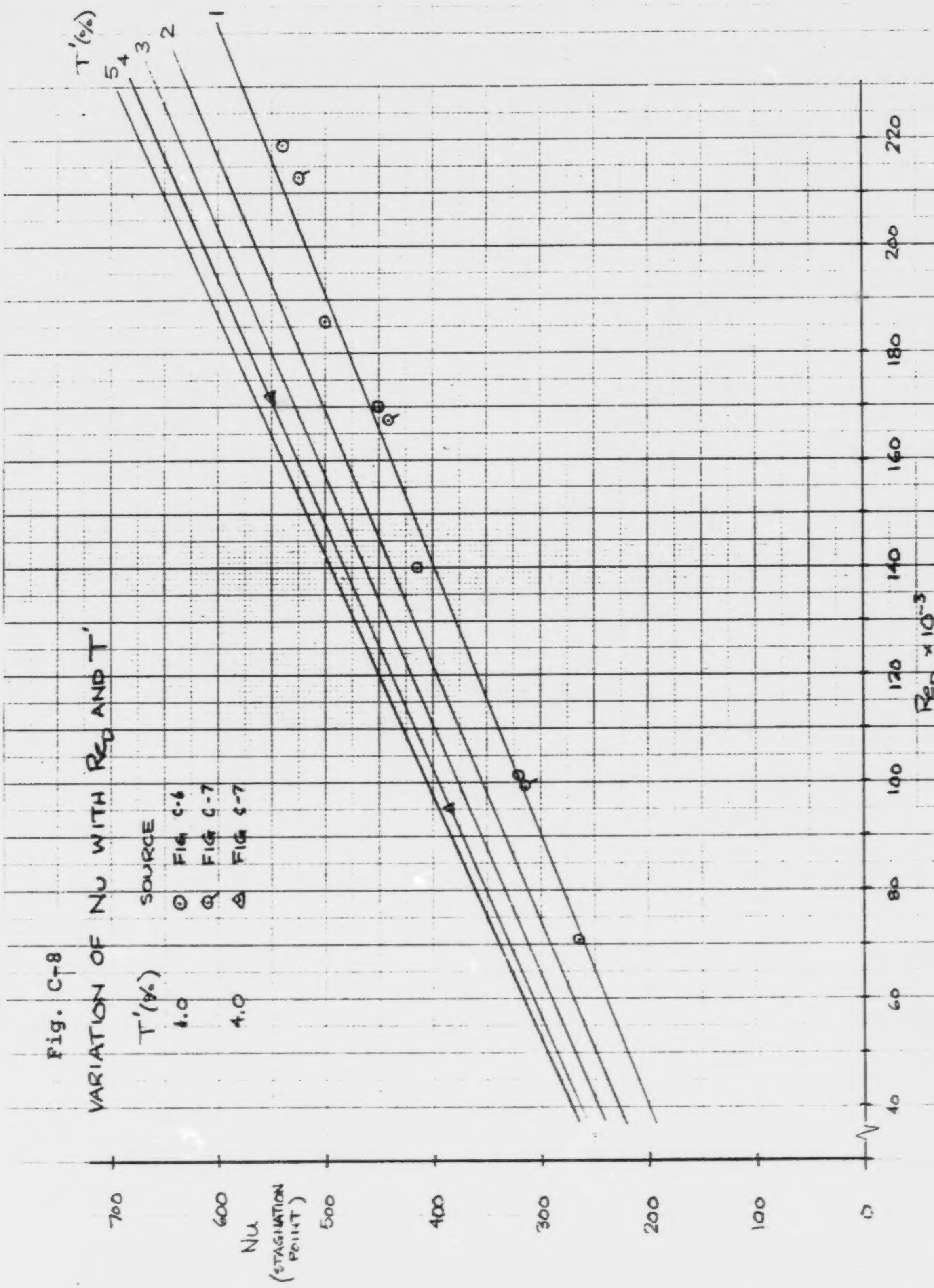

Fig. C-8

VARIATION OF NU WITH Re_D AND T'

C-3.0 ESTIMATED CONVECTIVE HEAT TRANSFER COEFFICIENTS

The flow around the tank car (which is assumed level and neglecting end effects) should appear roughly as shown in Fig. C-9.

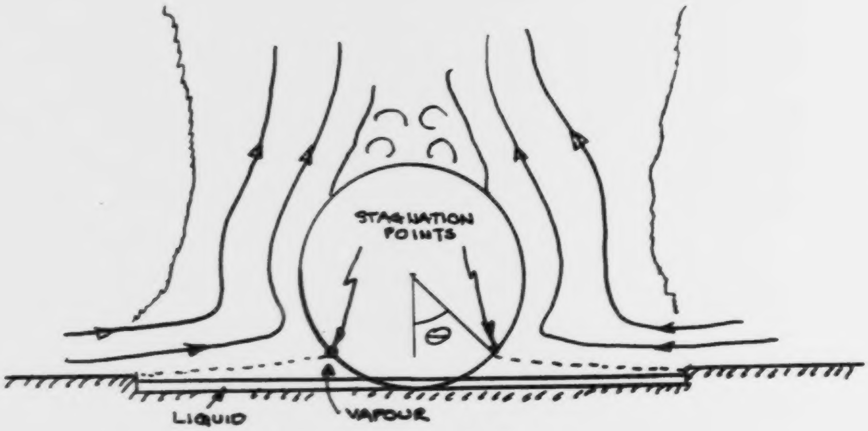

FIG. C-9: FLOW AROUND TANK CAR

Near the bottom, the tank should be exposed to unburned propane vapour. There will therefore be two stagnation lines where the induced upflow of air, combustion products and unburned vapour attaches to the tank. The circumferential location of these stagnation lines is unknown but $\theta \simeq 45^{\circ}$ might be a reasonable guess.

Obviously, the flow field is somewhat different from that which occurs in a uniform infinite stream. Nevertheless, it seems reasonable to assume that above the stagnation lines the two flows are very similar. However, since the gas boundary layers will essentially start at the stagnation lines, they will be thinner than if they had started at the front stagnation point. This effect can be taken into account approximately by incrementing the nominal Re since higher Re results in thinner boundary layers. It would be difficult to estimate the size of the increment and in view of the other approximations it is probably pointless to try. Instead a small amount will be added to the assumed turbulence irtensity to produce an additional increase in Re.

It is assumed that the pool fire is large enough so that the plume is not significantly distorted by the presence of the tank. The nominal Reynolds number will then be evaluated (somewhat arbitrarily) for the velocity and temperature conditions at half the tank height.

To see the effect of the size of the pool and other factors, the heat transfer coefficients will be estimated for several cases; specifically for pool diameters of 9 m and 15 m and ignition temperatures (T_o) of 500°K and 743°K since the latter values are roughly the ignition temperatures of JP-4 fuel and propane vapor respectively at atmospheric pressure. Vaporizing liquid propane could feed the pool fire if the tank car relief valve was located below the surface of the liquid propane and hence discharging a vapor liquid mixture. Results of the analysis with the two pool diameters and the two ignition temperatures are given below.

Case (a) $D_{pool} = 9m (\approx 3D_{tank})$; $T_o = 743^{\circ}K$.

$$\xi = \frac{z}{r_p} = \frac{1.51}{4.5} = 0.336,$$

then from Fig. C-5 $\frac{T}{T_o} \cong 2.23$, $\frac{V}{V_{ch}} = 0.78$,

and

$$V_{ch} = \sqrt{gr_p} = \sqrt{9.81 \times 4.5} = 6.64 \text{ m/s};$$

since $T_o = 743^oK$,

$$T \simeq 2.23 \times 743 \simeq 1657^oK \cdot$$

Since the vapour and combustion products are very dilute, the properties of air at the same temperature will be used

At $T = 1657^oK$, $P = 101.325 \text{ kP}_a$

$\nu = 27.1 \times 10^{-5} \text{ m}^2/\text{s}$, $k = 10.3 \times 10^{-2} \frac{W}{m^oK}$

$$\therefore \quad Re_{D_{nominal}} \quad \frac{VD}{\nu} = \frac{6.64 \times 3.02}{27.1 \times 10^{-5}}$$

$$= 74{,}000 \cdot$$

Also,

- for freestream turbulence, assume T' = 3% (a reasonably high value)
- add 1% shifted stagnation point.
- then $T' = 4\%$, and since the data platted in Fig. C-6, from which the Nu distribution will be obtained, corresponds to an assumed turbulence level (T') of 1%, Fig. C-8 is used to calculate the Reynolds number at which a freestream with T' = 1% would give the same stagnation point Nusselt number as a freestream with the Reynolds number of 74000, obtained previously, and T' = 4%. The former "effective Reynolds number" is seen from the dashed line in Fig. C-10 to be:

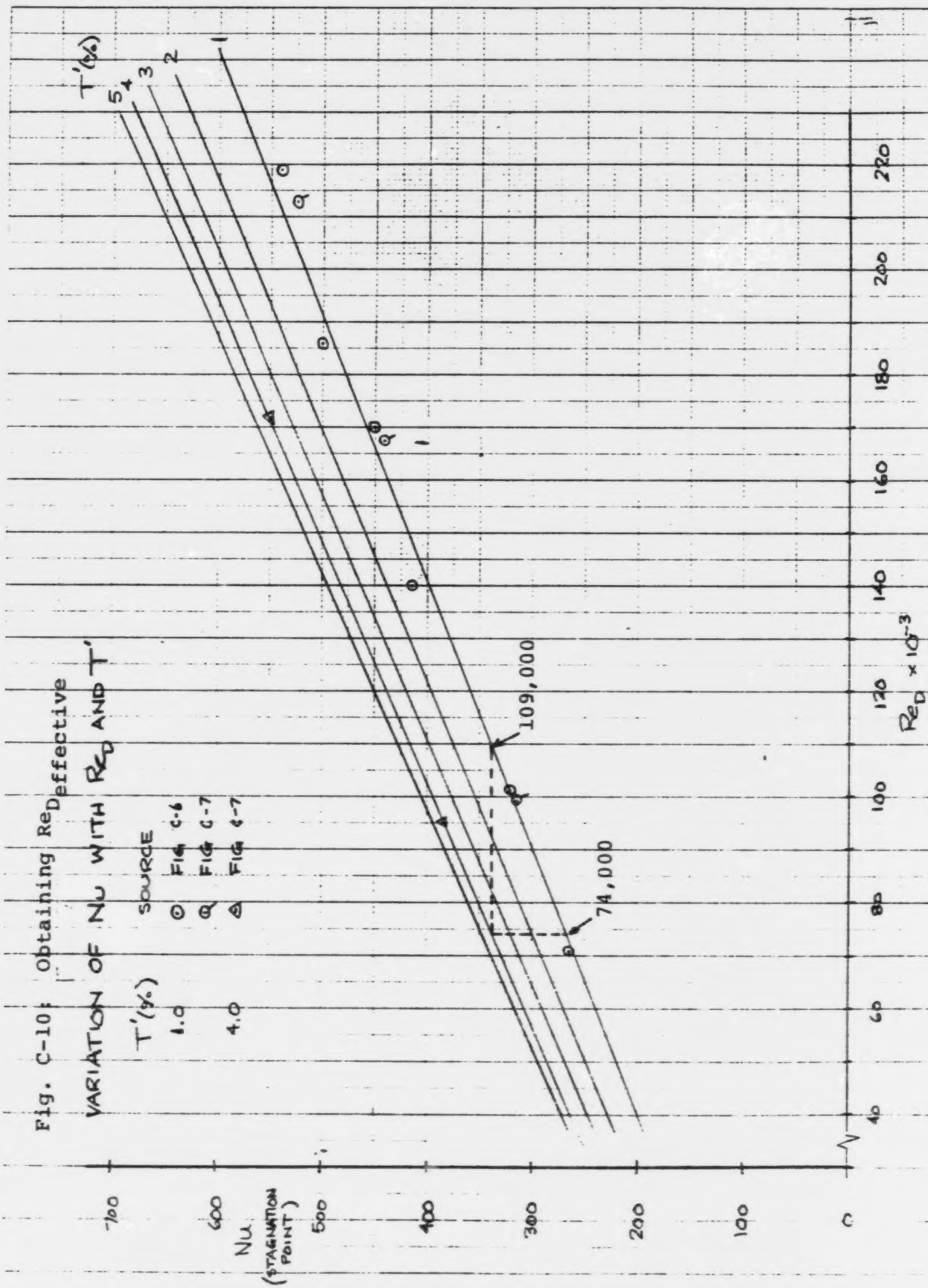

Fig. C-10: Obtaining $Re_{D_{effective}}$

$Re_{D_{effective}}=109{,}000$

- then estimating the Nu distribution from Fig. C-6, the results tabulated below are obtained.

θ ($^\circ$)	Nu ($= \frac{hD}{k}$)	h ($\frac{W}{m^{2\,\circ}K}$)
50	320	10.9
60	280	9.5
80	170	5.8
100	275	9.4
120	250	8.5
140	240	8.2
160	275	9.4
180	300	10.2

- the values of h have been calculated neglecting the circumferential variation in k
- to see the effect of varying k, consider the $\theta = 180^\circ$ position

$$\xi = \frac{3.02}{4.5} = 0.671\ , \quad \text{and} \quad \frac{T}{T_o} = 2.53\ ; \quad \therefore \quad T \simeq 1880^\circ K\ ,$$

then $k = 11.6 \times 10^{-2} \ \frac{W}{m^\circ K}$

$$h = Nu.\frac{k}{D} = 300 \times \frac{11.6}{3.02} \times 10^{-2}$$

$$= 11.5 \ \frac{W}{m^{2\,\circ}K} \qquad \left(\text{cf. } 10.2 \ \frac{W}{m^{2\,\circ}K}\right)$$

- relative to the uncertainties, the difference is not great.

Case (b) $D_{pool} = 9$ m; $T_o = 500^{o}K$

Since $T_o = 500^{o}K$ in the case,

$T = 2.23 \times 500 = 1115^{o}K$

$\nu = 14.1 \times 10^{-5}$ m^2/s

$k = 74 \times 10^{-3}$ $W/m^{o}K$

$$Re_{D_{nominal}} = \frac{6.64 \times 3.02}{14.1 \times 10^{-5}}$$

$$= 142000$$

$$Re_{D_{effective}} = 184000$$ (taking T' = 4% again)

Results

θ (°)	Nu $(=\frac{hD}{k})$	h $(\frac{W}{m^{2o}K})$
50	465	11.4
60	435	10.7
80	335	8.2
100	405	9.9
120	560	13.7
130	620	15.2
140	425	10.4
160	480	11.8
180	530	13.0

Case (c) $D_{pool} = 15$ m ($\approx 5\ D_{tank}$); $T_o = 743^oK$

- considering the effect of varying pool size

$$\xi = \frac{z}{r_p} = \frac{1.51}{7.5} = 0.201$$

- then from Fig. C-5, $\frac{T}{T_o} = 1.86$, $\frac{V}{V_{ch}} = 0.42$,

and

$$V_{ch} = \sqrt{g r_p} = \sqrt{9.81 \times 7.5} = 8.58 \text{ m/s}$$

$T = 1.86 \times 743 = 1380^oK$

$V = 0.42 \times 8.58 = 3.60$ m/s

$\nu = 20.0 \times 10^{-5}$ m^2/s

$k = 88.0 \times 10^{-3}$ W/m^oK

$$Re_{D_{nominal}} = \frac{3.60 \times 3.02}{20.0 \times 10^{-5}}$$

$$= 54400$$

$Re_{D_{effective}} = 88000$ (T' = 4%)

Results

θ (°)	Nu $\left(= \frac{hD}{k}\right)$	h $\left(\frac{W}{m^2\,{}^\circ K}\right)$
50	265	7.7
60	235	6.8
80	120	3.5
100	160	4.7
120	175	5.1
140	180	5.2
160	220	6.4
180	235	6.8

Case (d) $D_{pool} = 15\ m,\ T_o = 500^{\circ}K$

$T = 1.86 \times 500 \quad 930^{\circ}K$

$\nu = 10.5 \times 10^{-5}\ m^2/s$

$k = 63.9 \times 10^{-3}\ W/m^{\circ}K$

$$Re_{D_{nominal}} = \frac{3.60 \times 3.02}{10.5 \times 10^{-5}}$$

$$= 104000$$

$$Re_{D_{effective}} = 143000$$

Results

θ (°)	Nu ($\frac{hD}{k}$)	h ($\frac{W}{m^2 {}^{\circ}K}$)
50	375	7.9
60	350	7.4
80	245	5.2
100	450	9.5
120	425	9.0
140	325	6.9
160	370	7.8
180	400	8.5

The results are summarized in Figs. C-11 and C-12.

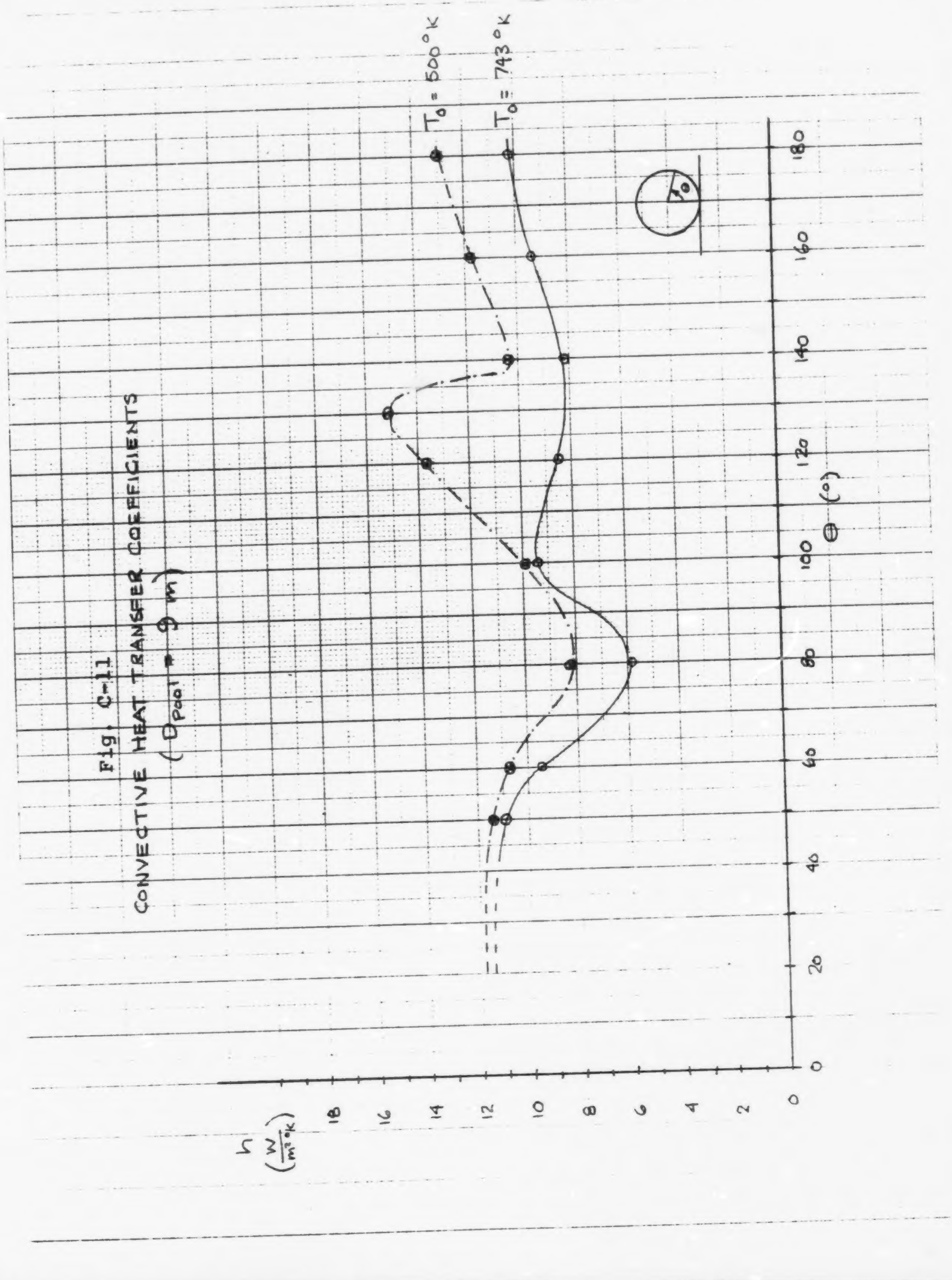

Fig. C-11

CONVECTIVE HEAT TRANSFER COEFFICIENTS

(D_{pool} = 9 m)

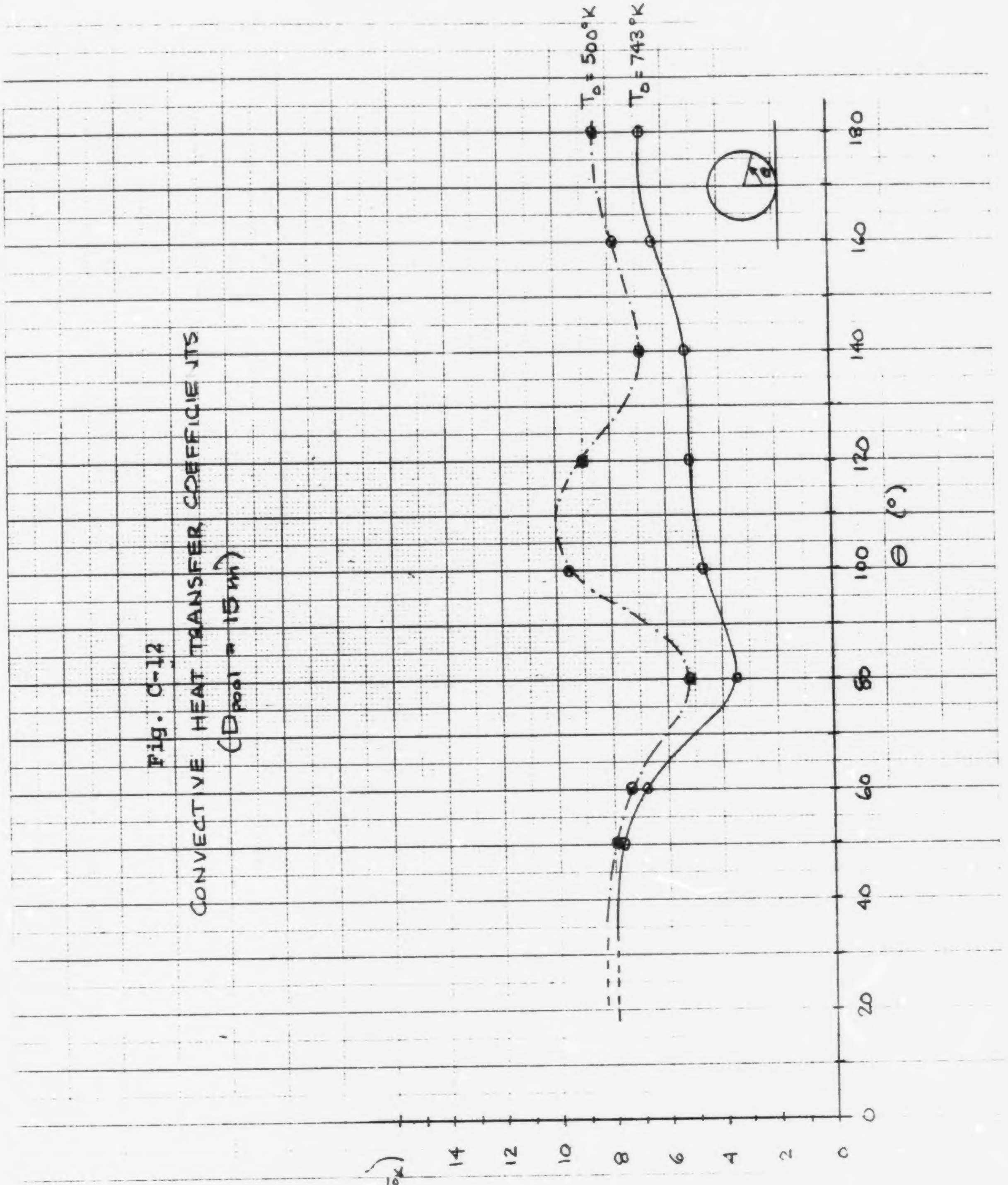

Fig. C-12

CONVECTIVE HEAT TRANSFER COEFFICIENTS (D_{pool} = 15 m)

C-4.0 CONCLUDING REMARKS

In view of the large number of assumptions and approximations made, the heat transfer coefficient distributions should obviously be regarded as reasonable estimates rather than precise predictions. The differences between the various curves should be taken more as a measure of the uncertainties than, say, an accurate indication of the effects of pool size.

The uncertainties are probably greatest for the upper half of the tank. From the calculations it appears that the flow lies in the Reynolds number range where modest variations in the flow conditions can produce substantial changes in the locations of the boundary layer transition and separation points. Such changes can, as seen from Fig. C-6, considerably alter the heat transfer coefficients on the leeward side of the cylinder.

The results are of course most directly applicable to the inboard portions of level tanks. There will be three-dimensional effects near and on the end-caps, but it is felt that the heat transfer coefficients will not be drastically different from those estimated here. There will likewise be three-dimensional effects on titled tanks due to axial flow. According to Morgan (1975) the heat transfer is in fact reduced somewhat by yawing the cylinder. For small angles of tilt (α), the effect can be taken into account approximately by basing the heat transfer calculation on the circumferential component of the velocity, $V_t (= V\cos\alpha)$, shown in Fig. C-13.

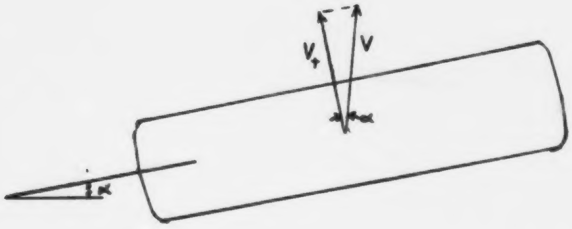
V_t
V
α
α

Fig. C-13: Circumferential velocity component (V_t) for a tilted tank

References

C-1.	Russell, L.H. Cranfield, J.A.	Experimental Measurement of Heat Transfer to a Cylinder Immersed in a Large Aviation-Fuel Fire. ASME J. Heat Trans., Aug. 1973, pp. 397-404.
C-2.	Raj, P.K.	Analysis of JP-4 Fire Test Data and Development of a Simple Fire Model. ASME Paper 81-HT-17, Aug. 1981.
C-3.	Morgan, V.T.	The Overall Convective Heat Transfer from Smooth Circular Cylinders. Advances in Heat Transfer, Vol. 11, Academic, New York, 1975, pp. 199-264.
C-4.	Giedt, W.H.	Investigation of Variation of Point Unit Heat Transfer Coefficient Around a Cylinder Normal to an Air Stream. Trans. ASME, May 1949, pp. 375-381.
C-5.	Giedt, W.H.	Effect of Turbulence Level of Incident Air Stream on Local Heat Transfer and Skin Friction on a Cylinder. J. Aero-Sciences, Nov. 1951, pp. 725-730.

APPENDIX D: ESTIMATING CONVECTIVE HEAT TRANSFER COEFFICIENTS ON THE INNER WALL OF A PROPANE TANK LYING IN A POOL FIRE

INTRODUCTION

This appendix makes initial estimates of the convective heat transfer coefficients on the inner wall of an unruptured, partially-filled propane tank which is lying in a pool fire. In addition, recommendations are made concerning methods of calculating the coefficients as part of a more comprehensive modelling of the internal and external fluid mechanics of burning tank cars.

The flow inside the tank is assumed to be dominated by the outflow of boiled-off propane through the relief valve. Natural convection effects are neglected. The wall flow is therefore treated as a conventional velocity boundary layer.

CONTENTS

D-1.0 General Assumptions
D-2.0 Level Tank
  D-2.1 Laminar Boundary Layer Development
  D-2.2 Possibility of Transition
  D-2.3 Convective Heat Transfer Coefficient
  D-2.4 Flow Behaviour in Model Tank
  D-2.5 Explosafe-Lined Tank
  D-2.6 Summary and Recommendations
D-3.0 Tilted Tank
  D-3.1 Freestream Flow
  D-3.2 Convective Heat Transfer Coefficient
  D-3.3 Possibility of Transition
  D-3.4 Summary and Recommendations
D-4.0 References
D-5.0 Properties of Propane

D-1.0 GENERAL ASSUMPTIONS

The following general assumptions are made concerning the flow inside the tank:

i) The flow is assumed quasi-steady even though it is recognized that the relief value will be cycling on and off.

ii) The propane is assumed to be superheated only in the boundary layer. In the rest of the vapour space, fluid properties are assumed uniform at the saturation conditions corresponding to the pressure setting of the relief valve.

iii) The boundary layer is assumed to be two-dimensional; that is, circumferential flow due to natural convection and other effects is assumed to be negligible. This should be valid except close to the outlet.

iv) The wall temperature is assumed to be the same throughout the vapour space.

D-2.0 LEVEL TANK

As a representative case, the flow is calculated for an 80% full, unlined, full-scale DOT 112A tank car with the relief value at the top centre. The tank dimensions used in the analysis are shown in Fig. D-1.

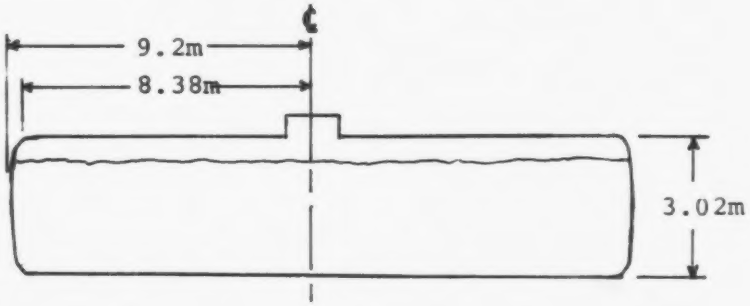

Fig. D-1: Full size tank car

For the purposes of this analysis it is assumed that the heat flux incident on the tank outer surface is the pool fire standard value (maximum) of 108,800 W/m^2 (34,500 $BTU/hrft^2$). It can be shown that the vapour evolution rate for one-half of the tank will be approximately 31.09 kg/sec. (68.48 lbm/sec. in this case. Other assumed conditions are as follows,

a) Saturated vapour conditions

$P \simeq 280$ psia (relief valve setting)
$T \simeq 55.5^{\circ}C$ (saturation temperature)
$v = 0.333\ ft^3/lb_m$
$\rho v = 3.0\ lb_m/ft^3$
$= 48.11\ kg/m^3$

b) Film conditions

$T \simeq 411^{\circ}C$ ($356^{\circ}C$ superheat)
(for additional data see Sect. D-5.0)

Assuming uniform vapour evolution at the liquid surface, the vapour velocity will vary linearly along the tank since the flow area for the vapour is constant. Thus half way along the tank,

$$U = \frac{\dot{m}}{\rho_v A_{flow}} ,$$

where,

$$A_{flow} = 0.2\ A_{tank} = 0.2 \quad \frac{\pi}{4}(3.02)^2 = 1.433m^2,$$

so,

$$U = \frac{31.09}{48.11x1.433} = 0.452m/s$$

The vapour axial velocity profile in the tank is sketched in Fig. D-2.

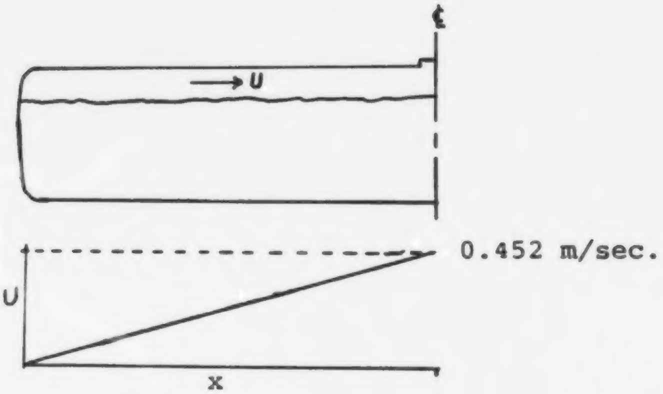

Fig. D-2: Vapour axial velocity profile

D-2.1 Laminar Boundary Layer Development

The wall boundary layer develops under conditions which closely approximate those occurring at a plane stagnation point, with the stagnation point being at the end cap, as shown in Fig. D-3.

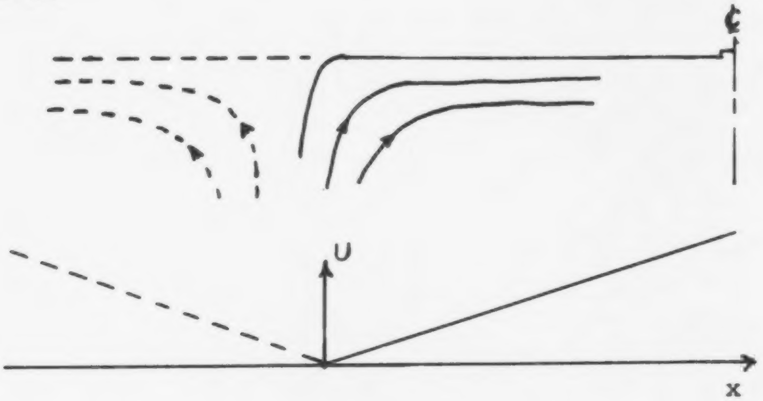

Fig. D-3: Stagnation point flow with the stagnation point at the tank end cap

In both cases, the freestream velocity varies linearly away from the stagnation point.

The boundary layer will be laminar initially and at some distance downstream may undergo transition to turbulence, depending on the Reynolds number and freestream conditions. The flow is therefore first analysed as a laminar boundary layer and an estimate is then made as to whether transition will occur along its length.

The plane stagnation point flow is in fact one of the Falkner-Skan wedge flows for which exact analytical solutions exist (eg. see Schlichting, 1979; White, 1974; Curle, 1962). The freestream velocity over the wedge surface (U(x)) is defined by the expression:

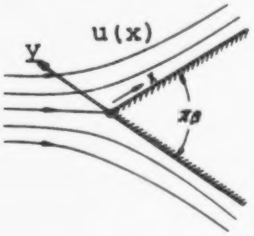

Fig. D-4: Wedge geometry

$$U(x) = Kx^{m}$$

where $m = \frac{\beta}{2-\beta}$

and for the plane stagnation point $\beta = 1$, $m = 1$.
The wedge geometry is shown in Fig. D-4.

Similarity solutions for the boundary layer equations are obtained by replacing y with

$$\eta = y \sqrt{\frac{m \;\; 1}{2} \cdot \frac{U(x)}{\gamma(x)}} \, ,$$

and the conventional boundary length scales (ie. thickness) are then given by

$$\eta_{\delta_{0.99}} = \delta \sqrt{\frac{m+1}{2} \frac{U(x)}{\nu x}}$$ (boundary layer thickness)

$$\eta_{\delta^*} = \delta^* \sqrt{\frac{m+1}{2} \frac{U(x)}{\nu x}}$$ (displacement thickness)

$$\eta_{\theta} = \theta \sqrt{\frac{m+1}{2} \frac{U(x)}{\nu x}}$$ (momentum thickness)

where $\eta_{\delta_{0.99}}$, η_{δ^*} and η_{θ} are constants which arise from the solution of the equations (η_{δ^*} and η_{θ} can be found tabulated as a function of m in the references mentioned earlier)

With $m = 1$ and $U(x) = Kx^m = Kx$,

$$\eta_{\delta_{0.99}} = \delta_{0.99} \sqrt{\frac{K}{\nu}} = 2.4$$

$$\eta_{\delta^*} = \delta^* \sqrt{\frac{K}{\nu}} = 0.64790$$

$$\eta_{\theta} = \theta \sqrt{\frac{K}{\nu}} = 0.29235$$

Note that this case is unusual in that the boundary layer has constant thickness because the thinning of the layer due to acceleration precisely balances the growth due to entrainment of freestream fluid. This effect causes the heat transfer coefficient to be constant also, as will be seen later.
For the full-scale tank car

$$K = \frac{\Delta U}{\Delta x} = \frac{0.452}{8.38} = 0.0539 \text{ s}^{-1} ,$$

and at the film temperature of the propane

$$\nu = 11.56 \times 10^{-7} \text{m}^2/\text{s} .$$

Thus $$\sqrt{\frac{K}{\nu}} = \sqrt{\frac{0.0539}{11.56\text{x}10^{-7}}} = 216.0\text{m}^{-1} \; ,$$

and $$\delta_{0.99} = \frac{2.4}{216.0} = 0.0111\text{m} \; , \qquad (\simeq 11\text{mm})$$

$$\delta^* = 0.0030 \qquad (\simeq 3\text{mm})$$

$$\theta = 0.00135 \qquad (\simeq 1.4\text{mm})$$

These figures indicate that the boundary layer on the inside wall is extremely thin. Although the boundary layer thickness is constant, the Reynolds number does of course change due to the variation in velocity along the flow. The Reynolds numbers based on x (ie. Re_x) and the momentum thickness (ie. Re_θ) are given by the expressions,

$$Re_x = \frac{Ux}{\nu} = \frac{Kx^2}{\nu} = (4.67\times10^4)x^2 \; ; \; Re_\theta = \frac{U\theta}{\nu} = \frac{K\theta x}{\nu} = 63.1x$$

Re_x, Re_θ and $\log_{10}Re_x$ are tabulated as a functions of x in Table D-1.

TABLE D-1: REYNOLDS NUMBERS AS FUNCTIONS OF X

x (m)	Re_x	$\log_{10}Re_x$	Re_θ
0.1	$4.67\text{x}10^2$	2.669	6.3
0.5	$1.17\text{x}10^4$	4.067	31.6
1.0	$4.67\text{x}10^4$	4.669	63.1
2.0	$1.87\text{x}10^5$	5.271	126.2
4.0	$7.47\text{x}10^5$	5.873	252.4
6.0	$1.68\text{x}10^6$	6.226	378.6
8.0	$2.99\text{x}10^6$	6.475	504.8
8.38	$3.28\text{x}10^6$	6.516	528.8

In the absence of disturbances, a laminar boundary layer can be expected to undergo transition to turbulence at about $Re_\theta = 600$, which suggests that transition could occur here before the layer reaches the outlet. The possibility of transition will therefore have to be examined before solving for the heat transfer coefficient.

D-2.2 Possibility of Transition

The location of the transition point is influenced by a number of factors:

(a) Wall Roughness

Rough walls will cause early transition. However, in the absence of other information, the walls of the unlined tank are assumed to be smooth.

(b) Wall Temperature

For gas flows, heated walls are known to be destabilizing. For example, for a constant speed flow with

$$\frac{T_{wall}}{T_{freestream}} = 1.25 ,$$

the Reynolds number at first onset of instability can be reduced by as much as a factor of 2 (eg. see White, 1974). For the present flow

$$\frac{T_{wall}}{T_{freestream}} \simeq \frac{1040^{\circ}K}{411^{\circ}K} \simeq 2.5$$

so that some effect on transition must be assumed. Unfortunately, stability calculations do not appear to have been made for accelerating flows and we can therefore only guess at the magnitude of the effect.

(c) Noise

The boundary layer undoubtedly experiences a high level of noise due to the turbulent combustion outside the tank. Noise (pressure fluctuations) will promote early transition but the effect is to some extent frequency dependent. That is, the wavelength of the pressure disturbances should be the same order of magnitude as the boundary layer thickness for strong coupling to occur. Intuition suggests that much of the acoustic energy generated by the fire will be at lower frequencies with corresponding wavelengths of metres rather than millimetres. In view of the extreme thinness of the boundary layer here, the effect of the noise on the transition location may in fact be fairly small.

(d) Freestream Turbulence

Like noise, freestream turbulence can promote early transition. Due to non-uniform boil-off and other effects it is likely that the freestream flow inside the tank will be fairly turbulent. On the other hand, if the eddy scales of the turbulence are large compared with the boundary layer length scales, the effect on transition can be considerably reduced.

Assuming the turbulence length scales are in the appropriate range, the approximate location of transition for the Falkner-Skan flows is given by (see White, 1974):

$$\frac{1690}{Re_{x,tr}^{\frac{1}{2}}} \simeq 0.312(m+0.11)^{-0.528} + 1.6\,\eta_{\delta_{0.99}}^{2} \quad Re_{x,tr}^{\frac{1}{2}} \; T'^{2},$$

where T'= turbulence intensity.

For the present flow, m = 1 and

$$\eta_{\delta_{0.99}} = 2.4, \text{ so that } \quad Re_{x,tr}^{\frac{1}{2}} = \frac{-0.2953 + \sqrt{0.08720 + 62300T'^{2}}}{18.432T'^{2}} .$$

Values of $Re_{x,tr}$ and its logarithm are tabulated as functions of T' in Table D-2.

TABLE D-2: TRANSITION REYNOLDS NUMBER ($Re_{x,tr}$) AS A FUNCTION OF THE TURBULENCE INTENSITY (T')

T'	$Re_{x_1 tr}$	$\log_{10} Re_{x_1 tr}$
0.001	2.46×10^7	7.391
0.005	4.59×10^6	6.662
0.01	1.45×10^6	6.161
0.02	4.07×10^5	5.610
0.03	1.88×10^5	5.274

The location of the transition points for various levels of turbulence are shown in Fig. D-5. As seen, transition will occur before the outlet if the turbulence intensity is greater than about 0.5% (T' = 0.005). We have no idea of the level of turbulence inside the tank, but the general observation can be made that T' = 0.03 is a very high level and it is probably lower here. This together with the likely mismatch of length means that a reasonable guess for the effective turbulence inside the tank might be 1% or lower. On this basis, the boundary layer should remain laminary for at least 2/3's of the distance to the outlet.

Fig. D-5: LEVEL TANK
VARIATION OF Re_x WITH X
(AND LOCATION OF TRANSITION FOR VARIOUS LEVELS OF TURBULENCE)

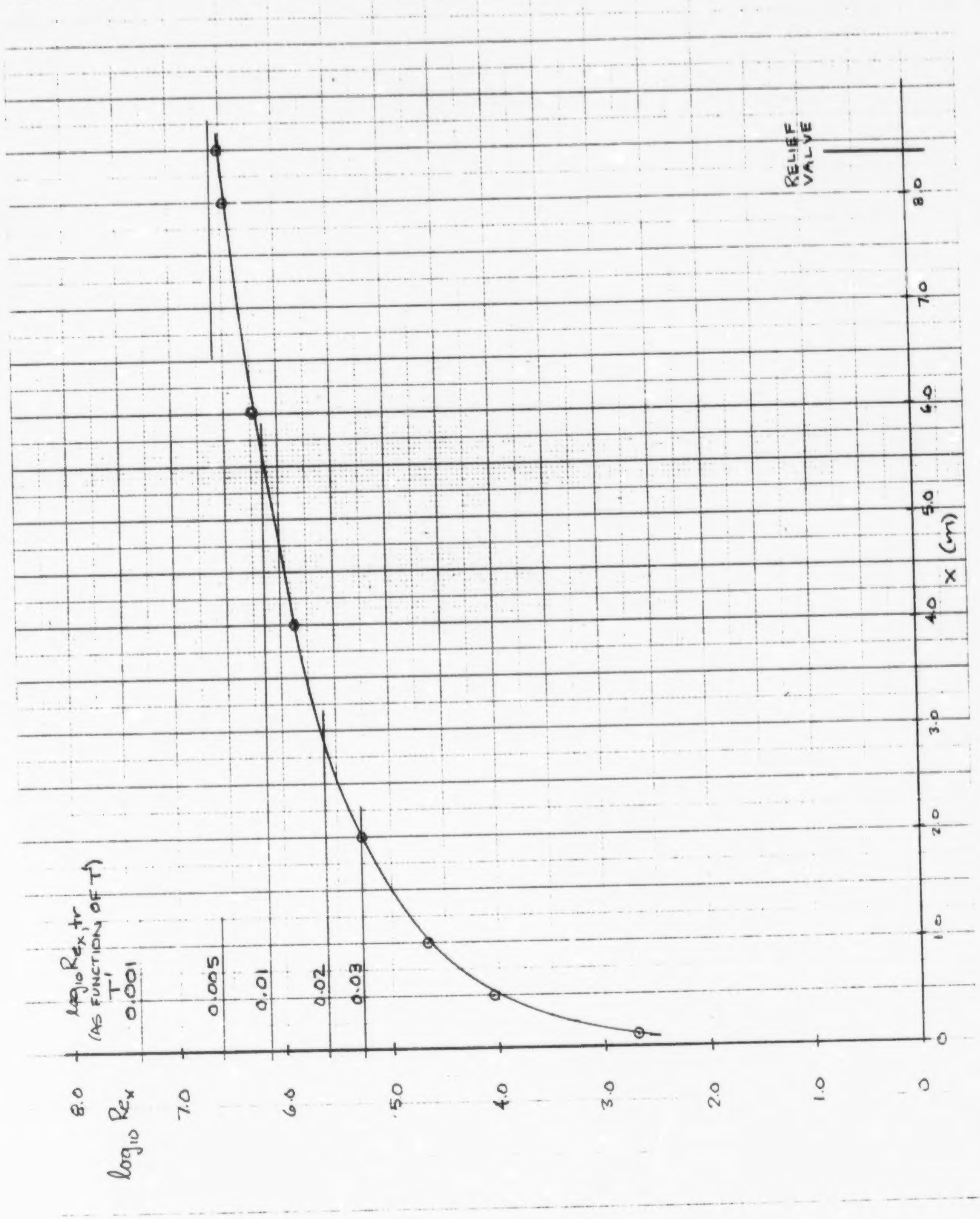

With the combined effect of the factors discussed above it seems probable that transition will occur before the flow reaches the outlet. However, based on the available information it is obviously impossible to predict its precise location.

For purposes of the present report the heat transfer coefficient will be calculated initially on the assumption that the layer remains laminar. Qualitative arguments will then be used to estimate how much it would increase if transition occured.

For future more detailed calculations it is suggested that the various factors promoting transition be lumped together as an "effective" turbulence intensity. The transition point can then be calculated from the formula quoted earlier. Downstream of the transition point the heat transfer coefficient will then be predicted from a turbulent boundary layer calculation. See section D-2.6 for more detailed recommendations.

D-2.3 Convective Heat Transfer Coefficient

For a constant wall temperature, the convective heat transfer coefficient for the Falkner-skan flows is given by

$$St(x) = \frac{G(P_r,\beta)}{P_r\sqrt{\frac{2Re_x}{1+m}}}$$

where $St = \frac{h_i}{\rho_v U C_\rho}$ (Stanton number)

$h_i = \frac{\dot{q}}{A(T_w - T_\infty)}$ (Convective heat transfer coefficient)

$$Pr = \frac{C_p \mu}{k} \qquad \text{(Prandtl number)}$$

and $G(Pr,\beta)$ follows from the solution of the equations (see White, 1974, Table 4-5)

$$\text{for } \beta = m = 1, \quad Pr = 0.81$$

$$G(Pr,\beta) = 0.524$$

(values of $G(Pr,1) = G(Pr)$ are tabulated in Table 2-3)

At the assumed film conditions,

$$C_p = 3.187\times10^{3}\ \text{J/kg}^{\circ}\text{K} \qquad \rho_v = 14.97\text{kg/m}^3$$

$$= 1.73\times10^{-5}\ \text{N-s/m}^2 \qquad \nu = 11.56\times10^{-7}\text{m}^2\text{/s}$$

$$k = 6.8\times10^{-2}\text{W/m}^{\circ}\text{K}$$

$$\text{so, } St\ (x) = \frac{0.524}{0.81\sqrt{\frac{2\ Re_x}{2}}} = \frac{0.647}{\sqrt{Re_x}}$$

$$\text{and, } h_i = St\ (x)\rho_v U C_p$$

$$= 0.647\rho_v C_p \frac{Kx}{\sqrt{\frac{Kx.x}{\nu}}}$$

$$= 0.647\rho_v C_p \sqrt{K\nu}$$

The last equation indicates that h_i is not a function of x, which is consistent with the fact that the boundary layer has constant thickness and therefore constant wall shear stress. For the vapor properties given previously we obtain,

$$h_i = 7.71\ \text{W/m}^{2\circ}\text{C}$$

At transition, both the wall shear stress and the heat transfer coefficient will increase. Figure D-6 (taken from Blair,

1982) shows the St distributions for two accelerated flows

$$\left(K = \frac{\nu}{U^2}\ \frac{dU}{dx}\right)$$

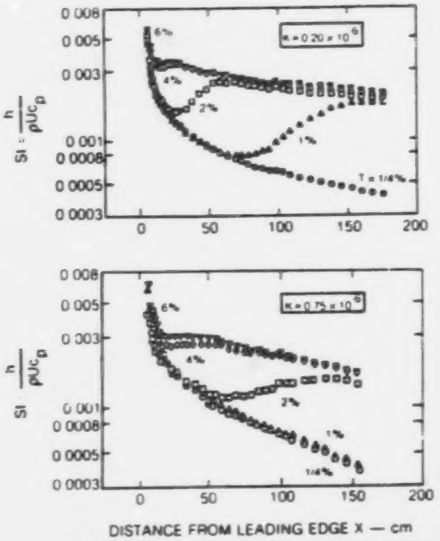

Heat-transfer distributions for accelerating flows

Fig. D-6: STANTON NUMBER DISTRIBUTIONS FOR ACCELERATED FLOWS

As seen in Fig. D-6, the rise in St varies with x (that is, with $Re_{x,tr}$) but lies roughly in the range.

$$St_{turbulent}/St_{laminar} \cong 2\text{-}4$$

so for the flow in the tank it is therefore reasonable to expect

$$h_i \simeq 20 W/m^{2\,o}K \quad \text{after transition}$$

D-2.4 Flow Behaviour in Model Tank

It can be shown that the vapor velocity at the center of a

1/5 scale tank will be the same as that given previously for the full-scale tank (ie. 0.452m/sec) when the tank pressure, the incident heat flux and the % liquid by volume are the same.

thus $$K = \frac{\Delta U}{\Delta x} = \frac{0.452}{8.38 x 1/5} = 0.270 \ s^{-1}$$

so $$\sqrt{\frac{K}{\nu}} = \sqrt{\frac{0.270}{11.56 x 10^{-7}}} = 483.0$$

and, $$\delta_{0.99} = \frac{2.4}{483.0} = 0.00497m \quad (= 5mm)$$

$$\delta^* = 0.00134m$$
$$\theta = 0.00061m$$

Relative to the tank diameter the boundary layer is therefore thicker in the model tank by a factor $\sqrt{5}$

At the outlet,

$$Re_x = \frac{Ux}{\nu} = \frac{0.452 x 1.676}{11.56 x 10^{-7}} = 6.55 x 10^5$$

$$Re_x = \frac{U\theta}{\nu} = 238.5$$

so the outlet Reynolds numbers are lower for the 1/5 scale tank than for the full-scale tank. The lower Reynolds numbers mean that transition is less likely in the model tank.

For the heat transfer coefficient,

$$h_i = 0.647 \rho_v C_p \sqrt{K\nu}$$

so, $$h_i = 7.7 x \sqrt{5}$$
$$= 17.2 \ W/m^2 {}^oK$$

D-2.5 Explosafe-Lined Tank

Having the tank lined with Explosafe mesh complicates the analysis considerably. In fact, no attempt has been made to calculate the boundary layer development because several essential pieces of information are not known at this stage. Only a brief qualitative discussion will be given here.

Since the boundary layer will be seeing essentially a very rough wall with EXPLOSAFE in the tank, an estimate will have to be made of the effective roughness height for the mesh. This could be done by making windtunnel measurements of the development of the boundary layer over an EXPLOSAFE mesh. The rough wall will result in early transition. In fact, it seems likely the boundary layer will be turbulent for most of its length in both the full-scale and model tanks. This, together with the enhanced mixing due to the roughness should result in considerably higher convective heat transfer coefficients than for the smooth tanks.

D-2.6 Summary and Recommendations

The following values of convective heat transfer coefficient are estimated for the unlined tanks under the assumed conditions.

(i) Full scale

$$h_i \cong 7.7 \ \frac{W}{m^2 {}^\circ K} \qquad \text{(laminar flow)}$$

$$h_i \cong 20 \ \frac{W}{m^2 {}^\circ K} \qquad \text{(turbulent flow)}$$

- where transition to turbulence probably occurs at about 5.5m from the end cap (ie. about 2/3's of the distance along the flow)

(ii) 1/5- scale

$$h_i \cong 17.2 \ \frac{W}{m^2 {}^oK} \qquad \text{(laminar flow)}$$

- and transition is not expected for this case

The need to improve on the present analysis will have to be determined in the contex of the complete problem. If it is found that the convective heat transfer on the inner surface is a minor factor, then the approximate method used here may be sufficient. However, if it is concluded that more detailed predictions are needed, the following procedures are recommended:

(i) For the laminar portion of the flow, no improvements should be necessary. The exception to this would be if it is found that the wall temperature varies substantially along the length of the flow. The Falkner-Skan similarity solutions do not apply for arbitrarily varying temperature distributions. For this situation, the approximate method of Spalding (see Curle, 1962) is recommended.

(ii) The location of the transition point can be predicted as outlined in section 2.2. As a starting value, an effective turbulence intensity of 1% is suggested.

(iii) For the turbulent boundary layer, it will be necessary to solve the momentum and heat transfer problems separately.

For calculating the velocity boundary layer development, the entrainment method of Head & Patel (1969) is recommended. This has been shown to be one of the most reliable of the integral methods and it is one of the simplest to apply. A description of the method and a Fortran program can also be found in Cebeci & Bradshaw (1977).

With the skin friction distribution, $C_f(x)$, known from the boundary layer solution, the heat transfer coefficient can be calculated from a turbulent form of the Reynolds analogy. The following expression gives reasonable results for gas flows:

$$St = \frac{\sqrt{\frac{C_f}{2}}}{\left[5Pr \pm 5\ln(5Pr + 1) \pm \frac{1}{\sqrt{\frac{C_f}{2}}} - 14\right]}$$

For further details, see Kays (1966).

The above discussion applies to the unlined tank. The entrainment method has not been applied to rough wall flows although it could perhaps be adapted. For initial estimates, the following approach is suggested.

The skin friction distribution is first calculated for the smooth-walled flow using the entrainment method. It is then assumed that the C_f is increased due to the roughness by the same amount as in the flat plate boundary layer with the same Reynolds number. Flat-plate data is readily available in the literature: see for example Schlichting (1979). Figure D-7 (taken from Cebeci & Bradshaw, 1979) summarizes the effect:

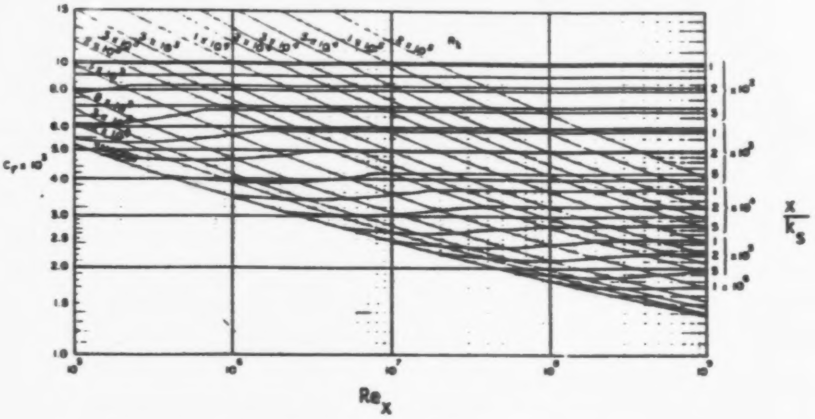

Local skin-friction coefficient on sand-roughened flat plate.

$R_k = \frac{kU}{\nu}$

k = roughness height

Fig. D-7: LOCAL SKIN-FRICTION COEFFICIENT ON SAND-ROUGHENED FLAT PLATE

Having determined the increase in C_f, the Stanton number, and then convective heat transfer coefficient can be calculated from the formula quoted above.

D-3.0 TILTED TANK

With the tank tilted, the flow area decreases toward the outlet, resulting in greater flow acceleration than for the level tank. This will increase the heat transfer coefficient. The liquid surface in a tilted tank might appear as shown in Fig. D-8.

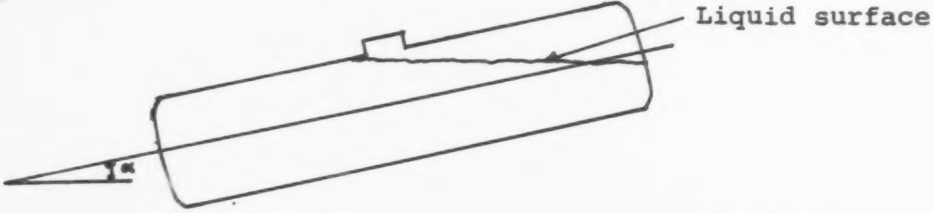

Fig. D-8: TILTED TANK

The end cap becomes uncovered for,

$$\alpha = \arctan\left(\frac{3.02}{8.38}\right) \simeq 19.8^{\circ}$$

As an example, an unlined tank tilted at 15° will be considered.

D-3.1 Freestream Flow

In the tilted tank case, vapour is evolved at the tilted free surface due to heating of the entire tank so the total mass flow of vapour is

$$\begin{aligned} \dot{m} &= 2(31.09) \\ &= 62.18\text{kg/sec} \end{aligned}$$

and the free surface area (A_{surf}) can be derived in the manner shown in Fig. D-9.

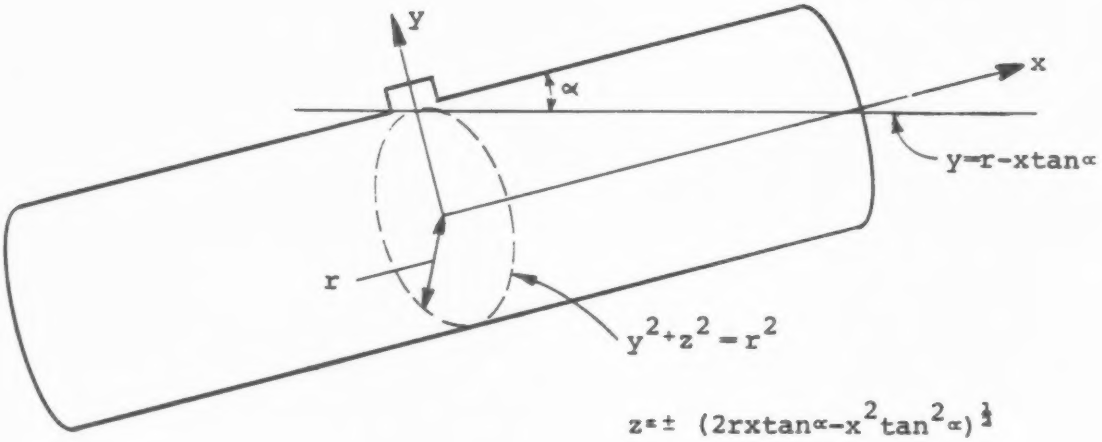
y
x
α
y=r-xtanα
r
$y^2+z^2=r^2$

$$z = \pm\ (2rx\tan\alpha - x^2\tan^2\alpha)^{\frac{1}{2}}$$

$$dw = \frac{dx}{\cos\alpha}$$

$$dA = 2\ z\,dw = 2z\frac{dx}{\cos\alpha}$$

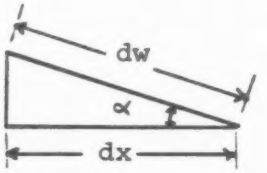

$$\therefore\ A_{surf.} = \int_0^{x_0} \frac{2}{\cos\alpha}(2r\tan\alpha x - \tan^2\alpha x^2)^{\frac{1}{2}}\ dx$$

Fig. D-9: Free surface area calculations

For $\alpha=15^{\circ}$, $r(=R_{it}) = 1.51m$, $x_o = 8.38m$ (neglecting curvature of the end cap)

$$A_{surf} = 22.05m^2$$

and assuming vapour evolution occurs uniformly over the free surface,

$$\frac{\dot{m}}{A} = \frac{62.18}{22.05} = 0.820kg/m^2$$

The velocity distribution along the wall of the tank can now be calculated as described below for the ullage geometry shown in Fig. D-10.

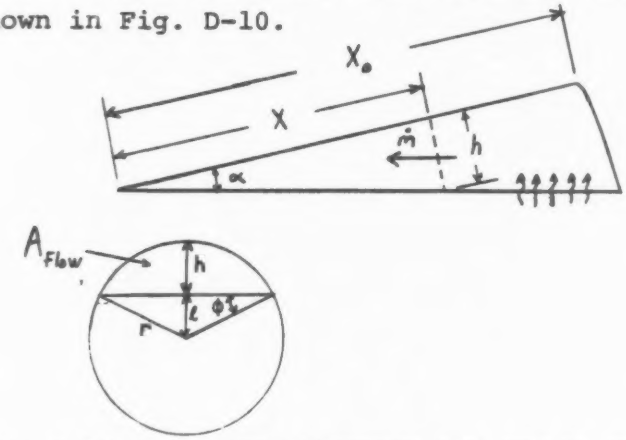

Fig. D-10: ULLAGE GEOMETRY AND VAPOR FLOW AREA (A_{flow})

For the flow area geometry shown in Fig. D-10

$$h = x \tan\alpha$$

$$= \arcsin\left(\frac{r - x\tan\alpha}{r}\right)$$

$$w = r - h/\tan\phi$$

$$A_{flow} = \pi r^2 - \pi r^2\left(\frac{180+2\phi}{360}\right) - \tfrac{1}{2}(2w)\,\ell$$

$$= \pi r^2\left(\tfrac{1}{2} - \frac{\phi}{180}\right) - w\ell$$

and through this surface

$$\dot{m} = \left(\frac{\dot{m}}{A}\right) A_{surface} \Big|_{x}^{x_o}$$

$$= \left(\frac{\dot{m}}{A}\right) \int_{x}^{x_o} \frac{2}{\cos\alpha} \left(2r\tan\alpha x - \tan^2\alpha x^2\right)^{\frac{1}{2}} dx$$

then $U_{flow} = \frac{\dot{m}}{\rho A_{flow}}$

where $\rho = 48.11 kg/m^3$ as before.

Results of the surface area, flow area and freestream velocity calculations for the conditions in the sample analysis are tabulated in Table D-2.

TABLE D-2: RESULTS OF THE VELOCITY, SURFACE AND FLOW AREA CALCULATIONS FOR THE SAMPLE PROBLEM

x (m)	$x_{bl} = 8.38 - x$ (m)	$\log_{10} x_{bl}$	$A_{surface}$ (m^2)	A_{flow} (m^2)	U_{flow} (m/sec)	$\log_{10} U_{flow}$
8.0	0.38	-0.420	1.057	5.434	0.0114	-1.943
7.0	1.38	0.1399	3.999	4.672	0.0502	-1.300
6.0	2.38	0.3766	7.081	3.874	0.1071	-0.970
5.0	3.38	0.5289	10.200	3.067	0.1949	-0.710
4.0	4.38	0.6415	13.256	2.276	0.3414	-0.467
3.0	5.38	0.7308	16.143	1.529	0.6189	-0.208
2.0	6.38	0.8048	18.732	0.859	1.2787	0.107
1.5	6.88	0.8376	19.862	0.566	2.0568	0.313
1.0	7.38	0.8681	20.842	0.313	3.9084	0.592
0.5	7.88	0.8965	21.616	0.112	11.306	1.053

The velocity distribution given in Table D-2 will be checked to see how well it approximates one of the Falkner-Skan flows. Since

$$U = Kx^m,$$

$$\log_{10}U = \log_{10}K + m \log_{10}x$$

then $$m = \frac{\Delta(\log_{10}U)}{\Delta(\log_{10}x)}$$

so, as shown in Fig. D-11

$m \cong 1.3$ $\beta \cong 1.13$ near start of flow

$m \cong 8.0$ $\beta \cong 1.78$ near outlet

While these results show that the Falkner-Skan solutions cannot be applied directly, they can be used to obtain an approximate solution using a procedure developed by Eckert (see Kays (1966) for details).

D-3.2 Convective Heat Transfer Coefficient For A Tilted Tank

Following the method of Eckert (see Kays, 1966), it is assumed that the various thermal boundary layer thicknesses are a function of local parameters only

-thus for $\Delta_4 = \frac{k}{h}$

$$\frac{d\Delta_4}{dx} = f\left(\Delta_4, U, \frac{dU}{dx}, \nu, Pr\right)$$

Fig. D-11

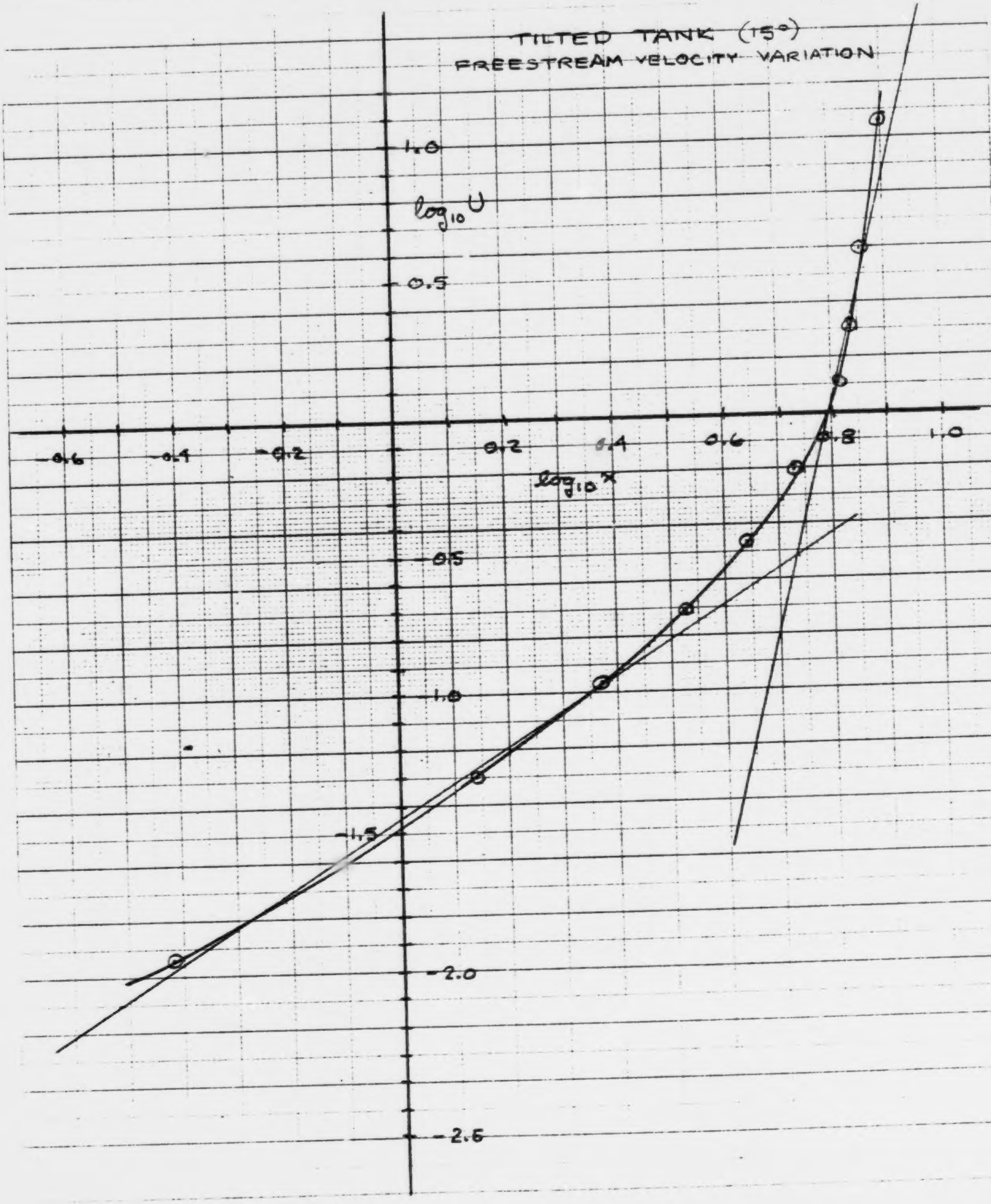
TILTED TANK (15°)
FREESTREAM VELOCITY VARIATION
log10 U
log10 x
1.0
0.5
-0.5
-1.0
-1.5
-2.0
-2.5
-0.6
-0.4
-0.2
0.2
0.4
0.6
0.8
1.0

or, from dimension analysis $\frac{U}{\nu}\frac{d\Delta_4^2}{dx} = f\left(\frac{\Delta_4^2}{\nu}\frac{dU}{dx}, Pr\right)$

It is then assumed that f for an arbitrary variation of free-stream velocity is the same as for the Falkner-Skan flows, where it can be shown for those flows that:

$$\frac{U}{\nu}\frac{d\Delta_4^2}{dx} = \frac{1-m}{C_1^2}$$

$$\frac{\Delta_4^2}{\nu}\frac{dU}{dx} = \frac{m}{C_1^2}$$

where $C_1 = Nu_x \, Re_x^{-\frac{1}{2}}$

and $Nu_x = \frac{hx}{k}$ (Nusselt number)

For a given Pr and m, a plot of f can be prepared and the resulting function integrated numerically to obtain the thermal boundary layer development for any specified velocity distribution. Alternatively, if a linear approximation is made, the function can be integrated analytically

That is if $\frac{U}{\nu}\frac{d\Delta_4^2}{d_x} = A - B \frac{\Delta_4^4}{\nu}\frac{dU}{dx}$

then $\Delta_4^2 = \frac{A\nu \int_0^x U^{B-1}\, dx}{U^B}$

The latter approach will be used here. The value of C_1 for $Pr = 0.81$ can be obtained from the values given in Table D-3 (taken from Kays, 1966) by interpolation.

TABLE D-3: TABLE 10-2 FROM KAYS, 1966

m	$C_1 = Nu_x Re_x^{-\frac{1}{2}}$			$\frac{U}{\nu}\frac{d\Delta_4{}^2}{dx}$	$\frac{\Delta_4{}^2}{\nu}\frac{dU}{dx}$
	Pr				
	0.8	1.0	0.81	$(=\frac{1-m}{C_1{}^2})$	$(=\frac{m}{C_1{}^2})$
-0.0753	0.253	0.272	0.254	16.67	-1.167
0	0.307	0.332	0.309	10.47	0
0.111	0.348	0.378	0.350	7.257	0.9061
0.333	0.403	0.440	0.405	4.066	2.030
1.0	0.523	0.570	0.526	0	3.614
4.0	0.858	0.938	0.863	-4.028	5.371

The values of $\frac{U}{\nu}\frac{d\Delta_4{}^2}{dx}$ and $\frac{\Delta_4{}^2}{\nu}\frac{dU}{dx}$ given in Table D-3 are plotted against each other in Fig. D-12 for $m \geq 0.111$. Fitting a straight line to the relationship for large m gives.

$$\frac{U}{\nu}\frac{d\Delta_4{}^2}{dx} \cong 8.15 - 2.27\frac{\Delta_4{}^2}{\nu}\frac{dU}{dx}$$

$$\text{so } \Delta_4{}^2 = \left(\frac{k}{h}\right)^2 = \frac{8.15\nu\int_0^x U^{1.27}dx}{U^{2.27}}$$

$$\text{or} \qquad h_i = \left[\frac{k^2U^{2.27}}{8.15\nu\int_0^x U^{1.27}dx}\right]^{\frac{1}{2}}$$

and at the assumed film conditions

$$k = 6.8\text{x}10^{-2}\text{J/ms}^{\text{o}}\text{K} \quad , \quad \nu = 11.56\text{x}10^{-7}\text{m}^2\text{/s}$$

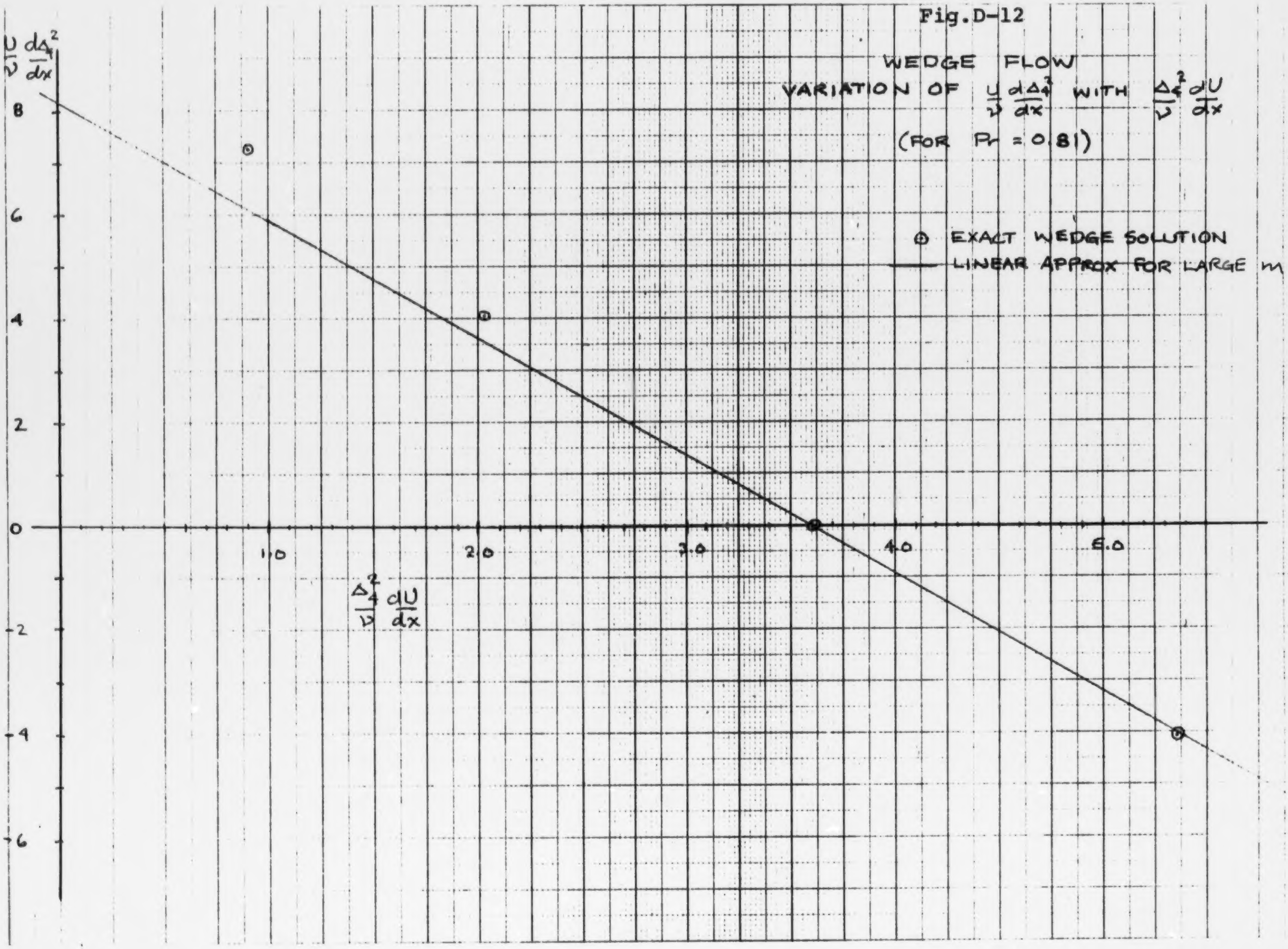

Fig.D-12

WEDGE FLOW

VARIATION OF $\frac{U}{\nu}\frac{d\Delta_4^2}{dx}$ WITH $\frac{\Delta_4^2}{\nu}\frac{dU}{dx}$

(FOR $Pr = 0.81$)

$$h_i = \left[\frac{490.8\ U^{2.27}}{\int_0^x U^{1.27}dx}\right]^{\frac{1}{2}}$$

The integral in the denominator of the expression defining h_i can be evaluated numerically. Simpson's rule was used to obtain the results given in Table D-3 for the sample problem.

TABLE D-3: HEAT TRANSFER COEFFICIENTS FOR THE SAMPLE PROBLEM

x (m)	U (m/sec)	$U^{1.27}$	$\int_0^x U^{1.27}dx$	h_i $(W/m^2\,{}^oK$
0.0	0.0	0.0		
0.38	0.0114	0.00341	0.000648	5.42
1.38	0.0502	0.02238		
2.38	0.1071	0.05859	0.051154	7.76
3.38	0.1949	0.12533		
4.38	0.3414	0.25541	0.32293	11.5
5.38	0.6189	0.54370		
6.38	1.2787	1.36646	1.58848	23.2
6.88	2.0568	2.49893	2.55483	31.4
7.38	3.9084	5.64727	4.42339	49.5
7.88	11.306	21.76218	10.36320	107.9

The results shown in Table D-3, which are also plotted in Fig. D-13, appear reasonable since at low values of x, values of m are comparable with those in the level tank and the heat transfer coefficients are similar, as they should be. As expected, the strong acceleration towards the outlet results in a substantial increase in heat transfer coefficient.

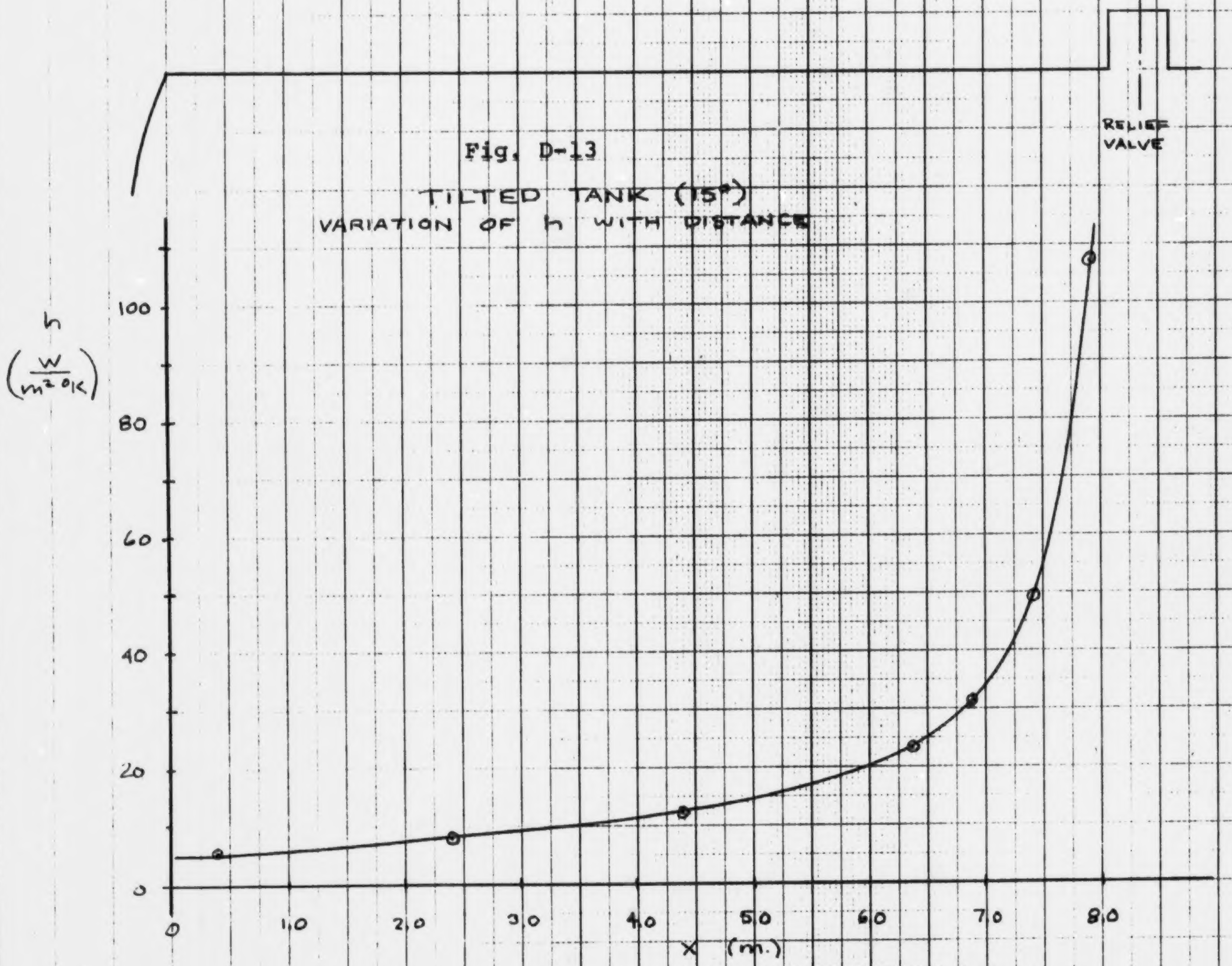

Fig. D-13

TILTED TANK (15°)
VARIATION OF h WITH DISTANCE

D-3.3 Possibility Of Transition

Strong acceleration has the effect of stabilizing laminar boundary layers. For example, the formula quoted earlier shows that increasing m from 1.0 to 4.0 increases the transition Reynolds number by a factor of about 5 to 6. It is therefore likely that layers will remain laminar in tilted tanks, providing they are unlined. If the tank is lined with Explosafe mesh, the roughness will again trigger transition near the start of the flow.

D-3.4 Summary and Recommendations

For the case considered (15^{o} of tilt, unlined tank) the convective heat transfer coefficient was found to be

$h_i \cong 5$ $W/m^{2\,o}K$ near the end cap

$h_i \cong 100$ $W/m^{2\,o}K$ near the outlet

For the unlined tank, the boundary layer is expected to remain laminar. In general, the approximate procedure based on the Falkner-Skan solutions, as used here, is thought to give reasonable accuracy and could be used for future predictions.

For tanks lined with Explosafe mesh, the location of transition and the development of the turbulent boundary layer should be predicted using the methods discussed in sections D-2.2 and D-2.6.

D-4.0 REFERENCES

1. Schlichting, H — *Boundary-Layer Theory*, 7th ed.
McGraw-Hill, New York, 1979.

2. White, F.M. — *Viscous Fluid Flow*
McGraw-Hill, New York, 1974.

3. Curle, N. — *The Laminar Boundary Layer Equations*
Clarendon Press, Oxford, 1962.

4. Head, M.R.
Patel, V.C. — Improved Entrainment Method for Calculating Turbulent Boundary Layer Development.
ARC R&M 3643, 1969.

5. Cebeci, T.
Bradshaw, P. — *Momentum Transfer in Boundary* Layers.
Hemisphere, Washington, 1977.

6. Kays, W.M. — *Convective Heat and Mass Transfer*
McGraw-Hill, New York, 1966.

7. Blair, M.F. — Influence of Free-Stream Turbulence on Boundary Layer Transition in Favorable Pressure Gradients.
ASME Paper 82-GT-4, April 1982.
(to be published ASME J. Eng. for Power).

D-5 PROPERTIES OF PROPANE

- assumed film conditions

$T = 356 + 55 + 273$ (356°C superheat)

$= 684^{o}K$

$P = 280psia$

$= 19.305x10^{5}N/m^{2}$

(i) Density, ρ

- assume the superheated vapour behaves as a perfect gas

$M = 44.094gm/mole$ $R_u = 1.986 \frac{cal}{gm\ mole^{o}K}$

$$\therefore\ R = \frac{1.986x4.186}{44.093x10^{-3}} = 188.5J/kg^{o}K$$

$$\text{then}\ \rho = \frac{P}{RT} = \frac{19.305x10^{5}}{188.5x684} = 14.97kg/m^{3}$$

(ii) Viscosity, μ

- tabulated values are available only up to $523.15^{o}K$ and have to be extrapolated from tabulated data for 20 bars

T (^{o}K)	μ poise	 Ns/m^2
373.95	$10.70x10^{-5}$	$1.070x10^{-5}$
424.15	$11.75x10^{-5}$	$1.175x10^{-5}$
474.15	$12.85x10^{-5}$	$1.285x10^{-5}$
523.15	$13.90x10^{-5}$	$1.390x10^{-5}$

- using a linear extrapolation (see Figure D-14)

$$\text{at } T = 684^{\circ}K \qquad \mu = 1.73\text{x}10^{-5} Ns/m^2$$

- and kinematic viscosity, ν

$$\nu = \frac{\mu}{\rho} = \frac{1.73\text{x}10^{-5}}{14.97}$$

$$= 11.56\text{x}10^{-7} m^3/s$$

(iii) Thermal Conductivity, k

- again tabulated data will have to be extrapolated

T ($^{\circ}K$)	k	
	cal/cms$^{\circ}$K	J/ms$^{\circ}$K
333.15	$6.07\text{x}10^{-5}$	$2.54\text{x}10^{-2}$
353.15	$6.57\text{x}10^{-5}$	$2.75\text{x}10^{-2}$
373.15	$7.15\text{x}10^{-5}$	$2.99\text{x}10^{-2}$
393.15	$7.70\text{x}10^{-5}$	$3.22\text{x}10^{-2}$
413.15	$8.34\text{x}10^{-5}$	$3.49\text{x}10^{-2}$

(data for p=20 bars)

- using linear extrapolation (see Figure D-15)

$$\text{at } T = 684^{\circ}K \qquad k = 6.8\text{x}10^{-2} J/ms^{\circ}K$$

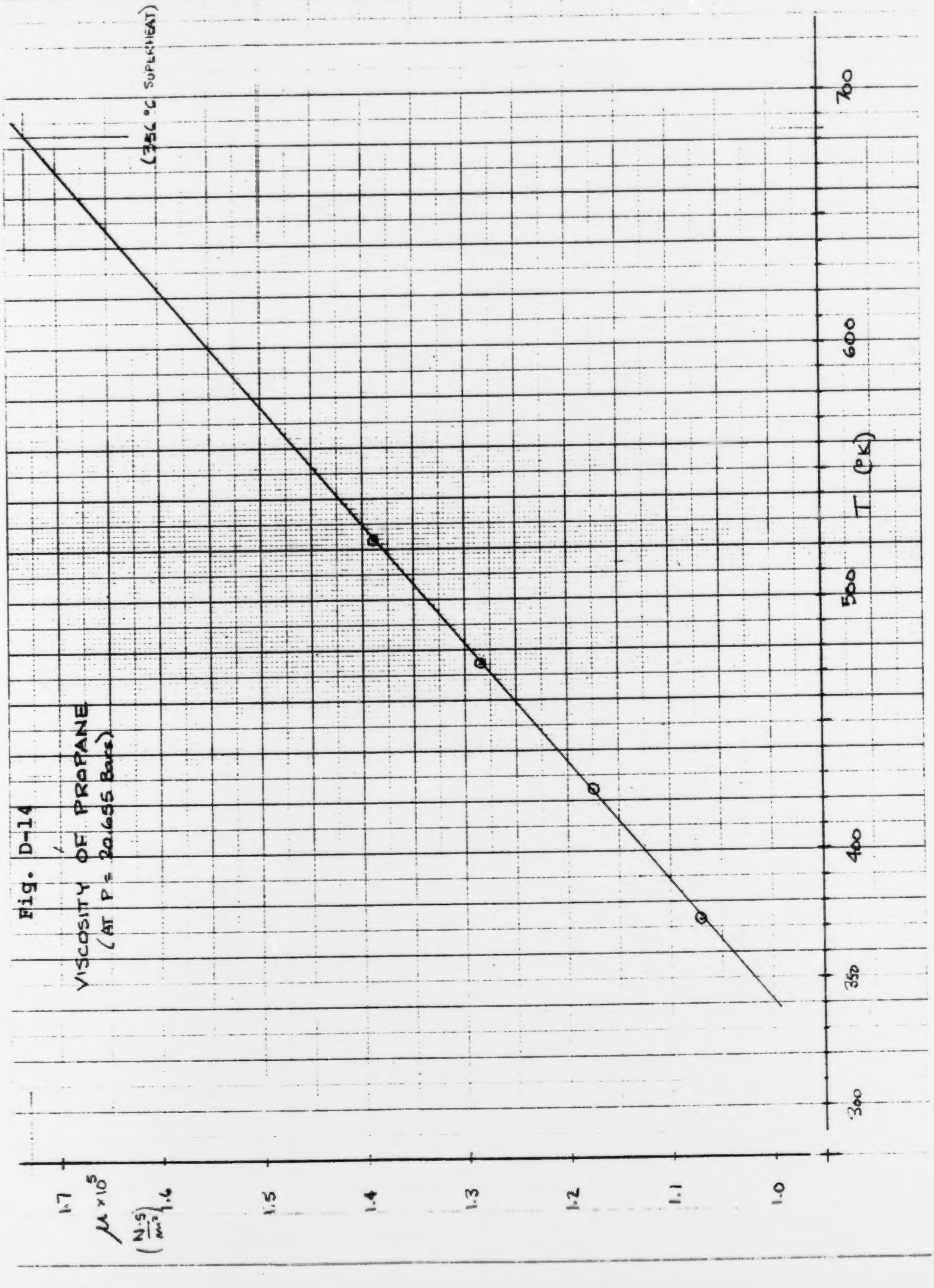

Fig. D-14

VISCOSITY OF PROPANE
(AT P = 20.655 Bars)

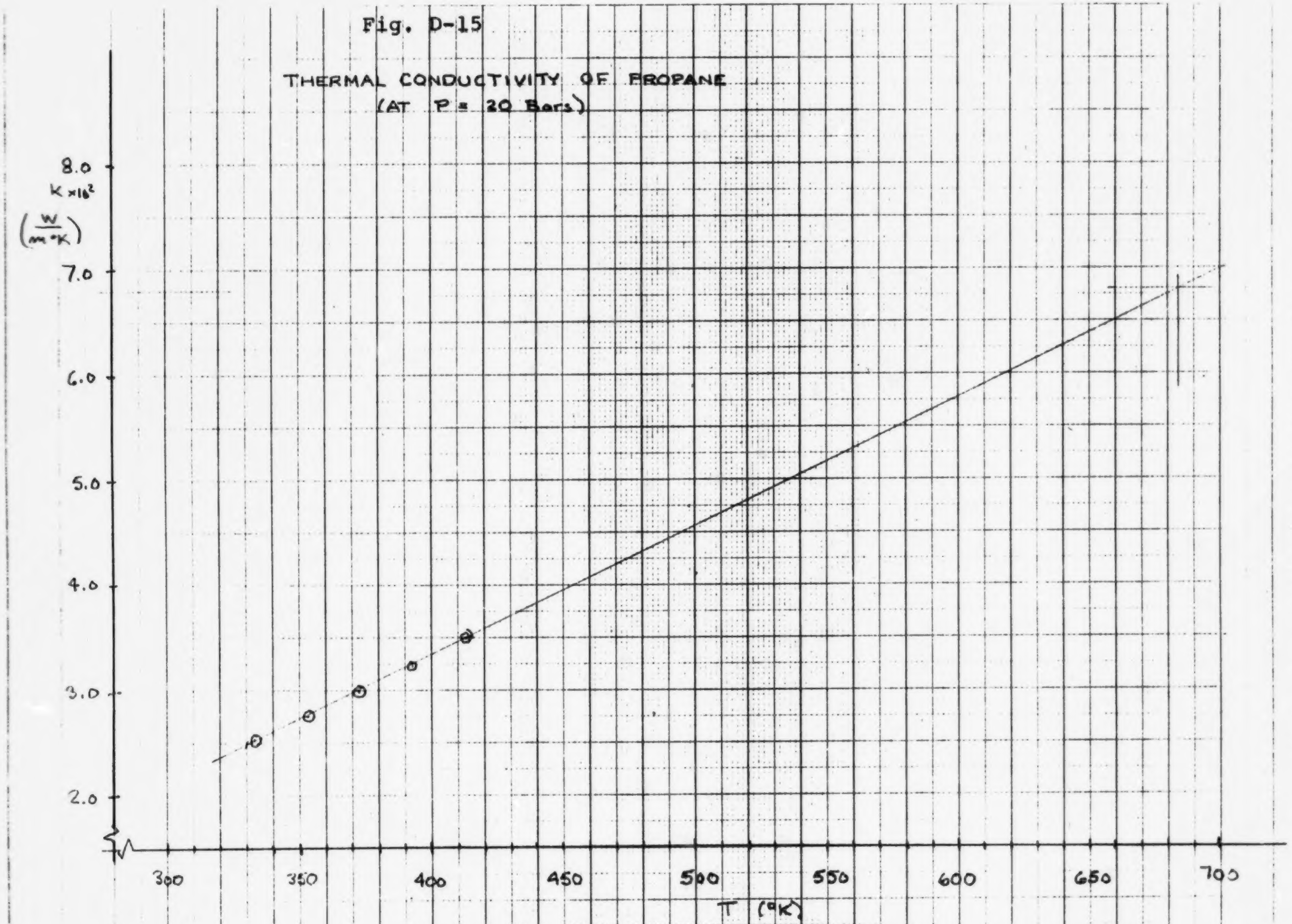

Fig. D-15

THERMAL CONDUCTIVITY OF PROPANE
(AT P = 20 Bars)

(iv) Specific Heat, C_p

- in this case, tabulated values cover the required temperature range

T ($^\circ$K)	C_p	
	$\frac{\text{cal}}{\text{mole}}\ ^\circ\text{K}$	$\frac{\text{J}}{\text{kg}^\circ\text{K}}$
600	30.76	2.923×10^3
700	34.10	3.241×10^3

conversion factors
4.186J/cal
44.049×10^{-3}kg/mole

- using linear interpolation

at $T = 684^\circ K$ $C_p = 3.190\times10^3$ J/kg$^\circ$K

(v) Prandtl Number, Pr

$$Pr = \frac{C_p \mu}{k}$$

- then at $T = 684^\circ K$

$$Pr = \frac{3.190\times10^3 \times 1.73\times10^{-5}}{6.8\times10^{-2}} = 0.812$$

- which looks reasonable (and suggests that the extrapolated values of μ and k are also fairly reasonable).

APPENDIX E: SAMPLE TANK CAR THERMAL ANALYSIS PROGRAM

E.1 INTRODUCTION

A simple FORTRAN IV computer program for predicting the wall temperature distribution in a tank car in a fire as a function of time is given in this appendix. Only vapor-covered parts of the tank wall are modelled and the liquid level is held constant throughout the transient. The program is set up so that the Newton-Raphson method can be used in either its normal or modified form to solve the non-linear finite-difference equations at each time step. The time derivative in the heat-conduction equation is backward-differenced in the program (ie. the implicit time integration procedure is used) and axial conduction in the tank wall is modelled. It is assumed that the plane A-A shown in Fig. 2-3 and the $r-\theta$ plane at the tank's axial midpoint are planes of thermal symmetry. The program currently uses one node across the thickness of the tank wall but it could easily be modified to permit the use of more nodes across the wall thickness.

The entire program consists of ten routines specifically the main program TANKS and the subroutines QFORM, DTHW, DZR, VIEWFA, TINITL, ZERO, CONMAG, CHLSKI and SUB. Finite-difference equations for nodes in the cylindrical shell and the endcaps are assembled in the main program TANKS which also controls the iterative procedure needed to solve the non-linear equations, selects time steps, controls the time marching process, and prints results. Subroutine QFORM updates the right-hand side vector for the system of finite-difference equations at any iteration or time step performed without recalculating the Jacobian matrix (ie. subroutine QFORM updates the right-hand side vector at each iteration or time step when the modified

Newton-Raphson method is used). The axial and circumferential mesh structures are defined in subroutines DTHW and DZR respectively and the view factor for each node in the tank wall viewing the liquid surface is calculated in VIEWFA. Nodal temperatures are initialized to the proper, user-specified, value at the start of the analysis (ie. at $t=0$) in subroutine TINITL and the Jacobian matrix and right-hand side vector are zeroed in subroutine ZERO whenever the Jacobian is recalculated. Subroutine CONMAG takes the finite-difference coefficients calculated in the main program (TANKS) for the cylindrical shell and endcap nodes and inserts them into the proper locations in the Jacobian matrix. Subroutine CHLSKI uses Cholesky's algorithm to factor the symmetric Jacobian matrix into the product of a lower triangular matrix and its transpose and subroutine SUB performs the forward and back substitutions needed to obtain the nodal temperatures from the previously factored Jacobian matrix and the right-hand side vector. All of the routines in the program are described in greater detail in Section E-2.

Input data not related to the definition of the circumferential and axial mesh structures are read by the main program, TANKS, and descriptions of all of the variables included in that category are given at the beginning of TANKS. Data describing the circumferential and axial mesh structures are subsequently read by subroutines DTHW and DZR respectively, in that order.

The results of sample analyses performed using the computer program described in this appendix are given in Sect. E-3. Solutions obtained using the normal and modified versions of the Newton-Raphson method are compared in that section and the results of an analysis performed to determine the size of the region affected by high convective heat transfer rates around a venting relief valve are also given.

E.2 DESCRIPTION OF ROUTINES

E.2.1 Main Program - TANKS

The main routine, TANKS, which is included as listing 1, reads most of the input data required by the tank car analysis program and calculates all of the coefficients in the Jacobian matrix (CX) and all of the terms in the right-hand side vector (D) whenever the Jacobian matrix is changed. It also controls the iterative procedure needed to solve the finite-difference equations at each time step by checking the results after every iteration (past the first) to see if the solution has converged. The main program, TANKS, controls the time-marching process and determines which user-specified time step size (DT) is to be used at any given time step number (NTS) (NTS = 1,2...; for the first, second, ..., etc. time steps). TANKS also controls the printing of results.

With reference to the listing of TANKS (Listing 1), line (TANK) 61 reads the first sixteen variables described at the top of the program (ie. the variables EPSI to HXOUT inclusive). Most of the variables require no explanation (other than the explanations already given in TANKS) but the significance of FEL, EPSLN, REXCO and MAXIT may not be clear. The variable FEL, which is the view factor for the end cap viewing the liquid surface (assumed the same at all of the nodes on the endcap) can be estimated from Fig. E.1 if the endcap is approximated by a rectangle. The rectangles A_1 and A_2 in Fig. E.1 represent the endcap and the liquid surface respectively. If it is assumed, for simplicity, that the dimension L_1 (see Fig. E.1) is the vertical distance from the liquid surface to the top of the endcap (ie. to the cylindrical shell), then $L_1/W = 0.5$ for a tank car half full of liquid.

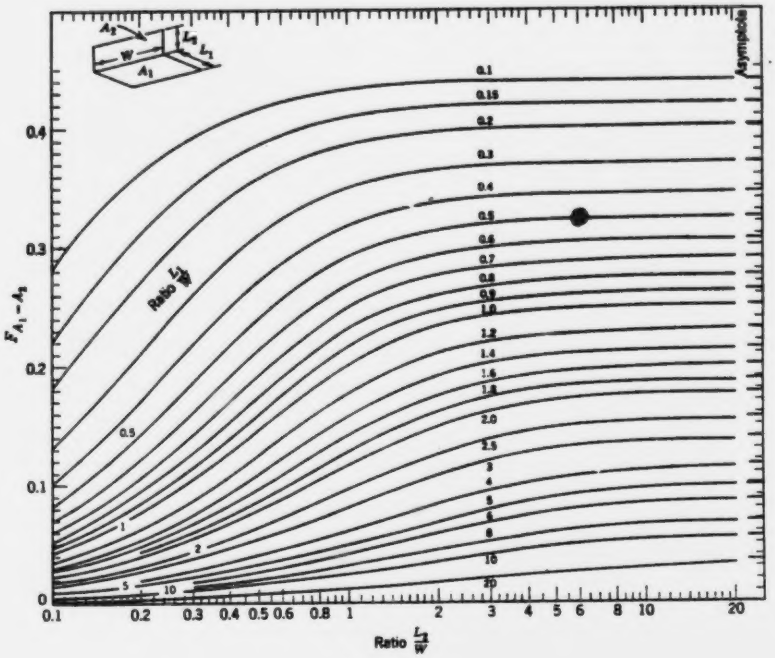

Fig. E-1: View factor for rectangle A_1 viewing rectangle A_2.

Also, $L_2/W = 18.4\ \mathrm{m}/3\ \mathrm{m} \approx 6$ for a DOT 112A tank car so $F_{A1-A2} = \mathrm{FEL} \approx 0.32$ from Fig. E.1 in that case. This value was assigned to FEL in the sample analyses described in Sect. E-3.

The variables EPSLN and MAXIT are needed in the convergence tests since it is assumed that the iterative procedure used to determine the nodal temperatures at each time step has converged when all of the nodal temperatures change by an amount less than EPSLN from one iteration to the next. If the number of iterations performed at any time step exceeds MAXIT, it is assumed that the solution is not converging and program exectuion is halted.

The variable REXCO, which is used in the flame-to-tank radiative heat transfer calculations, is defined by the expression,

$$\mathrm{REXCO} = \frac{\sigma}{1/\varepsilon_f + 1/\varepsilon_s - 1}$$

where σ is the Stefan-Boltzmann constant ($5.669 \times 10^{-8}\ \mathrm{W/m^2K^4}$), ε_f is the flameemissivity and ε_s is the emissivity of the tank's outer surface.

Time step sizes (DT (NDT)) and the time step numbers between which the different time step sizes are to be used are read by the program segment between lines 75 and 83. The user can enter any number of values for DT(NDT), NTC(NDT) and NEXT. The program stops reading values for DT, NTC and NEXT when NEXT is assigned a value other than unity by the user.

Additional variables, defined at the top of the listing, are read by line 86. Subroutines DTHW and DZR, in which input data defining the circumferential and axial mesh structures are read in (see the descriptions of those routines), are called next. Lines 112 to 120 calculate the radial subdivision size that will be used on the endcap (DR) and the radii of the endcap nodes (RAD(N)). Miscellaneous areas and radiative surface resistances (actually their inverses) are calculated in lines 126 to 146 and subroutine TINITL is called in line 150 to initialize the nodal temperatures. Values are assigned to the inner and outer surface heat transfer coefficients at each node J,K in lines 155 to 160 and VIEWFA is called to calculate the tank wall-to-liquid surface view factors (F(J)) using Hottels crossed-string method.

The time step number (NTS), time (TIME), time step size (DTAU), etc. are initialized in lines 172 to 175, after which the time step count (NTS) is incremented by one in line 176. The DO loop between lines 183 and 185 checks to see if the time step size (DTAU) should be changed to DT (NDT+1) and, if the check gives an affirmative answer, control is transferred to statement 14 to start the procedure by which the Jacobian matrix and the right-hand side vector are recalculated. If the time step size is not changed, the Jacobian matrix is not recalculated unless NSPEC time steps have elapsed since the last time it was calculated (this is the case if the check in line 213 gives an affirmative answer, in other words if NSTEP = NSPEC). If the Jacobian matrix does not have to be recalculated, subroutine QFORM is called to update only the right-hand side vector (D). Subroutine SUB is called after D has been recalculated to compute the nodal temperatures using the previously factored Jacobian matrix (CX) and the new right-hand side vector. Control is then transferred to statement 150 to perform the convergence tests and print the results, if required.

The DO loop starting at line 246 sweeps through all of the axial nodes (K) in the cylindrical shell and an inner DO loop starting at line 251 sweeps through all of the circumferential (azimuthal) nodes (J). Inner and outer surface areas and the volume and thermal capacity of the J,Kth node are calculated in lines 256 to 260 and the variable FACT, which is equivalent to the factor ω in Eq. 2-82, is calculated in line 269. The finite-difference coefficients (internodal conductances) for the J,Kth node are then calculated in lines 282 to 305. Coefficients to the left of the diagonal entry for the J,Kth node in the Jacobian matrix are stored temporarily in a vector CBW for transferral later to the Jacobian matrix (CX) in subroutine CONMAG. The diagonal entry for the J,Kth node in the cylindrical shell is calculated in lines 312 to 322 and the corresponding right-hand side term is calcualted in lines 326 to 334. Subroutine CONMAG is called at that time to transfer the entries in CBW to the Jacobian matrix CX.

The DO loop starting at line 347 sweeps through all of the radial nodes (K) in the tank endcap and an inner DO loop starting at line 352 sweeps through all of the circumferential nodes (J). Finite-difference equations for those nodes are assembled in the manner discribed previously for nodes in the cylindrical shell.

Temperatures needed to evaluate terms in the Jacobian matrix in later time steps or iterations are stored in the array TJAC by the program segment between lines 435 and 436 after the Jacobian matrix (CX) and right-hand side vector (D) have been calculated. The temperatures stored in the array TJAC are used in subroutine QFORM to update entries in D when the Jacobian matrix is not recalculated.

Subroutines CHLSKI and SUB are called by lines 440 and 446 respectively to solve for the nodal temperatures. The nodal temperatures are returned from SUB stored in the vector D so the entries in T, which is the vector of current nodal temperatures, are equated to those in D in lines 447 to 448.

A convergence indicator, NCONT, is set equal to zero in line 450. The program segment between lines 457 and 468 then examines the absolute value of the difference between the current temperature of each node and its value at the end of the previous iteration (stored as TPREV(J,K)) to see if any of the nodal temperatures have changed in value by an amount more than EPSLN. If any nodal temperatures changed by an amount more than EPSLN from the previous iteration to the current one, the convergence indicator (NCONT) is set equal to one in line 464 and the program is returned by line 477 to statement 5 (line 210) to start another iteration. The program is not returned to statement 5 if the current iteration count (NITER) is greater than the maximum permissible value (MAXIT), however, and program execution is halted if that is the case.

If the program reaches line 481, convergence has been achieved and the analysis is almost ready to proceed to the next time step. The current nodal temperatures are than stored as the previous nodal temperatures (i.e., the nodal temperatures at the previous time step) in the array TPRTS by the program segment between lines 490 and 498, which also causes nodal temperatures to be printed if required. Line 504 checks to see if the final time has been reached and causes the program to return to statement 8 (line 176) to start another time step if it has not.

E.2.2 Grid Definition Routines

The circumferential mesh structure for the finite-difference model of the tank car is defined in subroutine DTHW, where the circumferential mesh spacings $\Delta\theta_a$ and $\Delta\theta_b$, shown in Fig. 2-2, are either read in or calculated by the routine. The angular increments $\Delta\theta_a$ and $\Delta\theta_b$ can be varied in different intervals of the azimuthal coordinate (θ) to give finer spatial discretization in regions where temperature gradients are expected to be large, such as near the line of intersection of the shell and the liquid surface, than in other regions. Values of θ_j are also defined in DTHW for all of the azimuthal nodes (j). A detailed description of subroutine DTHW is given in the next section.

The axial mesh structure in the cylindrical shell of the tank car is defined in subroutine DZR, where the axial mesh spacings Δz_a and Δz_b shown in Fig. 2-2 are either read in or calculated by the routine. The axial coordinates (z_k) of the nodes are also calculated in subroutine DZR, although the coordinate $z = 0$ is located at the tank's axial midpoint instead of at one end as it will be in the tank car centered coordinate system used in the final model. Different values of Δz_a and Δz_b can be used in different axial segments of the tank, allowing finer spatial discretization to be used in regions where high temperature gradients are anticipated, such as around the relief value for instance, while still allowing coarse axial subdivisions to be used in regions where temperature gradients are expected to be small. Subroutine DZR is described in detail, with reference to the coding in the routine, in Sect. E.2.2.2.

E.2.2.1 Subroutine DTHW

The values of $\Delta\theta_a$ and $\Delta\theta_b$ at each circumferential mesh point

I*, designated DTHA(I) and DTHB(I) respectively, are defined in subroutine DTHW for I = 1,2, ... JTOT. The value of θ at each circumferential mesh point I, designated, AN(I), is also defined in this subroutine. The first variable read by the subroutine is JTOT, which is the total number of circumferential mesh points in the grid while the second variable read, ATOT, is the total included angle, measured in the $+\theta$ direction, between the first and last circumferential (constant θ) grid lines at I = 1 and I = JTOT respectively, as shown in Fig. E.2.

The READ statement in subroutine DTHW for the variables JTOT and ATOT is line (DTHW) 29 in the listing of that subroutine (Listing 2) after reading JTOT and ATOT the subroutine initializes a counter, N, in line 41 and subsequently reads three more variables, DTH, IN(N) (where N = 1 at this point) and NEXT, in line 43. The variable DTH is an angular subdivision size which, when N = 1, is used between circumferential nodes 1 and IN(1) (ie. from I = 1 to I = IN(1)), as seen in Fig. E.2. Lines 50 to 67 subsequently assign appropriate values of DTHA(I) and DTHB(I) to the nodes (I) in that range and calculate the value of θ (AN(I)) at each node. A check on the value of NEXT follows in line 72 and, if NEXT = 1, the value of the counter (N) is increased by one and new values of DTH, IN(N) andNEXT are read by line 43, as before. Lines 50 to 67 are then re-executed and the new subdivision size, DTH, is used to define values of DTHA(I), DTHB(I) and AN(I) for I between IN(N-1) and IN(N) (note that the circumferential nodes at which the use of DTH begins and ends are designated NIP and IN2 respectively in the program). If NEXT =1 again, the whole procedure is repeated.

---

* The subscript I is used for the circumferential node subscript, instead of J, in the routine.

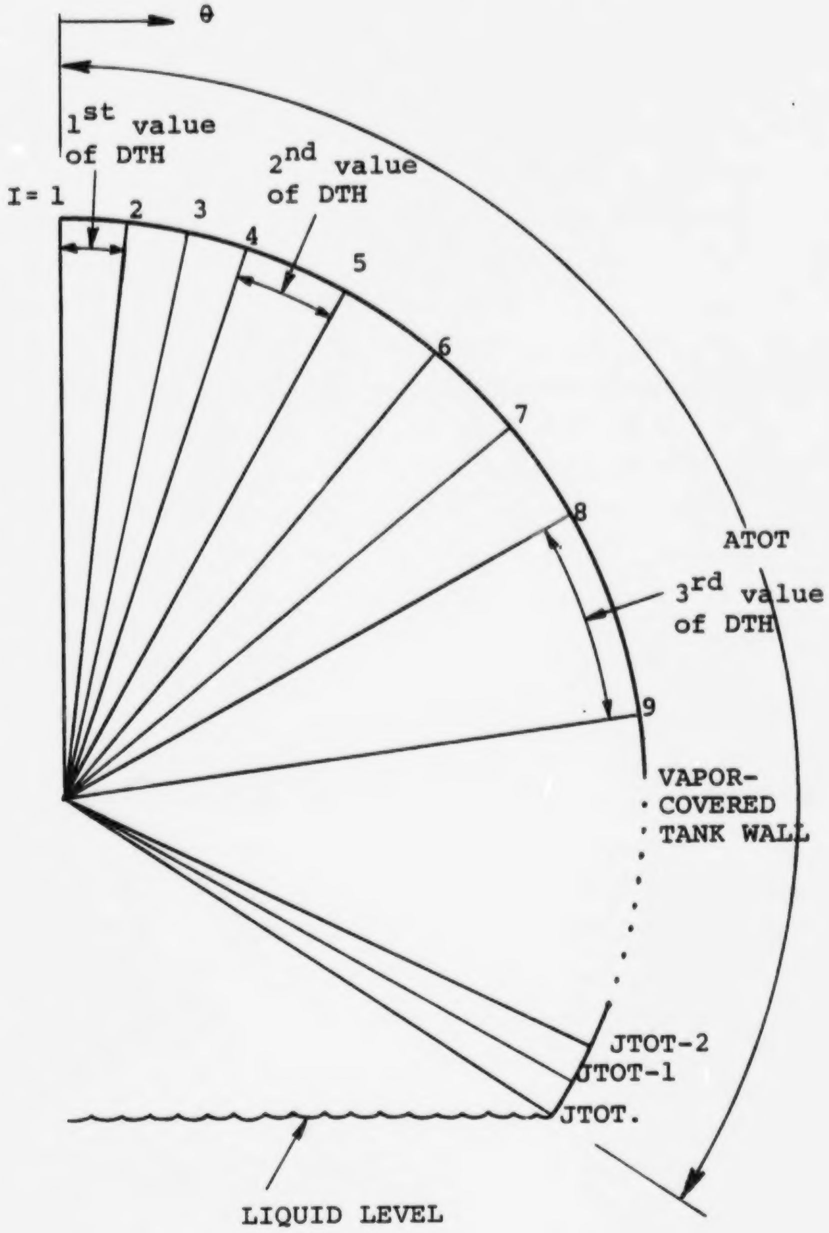
θ
1st value of DTH
2nd value of DTH
I = 1
2
3
4
5
6
7
8
9
ATOT
3rd value of DTH
VAPOR-COVERED TANK WALL
JTOT-2
JTOT-1
JTOT.
LIQUID LEVEL

Fig. E-2 : Tank car circumferential mesh structure

The process described above continues until NEXT is assigned a value other than 1 by the user and the comparison in line 72 no longer gives an affirmative answer. If the accumulated value of θ at this time (ie. the value of θ at the last value of IN(N)), designated ANG, is greater than ATOT an error message is printed and program execution is stopped, otherwise a final angular subdivision size for use at nodes (I) between the last value of IN(N) and I = JTOT is evaluated in line 84 by dividing the total remaining angle (ATOT-ANG) by the number of remaining subdivisions (JTOT-IN(N)). Lines 90 to 97 then define DTHA(I), DTHB(I) and AN(I) at the remaining nodes between the last value of IN(N) and JTOT.

E.2.2.2 Subroutine DZR

The values of Δz_a, Δz_b and z at each axial node KK, designated DZA(KK), DZB(KK) and AXPOS(KK) respectively in the program, are defined in subroutine DZ for KK = 1,2,... KTOT, where KTOT is the largest axial node number (at the end of the cylindrical tank shell). The manner in which the axial mesh structure is defined in subroutine DZR is similar to the way in which the circumferential mesh structure was defined in subroutine DTHW, as described below.

With reference to the listing of subroutine DZR provided as listing 3, computations start with the initialization of a counter, K, in line (DZR) 26 and the reading of three variables, DZ, KCH(K) (where K = 1 at this point) and NEXT in line 31. The variable DZ is an axial subdivision size which, when K = 1, is used between axial nodes 1 and KCH(1) (ie. from KK = 1 to KK = KCH(1)), as seen in Fig. E.3. Lines 39 to 54 subsequently assign appropriate values of DZA(KK)

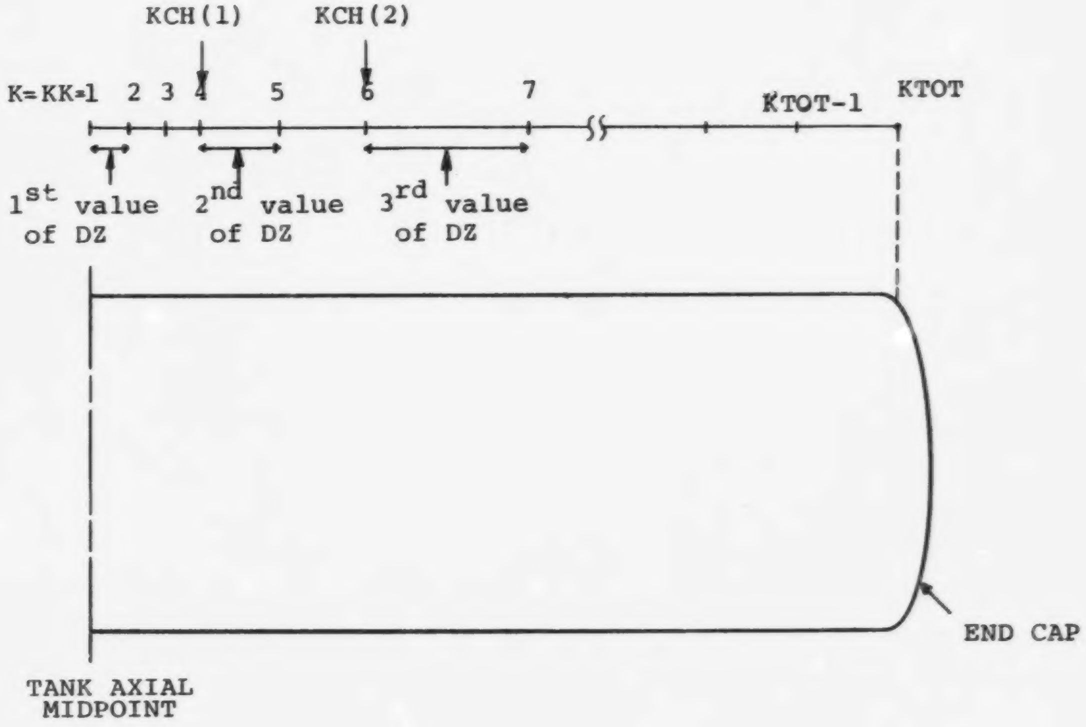
KCH(1)
KCH(2)
K=KK=1
2
3
4
5
6
7
KTOT-1
KTOT
1st value of DZ
2nd value of DZ
3rd value of DZ
TANK AXIAL MIDPOINT
END CAP

Fig. E-3: Tank car axial mesh structure.

and DZB(KK) to the nodes (KK) in that range and calculate the axial position (AXPOS(KK)) of each node. The value of the counter, K, is then increased by one and the value of NEXT is examined in line 61. If NEXT = 1, the program returns to statement 10 (line 31) where it reads new values for DZ, KCH(K) and NEXT as before. Lines 39 to 54 are then re-executed and the new subdividion size, DZ, is used to define values of DZA(KK), DZB(KK) and AXPOS(KK) for KK between KCH(K-1) and KCH(K) (note that the axial nodes at which the use of DZ begins and ends are designated NKP and KKF respectively in the program). If NEXT = 1 again, the whole procedure is repeated.

The process described above continues until NEXT is assigned a value other than 1 by the user and the comparision in line 64 no longer gives an affirmative answer. The last value of KCH(K) entered is, at that time, used to define the largest axial node number, KTOT, in line 68.

E.2.3 Remaining Routines

E.2.3.1 Subroutine QFORM

The right-hand side vector (D) for the system of finite-difference equations is updated in subroutine QFORM when the Jacobian matrix is not recalculated. The DO loop starting at line 20 in the listing of QFORM (listing 4) sweeps through all of the axial nodes (K) in the cylindrical shell and the inner DO loop starting at line 25 sweeps through all of the circumferential nodes (J). The right-hand side entry in the finite-difference equation for the J,Kth node in the cylindrical shell is calculated by the program segment between lines 30 and 58 using the temperatures stored in the array TJAC to update non-linear terms. This procedure is repeated for the endcap nodes in the program segment between lines 65 and 95.

E.2.3.2 Subroutine VIEWFA

Subroutine VIEWFA included as Listing 5, calculates the view factor (F(J)) for each azimuthal node (J) viewing the liquid surface. The DO loop starting at line 12 in the routine sweeps through all the azimuthal nodes and the program segment between lines 17 and 39 calculates the view factor for each node using Hottel's crossed-string method, described in Sect. 2.3.2.5. The angles θ_{1i}, θ_{1f}, θ_{2i} and θ_{2f} shown in Fig. 2-29, which are designated THET1I, THET1F, THET2I and THET2F respectively in the program, are calculated by lines 17 to 26 and Equ. 2-81 is then used in line 39 to calculate the view factor F_{1-2} = (F(J)).

E.2.3.3 Subroutines TINITL and ZERO

Entries in the temperature arrays T and TPRTS are equated to the user-specified initial temperature (TINIT) in subroutine TINITL, provided as listing 6. Subroutine ZERO, provided as listing 7, is simply used to zero entries in the Jacobian matrix CX and the right-hand side vector D before those arrays are recalculated.

E.2.3.4 Subroutine CONMAG

Subroutine CONMAG, provided as listing 8, transfers elements of the vector CBW, which contains finite-difference coefficients found within the left-hand bandwidth of a particular row (L) in the conductance matrix, to a singly-subscripted form of the banded, symmetric, conductance matrix (CX). Only the elements from the first non-zero entry in each row up to and including the diagonal term are stored and the rows are lined up end to end in CX. The Nth entry in a pointer vector, NDIAG, indicates the location of the diagonal coefficient for the Nth finite-difference equation in CX. This storage mode, termed profile storage, is described in greater detail by Jennings (7).

The finite-difference coefficients found within the left-hand bandwidth of each row in the conductance (Jacobian) matrix are computed in the main program, TANKS. The coefficients for the Lth node are stored at the end of CBW rather than at the beginning (ie. the diagonal coefficient for the node is stored as CBW (MBW), where MBW is an input variable) because it is not known when the computation of terms in the Lth finite-difference equation starts what the left-hand bandwidth of the equation will be. If the diagonal coefficient is stored as CBW (MBW), the coefficients to the left of the diagonal will not extend beyond the beginning of CBW unless the user has underestimated MBW.

Lines 15 to 19 in subroutine CONMAG determine the left-hand bandwith (-1) of the Lth finite-difference equation, designated NBW, from the values of JP(JJ) defined in TANKS. The location of the first non-zero entry in CBW (entry LM) is subsequently calculated from the values of MBW and NBW in line 20. Lines 21 to 27 then insert the entries in CBW between and including the entries LM and MBW into the conductance vector, CX. The location in CX of the diagonal element for the Lth row is stored as NDIAG(L) in line 29.

E.2.3.5 Subroutines CHLSKI and SUB

Subroutine CHLSKI, included as listing 9, uses Cholesky's algorithm to factor a positive-definite matrix, in this case the left-hand side conductance matrix for a system of finite-difference equations (CX), into the product of a lower triangular matrix (L) and the transpose of that matrix (L^T) (ie. $CX = LL^T$). The conductance matrix (CX) is actually designated A in subroutines CHLSKI and SUB. The conductance matrix is stored as a vector (ie. singly-subscripted array) in the profile storage mode described by Jennings (7). Only the elements from the first non-zero entry in each row up to and including the diagonal term are stored and the rows are lined up end to end in the coefficient vector. A pointer vector, KDIAG (or NDIAG in subroutine CONMAG), provides the location of each diagonal element in the coefficient vector. Subroutine SUB, included as listing 10, performs the forward and backward substitutions needed to obtain the solution vector (T) from the factored conductance matrix (A) and the right-hand side heat flow vector (D, or B in subroutine SUB). The solution vector (T) is obtained by solving the triangular system $LY = B$ for Y by forward substitution and then solving another triangular system, $L^T T = Y$, for T by backward substitution.

Subroutines CHLSKI and SUB were both written by Jennings and are described in more detail in (7).

E.3 RESULTS OF SAMPLE ANALYSES

The computer program described in the preceding sections of this appendix was used to compute the tank wall temperature distribution in a full-size DOT 112A tank car in a fire as a function of time. The tank was assumed to be half-full of liquid and exchanging heat with a flame at 1200 K. The flame emissivity (ε_f) and the tank outer surface emissivity (ε_s) were both assumed to be 0.9 in the analyses. A time step size of 10 seconds was used for the first 39 time steps (ie. for the first 390 seconds) and then changed to 20 seconds for the remaining time steps in each analysis. Tank temperatures did not change after approximately 1000 seconds so the analyses were stopped at 1100 seconds:

The angular subdivisions read by subroutine DTHW were varied to give finer spatial discretization in regions near the line of intersection of the liquid surface and the tank shell and near the relief valve than in other regions. The subdivisions used can be found on the printouts included in this appendix. The axial subdivisions read by subroutine DZR were also varied to give finer spatial discretization in regions near the relief valve than in regions remote from it. Those subdivisions can also be found on the printouts.

Solutions to a case with uniform convective heat transfer coefficients prescribed over the inner and outer surfaces of the tank car were obtained with the conventional Newton-Raphson method, in which the Jacobian matrix is recalculated every time step and every iteration, as well as with the modified Newton-Raphson method with the Jacobian matrix updated once every 20 time steps (ie. the Jacobian matrix would have been calculated and factored at times of approximately

0 seconds, 200 seconds, 400 seconds and 800 seconds within the 0-1100 second time period in this case). Essentially identical results were obtained in the two analyses, as can be seen by examining the printouts* for the two cases included in this appendix. The temperature of the tank wall at the top center (ie. $J = 1$, $K = 1$) is plotted against time in Fig. E.4. The computing time needed to obtain the solution using the modified Newton-Raphson method was only 24% of the computing time required by the conventional algorithm, thus proving the superiority of the former method.

The two analyses just mentioned were performed with a convective heat transfer coefficient of 10 $W/m^2{}^\circ C$ prescribed over the inner and outer surfaces of the tank. The thermal analysis was repeated with the inner surface convective heat transfer coefficient at nodes ($J = 1$, $K = 1$), ($J = 1$, $K = 2$), ($J = 2$, $K = 1$) and ($J = 2$, $K = 2$) set at the arbitrarily high value of 2500 $W/m^2{}^\circ C$ to simulate the high convective heat transfer coefficients that will be present around a venting relief valve. Prescribing high convective heat transfer coefficients over the inner surface areas of the nodes around the relief valve reduced the tank wall temperature in that region, as can be seen in the printout for the analysis included in this appendix, but the region affected appeared to extend, typically, to only about the sixth axial node (ie. to $K = 6$) along the top of the tank (ie. at 12 o'clock), which corresponds to a point located about 0.3 m (ie. one-tenth of a tank diameter or twenty tank wall thicknesses) from the relief valve. The results of this analysis indicate,

---

* Only the temperatures of the circumferential nodes ($1 \leqslant J \leqslant 17$) at the tank's axial midpoint (ie. at $K = 1$) and the temperatures of the axial nodes ($1 \leqslant K \leqslant 31$) at 12 o'clock (ie. $J = 1$) are given.

Fig. E-4: Tank wall temperature (at top center) vs. time

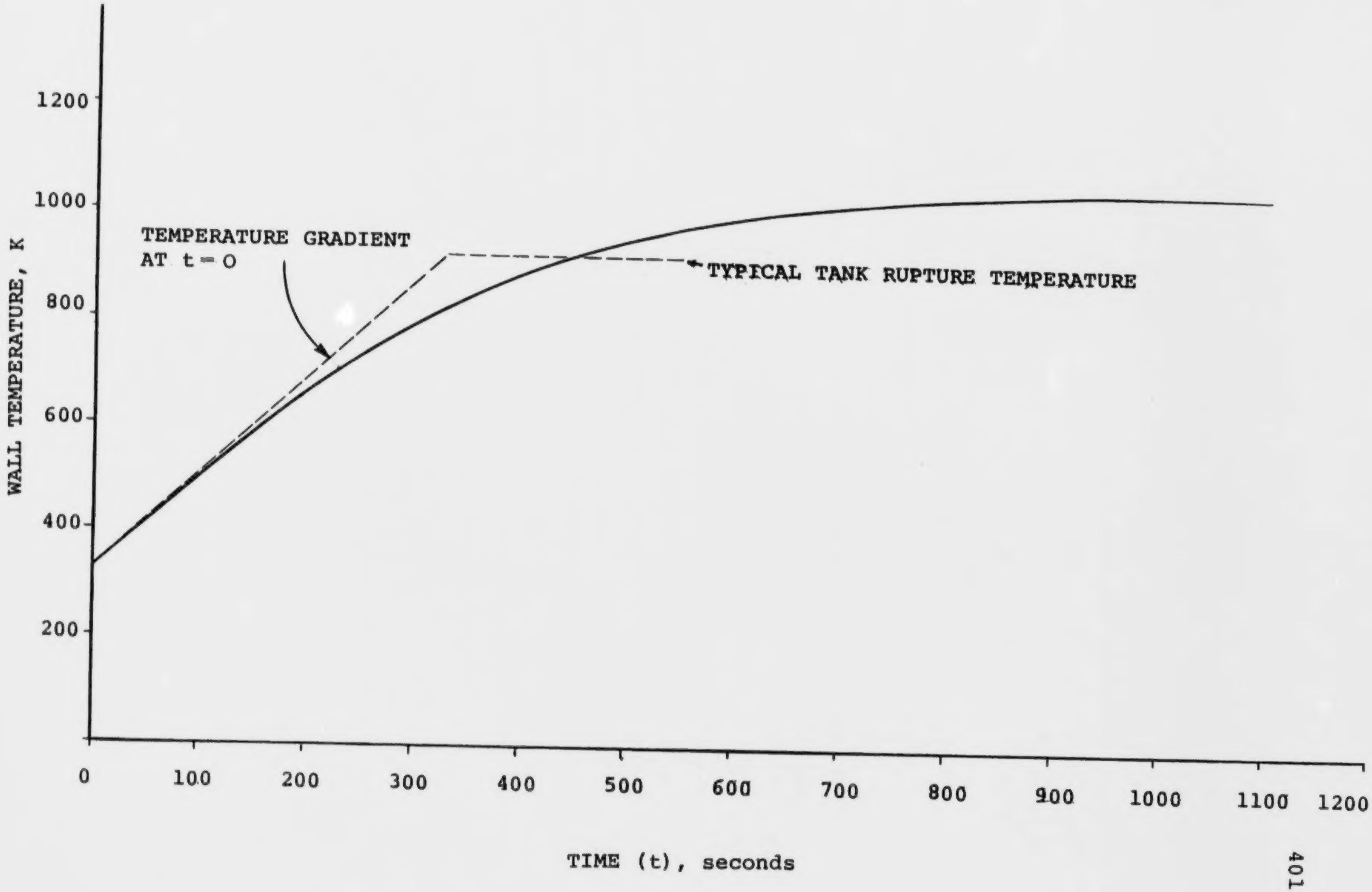

therefore, that high convective heat transfer rates around a venting relief valve will probably cause tank wall temperatures to be depressed only in a very small region around the valve.

19:41 OCT 06 '82 TANKS.XCCDAVIS

LISTING 1

```
C                                                                          TANK0000
C   This program computes the tank wall temperature distribution in the  TANK0001
C   ullage space of a tank car in a fire as a function of time.            TANK0002
C                                                                          TANK0003
      DIMENSION DZA(32),DZB(32),DTHA(20),DTHR(20),CC(10),CE(10)            TANK0004
      DIMENSION T(600),CX(12000),D(600),TPRTS(20,32),DT(10),NTC(10),       TANK0005
     $AXPOS(32),F(32),RAD(32),TPREV(20,32),HXO(20,32),HXI(20,32),          TANK0006
     $AN(30),TJAC(600),CRW(100),NDIAG(600),JP(3)                           TANK0007
C                                                                          TANK0008
      COMMON /DBOF/RI,SR,TC,FEL,RAV,RO,SRL,TF,TPROP,DR,REXCO,SIGMA,       TANK0009
     $SRLA,THK,WL,D,DTHA,DTHR,DZA,DZB,HXI,HXO,RAD,T,JTOT,JTOT1,           TANK0010
     $KTOT,KTOT1,KTTOT,THCAP,TPRTS,TJAC,F,AXLTH,AXPOS,AN                  TANK0011
C                                                                          TANK0012
C   Input variables read by main program                                   TANK0013
C                                                                          TANK0014
C     EPSI - Emissivity of tank inside surface                             TANK0015
C     EPSL - Emissivity of liquid propane                                  TANK0016
C     FEL  - View factor for surface elements on tank end cap viewing      TANK0017
C            liquid propane                                                TANK0018
C     EPSLN - Convergence parameter                                        TANK0019
C     THK - Tank wall thickness (m)                                        TANK0020
C     RO - Tank outer radius (m)                                           TANK0021
C     RI - Tank inner radius (m)                                           TANK0022
C     TC - Thermal conductivity of tank wall material (W/mK)               TANK0023
C     TPROP - Temperature of liquid propane (K)                            TANK0024
C     TF - Flame temperature (assumed uniform) (K)                         TANK0025
C     TINIT - Initial estimate of tank wall node temperature (K)           TANK0026
C     REXCO - Radiation exchange coefficient for radiation between         TANK0027
C                the tank wall and the flame                               TANK0028
C     MAXIT - Maximum number of iterations to be allowed for convergenceTANK0029
C     NRNOD - Number of radial nodes on tank endcap                        TANK0030
C     HXIN - Convective heat transfer coefficient on the inside of         TANK0031
C              the tank (in the ullage space) (W/(M**2)K)                  TANK0032
C     HXOUT - Convective heat transfer coefficient on the outside of       TANK0033
C             the tank (w/(m**2)k)                                         TANK0034
C                                                                          TANK0035
C    DT(NDT) - NDTth time step size (seconds)                              TANK0036
C    NTC(NDT) - the number of the time step at which use of the NDTth      TANK0037
C               time step size is terminated                               TANK0038
C    NEXT - =1,another set of values for DT(NDT)is  provided               TANK0039
C           =0,no more values for DT(NDT) and NTC(NDT) are                 TANK0040
C            provided                                                      TANK0041
C                                                                          TANK0042
C    DENS - density of tank wall material (kg/m3)                          TANK0043
C    SPHT - specific heat of tank wall material (J/kg k)                   TANK0044
C    TFINAL - time at which analysis is to be terminated                   TANK0045
C    NUPDAT - update option:                                               TANK0046
C               =1,jacobian matrix is updated every time step and every    TANK0047
C                iteration.                                                TANK0048
C               =0,jacobian matrix is updated every nth time step          TANK0049
C                where N=NSPEC (see next input variable)                   TANK0050
C    NSPEC - number of time steps between consecutive updatings            TANK0051
C            of the jacobian matrix (if NSPEC =1, the jacobian             TANK0052
C            matrix is updated every time step)                            TANK0053
C    NSKIP - print control variable. if NSKIP=1, results are printed       TANK0054
C            every time step; if NSKIP =n, results are printed             TANK0055
every nth time step                                                        TANK0056
C    NBW - number greater than the maximum row bandwidth                   TANK0057
```

```
C                                                                       TANK0058
C                                                                       TANK0059
      SIGMA = 5.669E-8                                                  TANK0060
      READ(5,900) EPSI,EPSL,FEL,EPSLN,THK,RO,RI,TC,TPROP,TF             TANK0061
     $      ,TINIT,REXCO,MAXIT,NRNOD,HXIN,HXOUT                         TANK0062
900   FORMAT(7F10.5/4F10.5,E12.6/2I5,2F10.5)                            TANK0063
      WRITE(6,901) EPSI,EPSL,FEL,EPSLN,THK,RO,RI,TC,TPROP,TF            TANK0064
     $      ,TINIT,REXCO,MAXIT,NRNOD,HXIN,HXOUT                         TANK0065
901   FORMAT(1X,'EPSI = ',F10.5,'EPSL = ',F10.5,'FEL = ',F10.5,         TANK0066
     $ 'EPSLN = ',F10.5,'THK = ',F10.5/1X,'RO = ',F10.5,                TANK0067
     $ 'RI = ',F10.5,'TC = ',F10.5,'TPROP = ',F10.5,                    TANK0068
     $ 'TF = ',F10.5/1X,'TINIT = ',F10.5,'REXCO = ',E12.6,              TANK0069
     $ 'MAXIT = ',I5,'NRNOD = ',I5,'HXIN = ',F10.5,                     TANK0070
     $ 'HXOUT = ',F10.5)                                                TANK0071
C                                                                       TANK0072
C   Read time step data.                                                TANK0073
C                                                                       TANK0074
      NDT=1                                                             TANK0075
7     READ(5,904) DT(NDT),NTC(NDT),NEXT                                 TANK0076
904   FORMAT (F10.5,2I5)                                                TANK0077
      WRITE(6,905) NDT,DT(NDT),NTC(NDT),NEXT                            TANK0078
905   FORMAT (1X,'NDT=',I3,10X,'DT(NDT)=',F10.5,10X,'NTC(NDT)='         TANK0079
     $,I3,10X,'NEXT=',I3,/)                                             TANK0080
      NDT=NDT+1                                                         TANK0081
      IF(NEXT.EQ.1) GO TO 7                                             TANK0082
      NTDT=NDT-2                                                        TANK0083
C                                                                       TANK0084
C                                                                       TANK0085
      READ(5,906) DENS,SPHT,TFINAL,NUPDAT,NSPEC,NSKIP,MBW               TANK0086
906   FORMAT (3F10.5,4I5)                                               TANK0087
      WRITE (6,907) DENS,SPHT,TFINAL,NUPDAT,NSPEC                       TANK0088
907   FORMAT (1X,'DENS=',F10.5,7X,'SPHT=',F10.5,7X,'FINAL TIME=',       TANK0089
     $F10.5,' SECS.',7X,'NUPDAT=',I3,7X,'NSPEC=',I3,/)                  TANK0090
C                                                                       TANK0091
      NPRINT=0                                                          TANK0092
      THCT=DENS*SPHT                                                    TANK0093
C                                                                       TANK0094
C                                                                       TANK0095
C   Call routine to define circumferential mesh structure               TANK0096
C                                                                       TANK0097
      CALL DTHW(DTHA,DTHB,AN,JTOT)                                      TANK0098
      JTOT1 = JTOT - 1                                                  TANK0099
C                                                                       TANK0100
C   Call routine to define the axial mesh structure                     TANK0101
C                                                                       TANK0102
      CALL DZR(DZA,DZB,AXLTH,KTOT,AXPOS)                                TANK0103
C                                                                       TANK0104
      KTTOT = KTOT + NRNOD                                              TANK0105
      KTOT1 = KTOT + 1                                                  TANK0106
      RAV = (RO + RI) / 2.0                                             TANK0107
C                                                                       TANK0108
C   Calculate the radial subdivision size that will be used on the     TANK0109
C   endcap                                                              TANK0110
C                                                                       TANK0111
      DR = RAV / NRNOD                                                  TANK0112
C                                                                       TANK0113
C   Calculate the radii of the radial nodes on the endcap               TANK0114
C                                                                       TANK0115
      RADIUS = -DR/2.0                                                  TANK0116
C                                                                       TANK0117
```

```
      DO 3 N=1,NRNOD
         RADIUS = RADIUS + DR
3     RAD(N) = RADIUS
C
C     Calculate inverses of radiative surface resistances (excluding area
C     terms), designated SR and SRL for the tank inner surface and the
C     liquid surface respectively.
C
      SR = EPSI / (1.0 - EPSI)
      SRL = EPSL / (1.0 - EPSL)
C
C     Calculate the width of the liquid surface (WL) from the angle
C     at which the liquid surface intersects the tank wall (AN(JTOT))
C
      WL = 2.0*RI*SIN(AN(JTOT))
C
C     Calculate the total area of the liquid surface (AREAL)
C
      AREAL = WL*AXLTH
C
C     Calculate the radiative resistance of the liquid surface (SRLA)
C
      SRLA = 1.0 / (AREAL*SRL)
C
C     Calculate an upper limit for the total number of nodes in the grid
C     (NNUM)
C
      NNUM = JTOT1*KTTOT
      NPAR=NNUM*JTOT
C
C     Call a routine to initialize the nodal temperatures.
C
      CALL TINITL(TINIT,T,TPRTS,JTOT,KTOT,JTOT1,KTTOT)
C
C     Assign values to the tank inner and outer surface convective
C     heat transfer coefficients.
C
      DO 1 J=1,JTOT1
         DO 2 K=1,KTTOT
            HXI(J,K) = HXIN
            HXO(J,K) = HXOUT
2        CONTINUE
1     CONTINUE
C
C     call VIEWFA to calculate the view factor between each node on
C     the tank inner surface and the liquid surface.
C
      CALL VIEWFA(AN,F ,JTOT)
C
C     initialize the number of time steps taken since the Jacobian
C     was updated (NSTEP), the number of time steps taken so far
C     in the analysis (NTS), the time (TIME) and the time step
C     size (DTAU)
C
      NSTEP=0
      NTS=0
      TIME=0.0
      DTAU=DT(1)
8     NTS=NTS+1
      NSTEP=NSTEP+1
```

```
C                                                                       TANK0178
C   check to see if the current time step number (NTS) is one           TANK0179
C   at which the time step size (DTAU) should be changed to             TANK0180
C   DT(NDT+1)                                                           TANK0181
C                                                                       TANK0182
      DO 9 NDT=1,NTDT                                                   TANK0183
      IF(NTS.EQ.NTC(NDT)) GO TO 11                                      TANK0184
9     CONTINUE                                                          TANK0185
      GO TO 12                                                          TANK0186
C                                                                       TANK0187
C   time step size has changed. advance time, initialize                TANK0188
C   iteration counter (NITER) and go to statement 14 to                 TANK0189
C   recalculate the jacobian matrix CX and the right-hand               TANK0190
C   side vector D.                                                      TANK0191
C                                                                       TANK0192
11    DTAU=DT(NDT+1)                                                    TANK0193
      TIME=TIME+DTAU                                                    TANK0194
      NITER=1                                                           TANK0195
      GO TO 14                                                          TANK0196
C                                                                       TANK0197
C   the time step size hasn't changed so the jacobian                   TANK0198
C   matrix CX will not be recalculated unless the conditions            TANK0199
C   in one of the three IF statements below are satisfied.              TANK0200
C                                                                       TANK0201
12    TIME=TIME+DTAU                                                    TANK0202
C                                                                       TANK0203
C   initialize the iteration counter.                                   TANK0204
C                                                                       TANK0205
      NITER=0                                                           TANK0206
C                                                                       TANK0207
C   increment the iteration counter (NITER)                             TANK0208
C                                                                       TANK0209
5     NITER=NITER+1                                                     TANK0210
      IF(NUPDAT.EQ.1) GO TO 14                                          TANK0211
      IF(NTS.EQ.1.AND.NITER.EQ.1) GO TO 14                              TANK0212
      IF(NSTEP.EQ.NSPEC) GO TO 14                                       TANK0213
C                                                                       TANK0214
C   call the routine DFORM to update the right-hand side vector         TANK0215
C   D since CX is not being recalculated and refactored.                TANK0216
C                                                                       TANK0217
      CALL DFORM                                                        TANK0218
C                                                                       TANK0219
C   call the routine SUB to perform the forward and backsubsti-         TANK0220
C   tutions needed to obtain the vector of nodal temperatures           TANK0221
C   from the factored form of CX and the right-hand side                TANK0222
C   vector D that was just recalculated in DFORM                        TANK0223
C                                                                       TANK0224
      CALL SUB(CX,D,NDIAG,NEQU)                                         TANK0225
C                                                                       TANK0226
C   go to statement 150 to check for convergence and to print           TANK0227
C   the nodal temperatures if convergence has been achieved.            TANK0228
C                                                                       TANK0229
      GO TO 150                                                         TANK0230
14    NSTEP=0                                                           TANK0231
      THCAP=THCT/DTAU                                                   TANK0232
C                                                                       TANK0233
C   zero CX and D since they will be recalculated                       TANK0234
C                                                                       TANK0235
      CALL ZERO(CX,D,NPAR,NNUM)                                         TANK0236
C                                                                       TANK0237
```

```
C                                                                       TANK0238
C     Initialize the total node counter (L)                             TANK0239
C                                                                       TANK0240
        L = 0                                                           TANK0241
        KI =0                                                           TANK0242
C                                                                       TANK0243
C     Sweep through the axial nodes (K)                                 TANK0244
C                                                                       TANK0245
        DO 10 K=1,KTOT                                                  TANK0246
           DZTOT = (DZA(K) + DZB(K))/2.0                                TANK0247
C                                                                       TANK0248
C     Sweep through the circumferential nodes (J) in the tank wall.    TANK0249
C                                                                       TANK0250
           DO 20 J=1,JTOT1                                              TANK0251
C                                                                       TANK0252
C     Increment the total node count (L)                                TANK0253
C                                                                       TANK0254
              L = L + 1                                                 TANK0255
              ANTOT = (DTHA(J) + DTHB(J))/2.0                           TANK0256
              SAREAO = RO*ANTOT*DZTOT                                   TANK0257
              SAREAI = RI*ANTOT*DZTOT                                   TANK0258
              VOLUM=RAV*ANTOT*THK*DZTOT                                 TANK0259
              CAP=THCAP*VOLUM                                           TANK0260
C                                                                       TANK0261
C     calculate the factor (FACT) that multiplies Hottel's crossed     TANK0262
C     string view factor to account for axial position of surface      TANK0263
C     element                                                           TANK0264
C                                                                       TANK0265
              HEIGHT=RI*(COS(AN(J))-COS(AN(JTOT)))                      TANK0266
              THII=ATAN((AXLTH-AXPOS(K))/HEIGHT)                        TANK0267
              BETA=ATAN((AXLTH+AXPOS(K))/HEIGHT)                        TANK0268
              FACT=0.5*(SIN(THII)+SIN(BETA))                            TANK0269
C                                                                       TANK0270
C     zero the vector (CBW) used to store the finite difference        TANK0271
C     coefficients in the Lth row                                       TANK0272
C                                                                       TANK0273
              DO 21 NS=1,MBW                                            TANK0274
21            CBW(NS)=0.0                                               TANK0275
              DO 22 JJ=1,3                                              TANK0276
22            JP(JJ)=0                                                  TANK0277
C                                                                       TANK0278
C     Define the internodal conductances (CC(I)) and place them in     TANK0279
C     the appropriate locations in CBW                                  TANK0280
C                                                                       TANK0281
              CC(1) = 0.0                                               TANK0282
              IF (J .EQ. 1) GOTO 25                                     TANK0283
              CC(1) = TC*THK*DZTOT / (RAV*DTHA(J))                      TANK0284
              JP(1)=1                                                   TANK0285
              CBW(MBW-1)=-CC(1)                                         TANK0286
C                                                                       TANK0287
25            CC(2) = TC*THK*DZTOT / (RAV*DTHB(J))                      TANK0288
C                                                                       TANK0289
              CC(4) = 0.0                                               TANK0290
              IF (K .EQ. 1) GOTO 26                                     TANK0291
              CC(4) = TC*THK*RAV*ANTOT / DZA(K)                         TANK0292
              JP(2)=JTOT1                                               TANK0293
              CBW(MBW-JTOT1)=-CC(4)                                     TANK0294
C                                                                       TANK0295
26            CC(5) = 0.0                                               TANK0296
              IF (K .EQ. KTOT) GOTO 27                                  TANK0297
```

```
      CC(5) = TC*THK*RAV*ANTOT / DZR(K)
C
27    CC(6) = 0.0
      IF (K .NE. KTOT) GOTO 28
      CC(6) = TC*THK*(RAV - DR/4.0)*ANTOT/(0.5*DR)
C
28    CC(7) = SAREAI*HXI(J,K)
      CC(8) = SAREAO*HXO(J,K)
      CPROP=SIGMA/(1.0/(SR*SAREAI)+1.0/(SRL*AREAL)+1.0/(F(J)
     $      *FACT*SAREAI))
C
C   Calculate the diagonal coefficient (CTOT) by first summing
C   the linear finite-difference coefficients.
C
      CTOT = CC(1) + CC(2) + CC(4) + CC(5) + CC(6) + CC(7) + CC(8)
     $+CAP
C
C   Add the non-linear (radiative) terms.
C
      CTOT = CTOT + 4.0*REXCO*SAREAO*(T(L)**3)
      CTOT = CTOT + 4.0*CPROP*(T(L)**3)
C
C   Store CTOT in the appropriate location in CRW
C
      CBW(NRW)=CTOT
C
C   Calculate the Lth entry in the right-hand side vector.
C
      D(L) = -REXCO*SAREAO*((T(L)**4 - TF**4)-4.*(T(L)**4))
     $      + CC(7)*TPROP + CC(8)*TF
      D(L)=D(L)-CPROP*((T(L)**4-TPROP**4)-4.*(T(L)**4.)) +
     $CAP*TPRTS(J,K)
C
C   Include the term for conduction in the wall to the liquid propane
C   if necessary.
C
      IF (J .EQ. JTOT1) D(L) = D(L) + CC(2)*TPROP
C
C   call CONMAG to transfer finite-difference coefficients in
C   the vector CBW to the Jacobian matrix CX
C
      CALL CONMAG(CBW,CX,NRW,KL,L,NDIAG,JTOT1,JP)
C
20      CONTINUE
10    CONTINUE
C
C   Assemble the finite-difference equations for nodes in the endcap.
C   Sweep through the radial nodes (K).
C
      DO 80 K=KTOT1,KTTOT
        I = KTTOT - K + 1
C
C   Sweep through the circumferential nodes (J).
C
        DO 90 J=1,JTOT1
C
C   Increment the total node count (L)
C
      L = L + 1
      ANTOT = (DTHA(J) + DTHB(J))/2.0
```

```
          SAREA = DR*RAD(I)*ANTOT
          VOLUM=SAREA*THK
          CAP=THCAP*VOLUM
          DO 91 NS=1,MBW
91        CBW(NS)=0.0
          DO 92 JJ=1,3
92        JP(JJ)=0
C
C   Calculate the internodal conductances for the end cap nodes and
C   insert them into the appropriate locations in CBW
C
          CE(1) = 0.0
          IF (I .EQ. NRNOD) GOTO 94
          CE(1) = TC*THK*(RAD(I)+DR/2.0)*ANTOT/DR
          JP(1)=JTOT1
          CBW(MBW-JTOT1)=-CE(1)
C
94        CE(2) = 0.0
          IF (I .EQ. 1) GOTO 95
          CE(2) = TC*THK*(RAD(I)-DR/2.)*ANTOT/DR
C
95        CE(3) = 0.0
          IF (J .EQ. 1) GOTO 100
          CE(3) = TC*THK*DR / (RAD(I)*DTHA(J))
          JP(2)=1
          CBW(MBW-1)=-CE(3)
C
100       CE(4) = TC*THK*DR / (RAD(I)*DTHB(J))
          CE(5) = SAREA*HXO(J,K)
          CE(6) = SAREA*HXI(J,K)
C
          CE(7) = 0.0
          IF (I .NE. NRNOD) GOTO 101
          CE(7) = TC*THK*(RAV-DR/4.)*ANTOT/(0.5*DR)
          JP(3)=JTOT1
          CBW(MBW-JTOT1)=-CE(7)
C
C   Calculate the diagonal coefficient by first summing all of the
C   linear coefficients.
C
101       CETOT = CE(1) + CE(2) + CE(3) + CE(4) + CE(5) + CE(6)+CE(7)
     $+CAP
C
C   Add the non-linear (radiative) terms.
C
          CETOT = CETOT + 4.*REXCO*SAREA*(T(L)**3)
          RADEX = SIGMA / (SRLA+1.0/(SAREA*FEL)+1.0/(SR*SAREA))
          CETOT = CETOT + 4.0*RADEX*(T(L)**3)
C
C   store CETOT in the appropriate location in CBW
C
          CBW(MBW)=CETOT
C
C   Calculate the right-hand side term in the finite-difference
C   equation for the Lth node.
C
          D(L) = -REXCO*SAREA*((T(L)**4-TF**4)-4.*(T(L)**4))
     $    -RADEX*((T(L)**4-TPROP**4)-4.*(T(L)**4))
     $    +CE(5)*TF+CE(6)*TPROP+CAP*TPRTS(J,K)
C
```

```
C     Include the term for conduction into the liquid propane, if necessarTANK0418
C                                                                       TANK0419
          IF (J .EQ. JTOT1) D(L) = D(L) + CE(4)*TPROP                   TANK0420
C                                                                       TANK0421
C     call CONMAG to transfer finite-difference coefficients in         TANK0422
C     CBW to CX                                                         TANK0423
C                                                                       TANK0424
          CALL CONMAG(CBW,CX,MBW,KL,L,NDIAG,JTOT1,JP)                   TANK0425
90      CONTINUE                                                        TANK0426
80    CONTINUE                                                          TANK0427
C                                                                       TANK0428
      NEQU=L                                                            TANK0429
C                                                                       TANK0430
C     store current nodal temperatures(T(L)) for use in sub-            TANK0431
C     sequent updates of the right-hand side vector D performed         TANK0432
C     without recalculating the jacobian matrix CX                      TANK0433
C                                                                       TANK0434
      DO 147 L=1,NEQU                                                   TANK0435
147   TJAC(L)=T(L)                                                      TANK0436
C                                                                       TANK0437
C     call CHLSKI to factor the jacobian matrix.                        TANK0438
C                                                                       TANK0439
      CALL CHLSKI(CX,NDIAG,NEQU)                                        TANK0440
C                                                                       TANK0441
C     call Sub to perform forward and backward substitutions.           TANK0442
C     The solution vector is returned in D so entries in T must be      TANK0443
C     be equated to those in D.                                         TANK0444
C                                                                       TANK0445
      CALL SUB (CX,D,NDIAG,NEQU)                                        TANK0446
150   DO 149 L=1,NEQU                                                   TANK0447
149   T(L)=D(L)                                                         TANK0448
      L=0                                                               TANK0449
      NCONT=0                                                           TANK0450
C                                                                       TANK0451
C     check for convergence by comparing the nodal temperatures         TANK0452
C     from the preceding iteration (stored as TPREV(J,K) to the         TANK0453
C     current values. The variable NCONT is set to unity if the         TANK0454
C     temperature at any node has not converged.                        TANK0455
C                                                                       TANK0456
      DO 110 K=1,KTTOT                                                  TANK0457
         IF (K.LE.KTOT) DZTOT = (DZA(K) + DZB(K))/2.                    TANK0458
         DO 120 J=1,JTOT1                                               TANK0459
           ANTOT = (DTHA(J) + DTHB(J))/2.                               TANK0460
           L = L + 1                                                    TANK0461
125        IF (NITER-1) 130,130,140                                     TANK0462
140        DIFF = T(L) - TPREV(J,K)                                     TANK0463
           IF (ABS(DIFF) .GT. EPSLN) NCONT = 1                          TANK0464
130        TPREV(J,K) = T(L)                                            TANK0465
120      CONTINUE                                                       TANK0466
C                                                                       TANK0467
110   CONTINUE                                                          TANK0468
C                                                                       TANK0469
C     check to see if the number of iterations has exceeded the        TANK0470
C     user-specified maximum (MAXIT)                                    TANK0471
C                                                                       TANK0472
      IF (NITER .GT. MAXIT) GOTO 131                                    TANK0473
C                                                                       TANK0474
C     Check for convergence                                             TANK0475
C                                                                       TANK0476
      IF (NITER .EQ. 1 .OR. NCONT .EQ. 1) GOTO 5                        TANK0477
```

```
C                                                                       TANK0478
C   increment the print control variable (NPRINT)                       TANK0479
C                                                                       TANK0480
      NPRINT=NPRINT+1                                                   TANK0481
      WRITE(6,800) TIME,NITER                                           TANK0482
C                                                                       TANK0483
C   set the nodal temperatures for the preceding time step              TANK0484
C   (TPRTS(J,K)) to the current values in preparation for               TANK0485
C   advancing to the next time step. Also print the nodal               TANK0486
C   temperatures if NSKIP time steps have passed since the              TANK0487
C   last printing.                                                      TANK0488
C                                                                       TANK0489
      L=0                                                               TANK0490
      DO 151 K=1,KTTOT                                                  TANK0491
      DO 152 J=1,JTOT1                                                  TANK0492
        L=L+1                                                           TANK0493
      IF(NPRINT.EQ.NSKIP.AND.J.EQ.1) WRITE (6,801) K,J,T(L)             TANK0494
      IF(NPRINT.EQ.NSKIP.AND.J.NE.1.AND.K.EQ.1) WRITE (6,801) K,J,T(L)  TANK0495
        TPRTS(J,K)=T(L)                                                 TANK0496
152     CONTINUE                                                        TANK0497
151   CONTINUE                                                          TANK0498
      IF(NPRINT.EQ.NSKIP) NPRINT=0                                      TANK0499
C                                                                       TANK0500
C   advance to the next time step unless the final time has             TANK0501
C   been reached.                                                       TANK0502
C                                                                       TANK0503
      IF(TIME.LT.TFINAL) GO TO 8                                        TANK0504
C                                                                       TANK0505
801   FORMAT(1X,'K = ',I5,10X,'J = ',I5,10X,'T = ',F11.5)               TANK0506
C                                                                       TANK0507
131   STOP                                                              TANK0508
      END                                                               TANK0509
```

LISTING 2

```
20:59 SEP 28 '82 DTHW.XCCDAVIS
      SUBROUTINE DTHW (DTHA,DTHB,AN,JTOT)
C
C   THIS SUBROUTINE COMPUTES THE ANGULAR MESH INCREMENTS
C   BEFORE AND AFTER EACH CIRCUMFERENTIAL MESH POINT I
C   DESIGNATED DTHA(I)  AND DTHB(I)  RESPECTIVELY , FOR GRID
C   OPTIONS 0 AND 1 (IE., NGROPT=0 OR 1). THE VALUE OF
C   THETA AT EACH CIRCUMFERENTIAL MESH POINT I,  DESIGNATED
C   AN(I),  IS ALSO COMPUTED.
C
C               ***** INPUT VARIABLES READ BY SUB. DTH01 *****
C
C               JTOT    - TOTAL NUMBER OF CIRCUMFERENTIAL MESH POINTS
C               ATOT  - TOTAL INCLUDED ANGLE BETWEEN FIRST AND LAST
C                       CIRCUMFERENTIAL MESH POINTS (I=1  AND I=JTOT
C                       RESPECTIVELY ).
C               DTH   - SIZE OF ANGULAR SUBDIVISION.
C               IN(N) - CIRCUMFERENTIAL MESH POINT AT WHICH USE OF
C                       SUBDIVISION SIZE READ PREVIOUSLY (DTH) IS
C                       TERMINATED.
C               NEXT  - CONTROL VARIABLE ; NEXT=0 SIGNALS THAT NO MORE
C                       VALUES OF DTH AND IN(N) FOLLOW WHILE NEXT=1
C                       SIGNALS THAT THE STATEMENT WHICH READS  VALUES
C                       OF DTH ,IN(N), AND NEXT SHOULD BE RE-EXECUTED
C                       BECAUSE MORE VALUES ARE SUPPLIED.
C
C
      DIMENSION IN(10),AN(30),DTHA(20),DTHB(20)
      WRITE (6,881)
C
      READ (5,991) JTOT,ATOT
C
      WRITE (6,882) JTOT,ATOT
C
C   INITIALIZE VARIABLES.
C
      AN(1)=0.0
      N=0
C
C    INCREMENT COUNTER (N) FOR NUMBER OF DIFFERENT SETS OF
C   VALUES FOR DTH,IN(N) AND NEXT PROVIDED.
C
10    N=N+1
C
      READ (5,992) DTH,IN(N),NEXT
C
      WRITE (6,883) N,DTH,IN(N),NEXT
C
C   DETERMINE CIRCUMFERENTIAL MESH POINT WHERE USE OF
C   ANGULAR SUBDIVISION DTH BEGINS (NIP).
C
      NIP=1
      IF(N.NE.1) NIP=IN(N-1)
C
C   DETERMINE CIRCUMFERENTIAL MESH POINT WHERE USE OF
C   ANGULAR SUBDIVISION DTH ENDS (IN2)
C
      IN2=IN(N)
C
```

```
C     SET VALUES OF DTHA(I)  AT I  BETWEEN NIP+1 AND IN2 AND              DTHW0058
C     VALUES OF DTHB(I)  AT I  BETWEEN NIP AND IN2-1 TO DTH.              DTHW0059
C     CALCULATE AN(I).                                                    DTHW0060
C                                                                         DTHW0061
        DO 15 I-NIP,IN2                                                   DTHW0062
         IF(I.NE.NIP)  AN(I)=ANG+DTH                                      DTHW0063
         ANG=AN(I)                                                        DTHW0064
         IF(I.NE.NIP)  DTHA(I)-DTH                                        DTHW0065
         IF(I.NE.IN(N))  DTHB(I)=DTH                                      DTHW0066
15      CONTINUE                                                          DTHW0067
C                                                                         DTHW0068
C     CHECK TO SEE IF MORE VALUES OF DTH,IN(N) AND NEXT ARE               DTHW0069
C     PROVIDED.                                                           DTHW0070
C                                                                         DTHW0071
        IF(NEXT.EQ.1) GO TO 10                                            DTHW0072
C                                                                         DTHW0073
C     CALCULATE THE INCLUDED ANGLE OF THE CYLINDRICAL SEGMENT             DTHW0074
C     REMAINING BY SUBTRACTING THE LAST VALUE OF IN(N) FROM               DTHW0075
C     ATOT AND THEN DIVIDE THE ANGLE REMAINING BY THE NUMBER              DTHW0076
C     OF SUBDIVISIONS REMAINING (=JTOT-IN(N)) TO OBTAIN THE               DTHW0077
C     SUBDIVISION SIZE TO BE USED IN THE REST OF THE SEGMENT.             DTHW0078
C                                                                         DTHW0079
        IF(IN(N).EQ.JTOT) GO TO 25                                        DTHW0080
        IF(ANG-ATOT) 16,17,17                                             DTHW0081
17      OUTPUT  'TOTAL ANGLE EXCEEDED'                                    DTHW0082
        STOP                                                              DTHW0083
16      DTH=(ATOT-ANG)/(JTOT-IN(N))                                       DTHW0084
        OUTPUT DTH                                                        DTHW0085
C                                                                         DTHW0086
C     ASSIGN VALUES OF DTHA(I)  AND DTHB(I)  TO THE REMAINING             DTHW0087
C     VALUES OF I.                                                        DTHW0088
C                                                                         DTHW0089
        IN1=IN(N)                                                         DTHW0090
        DO 20 I=IN1,JTOT                                                  DTHW0091
         IF(I.NE.IN(N))  AN(I)=AN(I-1)+DTH                                DTHW0092
         IF(I.NE.IN(N))  DTHA(I)=DTH                                      DTHW0093
         DTHB(I)=DTH                                                      DTHW0094
20      CONTINUE                                                          DTHW0095
25      DTHA(1)=0.0                                                       DTHW0096
        DTHB(JTOT)=0.0                                                    DTHW0097
C                                                                         DTHW0098
30      RETURN                                                            DTHW0099
991     FORMAT (I5,F10.5)                                                 DTHW0100
992     FORMAT (F10.5,2I5)                                                DTHW0101
881     FORMAT ('0****** DATA READ IN SUBROUTINE DTH01 ******',/)         DTHW0102
882     FORMAT (1X,'JTOT=',I3,10X,'ATOT=',F10.5,/)                        DTHW0103
883     FORMAT (1X,'N=',I3,10X,'DTH=',F10.5,10X,'IN(N)=',I3,10X,'NEXT=',I3DTHW0104
       $,/)                                                               DTHW0105
        END                                                               DTHW0106
```

```
      SUBROUTINE DZR(DZA,DZB,AXLTH,KTOT,AXPOS)
C
C   THIS SUBROUTINE COMPUTES THE AXIAL NODE SPACINGS BEFORE
C   AND AFTER EACH AXIAL NODE KK, DESIGNATED DZA(KK) AND
C   DZB(KK) RESPECTIVELY, AS WELL AS THE AXIAL COORDINATE
C   AT KK, AXPOS(KK). THE SUBDIVISIONS DZA(KK) AND DZB(KK)
C   ARE FUNCTIONS OF AXIAL POSITION ONLY.
C
C       ***** INPUT VARIABLES READ IN SUB. DZ *****
C
C               DZ     - SIZE OF AXIAL MESH SUBDIVISION.
C               KCH(K) - NUMBER OF AXIAL NODE AT WHICH USE OF
C                        SUBDIVISION DZ READ PREVIOUSLY IS TERMINATED.
C               NEXT   - CONTROL VARIABLE ; NEXT=0 SIGNALS THAT NO MORE
C                        VALUES OF DZ, KCH(K)  AND NEXT FOLLOW WHILE
C                        NEXT=1 INDICATES THAT THE READ STATEMENT WHICH
C                        READS DZ, KCH(K)  AND NEXT SHOULD BE RE-
C                        EXECUTED BECAUSE ADDITIONAL VALUES OF THESE
C                        VARIABLES ARE PROVIDED.
C
      DIMENSION DZA(32),DZB(32),KCH(11),AXPOS(20)
      WRITE (6,881)
C
C   INITIALIZE COUNTER FOR NUMBER OF DIFFERENT SETS OF
C   VALUES OF DZ, KCH(K)  AND NEXT PROVIDED.(K)
C
      K=1
      AXLTH=0.0
C
C               READ INPUT VARIABLES.
C
10    READ (5,991) DZ,KCH(K),NEXT
C
      WRITE (6,882) K,DZ,KCH(K),NEXT
C
C   CALCULATE NUMBER OF NODE AT START OF REGION IN WHICH
C   SUBDIVISION DZ IS USED (NKP). NODE AT END OF REGION IS
C   KKF (=KCH(K)).
C
      NKP=1
      IF(K.NE.1) NKP=KCH(K-1)
      KKF=KCH(K)
C
```

```
C     SET DZA(KK)=DZ AT KK BETWEEN NKP+1 AND KKF AND SET
C     DZB(KK)=DZ AT KK RETWEEN NKP AND KKF-1.
C
        DO 5 KK=NKP,KKF
         IF(KK.NE.NKP) DZA(KK)=DZ
         IF(KK.NE.KCH(K)) DZB(KK)=DZ
C
C     CALCULATE  AXIAL POSITION AT KK (AXPOS(KK)).
C
         IF(KK.NE.NKP) AXLTH=AXLTH+DZ
         AXPOS(KK)=AXLTH
5       CONTINUE
C
C     INCREMENT COUNTER FOR NUMBER OF SETS OF VALUES FOR
C     DZ, KCH(K) AND NEXT READ.




C
        K=K+1
C
C     CHECK WHETHER MORE INPUT DATA ARE PROVIDED . RETURN TO
C     STATEMENT 10 IF ANSWER IS AFFIRMATIVE.
C
        IF(NEXT.EQ.1) GO TO 10
C
C    STORE LARGEST NODE NUMBER AS KTOT.
C
        KTOT=KCH(K-1)
        DZA(1)=0.0
        DZB(KTOT)=0.0
C
        RETURN
C
991     FORMAT (F10.5,2I5)
881     FORMAT ('0****** AXIAL GRID DATA READ IN SUBROUTINE DZ ******',/)
882     FORMAT (1X,'K=',I3,10X,'DZ=',F10.7,10X,'KCH(K)=',I3,10X,'NEXT=',I2
       $,/)
        END
```

LISTING 4

```
[illegible] SEP 29 '82 QFM.X[illegible]DAVIS

      SUBROUTINE QFORM                                                  QFOM0000
C                                                                       QFOM0001
C     This subroutine computes entries in the right-hand side           QFOM0002
C     vector D when the Jacobian matrix is not recalculated.            QFOM0003
C                                                                       QFOM0004
      DIMENSION DZA(32),DZB(32),DTHA(20),DTHB(20),CC(10),CE(10)         QFOM0005
      DIMENSION T(600),D(600),RAD(32),TFRTS(20,32),HXO(20,32),          QFOM0006
     *HXI(20,32),TJAC(600),F(32),AN(30),AXPOS(32)                       QFOM0007
      COMMON /DBOF/RI,SR,TC,FEL,RAV,RO,SRI,TF,TPROP,DR,REXCO,SIGMA,     QFOM0008
     *SRLA,THK,WL,D,DTHA,DTHB,DZA,DZB,HXI,HXO,RAD,T,JTOT,JTOT1,         QFOM0009
     *KTOT,KTOT1,KTTOT,THCAP,TFRTS,TJAC,F,AXLTH,AXPOS,AN                QFOM0010
      SIGMA = 5.669E-8                                                  QFOM0011
C                                                                       QFOM0012
C                                                                       QFOM0013
C     Initialize the total node counter (L)                             QFOM0014
C                                                                       QFOM0015
      L = 0                                                             QFOM0016
C                                                                       QFOM0017
C     Sweep through the axial nodes (K)                                 QFOM0018
C                                                                       QFOM0019
      DO 10 K=1,KTOT                                                    QFOM0020
         DZTOT = (DZA(K) + DZB(K))/2.0                                  QFOM0021
C                                                                       QFOM0022
C     Sweep through the circumferential nodes (J) in the tank wall.     QFOM0023
C                                                                       QFOM0024
         DO 20 J=1,JTOT1                                                QFOM0025
C                                                                       QFOM0026
C     Increment the total node count (L)                                QFOM0027
C                                                                       QFOM0028
            L = L + 1                                                   QFOM0029
            ANTOT = (DTHA(J) + DTHB(J))/2.0                             QFOM0030
            SAREAO = RO*ANTOT*DZTOT                                     QFOM0031
            SAREAI = RI*ANTOT*DZTOT                                     QFOM0032
            VOLUM=RAV*ANTOT*THK*DZTOT                                   QFOM0033
C                                                                       QFOM0034
C     Calculate the factor (FACI) that multiplies Hottel's crossed      QFOM0035
C     string view factor to account for axial position of surface       QFOM0036
C     element.                                                          QFOM0037
C                                                                       QFOM0038
            HEIGHT=RI*(COS(AN(J))-COS(AN(JTOT)))                        QFOM0039
            THII=ATAN((AXLTH-AXPOS(K))/HEIGHT)                          QFOM0040
            BETA=ATAN((AXLTH+AXPOS(K))/HEIGHT)                          QFOM0041
            FACI=0.5*(SIN(THII)+SIN(BETA))                              QFOM0042
            CAP=THCAP*VOLUM                                             QFOM0043
C                                                                       QFOM0044
C     Calculate conductances to prescribed boundary temperatures.       QFOM0045
C                                                                       QFOM0046
            CC(2)=0.0                                                   QFOM0047
            IF(J.EQ.JTOT1) CC(2)=TC*THK*DZTOT/(RAV*DTHB(J))             QFOM0048
            CC(7) = SAREAI*HXI(J,K)                                     QFOM0049
            CC(8) = SAREAO*HXO(J,K)                                     QFOM0050
            CPROP=SIGMA/(1.0/(SR*SAREAI)+1.0/(SRL*AREAL)+1.0/(F(J)      QFOM0051
     +      *FACI*SAREAI))                                              QFOM0052
C                                                                       QFOM0053
C     Calculate the Lth entry in the right-hand side vector.            QFOM0054
C                                                                       QFOM0055
            D(L) = -REXCO*SAREAO*((T(L)**4-TF**4)-4.*((TJAC(L)**3)*     QFOM0056
     *[illegible]*TPROP*CC(7)*(T-CPROP*((T(L)**4-TPROP**4)-4.*          QFOM0057
     $((TJAC(L)**3.*T(L))) + CAP*TPRTS(J,K) + CC(2)*TPROP             QFOM0058
   60      CONTINUE                                                     QFOM0059
   70    CONTINUE                                                       QFOM0060
C                                                                       QFOM0061
C     Sweep through the radial nodes (K) in the endcap.                 QFOM0062
C                                                                       QFOM0063
        DO 80 K=KTOT1,KTTOT                                             QFOM0064
           I = KTTOT - K + 1                                            QFOM0065
C                                                                       QFOM0066
C     Sweep through the circumferential nodes (J).                      QFOM0067
C                                                                       QFOM0068
           DO 90 J=1,JTOT1                                              QFOM0069
C                                                                       QFOM0070
C     Increment the total node count (L)                                QFOM0071
C                                                                       QFOM0072
              L = L + 1                                                 QFOM0073
              ANTOT = (DTHA(J) + DTHB(J))/2.0                           QFOM0074
              SAREA = DR*RAD(I)*ANTOT                                   QFOM0075
              VOLUM=SARFA*THK                                           QFOM0076
              CAP=THCAP*VOLUM                                           QFOM0077
C                                                                       QFOM0078
C     Calculate conductances to prescribed boundary temperatures.       QFOM0079
C                                                                       QFOM0080
              CE(4)=0.0                                                 QFOM0081
              IF(J.EQ.JTOT1) CE(4)=TC*THK*DR/(RAD(I)*DTHB(J))           QFOM0082
              CE(5) = SAREA*HXO(J,K)                                    QFOM0083
              CE(6) = SAREA*HXI(J,K)                                    QFOM0084
              RADFX = SIGMA / (SRLA+1.0/(SAREA*FEI)+1.0/(SR*SARFA))     QFOM0085
C                                                                       QFOM0086
C     Calculate the right-hand side term in the finite-difference       QFOM0087
C     equation for the Lth node.                                        QFOM0088
C                                                                       QFOM0089
              B(L) = -REXCO*SARFA*((T(L)**4-TF**4)-4.*((TJAC(L)**3)*T(L))QFOM0090
     $        -RADEX*((T(L)**4-TPROP**4)-4.*((TJAC(L)**3)*T(L)))QFOM0091
     $        +CE(5)*TF+CE(6)*TPROP+CAP*TPRTS(J,K)                      QFOM0092
   90      CONTINUE                                                     QFOM0093
   80    CONTINUE                                                       QFOM0094
C                                                                       QFOM0095
         RETURN                                                         QFOM0096
         END                                                            QFOM0097
                                                                        QFOM0098
```

LISTING 5

```
17:44 SEP 29 '82 VIEWFJ.XCCDAVIS
      SUBROUTINE VIEWFA(AN,F ,JTOT)
C
C   This subroutine calculates view factors for circumferential
C   nodes in the vapor-covered tank wall viewing the liquid
C   surface. Hottel's crossed string method is used for this purpose.
C
      DIMENSION AN(30),F(20)
       JTOT1=JTOT-1
C
C   Sweep through circumferential nodes (J). The last node, JTOT1, is
C   the node just above the liquid surface.
C
      DO 5 J=1,JTOT1
C
C   Calculate the initial and final angles, designated THET1I and
C   THET1F respectively, bounding the Jth surface element.
C
         THET1I = 0.0
         IF (J .NE. 1) THET1I = (AN(J) + AN(J-1))/2.0
         THET1F = (AN(J) + AN(J+1))/2.0
         ARCLNJ = THET1F - THET1I
C
C   Calculate the initial and final angles at which the liquid surface
C   intersects the tank wall.
C
           THET2I = AN(JTOT)
           THET2F = 6.28318 - AN(JTOT)
C
C   Calculate normalized crossed and uncrosed string lengths for the
C   Jth surface element viewing the liquid surface..
C
           CSFF = SQRT(1. - COS(THET2F-THET1F))
           CSII = SQRT(1. - COS(THET2I-THET1I))
           CSFI = SQRT(1. - COS(THET2F-THET1I))
           CSIF = SQRT(1. - COS(THET2I-THET1F))
C
C   Calculate the view factor for the Jth surface element viewing the
C   liquid surface.
C
           F(J) = (CSFF+CSII-CSFI-CSIF)/(1.4142*(ARCLNJ))
C
5     CONTINUE
C
      RETURN
      END
```

```
18:22 SEP 29 '82 TINITL.XCCDAVIS
      SUBROUTINE TINITL(TINIT,T,IPRTS,JTOT,KTOT,JTOT1,KTTOT)         TINI0000
C                                                                    TINI0001
C     This subroutine initializes the temperatures of the nodes in the TINI0002
C     tank car for the first time step.                              TINI0003
C                                                                    TINI0004
      DIMENSION T(600),IPRTS(20,32)                                  TINI0005
C                                                                    TINI0006
      L=0                                                            TINI0007
C                                                                    TINI0008
      DO 1 K=1,KTTOT                                                 TINI0009
         DO 2 J=1,JTOT1                                              TINI0010
            L=L+1                                                    TINI0011
         IPRTS(J,K)=TINIT                                            TINI0012
2        T(L) = TINIT                                                TINI0013
1     CONTINUE                                                       TINI0014
C                                                                    TINI0015
      RETURN                                                         TINI0016
      END                                                            TINI0017
```

LISTING 6

```
18:22 SEP 29 '82 ZERJ.XCCDAVIS
      SUBROUTINE ZERO (CX,D,NPAR,NNUM)                                  ZER00000
C                                                                       ZER00001
C   THIS SUBROUTINE ZEROES THE COEFFICIENT AND RIGHT-HAND SIDE MATRICES ZER00002
C   FOR THE SYSTEM OF FINITE-DIFFERENCE EQUATIONS.                      ZER00003
C                                                                       ZER00004
      DIMENSION CX(12000),D(600)                                        ZER00005
C                                                                       ZER00006
      DO 10 I=1,NNUM                                                    ZER00007
         D(I) = 0.0                                                     ZER00008
10    CONTINUE                                                          ZER00009
C                                                                       ZER00010
         DO 15 J=1,NPAR                                                 ZER00011
         CX(J)=0.0                                                      ZER00012
15       CONTINUE                                                       ZER00013
C                                                                       ZER00014
      RETURN                                                            ZER00015
      END                                                               ZER00016
```

LISTING 7

LISTING 8

```
21:00 SEP 28 '82 CONMAG.XCCDAVIS

      SUBROUTINE CONMAG (CBW,CX,MBW,KL,L,NDIAG,JTOT1,JP)
C   SUBROUTINE CONMAG (ACRONYM FOR 'CONDUCTANCE MATRIX GENERATION')
C   TRANSFERS ELEMENTS OF THE VECTOR CBW, WHICH CONTAINS ENTRIES
C   FOUND WITHIN THE LEFT-HAND BANDWIDTH OF A PARTICULAR ROW (L) IN
C   THE CONDUCTANCE MATRIX, TO A SINGLY-SUBSCRIPTED FORM OF THE BANDED
C   CONDUCTANCE MATRIX (CX). A POINTER VECTOR (NDIAG) LOCATES DIAGONAL
C   ELEMENTS WITHIN CX. THE NTH ELEMENT OF NDIAG IDENTIFIES THE
C   LOCATION OF THE NTH DIAGONAL ELEMENT IN THE ARRAY CX. ELEMENTS
C   CONTAINED WITHIN THE LEFT-HAND BANDWIDTH OF A PARTICULAR ROW IN
C   THE CONDUCTANCE MATRIX ARE STORED AT THE END OF CBW RATHER THAN
C   AT THE BEGINNING (IE. THE DIAGONAL ELEMENT OF THE ROW IS FOUND IN
C   THE LOCATION CBW(MBW)).
      DIMENSION CBW(100),CX(12000),NDIAG(600),JP(3)
C   CALCULATE (LEFT-HAND BANDWIDTH - 1) OF ROW L (NBW) BY FINDING
C   THE LARGEST JP(JJ).
      NBW=1
      IF(L.EQ.1) NBW=0
      DO 10 JJ=1,3
       IF(JP(JJ).GT.NBW) NBW=JP(JJ)
10    CONTINUE
      LM=MBW-NBW
      LX=0
C   TRANSFER ELEMENTS IN CBW TO CX.
      DO 20 JJ=LM,MBW
       LX=LX+1
       CX(KL+LX)=CBW(JJ)
20    CONTINUE
      KL=KL+LX
C   STORE POSITION OF DIAGONAL ELEMENT OF ROW L IN NDIAG(L).
      NDIAG(L)=KL
      RETURN
      END
```

LISTING 9

```
20:59 SEP 28 '82 CHLSKI.XCCDAVIS

      SUBROUTINE CHLSKI(A,KDIAG,N)                                      CHLS0000
C                                                                       CHLS0001
C  THIS SUBROUTINE USES CHOLESKY'S ALGORITHM TO FACTOR A MATRIX 'A'     CHLS0002
C  INTO THE PRODUCT OF A LOWER TRIANGULAR MATRIX AND ITS TRANSPOSE.     CHLS0003
C  THE MATRIX 'A', WHICH MUST BE POSITIVE-DEFINITE, IS STORED AS A      CHLS0004
C  VECTOR IN JENNING'S PROFILE STORAGE MODE. ONLY THE ELEMENTS FROM     CHLS0005
C  THE 1ST NON-ZERO ENTRY IN EACH ROW UP TO AND INCLUDING THE DIAGONAL  CHLS0006
C  TERM ARE STORED AND THE ROWS ARE LINED UP END TO END IN 'A'. A       CHLS0007
C  POINTER VECTOR KDIAG PROVIDES THE LOCATION OF EACH DIAGONAL ELEMENT  CHLS0008
C  IN 'A'. THE LOWER TRIANGULAR MATRIX OBTAINED FROM THE FACTORIZATION  CHLS0009
C  OF 'A' OVERWRITES 'A' IN THIS SUBROUTINE.                            CHLS0010
C                                                                       CHLS0011
      DIMENSION KDIAG(600),A(12000)                                     CHLS0012
      A(1)=SQRT(A(1))                                                   CHLS0013
      DO 1 I=2,N                                                        CHLS0014
       KI=KDIAG(I)-I                                                    CHLS0015
       L=KDIAG(I-1)-KI+1                                                CHLS0016
       DO 2 J=L,I                                                       CHLS0017
        X=A(KI+J)                                                       CHLS0018
        KJ=KDIAG(J)-J                                                   CHLS0019
        IF(J.EQ.1) GO TO 2                                              CHLS0020
        LBAR=KDIAG(J-1)-KJ+1                                            CHLS0021
        LBAR=MAX0(L,LBAR)                                               CHLS0022
        IF(LBAR.EQ.J) GO TO 2                                           CHLS0023
        MM=J-1                                                          CHLS0024
        DO 3 K=LBAR,MM                                                  CHLS0025
3        X=X-A(KI+K)*A(KJ+K)                                            CHLS0026
2      A(KI+J)=X/A(KJ+J)                                                CHLS0027
1     A(KI+I)=SQRT(X)                                                   CHLS0028
      RETURN                                                            CHLS0029
      END                                                               CHLS0030
```

```
21:00 SEP 28 '82 SUBSTI.XCCDAVIS
      SUBROUTINE SUB (A,B,KDIAG,N)                                      SUBS0000
C                                                                       SUBS0001
C  THIS SUBROUTINE PERFORMS THE FORWARD AND BACKWARD SUBSTITUTIONS      SUBS0002
C  NEEDED TO OBTAIN THE SOLUTION VECTOR (T) FROM THE FACTORED           SUBS0003
C  COEFFICIENT MATRIX 'A' AND THE RIGHT-HAND SIDE VECTOR 'B'.           SUBS0004
C                                                                       SUBS0005
      DIMENSION KDIAG(600),A(12000),B(600),T(600)                       SUBS0006
      B(1)=B(1)/A(1)                                                    SUBS0007
      DO 4 I=2,N                                                        SUBS0008
       KI=KDIAG(I)-I                                                    SUBS0009
       L=KDIAG(I-1)-KI+1                                                SUBS0010
       X=B(I)                                                           SUBS0011
       IF(L.EQ.I) GO TO 4                                               SUBS0012
       MM=I-1                                                           SUBS0013
       DO 5 J=L,MM                                                      SUBS0014
5       X=X-A(KI+J)*B(J)                                                SUBS0015
4     B(I)=X/A(KI+I)                                                    SUBS0016
      DO 6 IT=2,N                                                       SUBS0017
       I=N+2-IT                                                         SUBS0018
       KI=KDIAG(I)-I                                                    SUBS0019
       X=B(I)/A(KI+I)                                                   SUBS0020
       B(I)=X                                                           SUBS0021
       L=KDIAG(I-1)-KI+1                                                SUBS0022
       IF(L.EQ.I) GO TO 6                                               SUBS0023
       MM=I-1                                                           SUBS0024
       DO 7 K=L,MM                                                      SUBS0025
7       B(K)=B(K)-X*A(KI+K)                                             SUBS0026
6     CONTINUE                                                          SUBS0027
      B(1)=B(1)/A(1)                                                    SUBS0028
      RETURN                                                            SUBS0029
      END                                                               SUBS0030
```

LISTING 10

```
EPSI =     .60000EPSL =     .80000FEL =     .32000EPSLN =     .50000THK =     .01588
EO =    1.52440RI =    1.50980IC =    30.00000TPROP =   325.00000TF =  1200.00000
TINIT =  325.00000REXCO =  .463800E-07MAXIT =    15NRNUD =     6HXIN =   10.00000HXOUT =    10.00000
NDT=  1            DT(NDT)=  10.00000          NTC(NDT)= 40           NEXT=  1

NDT=  2            DT(NDT)=  20.00000          NTC(NDT)=120           NEXT=  0

DENS=7800.00000       SPHT= 470.00000       FINAL TIME=1120.00000 SECS.      NUPDAT=  1       NSPEC= 20

****** DATA READ IN SUBROUTINE DTH01 ******

JTOT= 18            ATOT=   1.57000

N=  1           DTH=     .03330          IN(N)=  4           NEXT=  1

N=  2           DTH=     .06660          IN(N)=  7           NEXT=  1

N=  3           DTH=     .13330          IN(N)= 10           NEXT=  1

N=  4           DTH=     .28500          IN(N)= 12           NEXT=  1

N=  5           DTH=     .06660          IN(N)= 15           NEXT=  0

****** AXIAL GRID DATA READ IN SUBROUTINE DZ ******

K=  1           DZ=  .0500000         KCH(K)=  6          NEXT= 1

K=  2           DZ=  .1000000         KCH(K)= 11          NEXT= 1

K=  3           DZ=  .2000000         KCH(K)= 16          NEXT= 1

K=  4           DZ=  .4000000         KCH(K)= 21          NEXT= 1

K=  5           DZ= 1.3125000         KCH(K)= 25          NEXT= 0

TIME=  10.00000SECS            NO. OF ITERATIONS=     2

TIME=  20.00000SECS            NO. OF ITERATIONS=     2

TIME=  30.00000SECS            NO. OF ITERATIONS=     2

TIME=  40.00000SECS            NO. OF ITERATIONS=     2

TIME=  50.00000SECS            NO. OF ITERATIONS=     2
K =      1          J =      1           T =     413.56308
K =      1          J =      2           T =     413.56317
K =      1          J =      3           T =     413.56323
K =      1          J =      4           T =     413.56317
K =      1          J =      5           T =     413.56339
K =      1          J =      6           T =     413.56406
K =      1          J =      7           T =     413.56497
```

RESULTS OF SAMPLE ANALYSIS
PERFORMED WITH THE
CONVENTIONAL NEWTON-RAPHSON
METHOD.

```
K =  1        J =  8        T =  413.56647
K =  1        J =  9        T =  413.56882
K =  1        J = 10        T =  413.57291
K =  1        J = 11        T =  413.58075
K =  1        J = 12        T =  413.59045
K =  1        J = 13        T =  413.59650
K =  1        J = 14        T =  413.59992
K =  1        J = 15        T =  413.58420
K =  1        J = 16        T =  413.12561
K =  1        J = 17        T =  406.34473
K =  2        J =  1        T =  413.56320
K =  3        J =  1        T =  413.56326
K =  4        J =  1        T =  413.56329
K =  5        J =  1        T =  413.56326
K =  6        J =  1        T =  413.56290
K =  7        J =  1        T =  413.56278
K =  8        J =  1        T =  413.56281
K =  9        J =  1        T =  413.56284
K = 10        J =  1        T =  413.56284
K = 11        J =  1        T =  413.56357
K = 12        J =  1        T =  413.56363
K = 13        J =  1        T =  413.56372
K = 14        J =  1        T =  413.56372
K = 15        J =  1        T =  413.56378
K = 16        J =  1        T =  413.56369
K = 17        J =  1        T =  413.56372
K = 18        J =  1        T =  413.56384
K = 19        J =  1        T =  413.56412
K = 20        J =  1        T =  413.56439
K = 21        J =  1        T =  413.56461
K = 22        J =  1        T =  413.56607
K = 23        J =  1        T =  413.57138
K = 24        J =  1        T =  413.58890
K = 25        J =  1        T =  413.65195
K = 26        J =  1        T =  413.24454
K = 27        J =  1        T =  413.24124
K = 28        J =  1        T =  413.24118
K = 29        J =  1        T =  413.24164
K = 30        J =  1        T =  413.24231
K = 31        J =  1        T =  413.24918
TIME=  60.00000SECS          NO. OF ITERATIONS=    2

TIME=  70.00000SECS          NO. OF ITERATIONS=    2

TIME=  80.00000SECS          NO. OF ITERATIONS=    2

TIME=  90.00000SECS          NO. OF ITERATIONS=    2

TIME= 100.00000SECS          NO. OF ITERATIONS=    2
K =  1        J =  1        T =  498.96341
K =  1        J =  2        T =  498.96375
K =  1        J =  3        T =  498.96396
K =  1        J =  4        T =  498.96417
```

```
K =    1        J =    5        T =   498.96567
K =    1        J =    6        T =   498.96808
K =    1        J =    7        T =   498.97180
K =    1        J =    8        T =   498.97882
K =    1        J =    9        T =   498.98959
K =    1        J =   10        T =   499.00839
K =    1        J =   11        T =   499.01450
K =    1        J =   12        T =   499.08966
K =    1        J =   13        T =   499.11801
K =    1        J =   14        T =   499.13168
K =    1        J =   15        T =   498.98416
K =    1        J =   16        T =   496.61087
K =    1        J =   17        T =   475.40265
K =    2        J =    1        T =   498.96375
K =    3        J =    1        T =   498.96381
K =    4        J =    1        T =   498.96387
K =    5        J =    1        T =   498.96378
K =    6        J =    1        T =   498.96304
K =    7        J =    1        T =   498.96405
K =    8        J =    1        T =   498.96375
K =    9        J =    1        T =   498.96381
K =   10        J =    1        T =   498.96387
K =   11        J =    1        T =   498.96448
K =   12        J =    1        T =   498.96469
K =   13        J =    1        T =   498.96484
K =   14        J =    1        T =   498.96500
K =   15        J =    1        T =   498.96524
K =   16        J =    1        T =   498.96518
K =   17        J =    1        T =   498.96558
K =   18        J =    1        T =   498.96631
K =   19        J =    1        T =   498.96735
K =   20        J =    1        T =   498.96866
K =   21        J =    1        T =   498.97025
K =   22        J =    1        T =   498.97879
K =   23        J =    1        T =   499.00296
K =   24        J =    1        T =   499.08374
K =   25        J =    1        T =   499.37460
K =   26        J =    1        T =   498.61345
K =   27        J =    1        T =   498.60431
K =   28        J =    1        T =   498.60422
K =   29        J =    1        T =   498.60510
K =   30        J =    1        T =   498.60611
K =   31        J =    1        T =   498.61459
TIME= 110.00000SECS         NO. OF ITERATIONS=    2

TIME= 120.00000SECS         NO. OF ITERATIONS=    2

TIME= 130.00000SECS         NO. OF ITERATIONS=    2

TIME= 140.00000SECS         NO. OF ITERATIONS=    2

TIME= 150.00000SECS         NO. OF ITERATIONS=    2

K =    1        J =    1        T =   580.18536
```

```
K =     1         J =    2         T =   580.18585
K =     1         J =    3         T =   580.18652
K =     1         J =    4         T =   580.18765
K =     1         J =    5         T =   580.19165
K =     1         J =    6         T =   580.19760
K =     1         J =    7         T =   580.20743
K =     1         J =    8         T =   580.22583
K =     1         J =    9         T =   580.25479
K =     1         J =   10         T =   580.30502
K =     1         J =   11         T =   580.40134
K =     1         J =   12         T =   580.52252
K =     1         J =   13         T =   580.59769
K =     1         J =   14         T =   580.62677
K =     1         J =   15         T =   580.09314
K =     1         J =   16         T =   574.07687
K =     1         J =   17         T =   534.49219
K =     2         J =    1         T =   580.18343
K =     3         J =    1         T =   580.18567
K =     4         J =    1         T =   580.18567
K =     5         J =    1         T =   580.18546
K =     6         J =    1         T =   580.18506
K =     7         J =    1         T =   580.18713
K =     8         J =    1         T =   580.18686
K =     9         J =    1         T =   580.18695
K =    10         J =    1         T =   580.18707
K =    11         J =    1         T =   580.18729
K =    12         J =    1         T =   580.18756
K =    13         J =    1         T =   580.18796
K =    14         J =    1         T =   580.18839
K =    15         J =    1         T =   580.18897
K =    16         J =    1         T =   580.18921
K =    17         J =    1         T =   580.19009
K =    18         J =    1         T =   580.19235
K =    19         J =    1         T =   580.19507
K =    20         J =    1         T =   580.19846
K =    21         J =    1         T =   580.20294
K =    22         J =    1         T =   580.22769
K =    23         J =    1         T =   580.29224
K =    24         J =    1         T =   580.30790
K =    25         J =    1         T =   581.28824
K =    26         J =    1         T =   580.25919
K =    27         J =    1         T =   580.23688
K =    28         J =    1         T =   580.23676
K =    29         J =    1         T =   580.23822
K =    30         J =    1         T =   580.23950
K =    31         J =    1         T =   580.21954
TIME= 160.00000SECS          NO. OF ITERATIONS=    2


TIME= 170.00000SECS          NO. OF ITERATIONS=    2


TIME= 180.00000SECS          NO. OF ITERATIONS=    2


TIME= 190.00000SECS          NO. OF ITERATIONS=    2
```

```
                                  .
                                  .
                                  .
                                  .
                                  .
K =    21          J =     1           T =  1023.52988
K =    22          J =     1           T =  1024.19247
K =    23          J =     1           T =  1025.88913
K =    24          J =     1           T =  1031.65588
K =    25          J =     1           T =  1054.05975
K =    26          J =     1           T =  1056.41711
K =    27          J =     1           T =  1056.46182
K =    28          J =     1           T =  1056.46121
K =    29          J =     1           T =  1056.45978
K =    30          J =     1           T =  1056.36002
K =    31          J =     1           T =  1047.81055
TIME= 730.00000SECS          NO. OF ITERATIONS=    2

TIME= 750.00000SECS          NO. OF ITERATIONS=    2

TIME= 770.00000SECS          NO. OF ITERATIONS=    2

TIME= 790.00000SECS          NO. OF ITERATIONS=    2

TIME= 810.00000SECS          NO. OF ITERATIONS=    2
K =     1          J =     1           T =  1037.15353
K =     1          J =     2           T =  1037.16022
K =     1          J =     3           T =  1037.18201
K =     1          J =     4           T =  1037.22281
K =     1          J =     5           T =  1037.32507
K =     1          J =     6           T =  1037.49091
K =     1          J =     7           T =  1037.76514
K =     1          J =     8           T =  1038.30637
K =     1          J =     9           T =  1039.14456
K =     1          J =    10           T =  1040.59500
K =     1          J =    11           T =  1043.43695
K =     1          J =    12           T =  1047.01880
K =     1          J =    13           T =  1049.04144
K =     1          J =    14           T =  1049.07016
K =     1          J =    15           T =  1036.33932
K =     1          J =    16           T =   985.87973
K =     1          J =    17           T =   819.03607
K =     2          J =     1           T =  1037.15292
K =     3          J =     1           T =  1037.15292
K =     4          J =     1           T =  1037.15326
K =     5          J =     1           T =  1037.15387
K =     6          J =     1           T =  1037.15524
K =     7          J =     1           T =  1037.15939
K =     8          J =     1           T =  1037.16171
K =     9          J =     1           T =  1037.16449
K =    10          J =     1           T =  1037.16776
K =    11          J =     1           T =  1037.17133
K =    12          J =     1           T =  1037.18344
K =    13          J =     1           T =  1037.19519
K =    14          J =     1           T =  1037.20926
K =    15          J =     1           T =  1037.22595
K =    16          J =     1           T =  1037.24442
K =    17          J =     1           T =  1037.29199
```

```
K =    18          J =    1          T =  1037.35394
K =    19          J =    1          T =  1037.43298
K =    20          J =    1          T =  1037.33271
K =    21          J =    1          T =  1037.66403
K =    22          J =    1          T =  1038.39056
K =    23          J =    1          T =  1040.25156
K =    24          J =    1          T =  1046.58786
K =    25          J =    1          T =  1071.37558
K =    26          J =    1          T =  1074.31506
K =    27          J =    1          T =  1074.39505
K =    28          J =    1          T =  1074.39560
K =    29          J =    1          T =  1074.39291
K =    30          J =    1          T =  1074.27289
K =    31          J =    1          T =  1064.93271
TIME= 830.00000SECS          NO. OF ITERATIONS=    2

TIME= 850.00000SECS          NO. OF ITERATIONS=    2

TIME= 870.00000SECS          NO. OF ITERATIONS=    2

TIME= 890.00000SECS          NO. OF ITERATIONS=    2

TIME= 910.00000SECS          NO. OF ITERATIONS=    2
K =     1          J =    1          T =  1045.16486
K =     1          J =    2          T =  1045.17200
K =     1          J =    3          T =  1045.19495
K =     1          J =    4          T =  1045.23807
K =     1          J =    5          T =  1045.34628
K =     1          J =    6          T =  1045.52167
K =     1          J =    7          T =  1045.81131
K =     1          J =    8          T =  1046.38391
K =     1          J =    9          T =  1047.27060
K =     1          J =   10          T =  1048.80371
K =     1          J =   11          T =  1051.81140
K =     1          J =   12          T =  1055.60678
K =     1          J =   13          T =  1057.74286
K =     1          J =   14          T =  1057.81064
K =     1          J =   15          T =  1044.99051
K =     1          J =   16          T =   994.16632
K =     1          J =   17          T =   825.42679
K =     2          J =    1          T =  1045.16431
K =     3          J =    1          T =  1045.16400
K =     4          J =    1          T =  1045.16449
K =     5          J =    1          T =  1045.16528
K =     6          J =    1          T =  1045.16653
K =     7          J =    1          T =  1045.17102
K =     8          J =    1          T =  1045.17346
K =     9          J =    1          T =  1045.17645
K =    10          J =    1          T =  1045.17981
K =    11          J =    1          T =  1045.18384
K =    12          J =    1          T =  1045.19672
K =    13          J =    1          T =  1045.20901
K =    14          J =    1          T =  1045.22394
```

```
K =    15          J =     1          T =  1045.24152
K =    16          J =     1          T =  1045.26126
K =    17          J =     1          T =  1045.31152
K =    18          J =     1          T =  1045.37711
K =    19          J =     1          T =  1045.46048
K =    20          J =     1          T =  1045.56592
K =    21          J =     1          T =  1045.70453
K =    22          J =     1          T =  1046.47265
K =    23          J =     1          T =  1048.44049
K =    24          J =     1          T =  1055.14920
K =    25          J =     1          T =  1081.52100
K =    26          J =     1          T =  1084.85983
K =    27          J =     1          T =  1084.96762
K =    28          J =     1          T =  1084.96948
K =    29          J =     1          T =  1084.96685
K =    30          J =     1          T =  1084.83243
K =    31          J =     1          T =  1075.08572
TIME= 930.00000SECS            NO. OF ITERATIONS=    2

TIME= 950.00000SECS            NO. OF ITERATIONS=    2

TIME= 970.00000SECS            NO. OF ITERATIONS=    2

TIME= 990.00000SECS            NO. OF ITERATIONS=    2

TIME=1010.00000SECS            NO. OF ITERATIONS=    2
K =     1          J =     1          T =  1049.66763
K =     1          J =     2          T =  1049.67490
K =     1          J =     3          T =  1049.69879
K =     1          J =     4          T =  1049.74310
K =     1          J =     5          T =  1049.85498
K =     1          J =     6          T =  1050.03635
K =     1          J =     7          T =  1050.33569
K =     1          J =     8          T =  1050.92783
K =     1          J =     9          T =  1051.84479
K =     1          J =    10          T =  1053.43021
K =     1          J =    11          T =  1056.54263
K =     1          J =    12          T =  1060.47345
K =     1          J =    13          T =  1062.68103
K =     1          J =    14          T =  1062.78671
K =     1          J =    15          T =  1049.99487
K =     1          J =    16          T =   999.06455
K =     1          J =    17          T =   829.30216
K =     2          J =     1          T =  1049.66699
K =     3          J =     1          T =  1049.66656
K =     4          J =     1          T =  1049.66696
K =     5          J =     1          T =  1049.66776
K =     6          J =     1          T =  1049.66916
K =     7          J =     1          T =  1049.67374
K =     8          J =     1          T =  1049.67636
K =     9          J =     1          T =  1049.67938
K =    10          J =     1          T =  1049.68292
K =    11          J =     1          T =  1049.68719
```

```
K =   12        J =   1        T =  1049.70035
K =   13        J =   1        T =  1049.71335
K =   14        J =   1        T =  1049.72870
K =   15        J =   1        T =  1049.74692
K =   16        J =   1        T =  1049.76740
K =   17        J =   1        T =  1049.81946
K =   18        J =   1        T =  1049.88681
K =   19        J =   1        T =  1049.97327
K =   20        J =   1        T =  1050.08212
K =   21        J =   1        T =  1050.22528
K =   22        J =   1        T =  1051.01962
K =   23        J =   1        T =  1053.05472
K =   24        J =   1        T =  1059.99835
K =   25        J =   1        T =  1087.38574
K =   26        J =   1        T =  1090.78624
K =   27        J =   1        T =  1091.11505
K =   28        J =   1        T =  1091.11740
K =   29        J =   1        T =  1091.11362
K =   30        J =   1        T =  1090.97147
K =   31        J =   1        T =  1081.04825

TIME=1030.00000SECS          NO. OF ITERATIONS=    2

TIME=1050.00000SECS          NO. OF ITERATIONS=    2

TIME=1070.00000SECS          NO. OF ITERATIONS=    2

TIME=1090.00000SECS          NO. OF ITERATIONS=    2

TIME=1110.00000SECS          NO. OF ITERATIONS=    2
K =    1        J =   1        T =  1052.18146
K =    1        J =   2        T =  1052.18884
K =    1        J =   3        T =  1052.21338
K =    1        J =   4        T =  1052.25848
K =    1        J =   5        T =  1052.37256
K =    1        J =   6        T =  1052.55786
K =    1        J =   7        T =  1052.84292
K =    1        J =   8        T =  1053.46722
K =    1        J =   9        T =  1054.40283
K =    1        J =  10        T =  1056.02017
K =    1        J =  11        T =  1059.19693
K =    1        J =  12        T =  1063.21185
K =    1        J =  13        T =  1065.46448
K =    1        J =  14        T =  1065.60245
K =    1        J =  15        T =  1052.87601
K =    1        J =  16        T =  1001.94009
K =    1        J =  17        T =   831.62515
K =    2        J =   1        T =  1052.18073
K =    3        J =   1        T =  1052.18051
K =    4        J =   1        T =  1052.18088
K =    5        J =   1        T =  1052.18182
K =    6        J =   1        T =  1052.18326
K =    7        J =   1        T =  1052.18781
K =    8        J =   1        T =  1052.19043
```

```
K =     9           J =     1.          T =  1052.19339
K =    10           J =     1           T =  1052.19705
K =    11           J =     1           T =  1052.20148
K =    12           J =     1           T =  1052.21478
K =    13           J =     1           T =  1052.22830
K =    14           J =     1           T =  1052.24374
K =    15           J =     1           T =  1052.26248
K =    16           J =     1           T =  1052.28354
K =    17           J =     1           T =  1052.33658
K =    18           J =     1           T =  1052.40330
K =    19           J =     1           T =  1052.49326
K =    20           J =     1           T =  1052.60443
K =    21           J =     1           T =  1052.75018
K =    22           J =     1           T =  1053.56067
K =    23           J =     1           T =  1055.63730
K =    24           J =     1           T =  1062.72589
K =    25           J =     1           T =  1090.74927
K =    26           J =     1           T =  1094.51642
K =    27           J =     1           T =  1094.66016
K =    28           J =     1           T =  1094.66318
K =    29           J =     1           T =  1094.65909
K =    30           J =     1           T =  1094.31215
K =    31           J =     1           T =  1084.53348
TIME=1130.00000SECS           NO. OF ITERATIONS=    2
```

```
EPSI =     .60000EPSL =     .80000FEL =     .32000EPSLN =     .50000THK =     .01588
RO =    1.52440RI =    1.50980TC =   30.00000TPRUP =  325.00000TF = 1200.00000
TINIT =  325.00000REXCO =  .463800E-07MAXIT =      15NRNOD =      6HXIN =   10.00000HXOUT =   10.00000
NDT=  1           DT(NDT)=  10.00000         NTC(NDT)= 40          NEXT=  1

NDT=  2           DT(NDT)=  20.00000         NTC(NDT)=120          NEXT=  0

DENS=7800.00000      SPHT= 470.00000      FINAL TIME=1120.00000 SECS.      NUPDAT=  0      NSPEC= 20

****** DATA READ IN SUBROUTINE DTH01 ******

JTOT= 18          ATOT=   1.57000

N=  1           DTH=     .03330          IN(N)=  4          NEXT=  1

N=  2           DTH=     .06660          IN(N)=  7          NEXT=  1

N=  3           DTH=     .13330          IN(N)= 10          NEXT=  1

N=  4           DTH=     .28500          IN(N)= 12          NEXT=  1

N=  5           DTH=     .06660          IN(N)= 15          NEXT=  0

****** AXIAL GRID DATA READ IN SUBROUTINE DZ ******

K=  1           DZ=  .0500000          KCH(K)=  6          NEXT= 1

K=  2           DZ=  .1000000          KCH(K)= 11          NEXT= 1

K=  3           DZ=  .2000000          KCH(K)= 16          NEXT= 1

K=  4           DZ=  .4000000          KCH(K)= 21          NEXT= 1

K=  5           DZ= 1.3125000          KCH(K)= 25          NEXT= 0

TIME=  10.00000SECS          NO. OF ITERATIONS=     3


TIME=  20.00000SECS          NO. OF ITERATIONS=     2


TIME=  30.00000SECS          NO. OF ITERATIONS=     2


TIME=  40.00000SECS          NO. OF ITERATIONS=     2


TIME=  50.00000SECS          NO. OF ITERATIONS=     2

K =     1          J =     1          T =   413.36456
K =     1          J =     2          T =   413.36453
K =     1          J =     3          T =   413.36453
K =     1          J =     4          T =   413.36462
K =     1          J =     5          T =   413.36502
K =     1          J =     6          T =   413.36591
K =     1          J =     7          T =   413.36774
```

RESULTS OF SAMPLE ANALYSIS
PERFORMED WITH THE MODIFIED
NEWTON-RAPHSON METHOD.

```
K =    1        J =    8        T =   413.37051
K =    1        J =    9        T =   413.37494
K =    1        J =   10        T =   413.38278
K =    1        J =   11        T =   413.39752
K =    1        J =   12        T =   413.41583
K =    1        J =   13        T =   413.42722
K =    1        J =   14        T =   413.43399
K =    1        J =   15        T =   413.42148
K =    1        J =   16        T =   412.96661
K =    1        J =   17        T =   406.20664
K =    2        J =    1        T =   413.36447
K =    3        J =    1        T =   413.36450
K =    4        J =    1        T =   413.36453
K =    5        J =    1        T =   413.36453
K =    6        J =    1        T =   413.36417
K =    7        J =    1        T =   413.36392
K =    8        J =    1        T =   413.36404
K =    9        J =    1        T =   413.36408
K =   10        J =    1        T =   413.36414
K =   11        J =    1        T =   413.36484
K =   12        J =    1        T =   413.36490
K =   13        J =    1        T =   413.36508
K =   14        J =    1        T =   413.36502
K =   15        J =    1        T =   413.36517
K =   16        J =    1        T =   413.36511
K =   17        J =    1        T =   413.36527
K =   18        J =    1        T =   413.36566
K =   19        J =    1        T =   413.36603
K =   20        J =    1        T =   413.36655
K =   21        J =    1        T =   413.36694
K =   22        J =    1        T =   413.37051
K =   23        J =    1        T =   413.38034
K =   24        J =    1        T =   413.41333
K =   25        J =    1        T =   413.53299
K =   26        J =    1        T =   413.24283
K =   27        J =    1        T =   413.24118
K =   28        J =    1        T =   413.24112
K =   29        J =    1        T =   413.24161
K =   30        J =    1        T =   413.24231
K =   31        J =    1        T =   413.24789
TIME=  60.00000SECS          NO. OF ITERATIONS=    2

TIME=  70.00000SECS          NO. OF ITERATIONS=    2

TIME=  80.00000SECS          NO. OF ITERATIONS=    2

TIME=  90.00000SECS          NO. OF ITERATIONS=    2

TIME= 100.00000SECS          NO. OF ITERATIONS=    2
K =    1        J =    1        T =   498.77216
K =    1        J =    2        T =   498.77240
K =    1        J =    3        T =   498.77252
K =    1        J =    4        T =   498.77280
```

```
K =      1          J =     5          T =    498.77435
K =      1          J =     6          T =    498.77692
K =      1          J =     7          T =    498.78180
K =      1          J =     8          T =    498.78989
K =      1          J =     9          T =    498.80267
K =      1          J =    10          T =    498.82526
K =      1          J =    11          T =    498.86807
K =      1          J =    12          T =    498.92133
K =      1          J =    13          T =    498.95432
K =      1          J =    14          T =    498.97122
K =      1          J =    15          T =    498.82758
K =      1          J =    16          T =    496.46072
K =      1          J =    17          T =    475.28430
K =      2          J =     1          T =    498.77225
K =      3          J =     1          T =    498.77231
K =      4          J =     1          T =    498.77240
K =      5          J =     1          T =    498.77231
K =      6          J =     1          T =    498.77155
K =      7          J =     1          T =    498.77139
K =      8          J =     1          T =    498.77158
K =      9          J =     1          T =    498.77158
K =     10          J =     1          T =    498.77170
K =     11          J =     1          T =    498.77307
K =     12          J =     1          T =    498.77332
K =     13          J =     1          T =    498.77371
K =     14          J =     1          T =    498.77371
K =     15          J =     1          T =    498.77402
K =     16          J =     1          T =    498.77396
K =     17          J =     1          T =    498.77438
K =     18          J =     1          T =    498.77551
K =     19          J =     1          T =    498.77667
K =     20          J =     1          T =    498.77820
K =     21          J =     1          T =    498.77976
K =     22          J =     1          T =    498.79053
K =     23          J =     1          T =    498.81894
K =     24          J =     1          T =    498.91461
K =     25          J =     1          T =    499.25983
K =     26          J =     1          T =    498.61173
K =     27          J =     1          T =    498.60361
K =     28          J =     1          T =    498.60349
K =     29          J =     1          T =    498.60437
K =     30          J =     1          T =    498.60535
K =     31          J =     1          T =    498.57944
TIME= 110.00000SECS          NO. OF ITERATIONS=    2

TIME= 120.00000SECS          NO. OF ITERATIONS=    2

TIME= 130.00000SECS          NO. OF ITERATIONS=    2

TIME= 140.00000SECS          NO. OF ITERATIONS=    2

TIME= 150.00000SECS          NO. OF ITERATIONS=    2
K =      1          J =     1          T =    580.00156
```

```
K =     1          J =     2          T =    580.00198
K =     1          J =     3          T =    580.00263
K =     1          J =     4          T =    580.00372
K =     1          J =     5          T =    580.00742
K =     1          J =     6          T =    580.01367
K =     1          J =     7          T =    580.02478
K =     1          J =     8          T =    580.04431
K =     1          J =     9          T =    580.07504
K =     1          J =    10          T =    580.12903
K =     1          J =    11          T =    580.23175
K =     1          J =    12          T =    580.36029
K =     1          J =    13          T =    580.43955
K =     1          J =    14          T =    580.47180
K =     1          J =    15          T =    579.94281
K =     1          J =    16          T =    573.93610
K =     1          J =    17          T =    534.38944
K =     2          J =     1          T =    580.00150
K =     3          J =     1          T =    580.00165
K =     4          J =     1          T =    580.00171
K =     5          J =     1          T =    580.00168
K =     6          J =     1          T =    580.00089
K =     7          J =     1          T =    580.00082
K =     8          J =     1          T =    580.00104
K =     9          J =     1          T =    580.00107
K =    10          J =     1          T =    580.00140
K =    11          J =     1          T =    580.00333
K =    12          J =     1          T =    580.00378
K =    13          J =     1          T =    580.00455
K =    14          J =     1          T =    580.00476
K =    15          J =     1          T =    580.00537
K =    16          J =     1          T =    580.00552
K =    17          J =     1          T =    580.00644
K =    18          J =     1          T =    580.00903
K =    19          J =     1          T =    580.01190
K =    20          J =     1          T =    580.01544
K =    21          J =     1          T =    580.01968
K =    22          J =     1          T =    580.04688
K =    23          J =     1          T =    580.11511
K =    24          J =     1          T =    580.34515
K =    25          J =     1          T =    581.17722
K =    26          J =     1          T =    580.25198
K =    27          J =     1          T =    580.23383
K =    28          J =     1          T =    580.23377
K =    29          J =     1          T =    580.23511
K =    30          J =     1          T =    580.23584
K =    31          J =     1          T =    579.99674
TIME= 160.00000SECS          NO. OF ITERATIONS=    2

TIME= 170.00000SECS          NO. OF ITERATIONS=    2

TIME= 180.00000SECS          NO. OF ITERATIONS=    2

TIME= 190.00000SECS          NO. OF ITERATIONS=    2
                               .
                               .
                               .
                               .
```

```
K =    21          J =     1          T =  1023.48041
K =    22          J =     1          T =  1024.15134
K =    23          J =     1          T =  1025.84665
K =    24          J =     1          T =  1031.60971
K =    25          J =     1          T =  1053.99655
K =    26          J =     1          T =  1056.36111
K =    27          J =     1          T =  1056.40756
K =    28          J =     1          T =  1056.40463
K =    29          J =     1          T =  1056.40366
K =    30          J =     1          T =  1056.17328
K =    31          J =     1          T =  1038.93802
TIME= 730.00000SECS          NO. OF ITERATIONS=    2

TIME= 750.00000SECS          NO. OF ITERATIONS=    2

TIME= 770.00000SECS          NO. OF ITERATIONS=    2

TIME= 790.00000SECS          NO. OF ITERATIONS=    2

TIME= 810.00000SECS          NO. OF ITERATIONS=    3
K =     1          J =     1          T =  1037.10291
K =     1          J =     2          T =  1037.10974
K =     1          J =     3          T =  1037.13147
K =     1          J =     4          T =  1037.17261
K =     1          J =     5          T =  1037.27530
K =     1          J =     6          T =  1037.44150
K =     1          J =     7          T =  1037.71674
K =     1          J =     8          T =  1038.25873
K =     1          J =     9          T =  1039.09683
K =     1          J =    10          T =  1040.54901
K =     1          J =    11          T =  1043.39243
K =     1          J =    12          T =  1046.97000
K =     1          J =    13          T =  1048.98969
K =     1          J =    14          T =  1049.01889
K =     1          J =    15          T =  1036.29520
K =     1          J =    16          T =   985.84644
K =     1          J =    17          T =   819.01804
K =     2          J =     1          T =  1037.10226
K =     3          J =     1          T =  1037.10236
K =     4          J =     1          T =  1037.10291
K =     5          J =     1          T =  1037.10342
K =     6          J =     1          T =  1037.10498
K =     7          J =     1          T =  1037.10974
K =     8          J =     1          T =  1037.11227
K =     9          J =     1          T =  1037.11490
K =    10          J =     1          T =  1037.11801
K =    11          J =     1          T =  1037.12268
K =    12          J =     1          T =  1037.13614
K =    13          J =     1          T =  1037.14777
K =    14          J =     1          T =  1037.16254
K =    15          J =     1          T =  1037.17892
K =    16          J =     1          T =  1037.19943
K =    17          J =     1          T =  1037.24957
```

```
K =    18          J =    1          T =  1037.31161
K =    19          J =    1          T =  1037.39014
K =    20          J =    1          T =  1037.49036
K =    21          J =    1          T =  1037.63092
K =    22          J =    1          T =  1038.36694
K =    23          J =    1          T =  1040.22650
K =    24          J =    1          T =  1046.55792
K =    25          J =    1          T =  1071.32303
K =    26          J =    1          T =  1074.26370
K =    27          J =    1          T =  1074.34439
K =    28          J =    1          T =  1074.34268
K =    29          J =    1          T =  1074.34012
K =    30          J =    1          T =  1074.08450
K =    31          J =    1          T =  1056.35696

TIME= 830.00000SECS          NO. OF ITERATIONS=    2

TIME= 850.00000SECS          NO. OF ITERATIONS=    2

TIME= 870.00000SECS          NO. OF ITERATIONS=    2

TIME= 890.00000SECS          NO. OF ITERATIONS=    2

TIME= 910.00000SECS          NO. OF ITERATIONS=    2
K =     1          J =    1          T =  1045.13681
K =     1          J =    2          T =  1045.14423
K =     1          J =    3          T =  1045.16733
K =     1          J =    4          T =  1045.21106
K =     1          J =    5          T =  1045.31952
K =     1          J =    6          T =  1045.49545
K =     1          J =    7          T =  1045.78622
K =     1          J =    8          T =  1046.36011
K =     1          J =    9          T =  1047.24673
K =     1          J =   10          T =  1048.78256
K =     1          J =   11          T =  1051.79227
K =     1          J =   12          T =  1055.58304
K =     1          J =   13          T =  1057.71460
K =     1          J =   14          T =  1057.78262
K =     1          J =   15          T =  1044.96619
K =     1          J =   16          T =   994.14661
K =     1          J =   17          T =   825.41464
K =     2          J =    1          T =  1045.13608
K =     3          J =    1          T =  1045.13623
K =     4          J =    1          T =  1045.13705
K =     5          J =    1          T =  1045.13779
K =     6          J =    1          T =  1045.13974
K =     7          J =    1          T =  1045.14432
K =     8          J =    1          T =  1045.14725
K =     9          J =    1          T =  1045.15012
K =    10          J =    1          T =  1045.15356
K =    11          J =    1          T =  1045.15903
K =    12          J =    1          T =  1045.17355
K =    13          J =    1          T =  1045.18588
K =    14          J =    1          T =  1045.20102
```

```
K =   15        J =    1        T =  1045.21832
K =   16        J =    1        T =  1045.24094
K =   17        J =    1        T =  1045.29468
K =   18        J =    1        T =  1045.35999
K =   19        J =    1        T =  1045.44296
K =   20        J =    1        T =  1045.54892
K =   21        J =    1        T =  1045.70013
K =   22        J =    1        T =  1046.48138
K =   23        J =    1        T =  1048.44769
K =   24        J =    1        T =  1055.15033
K =   25        J =    1        T =  1081.49475
K =   26        J =    1        T =  1084.82974
K =   27        J =    1        T =  1084.93835
K =   28        J =    1        T =  1084.93857
K =   29        J =    1        T =  1084.93384
K =   30        J =    1        T =  1084.66635
K =   31        J =    1        T =  1066.95923
TIME= 930.00000SECS          NO. OF ITERATIONS=    2

TIME= 950.00000SECS          NO. OF ITERATIONS=    2

TIME= 970.00000SECS          NO. OF ITERATIONS=    2

TIME= 990.00000SECS          NO. OF ITERATIONS=    2

TIME=1010.00000SECS          NO. OF ITERATIONS=    2
K =    1        J =    1        T =  1049.65234
K =    1        J =    2        T =  1049.65997
K =    1        J =    3        T =  1049.68405
K =    1        J =    4        T =  1049.72925
K =    1        J =    5        T =  1049.84137
K =    1        J =    6        T =  1050.02353
K =    1        J =    7        T =  1050.32391
K =    1        J =    8        T =  1050.91779
K =    1        J =    9        T =  1051.83524
K =    1        J =   10        T =  1053.42343
K =    1        J =   11        T =  1056.53842
K =    1        J =   12        T =  1060.46365
K =    1        J =   13        T =  1062.66653
K =    1        J =   14        T =  1062.77200
K =    1        J =   15        T =  1049.98178
K =    1        J =   16        T =   999.05319
K =    1        J =   17        T =   829.29434
K =    2        J =    1        T =  1049.65186
K =    3        J =    1        T =  1049.65152
K =    4        J =    1        T =  1049.65253
K =    5        J =    1        T =  1049.65347
K =    6        J =    1        T =  1049.65555
K =    7        J =    1        T =  1049.66031
K =    8        J =    1        T =  1049.66321
K =    9        J =    1        T =  1049.66626
K =   10        J =    1        T =  1049.66986
K =   11        J =    1        T =  1049.67590
```

```
K =    9          J =    1          T =  1052.18765
K =   10          J =    1          T =  1052.19141
K =   11          J =    1          T =  1052.19788
K =   12          J =    1          T =  1052.21356
K =   13          J =    1          T =  1052.22656
K =   14          J =    1          T =  1052.24228
K =   15          J =    1          T =  1052.26062
K =   16          J =    1          T =  1052.28537
K =   17          J =    1          T =  1052.34259
K =   18          J =    1          T =  1052.41132
K =   19          J =    1          T =  1052.49869
K =   20          J =    1          T =  1052.61041
K =   21          J =    1          T =  1052.77261
K =   22          J =    1          T =  1053.59952
K =   23          J =    1          T =  1055.67413
K =   24          J =    1          T =  1062.75610
K =   25          J =    1          T =  1090.74762
K =   26          J =    1          T =  1094.50665
K =   27          J =    1          T =  1094.65063
K =   28          J =    1          T =  1094.65262
K =   29          J =    1          T =  1094.64682
K =   30          J =    1          T =  1094.37689
K =   31          J =    1          T =  1077.20422
TIME=1130.00000SECS          NO. OF ITERATIONS=    2
```

```
K =   12        J =   1        T =  1049.69116
K =   13        J =   1        T =  1049.70392
K =   14        J =   1        T =  1049.71930
K =   15        J =   1        T =  1049.73727
K =   16        J =   1        T =  1049.76123
K =   17        J =   1        T =  1049.81711
K =   18        J =   1        T =  1049.88461
K =   19        J =   1        T =  1049.97031
K =   20        J =   1        T =  1050.07983
K =   21        J =   1        T =  1050.23785
K =   22        J =   1        T =  1051.04749
K =   23        J =   1        T =  1053.08084
K =   24        J =   1        T =  1060.01797
K =   25        J =   1        T =  1087.37503
K =   26        J =   1        T =  1090.96899
K =   27        J =   1        T =  1091.09818
K =   28        J =   1        T =  1091.09955
K =   29        J =   1        T =  1091.09390
K =   30        J =   1        T =  1090.82275
K =   31        J =   1        T =  1073.35617
TIME=1030.00000SECS        NO. OF ITERATIONS=    2

TIME=1050.00000SECS        NO. OF ITERATIONS=    2

TIME=1070.00000SECS        NO. OF ITERATIONS=    2

TIME=1090.00000SECS        NO. OF ITERATIONS=    2

TIME=1110.00000SECS        NO. OF ITERATIONS=    2
K =    1        J =   1        T =  1052.17355
K =    1        J =   2        T =  1052.18134
K =    1        J =   3        T =  1052.20596
K =    1        J =   4        T =  1052.25195
K =    1        J =   5        T =  1052.36655
K =    1        J =   6        T =  1052.55255
K =    1        J =   7        T =  1052.85880
K =    1        J =   8        T =  1053.46478
K =    1        J =   9        T =  1054.40088
K =    1        J =  10        T =  1056.02167
K =    1        J =  11        T =  1059.20132
K =    1        J =  12        T =  1063.21014
K =    1        J =  13        T =  1065.45746
K =    1        J =  14        T =  1065.59540
K =    1        J =  15        T =  1052.86938
K =    1        J =  16        T =  1001.93369
K =    1        J =  17        T =   831.62045
K =    2        J =   1        T =  1052.17294
K =    3        J =   1        T =  1052.17282
K =    4        J =   1        T =  1052.17392
K =    5        J =   1        T =  1052.17490
K =    6        J =   1        T =  1052.17722
K =    7        J =   1        T =  1052.18173
K =    8        J =   1        T =  1052.18466
```

RESULTS OF RELIEF VALVE
VENTING HEAT TRANSFER ANALYSIS

```
EPSI =     .60000EPSL =     .06000FEL =     .32000FPSLN =     .50000THK =     .01588
RO =    1.52440RI =    1.50980TC =    30.00000TPROP =  325.00000TF = 1200.00000
TINIT =  325.00000REXCO =  .463800E 07MAXIT =     15NRNOD =     6HXIN =    10.00000HXOUT =    10.00000
NDT=  1            DT(NDT)=  10.00000           NTC(NDT)= 40            NEXT=  1

NDT=  2            DT(NDT)=  20.00000           NTC(NDT)=120            NEXT=  0

DENS=7800.00000       SPHT= 470.00000       FINAL TIME=1120.00000 SECS.       NUPDAT=  0       NSPEC= 20


****** DATA READ IN SUBROUTINE DTH01 ******

JT01= 16          AT01=   1.57000

N=  1           DTH=    .03330          IN(N)=  4          NEXT=  1

N=  2           DTH=    .06660          IN(N)=  7          NEXT=  1

N=  3           DTH=    .13330          IN(N)= 10          NEXT=  1

N=  4           DTH=    .28500          IN(N)= 12          NEXT=  1

N=  5           DTH=    .06660          IN(N)= 15          NEXT=  0


****** AXIAL GRID DATA READ IN SUBROUTINE DZ ******
K=  1           DZ=  .0500000          KCH(K)=  6          NEXT= 1

K=  2           DZ=  .1000000          KCH(K)= 11          NEXT= 1

K=  3           DZ=  .2000000          KCH(K)= 16          NEXT= 1

K=  4           DZ=  .4000000          KCH(K)= 21          NEXT= 1

K=  5           DZ= 1.3125000          KCH(K)= 25          NEXT= 0


TIME=  10.00000SECS           NO. OF ITERATIONS=     3


TIME=  20.00000SECS           NO. OF ITERATIONS=     2


TIME=  30.00000SECS           NO. OF ITERATIONS=     2


TIME=  40.00000SECS           NO. OF ITERATIONS=     2


TIME=  50.00000SECS           NO. OF ITERATIONS=     2
K =       1           J =     1           I =    360.09052
K =       1           J =     2           I =    361.88437
K =       1           J =     3           I =    409.68225
K =       1           J =     4           I =    413.20764
K =       1           J =     5           I =    413.36276
K =       1           J =     6           I =    413.36591
K =       1           J =     7           I =    413.36774
```

```
K =     1        J =    8        T =   413.37051
K =     1        J =    9        T =   413.37494
K =     1        J =   10        T =   413.38278
K =     1        J =   11        T =   413.39752
K =     1        J =   12        T =   413.41583
K =     1        J =   13        T =   413.42722
K =     1        J =   14        T =   413.43399
K =     1        J =   15        T =   413.42148
K =     1        J =   16        T =   412.96661
K =     1        J =   17        T =   406.20664
K =     2        J =    1        T =   361.91455
K =     3        J =    1        T =   409.61169
K =     4        J =    1        T =   413.13257
K =     5        J =    1        T =   413.35172
K =     6        J =    1        T =   413.36374
K =     7        J =    1        T =   413.36392
K =     8        J =    1        T =   413.36404
K =     9        J =    1        T =   413.36408
K =    10        J =    1        T =   413.36414
K =    11        J =    1        T =   413.36484
K =    12        J =    1        T =   413.36490
K =    13        J =    1        T =   413.36508
K =    14        J =    1        T =   413.36502
K =    15        J =    1        T =   413.36517
K =    16        J =    1        T =   413.36511
K =    17        J =    1        T =   413.36527
K =    18        J =    1        T =   413.36566
K =    19        J =    1        T =   413.36603
K =    20        J =    1        T =   413.36655
K =    21        J =    1        T =   413.36694
K =    22        J =    1        T =   413.37051
K =    23        J =    1        T =   413.38034
K =    24        J =    1        T =   413.41333
K =    25        J =    1        T =   413.53299
K =    26        J =    1        T =   413.24283
K =    27        J =    1        T =   413.24118
K =    28        J =    1        T =   413.24112
K =    29        J =    1        T =   413.24161
K =    30        J =    1        T =   413.24231
K =    31        J =    1        T =   413.24789
TIME=  60.00000SECS           NO. OF ITERATIONS=    2

TIME=  70.00000SECS           NO. OF ITERATIONS=    2

TIME=  80.00000SECS           NO. OF ITERATIONS=    2

TIME=  90.00000SECS           NO. OF ITERATIONS=    2

TIME= 100.00000SECS           NO. OF ITERATIONS=    2
K =     1        J =    1        T =   366.77750
K =     1        J =    2        T =   372.10333
K =     1        J =    3        T =   483.50940
K =     1        J =    4        T =   497.69318
```

```
K =     1         J =    5          T =   498.74921
K =     1         J =    6          T =   498.77643
K =     1         J =    7          T =   498.78177
K =     1         J =    8          T =   498.78989
K =     1         J =    9          T =   498.80267
K =     1         J =   10          T =   498.82526
K =     1         J =   11          T =   498.86807
K =     1         J =   12          T =   498.92133
K =     1         J =   13          T =   498.95432
K =     1         J =   14          T =   498.97122
K =     1         J =   15          T =   498.82758
K =     1         J =   16          T =   496.46072
K =     1         J =   17          T =   475.28430
K =     2         J =    1          T =   372.18341
K =     3         J =    1          T =   483.21372
K =     4         J =    1          T =   497.22238
K =     5         J =    1          T =   498.63983
K =     6         J =    1          T =   498.76431
K =     7         J =    1          T =   498.77130
K =     8         J =    1          T =   498.77158
K =     9         J =    1          T =   498.77158
K =    10         J =    1          T =   498.77170
K =    11         J =    1          T =   498.77307
K =    12         J =    1          T =   498.77332
K =    13         J =    1          T =   498.77371
K =    14         J =    1          T =   498.77371
K =    15         J =    1          T =   498.77402
K =    16         J =    1          T =   498.77396
K =    17         J =    1          T =   498.77438
K =    18         J =    1          T =   498.77551
K =    19         J =    1          T =   498.77667
K =    20         J =    1          T =   498.77820
K =    21         J =    1          T =   498.77976
K =    22         J =    1          T =   498.79053
K =    23         J =    1          T =   498.81894
K =    24         J =    1          T =   498.91461
K =    25         J =    1          T =   499.25983
K =    26         J =    1          T =   498.61173
K =    27         J =    1          T =   498.60361
K =    28         J =    1          T =   498.60349
K =    29         J =    1          T =   498.60437
K =    30         J =    1          T =   498.60535
K =    31         J =    1          T =   498.57944
TIME= 110.00000SECS          NO. OF ITERATIONS=    2

TIME= 120.00000SECS          NO. OF ITERATIONS=    2

TIME= 130.00000SECS          NO. OF ITERATIONS=    2

TIME= 140.00000SECS          NO. OF ITERATIONS=    2

TIME= 150.00000SECS          NO. OF ITERATIONS=    2
K =     1         J =    1          T =   368.80386
```

```
K =    1          J =   2          T =  377.72330
K =    1          J =   3          T =  547.18970
K =    1          J =   4          T =  576.79572
K =    1          J =   5          T =  579.90448
K =    1          J =   6          T =  580.01086
K =    1          J =   7          T =  580.02472
K =    1          J =   8          T =  580.04431
K =    1          J =   9          T =  580.07504
K =    1          J =  10          T =  580.12903
K =    1          J =  11          T =  580.23175
K =    1          J =  12          T =  580.36029
K =    1          J =  13          T =  580.43955
K =    1          J =  14          T =  580.47180
K =    1          J =  15          T =  579.94281
K =    1          J =  16          T =  573.93610
K =    1          J =  17          T =  534.38944
K =    2          J =   1          T =  377.84363
K =    3          J =   1          T =  546.52930
K =    4          J =   1          T =  575.51379
K =    5          J =   1          T =  579.49030
K =    6          J =   1          T =  579.96344
K =    7          J =   1          T =  579.99985
K =    8          J =   1          T =  580.00104
K =    9          J =   1          T =  580.00107
K =   10          J =   1          T =  580.00140
K =   11          J =   1          T =  580.00333
K =   12          J =   1          T =  580.00378
K =   13          J =   1          T =  580.00455
K =   14          J =   1          T =  580.00476
K =   15          J =   1          T =  580.00537
K =   16          J =   1          T =  580.00552
K =   17          J =   1          T =  580.00644
K =   18          J =   1          T =  580.00903
K =   19          J =   1          T =  580.01190
K =   20          J =   1          T =  580.01544
K =   21          J =   1          T =  580.01968
K =   22          J =   1          T =  580.04688
K =   23          J =   1          T =  580.11511
K =   24          J =   1          T =  580.34515
K =   25          J =   1          T =  581.17722
K =   26          J =   1          T =  580.25198
K =   27          J =   1          T =  580.23383
K =   28          J =   1          T =  580.23377
K =   29          J =   1          T =  580.23511
K =   30          J =   1          T =  580.23584
K =   31          J =   1          T =  579.99674
 TIME= 160.00000SECS          NO. OF ITERATIONS=   2


 TIME= 170.00000SECS          NO. OF ITERATIONS=   2


 TIME= 180.00000SECS          NO. OF ITERATIONS=   2


 TIME= 190.00000SECS          NO. OF ITERATIONS=   2
```

```
                              .
                              .
                              .
                              .
K =     21          J =     1           T =  1023.48041
K =     22          J =     1           T =  1024.15134
K =     23          J =     1           T =  1025.84665
K =     24          J =     1           T =  1031.60971
K =     25          J =     1           T =  1053.99655
K =     26          J =     1           T =  1056.36111
K =     27          J =     1           T =  1056.40756
K =     28          J =     1           T =  1056.40463
K =     29          J =     1           T =  1056.40366
K =     30          J =     1           T =  1056.17328
K =     31          J =     1           T =  1038.93802
TIME= 730.00000SECS          NO. OF ITERATIONS=    2

TIME= 750.00000SECS          NO. OF ITERATIONS=    2

TIME= 770.00000SECS          NO. OF ITERATIONS=    2

TIME= 790.00000SECS          NO. OF ITERATIONS=    2

TIME= 810.00000SECS          NO. OF ITERATIONS=    3
K =      1          J =     1           T =   375.00305
K =      1          J =     2           T =   402.41330
K =      1          J =     3           T =   856.86600
K =      1          J =     4           T =   997.89398
K =      1          J =     5           T =  1033.63315
K =      1          J =     6           T =  1037.11624
K =      1          J =     7           T =  1037.69675
K =      1          J =     8           T =  1038.25812
K =      1          J =     9           T =  1039.09683
K =      1          J =    10           T =  1040.54901
K =      1          J =    11           T =  1043.39243
K =      1          J =    12           T =  1046.97000
K =      1          J =    13           T =  1048.98969
K =      1          J =    14           T =  1049.01889
K =      1          J =    15           T =  1036.29520
K =      1          J =    16           T =   985.84644
K =      1          J =    17           T =   819.01804
K =      2          J =     1           T =   402.56778
K =      3          J =     1           T =   851.89078
K =      4          J =     1           T =   987.92722
K =      5          J =     1           T =  1024.55576
K =      6          J =     1           T =  1034.46869
K =      7          J =     1           T =  1036.87494
K =      8          J =     1           T =  1037.09274
K =      9          J =     1           T =  1037.11340
K =     10          J =     1           T =  1037.11823
K =     11          J =     1           T =  1037.12268
K =     12          J =     1           T =  1037.13614
K =     13          J =     1           T =  1037.14777
K =     14          J =     1           T =  1037.16254
K =     15          J =     1           T =  1037.17892
K =     16          J =     1           T =  1037.19943
K =     17          J =     1           T =  1037.24957
```

```
K =   18        J =   1        T =  1037.31161
K =   19        J =   1        T =  1037.39014
K =   20        J =   1        T =  1037.49036
K =   21        J =   1        T =  1037.63097
K =   22        J =   1        T =  1038.36694
K =   23        J =   1        T =  1040.22650
K =   24        J =   1        T =  1046.55792
K =   25        J =   1        T =  1071.37303
K =   26        J =   1        T =  1074.26370
K =   27        J =   1        T =  1074.34439
K =   28        J =   1        T =  1074.34268
K =   29        J =   1        T =  1074.34012
K =   30        J =   1        T =  1074.08450
K =   31        J =   1        T =  1056.35696
TIME = 830.00000SECS          NO. OF ITERATIONS=    2

TIME = 850.00000SECS          NO. OF ITERATIONS=    2

TIME = 870.00000SECS          NO. OF ITERATIONS=    2

TIME = 890.00000SECS          NO. OF ITERATIONS=    2

TIME = 910.00000SECS          NO. OF ITERATIONS=    2

K =    1        J =   1        T =   375.13699
K =    1        J =   2        T =   402.93680
K =    1        J =   3        T =   863.17813
K =    1        J =   4        T =  1005.64624
K =    1        J =   5        T =  1041.61945
K =    1        J =   6        T =  1045.15619
K =    1        J =   7        T =  1045.76462
K =    1        J =   8        T =  1046.35937
K =    1        J =   9        T =  1047.24673
K =    1        J =  10        T =  1048.78256
K =    1        J =  11        T =  1051.79227
K =    1        J =  12        T =  1055.58304
K =    1        J =  13        T =  1057.71460
K =    1        J =  14        T =  1057.78262
K =    1        J =  15        T =  1044.96619
K =    1        J =  16        T =   994.14661
K =    1        J =  17        T =   825.41464
K =    2        J =   1        T =   403.09317
K =    3        J =   1        T =   858.13953
K =    4        J =   1        T =   995.59903
K =    5        J =   1        T =  1032.47363
K =    6        J =   1        T =  1042.44391
K =    7        J =   1        T =  1044.89624
K =    8        J =   1        T =  1045.12555
K =    9        J =   1        T =  1045.14841
K =   10        J =   1        T =  1045.15375
K =   11        J =   1        T =  1045.15903
K =   12        J =   1        T =  1045.17355
K =   13        J =   1        T =  1045.18588
K =   14        J =   1        T =  1045.20102
```

```
K =    15          J =    1          T =  1045.21832
K =    16          J =    1          T =  1045.24094
K =    17          J =    1          T =  1045.29468
K =    18          J =    1          T =  1045.35999
K =    19          J =    1          T =  1045.44296
K =    20          J =    1          T =  1045.54892
K =    21          J =    1          T =  1045.70013
K =    22          J =    1          T =  1046.48138
K =    23          J =    1          T =  1048.44769
K =    24          J =    1          T =  1055.15033
K =    25          J =    1          T =  1081.49475
K =    26          J =    1          T =  1084.82974
K =    27          J =    1          T =  1084.93835
K =    28          J =    1          T =  1084.93857
K =    29          J =    1          T =  1084.93384
K =    30          J =    1          T =  1084.66635
K =    31          J =    1          T =  1066.95923
TIME= 930.00000SECS          NO. OF ITERATIONS=    2

TIME= 950.00000SECS          NO. OF ITERATIONS=    2

TIME= 970.00000SECS          NO. OF ITERATIONS=    2

TIME= 990.00000SECS          NO. OF ITERATIONS=    2

TIME=1010.00000SECS          NO. OF ITERATIONS=    2
K =     1          J =    1          T =   375.21640
K =     1          J =    2          T =   403.24551
K =     1          J =    3          T =   866.88684
K =     1          J =    4          T =  1010.11841
K =     1          J =    5          T =  1046.12964
K =     1          J =    6          T =  1049.67841
K =     1          J =    7          T =  1050.30133
K =     1          J =    8          T =  1050.91693
K =     1          J =    9          T =  1051.83524
K =     1          J =   10          T =  1053.42343
K =     1          J =   11          T =  1056.53842
K =     1          J =   12          T =  1060.46365
K =     1          J =   13          T =  1062.66653
K =     1          J =   14          T =  1062.77200
K =     1          J =   15          T =  1049.98178
K =     1          J =   16          T =   999.05319
K =     1          J =   17          T =   829.29434
K =     2          J =    1          T =   403.40341
K =     3          J =    1          T =   861.81793
K =     4          J =    1          T =  1000.03287
K =     5          J =    1          T =  1036.98120
K =     6          J =    1          T =  1046.94501
K =     7          J =    1          T =  1049.40576
K =     8          J =    1          T =  1049.64029
K =     9          J =    1          T =  1049.66446
K =    10          J =    1          T =  1049.67001
K =    11          J =    1          T =  1049.67590
```

```
K =    12          J =    1          T =  1049.69116
K =    13          J =    1          T =  1049.70392
K =    14          J =    1          T =  1049.71930
K =    15          J =    1          T =  1049.73727
K =    16          J =    1          T =  1049.76123
K =    17          J =    1          T =  1049.81711
K =    18          J =    1          T =  1049.88461
K =    19          J =    1          T =  1049.97031
K =    20          J =    1          T =  1050.07983
K =    21          J =    1          T =  1050.23785
K =    22          J =    1          T =  1051.04749
K =    23          J =    1          T =  1053.08084
K =    24          J =    1          T =  1060.01797
K =    25          J =    1          T =  1087.37503
K =    26          J =    1          T =  1090.96899
K =    27          J =    1          T =  1091.09818
K =    28          J =    1          T =  1091.09955
K =    29          J =    1          T =  1091.09390
K =    30          J =    1          T =  1090.82275
K =    31          J =    1          T =  1073.35617
TIME=1030.00000SECS          NO. OF ITERATIONS=    2

TIME=1050.00000SECS          NO. OF ITERATIONS=    2

TIME=1070.00000SECS          NO. OF ITERATIONS=    2

TIME=1090.00000SECS          NO. OF ITERATIONS=    2

TIME=1110.00000SECS          NO. OF ITERATIONS=    2
K =     1          J =    1          T =   375.26273
K =     1          J =    2          T =   403.42529
K =     1          J =    3          T =   869.04126
K =     1          J =    4          T =  1012.68033
K =     1          J =    5          T =  1048.66190
K =     1          J =    6          T =  1052.20563
K =     1          J =    7          T =  1052.83557
K =     1          J =    8          T =  1053.46405
K =     1          J =    9          T =  1054.40088
K =     1          J =   10          T =  1056.02167
K =     1          J =   11          T =  1059.20132
K =     1          J =   12          T =  1063.21014
K =     1          J =   13          T =  1065.45746
K =     1          J =   14          T =  1065.59540
K =     1          J =   15          T =  1052.86938
K =     1          J =   16          T =  1001.93369
K =     1          J =   17          T =   831.62045
K =     2          J =    1          T =   403.58432
K =     3          J =    1          T =   863.95804
K =     4          J =    1          T =  1002.57565
K =     5          J =    1          T =  1039.53299
K =     6          J =    1          T =  1049.47073
K =     7          J =    1          T =  1051.92480
K =     8          J =    1          T =  1052.16101
```

```
K =     9          J =     1          T =  1052.18591
K =    10          J =     1          T =  1052.19162
K =    11          J =     1          T =  1052.19788
K =    12          J =     1          T =  1052.21356
K =    13          J =     1          T =  1052.22656
K =    14          J =     1          T =  1052.24228
K =    15          J =     1          T =  1052.26062
K =    16          J =     1          T =  1052.28537
K =    17          J =     1          T =  1052.34259
K =    18          J =     1          T =  1052.41132
K =    19          J =     1          T =  1052.49869
K =    20          J =     1          T =  1052.61041
K =    21          J =     1          T =  1052.77261
K =    22          J =     1          T =  1053.59952
K =    23          J =     1          T =  1055.67413
K =    24          J =     1          T =  1062.75610
K =    25          J =     1          T =  1090.74762
K =    26          J =     1          T =  1094.50665
K =    27          J =     1          T =  1094.65063
K =    28          J =     1          T =  1094.65262
K =    29          J =     1          T =  1094.64682
K =    30          J =     1          T =  1094.37689
K =    31          J =     1          T =  1077.20422

TIME=1130.00000SECS          NO. OF ITERATIONS=    2
```

APPENDIX F: COMPUTER PROGRAM FOR PREDICTING THE RESISTANCE OF THE STRIP AB SHOWN IN FIG. 2-36

A listing of a FORTRAN IV computer program for predicting the thermal resistance of the strip AB shown in Figs. 2-36 and 2-37 is provided in this Appendix. The resistance of the strip, designated RESIST in the program, is calculated between the isothermal patches shown at temperatures T_o and T_1 in Figs. 2-36 and 2-37. This resistance, denoted R_s in Sect. 2.3.4.1, is needed to calculate the effective thermal conductivity of Style II EXPLOSAFE. The variables L_1,w,t and $\bar{S}$ identified in Fig. 2-37 are designated LENGTH, WIDTH, THICK and PW (acronym for "patch width") in the program.

The program is very simple to use in that only seven variables, listed in Table F-1, are required as input. The program divides the strip into NX subdivisions along its length and NY subdivisions along its width (see input variables 1 and 2) and obtains finite-difference equations for all of the nodes at the grid line intersections. The boundaries of the strip are modelled as being adiabatic except over the lower isothermal patch (of width PW), where a temperature of 0 is prescribed, and the upper isothermal patch, where a temperature of 100 is prescribed. The program solves the finite-difference equations for all of the nodes in the grid simultaneously to obtain the nodal temperatures, stored in the vector T, and then uses those temperatures to calculate the heat flow rate through the lower patch (QFL) and the heat flow rate through the upper patch (QFU). The resistance of the patch is then calculated from the expression,

RESIST =100.0/QFU

and printed out along with the heat flows QFL and QFU. The numerator in the expression for RESIST is 100.0 because the temperature difference between the upper and lower isothermal patches is set at 100.0, as mentioned previously. The heat flows printed out, QFL and QFU, should be the same of course.

The finite-difference equations for the nodes in the strip are solved simultaneously by subroutine GEBS (also included), which is applicable to banded positive-definite systems of equations. A positive-definite matrix is always symmetric so only the finite-difference coefficients (internodal conductances) within the left-hand bandwidth (=NBAND) of the conductance matrix are stored in the banded representation of that matrix (CO). Right-hand side constants are stored in the vector Q.

The results of a sample analysis performed with,

NX =50
NY =10
LENGTH =1.0(cm)
WIDTH =0.14(cm)
THICK =0.0075(cm)
PW =0.15(cm)
TCAL =1.80(W/cm°C)

are included after the program listing. These input values apply to the EXPLOSAFE foil used in the experimental program (thermal conductivity tests).

TABLE F-1: Input variables for program RESIST

VARIABLE #	VARIABLE NAME	FORMAT	DATA CARD #	DESCRIPTION
1	NX	I5	1	Number of subdivisions used along the length of the strip
2	NY	I5	1	Number of subdivisions used across the width of the strip
3	LENGTH	F10.5	1	Length of strip
4	WIDTH	F10.5	1	Width of strip
5	THICK	F10.5	1	Thickness of strip
6	PW	F10.5	1	Width of isothermal patches shown at temperatures T_o and T_1 in Figs. 2-36 and 2-37
7	TCAL	F10.5	1	Thermal conductivity of strip material (ie. EXPLOSAFE foil)

NOTE: Program RESIST can be used with any set of units but the units for the input variables must be consistent.

```
0001        PROGRAM RESIST
      C
      C
      C*********************************************************************
      C*********************************************************************
      C
      C
0002        REAL LENGTH
      C
0003        DIMENSION FNAME(4),CO(12,570),T(570),Q(570),C(5)
      C
      C
      C*******************************************************************
      C*******************************************************************
      C
      C
0004        IR=5
      C
      C     GET INPUT FILE NAME
      C
0005        WRITE(7,7)
0006  7     FORMAT(1X,'ENTER FILE NAME'$)
0007        READ(7,8) FNAME
0008  8     FORMAT(4A4)
0009        OPEN(UNIT=5,TYPE='OLD',NAME=FNAME)
      C
      C     GET OUTPUT DEVICE
      C
0010        WRITE(7,17)
0011  17    FORMAT(1X,'ENTER OUTPUT DEVICE (6=LP,7=TT,8=DYO:RESIST.LST) '$)
0012        READ(7,18)I
0013  18    FORMAT(I1)
0014        IW=I
0015        IF(I.EQ.0)IW=7
0017        IF(IW.EQ.8)OPEN(UNIT=8,TYPE='UNKNOWN',NAME='DYO:RESIST.LST')
      C
      C     READ INPUT DATA
      C
0019        READ(IR,800)NX,NY,LENGTH,WIDTH,THICK,PW,TCAL
0020  800   FORMAT(2I5,5F10.5)
      C
      C     CALCULATE NUMBER OF NODES ON X-AXIS(NNX) AND Y-AXIS(NNY)
      C
0021        NNX=NX+1
0022        NNY=NY+1
      C
      C     CALCULATE MESH SPACING ON X-AXIS(DX) AND Y-AXIS(DY)
      C
0023        DX=LENGTH/NX
0024        DY=WIDTH/NY
      C
      C     FIND NODES (ON X-AXIS) AT THE ENDS OF THE ISOTHERMAL PATCHES
      C     ON THE UPPER AND LOWER SURFACES OF THE STRIP (NPU & NPL RESPECTIVELY)
      C
```

```
0025            XL=LENGTH-PW
0026            X=0.0
          C
0027            DO 20 I=2,NNX
0028              X=X+DX
0029      20    IF(X.GT.PW)GO TO 25
          C
0031            WRITE(IW,801)
0032      801   FORMAT(1X,'END OF UPPER ISOTHERMAL PATCH NOT FOUND')
0033            STOP
          C
0034      25    NPU=I-1
0035            NPU2=NPU+2
0036            DO 30 I=NPU2,NNX
0037              X=X+DX
0038      30    IF(X.GT.XL)GO TO 35
          C
0040            WRITE(IW,802)
0041      802   FORMAT(1X,'END OF LOWER ISOTHERMAL PATCH NOT FOUND')
0042            STOP
          C
0043      35       NPL=I
          C
          C     CALCULATE INTERNODAL CONDUCTANCE IN THE Y-DIRECTION (CY)
          C     AND THE X-DIRECTION (CX)
          C
0044            CY=TCAL*THICK*DX/DY
0045            CX=TCAL*THICK*DY/DX
0046            CCOND=TCAL*100.0/WIDTH
          C
          C     CALCULATE HALF-BANDWIDTH OF BANDED COEFFICIENT MATRIX (MBAND)
          C     AND TOTAL NUMBER OF FINITE-DIFFERENCE EQUATIONS (NEQU)
          C
0047            MBAND=NNY+1
0048            NEQU=NNY*NNX
          C
          C     ZERO COEFFICIENT MATRIX (CO) AND RIGHT-HAND SIDE VECTOR (Q)
          C
0049            DO 45 J=1,NEQU
0050            DO 46 I=1,MBAND
0051      46    CO(I,J)=0.0
0052      45    Q(J)=0.0
          C
          C     SWEEP THROUGH NODES IN FINITE-DIFFERENCE GRID AND ASSEMBLE F-D
          C     EQUATIONS (IE, ASSEMBLE COEFFICIENT MATRIX CO AND RIGHT-HAND
          C     SIDE HEAT FLOW VECTOR Q)
          C
0053            L=0
          C
0054            DO 50 I=1,NNX
0055              C1=1.0
0056              IF(I.EQ.1.OR.I.EQ.NNX)C1=0.5
          C
0058            DO 55 J=1,NNY
```

```
0059             L=L+1
0060             C2=1.0
0061             IF(J.EQ.1.OR.J.EQ.NNY) C2=0.5
      C
0063             C(1)=0.0
0064             IF(I.EQ.1)GO TO 60
0066             C(1)=C2*CX
0067             CO(MBAND,L-NNY)=-C(1)
      C
0068  60         C(2)=0.0
0069             IF(I.EQ.NNX)GO TO 65
0071             C(2)=C2*CX
      C
0072  65            C(3)=0.0
0073             IF(J.EQ.1)GO TO 70
0075             C(3)=C1*CY
0076             CO(2,L-1)=-C(3)
      C
0077  70         C(4)=0.0
0078             IF(J.EQ.NNY)GO TO 75
0080             C(4)=C1*CY
      C
0081  75         C(5)=0.0
0082             IF((J.EQ.1.AND.I.GE.NPL).OR.(J.EQ.NNY.AND.I.LE.NPU))GO TO 80
0084             GO TO 85
      C
0085  80         C(5)=C1*THICK*DX*CCOND
0086             IF(J.EQ.NNY) Q(L)=100.0*C(5)
0088  85         CO(1,L)=C(1)+C(2)+C(3)+C(4)+C(5)
      C
0089  55       CONTINUE
0090  50       CONTINUE
      C
      C        CALL EQUATION SOLVING ROUTINE
      C
0091           CALL GEBS(Q,T,CO,MBAND,NEQU)
      C
      C        PRINT NODAL TEMPERATURES AND CALCULATE HEAT FLOW RATE THROUGH STRIP
      C
0092           L=0
0093           QFL=0.0
0094           QFU=0.0
      C
0095           DO 90 I=1,NNX
0096             C1=1.0
0097             IF(I.EQ.1.OR.I.EQ.NNX) C1=0.5
      C
0099           DO 95 J=1,NNY
0100             L=L+1
0101             IF((J.EQ.1.AND.I.GE.NPL).OR.(J.EQ.NNY.AND.I.LE.NPU)) GO TO 100
0103             GO TO 95
      C
0104  100        C5=C1*THICK*DX*CCOND
0105             IF(J.EQ.1)QFL=QFL+C5*T(L)
```

```
      C
0107            IF(J.EQ.NNY)QFU=QFU+C5*(100.0-T(L))
      C
0109  95     CONTINUE
0110  90     CONTINUE
      C
      C      CALCULATE AND PRINT RESISTANCE OF STRIP (RESIST)
      C
0111         RESIST=100.0/QFU
0112         WRITE(IW,805)QFL,QFU,RESIST
0113  805    FORMAT(1X,'QFL=',E12.5,4X,'QFU=',E12.5,4X,'RESIST=',E12.5)
      C
0114         STOP
0115         END
      C
      C***********************************************************************
      C************************************************************************
      C
      C
      C      THIS SUBROUTINE SOLVES BANDED SYMMETRIC SYSTEMS OF LINEAR
      C      EQUATIONS.
      C
             SUBROUTINE GEBS (Q,T,CO,NBAND,LMAX)
             DIMENSION CO(12,570),Q(570),T(570)
             IJ=1
             NA=NBAND
             NR=LMAX-NBAND
      10     RGE=1.0/CO(1,IJ)
             Q(IJ)=RGE*Q(IJ)
             IF(NA-1) 30,30,12
      12     DO 20 II=2,NA
             CX=CO(II,IJ)
             CO(II,IJ)=RGE*CO(II,IJ)
             DO 18 JJ=2,II
             I=II+1-JJ
             J=IJ-1+JJ
      18     CO(I,J)=CO(I,J)-CX*CO(JJ,IJ)
             IIF=IJ-1+II
      20     Q(IIF)=Q(IIF)-CX*Q(IJ)
             NR=NR-1
             IF(NR) 22,24,24
      22     NA=NA-1
      24     IJ=IJ+1
             GO TO 10
      30     NA=1
             IJ=LMAX
             T(IJ)=Q(IJ)
      32     IJ=IJ-1
             IF(IJ) 34,34,36
      34     RETURN
      36     IF(NA-NBAND) 38,40,40
      38     NA=NA+1
      40     CX=Q(IJ)
             DO 44 I=2,NA
             J=IJ-1+I
      44     CX=CX-CO(I,IJ)*T(J)
             T(IJ)=CX
             GO TO 32
             END
```

SAMPLE OUTPUT

```
QFL= 0.22423E+00    QFU= 0.22422E+00    RESIST= 0.44599E+03
```

APPENDIX G: CALCULATION OF THE NOZZLE DISCHARGE CONDITIONS FOR A MIDLAND A-3480 RELIEF VALVE

The mass flowrate of propane vapor ($\dot{m}$) discharged through a choked relief valve is given by the expression,

$$\dot{m} = C_D A_t G \qquad \text{G-1}$$

where C_D is the flow coefficient of the valve, A_t is the valve's minimum flow area (throat area) and G is the critical mass flux for an isentropic discharge, defined by the equation.

$$G = 0.637 \sqrt{\frac{p_o}{v_o}} \quad (\text{kg/m}^2\ \text{sec.}) \quad (\text{see. Eq. 3-40}) \qquad \text{G-2}$$

for propane when p_o is in P_a and v_o is in m^3/kg. At a tank pressure (p_o) of 2.07 MPa (300 psia), $v_o = 0.0206\ m^3/kg$ (value obtained from thermodynamic tables for propane) so $G = 6390\ kg/m^2$ sec. from Eq. G-2. The minimum flow area (A_t) for a Midland A-3480 relief valve is $5.074 \times 10^{-3} m^2$ so, for $C_D = 0.87$, Eq. G-1 predicts a vapor mass flowrate ($\dot{m}$) of 28.2 kg/sec. Referring to the geometry of a Midland A-3480 relief valve shown in Fig. 3-9, the valve will effectively act as a crude convergent-divergent nozzle when the flow is choked at the poppet valve part because the final flow area of the valve (ie. the area of the annulus with an outer diameter of 7.1" and an inner diameter of 2.8") is, at $2.166 \times 10^{-2} m^2$, greater than the port area of $5.074 \times 10^{-3} m^2$. The ratio of the discharge area (A_d) to the throat area (A_t) is 4.27 in this case and the pressure at the discharge (p_d) will be either greater than atmospheric if the nozzle is underexpanding or equal to atmospheric if the nozzle is fully expanding or overexpanding. For the purpose of estimating the nozzle discharge conditions it will be assumed that:

a) the flow in the nozzle is isentropic. This assumption is obviously very unrealistic because friction losses will be high in the nozzle but it allows an approximate estimate of the nozzle discharge conditions to be obtained very easily.

b) the propane vapor can be treated as a perfect gas.

With these assumptions, the discharge pressure that would be obtained if the nozzle was fully expanding or underexpanding is equal to the smaller root of the isentropic flow relation,

$$\left(\frac{A_d}{A_t}\right)^2 = \frac{\gamma-1}{2} \frac{\left(\frac{2}{\gamma+1}\right)^{(\gamma+1)/\gamma-1}}{\left[1-\frac{p_d}{p_o}^{(\gamma-1)/\gamma}\right]\left(\frac{p_d}{p_o}\right)^{2/\gamma}}$$

where the ratio of specific heats, γ, is approximately 1.14 for propane and p_o is the reservoir pressure (2.07 MPa). Solving Eq. G-3 for p_d by iteration (with $A_d/A_t = 4.27$) we obtain $p_d = 93$ kPa. Since p_d is less than atmospheric pressure ($\approx$101 kPa), a very weak shock will form, according to this analysis, near the nozzle exit so that the pressure at the discharge will be atmospheric. The nozzle will be assumed to be fully expanding, however, because the value of p_d obtained from Eq. G-3 is so close to atmospheric pressure. With this assumption, the Mach number (Ma) at the flow at the nozzle discharge can be calculated from another isentropic flow relation, viz.

$$\mathrm{Ma} = \sqrt{\frac{2}{\gamma-1}\left[\left(\frac{p_d}{p_o}\right)^{(1-\gamma)/\gamma} - 1\right]} \qquad \text{G-4}$$

which for $p_d/p_o = 0.0448$, gives Ma = 2.57. The density of the vapor at the nozzle discharge (ρ_d) is given in terms of the vapor density at the reservoir conditions (ρ_o) and the Mach number by the expression,

$$\frac{\rho_d}{\rho_o} = (1 + \frac{\gamma - 1}{2} Ma^2)^{1/1-\gamma} \qquad \text{G-5}$$

which, for a reservoir density ρ_o (= $1/v_o$) of approximately 48.6 kg/m^3, gives $\rho_d = 3.19$ kg/m^3. For a mass flowrate ($\dot{m}$) of 28.2 kg/sec., the vapor velocity at the nozzle discharge (V_d) will be,

$$V_d = \frac{\dot{m}}{\rho_d A_d} = \frac{28.2}{3.19 \times 2.166 \times 10^{-2}} = 408 \text{ m/sec.}$$